

**Newcastle**  
University

Investigation of the zinc-ZIP8-MTF1 signalling pathway in  
human OA chondrocytes

**Will Thompson 150501176**

*A thesis submitted in fulfilment of the requirements for the degree of  
Doctor of Philosophy*

*in the*

**Biosciences Institute  
International Centre for Life  
NE1 3BZ**

Supervisor:

Dr. Louise Reynard

Co-supervisors:

Prof. John Loughlin & Dr. Catharien Hilkens

December 2020



## ABSTRACT

Osteoarthritis (OA) is a common musculoskeletal disease characterised by articular cartilage loss resulting in severe joint pain, chronic morbidity, and premature mortality. There are no licensed OA drugs and current treatments involve pain relief with analgesics and joint replacement surgery.

In murine cartilage chondrocytes the zinc-ZIP8-MTF1 signalling pathway causes cartilage breakdown. Pathway activation by interleukin-1 $\beta$  (IL-1 $\beta$ ) stimulates upregulation of zinc transporter gene *Slc39a8* (coding for ZIP8), increased intracellular zinc levels, nuclear translocation of the zinc-dependent MTF1 transcription factor and upregulation of genes encoding cartilage matrix-degrading proteins including *Mmp13* and *Adam-ts5*.

This thesis aimed to investigate if the IL-1-mediated zinc-ZIP8-MTF1 pathway is active in human chondrocytes and if this pathway contributes to OA pathogenesis.

Analysis of OA-related transcriptomic datasets revealed that *SLC39A14* but not *SLC39A8*, was dysregulated in human OA cartilage and mouse OA models. Human articular chondrocytes (HACs), and the chondrocyte cell lines SW1353 and T/C-28a2, were cultured in monolayer and treated with IL-1 $\alpha$  and/or ZnCl<sub>2</sub> or IL-1 $\beta$ . Genes involved in inflammation, zinc homeostasis and cartilage degradation were measured by quantitative PCR. MTF1 activity and subcellular localisation were evaluated using luciferase reporter assays, immunocytochemistry (ICC) and western blots.

*SLC39A8* and *SLC39A14* were upregulated in IL-1 $\alpha$ -treated HACs 5.5 and 2.9-fold respectively but were selectively elevated in SW1353 (*SLC39A8*,  $p < 0.0001$ ) and T/C-28a2 cells (*SLC39A14*,  $p = 0.0001$ ). IL-1 raised intracellular zinc ion levels in HACs ( $p = 0.0004$ ) but not in the cell lines. IL-1 upregulated *MMP13* in T/C-28a2 lines and SW1353 cells, while both *MMP13* and *ADAM-TS5* were upregulated in T/C-28a2 cells. *MMP13* and *ADAM-TS5* expression was non-significant after IL-1 treatment in HACs. IL-1 repressed MTF1 transactivation activity in SW1353 cells (14.5%,  $p = 0.0114$ ), even when MTF1 itself was overexpressed (17.2%  $p < 0.0001$ ). Western blotting and ICC results were non-correlative.

Zinc-ZIP8-MTF1-mediated cartilage matrix-degrading gene upregulation induced through IL-1 $\alpha$  as a contributing factor to human OA pathogenesis was inconclusive.

## **ACKNOWLEDGEMENTS**

I would like to thank my supervisors Dr. Louise Reynard, Professor John Loughlin and Dr. Catharien Hilkens for their knowledge, commitment, and support throughout my academic studies. I would like to extend thanks to colleagues formerly of the Institute of Cellular Medicine, especially Dr. David Swan with whom many engaging conversations on zinc transporters were had. I am grateful to everyone in the Skeletal Research Group and Centre for Life who have supported or helped me develop scientifically and professionally.

A note of personal thanks to my close circle of friends and family who have provided much emotional support and especially my parents whose sustained encouragement helped me reach this project's conclusion. Finally, I would like to dedicate this PhD to my grandparents who sadly passed away during the coronavirus pandemic.

# TABLE OF CONTENTS

TABLE OF CONTENTS .....	i
LIST OF TABLES.....	vii
LIST OF FIGURES.....	ix
ABBREVIATIONS.....	xvi
<b>Chapter 1. INTRODUCTION .....</b>	<b>1</b>
<b>1.1 Synovial joint and long bone biology .....</b>	<b>1</b>
<b>1.1.1 <i>The synovial joint structure and function</i>.....</b>	<b>1</b>
1.1.1.1 Articular cartilage .....	3
<b>1.1.2 <i>Long bone and joint development</i> .....</b>	<b>5</b>
1.1.2.1 Endochondral ossification.....	5
1.1.2.2 Synovial joint development.....	6
<b>1.1.3 <i>Joint homeostasis</i>.....</b>	<b>8</b>
1.1.3.1 Anabolic matrix proteins and growth factors .....	8
1.1.3.2 Metalloproteinase-mediated matrix turnover.....	10
1.1.3.3 Tissue inhibitors of metalloproteinases .....	13
<b>1.2 Osteoarthritis .....</b>	<b>14</b>
<b>1.2.1 <i>Risk Factors</i> .....</b>	<b>15</b>
1.2.1.1 Age .....	15
1.2.1.2 Biological sex.....	16
1.2.1.3 Obesity .....	17
1.2.1.4 Joint injury.....	18
1.2.1.5 Genetics .....	19
1.2.1.6 Therapeutics.....	21
<b>1.2.2 <i>Role of MMPs and ADAM-TSs in osteoarthritis cartilage destruction</i>.....</b>	<b>22</b>
1.2.2.1 Evidence from animal models .....	22
1.2.2.2 Matrix fragments provide positive feedback pro-inflammatory chondrocyte responses.....	24
<b>1.3 Molecular drivers of cartilage destruction in osteoarthritis.....</b>	<b>25</b>
<b>1.3.1 <i>Inflammation and IL-1 in osteoarthritis pathogenesis</i>.....</b>	<b>25</b>
1.3.1.1 The IL-1 signalling pathway.....	25
1.3.1.2 IL-1 and other inflammatory mediators can stimulate cartilage destruction in vitro.....	26

1.3.1.3 In vivo evidence of inflammatory component to OA from genome-wide association studies and transcriptomics.....	28
1.4 Disrupted chondrocyte zinc homeostasis as a potential driver of osteoarthritis .....	32
1.4.1 Cellular zinc homeostasis .....	32
1.4.1.1 Zinc as an essential nutrient .....	32
1.4.1.2 Zinc transporters.....	33
1.4.1.3 Metallothioneins .....	35
1.4.1.4 Metal-sensing transcription factor 1.....	38
1.4.2 Does disrupted zinc homeostasis contribute to osteoarthritis pathogenesis? .....	39
1.4.2.1 The zinc-ZIP8-MTF1 signalling axis in osteoarthritis .....	39
1.4.3 The role of MTs in osteoarthritis .....	42
1.4.4 Several human OA loci encompass or are near to zinc transporter genes.....	44
1.4.5 Several zinc transporter genes are upregulated in a group of OA hip patients .....	45
1.5 Thesis aims .....	46
<b>Chapter 2. METHODS .....</b>	<b>47</b>
2.1 SkeletalVis database .....	47
2.1.1 Search term and inclusion/exclusion criteria for selection of human and murine cartilage and chondrocyte gene expression datasets .....	47
2.1.2 Extraction of target genes from datasets using R studio .....	47
2.1.3 Identifying replicable gene expression patterns between datasets, enabling selection of normalised read counts or normalised microarray signals for individual samples .....	48
2.2 LDlink and GTEx databases to assess genotype and tissue-specific gene expression correlations .....	49
2.3 Cell line culture .....	51
2.3.1 SW1353 and T/C-28a2 cell culture .....	51
2.3.2 IL-1 $\alpha$ concentration optimisation .....	52
2.3.3 SW1353 and T/C-28a2 IL-1 treatment .....	52
2.3.4 SW1353 and T/C-28a2 zinc chloride treatment .....	53
2.4 Human articular chondrocyte isolation from cartilage and IL-1 treatment .....	54
2.4.1 Cartilage tissue collection .....	54
2.4.2 Cartilage tissue digestion and extraction of human articular chondrocytes .....	54
2.4.3 HAC IL-1 treatment .....	55
2.5 Nucleic acid extraction and cDNA synthesis.....	56
2.5.1 Nucleic acid from cell lines .....	56
2.5.2 RNA extraction for HACs .....	57
2.5.3 Quantification of nucleic acid .....	57
2.5.4 Gel electrophoresis .....	58
2.5.5 cDNA synthesis .....	59
2.6 Gene expression quantification by qPCR .....	60

2.6.1	<i>Primer assay design for cDNA &amp; plate set-up</i>	60
2.6.2	<i>Primer validation</i>	61
2.6.3	<i>qPCR analysis</i>	61
2.7	<b>Zinc quantification assay</b>	63
2.7.1	<i>Testing kit specificity against biologically relevant metal ions</i>	64
2.7.2	<i>Inhibiting Fe<sup>2+</sup> influence on absorbance using 2,2'-bipyridine chelator</i>	64
2.8	<b>Cloning</b>	65
2.8.1	<i>Generation of an empty control pGL4.40 plasmid from the pGL4.40[luc2P/MRE/Hygro] plasmid</i>	66
2.8.2	<i>Preparing agar plates</i>	66
2.8.3	<i>Transformation reaction</i>	67
2.8.4	<i>Picking bacterial colonies</i>	67
2.8.5	<i>Miniprep &amp; glycerol stocks</i>	67
2.8.6	<i>Genotyping of plasmid DNA using restriction digestion</i>	69
2.8.7	<i>Sanger sequencing of miniprep DNA</i>	69
2.8.8	<i>Midiprep</i>	70
2.8.9	<i>Restriction digestion pre-transfection</i>	71
2.8.9.1	<i>Qiaquick DNA clean-up</i>	72
2.8.9.2	<i>Transient transfection of SW1353 cells with pCMV6-MTF1 plasmid or GFP</i>	72
2.9	<b>Generation of MTF1 and luciferase expressing stable cell lines</b>	73
2.9.1	<i>Hygromycin B kill curve for pGL4.40[luc2P/MRE/Hygro] plasmid transfection</i>	73
2.9.2	<i>Geneticin (G418) selection of pCMV6-MTF1 plasmid in SW1353 cells</i>	73
2.9.3	<i>Transfection, selection and expansion of MTF1 or luciferase overexpression cell lines</i>	73
2.9.4	<i>Storage and propagation of stable cells</i>	74
2.9.5	<i>Confirmation that stable cells express the fusion protein</i>	74
2.10	<b>Protein extraction</b>	76
2.10.1	<i>Whole protein extraction</i>	76
2.10.2	<i>NE-PER nuclear and cytoplasmic extraction kit</i>	76
2.10.3	<i>Protein quantification by Bradford assay</i>	77
2.11	<b>Western blot</b>	78
2.11.1	<i>SDS polyacrylamide gel electrophoresis</i>	78
2.11.2	<i>Blotting and probing</i>	79
2.11.3	<i>Densitometry analysis of western blot data</i>	81
2.12	<b>Immunocytochemistry (ICC)</b>	82
2.12.1	<i>ICC detection of c-myc-FLAG-tagged MTF1 protein in cells transiently transfected with the pCMV6-MTF1 c-myc-FLAG plasmid</i>	82
2.12.2	<i>Detection of c-myc-FLAG-tagged MTF1 protein in stable MTF1 overexpressing SW1353 cells</i>	83

2.12.3 <i>Determining MTF1 cellular localisation following IL-1<math>\alpha</math> and/or ZnCl<sub>2</sub> treatment of linear MTF1 overexpressing SW1353 cell line for 24 or 72 hours</i> .....	84
2.12.4 <i>Zeiss Axioplan fluorescence microscope calibration</i> .....	84
2.13 <i>Luciferase assays</i> .....	85
2.13.1 <i>SW1353 &amp; T/C-28a2 luciferase assays</i> .....	85
2.13.2 <i>Luciferase activity comparing MTF1 overexpression and endogenous MTF1 activity in SW1353 cells</i> .....	86
<b>Chapter 3: <i>IN SILICO</i> ANALYSIS OF GENES INVOLVED IN THE CELLULAR HOMEOSTASIS OF ZINC</b> .....	87
3.1 <i>Introduction</i> .....	87
3.2 <i>Chapter aims</i> .....	88
3.3 <i>Transcriptomic datasets</i> .....	88
3.4 <i>Several zinc transporters are differentially expressed in OA cartilage compared to non-OA cartilage</i> .....	90
3.5 <i>SLC39A14, MTIF, MTIG and MTIM are upregulated in damaged OA cartilage</i> .....	95
3.6 <i>Influence of IL-1 signalling pathway on zinc homeostasis genes in human and murine chondrocytes</i> .....	99
3.6.1 <i>Human chondrocytes treatment with different IL-1 receptor ligands up to four hours</i> ...	99
3.6.2 <i>Treatment of human and mouse chondrocytes with different IL-1 receptor ligands for 24 hours</i> .....	108
3.7 <i>Trauma-induced DMM model of OA induction in mice</i> .....	115
3.8 <i>Ageing model of OA in mice</i> .....	118
3.9 <i>Summary of SkeletalVis analysis on zinc homeostasis genes</i> .....	120
3.10 <i>Do human genetic studies implicate zinc homeostasis in OA pathogenesis?</i> .....	122
3.11 <i>Utilising existing RNA-Seq hip and knee OA cartilage data to identify zinc homeostasis genes for laboratory-based analyses</i> .....	126
3.12 <i>Chapter summary</i> .....	128
<b>Chapter 4: ESTABLISHING ACTIVITY OF THE ZINC-ZIP8-MTF1 AXIS IN HACs</b> .....	129
4.1 <i>Introduction</i> .....	129
4.2 <i>Aims</i> .....	129
4.3.1 <i>Do IL-1<math>\alpha</math> and IL-1<math>\beta</math> stimulate the same gene expression changes in human OA chondrocytes for a defined gene panel?</i> .....	130
4.3.2 <i>IL-1<math>\alpha</math>-mediated HAC qPCR expression responses</i> .....	131
4.3.2.1 <i>IL-1<math>\alpha</math> reduces HAC cell number for one or more passages with consequences for cellular proliferation but not senescence marker gene expression</i> .....	131
4.3.2.2 <i>Positive control genes IL-6, CXCL8 and CCL2</i> .....	134
4.3.2.3 <i>SLC39A8 and SLC39A14 are upregulated in response to IL-1<math>\alpha</math> in human OA knee chondrocytes</i> .....	135
4.3.3 <i>Do intracellular zinc levels in OA knee HACs change after IL-1<math>\alpha</math> treatment?</i> .....	138
4.3.3.1 <i>Non-specificity of zinc spectrophotometry kit in a cell-free experiment testing biologically relevant metal ions</i> .....	138

4.3.3.2 Attempted correction for iron's influence on metal ion absorbance using 2,2'-bipyridine .....	140
4.3.3.3 Zinc is specifically upregulated in IL-1 $\alpha$ -treated HACs but not downregulated in matched IL-1 $\alpha$ spent cultured HAC medium .....	142
4.3.4 MTF1 mRNA expression levels are unchanged following IL-1 $\alpha$ treatment in HACs....	144
4.3.5 Does IL-1 $\alpha$ trigger nuclear translocation of MTF1 in OA knee HACs? .....	145
4.3.5.1 Screening HAC nuclear, cytoplasmic and whole protein lysates with N-terminal targeting MTF1 antibody.....	145
4.3.5.2 Comparison of N and C-terminal targeting MTF1 antibodies in HAC lysates stimulated for six hours with or without IL-1 $\alpha$ and OSM.....	146
4.3.6 Metallothioneins are upregulated following IL-1 $\alpha$ stimulation for one passage in HACs .....	150
4.3.7 Cartilage matrix-degrading gene expression.....	153
4.4 Chapter summary.....	155
<b>Chapter 5: INVESTIGATING THE ZINC-ZIP8-MTF1 AXIS IN T/C-28A2 RIB CHONDROCYTES.....</b>	<b>157</b>
5.1 Introduction .....	157
5.2 Aims .....	158
5.3.1 IL-1 $\alpha$ concentration evaluation for T/C-28a2 cells.....	159
5.3.2 Do T/C-28a2 cells respond in the same manner to IL-1 $\alpha$ as IL-1 $\beta$ ? .....	160
5.3.3 SLC39A14 but not SLC39A8 is upregulated after one passage with IL-1 $\alpha$ .....	161
5.3.4 What effect does IL-1 $\alpha$ treatment have on T/C-28a2 intracellular and extracellular zinc levels? .....	169
5.3.5 Is MTF1 gene expression upregulated in response to IL-1 $\alpha$ in T/C-28a2 cells? .....	170
5.3.6 How do C and N-terminal MTF1 antibodies perform in western blots using untreated T/C-28a2 nuclear and whole protein lysates? .....	171
5.3.7 What are the effects of IL-1 $\alpha$ and/or ZnCl <sub>2</sub> treatment on MTF1 activity?.....	172
5.3.8 Does IL-1 $\alpha$ upregulate metallothionein gene expression in T/C-28a2 cells? .....	178
5.3.9 Does cartilage matrix-degrading gene expression change in response to IL-1 $\alpha$ and/or ZnCl <sub>2</sub> stimulation in T/C-28a2 cells? .....	181
5.4 Chapter summary.....	183
<b>Chapter 6: INVESTIGATING THE ZINC-ZIP8-MTF1 AXIS IN SW1353 CHONDROCYTES .....</b>	<b>185</b>
6.1 Introduction .....	185
6.2 Aims .....	186
6.3.1 Do IL-1 $\alpha$ and IL-1 $\beta$ stimulate the same gene expression changes in SW1353 cells?.....	187
6.3.2 Are zinc homeostasis genes upregulated in SW1353 cells after stimulation with or without IL-1 $\alpha$ and/or ZnCl <sub>2</sub> treatment? .....	188
6.3.2.1 SLC39A8 and SLC39A14 are upregulated after one passage with IL-1 $\alpha$ .....	188

6.3.3 <i>What effect does IL-1<math>\alpha</math> treatment have on SW1353 intracellular and extracellular zinc levels?</i> .....	196
6.3.4 <i>Is MTF1 gene expression upregulated in response to IL-1<math>\alpha</math> in SW1353 cells?</i> .....	197
6.3.5 <i>Does IL-1<math>\alpha</math> stimulation trigger MTF1 nuclear translocation in SW1353 cells?</i> .....	198
6.3.5.1 <i>Optimising the nuclear and cytoplasmic fraction extractions for western blot analysis</i> .....	198
6.3.5.2 <i>Detection of MTF1 protein in untreated SW1353 lysates using N and C-terminal targeting antibodies</i> .....	199
6.3.5.3 <i>Overexpression of c-myc-FLAG-tagged MTF1 in SW1353 cells</i> .....	203
6.3.6 <i>Production of an MTF1 overexpressing SW1353 cell line</i> .....	206
6.3.6.1 <i>MTF1 overexpression confirmation by western blot</i> .....	208
6.3.6.2 <i>Do IL-1<math>\alpha</math> and/or zinc stimulate MTF1 nuclear translocation?</i> .....	209
6.3.6.3 <i>Detecting endogenous and plasmid-encoded MTF1 using immunocytochemistry</i> .....	214
6.3.7 <i>What are the effects of IL-1<math>\alpha</math> and/or ZnCl<sub>2</sub> treatment on MTF1 activity?</i> .....	222
6.3.8 <i>Does metallothionein gene expression change in response to IL-1<math>\alpha</math> stimulation in SW1353 cells?</i> .....	230
6.3.9 <i>Does cartilage matrix-degrading gene expression change in response to IL-1<math>\alpha</math> and ZnCl<sub>2</sub> stimulation in SW1353 cells?</i> .....	233
6.4 Chapter summary .....	237
Chapter 7. DISCUSSION .....	239
Chapter 8. BIBLIOGRAPHY .....	253
Chapter 9. APPENDIX .....	275

## LIST OF TABLES

<b>Table 2.1 - Human and mouse gene names assessed in transcriptomic datasets using the SkeletalVis data portal.....</b>	<b>48</b>
<b>Table 2.2 – SNPs associated with OA susceptibility and reduced hip joint space width in four GWAS at loci nearby zinc transporters.....</b>	<b>50</b>
<b>Table 2.3 –TaqMan and IDT qPCR assays .....</b>	<b>62</b>
<b>Table 2.4- Plasmid-specific qPCR primer assays.....</b>	<b>75</b>
<b>Table 2.5 – Primary and secondary antibodies .....</b>	<b>80</b>
<b>Table 3.1 – Human (1-9) and murine (10-13) OA transcriptomics datasets identified through SkeletalVis.....</b>	<b>89</b>
<b>Table 3.2 - SkeletalVis data from four human preserved OA cartilage versus non-OA cartilage datasets for genes involved in zinc homeostasis .....</b>	<b>91</b>
<b>Table 3.3 – SkeletalVis data from two human ipsilateral damaged OA versus intact OA cartilage datasets for genes involved in zinc homeostasis. ....</b>	<b>96</b>
<b>Table 3.4 - SkeletalVis data from three human IL-1-treated chondrocyte datasets treated acutely (1, 1.25 or 4 hours) with IL-1 receptor ligands for genes involved in zinc homeostasis .....</b>	<b>101</b>
<b>Table 3.5 - SkeletalVis data from two human chondrocyte datasets IL-1-treated 24 hour and one murine IL-1-treated 24 hour chondrocyte dataset for genes involved in zinc homeostasis .....</b>	<b>109</b>
<b>Table 3.6 – SkeletalVis data from two murine destabilisation of the medial meniscus (DMM) OA datasets for genes involved in zinc homeostasis .....</b>	<b>116</b>
<b>Table 3.7 – SkeletalVis data from a single study of a spontaneous OA ageing mouse model using STR/ort mice .....</b>	<b>119</b>
<b>Table 3.8 – Summary of zinc homeostasis genes significantly and differentially expressed in iOA or dOA cartilage, IL-1-treated chondrocytes, DMM or STR/ort mice .....</b>	<b>121</b>
<b>Table 3.9– List of zinc homeostasis and inflammation-associated genes investigated for appreciable cartilage tissue expression (TPM) in two RNA-Seq datasets of hip and knee respectively .....</b>	<b>127</b>
<b>Table 8.1 – eQTLs for recently identified OA or hip mjsw-associated risk in proximity to zinc transporters .....</b>	<b>241</b>

**Table 8.2 – Gene expression information for each eQTL associated with SNPs in proximity to zinc transporters in hip and knee OA cartilage and hip OA chondrocytes.**  
.....245

## LIST OF FIGURES

Figure 1.1 – The synovial joint and associated tissues.....	2
Figure 1.2 – The zones of articular cartilage. ....	4
Figure 1.3– Aggrecan is the major proteoglycan component of cartilage. ....	9
Figure 1.4 – Aggrecan core protein is the target of aggrecanases at multiple sites. Replicated from Fosang <i>et al.</i> ,2008.....	12
Figure 1.5 – Schematic of ADAM-TS5 domain structure. ....	13
Figure 1.6- Diagram of an advanced osteoarthritic joint. ....	14
Figure 1.7 – Example mechanism of a single nucleotide polymorphism impacting on gene expression.....	20
Figure 1.8 – Intracellular localisation of Zrt/Irt-like (ZIP) and Zn <sup>2+</sup> transporter (ZnT) proteins with the plasma membrane or organelles of the cell.....	33
Figure 1.9 – Relationship between metallothionein protein states, oxidative status, and the reduced glutathione:glutathione disulfide ratio in chondrocytes.....	37
Figure 1.10 – Proposed mode of action of the zinc-ZIP8-MTF1 axis in chondrocytes....	41
Figure 2.1 – Serial IL-1 $\alpha$ treatment of cell lines for 24 hours, three subsequent passages (P1-P3) and removal of IL-1 $\alpha$ at P4. ....	53
Figure 2.2 - Time course of HAC treatment with or without IL-1 $\alpha$ between passages two and three and its removal for a final passage. ....	56
Figure 3.1 – <i>SLC30A2</i> , <i>SLC39A3</i> , <i>SLC39A7</i> and <i>SLC39A14</i> zinc transporters are significantly and differentially regulated in intact knee, hip or knee and hip OA cartilage versus non-OA cartilage. ....	93
Figure 3.2 – <i>MT1A</i> and <i>MT1X</i> are significantly and differentially expressed in iOA cartilage versus non-OA cartilage. ....	94
Figure 3.3 – <i>SLC39A14</i> is significantly and differentially expressed in dOA versus iOA knee cartilage of the same knee joint by RNA-Seq (Dunn <i>et al.</i> , 2016) and in matched knee or hip OA joints by microarray (Ramos <i>et al.</i> , 2014).....	97
Figure 3.4 – Metallothioneins significantly and differentially expressed in dOA versus iOA knee cartilage in RNA-Seq (Dunn <i>et al.</i> , 2016) and dOA knee and hip joints (Ramos <i>et al.</i> ,2014) from different patients. ....	98

<b>Figure 3.5 - <i>IL-6</i>, <i>CXCL8</i> and <i>CCL2</i> are differentially expressed in human chondrocytes treated with or without IL-1 for one, 1.25 or four hours in RNA-Seq (Pearson <i>et al.</i>, 2016) and microarray (Chan <i>et al.</i>, 2017; Moazedi-Fuerst <i>et al.</i>, 2016) datasets.....</b>	<b>103</b>
<b>Figure 3.6 – <i>SLC39A14</i> is significantly and differentially expressed in human chondrocytes after four hours IL-1<math>\beta</math> in microarray (Moazedi-Fuerst <i>et al.</i>, 2016) and RNA-Seq (Pearson <i>et al.</i>, 2016) datasets.....</b>	<b>104</b>
<b>Figure 3.7 – <i>MTF1</i> is significantly and differentially expressed in human chondrocytes after four hours IL-1<math>\beta</math> in microarray (Moazedi-Fuerst <i>et al.</i>, 2016) and RNA-Seq (Pearson <i>et al.</i>, 2016) datasets.....</b>	<b>105</b>
<b>Figure 3.8 – <i>MT1E</i>, <i>MT1X</i>, and <i>MT2A</i> are significantly and differentially expressed in human chondrocytes after four hours IL-1<math>\beta</math> in microarray (Moazedi-Fuerst <i>et al.</i>,2016) and RNA-Seq (Pearson <i>et al.</i>, 2016) datasets. ....</b>	<b>106</b>
<b>Figure 3.9 – <i>MMP3</i>, <i>MMP12</i> and <i>MMP13</i> are differentially expressed in human chondrocytes after four hours IL-1<math>\beta</math> in microarray (Moazedi-Fuerst <i>et al.</i>,2016) and RNA-Seq (Pearson <i>et al.</i>,2016) datasets.....</b>	<b>107</b>
<b>Figure 3.10 – IL-1 positive control genes (<i>IL-6/Il-6</i>, <i>CXCL8</i> and <i>CCL2/Ccl2</i>) differential expression in human and murine chondrocytes treated <math>\pm</math> IL-1 for 24 hours. ....</b>	<b>111</b>
<b>Figure 3.11 – <i>SLC39A8/Slc39a8</i> and <i>SLC39A14/Slc39a14</i> are significantly and differentially upregulated in human and murine chondrocytes treated <math>\pm</math> IL-1 for 24 hours. ....</b>	<b>112</b>
<b>Figure 3.12 – <i>MT1A</i>, <i>MT1E</i>, <i>MT1F</i>, <i>MT1G</i>, <i>MT1H</i> and <i>MT1X</i> in human chondrocytes treated <math>\pm</math> IL-1 for 24 hours are significantly and differentially upregulated. ....</b>	<b>113</b>
<b>Figure 3.13 – <i>Mt1</i> and <i>Mt2</i> are differentially upregulated in murine chondrocytes treated <math>\pm</math> IL-1<math>\beta</math> for 24 hours. ....</b>	<b>114</b>
<b>Figure 3.14 – <i>MMP9/Mmp9</i>, <i>MMP12/Mmp12</i> and <i>MMP13/Mmp13</i> are differentially upregulated in human and murine chondrocytes treated <math>\pm</math> IL-1 for 24 hours.....</b>	<b>114</b>
<b>Figure 3.15 – <i>Slc39a14</i> is significantly and differentially overexpressed in cartilage of mice following DMM surgery acutely and up to two weeks.....</b>	<b>117</b>
<b>Figure 3.16 – Eleven SNPs associated with OA susceptibility nearby <i>SLC30A10</i> overlap with <i>SLC30A10</i> eQTLs in UV-exposed skin of the lower leg.....</b>	<b>124</b>
<b>Figure 3.17 - SNPs in LD with rs10471753 do not overlap with eQTLs for <i>SLC30A5</i> A) and SNPs in LD with rs13107325 do not overlap with eQTLs for <i>SLC39A8</i> in GTEx B). ....</b>	<b>125</b>

<b>Figure 4.1 – Comparison of IL-1<math>\alpha</math> or IL-1<math>\beta</math>-inducible positive control genes after one passage in two HAC donors. ....</b>	<b>131</b>
<b>Figure 4.2 – Dot plots of matched HAC donor cell counts in IL-1<math>\alpha</math>-treated or untreated control flasks treated consecutively for two passages and a final passage without IL-1<math>\alpha</math>. ....</b>	<b>132</b>
<b>Figure 4.3- Proliferation (<i>MKI67</i>, <i>TOP2A</i> and <i>TPX2</i>) and senescence-associated (<i>CDKN1A</i>, <i>CAMK2G</i>, and <i>PARP2</i>) gene expression after one passage of IL-1<math>\alpha</math>. ....</b>	<b>133</b>
<b>Figure 4.4 – <i>IL-6</i>, <i>CXCL8</i>, and <i>CCL2</i> are all significantly upregulated by IL-1<math>\alpha</math> in HACs. ....</b>	<b>134</b>
<b>Figure 4.5 – Zinc transporters that are significantly and differentially expressed after IL-1<math>\alpha</math> treatment of HACs for one passage. ....</b>	<b>136</b>
<b>Figure 4.6 – Heatmap of <i>SLC39A8</i> and <i>SLC39A14</i> log<sub>2</sub>-fold change gene expression after IL-1<math>\alpha</math> treatment (P2 and P3) and without IL-1<math>\alpha</math> (P4) in two HAC donors. ....</b>	<b>137</b>
<b>Figure 4.7 – Cell-free zinc assay measurements <math>\pm</math> TCA inclusion using MAK032 zinc assay kit. ....</b>	<b>139</b>
<b>Figure 4.8 – Attempted iron chelation in cell-free metal salt solutions using the iron chelator 2,2'-bipyridine. ....</b>	<b>141</b>
<b>Figure 4.9 – TCA use in untreated or IL-1<math>\alpha</math>-treated HAC medium led to ~ two-fold total metal ion concentration reduction. ....</b>	<b>142</b>
<b>Figure 4.10 – Metal ion content is significantly upregulated in matched HAC lysates but not HAC spent medium <math>\pm</math> IL-1<math>\alpha</math> treatment for one passage. ....</b>	<b>143</b>
<b>Figure 4.11 – <i>MTF1</i> transcript is not significantly and differentially altered after IL-1<math>\alpha</math> treatment of HACs for one passage. ....</b>	<b>144</b>
<b>Figure 4.12 – N-terminal MTF1 antibody detects multiple bands in 10<math>\mu</math>g untreated HAC nuclear and cytoplasmic lysates and GAPDH cytoplasmic protein marker found in both fractions. ....</b>	<b>146</b>
<b>Figure 4.13 – Western blots using C and N-terminal MTF1 antibodies in six-hour IL-1<math>\alpha</math> and oncostatin M-treated HAC nuclear, cytoplasmic and whole protein lysates and overexpressed MTF1 lysate. ....</b>	<b>147</b>
<b>Figure 4.14 – Predicted cleavage sites of multiple protease families for the human protein MTF1 using the database PROSPER. ....</b>	<b>149</b>
<b>Figure 4.15 – Metallothioneins including <i>MT1A</i>, <i>MT1F</i>, <i>MT1G</i>, <i>MT1H</i> and <i>MT2A</i> are all significantly and differentially upregulated after IL-1<math>\alpha</math> treatment in HAC donors. ....</b>	<b>151</b>
<b>Figure 4.16 – <i>ADAM-TS5</i> and <i>MMP13</i> are not significantly and differentially expressed after IL-1<math>\alpha</math> treatment. ....</b>	<b>154</b>

<b>Figure 4.17 – Summary of zinc-ZIP8-MTF1 axis exploration in HACs. ....</b>	<b>156</b>
<b>Figure 5.1 – <i>IL-6</i> and <i>CXCL8</i> gene expression in T/C-28a2 cells treated ± <i>IL-1α</i> for three passages and its removal for the fourth passage.....</b>	<b>159</b>
<b>Figure 5.2 – Normalised <i>IL-6</i>, <i>CXCL8</i> and <i>CCL2</i> gene expression responses in T/C-28a2 cells treated ± <i>IL-1α</i> or <i>IL-1β</i>. ....</b>	<b>160</b>
<b>Figure 5.3– <i>SLC39A14</i>, not <i>SLC39A8</i> is significantly upregulated by <i>IL-1α</i> in T/C-28a2 cells after 72 hours in six experiments and is also significantly different from control after <i>IL-1β</i> treatment. ....</b>	<b>163</b>
<b>Figure 5.4– Long-term exposure of T/C-28a2 cells to <i>IL-1α</i> does not lead to sustained and elevated <i>SLC39A8</i> or <i>SLC39A14</i> expression compared to control, nor does <i>ZnCl<sub>2</sub></i> influence <i>SLC39A8</i> or <i>SLC39A14</i> expression.....</b>	<b>164</b>
<b>Figure 5.5– Zinc exporter gene expression in T/C-28a2 cells treated ± <i>IL-1α</i> for 72 hours. ....</b>	<b>165</b>
<b>Figure 5.6– Zinc importer gene expression in T/C-28a2 cells treated ± <i>IL-1α</i> for 72 hours. ....</b>	<b>166</b>
<b>Figure 5.7- Zinc exporter gene expression in T/C-28a2 cells treated ± <i>IL-1α</i> for consecutive passages up to 216 hours (P3) and cell recovery for 72 hours (P4). ....</b>	<b>167</b>
<b>Figure 5.8– Zinc importer gene expression in T/C-28a2 cells treated ± <i>IL-1α</i> for consecutive passages up to 216 hours (P3) and cell recovery for 72 hours (P4). ....</b>	<b>168</b>
<b>Figure 5.9–Metal ion content determined using a spectrophotometric method in T/C-28a2 cells and spent medium ± <i>IL-1α</i> was not significantly different. ....</b>	<b>169</b>
<b>Figure 5.10–<i>MTF1</i> relative expression and fold change in T/C-28a2 cells treated ± <i>IL-1α</i>. ....</b>	<b>170</b>
<b>Figure 5.11– Western blot comparing C and N-terminal MTF1 antibody consecutively on untreated T/C-28a2 nuclear and cytoplasmic lysates. ....</b>	<b>171</b>
<b>Figure 5.12 – Raw firefly:renilla ratios from T/C-28a2 cells transiently transfected with empty control pGL4.40 and renilla luciferase or MRE pGL4.40 plasmid and renilla luciferase.....</b>	<b>173</b>
<b>Figure 5.13- Luciferase reporter assay measuring MTF1 activity in T/C-28a2 cells treated ± <i>IL-1α</i>, <i>IL-1β</i>, <i>ZnCl<sub>2</sub></i> or <i>IL-1α</i> + <i>ZnCl<sub>2</sub></i> for 24 hours. ....</b>	<b>174</b>
<b>Figure 5.14– Assessment of <i>luciferase</i> gene expression in stably selected NotI-digested linear or circular transfected pGL4.40 <i>luciferase</i> overexpressing T/C-28a2 cell line. ....</b>	<b>176</b>
<b>Figure 5.15- Normalised <i>MTF1</i> gene expression in NotI-digested linear pGL4.40 luciferase overexpressing T/C-28a2 cells transiently transfected for 24 hours ± MTF1 plasmid then treated ± <i>IL-1α</i> and/or <i>ZnCl<sub>2</sub></i> for 72 hours. ....</b>	<b>177</b>

<b>Figure 5.16– Normalised <i>Luciferase</i> gene expression in NotI-digested linear pGL4.40 luciferase T/C-28a2 cells transiently transfected for 24 hours ± MTF1 plasmid then treated ± IL-1<math>\alpha</math> alone and/or ZnCl<math>_2</math> for 72 hours. ....</b>	<b>178</b>
<b>Figure 5.17 – <i>MT1A</i> and <i>MT1G</i> are significantly upregulated by IL-1<math>\alpha</math> in T/C-28a2 cells after a 72 hour passage. ....</b>	<b>179</b>
<b>Figure 5.18 – <i>MT1A</i> was significantly upregulated by IL-1<math>\alpha</math> at multiple timepoints or not at all for <i>MT1G</i> and effects of ZnCl<math>_2</math> treatment alone were undetermined. ....</b>	<b>180</b>
<b>Figure 5.19 – <i>ADAM-TS5</i> and <i>MMP13</i> are significantly upregulated by IL-1<math>\alpha</math> in T/C-28a2 cells after a 72 hour passage.....</b>	<b>181</b>
<b>Figure 5.20 – <i>ADAM-TS5</i> was significantly upregulated by IL-1<math>\alpha</math> at multiple timepoints of a time course experiment or not at all for <i>MMP13</i>. Effects of ZnCl<math>_2</math> treatment alone were undetermined. ....</b>	<b>182</b>
<b>Figure 5.21- Summary of zinc-ZIP8-MTF1 axis exploration in T/C-28a2 cells.....</b>	<b>184</b>
<b>Figure 6.1 – Normalised <i>IL-6</i>, <i>CXCL8</i>, <i>CCL2</i> gene expression responses in SW1353 cells treated ± IL-1<math>\alpha</math> or IL-1<math>\beta</math>. ....</b>	<b>187</b>
<b>Figure 6.2 – <i>SLC39A8</i> and <i>SLC39A14</i> are among the most significantly upregulated zinc transporters after IL-1<math>\alpha</math> in SW1353 cells after 72 hours in five experiments. ....</b>	<b>189</b>
<b>Figure 6.3 – <i>SLC39A8</i>, not <i>SLC39A14</i> expression was not sustained beyond P1 by IL-1<math>\alpha</math> in SW1353 time course and ZnCl<math>_2</math> does not influence <i>SLC39A8</i> or <i>SLC39A14</i> expression. ....</b>	<b>191</b>
<b>Figure 6.4 - Zinc exporter gene expression in SW1353 cells treated ± IL-1<math>\alpha</math> for 72 hours. ....</b>	<b>192</b>
<b>Figure 6.5- Zinc importer gene expression in SW1353 cells treated ± IL-1<math>\alpha</math> for 72 hours. ....</b>	<b>193</b>
<b>Figure 6.6 - Zinc exporter gene expression in SW1353 cells treated ± IL-1<math>\alpha</math> for consecutive passages up to 216 hours (P3) and cell recovery for 72 hours (P4).....</b>	<b>194</b>
<b>Figure 6.7 - Zinc importer gene expression in SW1353 cells treated ± IL-1<math>\alpha</math> for consecutive passages up to 216 hours (P3) and cell recovery for 72 hours (P4).....</b>	<b>195</b>
<b>Figure 6.8 – Metal ion content determined using a spectrophotometric method in SW1353 cells and spent medium treated ± IL-1<math>\alpha</math> was not significantly different.....</b>	<b>196</b>
<b>Figure 6.9 –<i>MTF1</i> expression significantly elevated at P1 in SW1353 cells treated ± IL-1<math>\alpha</math>. ....</b>	<b>197</b>

<b>Figure 6.10 – Optimisation of untreated SW1353 nuclear and cytoplasmic proteins extracted 24 and 72 hours after plating with the NE-PER kit with an additional PBS wash. ....</b>	<b>200</b>
<b>Figure 6.11 – Western blot comparing C and N-terminal MTF1 antibody consecutively on untreated SW1353 nuclear and cytoplasmic lysates collected 72 hours after seeding. ....</b>	<b>200</b>
<b>Figure 6.12 – Twenty-four and 72 hour-treated SW1353 nuclear or cytoplasmic lysates probed consecutively on separate blots with C and N-terminal MTF1 antibody.....</b>	<b>202</b>
<b>Figure 6.13 – SW1353 cells expressing GFP 24 hours after transfection with short hairpin RNA encoding GFP. ....</b>	<b>203</b>
<b>Figure 6.14 – Western blots for MTF1 detection in transiently MTF1 overexpressing SW1353 cell lysates using FLAG or c-myc antibodies respectively.....</b>	<b>205</b>
<b>Figure 6. 15 – Western blot comparing commercially available anti-FLAG tag antibodies in SW1353 lysates overexpressing Cas9-FLAG fusion protein. ....</b>	<b>206</b>
<b>Figure 6.16 – <i>MTF1</i> gene expression in MTF1 overexpressing SW133 cells as fold change relative to untransfected SW1353 cells.....</b>	<b>207</b>
<b>Figure 6.17 – MTF1 protein overexpression confirmation in SW1353 cells transfected and selected with 1mg/ml G418 generating the MTF1 overexpression cell lines. ....</b>	<b>208</b>
<b>Figure 6.18 – Western blots highlighting biological replicates from one of three representative experiments for AgeI-digested linear MTF1 overexpressing SW1353 cells in nuclear and cytoplasmic lysates ± treatment for 24 hours.....</b>	<b>211</b>
<b>Figure 6.19 – Western blots highlighting biological replicate from one of three representative experiments for AgeI-digested linear MTF1 overexpressing SW1353 cells in nuclear and cytoplasmic lysates ± treatment for 72 hours.....</b>	<b>212</b>
<b>Figure 6.20 - Densitometry analysis of western blots determining MTF1 translocation between cytoplasmic and nuclear compartments 24 A) or 72 hours B) after treatment. ....</b>	<b>213</b>
<b>Figure 6.21 – ICC of untransfected or transiently transfected SW1353 cells with MTF1 plasmid and stained ± anti-c-myc or anti-MTF1 antibodies. ....</b>	<b>215</b>
<b>Figure 6.22 – ICC experiment using two strategies to detect MTF1 protein with C-terminal MTF1 antibody A) or FLAG antibody B). ....</b>	<b>218</b>
<b>Figure 6.23- ICC costaining with anti-MTF1 (GFP BP filter) and anti-FLAG (594 filter) antibodies of linear MTF1 overexpressing SW1353 cells treated for 24 A) or 72 hours B) ± IL-1<math>\alpha</math> and/or ZnCl<math>_2</math>.....</b>	<b>220</b>
<b>Figure 6.24 - Manual cell counts from an ICC experiment using linear MTF1 overexpressing SW1353 cells treated ± IL-1<math>\alpha</math> and/or ZnCl<math>_2</math> for 24 or 72 hours testing anti-FLAG and anti-beta-actin antibody costaining. ....</b>	<b>221</b>

Figure 6.25 - Raw firefly:renilla ratios from SW1353 cells transiently transfected with empty control pGL4.40 and renilla luciferase or MRE pGL4.40 plasmid and renilla luciferase. ....	223
Figure 6.26 – Luciferase reporter assay measuring MTF1 activity in SW1353 cells treated ± IL-1 $\alpha$ , IL-1 $\beta$ , ZnCl $_2$ or IL-1 $\alpha$ + ZnCl $_2$ for 24 hours.....	224
Figure 6.27 – Raw firefly:renilla ratios from SW1353 cells or linear MTF1 overexpressing SW1353 cells transiently transfected with empty control pGL4.40 and renilla luciferase or pGL4.40 plasmid and renilla luciferase.....	225
Figure 6.28 – Luciferase reporter assay comparing SW1353 cells against MTF1 overexpressing SW1353 cells ± IL-1 $\alpha$ alone and/or ZnCl $_2$ for 24 hours.....	226
Figure 6.29 – Assessment of <i>luciferase</i> gene expression in stably selected NotI-digested linear transfected pGL4.40 <i>luciferase</i> -overexpressing SW1353 cell line. ....	227
Figure 6.30 – Normalised <i>MTF1</i> gene expression in pGL4.40 luciferase overexpressing SW1353 cells transiently transfected ± MTF1 plasmid for 24 hours then treated ± IL-1 $\alpha$ alone and/or ZnCl $_2$ for 72 hours. ....	228
Figure 6.31 – Normalised <i>luciferase</i> gene expression in pGL4.40 luciferase overexpressing SW1353 cells transiently transfected ± MTF1 plasmid for 24 hours then treated ± IL-1 $\alpha$ alone and/or ZnCl $_2$ for 72 hours. ....	229
Figure 6.32 – <i>MT1A</i> and <i>MT1G</i> gene expression is significantly upregulated by IL-1 $\alpha$ after a 72 hour passage in SW1353 cells. ....	231
Figure 6.33 - <i>MT1G</i> and not <i>MT1A</i> was upregulated after P1 in IL-1 $\alpha$ time course experiments and effects of ZnCl $_2$ treatment alone or with IL-1 $\alpha$ on <i>MT1A</i> and <i>MT1G</i> expression were undetermined in SW1353 cells.....	232
Figure 6.34 – <i>MMP13</i> , but not <i>ADAM-TS5</i> is significantly upregulated by IL-1 $\alpha$ after a 72 hour passage in SW1353 cells. ....	234
Figure 6.35 - <i>MMP13</i> and <i>ADAM-TS5</i> were not upregulated in IL-1 $\alpha$ time course experiments and effects of ZnCl $_2$ treatment alone or with IL-1 $\alpha$ on matrix-degrading gene expression were undetermined in SW1353 cells.....	235
Figure 6.36 – Summary of zinc-ZIP8-MTF1 axis exploration in SW1353 cells.....	238

## ABBREVIATIONS

<b>ADAM-TS</b>	A disintegrin and metalloproteinase-thrombospondin proteinases
<b>ATCC</b>	American Type Culture Collection
<b>ACL</b>	Anterior cruciate ligament
<b>arcOGEN</b>	Arthritis research UK osteoarthritis genetics
<b>ARE</b>	Antioxidant response element
<b>BMI</b>	Body mass index
<b>BMP</b>	Bone morphogenetic protein
<b>BNC</b>	Bovine nasal cartilage
<b>BSA</b>	Bovine serum albumin
<b>CaCl<sub>2</sub></b>	Calcium chloride
<b>CS</b>	Chondroitin sulphate
<b>CRISPR</b>	Clusters of regularly interspaced palindromic repeats
<b>CuSO<sub>4</sub>.5H<sub>2</sub>O</b>	Copper sulphate pentahydrate
<b>DAMPs</b>	Damage-associated molecular pattern
<b>DNA</b>	Deoxyribonucleic acid
<b>DMM</b>	Destabilisation of the medial meniscus
<b>DEPC</b>	Diethylpyrocarbonate water
<b>DML</b>	Differentially methylated locus
<b>DHT</b>	Dihydrotestosterone
<b>DMSO</b>	Dimethylsulfoxide
<b>DTT</b>	Dithiothreitol (DTT)
<b>DMEM-F12</b>	Dulbecco's modified eagle's medium F12
<b>eQTL</b>	Expression quantitative trait locus
<b>ECM</b>	Extracellular matrix
<b>ERK</b>	Extracellular-mediated kinase
<b>FGF2</b>	Fibroblast growth factor 2
<b>GEMM</b>	Genetically engineered mouse mutant
<b>G418</b>	Geneticin antibiotic
<b>GWAS</b>	Genome-wide association study
<b>GTE<sub>x</sub></b>	Genotype tissue expression
<b>GSSG</b>	Glutathione disulfide
<b>GAGs</b>	Glycosaminoglycans
<b>GFP</b>	Green fluorescent protein
<b>HACs</b>	Human articular chondrocytes
<b>HNC</b>	Human nasal cartilage
<b>IL-1Ra</b>	IL-1 receptor antagonist
<b>IL-1R1</b>	IL-1 receptor type 1
<b>IRAK4</b>	IL-1 receptor-associated kinase 4
<b>ICC</b>	Immunocytochemistry
<b>iNOS</b>	Inducible nitric oxide synthase
<b>IDT</b>	Integrated DNA Technologies
<b>IGD</b>	Interglobular domain
<b>IL</b>	Interleukin
<b>Fe<sub>2</sub>SO<sub>4</sub>.7H<sub>2</sub>O</b>	Iron sulphate heptahydrate
<b>KS</b>	Keratan sulphate
<b>LD</b>	Linkage disequilibrium
<b>lncRNA</b>	Long non-coding ribonucleic acid
<b>LB</b>	Luria broth
<b>MgCl<sub>2</sub>.6H<sub>2</sub>O</b>	Magnesium chloride hexahydrate
<b>MRI</b>	Magnetic resonance imaging

<b>MMPs</b>	Matrix metalloproteinase
<b>MT-MMP</b>	Membrane-type matrix metalloproteinase
<b>MSCs</b>	Mesenchymal stem cells
<b>mRNA</b>	Messenger ribonucleic acid
<b>MRE</b>	Metal response element
<b>MT</b>	Metallothionein
<b>MTF1</b>	Metal-sensing transcription factor 1
<b>mBSA</b>	Methylated bovine serum albumin
<b>miRNA</b>	Micro ribonucleic acid
<b>MJSW</b>	Minimal joint-space width
<b>MAPK</b>	Mitogen-activated protein kinase
<b>MyD88</b>	Myeloid differentiating factor 88
<b>NOF</b>	Neck of femur
<b>NEB</b>	New England Biolabs
<b>NADPH</b>	Nicotinamide adenine dinucleotide phosphate
<b>NF<math>\kappa</math>B</b>	Nuclear factor kappa light chain activator of B cells
<b>OSM</b>	Oncostatin M
<b>OA</b>	Osteoarthritis
<b>OARSI</b>	Osteoarthritis research society international
<b>PAMPs</b>	Pathogen-associated molecular patterns
<b>PRR</b>	Pattern recognition receptor
<b>PBLs</b>	Peripheral blood leukocytes
<b>PBS</b>	Phosphate buffered saline
<b>PTOA</b>	Post-traumatic osteoarthritis
<b>PCA</b>	Principal component analysis
<b>PKC</b>	Protein Kinase C
<b>PDB</b>	Protein structure database
<b>qPCR</b>	Quantitative polymerase chain reaction
<b>RIPA</b>	Radioimmunoprecipitation assay buffer
<b>ROS</b>	Reactive oxygen species
<b>GSH</b>	Reduced glutathione
<b>RA</b>	Rheumatoid arthritis
<b>SNP</b>	Single nucleotide polymorphism
<b>siRNA</b>	Small inhibitory ribonucleic acid
<b>TUNEL</b>	Terminal deoxynucleotidyl transferase dUTP nick-end labelling
<b>TIMPs</b>	Tissue inhibitors of metalloproteinases
<b>TGF<math>\beta</math></b>	Transforming growth factor beta
<b>TAE</b>	Tris-acetate-EDTA
<b>TNF<math>\alpha</math></b>	Tumour necrosis factor alpha
<b>UKBB</b>	UK biobank data
<b>UPL</b>	Universal probe library
<b>UCSC</b>	University of Santa Cruz and California
<b>ZnCl<sub>2</sub></b>	Zinc chloride
<b>ZnTs</b>	Zinc ion transporters
<b>ZIPs</b>	Zrt/Irt-like proteins



# Chapter 1. INTRODUCTION

## 1.1 Synovial joint and long bone biology

### 1.1.1 *The synovial joint structure and function*

A joint is an articulation between two bones which permits differing ranges of movement (Lumen, 2019). These are classified into fibrous, cartilaginous, or synovial joints in order of increasing mobility. Of these, synovial joints are the most common type of joint in the human body and are distinguishable from the others because of the presence of a synovial cavity between the adjacent bones (Figure 1.1). There are six types of synovial joint which have distinct ranges of motion. These include pivot joints, (between C1 and C2 vertebrae, hinge joints (e.g. elbow and knee), saddle joint (e.g. thumb), ball-and-socket (e.g. hip and shoulder), plane (e.g. ankle) and condyloid (e.g. wrist). Interphalangeal joints of the fingers and toes are also examples of hinge joints and have two hinge regions as opposed to the thumbs one. Synovial joints consist of multiple tissues including bone, synovium, cartilage, ligaments, tendons and muscles (Figure 1.1). Ligaments provide stability and muscles allow for movement. The subchondral bone, where the two opposing bones of the joint meet, is lined with smooth articular cartilage and the encapsulated joint space is lined with a synovial membrane from which the synoviocytes exude synovial fluid. The cells responsible for the maintenance of the synovium, both in terms of removing cellular debris and in secretion of matrix components are type A and B synoviocytes respectively (Iwanaga *et al.*, 2000). The synovial fluid and cartilage synergistically reduce friction between the bones. The synovium nourishes the chondrocytes in the avascular articular cartilage through diffusion of oxygen and nutrients in exchange for carbon dioxide and waste metabolites, in part facilitated by hyaluronic acid and lubricin (Scanzello and Goldring, 2012; Gordon-Betts, 2013).

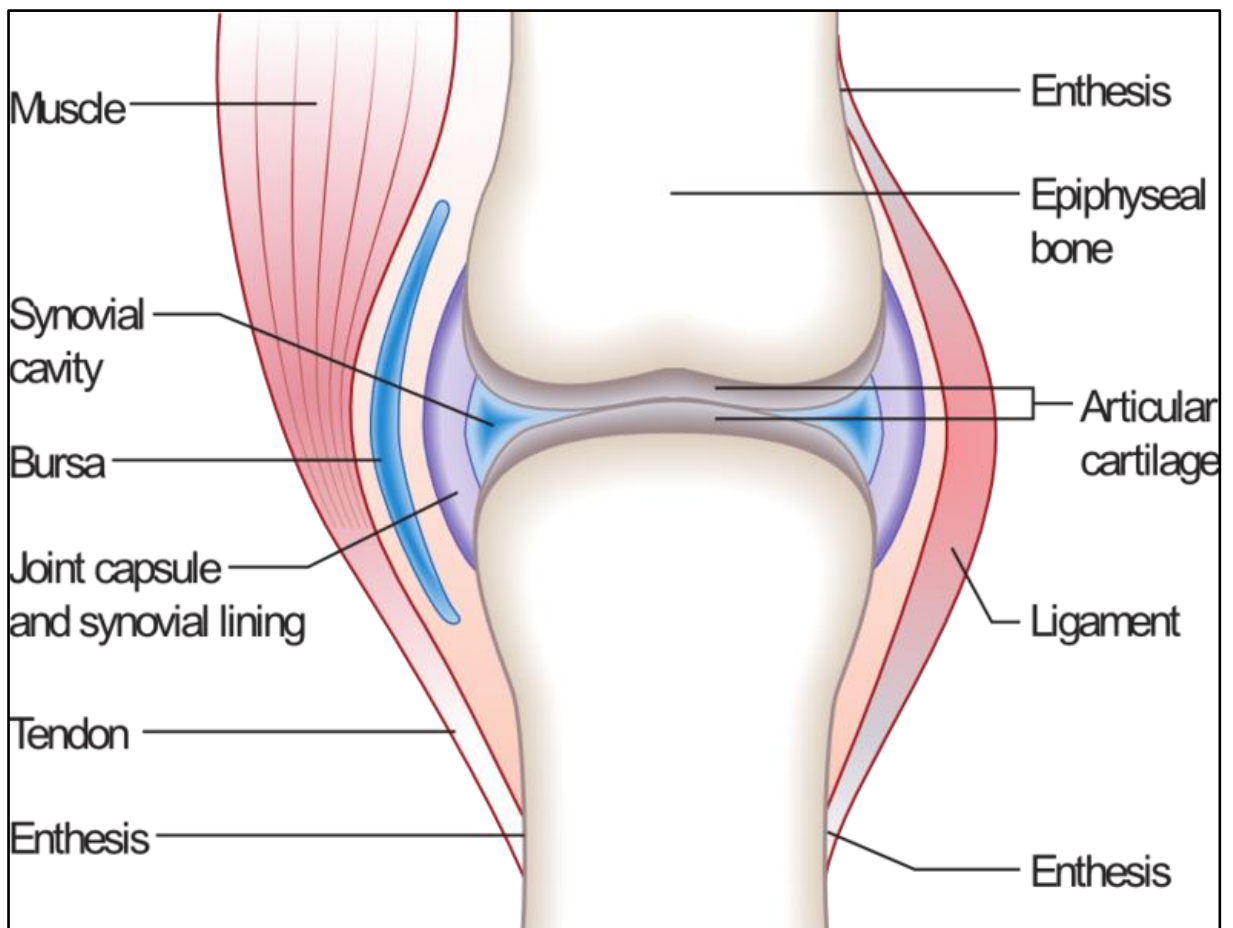


**Figure 1.1 – The synovial joint and associated tissues.**

This schematic of a healthy synovial joint highlights the different tissues and points of attachment (entheses) of tendons and ligaments to bone. The unique aspect of the synovial cavity is the avascular environment in which the synovial fluid provides nourishment to the cartilage through diffusion which supports cartilage function i.e. reducing bone-on-bone friction. Image copied from Wikimedia Commons Madhero88, 2010, *Joint.png* [online], Accessed 14/07/2020, URL: <https://commons.wikimedia.org/wiki/File:Joint.png>.

### **1.1.1.1 Articular cartilage**

Articular chondrocytes are a highly specialised and metabolically active cell type which is perhaps unusual due to being located in a hypoxic environment. Chondrocytes are the only cellular component in articular cartilage and their main function is to maintain or remodel cartilage through the release of anabolic matrix proteins and metalloproteinases in a regulated manner. Chondrocytes can respond to a plethora of different soluble mediators such as growth factors and cytokines and mechanical stresses mediated through integrin receptors. However, the chondrocytes rarely interact with one another for direct cell-to-cell communication to occur (Fox *et al.*, 2009).

The chondrocytes and the extracellular matrix (ECM) proteins within the articular cartilage are not randomly positioned but are in fact organised into different layers or zones with differing functionality in each zone (Figure 1.2). The chondrocytes in the superficial zone are flattened in appearance and produce lubricin which plays an essential role in boundary lubrication (Goldring and Goldring, 2010). This region protects from a combination of shear, tensile and compressive forces and makes up 10-20% of the articular thickness. The collagen fibres (types II and IX) are aligned parallel to the articular surface (Fox *et al.*, 2009). The middle zone comprises 40-60% of the total tissue volume and it contains proteoglycans and thicker collagen fibrils which are oblique in arrangement. The chondrocytes in the middle zone are spherical and are few in number and this zone functionally provides the first resistance to compressive load. In the deep zone, comprising 30% of the tissue, the chondrocytes are columnar in arrangement and are parallel to the collagen fibres, permitting the most resistance to compressive forces. The tidemark zone is between the deep and calcified zones, and this calcified zone anchors the cartilage to the subchondral bone (Fox *et al.*, 2009).

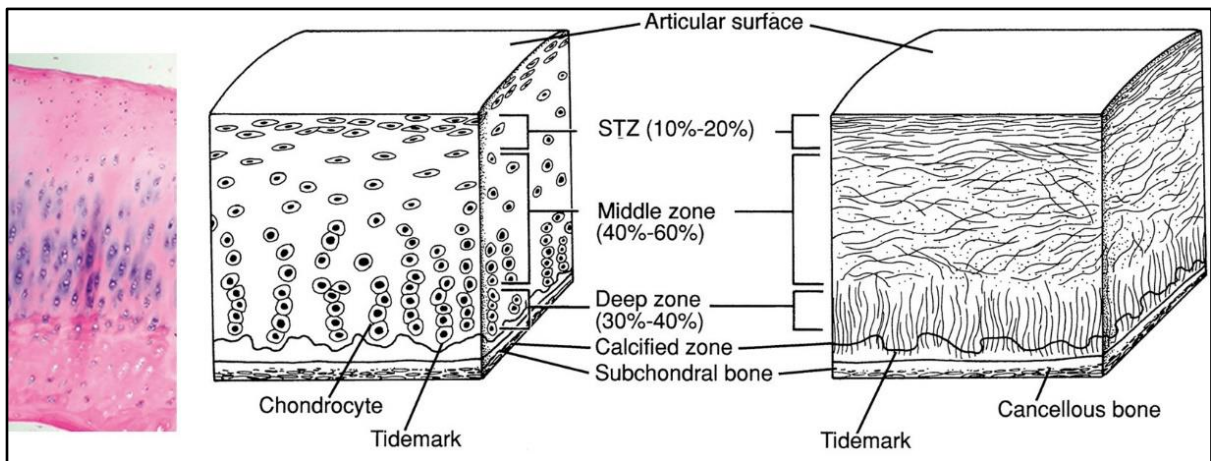


**Figure 1.2 – The zones of articular cartilage.**

From left to right, a histological slide of articular cartilage tissue stained with haematoxylin and eosin, the chondrocyte morphology and cellular organisation, and the collagen molecular arrangement in each of the zones of articular cartilage. Newman, A.P. 1998, Articular cartilage repair. *American Journal of Sports Medicine* 26(2) pp.309-324 [online], Accessed 17/07/2020].

In addition to the cartilage zones, there are different territories surrounding the chondrocytes distinguished by composition, collagen fibril diameter and organisation. These are pericellular, territorial, and the interterritorial environments, the first of which deals with mechanotransduction and has the fewest collagen fibres but many more glycoproteins. One receptor type on the surface of chondrocytes through which mechanotransduction is conveyed are the integrin receptors. These integrin receptors consist of  $\alpha$  and  $\beta$  subunits and bind to a variety of different proteins including collagen types II and IV ( $\alpha 1\beta 1$ ,  $\alpha 2\beta 1$ ,  $\alpha 11\beta 1$ ), vitronectin and osteopontin ( $\alpha V\beta 3$ ), laminin ( $\alpha 6\beta 1$ ) and most abundantly fibronectin ( $\alpha 5\beta 1$ ) (van der Kraan *et al.*, 2002). The mechanical signals conveyed from the collagen to the chondrocytes protects against apoptosis (Cao *et al.*, 1999). These integrin-mediated signals are necessary for the formation of intracellular focal adhesion plaques, a prerequisite for chondrocyte responsiveness to growth factors such as fibroblast growth factor and insulin growth factor 1 (Clancy *et al.*, 1997; Martin and Buckwalter, 1998). The pericellular matrix is encapsulated by the territorial matrix which is composed of many fine collagen fibrils (including collagen type VI and IX) forming a basketlike network around the cells (Fox *et al.*, 2009). This zone is functionally most resistant to compression loads. The interterritorial region is the largest of the three matrix territories, covering all zones of the articular cartilage with parallel or oblique collagen fibres with respect to the chondrocyte arrangement in each zone.

## **1.1.2 Long bone and joint development**

### **1.1.2.1 Endochondral ossification**

Long bone formation, also known as endochondral ossification, commences when mesenchymal stem cells (MSCs) undergo condensation to form distinctive limb buds in the embryo and subsequent formation of a hyaline cartilage framework (Mackie *et al.*, 2008). The production of this cartilage structure is mediated through the process of chondrogenesis, turning mesenchymal tissue into chondroblasts which secrete extracellular matrix (predominantly collagen type II and aggrecan) mediated by multiple transcription factors including SOX9 and RUNX2 (Goldring, 2012; Li and Dong, 2016). The chondroblasts become less metabolically active and differentiate within lacunae into chondrocytes undergoing proliferation, hypertrophy and apoptosis. This permits osteoblasts to produce trabecular bone at the site of primary ossification in the diaphysis of the structure. The trabecular bone becomes denser and stronger during development following calcification of the ECM which is converted into osteoid and is mineralised by osteoblasts. Secondary ossification centres in the epiphyses of the bone allow for continued endochondral ossification.

Most of the cartilage is replaced by bone apart from the growth plate and articular cartilage, situated between the epiphysis and metaphysis of long bones or covering the subchondral bone at the site of the synovial joint respectively. The growth plate is responsible for continued growth of the diaphysis of the long bone postnatally, until completion of puberty, when the growth plate fuses and the bone is skeletally mature. Fracture recovery following an injury to the bone does not require a cartilage model for repair and instead uses osteoblasts differentiated directly from MSCs to produce trabecular bone which is later replaced with lamellar bone in a process of intramembranous ossification (Mackie *et al.*, 2008).

### 1.1.2.2 Synovial joint development

Synovial joint formation occurs in tandem with long bone ossification in two main stages. These two phases are called interzone formation and cavitation. These refer to the creation of a non-chondrogenic layer of cells between the continuous hyaline cartilage core producing a presumptive joint site, and the processes involved in the separation of the two opposing skeletal elements to create the synovial joint respectively (Archer *et al.*, 2003).

The interzone is a non-chondrogenic region that forms after MSC condensation and differentiation and separates the two epiphyses of the bones opposite the presumptive joint. The morphology of the cells in this region adopt a flattened rather than a circular appearance and the interzone is only a few cell layers thick. The interzone is critical for synovial joint formation because its removal from elbow joints in chick (*Gallus gallus*) embryos' resulted in fusion of the humerus with the radius and ulna (Holder, 1977). The loss of chondrogenic markers such as *Sox9* and *Col2a1* and expression of *Gdf5*, *Wnt9a* (formerly *Wnt14*) and *Wnt4* characterise cells of the interzone and differential protein expression, and proliferation in this region is what gives rise to the interzone (Archer *et al.*, 2003). Interzone expression of bone morphogenetic proteins (BMPs) two and four are also present during the early stages of joint development, however BMPs are downregulated in later stages because of BMP antagonism from proteins like noggin. A null mutation was made by replacing the coding region of *Noggin* with a *lacZ* gene to determine the effects on skeletogenesis, effectively removing the inhibition of BMPs during this process (Brunet *et al.*, 1998). These mutant mice did not develop joints and had skeletal fusions strongly supporting the role of BMP antagonism in the development of functioning synovial joints. The presence of *chordin* messenger RNA (mRNA), another example of a BMP antagonist in the interzone, was additional evidence for the importance of BMP regulation in joint development. GDF5, a member of the transforming growth factor beta (TGF $\beta$ ) family and hence a prochondrogenic factor, is present at the interzone. This is paradoxical given this tissue is non-chondrogenic, however, years of research on this gene's role in joint development is justified from evidence of *Gdf5/GDF5* mutations in *brachypod* mice and humans causing appendicular skeletal defects and absence of joints (Storm *et al.*, 1994). GDF5 does not however specify joint formation as it has three major roles in initiating chondrogenesis, chondrocyte proliferation and in early joint maintenance (Storm and Kingsley, 1999; Archer *et al.*, 2003).

Cells at the centre of the interzone, named the intermediate zone, do not undergo apoptosis in order to generate the fluid-filled cavity that becomes the synovial joint (Chijimatsu and Saito, 2019). Instead, these cells upregulate their hyaluronic acid production, hyaluronic acid synthases, hyaluronic acid binding proteins (CD44) and the activity of uridine diphosphoglucose dehydrogenase prior to and during the detachment of cell-to-cell adhesion. Cavitation contributes to the formation of the articular cartilage and other synovial joint tissues (Chijimatsu and Saito, 2019), in fact there is evidence that growth plate and articular cartilage are derived from different cell lineages. For example, GDF5-expressing progenitor cells in mice have been shown to give rise to articular cartilage (Koyama *et al.*, 2008). Skeletal muscle paralysis in chick embryos results in failure of joint cavitation and these mice did not lose *Gdf5* expression in the interzone (which under normal conditions is gradually downregulated in the developing joint) but downregulated mitogen activated protein kinase (MAPK) signalling and hyaluronic acid synthesis was observed. This finding was complemented by similar or more severe phenotypes in muscle-less mice also known as splotted-delay mutants (Chijimatsu and Saito, 2019). These results point to the requirement of muscular contraction and MAPK signalling in proper joint development.

Two members of the odd-skipped family of zinc finger transcription factors (*Osr1* and *Osr2*) required for development of leg joints in *Drosophila melanogaster* are also implicated in synovial joint formation in mice (Gao *et al.*, 2011). They reported that *Osr1* and *Osr2* are required for expression of *Gdf5*, *Wnt4* and *Wnt9a*, which, as already discussed, are key to interzone formation and joint development. Hence, zinc association with these transcription factors is required for normal joint formation of these species, but their role in human embryogenesis is still to be determined.

### **1.1.3 Joint homeostasis**

#### **1.1.3.1 Anabolic matrix proteins and growth factors**

The principal collagen and proteoglycan in articular cartilage is collagen type II and aggrecan respectively, collectively accounting for most of the structural protein within the ECM.

Collagen type II is a helical molecule comprised of three identical  $\alpha 1$  polypeptide chains that intertwine, providing tensile strength. Collagen type II accounts for approximately 90-95% of collagen within the ECM with the minor collagens (type I, IV, VI, IX and XI) stabilising collagen type II fibrils in the ECM network. The collagen network resists the swelling pressure of proteoglycan through inherent tensile strength, ensuring resistance to compression and the redistribution of force under mechanical load (Fosang and Beier, 2011). Other than collagen, elastin is the major structural protein of the ECM and provides flexibility for the cartilage (Kim *et al.*, 2011).

Aggrecan consists of many monomers of core protein non-covalently attached to a hyaluronic acid backbone via LINK protein (Verma and Dalal, 2011) as shown in Figure 1.3. Aggrecan attracts water molecules indirectly through the negative charges on the side-chains of the glycosaminoglycans (GAGs), an important mechanism of nutrient acquisition for chondrocytes in this otherwise avascular tissue (Fosang and Beier, 2011). Other matrix proteins are present in the ECM at lower concentrations than the predominating collagen type II and aggrecan, many of which bind and store growth factors supporting normal tissue function (Grässel and Aszodi, 2017). For example, perlecan, another large multi-domain proteoglycan in the pericellular matrix, sequesters fibroblast growth factor 2 (FGF2) which regulates chondrocyte proliferation. Furthermore, a mechanical load applied to chondrocytes cultured in alginate beads resulted in pericellular perlecan and FGF2 accumulation and extracellular signal-regulated kinase (ERK) activation, suggesting a role for perlecan in conveying mechanically driven signal transduction (Vincent *et al.*, 2007). Biglycan is a small leucine-rich repeat proteoglycan capable of binding many substrates including collagen (types I, II, III and VI), BMPs (two, four and six), TGF $\beta$  and tumour necrosis factor  $\alpha$  (TNF $\alpha$ ) (Grässel and Aszodi, 2017). Biglycan deficient mice develop an osteoporotic-like phenotype and collagen fibril abnormalities (Xu *et al.*, 1998). Biglycan may mediate toll-like receptor activation in chondrocytes in response to physical injury, though evidence for this signalling pathway comes from macrophage toll-like receptor stimulation using soluble biglycan, and still awaits to be definitively proven in chondrocytes (Babelova *et al.*, 2009).

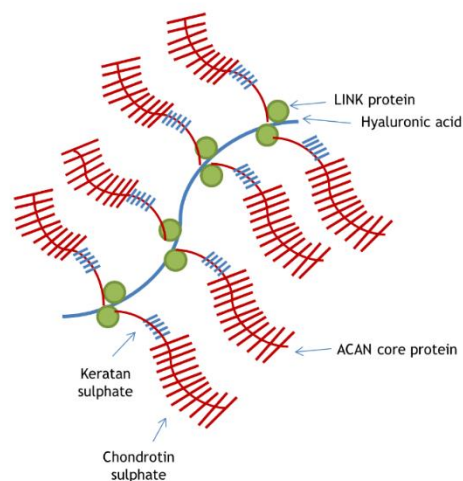


**Figure 1.3– Aggrecan is the major proteoglycan component of cartilage.**

Aggrecan is composed of multiple core protein monomers attached to a hyaluronic acid backbone via LINK protein. The core proteins are post-translationally modified with the addition of sulphated glycosaminoglycans, enabling water and associated nutrients to bathe the chondrocytes. This movement of water also enables cartilage to resist compression loads which is why aggrecan is necessary for functional articular cartilage. Aggrecan = ACAN.

### **1.1.3.2 *Metalloproteinase-mediated matrix turnover***

The family of proteins required for matrix turnover in embryogenesis, wound healing, and cartilage remodelling are the metzincin metalloproteases. The sub-families within the metzincin proteinases have low genetic sequence homology but share zinc dependency for their activity. The matrix metalloproteinases (MMPs) and a disintegrin and metalloproteinase-thrombospondin proteinases (ADAM-TS) are the most important proteinase families in articular cartilage which are responsible for remodelling and are discussed below.

The MMP family consists of 24 proteins in humans (Löffek *et al.*, 2011), seven of which (1, 2, 3, 8, 9, 13 and 14) have been shown to be expressed in articular cartilage under a range of conditions (Rose and Kooyman, 2016). Of these seven, four (1, 2, 13 and 14) are constitutively expressed, presumably participating in matrix turnover. There are numerous ways in which the MMPs are regulated to maintain normal physiological homeostasis. These include transcriptional/post-transcriptional regulation, extracellular localisation (compartmentalisation), pro-domain removal and inhibition by tissue inhibitor of matrix metalloproteinases (TIMPs) (Löffek *et al.*, 2011). Except for the membrane-type MMPs (MT-MMP), the MMPs are secreted with pro-domains, rendering them inactive zymogens until cleavage by pro-protein convertases or furins dependent on the MMP class. In the zymogen form, the cysteine residue PRCGxPD in the pro-domain interacts with a zinc ion of the catalytic domain, which would otherwise function to cleave substrates through interaction with the proline-rich hinge region and haemopexin domain (except MMP7 and 26). Zinc is an essential cofactor of metalloproteinase activity with its target substrates at the catalytic domain. The pro-domain, cleaved during transport through the golgi, is one of three common domains shared by all MMPs (except for MT-MMPs) in addition to the signal sequence and catalytic domain.

MMP1 and MMP13 both cleave collagen type II, with the latter one of the two receiving greater research attention because of its robust cleavage potential against this major collagen within the ECM of articular cartilage. MMP1 cleaves collagen type III and both enzymes can cleave the minor collagens type IV and IX, and glycoproteins like osteonectin (Shiomi *et al.*, 2010). MMP2, also known as gelatinase A, does not cleave either collagen type II or aggrecan, but does target collagen IV and is regarded as crucial for early wound healing (Salo *et al.*, 1994). *Mmp2* deletion in mice also causes intramembranous ossification defects, including growth delay and craniofacial abnormalities (Mosig *et al.*, 2007). MMP14 (also called MT1-MMP) targets aggrecan and cadherin for cleavage in the ECM (Rose and Kooyman, 2016), boosts postnatal bone formation through osteogenesis and chondrogenesis (Yang, 2015), and can activate both MMP2 (Esparza *et al.*, 1999) and MMP13 (Knäuper *et al.*, 1996). Collagen fragmentation is the irreversible step in cartilage degradation.

The degradation of aggrecan by the ADAM-TS family of aggrecanases is an important step in cartilage turnover. The core protein of aggrecan has three globular domains with sulphated chondroitin and keratan GAG residues between domains two and three, and an interglobular domain (IGD) between domains one and two. Cleavage of aggrecan by aggrecanases (ADAM-TS4 and/or ADAM-TS5) occurs between the different domains of the aggrecan protein, such that cartilage ECM can be remodelled during development or injury as illustrated in Figure 1.4. Aggrecanases that target the IGD cleave at position 373 generating the ARG peptide sequence. Aggrecanase cleavage also occurs at multiple sites within the chondroitin sulphate rich regions and there is a hierarchy of preferential cleavage sites at either the chondroitin sulphate regions or IGD for both ADAM-TS4 and ADAM-TS5 (Tortorella *et al.*, 2002). Though there is much evidence for ADAM-TS4 and 5 involvement in structural damage to the ECM, the question of which of these enzymes is more critical to cartilage damage in humans remains nuanced. For example, the ability of ADAM-TS4 to cleave in the IGD of aggrecan correlates with age in animal and human cartilage but does not with ADAM-TS5 (Roughley *et al.*, 2003). This may reflect the age-related changes in the glycosylation pattern of aggrecan (Pratta *et al.*, 2000; Miwa *et al.*, 2006). In fact, ADAM-TS4 has a much wider substrate specificity than ADAM-TS5 and can also cleave cartilage oligomeric matrix protein as well as fibromodulin and decorin (Apte, 2009). Unlike collagen loss, aggrecan breakdown is reversible, as proteoglycan can be resynthesized as observed when the turgor of rabbit ears was restored following cessation of papain aggrecanase injection in the ears (THOMAS, 1956).

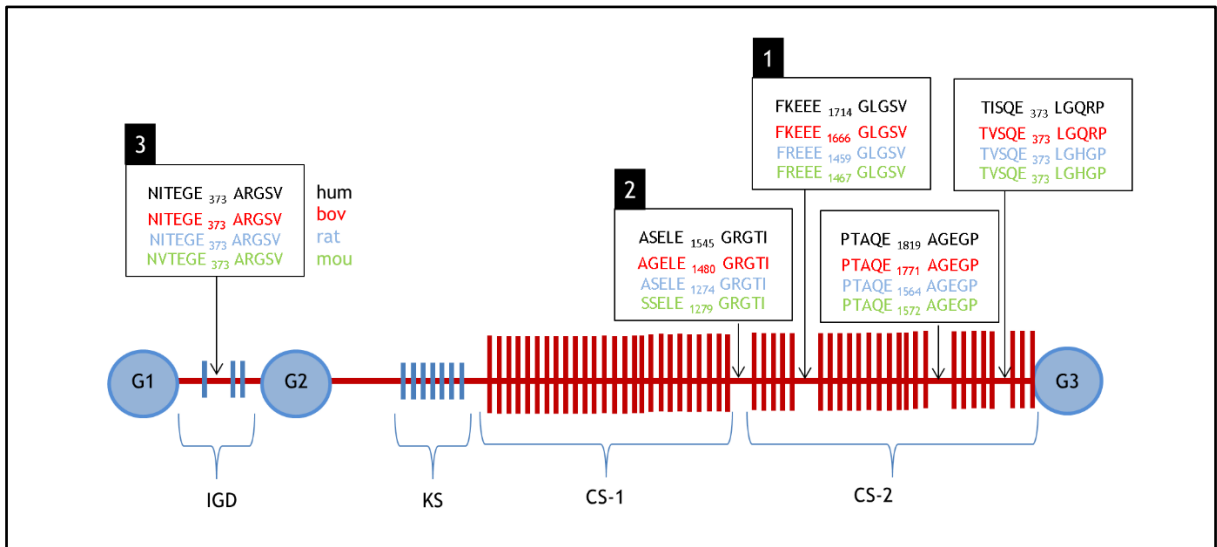


**Figure 1.4 – Aggrecan core protein is the target of aggrecanases at multiple sites. Replicated from Fosang *et al.*, 2008.**

Boxes above the aggrecan core protein indicate the known cleavage sites of the aggrecanases (ADAM-TS) in humans, cows, rats and mice in numerical order of preferential cleavage. Some keratan sulphate is present in the mouse IGD and is highlighted. A disintegrin and metalloproteinase-thrombospondin = ADAM-TS, Interglobular domain = IGD, Keratan sulphate = KS, Chondroitin sulphate = CS.

Like the MMPs, the ADAM-TS members are synthesised in zymogen form possessing a pro-domain and require pro-protein convertases to activate the catalytic domain. Unlike MMPs, the aggrecanases also have an ancillary domain consisting of disintegrin-like, thrombospondin, cysteine-rich and spacer domains involved in substrate recognition as illustrated for ADAM-TS5 in Figure 1.5.

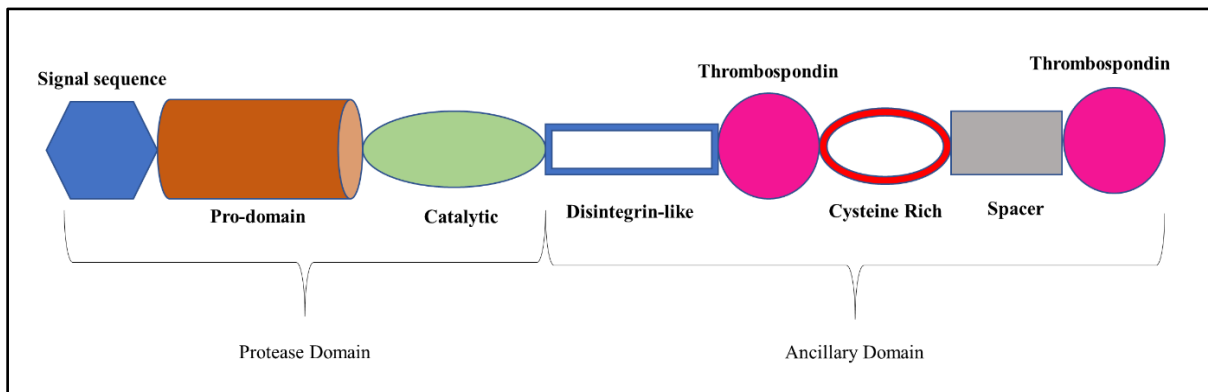


**Figure 1.5 – Schematic of ADAM-TS5 domain structure.**

The ADAM-TS5 protein can be divided in two halves e.g. the proteinase and ancillary domains and within each are distinct protein domains required for function. Edited from Fosang *et al.*, 2008.

### 1.1.3.3 Tissue inhibitors of metalloproteinases

Regulation of the metalloproteinases is clearly necessary in cartilage to avoid overactivity of these enzymes causing an imbalance in favour of chondrocyte catabolic activity, in turn contributing to pathogenesis. There are four TIMPs (1-4) in mammals that are thought to be products of gene duplication (Murphy, 2011). TIMPs are 184-194 amino acids long and inhibit their targets in a 1:1 stoichiometry by blocking pro-MMP cleavage thus preventing MMP target substrate cleavage (Fox *et al.*, 2009). In healthy cartilage from patients with neck of femur (NOF) fractures compared to age-matched hip osteoarthritic cartilage, *TIMP1* and *TIMP4* were overexpressed, suggesting that healthy individuals could regulate the cartilage MMP activities with these two proteins (Kevorkian *et al.*, 2004). Cawston and colleagues measured increased TIMP1 levels in cell culture medium from the T/C-28a4 chondrocyte cell line treated with growth factors (IL-4 and TGF- $\beta$ ) and retinoic acid for 24 hours compared to untreated cells, though this upregulation was not sustained. Using bovine nasal cartilage explants, this same group showed that addition of IL-4 to explants treated with interleukin-1 (IL-1) and oncostatin M (OSM) resulted in ~2% collagen release compared to >90% with these inflammatory mediators alone, thus protecting the cartilage from collagenases. No discernible difference in TIMP1 levels was measured and Cawston *et al.*, suggested this protective response was due to IL-4-mediated collagenase gene downregulation (Cawston *et al.*, 1999).

## 1.2 Osteoarthritis

Osteoarthritis (OA) is the most common musculoskeletal condition worldwide and the 11<sup>th</sup> leading cause of global disability. In the United Kingdom, over 8.75 million people have sought treatment for OA (Arthritis Research UK, 2013). Historically, OA was thought of as a ‘wear-and-tear’ disease associated with old age and characterised by cartilage destruction. However, within the last 15 years, it has become increasingly accepted that OA affects multiple tissues within the joints. The changes that occur within the joint include fibrillation and gradual loss of the articular cartilage (causing a reduction in the joint space), formation of osteophytes on the subchondral bone, synovitis, and increased synovial fluid volume (Figure 1.6). One or more of these clinical features may be present, but ultimately results in compromised joint function, loss of dexterity and pain from bone-on-bone grinding. The most affected joints are the knee and hip but also the hand, wrist, foot, and ankle. The fact that OA can occur in the hand, which is not weight-bearing, supports the notion that OA is not merely the result of abnormal mechanical loads caused by joint instability or misalignment (Arthritis Research UK, 2013).

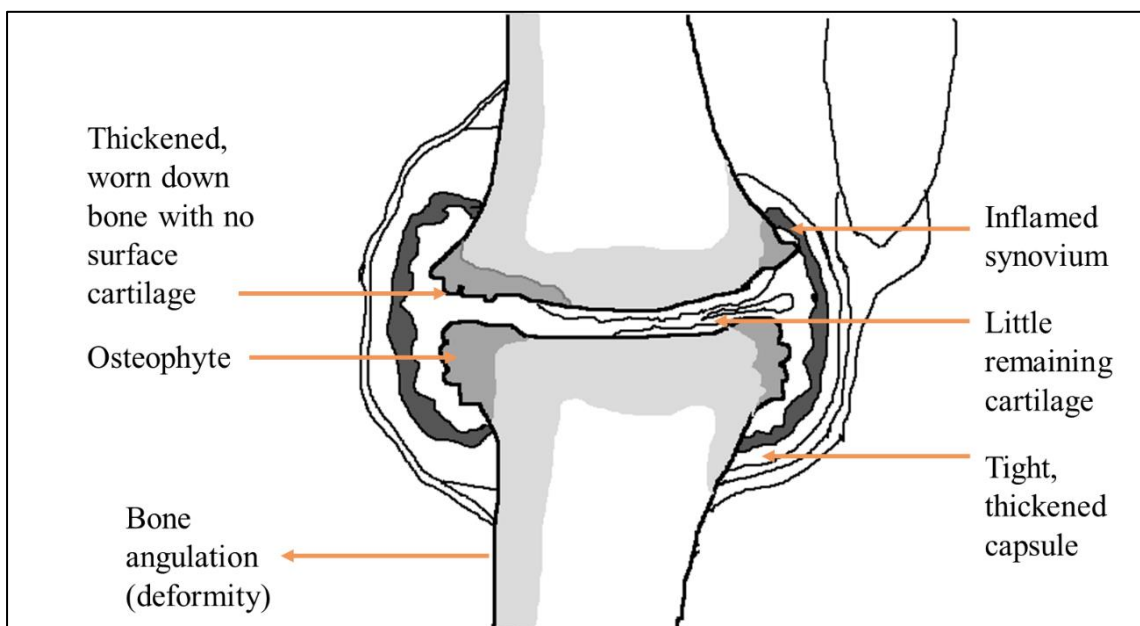


**Figure 1.6- Diagram of an advanced osteoarthritic joint.** Multiple tissues are affected in the pathogenesis of OA, but the distinctive feature is reduced joint space width following degradation of the articular cartilage. Other features which may present are the thickening of the synovium due to synovitis, increased synovial fluid volume and instability through ligament and tendon damage. Replicated from Arthritis Research UK, 2013, *Osteoarthritis in general practice report*. Accessed 29/07/20.

### **1.2.1 Risk Factors**

The aetiology of OA is unknown but its associated risk factors include age, biological sex (women have greater incidence), obesity, prior joint injury (including anterior cruciate ligament (ACL) tear), and bone density (Arthritis Research UK, 2013).

#### **1.2.1.1 Age**

People over 40 years typically present with OA and the reported prevalence of the disease is a function of multiple factors including OA diagnosis (radiographic, symptomatic or self-reported), age range, countries of origin and sex distribution of the study population (Hunter and Bierma-Zeinstra, 2019). For example, radiographic OA is more widespread than symptomatic OA across the age groups and knee and hand OA is more prevalent than hip OA in population-based studies. Incidence increases with increasing age but between the ages of 50-75, knee and hand OA incidence among women exceeds that of men with peak incidence at age 75 (Hunter and Bierma-Zeinstra, 2019). Aged cartilage and OA cartilage are distinct in their appearance (functional versus non-functional), yet the former can predispose to the latter should the accumulation of advanced glycation end-products overwhelm the structural integrity through increased brittleness (Verzijl *et al.*, 2002). Chondrocytes from elderly individuals are more likely to adopt a senescence-associated secretory phenotype which essentially switch from phosphoinositide 3 kinase-Akt anabolic cell signalling to activation of specific catabolic MAPK signalling pathways, resulting in cartilage matrix-degrading enzyme production and apoptosis. Increased mitochondrial dysfunction in aged chondrocytes causes greater reactive oxygen species (ROS) production, coupled with diminished glutathione anti-oxidant activity, compromising chondrocyte sensitivity to growth factors, leading to a phenotypic switch (Loeser, 2017).

### 1.2.1.2 *Biological sex*

Women over men are more likely to develop OA of the knee and hand but not hip (Boyan *et al.*, 2013b) across different age groups according to studies conducted in sponsorship with the Centers for Disease Control and the National Institutes of Health (Srikanth *et al.*, 2005; Loeser *et al.*, 2012). The severity of OA increases after the menopause in women but the supporting literature on how sex hormones may mediate OA risk in women is not clearly defined (Boyan *et al.*, 2013a). For example, male and female chondrocytes express oestrogen receptors (with fewer receptors overall in male cells), indicating chondrocytes are oestrogen responsive cells. However, male articular chondrocytes do not produce protein kinase C (PKC) activity nor are able to produce proteoglycans in response to  $17\beta$ -oestradiol unlike female articular chondrocytes, clearly indicating sexual dimorphism after treatment with  $17\beta$ -oestradiol (Kinney *et al.*, 2005). This paper also suggested that the  $17\beta$ -oestradiol-mediated effect was the result of rapid signal transduction following activation of the membrane-bound receptor (PKC activity) and not through activation of the nuclear receptor of oestrogen (proteoglycan measurement by  $^{35}\text{S}$ ]-sulphate incorporation).

While pre-menopausal concentrations of  $17\beta$ -oestradiol has a decelerating effect on telomere attrition (Breu *et al.*, 2011), no significant effect was observed with a reduced  $17\beta$ -oestradiol post-menopausal concentration. Diminishing oestrogen levels in menopause may influence the severity of OA by reducing chondrocyte proliferation and matrix production (Kinney *et al.*, 2005), and encouraging greater *MMP 1,3* and *13* transcription in 3D cultured chondrocytes (Claassen *et al.*, 2010). It should also be noted that male and female chondrocytes express androgen and dihydrotestosterone (DHT) receptors such that they are receptive to androgen stimulation. DHT has been shown to be produced from testosterone in rat growth plate chondrocytes by  $5\alpha$ -reductase (Raz *et al.*, 2005). Though less is known about the direct effects of testosterone on articular chondrocytes (Boyan *et al.*, 2013a), androgen studies have shown to be protective in cartilage studies of inflammation-induced rheumatoid arthritis (RA) (Da Silva *et al.*, 1993), though it is not known whether this was a direct effect, DHT-driven or even oestrogen-mediated, produced locally by aromatase conversion of testosterone. Whether this protective effect extends to OA cartilage is unknown but likely does not offset the consequences of post-menopausal oestrogen levels on the articular chondrocytes.

Bilateral oophorectomy or oophorectomy and hysterectomy in rodent (Yao *et al.*, 2006; McMillan *et al.*, 2007) and primate (Wentorf *et al.*, 2006) animal models are used to study the loss of oestrogens on connective tissue homeostasis in the joints. Osteopenia was a common phenotype in all animals receiving these surgeries but there was variation of such between animals and rates of its onset (Boyan *et al.*, 2013a). In primates, the decline in oestrogens did not result in changes to patellar tendon or ACL following mechanical load of the tissue post-sacrifice two years after surgery, therefore suggesting that not all joint tissues are affected equally following oestrogen removal (Wentorf *et al.*, 2006). A major limitation of these animal models, and hence the interpretation of these findings, was the use of young animals, removing the contribution of age in the pathogenesis of OA (Boyan *et al.*, 2013a). This variation in phenotypes/symptoms is also reflected in humans as not all post-menopausal women develop OA, but subchondral bone changes and general osteopenia may predispose to OA through abnormal mechanical loading, impacting articular cartilage.

### **1.2.1.3 Obesity**

Obesity is the greatest modifiable risk factor in OA and its association with OA in the literature is more robust for knee than hip joints, reflecting either joint-site specific effects or differences in the methodologies of the studies assessing these relationships (King *et al.*, 2013). One group investigated the relationship between body mass index (BMI) (among other anthropometric factors including height and weight) and risk for arthroplasty in a prospective cohort study of women, where a relative risk of 10.5 and 2.47 for knee and hip respectively was calculated in obese ( $\text{BMI} \geq 30 \text{kg/m}^2$ ) versus non obese ( $\text{BMI} \leq 22.5 \text{kg/m}^2$ ) individuals (Liu *et al.*, 2007). Liu *et al.*, 2007 estimated the percentage contribution of being overweight and obese on knee and hip arthroplasty in the UK as 69 and 27% respectively. In addition to weight and obesity as contributing factors for elective joint replacement, there are other influences such as patient and doctor preferences and socio-economic factors, for instance waiting lists and access to private healthcare. Thus, interpretation of joint replacement data needs to be carefully assessed.

Magnetic resonance imaging (MRI) has been used to screen 137 middle-aged individuals with associated knee OA risk factors but without radiographic knee OA at baseline and at a 36 months follow up (Laberge *et al.*, 2012). Subjects were grouped into three categories according to their BMI status ( $\leq 25\text{kg/m}^2$ ,  $25\text{-}29.9\text{kg/m}^2$  or  $\geq 30\text{kg/m}^2$ ) and those who were obese had higher prevalence and severity of cartilage lesions at baseline which were positively correlated with BMI and increased meniscal tears and high-grade defects compared to non-obese groups. At the 36 months follow up the number of new or worsening cartilage lesions was significantly higher in obese subjects ( $p=0.039$ ), but obesity did not confer greater risk of meniscal or bone marrow lesion progression. How obesity confers risk to OA is believed to be a consequence of increased mechanical loading and of metabolic factors (King *et al.*, 2013), as being obese can confer greater risk to hand OA which is non-load bearing. The low-grade inflammatory state that excess adipose tissue contributes towards is mediated in part by adipokines (leptin and adiponectin), the receptors for which are abundantly expressed on chondrocytes, synoviocytes and subchondral osteoblasts. Leptin regulates MMPs, pro-inflammatory cytokines and nitric oxide but less is known about the role of adiponectin and contrary evidence supporting both pro and anti-inflammatory effects have been reported in joint disease compared to its anti-inflammatory effects systemically (King *et al.*, 2013).

#### **1.2.1.4 Joint injury**

Post-traumatic osteoarthritis (PTOA) development of the knee tends to occur after a decade following an injury, the prevalence of which increases from 13% in patients with isolated ACL injury to 21-48% in people with combined ACL and meniscal injuries (Øiestad *et al.*, 2009). 50% of those with serious knee injury and > 25% of acetabular fractures of the hip progress to PTOA. A comparison of the prevalence of PTOA among patients after ACL reconstruction with those who were ACL deficient found greater rates of OA development in the reconstruction group (44% versus 37%). The prevalence was further influenced by time since injury (Luc *et al.*, 2014). No ACL reconstruction resulted in 34% greater PTOA prevalence than the reconstruction group by the 3<sup>rd</sup> decade after injury. All the factors following ACL and meniscal injury which cause PTOA are not known but can be influenced by BMI. In fact, 68% of patients classified as morbidly obese with acetabular fractures developed PTOA (Lawyer *et al.*, 2014). Direct tissue trauma causing ligament injuries may be sufficient to cause PTOA which is supported by 90% of ACL injuries being accompanied by osteochondral lesions, suggesting concomitant cartilage trauma (Thomas *et al.*, 2017).

### 1.2.1.5 Genetics

The genetic component to OA is estimated to be between 40-80% in twin studies. OA is typically considered a disease of the elderly, but there is a rare early-onset form typically occurring in families where a single mutation has a large effect on the function of gene/protein networks. For example, the gain of function mutation in *TNFRSF11B* encoding osteoprotegerin discovered through whole exome sequencing is causative of familial early-onset OA in multiple joints (Ramos *et al.*, 2015). The risk of developing an age-related OA phenotype correlates with specific DNA variants located at multiple different loci, reflecting the complex polygenic nature of OA. These DNA variants have modest effect size on the phenotype. Therefore, accrual of risk DNA variants in an individual's genome confers greater susceptibility to developing OA. DNA polymorphisms such as single nucleotide polymorphisms (SNPs) are the most common type of genetic variant and are defined once frequency across one percent of the population has been reached, distinguishing them from mutations which are far rarer. Many DNA polymorphisms are not located in the coding regions of genes but in intronic and other non-coding features like enhancers and insulators and so principally regulate gene expression. The mechanisms through which SNPs function include altering transcription factor binding impacting gene transcription (Figure 1.7), amino acid substitutions akin to missense mutation, and mRNA stability changes either repressing or enhancing microRNA (miRNA) activity (Bush and Moore, 2012).

Over the last decade our understanding of the OA risk SNPs and loci has vastly improved due to data generated from genome-wide association studies (GWAS) comparing allele frequencies for SNPs in OA patients versus healthy controls. Up until April 2017, only 19 OA-risk loci had been identified but now there are over 90 OA-risk loci with genome-wide significance  $p \leq 5 \times 10^{-8}$ . Many of these new loci have been validated in replication cohorts and this rapid increase in loci identification can in part be explained by the publication of several large scale, well powered OA GWAS (Reynard, 2019).

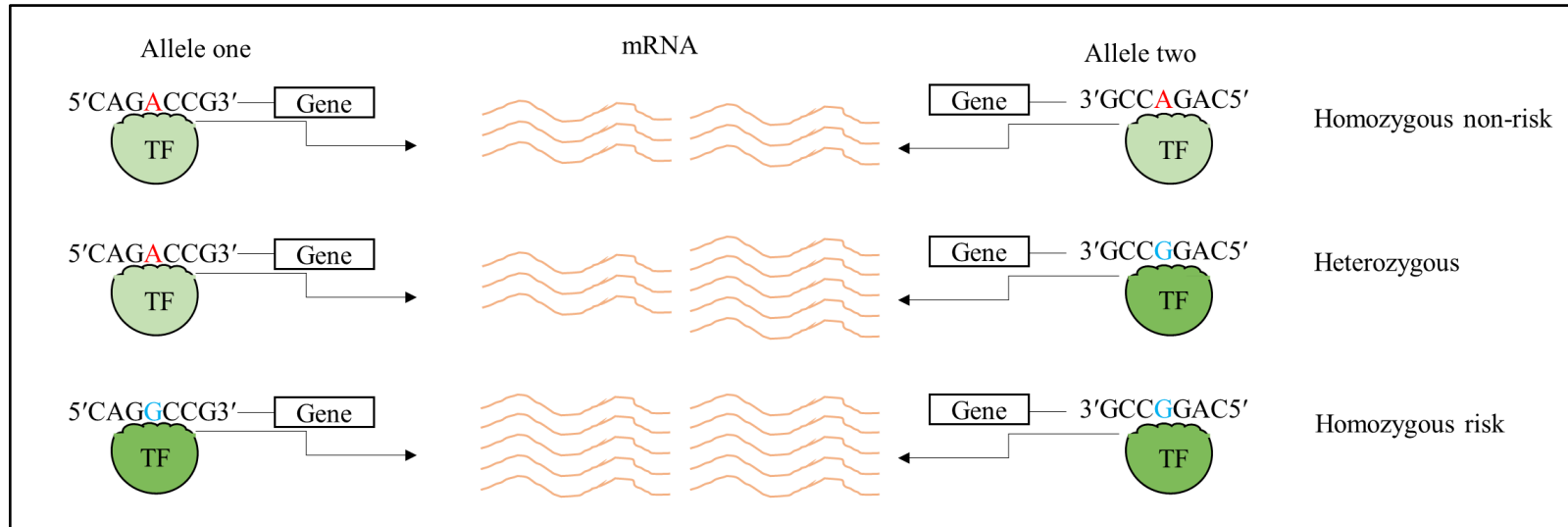


**Figure 1.7 – Example mechanism of a single nucleotide polymorphism impacting on gene expression.**

One of the principal mechanisms through which DNA polymorphisms influence gene expression is through increased transcription factor binding. Increased transcription factor (TF) binding (increasing green colour saturation) in individuals possessing the risk G compared to TFs binding at the same site with the A non-risk allele. The consequence of this increased TF binding is greater gene expression illustrated by more mRNA copies produced from individuals with the G-allele. This example is representative but not exhaustive of the potential mechanisms of SNPs conferring altered gene expression states.

The current challenge for translating GWAS results to clinical benefit is locating the causal SNP(s) from the association signal and discovering the mechanism through which the SNP regulates gene expression. Knowledge of the mechanism through which the SNP increases the disease risk provides a rationale for using genome editing to replace the risk allele with the non-risk allele, though this comes with obvious ethical considerations for editing the germ line. Initially it is important to determine if gene expression changes with the sentinel SNP genotype detected on the GWAS, also known as expression quantitative trait loci (eQTL). SNPs are commonly found in areas of high linkage disequilibrium (LD), so it is difficult to pinpoint the causal SNP at this stage. A state of LD is achieved when the allele of one SNP is inherited or correlates with an allele of another SNP within a population. When two SNPs on a contiguous stretch of DNA are inherited over generations and are not immediately segregated after meiotic recombination between homologous chromosomes, the two alleles of each SNP are dependent on each other. Assuming a fixed population size, random mating, and random recombination events, LD tends towards zero and the SNPs eventually enter linkage equilibrium or are independently associated (Bush and Moore, 2012). An alternative approach to unmask the risk SNP is to analyse the heterozygote population for allelic expression imbalance of a transcript SNP (coding variant) in LD with the sentinel SNP, and normalise the data to the individual's DNA before other SNPs within the risk locus are investigated (Pastinen, 2010). These approaches will help identify SNPs in the association locus which correlate with eQTLs, however both allelic forms of the SNPs need to be tested for influencing gene expression through one of the aforementioned mechanisms (Bush and Moore, 2012).

#### **1.2.1.6 Therapeutics**

Therapeutics for OA are largely dependent on the stage of the disease upon diagnosis. If the condition is detected early, which is more likely to be the case in individuals with a prior joint injury, then light exercise forms the core treatment. In individuals who also present with obesity, lifestyle changes in the form of diet and exercise to reduce impact forces on the joint are recommended and pain is managed pharmaceutically with non-steroidal anti-inflammatories or corticosteroid injections. For patients with more severe disease, joint arthroplasty is conducted. This effectively eliminates pain and restores joint mobility (Arthritis Research UK, 2013) and there are currently no disease-modifying anti-rheumatic drugs for OA.

### **1.2.2 Role of MMPs and ADAM-TSs in osteoarthritis cartilage destruction**

Loss of cartilage homeostasis occurs when members of the metalloproteinases are not just turning over ECM but begin to degrade it pathologically without regulation (Rose and Kooyman, 2016). Four (MMP1, 2, 13 and 14) of the 24 MMPs and principally ADAM-TS4 and ADAM-TS5 are associated with OA (Verma and Dalal, 2011; Rose and Kooyman, 2016). The mechanisms by which the metalloproteinases target their respective components of the ECM were outlined in 1.1.3.2. In these subsections I hope to outline which proteinases are specifically associated with OA from genetically engineered mouse models (GEMM) and what the consequence of ECM fragments production is for immune system-associated receptor activation.

#### **1.2.2.1 Evidence from animal models**

GEMM assess the effects of global gene knockout, tissue-specific gene knockout and even knock-in mutations in both surgical models and spontaneous models of OA (Miller *et al.*, 2013). For example, global gene knockout of *Mmp3* (Glasson, 2007), *Mmp12* (Glasson, 2007) or *Mmp17* (Clements *et al.*, 2011) and surgical destabilisation of the medial meniscus (DMM) did not influence OA progression assessed at 8 weeks post-surgery compared to sham-operated mice. In the *Mmp13* mouse global knockout there were no observed cartilage lesions on the tibial plateau but focal aggrecan loss on the femoral surface at 8 weeks and osteophytes observed as early as 4 weeks post-surgery (Little *et al.*, 2009). A decreased rate of cartilage degeneration was observed in a chondrocyte-specific *Mmp13* knockout mouse line receiving surgery (transection of the medial collateral ligament and partial medial meniscus removal) compared to sham-operated mice (Wang *et al.*, 2013). *Mmp14* global gene knockout has been assessed in mouse lines to study spontaneous OA in mice aged up to 40 days and these animals developed OA at an increased rate (Holmbeck *et al.*, 1999).

Catalytic domain exchange of ADAM-TS4 and ADAM-TS5 in chimeric protein and subsequent aggrecanolytic assessment resulted in a four-fold increase in ADAM-TS5 catalytic domain activity in the IGD over ADAM-TS4 and 2.5-fold in the chondroitin sulphate-2 region of aggrecan (Fushimi *et al.*, 2008). This set a precedent to explore the roles of ADAM-TS catalytic domains *in vivo* using a GEMM. ADAM-TS5 was proven to be the major aggrecanase in murine cartilage through Cre-loxp deletion of the catalytic domain *in vivo* resulting in protection from aggrecanolytic in an OA inflammatory model. Briefly, the mice were primed with intradermal injection of methylated bovine serum albumin (mBSA) on day zero, then at day seven, mice received intraarticular injection with another mBSA dose and tibiofemoral joints were collected three days later. There was no significant difference between the control strain (heterozygous loxp (exon3)) or the homozygous catalytic domain-excised strain in the severity of synovitis, joint space exudate, pannus-mediated erosion, or bone destruction. There was greater loss of aggrecan in the control mice compared to the homozygous catalytic domain-excised strain (Stanton *et al.*, 2005). A similar result with another transgenic mouse through Cre-loxp excision of *Adam-ts5* catalytic domain was achieved by Glasson *et al.*, who did not detect aggrecan neoepitopes in this strain by immunostaining compared to wild-type or *Adam-ts4* homozygous catalytic domain excision strain (Glasson *et al.*, 2005). Knock-in mutations in the IGD of the *Acan* gene have been carried out, preventing MMP or ADAM-TS-mediated aggrecan cleavage of the Asn<sup>341</sup>-Phe<sup>342</sup> (Little *et al.*, 2005) and Glu<sup>373</sup>-Ala<sup>374</sup> (Little *et al.*, 2007) sites respectively. This created the Chloe and Jaffa mice lines respectively. Cartilage degeneration of Chloe mice after DMM surgery was comparable to wild-type sham-operated mice, but Jaffa mice were protected from cartilage erosion comparable to the *Adam-ts5* knockout mouse (Glasson *et al.*, 2005). Comparison of the cartilage of *Adam-ts4* exon 4 catalytic domain deleted mutant mice with wild-type mice receiving DMM or sham-surgery at four or eight weeks after surgery revealed no difference in histological score (Glasson *et al.*, 2004).

#### ***1.2.2.2 Matrix fragments provide positive feedback pro-inflammatory chondrocyte responses***

The breakdown of structural protein components of the ECM by metalloproteinases in OA creates fragmented proteoglycans which act as damage-associated molecular patterns (DAMPs) to further exacerbate pro-catabolic responses in chondrocytes via pattern recognition receptors (PRRs) (Sokolove and Lepus, 2013). PRRs are composed of several families of cell surface, endosomal and cytosolic receptors and are principally involved in identifying foreign pathogens or pathogen-associated molecular patterns (PAMPs). For example, the toll-like receptors two and four are PRRs which recognise multiple ECM fragment components including fibronectin and hyaluronic acid (Sokolove and Lepus, 2013). Fibronectin fragments injected into the knee joints of rabbits resulted in cartilage damage through loss of up to 70% of proteoglycan (Homandberg *et al.*, 1993). The fibronectin injection was later shown to upregulate pro-inflammatory cytokines such as *TNF $\alpha$*  and *IL-1 $\beta$*  as well as *MMP1* and *13* (Homandberg and Hui, 1996).

### **1.3 Molecular drivers of cartilage destruction in osteoarthritis**

Molecular studies and clinical observations have indicated that OA is a heterogenous and multifactorial disease, with different pathophysiological pathways leading to the same end phenotype of cartilage destruction, synovial inflammation, bone changes and accompanying symptoms of pain and loss of joint function. The aetiology of OA is poorly understood, with little being known about the early molecular processes that mark the development and early progression of OA prior to the presence of radiographically detected joint damage. There are currently no disease-modifying drugs for OA, with the only treatment options being analgesia, physical therapy and joint replacement. To identify new therapeutic targets, discover biomarkers of disease and improve existing joint tissue regeneration approaches for OA treatment, understanding of the biological processes underlying OA development and progression needs to be improved. Several molecular pathways have been suggested to act as key drivers that disrupt the balance between cartilage synthesis and turnover, such that there is increased MMP and ADAMTS-mediated cartilage destruction, eventually leading to complete cartilage loss. These molecular drivers include unresolved inflammation and disrupted zinc homeostasis, which are discussed below or in 1.4.2.

#### **1.3.1 Inflammation and IL-1 in osteoarthritis pathogenesis**

##### **1.3.1.1 The IL-1 signalling pathway**

Interleukins (ILs) are a class of signalling molecule known as cytokines, enabling intercellular communication. The interleukin 1 family consists of 11 individual members, each with distinct biological functions despite the structural homology (Schett *et al.*, 2016). The IL-1 members' roles include resolution from sterile injury and infection by promoting downstream pro-inflammatory pathway activation, though IL-36Ra and IL-37 are anti-inflammatory IL-1 members. I will provide insight for three ligands which signal via the IL-1 receptor type 1 (IL-1R1) which are IL-1 $\alpha$ , IL-1 $\beta$  and IL-1 receptor antagonist (IL-1Ra).

IL-1 $\alpha$  can bind to IL-1R1 with 10-fold greater receptor affinity than IL-1 $\beta$  (Chin *et al.*, 1988) and is released following cell necrosis, acting as an alarmin to neighboring cells that sterile injury has occurred. In apoptosis, IL-1 $\alpha$  is directed to the nucleus through a nuclear localisation sequence in the IL-1 $\alpha$  precursor preventing its activity and propagating inflammation as the cell dies. Unlike IL-1 $\alpha$ , IL-1 $\beta$  requires activation from a 31kDa pro-protein form to a 17kDa active form. This can occur through inflammasome-dependent or independent pathways requiring neutrophil-derived serine proteases (Schett *et al.*, 2016). Neutrophil infiltration into the joint capsule is not common in OA (de Lange-Brokaar *et al.*, 2012) but does occur in some individuals and therefore activation of IL-1 $\beta$  through such proteases as cathepsin G or neutrophil elastase cannot be ruled out. IL-1Ra competes with IL-1 $\alpha$  and IL-1 $\beta$  for the IL-1R1 and does not lead to downstream intracellular signalling, effectively blocking the other two ligands (Schett *et al.*, 2016).

Following receptor activation, IL-1 receptor accessory protein interacts with multiple intracellular signalling molecules including myeloid differentiating factor 88 (MyD88), IL-1 receptor-associated kinase 4 (IRAK4) and tumour necrosis factor receptor-associated factor 6 (TNF6). Signalling through these pathways results in activation of nuclear factor kappa-light-chain-enhancer of activated B cells (NF $\kappa$ B), p38, ERK and MAPKs (Schett *et al.*, 2016). Activation of these networks leads to recruitment of transcription factors to the nucleus which promote pro-inflammatory gene expression.

### **1.3.1.2 IL-1 and other inflammatory mediators can stimulate cartilage destruction *in vitro***

The first experimental evidence identifying IL-1 $\beta$  (or catabolin as it was known at the time) in cartilage degradation was from *in vitro* porcine cartilage explants co-cultured with synovium (Fell and Jubb, 1977). This co-culture resulted in IL-1 $\beta$ -mediated cartilage degradation through loss of aggrecan (Tyler, 1985) and suppressed new proteoglycan synthesis. The importance of IL-1 $\beta$  in the discovery of the metalloproteinases responsible for cartilage degradation cannot be understated. Prior to the discovery of the aggrecanases, IL-1 had already been described as a key cytokine inducing *MMP* gene expression (Gadher *et al.*, 1988; Lefebvre *et al.*, 1990), and medium from IL-1 $\beta$  stimulated bovine nasal cartilage explants identified the first aggrecanase, *ADAM-TS4* (Tortorella *et al.*, 1999). *ADAM-TS4* mRNA is also inducible to other pro-catabolic agents such as TNF $\alpha$  (Moulharat *et al.*, 2004), whereas *ADAM-TS5* expression is both constitutive and inducible in human chondrocytes. *ADAM-TS5* has been shown to be inducible dependent on the species, cell type, culture format or treatment (Fosang *et al.*, 2008).

Another cytokine, OSM, was used in combination with IL-1 or TNF $\alpha$  in the study of ECM breakdown in *in vitro* human nasal cartilage (HNC) explants compared to bovine nasal and human articular cartilage explants (Morgan *et al.*, 2006). Collagenase production and ECM breakdown responses were similar in HNC explants treated with the IL-1 and OSM combination as the IL-1 and TNF $\alpha$  stimulus. The authors found that HNC explants' baseline proteoglycan release (a proxy measurement for aggrecanolytic activity) was 1/3 lower than human articular cartilage (12.5% versus 39%) but had similar proteoglycan release (69.2% versus 79.5%) following IL-1 and OSM treatment of HNC explants and human articular cartilage for 14 and 21 days respectively. The proteoglycan release experiments were conducted in three HNC and 43 OA human articular cartilage explants. Collagen release (a proxy measurement for collagenolysis) from the cartilage in HNC explants treated with IL-1 and OSM was comparable to bovine nasal cartilage after 14 days of stimulation but was greater than human articular cartilage after 21 days (59.6% versus 7%), the latter comparison using two donor HNC and 55 human articular cartilage explants. Human articular cartilage does not typically respond strongly to IL-1 and OSM stimulation, with 50% of donors responding with <15% collagenolysis (Cawston *et al.*, 1998). In this study (Morgan *et al.*, 2006), 30 of 55 (55%) human articular cartilage donors belonged to this group and it is thought that the reason for the differences between HNC and human articular cartilage explants is due to multiple factors including age, health and tissue permeability. For example, aged OA cartilage at the time of elective surgery is already structurally compromised because of chronic ECM degradation, so the tissue responsiveness to pro-inflammatory cytokines is reduced *in vitro*, which is compounded by the presence of advanced glycation end products and reduced tissue permeability, preventing metalloproteinase-mediated matrix release. HNC explants provide a model to study cartilage breakdown from healthy individuals using pro-inflammatory cytokines that overcomes the issues described with human articular cartilage. Both primary chondrocytes, SW1353 and T/C-28a4 chondrocyte cell lines treated with IL-1 $\alpha$  alone or IL-1 $\alpha$  and OSM also show metalloproteinase gene upregulation (Koshy *et al.*, 2002; Young *et al.*, 2005), indicating cells as well as tissue explants are responsive to pro-inflammatory stimuli *in vitro*.

### **1.3.1.3 *In vivo* evidence of inflammatory component to OA from genome-wide association studies and transcriptomics**

In recent years two of the largest OA analyses were published, collectively identifying 56 loci and 12 replicated genome-wide associations (Styrkarsdottir *et al.*, 2018; Tachmazidou *et al.*, 2019). Both studies performed a meta-analysis of the UK biobank data (UKBB) in addition to either the Icelandic deCODE genetics or UK arcOGEN datasets respectively. The deCODE-UKBB study (Styrkarsdottir *et al.*, 2018) included over 650000 British and Icelandic individuals and 11.6 million SNPs were analysed with separate meta-analyses for hip and knee OA (Reynard, 2019). The same OA definition was used for both cohorts and individuals with known causes of secondary OA were excluded, yielding 17151 OA hip cases, 23877 knee cases and up to 619289 controls. They identified 23 independent associations at 22 loci using an additive model (where possession of a risk allele increases OA risk in a linear fashion) with odds ratios 1.06-2.84 and two loci using a recessive model (homozygous risk allele genotype compared against compound heterozygotes and homozygous non-risk individuals) with odds ratios 1.95-5.89. This included 12 hip and four knee novel loci. The arcOGEN-UKBB study (Tachmazidou *et al.*, 2019) analysed up to 17.5 million SNPs in over 455000 UK individuals and 369983 controls, reporting 65 genome-wide significant SNPs mapping to 64 loci (Reynard, 2019). Separate meta-analyses were performed for four OA phenotypes; OA hip, OA knee, hip and/or knee OA, and OA at any site, although different OA definitions were used in the two cohorts.

Among the 12 signals that were replicated, the low-frequency (2.08%) missense variant rs4252548 in *IL-11* was associated with risk of hip OA ( $p=2.1 \times 10^{-11}$  (Styrkarsdottir *et al.*, 2018),  $p=1.96 \times 10^{-12}$  (Tachmazidou *et al.*, 2019)) and the same SNP is associated with decreased adult height ( $p=5.32 \times 10^{-81}$ ) (Marouli *et al.*, 2017). *IL-11* was elevated in hip and knee damaged OA cartilage compared to non-damaged OA cartilage regions from the same joint (Tachmazidou *et al.*, 2019). IL-11 is a potent stimulator of bone formation and is required for osteoclast differentiation. Increased IL-11 signalling in OA joints is not well understood and the amino acid substitution p.Arg112His, caused by the missense SNP, renders IL-11 thermally unstable, failing to support osteoclast progenitor cell survival (Lokau *et al.*, 2018). Overall, well-powered GWAS that include low frequency and common variants provide the best opportunity to detect marginal to moderate effect sizes of SNPs associated with inflammatory genes, but the evidence so far is that inflammation related genes are not relevant to the disease.

Microarray and RNA-Seq experiments assessing the transcriptome provides more compelling evidence for immune gene involvement in OA. These experiments assess gene expression in case-controls but also in terms of disease stage and in the study of healthy and diseased regions of the same tissue (Rogers *et al.*, 2015). The synovium is one of the most overtly inflamed tissues in the OA joint, though not to the same extent as in RA, but is often used as a negative control by RA researchers. Microarray analysis of OA synovium compared to non-OA synovium revealed upregulation of complement effector genes, downregulation of complement inhibitors and increased IL-1 $\beta$  activity (Wang *et al.*, 2011). IL-1 $\beta$ -mediated gene expression in knee-derived OA chondrocytes led to differential expression of 909 out of 3459 genes compared to untreated chondrocytes including numerous chemokines and inflammatory mediators such as *IL-11* and *CCL5* (Saas *et al.*, 2006). When whole tissue comparisons of lesioned OA cartilage against intact non-OA cartilage samples were made, an increase in *CXCL8* and leukaemia inhibitory factor was observed (Karlsson *et al.*, 2010). In terms of inflammatory gene signature overlap between joint sites (hip and knee) the genes involved in the TREM1 signalling pathway were upregulated (Xu *et al.*, 2012). Not only has there been evidence of inflammatory gene expression in a tissue-specific manner but there is evidence of systemic inflammation in the peripheral blood leukocytes (PBLs) of OA. One hundred and seventy-three genes were found differentially expressed in OA PBLs compared to non-OA PBLs and among them were many notable inflammatory mediators (Attur *et al.*, 2011). The identification of a subgroup within the OA blood characterised by 2-fold greater IL-1 $\beta$  expression than non-OA PBLs was correlated with higher knee pain scores and risk of radiographic OA progression.

The differential gene expression patterns in early OA are of particular interest as this precedes structural joint damage and may provide an option for effective therapeutic intervention (Rogers *et al.*, 2015). However, only synovium tissue or fluid is taken for early OA assessment from individuals who have had meniscal tears and later require arthroscopic meniscectomy or arthrocentesis, as the Multicentre Osteoarthritis Study identified that these people are at risk from later developing OA (Englund *et al.*, 2009). Microarray analysis of a meniscectomy group of patients identified 266 genes differentially expressed in inflamed synovium compared against synovium from individuals without inflammation. Chemokines and chemokine receptors were among those genes most enriched among the 266 genes (Scanzello *et al.*, 2011) and CCL-5 can induce *IL-6* in a concentration-dependent manner in synovial fibroblasts. *IL-6* was produced in OA human knee synovial fibroblasts (n=11 donors) in response to CCL-5 treatment compared to untreated OA synovial fibroblasts from the same donors in a concentration and time-dependent manner (Tang *et al.*, 2010). The early upregulation of chemokines in synovium may suggest pivotal roles in cytokine expression which propagates further inflammation exacerbating OA pathogenesis. A pilot study was conducted in meniscectomy patients who had synovial fluid collected at differing times since injury (injury duration defined as self-reported time of injury until date of partial meniscectomy procedure) and gene expression of cell pellets and supernatant was assessed by microarray and RNA-sequencing (Vance *et al.*, 2014). The researchers found that inflammatory gene expression patterns were greatest in the individuals whose injury duration was greater than two months compared to those who resolved their injury under two months. However, this pilot study was only conducted in eight individuals so care interpreting the results is needed. Finally, a study measuring gene expression in synovial membrane and fluid from early OA patients compared to end-stage OA patients found that levels of *TNF- $\alpha$* , *IL-1 $\beta$*  and *IL-6* were comparable (Scanzello *et al.*, 2009), lending support to the hypothesis that downstream effects on joint tissues mediated by inflammatory genes take effect early in the disease process.

Twenty two overlapping differentially expressed genes were identified in RNA-Seq (Dunn *et al.*, 2016) and microarray datasets (Ramos *et al.*, 2014; Snelling *et al.*, 2014) comparing damaged OA cartilage with intact OA cartilage from the same joint with a fold change >1.5 and adjusted p value  $\leq 0.1$ . Of these, only four were associated with roles in inflammation including *CD55*, *CRLF1*, *PTGES* and *TNFAIP6* and the remaining pathways identified through gene ontological pathway analysis are related to cell adhesion, ECM proteins and other previously validated OA gene networks. In the RNA-Seq study the expression of the soluble mediators *IL-1 $\beta$* , *OSM* and *TNF- $\alpha$*  were undetected in damaged OA cartilage yet there was some evidence of a chondrocyte inflammatory response for the aforementioned genes *PTGES* and *TNFAIP6*. Inducible nitric oxide synthase (*iNOS*) was also upregulated as part of the oxidative stress pathway. The authors proposed that the inflammatory gene signature was generated through increased *IL-11* and protease activity, rather than *IL-1 $\beta$* , *OSM* or *TNF- $\alpha$* , in turn generating damage associated molecular patterns (DAMPs) from fibronectin fragments (Dunn *et al.*, 2016).

In conclusion, evidence from *in vivo* transcriptomics analyses suggests inflammation does not play a pivotal role in OA pathogenesis, whereas the expression profiles observed are consistent with abnormal mechanical loading, and Wnt signalling (Soul *et al.*, 2018a). This is despite support for the role of pro-inflammatory cytokines in cartilage degradation *in vitro* albeit the pro-inflammatory gene changes in chondrocytes historically were observed with supraphysiologic cytokine concentrations.

## **1.4 Disrupted chondrocyte zinc homeostasis as a potential driver of osteoarthritis**

### **1.4.1 Cellular zinc homeostasis**

#### **1.4.1.1 Zinc as an essential nutrient**

The earliest description for the role of zinc in supporting organismal growth was in 1869 when Jules Raulin noticed improved *Aspergillus niger* growth using zinc in chemically defined medium (Raulin, 1869). More than half a century later in the 1930s and later still in the 1960s the importance of zinc in rats and humans was realised (Todd *et al.*, 1933; PRASAD *et al.*, 1961). Deficiencies in this essential nutrient was associated with hypogonadism, dwarfism and delayed sexual maturation, and these phenotypes are improved after zinc supplementation (PRASAD *et al.*, 1961). Three complementary bioinformatics approaches utilising a protein structure database (PDB, RCSB.org), gene annotation and a domain-based database (pfam.xfam.org) confirmed that zinc is bound by 10% of proteins in the human proteome (3207 proteins), and is required for enzyme catalysis, gene transcription via zinc-finger transcription factors, and other structural roles in proteins (Andreini *et al.*, 2006). For example, the catalytic domains of both ADAM-TS5 and MMPs require zinc to cleave their substrates. Furthermore, the zinc sensing transcription factor metal-sensing transcription factor 1 (MTF1) has six zinc-finger domains and binding of zinc to these domains enables cytoplasmic to nuclear translocation of MTF1 and transcription of MTF1 target genes (Hara *et al.*, 2017). Thus, available intracellular free zinc ions can trigger downstream signalling cascades.

The human body contains ~ 2-3 grams of zinc which is absorbed from whole grains, red meats and dairy products through the small intestine. Zinc is stored in the skeletal muscle (60%), bone (30%), and other organs (brain, kidney, liver, spleen, pancreas totalling 10%). Zinc is essential for the immune system and as a neuromodulator in synaptic transmission (Hara *et al.*, 2017). Assessments on total intracellular zinc concentration range from 10-100µM but this range accounts for both protein-bound and free-zinc levels (Hara *et al.*, 2017). The actual concentration of free zinc ions in the cytoplasm is buffered in the picomolar to low nanomolar range through the activities of zinc transporters and zinc sequestering proteins needed to maintain homeostasis and avoid zinc cytotoxicity.

### 1.4.1.2 Zinc transporters

Zinc homeostasis in mammals is coordinated by 24 zinc transporters embedded in either the plasma membrane or within intracellular vesicles as illustrated in the schematic in Figure 1.8. Zinc can be transported from the extracellular space or intracellular organelles into the cytosol by the 14 Zrt/Irt-like proteins (ZIPs/*SLC39A1-14* gene family), raising the intracellular zinc concentration. The 10 Zn<sup>2+</sup> transporters (ZnT/*SLC30A1-10*) family members transport zinc from the cytosol into the organelles or outside the cell lowering zinc concentration. ZnT9, although predicted to possess six transmembrane domains, actually associates with nuclear and cytoplasmic fractions and not membranes (Sim and Chow, 1999) and is not well studied, accounting for its lack of coverage in zinc homeostasis reports (Kimura and Kambe, 2016; Hara *et al.*, 2017). In addition to these transporters' unique positioning within cells the zinc transporters have a tissue specific pattern of expression. For example, ZnT8 is expressed in the pancreatic  $\beta$  cells and is involved in insulin secretion whereas ZnT1 is ubiquitously expressed in the plasma membranes (Kimura and Kambe, 2016).

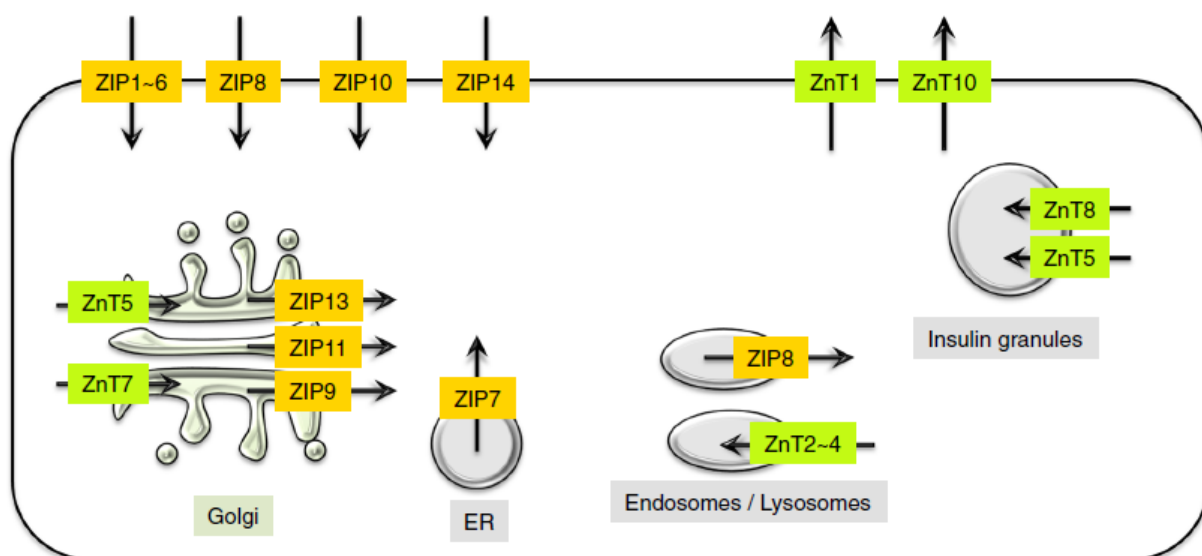


**Figure 1.8 – Intracellular localisation of Zrt/Irt-like (ZIP) and Zn<sup>2+</sup> transporter (ZnT) proteins with the plasma membrane or organelles of the cell.**

The diagram shows the localisation of ZnT (green) and ZIP (yellow) proteins, and the direction of Zn<sup>2+</sup> transport (black arrows) for each organelle and plasma membrane. In terms of Zn<sup>2+</sup> homeostasis, ZnT and ZIP maintain the influx and efflux of Zn<sup>2+</sup> ions between the cell and extracellular spaces, or between the cytosol and the organelle compartments, thereby maintaining appropriate Zn<sup>2+</sup> concentrations in the cell. ZnT9 does not associate with membranes. This figure is from (Hara *et al.*, 2017) and is free to use under Creative Commons License.

Loss of function missense, nonsense, insertion, deletions and splice-site mutations in the zinc importer gene *SLC39A4* underlie the condition acrodermatitis enteropathica which is inherited in an autosomal recessive manner (Schmitt *et al.*, 2009). This condition is recognisable in infants by the presence of symmetrical dermatosis and skin lesions and is caused by a decrease in zinc absorption through the duodenum and jejunum where the ZIP4 transporter is located, causing zinc deficiency. A different missense mutation in the zinc exporter ZnT2 is also associated with zinc deficiency in breast milk due to failed secretion, and this can cause zinc deficiency in newborns fed exclusively on breast milk (Chowanadisai *et al.*, 2006). A nine base pair loss-of-function deletion in the zinc importer *SLC39A13* gene causes a connective tissue disorder called spondylocheiro dysplastic Ehlers-Danlos syndrome (Giunta *et al.*, 2008). There are 13 types of Ehlers-Danlos syndrome with varying symptoms but common features are joint hypermobility and skin fragility, but the *SLC39A13* version of the disease is additionally associated with hand abnormalities. These include thenar hypotrophy, syndactyly and finger tapering (Giunta *et al.*, 2008). Knockout of the zinc importer *SLC39A14* by removing exons 5-8 and the two exon 4 splice variants was associated with stunted growth in mice and was a consequence of abnormal chondrocyte differentiation in the growth plate (Hojyo *et al.*, 2011). Autosomal recessively inherited loss of function mutations found in human *SLC39A14* cause childhood-onset Parkinsonism-dystonia by affecting homeostasis of the divalent metal cation manganese, transported by both ZIP14 and ZIP8 importers. These mutations can impair transporter function through nonsense-mediated decay, protein truncation or impairment of transporter activity leading to accumulation of manganese in the brain causing neurodegeneration (Tuschl *et al.*, 2016). A phylogenetic tree comparing ZIP protein domains curated from the National Center for Biotechnology Information (NCBI) website (<http://www.ncbi.nlm.nih.gov>) and built using ClustalW (<http://www.ebi.ac.uk/clustalw/index.html>) for multiple alignment of mice and human sequences revealed that ZIP8 and 14 are more closely related to each other than the other 12 members of this family (Girijashanker *et al.*, 2008).

### 1.4.1.3 Metallothioneins

Another key group of proteins involved in zinc homeostasis through the sequestration of intracellular zinc and free radical scavenging are the metallothioneins (MTs). These are small (7kDa) cysteine-rich proteins which primarily bind zinc and chaperone this metal ion to metalloproteinases or transcription factors. MT is able to bind a range of trace metals other than zinc including copper and cadmium (Miles *et al.*, 2000) and thus is important in the homeostasis of copper and defense against cadmium toxicity, topics that are beyond the scope and relevance to this thesis. There are four classes of MT (1-4) in mammals, *MT1* and *MT2* are expressed ubiquitously whereas *MT3* is restricted to the brain and *MT4* is present in epithelial tissues (Kimura and Kambe, 2016). *MT1B* among the *MT1* genes is not however ubiquitously expressed in a range of human tissues according to the genotype tissue expression (GTEx) website ([gtexportal.org/home/](http://gtexportal.org/home/)). There are 11 human *MT* genes in a cluster on chromosome 16 ((*MT1A*, *1B*, *1E*, *1F*, *1G*, *1H*, *1M*, *1X*, *MT2A*, *MT3* and *MT4*) and five *MT1* pseudogenes (*MT1C*, *1D*, *1I*, *1J* and *1L*) (Kimura and Kambe, 2016). In mice there are four *Mt* genes clustered on chromosome eight (*Mt1-4*) (Kimura and Kambe, 2016) and more *Mt* genes in humans than mice due to gene duplication (Moleirinho *et al.*, 2011). MTs have alpha and beta domains housing four or three sulfur atoms respectively for divalent metal ion binding. MTs are regulated by heavy metals, oxidative stress and cytokines and protect cells against these stressors to maintain cell viability. The promoter regions of *MTs* contain DNA regulatory elements associated with distinct types of stress stimuli. For example, there are response element sequences for glucocorticoids, metals (MREs), and antioxidants (AREs), which, after binding of the appropriate transcription factor(s), elicit gene expression.

As a general principle MTs exist in three forms intracellularly, but the relative abundance of each is dependent on the oxidation state of the cell. These are the fully oxidised thionins with a lower metal affinity, the reduced thioneins (apoprotein) and the zinc-bound MT (Ziller and Fraissinet-Tachet, 2018). Reduced glutathione (GSH) is an antioxidant required to recycle thionin into apoprotein and MT is stabilized at high GSH concentrations. In the presence of free radicals, GSH oxidises through the removal of an electron from a thiol group of a cysteine residue to neutralise a pro-oxidant molecule and reacts with another reactive GSH to form glutathione disulfide (GSSG) (Zhu *et al.*, 2020). GSSH is converted back to GSH by glutathione reductase which utilises nicotinamide adenine dinucleotide phosphate (NADPH) as an electron donor. Chondrocytes from the elderly are associated with a reduced GSH:GSSG ratio and a concomitant decrease of *SIRT3*, encoding a mitochondrial deacetylase (Carlo and Loeser, 2003). The reduced GSH:GSSG ratio may be partly explained by increases in mitochondrial protein acetylation (in part a consequence of decreased SIRT3 activity) of superoxide dismutase 2 and isocitrate dehydrogenase 2 as examples, the latter of which once acetylated is unable to synthesize NADPH for GSSG reduction (Zhu *et al.*, 2020). Thus, an oxidised environment does not support recycling of the thionin back to apoprotein enabling zinc sequestration, MT anti-oxidative activity and heavy metal sequestration to occur.

Decreased levels of GSH have also been detected in human OA synovial fluid compared to synovial fluid taken from patients in chronic pain, with meniscal tears or ACL injury (Regan *et al.*, 2008), suggesting that oxidation is a feature of OA and occurs in tissues other than cartilage in contact with joint capsule. However, an experimental rat model for studying GSH in oxidative stress addressing GSH and GSSG as regulators of oxidation, did not extend to the infrapatellar fat pad and meniscus compared to cartilage because absolute levels of these antioxidants in these tissues was greatly reduced (Zhu *et al.*, 2020). An attempt at illustrating the relationship between the three forms of MT and glutathione antioxidant activity in which a decreased GSH:GSSG ratio is a feature of aged chondrocytes and OA is depicted in Figure 1.9. Altered oxidative resistance in aged chondrocytes may impact the relative quantities of thionin, apoprotein and MT such that zinc homeostasis is disrupted and zinc intracellular concentration increases (Ruttkay-Nedecky *et al.*, 2013).

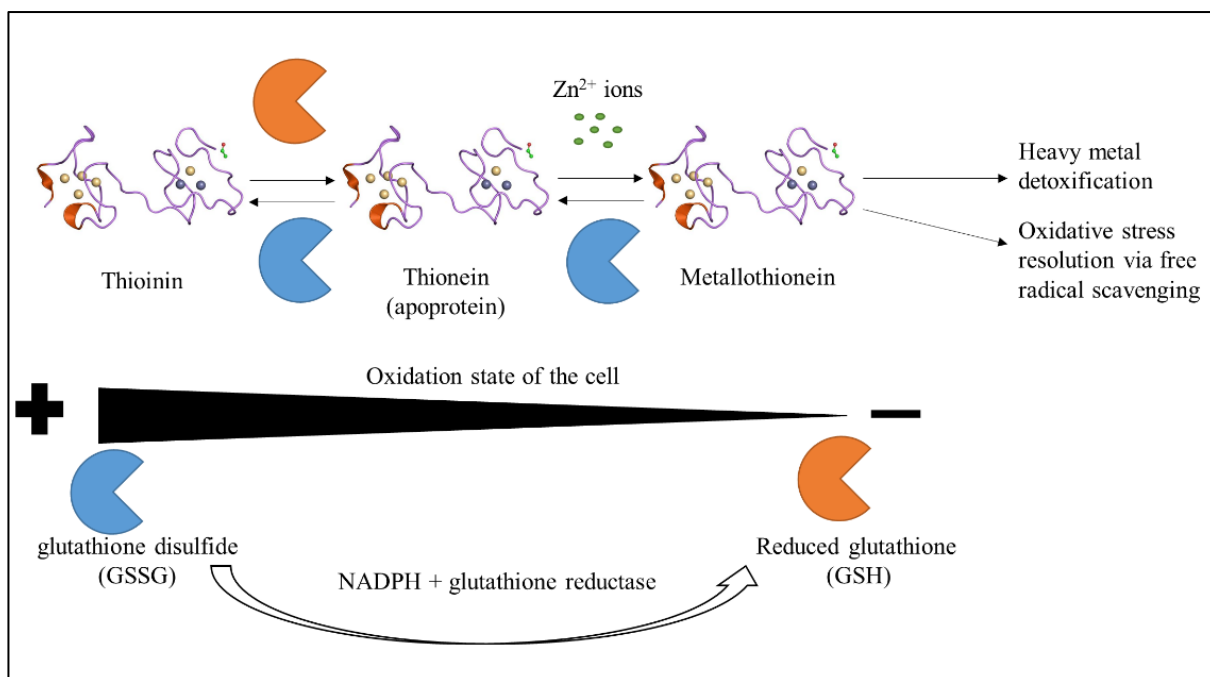


**Figure 1.9 – Relationship between metallothionein protein states, oxidative status, and the reduced glutathione:glutathione disulfide ratio in chondrocytes.**

Metallothioneins (MTs) are integral to cell survival in stress situations namely the presence of heavy metals and in free-radical scavenging. MT bound to zinc ions is stable at high levels of reduced glutathione and low oxidation state of the cell which is reversed in increased oxidative environments. Concomitant with increased oxidation is a decrease in SIRT3-mediated deacetylase activity in OA chondrocytes, an example target being isocitrate dehydrogenase 2 which synthesizes NADPH, a required electron donor for glutathione reductase conversion of GSSG back to GSH and enabling more apoprotein and zinc ion interaction. This figure has been created using information from Ziller and Fraissinet-Tachet 2018.

#### **1.4.1.4 Metal-sensing transcription factor 1**

MTF1 is an important regulator of heavy metal stress, hypoxia, oxidative stress and is also essential for embryonic liver development as evidenced by *Mtf1* knockout in mice which are non-viable because of liver degeneration (Günes *et al.*, 1998). The protein contains six Cys<sub>2</sub>His<sub>2</sub> zinc fingers with varying zinc binding affinities (within 10-50 fold of each other) in the nanomolar to sub micromolar range (Kimura and Kambe, 2016). Three transcriptional activation domains were discovered after cloning of the murine *Mtf1* cDNA and fusing of DNA segments to GAL4 DNA binding domain (Radtke *et al.*, 1995). These are acidic, proline-rich and serine-threonine-rich domains in the C-terminal region of the protein. Under physiologic conditions MTF1 shuttles between the cytoplasm and nucleus but accumulates in the nucleus upon diverse stresses, including heat shock, heavy metal overload and oxidative stress (Gunther *et al.*, 2012). This nuclear-cytoplasmic shuttling is possible through MTF1 possession of a nuclear export and nuclear localisation sequence located in the acidic transcriptional domain and in zinc finger one respectively. Pharmacological inhibition of the nuclear export receptor CRM1 with leptomycin B or mutation of the linker sequence between zinc fingers one and two of MTF1 in mice resulted in nuclear MTF1 retention but not DNA binding or transcriptional activity. However, when the same mutation in the linker sequence was made in human MTF1 it was still zinc-responsive and transcriptionally active, suggesting that metal inducibility of human MTF1 is more robust than mouse MTF1 (Gunther *et al.*, 2012). Additionally, the inducibility of MTF1 target genes is magnitudes greater than murine MTF1. Murine MTF1 can be ‘humanised’ by substituting three amino acids for the human equivalent of the nuclear export sequence in the acidic transcriptional domain which raises MTF1 activity comparable to the human counterpart.

*MTs* are a primary gene target of MTF1 via MTF1 interaction with one or more MREs in the promoter regions, enabling effective response to heavy metal intracellular changes or free-radical scavenging. Not all MTF1-MRE interactions are associated with increased transcriptional activity and this is despite the fact the consensus sequence of the MRE is conserved TGCRCNC where R is either adenine or guanine and N is any nucleotide. For example, cadmium-induced MTF1 binding to the MRE 17 base pairs downstream of the transcription start site in *Slc39a10* is associated with gene repression in mice (Wimmer *et al.*, 2005). Furthermore, MTF1 can repress redox sensing by inhibiting selenoprotein H and thioredoxin reductase two (Stoytcheva *et al.*, 2010).

## 1.4.2 Does disrupted zinc homeostasis contribute to osteoarthritis pathogenesis?

### 1.4.2.1 The zinc-ZIP8-MTF1 signalling axis in osteoarthritis

Serum zinc concentration was elevated in OA patients compared to synovial fluid (Krachler *et al.*, 2000; Ovesen *et al.*, 2009), though this was not an uncommon observation. However, these studies compared OA sera against knee effusions from the same OA individual (Krachler *et al.*, 2000), or against serum from osteoporotic patients (Ovesen *et al.*, 2009), rather than comparing age-matched healthy controls. One study in which plasma from OA patients was compared to non-OA and RA plasma controls found no difference in plasma zinc concentration (Yazar *et al.*, 2005). Zinc was shown to accumulate in the tidemark region of articular cartilage (Roschger *et al.*, 2013) and is broadly appreciated for matrix metalloproteinase catalysis, but whether zinc contributes to the progression of OA by altering the chondrocyte gene expression pattern towards catabolism was not addressed until 2014 (Kim *et al.*, 2014).

In this study, the authors (Kim *et al.*, 2014) investigated the role of zinc in different models of cartilage destruction using *in vitro* IL-1-treated mouse chondrocytes, transgenic mouse models and intra-articular injection of adenoviral constructs into mouse joints. Kim *et al.*, began by treating knee articular chondrocytes from mice with 1ng/ml IL-1 $\beta$  for 24 hours and measured the expression of genes encoding the 24 zinc transporters. Of these, *Slc39a8* was the most upregulated with no significant difference in *Slc39a14* gene expression and ZIP8 protein was produced by IL-1 $\beta$  in a concentration dependent manner. ZIP8 overexpression using an adenovirus (Ad-ZIP8) transduced for 24 hours increased chondrocyte zinc levels 2-fold. ZIP8 cartilage levels were significantly increased (10-fold,  $p < 0.001$ ) as were zinc levels (2.5-fold,  $n \geq 8$ ,  $p < 0.05$ ) following surgical DMM of mice compared to sham-operated controls. Ad-ZIP8 transduction and ZIP8 overexpression (~200-fold) of mice chondrocytes for 24 hours resulted in increased transcription of cartilage degrading genes including *Mmp3*, *9*, *12*, *13* and *Adam-ts5* relative to mice receiving the control adenovirus. This Ad-ZIP8-mediated metalloproteinase gene overexpression effect was translated to MMP3, 9 and ADAM-TS5 protein, detected by western blot and equivalent or greater metalloproteinase was produced with ZnCl<sub>2</sub> or IL-1 $\beta$  respectively. Furthermore, the dominant metal ion responsible for the metalloproteinase expression response in murine chondrocytes was ZnCl<sub>2</sub> and to a lesser extent iron ions. The metalloproteinase expression response was reduced with metal ion chelators that chelate zinc.

Through a series of *in vitro* and *in vivo* experiments using techniques already described, the authors were able to demonstrate that the transcription factor MTF1 was responsible for mediating the effects on matrix degrading gene expression after ZIP8-mediated zinc entry. Briefly, Ad-ZIP8 transduction in murine chondrocytes resulted in increased *Mtfl* activity (no change in gene or protein levels) relative to the control adenovirus, suggesting the cartilage matrix-degrading expression response from zinc was mediated via the zinc-sensitive transcription factor MTF1. The question as to whether MTF1 acted before or after zinc-mediated transport via ZIP8 was addressed using chondrocyte-specific *Slc39a8* or *Mtfl* knockout followed by DMM. Ad-ZIP8-mediated DMM damage is attenuated in mice with deletion of *Mtfl* whereas deletion of *Slc39a8* in cartilage of mice with Ad-MTF1 overexpression had no effect on DMM damage. This indicated MTF1 was acting downstream of ZIP8 but that other transcription factors were involved as damage was only attenuated and not prevented in cartilage lacking *Mtfl* and exposed to Ad-ZIP8 and DMM surgery. Interestingly, the transcription factor SP1, discovered among 37 other transcription factors in early screening after Ad-ZIP8 transduction, was also responsible for matrix-degrading gene expression as mithramycin A treatment attenuated these genes' expression. However, Kim *et al.*, 2014 decided to focus solely on MTF1 because of its defined role in responding to cellular heavy metal stress, though it does allow the possibility that SP1 is a potential but lesser-known target in the zinc-ZIP8-MTF1 signalling axis.

Three weeks post-injection, Ad-ZIP8 or Ad-MTF1-transduced mice had increased levels of cartilage destruction, indicated by loss of safranin O staining and increased Osteoarthritis Research Society International (OARSI) grade. Chondrocyte-specific expression of ZIP8 also showed enhanced cartilage damage after DMM surgery and spontaneous cartilage destruction after 12 months compared to age matched wild type mice. This suggested that cartilage overexpression of ZIP8 or MTF1 was sufficient to cause OA pathogenesis in mice. This was confirmed in mice with cartilage specific deletion of *Slc39a8* or *Mtfl*. Chondrocyte-specific knockouts were generated with the Cre/loxP system to address *Slc39a8* and *Mtfl* deletion. Chondrocyte-specific knockout resulted in increased safranin O staining compared to the floxed *Slc39a8* or *Mtfl* cre recombinase negative control strain after DMM surgery (n=10 and n≥14 respectively) and reduced zinc, MMP3 and MMP13 levels further implicating *Slc39a8* and *Mtfl* in OA pathogenesis.

Together this data indicates that the zinc-ZIP8-MTF1 axis acts as a catabolic regulator of OA pathogenesis in mice by upregulating cartilage matrix degrading enzymes. This is summarised as an adapted figure (Figure 1.10) from Virginia Kraus' Nature news and views article that accompanied the Kim *et al.*, 2014 paper. OA is hypothesised to be the result of an unresolved chronic wound healing response in the joint. The response begins with activation of cell signalling molecules such as IL-1 in chondrocytes. This stimulates upregulation of ZIP8 and cytoplasmic zinc influx, triggering nuclear translocation of the MTF1 transcription factor. MTF1 then enhances the transcription of zinc-dependent matrix degrading enzymes such as *Mmp13*, which once translated contributes to cartilage breakdown and release of disease associated molecular patterns or DAMPs into the joint. DAMPs are then recognised by immune cell or chondrocyte PRRs, leading to inflammation of the joint lining, which then feeds back to aggravate the response.

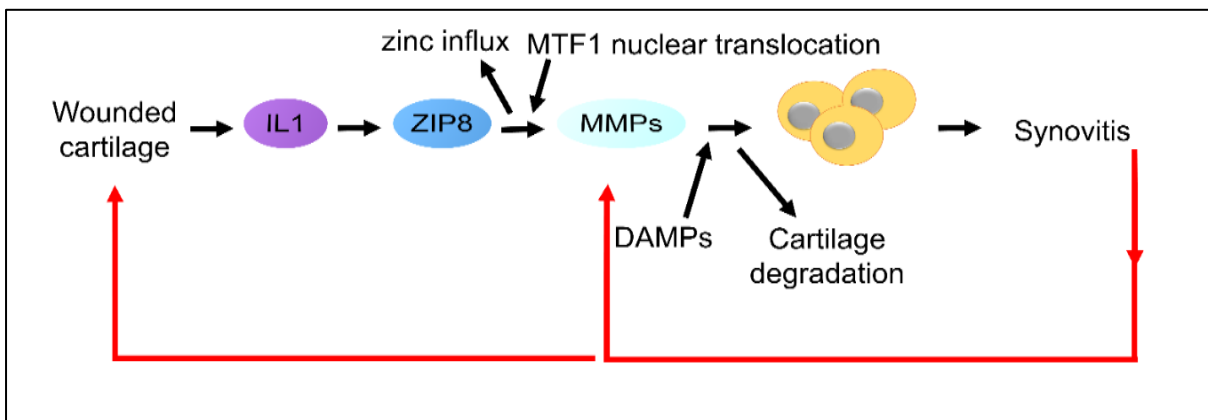


**Figure 1.10 – Proposed mode of action of the zinc-ZIP8-MTF1 axis in chondrocytes.**

OA cartilage is an avascular tissue and in the normal pattern of wound healing in response to injury cannot proceed beyond the initial inflammatory response, resulting in prolonged exposure to inflammatory mediators such as IL-1. This leads to increases in *Slc39a8* gene and protein expression, and ZIP8-mediated zinc import which is sensed by the transcription factor MTF1. MTF1 targets and upregulates *Mmp* expression which degrades cartilage, releasing damage-associated molecular patterns (DAMPs) further exacerbating the disease in a cyclical manner via immune cell involvement in the synovium. This figure is adapted from (Kraus, 2014).

### 1.4.3 The role of MTs in osteoarthritis

A few studies investigating the roles of MT1 and MT2 in mice models of PTOA have been conducted. Both *Mt1* and *Mt2* were upregulated in murine chondrocytes after Ad-ZIP8 or Ad-MTF1 transduction and after 100 $\mu$ M zinc treatment compared to the control adenovirus or cells cultured in medium alone (n $\geq$ 6). *In vivo* investigation using double *Mt1/2* knockout mice exacerbated DMM-mediated cartilage degradation as evidenced with reduced safranin O staining (n=13) (Kim *et al.*, 2014; Won *et al.*, 2016). This mechanism was investigated further by the same group in a later publication (Won *et al.*, 2016). Double knockout increased apoptosis in the articular chondrocytes compared to the wild type sham-operated mice, without affecting the levels of cartilage matrix-degrading or anabolic matrix proteins. Chondrocyte apoptosis, measured by terminal deoxynucleotidyl transferase dUTP nick-end labelling (TUNEL), was confined to the superficial/middle zones of cartilage and did not extend to the calcified region. Similarly, IL-1 $\beta$  treatment of either wild type or *Mt1/2* knockout chondrocytes had indistinguishable catabolic (*Mmp3*, *13* and *Adam-ts5*) and anabolic (*Sox9*, *Col2a1* and *Acan*) gene expression markers. The chondroprotective effect mediated by MT1 and MT2 proteins correlated with their capacity to regulate ROS, as Ad-MT2 and to a lesser extent Ad-MT1 transduction resulted in reduced oxidant levels in chondrocytes. Furthermore, basal ROS levels were greater before and after tert-butyl hydroperoxide treatment of *Mt1/2* double knockout chondrocytes compared to wild type chondrocytes receiving the same treatment. These data suggest that the cartilage degradation observed in the double *Mt1/2* knockout phenotype is a consequence of increased apoptosis and reduced anti-oxidative capacity.

However, MTs were shown to have pleiotropic roles as overexpression of MT2 but not MT1 resulted in matrix-degrading gene expression independently of the zinc-ZIP8-MTF1 axis (Won *et al.*, 2016), thus MT2 is chondroprotective via ROS scavenging up to a limit. Intraarticular injection of Ad-MT1 (n=14) or Ad-MT2 (n=12) compared to mice injected with a control adenovirus resulted in increased OARSI score and reduced safranin O staining in Ad-MT2 only. Chondrocyte-specific *Slc39a8* or *Mtf1* knockout in mice followed by intraarticular injection with Ad-MT2 and DMM resulted in comparable OA cartilage and synovitis progression as observed as Ad-MT2 and DMM in wild type mice. Conversely, Ad-ZIP8 or Ad-MTF1 overexpression in *Mt1/2* double knockout mutants and DMM surgery did not impact on OA progression compared to ZIP8 and MTF1 overexpression and DMM in wild type mice either, clearly indicating that MT2-mediated cartilage destruction is independent of the zinc-ZIP8-MTF1 axis.

A cDNA microarray analysis was performed from Ad-MT2, Ad-MTF1 or Ad-ZIP8-transduced murine chondrocytes to identify genes which were specific to MT2-mediated cartilage destruction, genes overlapping with either MTF1 or ZIP8-mediated cartilage destruction, and genes shared by all three (Won *et al.*, 2016). Three hundred and eighty-five genes were upregulated by more than 2-fold and 65 genes were downregulated more than 2-fold in response to *Mt2* overexpression. Two hundred and thirteen and 38 genes were up and downregulated respectively by *Slc39a8* overexpression and 189 and 18 genes were up and downregulated respectively by *Mtf1* overexpression with the same fold-change criteria as *Mt2* overexpression. Forty-two and 30 percent of genes were upregulated and downregulated respectively when the differentially expressed genes for all three adenoviruses carrying *SLC39A8*, *MTF1* or *Mt2* were compared. Forty-eight percent of genes were uniquely regulated by MT2 independent of the zinc-ZIP8-MTF1 axis. Cell cycle regulation and catalytic activity were ranked highest after pathway analysis of the MT2 upregulated genes and cartilage development and hormone binding placed highest among the MT2 downregulated genes. There were no overlapping upregulated or downregulated genes between Ad-MT1 and Ad-MT2 transduced chondrocytes.

Nine of 45 (20%) transcription factors showed transcriptional activity greater than 2-fold following Ad-MT2 transduction compared to control adenovirus transduction as well as mRNA upregulation of *Mmps 3,9,12,13* and *Adam-ts5*. Among these nine transcription factors, pharmacological inhibition of the NOTCH pathway (RBP-JK transcription factor) nor siRNA-mediated inhibition of *Stat1/2*, *Atf2* or *Irf1* affected MT2-induced expression of cartilage matrix-degrading or anabolic matrix genes. However, pharmacological inhibition of NFκB with SC-514 decreased cartilage matrix-degrading genes and reversed anabolic matrix gene downregulation (observed with NFκB alone) in a concentration dependent manner. AP-1 was another transcription factor among the nine which after inhibition with tanshinone IIA specifically inhibited *Mmp9* and *13* but not *Mmp3*, *12* or *Adam-ts5* gene expression and had no effect on anabolic matrix gene expression. The differential effects of MT1 and MT2 described by Won *et al.*, may reflect the MTs distinct physiological functions. For example, MT2 regulates the homeostasis of zinc and copper ions while MT1 has a distinctive detoxification function via its superior affinity for toxic heavy metals, such as cadmium (Artells *et al.*, 2013; Won *et al.*, 2016).

#### **1.4.4 Several human OA loci encompass or are near to zinc transporter genes**

Several GWAS have identified and validated SNPs that are correlated to either OA or minimal joint space width (mjsw) phenotypes (Castano-Betancourt *et al.*, 2016; Styrkarsdottir *et al.*, 2018; Zengini *et al.*, 2018; Tachmazidou *et al.*, 2019). These five SNPs are in proximity to the zinc transporters *SLC30A5* (rs10471753,  $p=3.8 \times 10^{-9}$ ), *SLC30A10* (rs2820436,  $p=2.1 \times 10^{-9}$ ; rs2820443,  $p=6.01 \times 10^{-11}$  and rs2785988,  $p=3.9 \times 10^{-9}$ ) and *SLC39A8* (rs13107325,  $p=8.29 \times 10^{-19}$ ). Although susceptibility to mjsw of the hip is not of itself OA, it is usually a key radiographic finding on diagnosis of OA and is included as part of my analysis (section 3.10) of these SNPs (and those in LD  $r^2 \geq 0.8$  with the sentinel SNP from each study) compared to SNPs with eQTLs for *SLC30A5*, *SLC30A10* and *SLC39A8* genes in healthy tissues provided on GTEx. So far, none of these SNPs have been studied in detail using methods or databases to assess allelic expression imbalance, chromatin interaction, clustered regularly interspaced short palindromic repeats (CRISPR) to determine if the genotype at these OA and hip mjsw loci is associated with gene expression of these zinc transporters.

### 1.4.5 Several zinc transporter genes are upregulated in a group of OA hip patients

Epigenetic gene expression regulation, specifically DNA methylation, has emerged as a powerful diagnostic tool in the identification of differentially methylated loci (DML). In this study, DML was defined as both greater than 10% methylation difference in the average beta value between groups at a specific locus and an adjusted Benjamini-Hochberg corrected p value <0.05 which could largely stratify hip OA (n=23) from NOF cartilage (n=21), define two subclusters within hip OA cartilage (cluster one n=11 and cluster two n=12) and reveal heterogeneous subclustering of knee OA cartilage (cluster one n=39 and cluster two n=34) into two groups (Rushton *et al.*, 2014). Comparison of the methylated loci between the two subclustered groups of hip or knee OA cartilage produced 15239 and 5769 DMLs by unsupervised hierarchical clustering respectively. These were compared to identify the percentage DML overlap contributing to the clustering of either hip or knee OA cartilage. Only 23 and 61% of hip and knee DMLs overlapped respectively, suggesting that the cartilage methylome of hip and knee are different and that other genes/pathways are involved in the observed stratification of each. Pathway analysis of the cluster two OA cartilage groups from either joint site revealed genes involved in the immune response and inflammation (Rushton *et al.*, 2014).

A follow up study was carried out using the previously generated methylation data from the stratified OA hip cartilage clusters (n=23 total) and NOF samples (n=21) to address promoter methylation status. Additionally, paired cartilage RNA was collected to assess gene expression related to pro-inflammatory and zinc-ZIP8-MTF1 signalling axis which was compared to the methylation status of the promoters (Rushton *et al.*, 2015). Promoter methylation of inflammatory genes (*TNF $\alpha$* , *CXCR2*, *CCL2*, *IL-6*, *CCL5* and *IL-1 $\alpha$* ) were all significantly reduced (apart from a single probe in *IL-6*) in hip OA cluster two compared to NOF and hip cluster one. The expression of these genes was measured in six samples from hip OA cluster two, five from hip OA cluster one and five NOF samples and were all found significantly upregulated for hip OA cluster two. *TNF $\alpha$*  and *CXCR2* were upregulated in hip OA cluster one only. *IL-1 $\beta$* , responsible for activation of the zinc-ZIP8-MTF1 axis in mice was significantly upregulated 8-fold in hip OA cluster two and of the zinc transporters expressed in human cartilage the importers (*SLC39A3,4,7,8,11,14*) and exporters (*SLC30A1,4,5,7,9*) were significantly upregulated in hip OA cluster two compared to NOF. This trend was observed for *MTF1* expression and its target MTs, (*MT1A*, *MT1G* and *MT1H*) and cartilage matrix-degrading genes (*MMP13* and *ADAM-TS5*).

## 1.5 Thesis aims

As discussed in section 1.4, studies in mice have implicated IL-1-mediated disruption of chondrocyte zinc homeostasis in the pathogenesis of OA. Furthermore, although the role of zinc homeostasis has not been studied in human OA, recent genetic and transcriptomic analysis has suggested that disrupted zinc homeostasis may also play a role in human OA development and/or progression. The aim of this thesis is to explore the role of cellular zinc homeostasis in human knee OA chondrocytes and relevant chondrocyte cell lines. I will extend my analysis of the zinc-ZIP8-MTF1 axis more broadly than in its original characterisation in mice for other zinc transporters, MTs and matrix metalloproteinases to discern whether the same signalling pathway already identified in mice cartilage and chondrocytes is comparable, or not, with human chondrocytes.

In the opening results chapter, I will use online bioinformatics tools to assess OA transcriptomics datasets (human and experimental OA mouse models) where IL-1 was used as a stimulus for components of the zinc-ZIP8-MTF1 axis and broader gene families involved in zinc homeostasis. I will also stratify the genotypes of recently identified SNPs in OA GWAS meta-analyses and associated SNPs in LD with gene expression data to detect eQTLs. Chapters four to six aim to address IL-1-mediated zinc transporter gene expression changes, intracellular zinc ion content, MTF1 expression, translocation and activity where possible, and changes in *MTs* and metalloproteinases expression in primary articular chondrocytes and cell line experiments separately.

## Chapter 2. METHODS

### 2.1 SkeletalVis database

#### 2.1.1 Search term and inclusion/exclusion criteria for selection of human and murine cartilage and chondrocyte gene expression datasets

In the ‘Explore’ section of SkeletalVis (Soul *et al.*, 2018b) , the experiments were initially filtered sequentially for human and then murine studies before the search terms “cartilage”, “chondrocyte” “IL-1” and “osteoarthritis” were used to identify potentially relevant transcriptomic datasets. A total of 17 human and eight murine datasets were identified based on these terms. After selecting an experiment, the factor(s) to be compared within the experiment were selected in the “Choose a Comparison” window and each microarray or RNA-Seq study was assessed for quality control, which was predominantly determined by viewing the principal component analysis (PCA) plots. George Dallas (Dallas, 2013) simplifies the mathematical concept of PCA for non-mathematicians and how PCA can be used in the analysis of microarray and RNA-Seq platforms is paraphrased using his article as reference. “PCA is a dimension reduction and visualisation technique that is used to project the multivariate data vector of each array into a two-dimensional plot, such that the spatial arrangement of the points in the plot reflects the overall data (dis)similarity between the arrays. Thus, well-defined clusters of the same biological sample are seen to group closely together and segregate from other unrelated samples”. Those studies without well-defined clusters were omitted from subsequent steps so that nine human (Ramos *et al.*, 2014; Comblain *et al.*, 2016; Dunn *et al.*, 2016; Moazedi-Fuerst *et al.*, 2016; Pearson *et al.*, 2016; Chan *et al.*, 2017; Fisch *et al.*, 2018; Soul *et al.*, 2018a; Ajekigbe *et al.*, 2019) and four murine studies remained (Burleigh *et al.*, 2012; Poulet *et al.*, 2012; Bateman *et al.*, 2013; Chun, 2017).

#### 2.1.2 Extraction of target genes from datasets using R studio

The results of the differential expression analysis were downloaded from SkeletalVis. R Studio version 1.0.153 was used to extract the genes, shown in Table 2.1, from the downloaded txt. files. For all the datasets, the log<sub>2</sub>-fold change and Benjamini-Hochberg p values calculated in SkeletalVis were used.

### 2.1.3 Identifying replicable gene expression patterns between datasets, enabling selection of normalised read counts or normalised microarray signals for individual samples

The extracted genes, using the gene panel (Table 2.1) were tabulated in Microsoft Excel 2016 with the associated log2fold change and adjusted p value generated by SkeletalVis. Statistical differential gene expression testing was conducted within the Limma (v3.26.0 for microarray) or DESeq2 (v1.18.1 for RNA-Seq) as part of the RGalaxy pipeline (Soul *et al.*, 2018b). Datasets were categorised according to similar study design in the following way; 1. Comparison of intact human OA and non-OA cartilage (knee and/or hip joints n = four datasets), 2. Ipsilateral damaged versus intact human OA cartilage (n = two datasets), 3. Murine DMM for PTOA (n = two datasets) 4. Murine ageing-OA model (n=one dataset) and 5. IL-1 treatment of isolated chondrocytes (human n = four datasets, murine n = one dataset). This enabled identification of directional gene expression changes which were consistent between studies or between different time points within a single study. Normalised microarray signals and read counts for significantly differentially expressed genes between datasets within the gene panel (Table 2.1) were requested for every sample derived from either the microarray or RNA-Seq datasets from the Bioinformatician, Dr. Jamie Soul (Newcastle University, Faculty of Medical Science), the creator of SkeletalVis. This data was graphed as dot plots.

**Table 2.1 - Human and mouse gene names assessed in transcriptomic datasets using the SkeletalVis data portal.**

Human gene names precede mouse gene names and are capitalised, whereas mouse gene names are lower case after initial upper-case letter.

IL1 target and cartilage degrading genes	Zinc importers	Zinc exporters	Metallothioneins	Transcription Factors
<i>IL6/Il6</i>	<i>SLC39A1/Slc39a1</i>	<i>SLC30A1/Slc30a1</i>	<i>MT1A</i>	<i>SP1/Sp1</i>
<i>CXCL8/Cxcl8</i>	<i>SLC39A2/Slc39a2</i>	<i>SLC30A2/Slc30a2</i>	<i>MT1B</i>	<i>MTF1/Mtf1</i>
<i>CCL2/Ccl2</i>	<i>SLC39A3/Slc39a3</i>	<i>SLC30A3/Slc30a3</i>	<i>MT1E</i>	<i>MTF2/Mtf2</i>
<i>ADAMTS5/Adamts5</i>	<i>SLC39A4/Slc39a4</i>	<i>SLC30A4/Slc30a4</i>	<i>MT1F</i>	
<i>MMP13/Mmp13</i>	<i>SLC39A5/Slc39a5</i>	<i>SLC30A5/Slc30a5</i>	<i>MT1G</i>	
	<i>SLC39A6/Slc39a6</i>	<i>SLC30A6/Slc30a6</i>	<i>MT1H</i>	
	<i>SLC39A7/Slc39a7</i>	<i>SLC30A7/Slc30a7</i>	<i>MT1M</i>	
	<i>SLC39A8/Slc39a8</i>	<i>SLC30A8/Slc30a8</i>	<i>MT1X</i>	
	<i>SLC39A9/Slc39a9</i>	<i>SLC30A9/Slc30a9</i>	<i>MT2A</i>	
	<i>SLC39A10/Slc39a10</i>	<i>SLC30A10/Slc30a10</i>	<i>MT3</i>	
	<i>SLC39A11/Slc39a11</i>		<i>MT4</i>	
	<i>SLC39A12/Slc39a12</i>		<i>Mt1</i>	
	<i>SLC39A13/Slc39a13</i>		<i>Mt2</i>	
	<i>SLC39A14/Slc39a14</i>			

## 2.2 LDlink and GTEx databases to assess genotype and tissue-specific gene expression correlations

To identify eQTLs with SNPs located proximal to or within zinc transporters and identified through GWAS of OA or hip mjsw, the websites [gtexportal.org/home/](http://gtexportal.org/home/) and [ldlink.nci.nih.gov](http://ldlink.nci.nih.gov) were used. Four separate GWAS (Castano-Betancourt *et al.*, 2016; Styrkarsdottir *et al.*, 2018; Zengini *et al.*, 2018; Tachmazidou *et al.*, 2019) have recently identified five SNPs (rs2820436, rs2785988, rs2820443, rs13107325, rs10471753) at three genomic loci nearby zinc transporters associated with OA or mjsw (Table 2.2). LDlink was used to identify all SNPs in LD with each of the five sentinel SNPs from the GWAS studies in all five available European populations with a  $r^2$  threshold of  $\geq 0.8$ . The nearest genes to each of the SNPs were either *SLC30A5*, *SLC39A8* and *SLC39A10*. Using the search box in GTEx each of these genes were searched to identify expression quantitative trait loci; SNPs that significantly correlate with gene expression in one or more of up to 54 non-diseased tissue sites in close to 1000 individuals.

The online tool ‘Venny’ (<https://bioninfogp.cnb.csic.es/tools/venny/index.html>) was used to overlap lists of each of the five OA and mjsw GWAS SNPs and proxy variants ( $r^2 \geq 0.8$ ) with corresponding eQTL SNP lists for the nearest zinc transporter to identify SNPs in common with eQTLs for that zinc transporter (*SLC30A5*, *SLC39A10* and *SLC39A8*).

**Table 2.2 – SNPs associated with OA susceptibility and reduced hip joint space width in four GWAS at loci nearby zinc transporters.**

Allele marked in red is the risk variant for each SNP for the associated trait, which is not always associated with the minor allele as for rs10471753 which was determined with the GWAS Catalog ([www.ebi.ac.uk/gwas/](http://www.ebi.ac.uk/gwas/)). Distances of the SNP from the promoter of each zinc transporter gene was determined using University of California and Santa Cruz (UCSC) genome browser. P values recorded are the meta-analysis combined discovery and replication cohort(s) for each genome-wide association study (GWAS). Ref = reference, Alt= alternative

SNP	Alleles (Ref/Alt)	Major allele	Distance (kb) to nearest zinc transporter	Location (hg38)	Trait	P Value	Publication
rs2820436	A/C	C	~445 from <i>SLC30A10</i>	chr1:219467338	OA (across any joint site)	$2.1 \times 10^{-9}$	Zengini, E <i>et al.</i> , 2018
rs2785988	C/A	C	~341 from <i>SLC30A10</i>	chr1:219570796	OA (hip)	$3.9 \times 10^{-10}$	Styrkarsdottir, U. <i>et al.</i> , 2018
rs2820443	T/C	T	~334 from <i>SLC30A10</i>	chr1:219580167	OA (knee and hip)	$6.01 \times 10^{-11}$	Tachmazidou, I. <i>et al.</i> , 2018
rs13107325	C/T	C	exon 7 <i>SLC39A8</i>	chr4:102267552	OA	$8.29 \times 10^{-19}$	Tachmazidou, I. <i>et al.</i> , 2018
rs10471753	C/G	C	~570 from <i>SLC30A5</i>	chr5:68523125	Hip minimal joint space width	$3.8 \times 10^{-9}$	Castaño-Betancourt, M.C. <i>et al.</i> , 2016

## 2.3 Cell line culture

### 2.3.1 SW1353 and T/C-28a2 cell culture

SW1353 human chondrosarcoma cells were purchased from American Type Culture Collection (ATCC) and T/C-28a2 human rib chondrocytes were a gift from Dr Mary Goldring, Hospital for Special Surgery, New York. SW1353 cells are derived from a 72-year-old female Caucasian with chondrosarcoma, a specific form of bone cancer arising from chondrocytes (ATCC). T/C-28a2 cells are derived from five-day old primary cultures of costal cartilage isolated from a 15-year-old female (Goldring *et al.*, 1994a). The simian V40 (SV40) large T antigen inserted in the retroviral neomycin-resistant pZipNeoSV (X) vector was transfected into the patient cells to generate the immortalised T/C-28a2 cell line (Goldring *et al.*, 1994a). IL-1 $\alpha$  used in this study was a gift from Dr. K. Ray of GlaxoSmithKline to Professor Andrew Rowan of Newcastle University, Faculty of Medical Science.

Cells were maintained in Dulbecco's Modified Eagle's Medium F12 (DMEM-F12) (Fisher Scientific, 11320074) supplemented with 2mM L-glutamine (Fisher Scientific, 25030024), 100U/ml penicillin/streptomycin (Fisher Scientific, 15140122), 10% foetal bovine serum (FBS) (Sigma, F9665) and 50U/ml nystatin (Sigma, N1638). When 90% confluent, cells were washed in phosphate buffered saline (PBS) (Fisher Scientific, 10010015) before detachment by incubation with 0.05% trypsin (Fisher Scientific, 25300054) for three minutes at 37°C. Trypsin was inactivated by adding DMEM-F12 and the cells pelleted by centrifugation at 280 xg for five minutes. Cells were resuspended in media, and the cell number quantified using a Fuchs Rosenthal haemocytometer.  $1 \times 10^6$  or  $1 \times 10^5$  cells were seeded per T75cm<sup>2</sup> or T25cm<sup>2</sup> flask respectively. Storage of SW1353 and T/C-28a2 lines was achieved by centrifugation of cells at 280 xg for five minutes to make pellets which were resuspended in a 95% FBS and 5% DMSO or 90% FBS and 10% DMSO freezing medium respectively at a density of  $1 \times 10^6$  cells/ml. The cellular suspension was added in 1ml volumes to cryovials and these were stored at -80°C overnight in polystyrene before long-term storage in liquid nitrogen. Cell lines were resurrected by placing a cryovial in a 37°C water bath for three minutes, removing the contents to a 50ml falcon tube containing 8ml medium and the cryovial was rinsed with 1ml medium and topped up with medium to a total of 10ml. This was centrifuged at 280 xg for five minutes, resuspended in 10ml fresh medium and was added to a T75cm<sup>2</sup> flask.

### ***2.3.2 IL-1 $\alpha$ concentration optimisation***

1x10<sup>6</sup> T/C-28a2 cells were seeded into four T75cm<sup>2</sup> flasks then incubated at 37°C. After four hours the media was removed from the flasks and replaced with 10ml of media containing 0, 1.5, 3.73 and 7.46 $\mu$ l of 667ng/ml IL-1 $\alpha$ , giving a final concentration of 0, 0.1, 0.25 and 0.5ng/ml IL-1 $\alpha$ . The cells were returned to the 37°C incubator and initially cultured for six days without media change until confluent. At day six, cells were split and the cultures were maintained for a further three passages, each lasting 72 hours after the first passage. IL-1 $\alpha$  was omitted from the fourth passage for a final 72 hours.

### ***2.3.3 SW1353 and T/C-28a2 IL-1 treatment***

Four hours after seeding the cells, the flasks were treated with or without IL-1 $\alpha$  by media replacement at final concentrations of 0.25ng/ml or 0.5ng/ml for T/C-28a2 lines and SW1353 respectively. Cells were exposed to IL-1 $\alpha$  for 24 hours, or one (72 hours), two (144 hours) or three (216 hours) passages, with IL-1 $\alpha$  replenished at the beginning of each passage (Figure 2.1). Cells collected after 216 hours were split and passaged for a further 72 hours in the absence of IL-1 $\alpha$  to recover (288 hours) and were then also collected. 10 $\mu$ g/ml IL-1 $\beta$  (Peprotek IL-1 $\beta$ , Cat: 200-O1Q), a gift from Dr. David Swan of the Inflammation Immunology and Immunotherapy group, Institute for Cellular Medicine, Newcastle University was used for one experiment for one passage (72 hours). A final concentration of 2.5ng/ml or 5ng/ml IL-1 $\beta$  was used for T/C-28a2 and SW1353 cells respectively following an initial four hour incubation at 37°C after seeding, with no replacement of media for the duration of the passage. Cells were collected from the flasks using 0.05% trypsin (Fisher Scientific, 25300054) and medium into 50ml falcon tubes. Falcon tubes were centrifuged at 241.5 xg for five minutes and the cells resuspended in fresh medium at 1x10<sup>6</sup> cells/ml. The cell suspension was aliquoted into 1.5ml Eppendorf tubes and the tubes were centrifuged at 4293 xg for three minutes on a Heraeus Pico17, the media discarded and the pellets were stored frozen at -80°C for subsequent extraction of the nucleic acid.

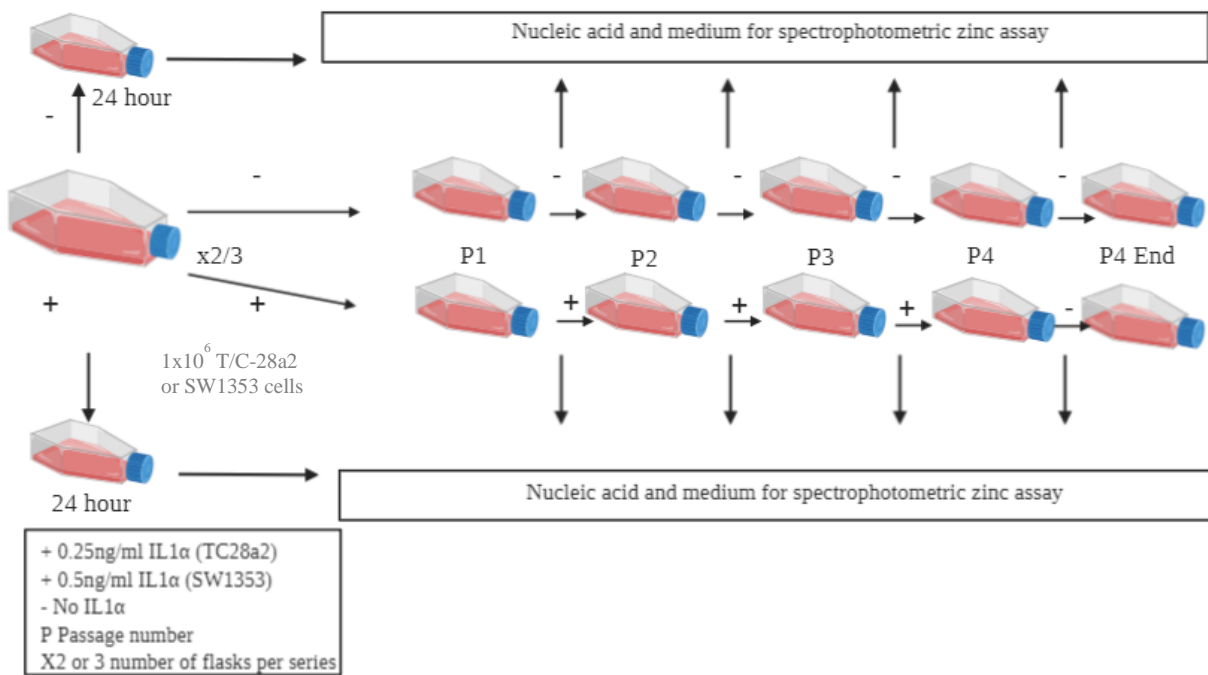


**Figure 2.1 – Serial IL-1 $\alpha$  treatment of cell lines for 24 hours, three subsequent passages (P1-P3) and removal of IL-1 $\alpha$  at P4.**

1x10<sup>6</sup> cells were seeded in biological duplicate or triplicate and four hours later treated with or without IL-1 $\alpha$ . Each passage was 72 hours in duration and some experiments were only passaged to P1 (72 hours). 1x10<sup>6</sup> cell pellets were collected at the end of each passage for nucleic acid extraction. P1 was used for qPCR analysis representing the first passage after IL-1 $\alpha$  treatment. Images were sourced from <https://biorender.com>.

### 2.3.4 SW1353 and T/C-28a2 zinc chloride treatment

A 50mM solution of zinc chloride (ZnCl<sub>2</sub>) (Sigma, 208086-100G) was prepared by dissolving 3.407g ZnCl<sub>2</sub> in 500ml of deionised water using a magnetic stirrer. Before use in tissue culture, 50ml of the solution was filtered with 0.2 $\mu$ M filter (Fisherbrand, 15206869) and a 50ml syringe (BD Plastipak™) into a 50ml falcon tube and this reagent stock was kept refrigerated until use. In all instances, whether ZnCl<sub>2</sub> was added to cells alone or in combination with IL-1 $\alpha$ , the final concentration of ZnCl<sub>2</sub> was 100 $\mu$ M. Twenty-four microlitres of 50mM stock was added to 11.976ml medium for ZnCl<sub>2</sub> alone or 24 $\mu$ l ZnCl<sub>2</sub> combined with 8.95 $\mu$ l 670ng/ml IL-1 $\alpha$  (for 0.5ng/ml + 100 $\mu$ M ZnCl<sub>2</sub> –SW1353 cells) or 4.48 $\mu$ l IL-1 $\alpha$  (for 0.25ng/ml IL-1 $\alpha$  +100 $\mu$ M ZnCl<sub>2</sub> T/C-28a2 cells) and the difference made up to 12ml with medium. 10ml of this solution was added to the relevant cell line in flasks containing 1x10<sup>6</sup> cells four hours after seeding, having first removed the media on the cells. SW1353 and T/C-28a2 cells were incubated for 72 hours in biological duplicate and triplicate respectively.

## **2.4 Human articular chondrocyte isolation from cartilage and IL-1 treatment**

### **2.4.1 *Cartilage tissue collection***

Informed written consent for the use of joint tissues was obtained from patients who had undergone knee arthroplasty for OA at the Freeman Hospital and the Royal Victoria Infirmary, Newcastle-upon-Tyne. Ethical approval was granted by the Newcastle and North Tyneside Research Ethics Committee (REC reference number 14/NE/1212). Patient ages ranged from 51-81 years old (mean age 62) and 75% of the cartilage samples were from females. Following surgery, samples were stored at 4°C in Hank's Balanced Salt Solution supplemented with nystatin, penicillin, and streptomycin and collected by a research technician and brought to the university laboratory no later than 48 hours after surgery.

### **2.4.2 *Cartilage tissue digestion and extraction of human articular chondrocytes***

This protocol was performed by a research technician. Cartilage was removed from joints by scalpel, washed in pre-warmed PBS (Fisher Scientific 10010015) to 37°C, and cut into small pieces. Tissue was transferred to a 50ml falcon tube and washed a further two times in PBS. Hyaluronidase (Sigma Aldrich, H3506) and trypsin (Sigma Aldrich, T7409) were prepared as 1mg/ml and 2.5mg/ml solutions respectively in PBS. Collagenase (Sigma Aldrich, C0130) was dissolved in pre-warmed DMEM medium containing 10% FBS (Fisher Scientific, 10270106), 100U/ml penicillin, 100µg/ml streptomycin, 2mM L-glutamine (Fisher Scientific, 25030024), and 50U/ml nystatin (Sigma, N1638). Hyaluronidase solution was filtered through a 0.2µM filter (Fisherbrand, 15206869) using a 50 ml syringe (BD Plastipak™) over the tissue and then incubated at 37°C for 15 minutes. The supernatant was removed and the sample washed twice in PBS. This process was repeated for the trypsin solution with an incubation time of 30 minutes and a wash using pre-warmed medium. Collagenase was filtered through a 0.2µM filter (Fisherbrand, 15206869) and incubated with the tissue overnight at 35°C on a roller.

After tissue digestion the chondrocytes separated passively into the supernatant while the matrix formed a sediment at the bottom of the tube. The supernatant, containing the cells, was removed from the falcon tube and passed through a 100 $\mu$ M cell strainer (BD Falcon, 352360) into a new falcon tube before centrifugation using a Heraeus Labofuge 400R at 241.5 xg for seven minutes to obtain a cell pellet which was resuspended in PBS. Cells were counted in equal volumes with trypan blue viability dye with a Fuchs Rosenthal haemocytometer and 1x10<sup>6</sup> human articular chondrocytes (HACs) were frozen down immediately post extraction from the cartilage in 4°C freezing medium containing 50% DMEM (Fisher Scientific, 11965092), 40% FBS and 10% DMSO in 1ml cryovials; these cells were considered P0. HACs were seeded (4-6x10<sup>6</sup>) in T175cm<sup>2</sup> flasks containing 25ml DMEM (Fisher Scientific, 11965092), 2mM L-glutamine (Fisher Scientific, 25030024), 100U/ml penicillin/streptomycin (Fisher Scientific, 15140122), 10% FBS (Fisher Scientific, 10270106) and 50U/ml nystatin (Sigma, N1638). Cells were incubated at 37°C for 7-20 days until confluency was reached before further use in experimental procedures.

### **2.4.3 HAC IL-1 treatment**

Following the 7-20 day culture, HACs were passaged, and 1x10<sup>6</sup> cells seeded into new T75cm<sup>2</sup> flasks, with the remaining cells collected for nucleic acid extraction (termed passage one cells). Cells adhered for 24 hours, before replacing the media with media  $\pm$  IL-1 $\alpha$  at 0.1ng/ml. The concentration of IL-1 $\alpha$  had been previously determined within the group. For six of the 16 HAC lines examined, HACs were stimulated with IL-1 $\alpha$  for two passages until flask confluency was reached (P2 10-13 days and P3 12-15 days dependent on donor). The IL-1 $\alpha$  was removed for the fourth and final passage (Figure 2.2). The medium was changed every four to five days and fresh 0.1ng/ml IL-1 $\alpha$  added to treated flasks. For one experiment in two HAC donors, cells were exposed to either 1ng/ml of IL-1 $\beta$  (Peprotek IL-1 $\beta$ , Cat: 200-O1Q) or 0.1ng/ml IL-1 $\alpha$  for 10 or 12 days respectively. This was introduced to the cells in fresh media following an overnight incubation at 37°C. At least 1x10<sup>6</sup> HACs were frozen (section 2.4.2) in 1.5ml Eppendorf tubes at -80°C for extraction of RNA at each passage end (P0-P4).

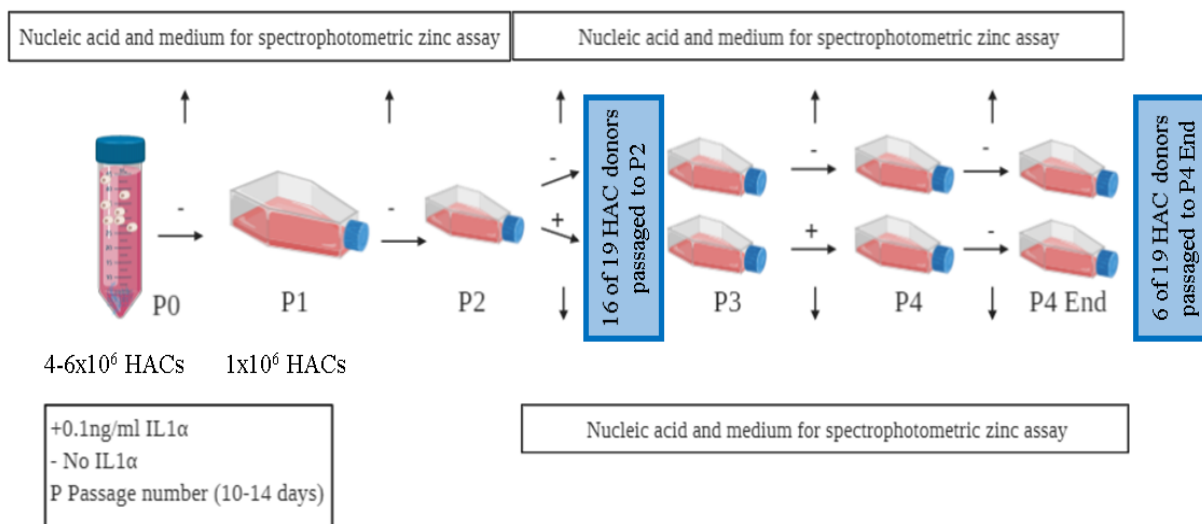


**Figure 2.2 - Time course of HAC treatment with or without IL-1 $\alpha$  between passages two and three and its removal for a final passage.**

HACs were seeded at high density and cultured in monolayer for 7-20 days (P1-P2). Thereafter,  $1 \times 10^6$  cells were split into two flasks and incubated 24 hours before treating one flask in the series with 0.1ng/ml IL-1 $\alpha$ . Flasks were cultured until confluent and treated with IL-1 $\alpha$  for one further passage before its removal at P4.  $1 \times 10^6$  cell pellets were collected into separate 1.5ml Eppendorf tubes at the end of each passage for extraction of nucleic acids using different methods. P2 was used for qPCR analysis representing the first passage after IL-1 $\alpha$  treatment. Graphics were sourced from <https://biorender.com>.

## 2.5 Nucleic acid extraction and cDNA synthesis

### 2.5.1 Nucleic acid from cell lines

Nucleic acid was extracted from frozen SW1353 and T/C-28a2 pellets using the omega BIO-TEK E.Z.N.A DNA/RNA Isolation Kit (R6731-01) according to the manufacturer's protocol. To increase the RNA yield from the columns, the RNA was either eluted in 70°C diethylpyrocarbonate (DEPC) water in two 25 $\mu$ l volumes allowing the column to stand for five minutes between elutions, or in 50 $\mu$ l DEPC water with the same volume passed down the column twice. The tube was pulse centrifuged to pool the RNA at the bottom of the Eppendorf tube and allowed to cool down before the RNA was quantified. The concentration, where possible, was adjusted to 250ng/ $\mu$ l in a separate tube and adjusted concentration confirmed by Nanodrop<sup>TM</sup>. 1.5 $\mu$ l of RNA was checked for integrity on a 1% tris-acetate ethylenediaminetetraacetic acid (TAE) agarose gel and stored at -80°C.

### ***2.5.2 RNA extraction for HACs***

Thawed pellets in 1.5ml Eppendorf tubes were resuspended in 500µl of TRIzol Reagent (Fisher Scientific, 15596026) before vigorous mixing with 100µl chloroform until both phases were combined. The solution was then incubated at room temperature for 10 minutes before centrifugation using a Heraeus Pico17 at 4°C for 15mins at 16249 xg. The upper aqueous phase was transferred to a new 1.5ml Eppendorf tube and 1.5µl GlycoBlue (Fisher Scientific, AM9516) added and mixed. Two hundred and fifty microlitres of isopropanol was added and the tube inverted 5-6 times followed by incubation at room temperature for 10 minutes. The tube was then centrifuged again at 16249 xg at 4°C but for 10 minutes and the supernatant discarded. 500µl of 75% ethanol (diluted in DEPC water) was added to the pellet and mixed up and down by pipette. The sample was then centrifuged at 9615 xg for five minutes at 4°C and the supernatant removed. The tube was briefly spun to remove further supernatant and the pellet allowed to dry for five minutes on ice. The pellet was dissolved in 15µl DEPC water and the sample incubated at 60°C for 10 minutes. The tube was pulse centrifuged to pool the RNA at the bottom of the tube and allowed to cool on ice before the RNA was quantified using a Nanodrop™ spectrophotometer. The concentration, where possible, was adjusted to 250ng/µl in a separate tube and adjusted concentration confirmed by Nanodrop™. 1.5µl of RNA was checked for integrity on a 1% TAE agarose gel and stored at -80°C.

### ***2.5.3 Quantification of nucleic acid***

RNA was quantified with a single or eight sample pedestal Nanodrop™ spectrophotometer 2000 or 8000 respectively (Fisher Scientific). All samples were measured twice, and the mean concentration taken. The 260/280 and 260/230 ratios were recorded in each instance to identify potential phenol or guanidine chemical carryover from TRIzol Reagent and column extraction methods respectively.

Several RNA samples were quantified with the Qubit® (Fisher Scientific) using the broad-range (BR) assay kit (Fisher Scientific, Q10210). This kit utilises a fluorescent dye tagging approach which has increased sensitivity than spectrophotometric approaches. Thin-wall clear 0.5ml tubes (Fisher Scientific, Q32856) were used to measure each sample and the Qubit® working solution was prepared by diluting the Qubit® RNA BR fluorescent reagent 200-fold in Qubit® RNA BR buffer. Each standard or sample tube contained 200µl reagent (190µl working solution and 10µl standards or 1-20µl sample and 199-180µl working solution). Each tube was briefly pulse centrifuged and checked for absence of bubbles before incubating at room temperature for two minutes. Once the machine was calibrated using the standards, the samples were measured. Both Nanodrop™ and Qubit® readings were used in the synthesis of cDNA.

#### ***2.5.4 Gel electrophoresis***

Molecular biology grade agarose (Sever Biotech Ltd, 30-10-50), was dissolved in 100ml of a 1x TAE buffer preparation (diluted in DEPC water) of a 50x stock (2M Tris, 1M acetic acid and 50mM EDTA). All RNA samples were observed on a 1% gel. The agarose-TAE solution was heated in the microwave until fully dissolved, the glass conical flask cooled, and 1% (v/v) ethidium bromide or SafeView (NBS Biologicals, NBS-SV1) added. The solution was mixed and poured into the casts with the appropriate well insert until set. Samples were mixed with bromophenol blue loading dye and DEPC water to a volume of 10µl and loaded on the gel alongside 5µl of a 2-log DNA ladder from New England Biolabs (NEB, N3200S). The gels were run in 1x TAE buffer at 70-80V for nucleic acid or 100V for digested products. Gels were visualised using a G Box Syngene imager or AzureC600 (Azure Biosystems) under UV light. RNA was visualised to check the integrity after extraction and suitability for cDNA synthesis.

### **2.5.5 cDNA synthesis**

Four microlitres of 250ng/ $\mu$ l RNA was reverse transcribed per sample. In instances where the RNA sample was less than 250ng/ $\mu$ l, the RNA was concentrated using a speedvac or by ethanol precipitation. If RNA from an experiment was still less than 250ng/ $\mu$ l, 4 $\mu$ l of this was used and became the standard amount of RNA reverse transcribed for every sample of the same experiment. Prior to cDNA synthesis, RNA was DNaseI treated to remove any DNA contamination. 1 $\mu$ l of a 1:1 Turbo DNase & DNase buffer (Fisher Scientific, AM2238) was added to 4 $\mu$ l RNA in a 0.2ml tube (VWR, 732-4836) and incubated at 37°C for 30 minutes. The DNaseI enzyme was inactivated by addition of 0.9 $\mu$ l of 0.1M EDTA (Fisher Scientific, AM9260G) and incubation at 75°C for 10 minutes, before being transferred to ice. RNA was reverse transcribed using the SuperScript II reverse transcriptase enzyme (Fisher Scientific, 18064014) according to the manufacturer's instructions. Briefly, 1 $\mu$ l of random hexamers (ThermoFisher Scientific, 48190011), 1 $\mu$ l of 10mM dNTPs (ThermoFisher Scientific, 18427-013) and 0.5 $\mu$ l of DEPC water were added. The RNA was incubated at 65°C for five minutes using the G storm thermal cycler (Agilegene Technologies) to allow the random hexamers to bind to the RNA. After incubating the RNA on ice for one minute, 11 $\mu$ l of master mix containing the following was added to each sample; 4 $\mu$ l of 5x reverse transcriptase buffer (Fisher Scientific, 18064014), 4 $\mu$ l 25mM MgCl<sub>2</sub> (ThermoFisher Scientific, N8080241), 2 $\mu$ l 0.1M DTT (Fisher Scientific, 18064014) and 1 $\mu$ l RNaseOUT (Fisher Scientific, 10777019). Samples were mixed by pipetting up and down then incubated at 25°C for one minute. 1 $\mu$ l of superscript II diluted three-fold in DEPC water was added to the mix and the whole mixture was pipetted up and down several times. The final reverse transcription cycling conditions were 25°C 10 minutes, 42°C 50 minutes and 70°C for 10 minutes. 20-fold dilutions of the cDNA in DEPC water were made for subsequent qPCR analysis and stored at -20°C.

## 2.6 Gene expression quantification by qPCR

### 2.6.1 Primer assay design for cDNA & plate set-up

Intron-spanning oligonucleotide primers were designed using the Roche ProbeLibrary Assay Design Software (Roche, Applied Science) using genomic DNA sequences from the University of California and Santa Cruz Genome Browser (UCSC, <https://genome.ucsc.edu/>) and ordered from Sigma or Integrated DNA Technologies (IDT). To normalise the different amounts of mRNA between the samples, qPCR assays for *18S* ribosomal RNA, *HPRT1* (Hs.PT.58v.45621572, RefSeqNM\_000194) and *GAPDH* (Hs.PT58.40035104, RefSeqNM\_002046) were used as reference housekeeping genes. Table 2.3 lists all qPCR assays used, including primer sequences, probe IDs or premade assay catalogue numbers. For Roche ProbeLibrary designed assays, master mixes were prepared with 5µl 2x Taqman fast universal PCR master mix (Fisher Scientific, 4444558), 0.2µl 10µM of each primer (200nM final concentration), 0.1µl 100nM probe, and 2µl DEPC water. For all assays, 7.5µl of master mix was added first to each well of a MicroAmp® Fast Optical 96-well Reaction Plate (Fisher Scientific, 4346906) followed by 2.5µl of 20-fold diluted cDNA for a total volume of 10µl. Primer concentrations for *18S* gene expression were 30µM. *ADAM-TS5* (Hs.PT58.20378240), *MMP13* (Hs.PT.58.4612796.g), *HPRT1* and *GAPDH* assays were all ordered from IDT as x10 assays and master mixes prepared with 1µl x10 IDT assay, 5µl 2x Taqman fast universal PCR master mix (4444558) and 1.5µl DEPC water. The plates were sealed with a MicroAmp Optical Adhesive Film (Fisher Scientific, 4311971) and centrifuged at 4.5 xg on a Thermo IEC Centra CL3 centrifuge for 20 seconds to ensure cDNA and master mix was at the bottom of the well. The plates were loaded into an ABI 7900HT Fast Real-time PCR system or the Quantstudio 3 Real-time PCR machine and were subjected to denaturation at 95°C for 20 seconds followed by 40 cycles of 95°C for one second and 60°C for 20 seconds.

### **2.6.2 Primer validation**

The efficiency of each Roche ProbeLibrary designed qPCR assay was evaluated across a range of cDNA dilutions and were validated prior to using them on valuable patient samples. *IL-6*, *CXCL8*, *MMP13* and *ADAM-TS5* assays had previously been validated by other laboratory members. Serial dilutions of 1:20, 1:80, 1:320 and 1:1280 SW1353 or T/C-28a2 cDNA were made by diluting cDNA in DEPC water. These dilutions were used as a template for a standard curve. Theoretically, each dilution should lead to a  $C_t$  increase of two and it is against this standard that the efficiency of the primer curve was assessed. Efficiency was calculated as  $10^{(-1/\text{gradient})-1}$  and expressed as a percentage. Dr. Louise Reynard, Newcastle University, Faculty of Medical Science optimised the *SLC30A* and *SLC39A* primers and determined the primer efficiency using the same protocol.

### **2.6.3 qPCR analysis**

Each cDNA sample was measured in technical triplicate generating a  $C_t$  value, defined as the number of cycles required for fluorescent signal to exceed background level, and the mean  $C_t$  for every sample for a specific gene calculated. If any  $C_t$  from a technical triplicate deviated by more than 0.5 cycles from each other, it was excluded from the mean and if all three  $C_t$ s were not replicable then the qPCR was repeated or the sample was not used. The method of data normalisation was to first calculate the mean of housekeepers (*18S*, *GAPDH*, *HPRT1*) for each sample, then calculate  $2^{-(\text{sample } C_t - \text{sample housekeeper } \bar{x})}$ , where  $\bar{x}$  is the sample housekeeper mean. This was calculated for every technical repeat for a sample, seeded in biological duplicate or triplicate per condition and the mean taken. For interpretation of gene expression fold change, the normalised data for treatments was divided by the normalised mean of the untreated controls at the same passage in the experiment. The heatmaps were created in Prism version 8.1.1 and the data is presented in the form of fold change or log<sub>2</sub>-fold change. Comparisons of means after one passage of treatment with IL-1 $\alpha$  in both cell lines (P1) and in HACs (P2) was either a paired or Wilcoxon t-test dependent on the outcome of normality assessment by either Shapiro Wilk ( $n < 8$  means) or D'Agostino-Pearson omnibus  $k_2$  ( $n \geq 8$  means) on a gene by gene basis. If the normalised gene expression data did not satisfy a normal distribution at first, a single attempt at data transformation by taking logarithm base two and repeating the same normality test was performed, the outcome of which dictated either a paired or Wilcoxon t-test. All analyses of the data were performed in Prism version 8.1.1.

**Table 2.3 –TaqMan and IDT qPCR assays.**

IDT = Integrated DNA Technologies UPL = Universal Probe Library. BLD = below limit of detection.

GENE	PRIMER SEQUENCE (5' to 3')	UPL PROBE NO. OR IDT PROBE SEQUENCE	EFFICENCY (%)
<i>18S</i>	CGAATGGCTCATTAAATCAGTTATGG TATTAGCTCTAGAATTACCACAGTTATCC	TCCTTTGGTCGCTCGCTCCTCTCCC	primers already validated
<i>HPRT1</i>	TGCTGAGGATTTGGAAAGGG ACAGAGGGCTACAATGTGATG	FAM/AGGACTGAACGCTTTGCTCGAGATG/ZEN/IBFQ	primers already validated
<i>GAPDH</i>	ACATCGCTCAGACACCATG TGTAAGTTGAGGTCAATGAAGGG	FAM/AAGGTCGGAGTCAACGGATTGGTC/ZEN/IBFQ	primers already validated
<i>CCL2</i>	AGTCTCTGCCGCCCTTCTG GTGACTGGGGCATTGATTGC	40	82
<i>IL-6</i>	CAGGAGCCCAGCTATGAACT GAAGGCAGCAGGCAACAC	45	primers already validated
<i>CXCL8</i>	AGACAGCAGAGCACACAAGC AGGAGGCTGCCAAGAGAG	72	primers already validated
<i>MTF1</i>	CACGTTCTGTACACATACTGGTG TGCTGAATGTTTTCTCACAGC	29	100
<i>MT1A</i>	TCCTGCAAATGCAAAGAGTG GCACATTGGCAGACTCAT	68	BLD
<i>MT1E</i>	TGCTTGTTCTGCTCACTGGT GCATTGCACTCTTTGCACT	67	80
<i>MT1F</i>	CCACTGCTTCTTCGCTTCTC GCAGGTGCAGGAGACACC	68	BLD
<i>MT1G</i>	CTAGTCTCGCTCGGGTTG GCATTGCACTCTTTGCACT	68	BLD
<i>MT1H</i>	TGGAATCCAGTCTCACCTC TGCATTGCACTTTTTGCAC	68	BLD
<i>MT1X</i>	CTTCTCCTTGCCCTCGAAATG ACAGGCACAGGACCAAC	15	99
<i>MT2A</i>	AACCTGTCCCGACTCTAGCC GCAGGTGCAGGAGTCACC	68	BLD
<i>SLC30A1</i>	TCACCACTTCTGGGGTTTTC CGACCAGGAGGAGACCAAC	49	107
<i>SLC30A5</i>	GGGATGGAGGAGAATACGG AAGTCCACAGCCTTCAAAA	70	94
<i>SLC30A6</i>	TGGAAGATACTGCTCTTTGGTG TGGTCAGGTAAGTATAGGCAGTTAAA	4	105
<i>SLC30A7</i>	AATGATGCTTTTCTCTATGGGTA AGATCAAAAATAGGCCATTGACA	20	108
<i>SLC30A9</i>	GCTCCAGAACAGCATCAGTG AATTTAAAGAAGCAGTTAATCCATTG	9	85
<i>SLC39A1</i>	TGACTACCTGGCTGCCATAGA ACTCTTGCAAGTGGGAAGTGG	81	83
<i>SLC39A3</i>	GTTTCTGGCCACGTGCTT AGGCTCAGGACCTTCTGGA	74	100
<i>SLC39A4</i>	TCTACGTAGCACTCTGCGACA CGTACAGGGACAGCAGCAGC	3	98
<i>SLC39A6</i>	ACTGGCCGTTGGGACTTT ATGGTGGTGACTTGCATGAG	9	101
<i>SLC39A7</i>	GTCGGAGACTTTGCCATCTT CAGTAGTTGCAGACGCATCG	71	98
<i>SLC39A8</i>	TTTTGGTGGGCAACAATTT CAGCATATCATTCTCTGGAAAC	67	106
<i>SLC39A9</i>	GATGTTACGTGGCCGGAAT CCAAAACAGTCACCAGCTT	6	102
<i>SLC39A10</i>	TGTAGCCTTGGTGGATATGCT CCACAGGACAAAAGCCATGT	9	106
<i>SLC39A11</i>	GATGGAAGTCTTGGCTTTC CAACAGCCACAGGGAAGAA	3	86
<i>SLC39A13</i>	GGCCAACACCATCGATAACT TTGTCAGGAGCCCGATCTT	5	98
<i>SLC39A14</i>	TCTCTGCCAACTGGATTTTTG CCTCATTCATCTCAGGGAAC	78	111
<i>MK167</i>	GAGGTGTGCAGAAAAATCCAAA CTGTCCCTATGACTTCTGGTCT	30	95
<i>MMP13</i>	AAATTATGGAGGAGATGCCATT TCCTTGGAGTGGTCAAGACCTAA	FAM/CTACAACCTGTTTCTTGTGCTGCGCATGA/ZEN/IBFQ	primers already validated
<i>ADAM-TS5</i>	CAAGTGGCGAGTATGTGGAG GTCTTTGGCTTTGAACTGTCG	FAM/TTTATGTGGGTTGCCCTTCAGGA/ZEN/IBFQ	primers already validated
<i>TOP2A</i>	CAGTGAAGAAGACAGCAGCAA AGCTGGATCCCTTTAGTTCCT	43	93
<i>TPX2</i>	ACATCTGAACTACGAAAGCATCC GGCTTAACAATGGTACATCCCTTA	51	85
<i>CDKN1A</i>	CACCTCACCTGCTCTGCTG GAGGCACAAGGGTACAAGACA	6	89
<i>CAMK2G</i>	CAGCACAAAGCTGTATCAGCAG TTACCGTGICCCATTCTGGT	19	71
<i>PARP2</i>	GCCAGAGACAGGAGTCGAAA ACAGCAAGGCCTTCACAGAT	5	99

## 2.7 Zinc quantification assay

A spectrophotometry assay suitable for the determination of zinc in serum and other biological samples was purchased from Sigma (MAK032). The kit was used to assess the abundance of zinc in spent medium and cell pellets from T/C-28a2, SW1353 and HACs treated  $\pm$  IL-1 $\alpha$  for one passage in monolayer.  $1.3 \times 10^6$  cell pellets and 300 $\mu$ l spent medium were collected for use with the kit. Briefly, the assay works by chelating zinc (zinc reagent A) and other interfering metal ions ( $\text{Cu}^{2+}$  and  $\text{Fe}^{2+}$ ) and by subsequent zinc demasking with chloral hydrate. This free  $\text{Zn}^{2+}$  is then able to bind to the pyridylazo ligand 2-(5-bromo-2-pyridylazo)-5-(N-n-propyl-N-3-sulfopropyl-amino)phenol (zinc reagent B) creating a coloured complex which absorbs light at 560nm (Homsher and Zak, 1985). Other interfering metal ions such as  $\text{Ca}^{2+}$  and  $\text{Mg}^{2+}$ , are not appropriately chelated thus their interference is controlled by maintaining the pH between 7.4-7.8.

Protein was not removed at the time of collection of the spent medium, thus 7% trichloroacetic acid (TCA) was added 1:1 to samples and centrifuged in an Eppendorf minispin bench-top centrifuge at 12045 xg for five minutes to precipitate and pellet the protein. The MAK032 kit protocol did not mandate the addition of TCA to standards, so initial experiments were done with or without TCA, and then from the preliminary results TCA was included in both the standards and samples.  $1.3 \times 10^6$  frozen cell pellets were lysed in 55 $\mu$ l deionised water and treated with 55 $\mu$ l 7% TCA and centrifuged as previous. For spent medium samples, 55 $\mu$ l of medium was mixed with 55 $\mu$ l of 7% TCA. Fifty microlitres of TCA-diluted sample and  $\text{ZnCl}_2$  standard was transferred to separate wells of a flat-bottom 96-well plate (Greiner Bio-One, 655101) before addition of 200 $\mu$ l zinc reagent (four parts zinc reagent A: one part zinc reagent B). The 50mM  $\text{ZnCl}_2$  standard provided was diluted 100-fold for a 0.5mM working standard solution and aliquots made and frozen at  $-20^\circ\text{C}$ . This was used to form six-point standard curves of ranges 0, 4, 8, 12, 16 and 20 $\mu$ M or in later experiments 0, 2, 4, 6, 8 and 10 $\mu$ M. For experiments completed in November and December 2017, the calculated concentration of different samples was consistently in the range of 0-4 $\mu$ M which is why the range of the standard curve was reduced in samples quantified in 2018. Cover seals were placed on plates then gently agitated, avoiding inclusion of bubbles, and incubated for 10 minutes at room temperature in the dark. The cover seal was removed, and the plates were read on a Varioskan Lux plate reader at 560nm.

The background (0 nanomoles/well standard) absorbance was removed from samples and standards before dividing the corrected absorbance by the gradient (m) of the linear regression equation  $y=mx$  of the standard curve to give x, which is equal to nanomoles/250 $\mu$ l when the standards are expressed in the same units. The concentration in  $\mu$ M was calculated by multiplying the nanomoles/250 $\mu$ l by four. All standards and samples were assayed in duplicate, except for the cell-free  $\text{ZnCl}_2 \pm$  other metal ions experiment, which was only performed in singlicate. The data was analysed by paired t-test in Prism version 8.1.1.

### ***2.7.1 Testing kit specificity against biologically relevant metal ions***

Five millimolar stock solutions of biologically relevant metal ions were prepared using deionised water for the following compounds:  $\text{Fe}_2\text{SO}_4 \cdot 7\text{H}_2\text{O}$  (Melford Laboratories, F0512),  $\text{Cu}_2\text{SO}_4 \cdot 6\text{H}_2\text{O}$  (Sigma, MKBF7872V),  $\text{CaCl}_2$  (Sigma, BCBN5264V) and  $\text{MgCl}_2$  (Sigma, BCBR4870V). These, and the 0.5mM  $\text{ZnCl}_2$  stock were diluted  $\pm$  7% TCA and deionised water to 40 $\mu$ M. 25 $\mu$ l of  $\text{ZnCl}_2$  and 25 $\mu$ l of one of the other metal compounds were combined in the assay plate and diluted 10-fold with 200 $\mu$ l zinc assay reagent for 4 $\mu$ M equimolar metal ion solutions. The 4 $\mu$ M  $\text{ZnCl}_2$  standard was used as the zinc alone measurement. Cover seals were placed on plates then gently agitated, avoiding inclusion of bubbles, and incubated for 10 minutes at room temperature in the dark. The cover seal was removed and the plates were read on a Varioskan Lux plate reader at 560nm. For this experiment the concentration of zinc in the assay plate was expressed as micromolar.

### ***2.7.2 Inhibiting $\text{Fe}^{2+}$ influence on absorbance using 2,2'-bipyridine chelator***

A metal ion chelator, 2,2'-bipyridine used as an inhibitor of iron ions (Kim *et al.*, 2014), was purchased from Sigma for attempted attenuation of the increased absorbance in the cell-free  $\text{ZnCl}_2 + \text{Fe}_2\text{SO}_4 \cdot 7\text{H}_2\text{O}$  condition described in 2.7.1. Deionised water was used for dilution of metal compounds in all instances. 2,2'-bipyridine,  $\text{ZnCl}_2$  and  $\text{Fe}_2\text{SO}_4 \cdot 7\text{H}_2\text{O}$  were diluted to a 25mM, 80 $\mu$ M and 80 $\mu$ M working stock respectively. 1.82 $\mu$ M zinc alone, 1.82 $\mu$ M iron alone or zinc and iron alone (both 1.82 $\mu$ M) were assayed in 96 well plates with or without 2,2'-bipyridine at 45, 227 or 450 $\mu$ M. Cover seals were placed on plates then gently agitated, avoiding inclusion of bubbles, and incubated for 10 minutes at room temperature in the dark. The cover seal was removed, and the plates were read on a Varioskan Lux plate reader at 560nm.

## 2.8 Cloning

The 6kb pGL4.40[luc2P/MRE/Hygro] plasmid (referred to outside the methods as MRE pGL4.40 plasmid) was purchased from Promega (E4131) to study MTF1 transcriptional activity in transiently transfected SW1353 and T/C-28a2 cell lines with or without cytokine and/or ZnCl<sub>2</sub> treatment. This construct contains five MRE copies in the promoter region required for MTF1 interaction with its target genes, driving the expression of luciferase protein. The 7.1kb pCMV6-MTF1 c-myc-FLAG-tagged plasmid construct (referred to outside the methods as MTF1 plasmid) was purchased from Origene (RC204861) for use in studying MTF1 localisation in SW1353 cells under conditions of IL-1 $\alpha$  stimulation and/or ZnCl<sub>2</sub> treatment. All restriction enzymes and buffers used for cloning were from NEB. The plasmid maps are in Appendices A and B.

### ***2.8.1 Generation of an empty control pGL4.40 plasmid from the pGL4.40[luc2P/MRE/Hygro] plasmid***

Cloning was necessary to generate a pGL4.40 plasmid which after transfection into SW1353 cells would not permit luciferase expression in the absence of the five MRE copies. The pGL4.40[luc2P/MRE/Hygro] plasmid was digested using XhoI and SacI restriction enzymes in CutSmart buffer which cut either side of the combined MRE sequences creating a linearised plasmid with overhangs. The digested products were separated by 1% TAE agarose gel electrophoresis and the MRE-excised pGL4.40 plasmid extracted and purified by Raul Fulea (a PhD student within the group) using the QIAquick Gel Extraction Kit (Qiagen, 28704) according to the manufacturer's instructions. The linearised plasmid was religated using a synthetic multiple cloning sequence (MCS) with complementary overhangs. The synthetic MCS was designed by Dr. Louise Reynard (Newcastle University, Faculty of Medical Science) and was comprised of two oligonucleotides (5'CACGCGTCATATGGCTAGCCACGTGC3' and 5'TCGAGCACGTGGCTAGCCATATGACGCGTGAGCT3') with multiple restriction sites (MluI, NdeI, NheI and PmII) specific to the MCS. 10µl of each 10µM oligonucleotide, combined with 10µl 10x annealing buffer (10mM Tris pH7.5, 50mM NaCl and 1mM EDTA) and 70µl DEPC water, was heated to 95°C for five minutes and cooled. The annealed MCS was ligated into the linear MRE-excised pGL4.40 plasmid using the T4 DNA ligase (NEB, M0202). A 3:1 insert:plasmid ratio based on the DNA concentration and insert and plasmid size was used, such that 124ng (2µl) of linearised MRE-excised pGL4.40 plasmid was mixed with or without 2.1ng (1µl) of MCS, 1µl T4 DNA ligase, 2µl 10x T4 DNA ligase buffer and 14µl nuclease-free water, then incubated overnight at room temperature. The T4 DNA ligase was heat inactivated at 65°C for 20 minutes. This plasmid is referred to outside the methods as the empty control pGL4.40 plasmid.

### ***2.8.2 Preparing agar plates***

Five hundred millilitres of agar were prepared by dissolving 10.3g luria broth (LB) and 7.5g agar in deionised water and then autoclaved for 45 minutes. The autoclaved agar was then cooled in a prewarmed 50°C water bath before adding ampicillin or kanamycin antibiotics at a final concentration of 100µg/ml ampicillin and 25µg/ml kanamycin and poured into petri dishes and left to cool on the bench. Plates were left in 4°C storage until required.

### **2.8.3 Transformation reaction**

Agar plates were removed from storage and allowed to reach room temperature before placing in a 37°C incubator downturned. All subsequent steps were performed by a bunsen burner. The plasmids were diluted to 1 or 5ng/μl from a 100ng/μl stock in DEPC water. 50μl vials of chemically competent One Shot TOP10 *E. coli* (Fisher Scientific, C404010) were thawed on ice and then split into 25μl volumes in Eppendorf tubes to receive 1μl plasmid from each concentration for both pCMV6-MTF1 c-myc-FLAG-tagged and pGL4.40[luc2P/MRE/Hygro] plasmids. The cells were transformed with either plasmid using 42°C heat shock as described in the manufacturers' instructions.

The cells were then streaked out in 25, 50 or 100μl volumes on to the agar plates containing the relevant antibiotic (ampicillin and kanamycin for pGL4.40[luc2P/MRE/Hygro] and pCMV6-MTF1 c-myc-FLAG-tagged transformed *E. coli* respectively) and incubated at 37°C overnight to pick single colonies afterwards and to assess transformation efficacy.

### **2.8.4 Picking bacterial colonies**

After 12-16 hours, individual colonies present on the plates were screened for transformants and absence of transformants on negative control dishes. LB broth medium prepared by dissolving 10.3g LB in 500ml deionised water and autoclaving, was prepared as a master mix with ampicillin or kanamycin at the same concentrations as described in 2.8.2. Three millilitre volumes of the master mix were dispensed into labelled 15ml falcon tubes to receive each colony and using a sterile 10μl filter tip a single colony was picked from the dish and the tip added to the tube. The tube was closed and incubated overnight at 37°C in the shaker at 225 rpm.

### **2.8.5 Miniprep & glycerol stocks**

The overnight bacterial cultures were divided into two 750μl volumes in 1.5ml Eppendorf tubes. The tubes were then centrifuged using an Eppendorf minispin at 4293 xg for three minutes to pellet the bacteria and the supernatant discarded to 1% virkon waste. Remaining solution was pipetted off to remove extra LB broth. The QIAprep Spin Miniprep Kit reagents (Qiagen, 27104) were used to extract DNA from the cells with modifications to the protocol.

The cell pellets were resuspended by vortexing in 100µl ice-cold P1 solution. The resuspended cells were then lysed in 200µl of P2 solution. The tube was inverted several times to mix without vortexing and left for three minutes. 150µl P3 solution was added to each tube, inverted several times to mix and tubes were centrifuged at 11337 xg for five minutes. Following centrifugation, a white precipitate formed on the side of the tube and the clear supernatant, containing the DNA, was removed and added to a new tube. The centrifugation was repeated as before for five minutes and the clear supernatant phase separated from any remaining precipitate into another tube. 1ml of 100% ethanol was added to the samples, mixed, and the tubes stored at -80°C for 15 minutes. Centrifugation at 11337 xg for 10 minutes was conducted to pellet the DNA and the ethanol was removed entirely and the tubes left open to air dry for 10-15 minutes. The DNA was resuspended in 80µl DEPC water, allowed to dissolve fully for 15 minutes at room temperature to then be quantified by nanodrop.

The PureYield™ Plasmid Miniprep System (Promega, A1221) is a ‘cleaner’ approach to DNA extraction with the use of silica membrane columns and was used once for miniprep of the pGL4.40[luc2P/MRE/Hygro] plasmid. Six hundred microlitres of bacterial culture was added to a 1.5ml Eppendorf tube and mixed with 100µl cell lysis buffer by inversion six times. The solution changed from opaque to clear blue, indicating complete lysis after which 350µl of ice-cold neutralisation solution was added and mixed well by inversion. The colour of the sample turned yellow when neutralisation was complete and after three final inversions the tube was centrifuged at 12045 xg in an Eppendorf minispin bench-top centrifuge for three minutes. The supernatant was transferred to a PureYield™ minicolumn. The minicolumn was inserted into a PureYield™ collection tube and centrifuged at 12045 xg for 15 seconds. The filtrate was discarded and the minicolumn replaced in the same collection tube. 200µl of endotoxin removal wash was added to the minicolumn and centrifuged at 12045 xg for 15 seconds. The filtrate was not discarded. 400µl column wash solution was then added to the minicolumn and centrifuged at 12045 xg for 30 seconds. The minicolumn was transferred to a clean 1.5ml Eppendorf tube and allowed five minutes to air-dry before eluting the DNA in 30µl elution buffer. The tube was centrifuged at 12045 xg for 15 seconds to collect the DNA which was quantified by nanodrop and visualised on 1% TAE agarose by electrophoresis.

Glycerol stocks were prepared by combining 300µl glycerol with 300µl of each individual colony originating from respective antibiotic agar plates transformed with either pCMV6-MTF1 c-myc-FLAG-tagged or pGL4.40[luc2P/MRE/Hygro] plasmids. The suspension was mixed thoroughly before storing at -80°C in 1.5ml Eppendorf tubes.

### **2.8.6 Genotyping of plasmid DNA using restriction digestion**

Restriction enzymes which cut the pCMV6-MTF1 c-myc-FLAG-tagged and pGL4.40[luc2P/MRE/Hygro] plasmids were identified using a publicly available tool (ApE, <http://jorgensen.biology.utah.edu/wayned/ap/>). NcoI and a combination of high-fidelity KpnI and XhoI were identified to digest pGL4.40[luc2P/MRE/Hygro] and pCMV6-MTF1 c-myc-FLAG-tagged plasmids respectively into three fragments identifiable after 1% TAE gel electrophoresis. NcoI cuts pGL4.40[luc2P/MRE/Hygro] plasmid to give predicted products 3689, 2094 and 296bp and the KpnI and XhoI combination cutters cut pCMV6-MTF1 c-myc-FLAG-tagged plasmid producing predicted products 4835, 1859 and 446bp. MluI was used to cut specifically in the MCS of the empty control pGL4.40 plasmid just once and was compared with full-length unmodified pGL4.40 plasmid to demonstrate specificity of the enzyme. High-fidelity versions of KpnI and XhoI were required so the same enzymatic buffer could be used to do a double digest.

### **2.8.7 Sanger sequencing of miniprep DNA**

Sanger sequencing of the miniprep DNA was necessary to ensure the *E. coli* had not altered the plasmid sequence and the plasmid was sequenced in both directions. Sanger sequencing was outsourced to Source BioScience (Cambridge) and 500ng of plasmid DNA and 16pmol primers were sent away. The sequences of the pCMV6-MTF1 c-myc-FLAG-tagged plasmid for VP1.5 forward primer and XL39 reverse primer were 5'GGACTTTCCAAAATGTGCG3' and 5'ATTAGGACAAGGCTGGTGGG3' respectively. The sequence of the pGL4.40[luc2P/MRE/Hygro] plasmid sequencing primer, RVprimer3 was 5'CTAGCAAAAATAGGCTGTCCC3'.

### **2.8.8 Midiprep**

Glycerol stocks of colonies which had the expected restriction digestion profile and unmutated plasmid sequence were selected for midipreps and one or two colonies were used for the initial growth phase. Stocks were thawed on ice and 30µl cells transferred to 5ml LB broth cultures in labelled 15ml falcon tubes containing either 100µg/ml ampicillin or 25µg/ml kanamycin and placed in a 37°C shaker at 225 rpm for six hours. Afterwards, the cultures were checked for their turbidity as an indicator of growth and then combined into a 500ml autoclaved Erlenmeyer flask containing 100ml LB broth with 100µg/ml ampicillin or 25µg/ml kanamycin for overnight incubation in a 37°C shaker at 225 rpm.

The PureYield™ Plasmid Midiprep System (Promega, A2492), containing all the columns and buffers necessary for the subsequent steps in the midiprep protocol, was utilised. The Erlenmeyer flask was removed from the 37°C shaker and divided into 25ml volumes in four 50ml falcon tubes, which were weighed and weight-adjusted with water prior to centrifugation. Tubes were centrifuged using a Hettich Rotanta 460 R at 5000 xg for 10 minutes and the supernatant discarded to virkon waste. The cells were resuspended in 3ml of resuspension buffer and the four tubes combined into one. Cells were lysed in 3ml lysis buffer for three minutes exactly at room temperature. 5ml neutralisation buffer was added and the tube inverted 5-10 times. The tube was then centrifuged at 15000 xg for 15 minutes.

During this time, the vacuum manifold was assembled, connected to a pump and the PureYield™ clearing columns (blue) inserted into the PureYield™ binding columns (white) atop the vacuum manifold. The cleared lysate was pipetted into the blue column and the vacuum applied until all liquid passed both columns. The vacuum was released and the clearing column disposed and then 5ml endotoxin removal wash applied to the binding column and the vacuum turned on. The vacuum was released and 20ml of column wash solution was added and the vacuum turned on. Once the solution had passed, the vacuum was left on for another five minutes to remove traces of ethanol. An Eppendorf tube was placed in the base of the Eluator™ device and the device attached to the vacuum manifold. The binding column was positioned above the Eppendorf tube in the Eluator™ device and 600µl nuclease-free water was added to the column and eluted by vacuum. The DNA was then quantified by nanodrop and visualised by 1% TAE gel electrophoresis then stored at -20°C.

### ***2.8.9 Restriction digestion pre-transfection***

Both linearised and circular forms of each plasmid were transfected into cell lines using restriction enzymes that cut each of the plasmids once in regions that would not disrupt transcription of native sequences. NotI cuts at position 5190 in the pGL4.40[luc2P/MRE/Hygro] plasmid (Appendix A) and AgeI cuts at position 3969 in the pCMV6-MTF1 c-myc-FLAG-tagged plasmid (Appendix B). 10µl reactions were prepared and digested at 37°C overnight with or without AgeI or NotI with a surplus of plasmid DNA. NotI was digested with NEB 3.1 buffer and AgeI with CutSmart buffer and 1µl of the overnight digests were visualised on 1% TAE agarose gels.

### **2.8.9.1 Qiaquick DNA clean-up**

After successful digestion confirmation by gel electrophoresis, the restriction enzymes were removed with the QIAquick Gel Extraction kit (Qiagen, 28704) prior to transfection. Three volumes of buffer QG and one volume of isopropanol was added to the digestion reaction and mixed well. A spin column was inserted into a 2ml collection tube and the solution added to the spin column. This was centrifuged for one minute at 12045 xg and the filtrate discarded. The spin column was placed back in the same collection tube and 750µl PE wash buffer applied and left to stand for five minutes before again centrifuging for one minute at 12045 xg. The filtrate was removed and spun again for one minute at 12045 xg before the column was transferred to a new labelled Eppendorf tube. The DNA was eluted in 30µl EB buffer, incubated for four minutes at room temperature and then centrifuged for one minute. The DNA was quantified by nanodrop.

### **2.8.9.2 Transient transfection of SW1353 cells with pCMV6-MTF1 plasmid or GFP**

SW1353 cells were seeded as  $0.5 \times 10^6$  cells in a 10cm dish (VWR, 7342321) for 24 hours and the next day at approximately 50% confluency were transfected with 5.6µg of pCMV6-MTF1 c-myc-FLAG-tagged plasmid for 48 hours. FuGENE transfection agent (Promega, E2311) was the lipid chemical used for transfection of SW1353 cells. Three times the volume of FuGENE was required for every µg of plasmid DNA transfected, thus 16.8µl FuGENE was used to transfect 5.6µg of pCMV6-MTF1 c-myc-FLAG-tagged plasmid. The mixture was incubated for 15 minutes at room temperature before adding to the cells. As a positive control to test that the SW1353 cells could successfully be transfected for 48 hours using FuGENE, a sample of short hairpin RNA vector containing green fluorescence protein (GFP) (Origene, TR30007) was kindly provided by Dr. Matt Barter, Newcastle University, Faculty of Medical Sciences and the GFP was visualised by fluorescence microscopy.

## **2.9 Generation of MTF1 and luciferase expressing stable cell lines**

### **2.9.1 Hygromycin B kill curve for pGL4.40[luc2P/MRE/Hygro] plasmid transfection**

Hygromycin B antibiotic inhibits protein synthesis by stabilising the tRNA-ribosomal acceptor site and was used to select SW1353 or T/C-28a2 cells transfected with the pGL4.40 luciferase plasmid. A hygromycin B kill curve had previously been carried out by Raul Fulea in SW1353 cells who deemed 200µg/ml was the minimum concentration required to kill all cells acutely with cytotoxicity observed at higher concentrations. Therefore 200µg/ml was used when creating the SW1353 pGL4.40 luciferase overexpression line. To generate a kill curve for T/C-28a2, the cells were seeded at  $5 \times 10^3$  cells per well into flat-bottom 96 well plates incubated at 37°C with hygromycin B at concentrations 0, 10, 20, 30, 40, 50 & 100µg/ml for eight days.

### **2.9.2 Geneticin (G418) selection of pCMV6-MTF1 plasmid in SW1353 cells**

G418 is an aminoglycoside antibiotic that blocks polypeptide synthesis by inhibiting transcript elongation. The gene which confers G418 resistance is *neo* which is present in the pCMV6-MTF1 plasmid sequence as a kanamycin/neo cassette. Yao Hao (Newcastle University, Faculty of Medical Science) had previously conducted a G418 kill curve in SW1353 cells and deemed 1mg/ml the optimum concentration to kill cells in a week without cytotoxicity and was the concentration used for selection of the plasmid in section 2.9.3.

### **2.9.3 Transfection, selection and expansion of MTF1 or luciferase overexpression cell lines**

$1.5 \times 10^5$  cells were seeded in 6-well plates (VWR, 7342323) overnight and incubated at 37°C. The next day cell lines were transfected with or without 1µg linear or circular plasmid as prepared in the sections 2.8.9 and 2.8.9.1. 5ul lipofectamine 2000 (Fisher Scientific, 10696343) was used per µg of plasmid transfected into T/C-28a2 cells only as described in online protocols. The media was supplemented 24 hours after transfection with or without 1mg/ml G418 for MTF1 overexpressing SW1353 cells. Final concentrations of 50µg/ml (T/C-28a2 cells) or 200µg/ml (SW1353 cells) hygromycin B were supplemented for pGL4.40 luciferase overexpressing cells. Cell growth was assessed daily and when confluent the linear and circular transfected and antibiotic-selected wells were trypsinised and seeded into T25cm<sup>2</sup> flasks maintaining the antibiotic concentrations. These were expanded until confluent and were trypsinised once more into T75cm<sup>2</sup> flasks maintaining the antibiotic concentrations.  $4 \times 10^5$  SW1353 cells were seeded in 6-well plates at in T25cm<sup>2</sup> for 24 hours and transfected 24 hours later with 2.7µg pCMV6-MTF1 plasmid and selected as described.

#### ***2.9.4 Storage and propagation of stable cells***

As for section 2.3.1, SW1353 cell pellets were frozen for later extraction of RNA to validate by qPCR which of the lines generated (linear or circular) would be taken forward for future experiments, dependent on the highest *MTF1* expression. SW1353 or T/C-28a2 cells were frozen down at  $1 \times 10^6$  cells per cryovial in FBS containing 5 or 10% DMSO respectively. Revived antibiotic-selected cells were incubated in media containing half the original concentration of antibiotic; 100 or 25  $\mu\text{g}/\text{ml}$  hygromycin B for SW1353 and T/C-28a2 cells respectively. 500  $\mu\text{g}/\text{ml}$  G418 was used for linear-transfected MTF1 overexpressing SW1353 cells.

#### ***2.9.5 Confirmation that stable cells express the fusion protein***

Primers that would amplify transcribed and non-transcribed regions of both plasmids were designed with defined DNA sequences from the supplier's sequence map using the Roche ProbeLibrary Assay Design Software (Roche, Applied Science). The oligonucleotides were purchased from Integrated DNA Technologies (IDT), resuspended in IDTE solution at 100  $\mu\text{M}$  and frozen at  $-20^\circ\text{C}$ . These were diluted for use at 10  $\mu\text{M}$  with DEPC water. Primer sequences are listed in Table 2.4 and their locations relative to the plasmids are highlighted in Appendices A and B.

Each plasmids DNA was diluted with deionised water 50-fold for four serial dilutions from 1  $\text{ng}/\mu\text{l}$  to  $8 \times 10^{-6}$   $\text{ng}/\mu\text{l}$  (or 0.02  $\text{ng}/\mu\text{l}$  to 0.16  $\text{fg}/\mu\text{l}$ ) and was used as a template for each of the primers presented in Table 2.4. Master mixes for each assay were prepared with 5  $\mu\text{l}$  Taqman Fast Universal PCR Master Mix (Fisher Scientific, 4444558), 0.2  $\mu\text{l}$  10  $\mu\text{M}$  primers, 0.1  $\mu\text{l}$  Taqman probe and 2  $\mu\text{l}$  DEPC water per reaction. qPCR reaction volume was 10  $\mu\text{l}$  (7.5  $\mu\text{l}$  master mix & 2.5  $\mu\text{l}$  DNA). The samples were then subject to denaturation at  $95^\circ\text{C}$  for 20 seconds followed by 40 cycles of  $95^\circ\text{C}$  for 1 second and  $60^\circ\text{C}$  for 20 seconds using the Quantstudio 3 Real-time PCR machine (Applied Biosystems, Fisher Scientific). In each instance where the relevant overexpressed mRNA from SW1353 or T/C-28a2 was determined, only the primer assays to transcribed regions (Table 2.4 primers highlighted in green) were used. Appendix C shows the qPCR validation for all assays in Table 2.4.

**Table 2.4- Plasmid-specific qPCR primer assays.**

Primers were validated against pCMV6-MTF1-c-myc-FLAG-tagged plasmid or pGL4.40[luc2P/MRE/Hygro] plasmid. Confirmation of *luciferase* gene overexpression in T/C-28a2 cells was confirmed using *luciferase* ORF assays and either MTF1-c-myc-FLAG or *luciferase* overexpression in SW1353 cells confirmed with *MTF1* ORF/c-myc-FLAG assays or *luciferase* ORF assays respectively. ORF= open reading frame. UPL = universal probe library.

<b>pCMV6-MTF1 C-MYC-FLAG-TAGGED PLASMID</b>	<b>PRIMER SEQUENCE (5'- 3')</b>	<b>UPL</b>
MTF1 ORF1 (assay 1)	TGGAAGTGTATTATGATAGGACCAC GTCCGTCGTCATCTTCATCC	15
MTF1 ORF2 (assay 2)	TGTTGTTGCTGGGGCTTC CTGGCAGGGGCTCAGTAGT	59
MTF1 c-myc-FLAG	CGCTCGAGCAGAACTCAT CGTCGTCATCCTTGTAATCCA	35
SV40 promoter	CGGGACTATGGTTGCTGACTA GCAACCAGGTGTGGAAAGTC	3
Kanamycin/neo resistance gene	CCACAGTCGATGAATCCAGA ATGCCTGCTTGCCGAATA	31
<b>pGL4.40[luc2P/MRE/HYGRO] PLASMID</b>	<b>PRIMER SEQUENCE (5'- 3')</b>	<b>UPL</b>
Min promoter	GGCCAAGCTTAGACTAGAGG TTACCAACAGTACCGGATTGC	11
Luc2 ORF1 (assay 1)	ACGCCGAGTACTTCGAGATG ATCAGCCCATAGCGCTTC	29
Luc2 ORF2 (assay 2)	CATGACCGAGAAGGAGATCG CAGCTTCTTGCGGTTGTA	20
SV40 early promoter	TGTGTCAGTTAGGGTGTGGAA CACCTGGTTGCTGACTAATTGA	29
Hygromycin B	AAGACCTCCCCGAAACAGAG GCAATAGCATCCATAGCTTCG	40
<b>CONTROL ASSAYS</b>	<b>PRIMER SEQUENCE (5'- 3')</b>	<b>UPL</b>
Genomic DNA primers (-ve control)	CCAGGACTCTGTCTGCATCA GCGTTTTAAAGGTACCTCCTATTTG	51
dCas9 assay (-ve control)	AGAAGAGAAAGGTAGACCCAAAGA TTTTTGTATAACTCGATCAAGACAGC	35
TET1 assay (-ve control)	GAAGTGTGGGTATCACCATTAT CCTTTGGCTTCGAGAAAGTC	17

## **2.10 Protein extraction**

### **2.10.1 Whole protein extraction**

Whole protein extractions were prepared from HACs and cell lines using ice-cold x1 radioimmunoprecipitation assay (RIPA) buffer (150mM NaCl, 1% TritonX-100, 12.7mM C<sub>24</sub>H<sub>39</sub>NaO<sub>4</sub> (sodium deoxycholate), 3.5mM sodium dodecyl sulphate (SDS), 50mM Tris pH8). cOmplete™ mini EDTA-free protease inhibitor cocktails (Sigma, 4693159001) were added to the RIPA buffer (1 tablet per 10ml x10 RIPA buffer). 1x RIPA buffer was diluted from the x10 stock using deionised water. Cells were briefly washed in PBS and then either trypsinised and pelleted in Eppendorf tubes before lysis or lysed directly in cell culture dishes. 200-300µl x1 RIPA was added to the cells in each instance and the homogenate passed up and down an 18-gauge needle (BD Bioscience) to aid complete lysis. Lysate was transferred to a 1.5ml Eppendorf tube and the tube centrifuged in a PrismR Labnet centrifuge for 15 minutes at 14000 xg at 4°C to pellet the debris. The supernatant was transferred to a new 1.5ml Eppendorf tube. Bradford assays were carried out the same day as extraction or samples were stored at -80° C for later quantification.

### **2.10.2 NE-PER nuclear and cytoplasmic extraction kit**

Nuclear and cytoplasmic protein extraction was conducted with the NE-PER™ Nuclear and Cytoplasmic Extraction Reagents kit (Fisher Scientific, 78833) suitable for 50 pellet extractions. Adherent SW1353 and T/C-28a2 cells treated with or without IL-1α for 24 or 72 hours were washed in PBS and then dislodged with either a cell scraper or 0.05% trypsin (Fisher Scientific, 25300054) and collected into 1.5ml Eppendorf tubes. The amount of lysis reagent to add per sample was determined from the packed cell volume (PCV). For example, the volume ratio of cytoplasmic extraction reagent I: cytoplasmic extraction reagent II: nuclear extraction reagent (CERI:CERII:NER) was maintained 200:11:100µl for 20µl (~2x10<sup>6</sup> cells) PCV. The CERI and NER reagents were supplemented with EDTA-free Halt protease inhibitor cocktail (ThermoFisher Scientific, 78425) at x1 concentration (100-fold dilution). The CERII reagent did not require supplementation with Halt protease inhibitor cocktail. All steps, including centrifugation in a PrismR Labnet centrifuge, were carried out on ice or at 4°C.

After addition of ice-cold CER I, the sample was vortexed vigorously on the highest setting for 15 seconds to fully resuspend the cell pellet, followed by incubation on ice for 10 minutes. 11  $\mu$ l ice-cold CER II was added and the sample vortexed for five seconds on the highest setting followed by another incubation on ice for one minute. Another five second vortex was performed followed by a five minute centrifugation at 15981 xg. The cytoplasmic protein fraction was transferred to a pre-chilled Eppendorf tube. The nuclear pellet was washed with PBS to remove excess cytoplasmic proteins and prevent carryover of cytoplasmic protein into the nuclear fraction before the nuclei were resuspended in 100  $\mu$ l ice-cold NER reagent. The sample was vortexed for 15 seconds, placed on ice and then vortexed for 15 seconds every 10 minutes for a total of 40 minutes. The tube was centrifuged at 15981 xg for 10 minutes and the supernatant containing nuclear extract transferred to a pre-chilled Eppendorf tube. Extracts were stored at -80°C until quantification by Bradford assay (section 2.10.3).

### **2.10.3 Protein quantification by Bradford assay**

All protein samples were thawed on ice and then diluted five-fold with either RIPA buffer, CER I or NER dependent on whether the sample was a whole protein lysate or a cellular fraction. Bovine serum albumin (BSA) standard (ThermoFisher Scientific, 23209) ampules were used for generation of 10-point standard curve (0, 0.04, 0.08, 0.12, 0.16, 0.2, 0.24, 0.28, 0.32, 0.36 and 0.4  $\mu$ g/ $\mu$ l). A negative control of lysis buffer diluted five-fold with water was also incorporated. 10  $\mu$ l of diluted protein or standards were added to flat-bottom 96 well plates (Greiner Bio-One, 655101) and 150  $\mu$ l Bradford Ultra reagent (Expedeon, BFU05L) added to each well in duplicate, and the plate developed for five minutes in the dark before quantification of proteins at 595nm with a Varioskan Lux plate reader. For later experiments the Bradford assay was modified to improve the linearity of the line of best fit of the standard curve by additionally measuring absorbance at 450nm. The ratio of absorbance between 595 and 450nm was plotted against the dilution series and the concentration of the samples calculated from the line of best fit equation. The samples were diluted in 2x Laemmli buffer (Sigma, S3401) and deionised water so that the same volume and hence same amount of total protein was loaded for a particular western blot experiment and the sample was again frozen at -80°C for use later.

## 2.11 Western blot

MTF1 overexpression lysate was purchased from Origene (LC401804) and used as a positive control. Lysates from the GFP-transfected cells (section 2.8.9.2) were used as negative controls in western blots to test specificity of the c-myc and FLAG (CST 2368) antibodies. A spare unprobed western blot containing Cas9-FLAG tag overexpressing SW1353 cells transfected with different pairs of guides targeting exon one of *SOX9* was provided by Dr. Matt Barter, Newcastle University. This was used to test some commercially available anti-FLAG antibodies for the detection of FLAG in the samples.

### 2.11.1 SDS polyacrylamide gel electrophoresis

10 or 12% SDS polyacrylamide gels were made with 3ml or 3.6ml 40% acrylamide/bisacrylamide solution (Sigma, 01709), 3ml of 4x lower gel buffer (final concentration: 375mM Tris and 0.1% SDS) and the difference made up to 12ml with deionised water. Gels were polymerised by the addition of 60µl 20% ammonium persulfate (APS) (Sigma, A3678) and 20µl N,N,N',N'-Tetramethylethylenediamine (Sigma, T9281) and quickly cast between glass plates of BioRad Mini-Protean tetra-cell apparatus. A thin layer of isopropanol was pipetted on top of the gel to exclude oxygen and remove air bubbles. The isopropanol was washed away after complete polymerisation and the gels washed with deionised water. 6ml of pre-made stacking gel (acrylamide 4.5%, 4x upper gel buffer; Tris 500mM SDS 0.4%) was polymerised with 30µl 20% APS and 10µl TEMED and ~3ml was added on top of the set lower gels. The combs were inserted until the gels had completely polymerised.

After protein extraction (section 2.10), the samples were passed through a 2ml syringe (BD Plastipak™) 25mmx25 gauge needle (Scientific Laboratory Supplies, HSWNH251-100EA) to shear DNA and denatured at 100°C for five minutes. The BioRad apparatus containing the gel was put in an electrophoresis tank. The inner chamber was first filled with x1 running buffer (25mM Tris, 192mM glycine and 0.1% SDS) and the rest of the tank for 1.5L total. 3-20µg protein was loaded for different experiments, with the same amount of protein loaded per well per experiment. The PageRuler™ prestained protein ladder (Thermofisher Scientific, 26616) was loaded to determine the size of target proteins. Electrophoresis was carried out at 100V until the protein resolved through the stacking gel and later at 160V until the loading dye ran to the end of the gel.

### ***2.11.2 Blotting and probing***

The gel was transferred to a polyvinylidene difluoride (PVDF) membrane by wet transfer using x1 Towbin's buffer (25mM Tris, 192mM glycine and 15% methanol) in a transfer tank at 80mA/gel for 90-120 minutes. For some experiments semi-dry transfer was employed as it gave improved transfer results over transfers from wet transfer. The PVDF membranes were stained with neat ponceau S solution (Santa Cruz, 301558) for five minutes followed by counter-stain in deionised water to visualise protein transfer. The membrane was then blocked in 25ml of x1 TBS-Tween (10mM Tris, 154mM NaCl and 1% Tween 20) containing 5% milk powder (Marvel Original, Waitrose) for one hour at room temperature on a rocker.

After blocking, the membrane was washed three times in x1 TBS-Tween for five minutes each. Primary antibodies were diluted accordingly (Table 2.5) for western blot in 5ml 1x TBS-Tween with 5% BSA and 0.02% sodium azide before addition to the membrane for incubation at 4°C overnight or for one hour on a rocker in the case of GAPDH. The primary antibodies were recovered for subsequent usage, in some but not all western blots, and the blot was again washed three times as before. Horseradish peroxidase (HRP)-conjugated polyclonal goat anti-rabbit (Agilent Dako, P0448) or anti-mouse (Agilent Dako, P0447) secondary antibodies were diluted 2000-fold in 10ml of TBS-Tween with 5% milk and incubated with the blots for one hour at room temperature. The secondary antibody was discarded and the blot washed three times again for five minutes each.

The substrate for the HRP-conjugated secondary antibody was either enhanced chemiluminescent substrate (ECL) normal (Sigma, GERPN2106), mid-sensitivity substrate (Millipore, WBKLS0500) or ECL select high sensitivity substrate (Sigma, GERPN2235) with each reagent from the kit mixed 1:1. The normal and mid-sensitivity substrates were added to the blot for 3-4 minutes or one minute using the high sensitivity substrate, and kept in the dark whilst the Azure C600 chemiluminescent imager was prepared. All images captured had a calculated auto exposure time, often with cumulative images taken to select best image avoiding saturation. PageRuler™ prestained ladder was imaged separately and then the ladder was copied and pasted on to the rest of the blot with the region of interest tool, generating the composite image.

**Table 2.5 – Primary and secondary antibodies.**

Antibodies in blue are primary and in orange are secondary. WB = western blot and ICC = Immunocytochemistry.

<b>Antibody Name</b>	<b>Species &amp; Clonality</b>	<b>Manufacturer</b>	<b>Catalogue Number</b>	<b>Application</b>	<b>Dilution</b>
MTF1 N-terminal	Rabbit polyclonal	Human Protein Atlas	HPA028689	WB	0.4µg/ml
MTF1 (H-6) C-terminal	Mouse monoclonal	Santa Cruz	SC-365090	WB/ICC	2µg/ml (WB) 1µg/ml (ICC)
Clone OTI4C5, Anti-DDK (FLAG)	Mouse monoclonal	Origene	TA50011-100	WB	0.5µg/ml
DDK (FLAG)	Mouse monoclonal	Origene	TA180144	WB	0.5µg/ml
DYKDDDDK Tag	Rabbit polyclonal	Cell Signalling Technology (CST)	2368	WB/ICC	42ng/ml (WB) 840ng/ml (ICC)
c-myc	Mouse monoclonal	Roche	11667149001	WB/ICC	1µg/ml (WB) 4µg/ml (ICC)
Calnexin	Rabbit polyclonal	Enzo	ADI-SPA-860	WB	50ng/ml
PCNA	Mouse monoclonal	Santa Cruz	SC-56	WB	1µg/ml
Lamin A/C	Mouse monoclonal	Santa Cruz	SC-7292	WB	1µg/ml
Histone 2A	Rabbit polyclonal	Cell Signalling Technology (CST)	2572	WB	2000-fold
Anti-glyceraldehyde-3-phosphate dehydrogenase clone 6C5	Mouse monoclonal	Millipore	MAB374	WB	0.025µg/ml
Beta-actin	Mouse monoclonal	ProteinTech	60008-1-IG	ICC	3.3µg/ml
Goat anti-rabbit HRP	Goat polyclonal	Agilent, DAKO	P0448	WB	2000-fold
Goat anti-mouse HRP	Goat polyclonal	Agilent, DAKO	P0447	WB	2000-fold
Goat anti-mouse af488	Goat polyclonal	Fisher Scientific	A11029	ICC	10µg/ml or 4µg/ml
Goat anti-rabbit af594	Goat polyclonal	Fisher Scientific	A11037	ICC	10µg/ml or 4µg/ml

### **2.11.3 Densitometry analysis of western blot data**

Densitometry analysis using the publicly available software ImageJ (Schneider *et al.*, 2012) permitted semi-quantitative analysis of the western blot data. No plug-ins were required for the analysis and only the built-in draw rectangles and area measurement tools were required. For each observed protein band, whether protein of interest (FLAG antibody, CST 2368) or loading control protein, a rectangle of fixed size was drawn around each band per lane (sample) and the area measurements, equivalent to the pixel density was taken. Then the background measurements calculated with rectangles of fixed size from the same lane was subtracted from each sample on the blot.

The western blots for which this analysis was performed contained nuclear and cytoplasmic lysates extracted at 24 or 72 hours after treatments with 0.5ng/ml IL-1 $\alpha$ , 100 $\mu$ M ZnCl<sub>2</sub> or 0.5ng/ml IL-1 $\alpha$  + 100 $\mu$ M ZnCl<sub>2</sub>. There was a total of three experiments conducted in technical duplicate for a total of six biological samples per time point or 12 western blots. There was much greater variation across treatments between the nuclear and cytoplasmic lysates after plotting the pixel measurements corrected for background. For example, the 24 hour experiments had greater variation in the cytoplasmic samples and at 72 hours greater variation was observed in the nuclear samples compared to cytoplasmic lysates. Therefore, the samples were divided by either the control cytoplasmic pixel density measurement for the FLAG protein band for the 24 hour experiments or by the control nuclear pixel density measurement for the FLAG protein band for the 72 hour experiments. Finally, the pixel intensity measurements for the FLAG antibody for the nuclear or cytoplasmic samples were divided by the measurements calculated for their respective loading control e.g. lamin AC for nuclear samples and GAPDH for cytoplasmic samples. The resulting densitometry data was analysed by Wilcoxon t-test comparing controls against treatment within the same protein fraction across both 24 and 72 hour time points.

## **2.12 Immunocytochemistry (ICC)**

### ***2.12.1 ICC detection of c-myc-FLAG-tagged MTF1 protein in cells transiently transfected with the pCMV6-MTF1 c-myc-FLAG plasmid***

Eleven thousand two hundred and fifty SW1353 cells were seeded into each well of a 4-well permanox-coated chamber slide (Fisher Scientific) in 400µl DMEM/F12 medium and incubated at 37°C overnight. The next day two wells were transfected with 1µg of MTF1 expression plasmid using FuGENE HD™ Transfection Reagent (Promega, E2311). Chamber slides were incubated at 37°C incubator for 48 hours before the medium was removed and the cells washed in PBS. Cells were fixed in 250µl 10% neutral buffered formalin solution containing 4% formaldehyde (Sigma, HT501128) for 10 minutes on the bench. The fixative was removed and the wells gently washed in PBS twice, with no incubation period or plate rocker between washes. The cells were then permeabilised in 250µl 0.2% Triton X-100 detergent (diluted with PBS) for five minutes and washed another three times in PBS. The cells were blocked with 250µl 10% goat serum (Vector Laboratories, S-1000) to prevent non-specific binding of the primary antibodies for one hour at room temperature. The block was removed, 4µg/ml mouse monoclonal anti-c-myc antibody (Roche, 11667149001) or 1µg/ml monoclonal mouse anti-MTF1 antibody (Santa Cruz, 365090) added to the chambers, and incubated at room temperature for an hour. Untransfected cells were incubated at room temperature for an hour with a 10% goat serum and PBS solution (absent primary antibody) to later stain with 10µg/ml goat anti-mouse IgG af488 (Fisher Scientific, A11029) or 4µg/ml mouse monoclonal anti-c-myc antibody to determine if this antibody is specific. The chamber slide was washed three times with PBS before addition of 10µg/ml goat anti-mouse IgG af488 (Fisher Scientific, A11029) diluted in 10% goat serum/PBS solution to all wells and incubated again at room temperature for 60 minutes. Unbound secondary antibody was discarded and after a final PBS wash the chamber was removed from the slide which was mounted in aqueous VECTASHIELD™ Antifade Mounting Medium with DAPI (H-1200). The slides were covered with a glass coverslip (VWR, 631-1574) and images captured with a Zeiss Axioplan fluorescent microscope. The percentage of localised nuclear protein was calculated as the sum of the nuclear only counts for a target protein divided by cytoplasmic and nuclear stained target protein multiplied by 100 from a total of three fields of view per well per condition.

### **2.12.2 Detection of c-myc-FLAG-tagged MTF1 protein in stable MTF1 overexpressing SW1353 cells**

The stably selected MTF1 overexpressing SW1353 cells generated previously (section 2.9.3) were assessed for production of the encoded MTF1-MYC-FLAG tagged protein by ICC. As a positive control for the transfection, HEK293 cells were also transfected with the pCMV6-MTF1 c-myc-FLAG plasmid in these experiments. HEK293 cells were cultured in 10cm dishes containing DMEM (Fisher Scientific, 11965092) with 2mM L-glutamine, 10% FBS (Sigma, F9665), 100U/ml penicillin/streptomycin and 50U/ml nystatin prior to seeding into chamber slides. Four wells of an eight-well chamber slide (Fisher Scientific, 154534) were seeded with  $7.5 \times 10^3$  SW1353 cells and the remaining four wells seeded in duplicate with either AgeI-digested MTF1 overexpressing SW1353 or HEK293 cells and incubated at 37°C for 24 hours. AgeI-digested MTF1 overexpressing SW1353 cells were supplemented with 500µg/ml G418 in the medium to maintain the selection pressure. One microgram MTF1 plasmid was transfected into two wells containing SW1353 or HEK293 cells were incubated at 37°C for 48 hours before immunostaining. Untransfected SW1353 wells had 100µl medium replaced instead of transfection. Cells were fixed, permeabilised, blocked and stained as described previously and the correct concentration of 0.5% TritonX-100 detergent for permeabilisation was used. The primary antibodies used in the detection of MTF1 were 1µg/ml monoclonal mouse anti-MTF1 antibody (Santa Cruz, 365090) or 840ng/ml polyclonal rabbit anti-FLAG antibody (CST, 2368) incubated at room temperature for one hour for four wells each per cell line. 10µg/ml of goat anti-mouse IgG af488 or goat anti-rabbit IgG af594 diluted in 10% goat serum/PBS solution was added to the appropriate wells for one hour at room temperature. The same experiment was repeated but substituting the AgeI-digested linear MTF1 overexpressing SW1353 cells with the circular MTF1 overexpression SW1353 line (Appendix D).

### ***2.12.3 Determining MTF1 cellular localisation following IL-1 $\alpha$ and/or ZnCl $_2$ treatment of linear MTF1 overexpressing SW1353 cell line for 24 or 72 hours***

Two eight-well chamber slides were seeded with  $7.5 \times 10^3$  linear MTF1 overexpressing SW1353 cells per well for four hours. The media from one chamber slide was removed and replaced with medium alone or medium containing 0.25ng/ml IL-1 $\alpha$ , 100 $\mu$ M ZnCl $_2$  or both 0.25ng/ml IL-1 $\alpha$  + 100 $\mu$ M ZnCl $_2$  and incubated for 72 hours at 37°C. Forty eight hours after treatment, the second chamber slide was also stimulated with 0.25ng/ml IL-1 $\alpha$ , 100 $\mu$ M ZnCl $_2$  or both 0.25ng/ml IL-1 $\alpha$  and 100 $\mu$ M ZnCl $_2$  for 24 hours, after which both chamber slides were fixed for 10 minutes in 10% neutral buffered formalin solution containing 4% formaldehyde on the bench followed by cell permeabilisation (0.5% Triton X-100) for five minutes. The primary antibody concentration for the anti-FLAG (CST, 2368) was 280ng/ml and cells were stained alone or in combination with 3.3 $\mu$ g/ml beta-actin antibody (ProteinTech, 60008-1-IG) as a cytoplasmic protein reference. The secondary antibodies were used at 4 $\mu$ g/ml rather than the 10 $\mu$ g/ml used previously which is still in the manufacturer's tested range for goat anti-mouse IgG af488 but the goat anti-rabbit IgG af594 specifically states 4 $\mu$ g/ml which was overlooked. The rest of the staining protocol was the same as in 2.12.1 except I increased the primary antibody incubation to overnight at 4°C and the secondary antibody incubation to two hours.

### ***2.12.4 Zeiss Axioplan fluorescence microscope calibration***

The GFP band pass filter was used to detect MTF1 in chamber slides stained either solely with green fluorochrome af488 IgG antibody or in combination with red fluorochrome af594 IgG antibody. However, in the first ICC experiment, the GFP long pass filter for wells stained with goat anti-mouse IgG af488 only was used. The af594 filter for any cells stained with the af594 IgG antibody was always used. Setting the exposure time for each channel across all samples of an experiment was dependent on whether HEK293 cells were used as a positive control. If HEK293 cells were used the exposure time in that well was reduced until the signal was undetected and that exposure time applied to all other samples. Alternatively, secondary antibody only controls were used where signal generated in the channel should not be observed and if detectable the exposure time decreased again until not visible and this time applied to all samples. Three or four images were captured per well after camera calibration and the cells were counted manually with help from Raul Fulea. Attempts were made to automate the counting procedure akin to methods for counting chondrocytes in the growth plate using ImageJ, however I found that the software would too easily amalgamate groups of cells which led to inaccurate measurements.

## 2.13 Luciferase assays

### 2.13.1 SW1353 & T/C-28a2 luciferase assays

SW1353 and T/C-28a2 cells were seeded into 96 well plates (Greiner Bio-One, 655101) at  $5 \times 10^3$  cells/well in 100 $\mu$ l DMEM/F12 medium (Fisher Scientific, 11320074) supplemented with 2mM L-glutamine (Fisher Scientific, 25030024), 10% FBS (Sigma, F9665), 100U/ml penicillin-streptomycin (Fisher Scientific, 15140122) and 50U/ml nystatin (Sigma, N1638) and incubated at 37°C. Twenty four hours later, cells were transfected with either 100ng/well of the pGL4.40[luc2P/MRE/Hygro] (Promega, E4131) or the empty control pGL4.40 luciferase plasmids. Six nanograms per well of *Renilla* luciferase TK control reporter vector (Promega, E2241) was used in all wells to normalise the data and control for the transfection efficiencies between wells.

Twenty-four hours after transfection the medium was removed from all wells and the cells were treated with medium alone, IL-1 $\alpha$  (0.5ng/ml-SW1353, 0.25ng/ml- T/C-28a2), IL-1 $\beta$  (5ng/ml-SW1353, 2.5ng/ml-T/C-28a2), 100 $\mu$ M ZnCl<sub>2</sub> or both IL-1 $\alpha$  (0.5ng/ml-SW1353, 0.25ng/ml- T/C-28a2) and 100 $\mu$ M ZnCl<sub>2</sub>. After a final 24 hours incubation the medium was removed and the cells rinsed once in PBS. The cells were lysed in fresh Passive Lysis Buffer (Promega, E1941) and the luciferase activity was determined using the Dual-Luciferase® Reporter Assay System (Promega, E1910) on a GloMax-Multi Detection System (Promega). The firefly luciferase activity was normalised against the activity of the renilla luciferase, and further normalised against the empty control pGL4.40 luciferase plasmid for the same treatment group. This was executed in case the treatments unexpectedly influenced the luciferase expression in cells transfected with the empty control pGL4.40 luciferase plasmid. Four biological and six technical repeats were performed for each cell line.

### **2.13.2 Luciferase activity comparing MTF1 overexpression and endogenous MTF1 activity in SW1353 cells**

The linear MTF1 overexpression SW1353 cell line generated in section 2.9.3 and untransfected SW1353 cells were seeded into 96 well plates (Greiner Bio-One, 655101) at  $5 \times 10^3$  cells/well in 100 $\mu$ l DMEM/F12 medium (Fisher Scientific, 11320074) supplemented with 2mM L-glutamine (Fisher Scientific, 25030024), 10% FBS (Sigma, F9665) , 100U/ml penicillin-streptomycin (Fisher Scientific, 15140122) and 50U/ml nystatin (Sigma, N1638). 24 hours later cells were transfected with either 100ng/well of the pGL4.40[luc2P/MRE/Hygro] plasmid (Promega, E4131) or the empty control pGL4.40 luciferase plasmid. Six nanograms per well of *Renilla* luciferase reporter plasmid (Promega) was used in all wells to normalise the data and control for the transfection efficiencies between wells.

Twenty-four hours after transfection the medium was removed from all wells and the cells were treated with medium alone, 0.5ng/ml IL-1 $\alpha$ , 100 $\mu$ M ZnCl<sub>2</sub> or both 0.5ng/ml IL-1 $\alpha$  and 100 $\mu$ M ZnCl<sub>2</sub>. After a final 24 hours incubation the medium was removed, and the cells rinsed once in PBS. The cells were lysed in fresh Passive Lysis Buffer (Promega) and the luciferase activity was determined using the Dual-Luciferase® Reporter Assay System (Promega, E1910) on a GloMax-Multi Detection System (Promega). The firefly luciferase activity was normalised against the activity of the renilla luciferase, and further normalised against the empty control pGL4.40 luciferase plasmid for the same treatment group. Four biological and six technical repeats were performed for each cell line. The luciferase data was first screened for normality by D'Agostino-Pearson omnibus k2 test ( $n \geq 8$  means) and control vs treatment pairings that passed were analysed by unpaired t-test with Welch's correction which does not assume equal variance of the groups, otherwise data was analysed by non-parametric Mann-Whitney test. Outliers in the raw firefly:renilla luciferase ratios were determined by addition or subtraction of 1.5 times the interquartile range of the 75<sup>th</sup> or 25<sup>th</sup> percentile respectively

## Chapter 3: *IN SILICO* ANALYSIS OF GENES INVOLVED IN THE CELLULAR HOMEOSTASIS OF ZINC

### 3.1 Introduction

As described in detail in section 1.4.2, the zinc-ZIP8-MTF1 axis was identified as a catabolic regulator of matrix metalloproteinase activity, contributing to OA pathogenesis (Kim *et al.*, 2014). *In vitro* and *in vivo* experiments together with transgenic mice models identified a key role for zinc homeostasis in OA pathogenesis. The zinc importer *Slc39a8* was upregulated in response to IL-1 treatment, leading to increased cytoplasmic levels of zinc which in turn triggered nuclear translocation of the MTF1 metal sensing transcription factor. MTF1 then upregulated the expression of several genes including *MTs*, *Mmp13* and *Adam-ts5*.

It is unknown if zinc homeostasis plays a role in human cartilage homeostasis and OA. Extrapolating these interesting mechanistic findings from mouse to human in relation to zinc homeostasis is challenging, not least because of the increase in *Mt* gene complexity from two in mice to 16 in humans, of which at least 11 are functional (Kimura and Kambe, 2016). However, the advent of SkeletalVis (<http://phenome.manchester.ac.uk/>), a new bioinformatics tool to analyse transcriptomic datasets from different species (including human and mouse) in different experimental contexts or diseases, allows one to perceive which genes are commonly associated with zinc homeostasis between different OA datasets. It also permits identification of overlapping transcriptomic signatures between species for an evolutionary appreciation of potentially common homeostatic mechanisms.

SkeletalVis is a publicly available repository of musculoskeletal transcriptomic datasets from microarrays and RNA-Seq platforms conducted across multiple tissues and species (Soul *et al.*, 2018b). This resource was created for two main purposes. Firstly, to increase the utility of published transcriptomics data using the entire dataset to identify previously over-looked features and secondly to standardise the analysis and integration of the data, enabling clear interpretation and to inform new promising avenues of research. The database can be mined for gene expression profiles and filtered by species, tissue, PubMed ID, expression platform and more. My approach was focussed to OA-relevant studies (Table 3.1) of both human and mice cartilage and chondrocytes, using the filtering tools in SkeletalVis (section 2.1.1).

### 3.2 Chapter aims

The aim of this chapter is to use *in silico* tools and existing datasets to examine if dysregulated zinc homeostasis may contribute to human OA pathogenesis.

Using SkeletalVis, the following questions were addressed:

- Are zinc homeostasis genes dysregulated in a human OA cartilage setting compared to non-OA controls?
- Are zinc homeostasis genes dysregulated in damaged versus intact human OA cartilage of the same joint?
- Do inflammatory mediators, namely IL-1 $\alpha$  or IL-1 $\beta$ , affect zinc homeostasis genes in human chondrocytes cultured *in vitro*?
- Do murine models of OA and cultured murine chondrocytes share any directionally dysregulated zinc gene signatures in common with human studies?

Using LDlink and GTEx databases:

- Identify and present SNP eQTL associations by plotting venn-diagrams of separate SNP lists for each of the five OA-susceptibility or mjsw width GWAS SNPs against the respective eQTL SNP lists for the corresponding genomic locus.

### 3.3 Transcriptomic datasets

Using the SkeletalVis ‘Explore’ tool, the 300 transcriptomic datasets were searched to identify relevant key words “osteoarthritis”, “cartilage”, “chondrocyte” and “IL-1”. A total of 17 human and eight murine datasets were identified based on these terms. After selecting an experiment, the factor(s) to be compared within the experiment were selected in the “Choose a Comparison” window and each microarray or RNA-Seq study was assessed for quality control, which was determined by viewing the principal component analysis (PCA) plots. Thus, a total of 13 datasets were chosen for further analysis. Data for all 24 zinc transporters, *MTF1*, *MTF2*, *SP1* and 11 *MTs* were extracted for each study. Additional genes of interest for chondrocyte studies were the pro-inflammatory genes *IL-6*, *CXCL8* (encoding IL-8), *CCL2*, the matrix metalloproteinases *MMP3*, *MMP9*, *MMP12*, *MMP13*, and the aggrecanase *ADAM-TS5*. Expression data relating to *Cxcl8* was unavailable for the murine chondrocyte microarrays. Differentially expressed genes between experiments of similar design, or different time points within the same experiment, were identified and recorded (Tables 3.2-3.7). The normalised microarray signals or read counts of the significantly and differentially expressed genes were obtained for every sample in each of the studies with assistance from Dr. Jamie Soul.

**Table 3.1 – Human (1-9) and murine (10-13) OA transcriptomics datasets identified through SkeletalVis.**

dOA = damaged OA cartilage, iOA = intact OA cartilage, DMM = destabilisation of the medial meniscus, OSM = oncostatin M, OA = osteoarthritis.

Study	Reference	Tissue	Type	Comparison	Sample Size (N)
1	(Fisch <i>et al.</i> , 2018)	knee cartilage	RNA-Seq	iOA vs non OA	20 iOA vs 18 non OA
2	(Soul <i>et al.</i> , 2018a)	knee cartilage	RNA-Seq	iOA vs non OA	60 iOA vs 10 non OA
3	(Dunn <i>et al.</i> , 2016)	knee cartilage	RNA-Seq	dOA vs iOA	8 dOA vs 8 iOA
4	(Xu <i>et al.</i> , 2012)	hip cartilage	microarray	iOA vs non OA	12 iOA vs 13 non OA
5	(Ramos <i>et al.</i> , 2014)	hip and knee cartilage	microarray	dOA vs iOA	33 dOA vs 33 iOA
				iOA vs non OA	33 iOA vs 7 non OA
6	(Pearson <i>et al.</i> , 2016)	hip chondrocytes	RNA-Seq	1ng/ml IL-1 $\beta$ vs control	3 donors (hip OA)
7	(Moazedi-Fuerst <i>et al.</i> , 2016)	knee chondrocytes	microarray	10ng/ml IL-1 $\beta$ vs control	4 donors (knee OA)
8	(Comblain <i>et al.</i> , 2016)	knee chondrocytes	microarray	10pM IL-1 $\beta$ vs control	12 donors (knee OA)
9	(Chan <i>et al.</i> , 2017)	knee chondrocytes	microarray	0.05ng/ml IL-1 $\alpha$ and 10 $\mu$ g/ml OSM vs control	3 donors (knee OA)
Study	Reference	Tissue	Type	Comparison	Sample Size (N)
10	(Burleigh <i>et al.</i> , 2012)	Whole-joint (excluding skin and skeletal muscle)	microarray	DMM vs sham (independent mice knee joints)	21 3 mice/group/time point
11	(Bateman <i>et al.</i> , 2013)	cartilage	microarray	DMM vs sham (contralateral knee)	12 4 mice/group/time point
12	(Poulet <i>et al.</i> , 2012)	cartilage	microarray	ageing OA model vs CBA mice	24 4 mice/group/time point
13	GSE104793 (unpublished)	chondrocytes	microarray	IL-1 $\beta$ vs control	6 3 mice/group

### 3.4 Several zinc transporters are differentially expressed in OA cartilage compared to non-OA cartilage

To investigate if genes involved in zinc homeostasis are dysregulated in undamaged intact OA cartilage, datasets that compared intact OA cartilage to cartilage from patients without OA were analysed. The experimental groups for the microarray and RNA-Seq comparing human cartilage with control knee cartilage (referred to as non-OA subsequently) can be classified as knee (Fisch *et al.*, 2018; Soul *et al.*, 2018a), hip (Xu *et al.*, 2012), or combined hip and knee (Ramos *et al.*, 2014) cartilage. The controls between each study are not all uniform and are worth defining herein. Firstly, Fisch *et al.*, 2018 used full-thickness intact OA knee cartilage (iOA) from patients undergoing joint replacement and sourced non-OA cartilage from cadavers 48 hours after death with no history of OA or joint trauma. Soul *et al.*, 2018 also used iOA knee cartilage sourced at time of surgery and used control articular cartilage of above knee amputees who had vascular disease but no history of OA (referred to as non-OA in figures). Xu *et al.*, 2012 compared iOA hip cartilage with cartilage from patients who had NOF fractures (also referred to as non-OA subsequently). Dunn *et al.*, 2016 performed ipsilateral analyses of damaged OA cartilage (dOA) against iOA regions of knee cartilage. Ramos *et al.*, 2014 compared hip and knee dOA or iOA against non-OA ‘healthy’ controls but there is no further description of these controls beyond this in the paper or supplementary data. Furthermore, the dOA versus non-OA comparison from Ramos *et al.*, 2014 was not assessed because this was a stand-alone cartilage study and the other groups had all used iOA cartilage.

The results of the OA vs non-OA gene expression analyses for each of the four studies are summarised for the genes of interest in Table 3.2. The log<sub>2</sub>-fold changes, fold changes and adjusted p-values generated by SkeletalVis are illustrated; for some genes, there were several probes on the microarray and the data for each is given. A gene was said to be differentially expressed in OA cartilage if it was significantly and differentially expressed (FDR p<0.05) in the same direction in at least three of the datasets. Using these criteria, the zinc exporter gene *SLC30A2* and the zinc importer genes *SLC39A3*, *SLC39A7* and *SLC39A14* were identified as differentially expressed (Figure 3.1). *SLC30A2* and *SLC39A14* were downregulated and *SLC39A3* and *SLC39A7* were upregulated. *SP1*, *MTF1* or *MTF2*, proposed to mediate zinc signalling, were not significantly altered. A number of class I MTs were down-regulated significantly in both iOA knee cartilage RNA-Seq datasets (Table 3.2) but only *MT1A* and *MT1X* were significantly down-regulated in three of four iOA knee or hip cartilage datasets compared to their respective non-OA controls (Figure 3.2).

**Table 3.2 - SkeletalVis data from four human preserved OA cartilage versus non-OA cartilage datasets for genes involved in zinc homeostasis.** The log<sub>2</sub>-fold change (log<sub>2</sub>FC), fold change (FC) and adjusted p-value (padj) is recorded for each gene entry and fold change is relative to the fold change has been formatted across all genes and datasets using a three colour scheme indicating differential gene downregulation in OA (blue), no change (white) and upregulation in OA (red). Expression data in bold are significantly and differentially expressed in OA for one or more datasets. Gene names in bold are significantly and differentially expressed unidirectionally in OA for 75% of datasets. Where there were fewer than four probes for a particular gene on the microarray NA was used to indicate this. If NA is confined to padj only column, then the p value was not calculated because of insufficient replicates.

Datasets	GSE114007			E-MTAB-6266			PMID:22659600									GSE57218 B														
References	Fisch <i>et al.</i> , 2018			Soul <i>et al.</i> , 2018			Xu <i>et al.</i> , 2012									Ramos <i>et al.</i> , 2014														
Platforms	RNA-Seq			RNA-Seq			Illumina HumanHT-12 V3.0 expression beadchip microarray									Illumina HumanHT-12 V3.0 expression beadchip microarray														
N numbers	20 OA knee vs 18 control knee			60 OA knee vs 10 control knee			12 OA hip vs 13 NOF									33 OA (67% hips and 33% knees <b>intact</b> ) vs 7 controls (29% hips and 71% knees)														
Control definitions	post-mortem tissue collected 48hours no history OA or joint trauma			above knee amputees of patients with vascular disease and no history or clinical sign of OA			patients with neck of femur fracture									non-OA 'described as 'healthy'														
Mean age groups	66 vs 38			72 vs 64			72 vs 76									66.2 vs 39.9														
% female	60 vs 28			45 vs 10			100 vs 100									61vs 86														
ZnT zinc exporter gene family																														
Gene name	log2 FC	FC	padj	log2 FC	FC	padj	probe 1			probe 2			probe 3			probe 4			probe 1			probe 2			probe 3			probe 4		
							log2 FC	FC	padj	log2 FC	FC	padj	log2 FC	FC	padj	log2 FC	FC	padj	log2 FC	FC	padj	log2 FC	FC	padj	log2 FC	FC	padj	log2 FC	FC	padj
<i>SLC30A1</i>	0.299	1.2	0.381	<b>-0.436</b>	<b>0.7</b>	<b>0.016</b>	-0.178	0.9	0.056	<b>-0.178</b>	<b>0.9</b>	<b>0.028</b>	NA			NA			0.020	1.0	0.885	0.035	1.0	0.668	NA			NA		
<i>SLC30A2*</i>	<b>-0.623</b>	<b>0.6</b>	<b>0.008</b>	<b>-0.994</b>	<b>0.5</b>	<b>0.003</b>	-0.064	1.0	NA	-0.367	0.8	0.172	NA			NA			<b>-0.169</b>	<b>0.9</b>	<b>0.004</b>	<b>-0.316</b>	0.8	<b>0.050</b>	NA			NA		
<i>SLC30A3</i>	0.427	1.3	0.330	-0.644	0.6	0.263	-0.016	1.0	0.814	NA			NA			NA			0.013	1.0	0.875	NA			NA			NA		
<i>SLC30A4</i>	0.180	1.1	0.291	0.227	1.2	0.125	-0.018	1.0	NA	-0.053	1.0	NA	NA			NA			-0.041	1.0	NA	-0.042	1.0	0.602	NA			NA		
<i>SLC30A5</i>	<b>0.548</b>	<b>1.5</b>	<b>0.006</b>	<b>0.274</b>	<b>1.2</b>	<b>0.023</b>	<b>0.427</b>	<b>1.3</b>	<b>0.000</b>	0.068	1.0	0.060	<b>0.182</b>	<b>1.1</b>	<b>0.036</b>	0.038	1.0	0.229	<b>0.222</b>	<b>1.2</b>	<b>0.020</b>	-0.096	0.9	NA	<b>-0.202</b>	<b>0.9</b>	<b>0.008</b>	-0.031	1.0	NA
<i>SLC30A6</i>	0.296	1.2	0.105	<b>0.383</b>	<b>1.3</b>	<b>0.000</b>	<b>-0.210</b>	<b>0.9</b>	<b>0.033</b>	0.002	1.0	0.966	NA			NA			0.020	1.0	NA	0.002	1.0	0.988	NA			NA		
<i>SLC30A7</i>	0.273	1.2	0.282	<b>0.370</b>	<b>1.3</b>	<b>0.012</b>	0.170	1.1	0.206	NA			NA			NA			0.109	1.1	0.464	NA			NA			NA		
<i>SLC30A8</i>	0.143	1.1	0.863	0.630	<b>1.5</b>	0.117	0.002	1.0	NA	NA			NA			NA			0.016	1.0	0.859	NA			NA			NA		
<i>SLC30A9</i>	0.207	1.2	0.426	0.058	1.0	0.690	<b>0.177</b>	<b>1.1</b>	<b>0.002</b>	NA			NA			NA			-0.113	0.9	0.206	NA			NA			NA		
<i>SLC30A10</i>	-0.107	0.9	0.818	0.218	1.2	NA	0.014	1.0	NA	NA			NA			NA			0.058	1.0	NA	NA			NA			NA		
ZIP zinc importer gene family																														
<i>SLC39A1</i>	0.074	1.1	0.834	<b>-0.245</b>	<b>0.8</b>	<b>0.004</b>	<b>-0.335</b>	<b>0.8</b>	<b>0.003</b>	NA			NA			NA			0.119	1.1	0.619	NA			NA			NA		
<i>SLC39A2</i>	0.185	1.1	NA	0.569	<b>1.5</b>	0.244	0.053	1.0	NA	NA			NA			NA			-0.004	1.0	NA	NA			NA			NA		
<i>SLC39A3*</i>	0.238	1.2	0.228	<b>0.363</b>	<b>1.3</b>	<b>0.031</b>	<b>0.171</b>	<b>1.1</b>	<b>0.023</b>	<b>0.419</b>	<b>1.3</b>	<b>0.002</b>	0.022	1.0	NA	0.058	1.0	0.834	<b>0.195</b>	<b>1.1</b>	<b>0.012</b>	<b>0.339</b>	<b>1.3</b>	<b>0.014</b>	0.000	1.0	0.996	NA		
<i>SLC39A4</i>	0.049	1.0	0.908	-0.054	1.0	0.827	-0.035	1.0	NA	0.009	1.0	0.834	NA			NA			-0.020	1.0	NA	-0.017	1.0	NA	0.035	1.0	0.745	NA		
<i>SLC39A5</i>	0.976	<b>2.0</b>	0.054	-0.376	0.8	0.800	0.015	1.0	NA	NA			NA			NA			-0.039	1.0	0.639	NA			NA			NA		
<i>SLC39A6</i>	0.315	1.2	0.076	<b>0.289</b>	<b>1.2</b>	<b>0.006</b>	0.151	1.1	0.127	0.165	1.1	0.225	NA			NA			0.016	1.0	0.907	0.084	1.1	0.579	NA			NA		
<i>SLC39A7*</i>	0.313	1.2	0.194	<b>0.570</b>	<b>1.5</b>	<b>0.000</b>	0.117	1.1	0.081	<b>0.068</b>	<b>1.0</b>	<b>0.050</b>	NA			NA			0.065	1.0	0.539	<b>0.177</b>	<b>1.1</b>	<b>0.006</b>	NA			NA		
<i>SLC39A8</i>	0.225	1.2	0.403	<b>0.289</b>	<b>1.2</b>	<b>0.006</b>	0.076	1.1	0.922	0.195	1.1	0.305	NA			NA			0.393	1.3	0.075	<b>0.361</b>	<b>1.3</b>	<b>0.002</b>	NA			NA		
<i>SLC39A9</i>	<b>0.457</b>	<b>1.4</b>	<b>0.002</b>	<b>0.472</b>	<b>1.4</b>	<b>0.000</b>	-0.005	1.0	0.966	NA			NA			NA			-0.002	1.0	0.988	NA			NA			NA		
<i>SLC39A10</i>	-0.344	0.8	0.060	0.087	1.1	0.733	<b>0.245</b>	<b>1.2</b>	<b>0.000</b>	NA			NA			NA			-0.015	1.0	0.883	NA			NA			NA		
<i>SLC39A11</i>	0.122	1.1	0.726	<b>0.800</b>	<b>1.7</b>	<b>0.000</b>	<b>0.617</b>	<b>1.5</b>	<b>0.000</b>	NA			NA			NA			-0.097	0.9	0.509	NA			NA			NA		
<i>SLC39A12</i>	1.259	<b>2.4</b>	0.230	-0.016	1.0	NA	0.018	1.0	NA	NA			NA			NA			0.003	1.0	NA	NA			NA			NA		
<i>SLC39A13</i>	0.331	1.3	0.323	<b>0.416</b>	<b>1.3</b>	<b>0.000</b>	-0.012	1.0	0.819	NA			NA			NA			0.007	1.0	0.964	NA			NA			NA		
<i>SLC39A14*</i>	<b>-1.349</b>	<b>0.4</b>	<b>0.000</b>	<b>-1.182</b>	<b>0.4</b>	<b>0.000</b>	<b>-1.674</b>	<b>0.3</b>	<b>0.000</b>	NA			NA			NA			0.115	1.1	0.759	NA			NA			NA		
Transcription factors																														
<i>SP1</i>	<b>-0.577</b>	<b>0.7</b>	<b>0.008</b>	-0.100	0.9	0.335	<b>0.182</b>	<b>1.1</b>	<b>0.000</b>	NA			NA			NA			0.030	1.0	0.804	NA			NA			NA		
<i>MTF1</i>	0.339	1.3	0.192	<b>0.402</b>	<b>1.3</b>	<b>0.002</b>	0.074	1.1	0.261	NA			NA			NA			-0.142	0.9	0.218	NA			NA			NA		
<i>MTF2</i>	<b>0.451</b>	<b>1.4</b>	<b>0.009</b>	0.219	1.2	0.114	-0.106	0.9	0.069	NA			NA			NA			0.061	1.0	0.420	NA			NA			NA		
Metallothioneins																														
<i>MT1A*</i>	<b>-1.626</b>	<b>0.3</b>	<b>0.001</b>	<b>-1.618</b>	<b>0.3</b>	<b>0.000</b>	<b>-1.108</b>	<b>0.5</b>	<b>0.000</b>	NA			NA			NA			-0.279	0.8	0.363	NA			NA			NA		
<i>MT1B</i>	0.096	1.1	NA	-0.010	1.0	NA	0.001	1.0	NA	NA			NA			NA			-0.032	1.0	NA	NA			NA			NA		
<i>MT1E</i>	-0.762	0.6	0.142	<b>-2.603</b>	<b>0.2</b>	<b>0.000</b>	<b>-0.634</b>	<b>0.6</b>	<b>0.007</b>	0.420	1.3	0.222	NA			NA			0.082	1.1	0.878	0.485	1.4	0.404	NA			NA		
<i>MT1F</i>	0.618	<b>1.5</b>	0.168	<b>-1.102</b>	<b>0.5</b>	<b>0.000</b>	-0.432	0.7	0.175	NA			NA			NA			0.381	1.3	0.369	NA			NA			NA		
<i>MT1G</i>	0.600	<b>1.5</b>	0.273	<b>-2.267</b>	<b>0.2</b>	<b>0.000</b>	<b>-1.952</b>	<b>0.3</b>	<b>0.000</b>	NA			NA			NA			0.205	1.2	0.834	NA			NA			NA		
<i>MT1H</i>	0.044	1.0	0.877	<b>-1.797</b>	<b>0.3</b>	<b>0.000</b>	<b>-1.529</b>	<b>0.3</b>	<b>0.000</b>	<b>-0.307</b>	<b>0.8</b>	<b>0.008</b>	NA			NA			0.267	1.2	0.708	0.004	1.0	0.969	NA			NA		
<i>MT1M</i>	-0.989	0.5	0.062	-2.671	<b>0.2</b>	<b>0.000</b>	<b>-1.668</b>	<b>0.3</b>	<b>0.000</b>	NA			NA			NA			-0.242	0.8	0.663	NA			NA			NA		
<i>MT1X*</i>	<b>-1.149</b>	<b>0.5</b>	<b>0.021</b>	<b>-2.229</b>	<b>0.2</b>	<b>0.000</b>	<b>-0.811</b>	<b>0.6</b>	<b>0.000</b>	NA			NA			NA			-0.483	0.7	0.060	NA			NA			NA		
<i>MT2A</i>	-0.836	0.6	0.084	<b>-2.552</b>	<b>0.2</b>	<b>0.000</b>	<b>-1.537</b>	<b>0.3</b>	<b>0.000</b>	NA			NA			NA			-0.211	0.9	0.604	NA			NA			NA		
<i>MT3</i>	<b>-1.279</b>	<b>0.4</b>	<b>0.029</b>	-0.314	0.8	0.730	<b>-0.306</b>	<b>0.8</b>	<b>0.050</b>	NA			NA			NA			<b>0.356</b>	<b>1.3</b>	<b>0.000</b>	NA			NA			NA		
<i>MT4</i>	0.022	1.0	NA	NA	NA	NA	0.029	1.0	NA	NA			NA			NA			0.013	1.0	NA	NA			NA			NA		

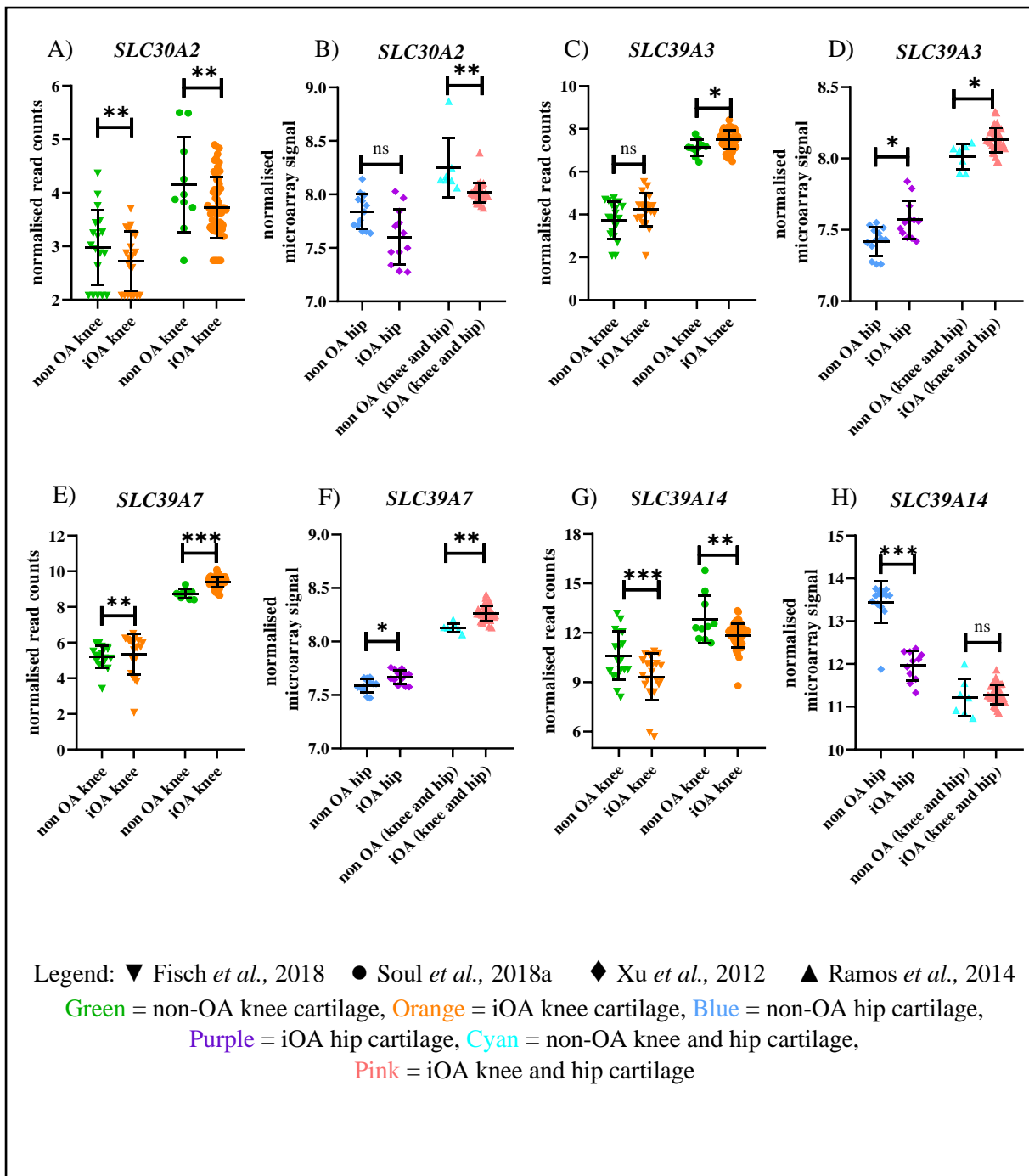


**Figure 3.1 – *SLC30A2*, *SLC39A3*, *SLC39A7* and *SLC39A14* zinc transporters are significantly and differentially regulated in intact knee, hip or knee and hip OA cartilage versus non-OA cartilage.**

Normalised data for *SLC30A2*, *SLC39A3*, *SLC39A7* or *SLC39A14* are expressed as read counts or (A, C, E and G) microarray signals (B, D, F and H) dependent on the platform used and were generated by Dr Jamie Soul upon request and are not provided by the SkeletalVis tool. The horizontal lines are the means of the samples with the standard deviation plotted. P values for significantly and differentially expressed genes were calculated in SkeletalVis (Soul *et al.*, 2018b). \*  $p < 0.05$  \*\*  $p < 0.01$  \*\*\*  $p < 0.001$ .

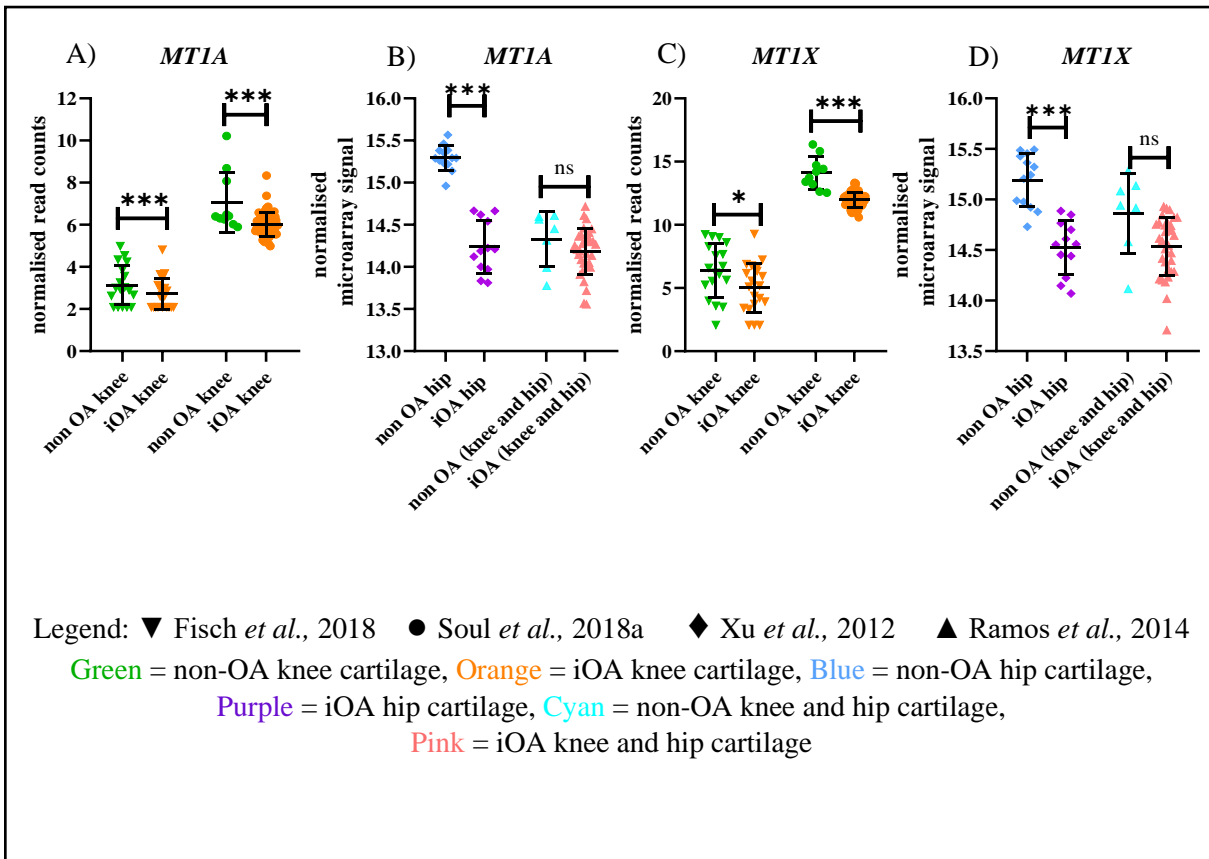


**Figure 3.2 – *MTIA* and *MTIX* are significantly and differentially expressed in iOA cartilage versus non-OA cartilage.**

Normalised data for *MTIA* and *MTIX* are expressed as read counts (A and C) or microarray signals B and D) dependent on the platform used by the research group specified in the legend and were generated by Dr Jamie Soul upon request and are not provided by the SkeletalVis tool. The horizontal lines are the means of the samples with the standard deviation plotted. P values for significantly and differentially expressed genes were calculated in SkeletalVis (Soul *et al.*, 2018b). \* p<0.05 \*\*\* p<0.001.

### 3.5 *SLC39A14*, *MT1F*, *MT1G* and *MT1M* are upregulated in damaged OA cartilage.

As several genes involved in zinc homeostasis are dysregulated in human OA cartilage, I examined whether these genes had altered expression in lesioned dOA cartilage compared to undamaged iOA cartilage from the same joint. Two transcriptomic datasets were available on SkeletalVis for analysis. These were the Dunn *et al.*, 2016 RNA-Seq dataset and the Ramos *et al.*, 2014 microarray dataset. The former performed ipsilateral analyses of dOA cartilage against iOA regions of knee cartilage, and the latter performed a similar analysis of OA knee and OA hip cartilage combined. A gene was said to be significantly and differentially expressed in dOA cartilage compared to iOA cartilage if the p-value generated in SkeletalVis was below the FDR  $p < 0.05$  threshold in the same direction in both Dunn *et al.*, 2016 and Ramos *et al.*, 2014 datasets. Fewer zinc homeostasis genes were significantly and differentially altered when the comparison being made was from a damaged region of an OA joint compared to an intact region (Table 3.3). For example, no zinc exporter genes were significantly and differentially expressed in both datasets, though *SLC30A1* almost reached significance ( $p=0.058$ ) for the Ramos *et al.*, 2014 comparison and was already significant ( $p=0.000$ ) for Dunn *et al.*, 2016. Among the zinc importers only *SLC39A14* (Figure 3.3) was altered in both datasets (Dunn *et al.*, 2016  $p=0.003$ ; Ramos *et al.*, 2014  $p=0.001$ ). The transcription factors *SPI1*, *MTF1* and *MTF2* were not significantly and differentially expressed. *MT1F*, *MT1G* and *MT1M* (Figure 3.4) were significantly and differentially expressed among the *MT* genes (Table 3.3). Compared to iOA cartilage versus non-OA cartilage datasets, *SLC39A14* and the *MTs* were differentially upregulated suggesting these genes may be more pertinent to OA progression in the establishment of tissue damage or after the event.

**Table 3.3 – SkeletalVis data from two human ipsilateral damaged OA versus intact OA cartilage datasets for genes involved in zinc homeostasis.**

The log<sub>2</sub>-fold change (log<sub>2</sub>FC), fold change (FC) and adjusted p-value (padj) is recorded for each gene entry and the fold change has been formatted across all genes and datasets using a three colour scheme indicating differential gene downregulation in dOA cartilage (blue), no change (white) and upregulation in dOA cartilage (red). Data in bold are significantly and differentially expressed in dOA for at least one dataset. Gene names in bold are significantly and differentially expressed unidirectionally in dOA for both datasets. Where there were fewer than four probes for a particular gene on the microarray NA was used to indicate this. If NA is confined to padj only column, then the p value was not calculated because of insufficient replicates.

Dataset	E-MTAB-4304			GSE57218 B											
Reference	Dunn <i>et al.</i> , 2016			Ramos <i>et al.</i> , 2014											
Platform	RNA-seq			Illumina HumanHT-12 V3.0 expression beadchip microarray											
N number	8 OA knee distal medial condyle vs posterior lateral condyle			33 OA (22 hips and 11 knees <b>damaged</b> ) vs 33 OA (22 hips and 11 knees <b>intact</b> )											
Mean age of groups	70.3			66.2											
% female	38			61											
<b>ZnT zinc exporter gene family</b>															
Gene name	log <sub>2</sub> FC	FC	padj	probe 1			probe 2			probe 3			probe 4		
				log <sub>2</sub> FC	FC	padj	log <sub>2</sub> FC	FC	padj	log <sub>2</sub> FC	FC	padj	log <sub>2</sub> FC	FC	padj
<i>SLC30A1</i>	<b>0.776</b>	<b>1.7</b>	<b>0.000</b>	0.071	1.1	0.058	0.021	1.0	NA	NA			NA		
<i>SLC30A2</i>	0.192	1.1	0.887	-0.002	1.0	0.974	-0.101	0.9	0.200						
<i>SLC30A3</i>	-0.097	0.9	NA	-0.004	1.0	0.946	NA			NA					
<i>SLC30A4</i>	0.177	1.1	0.431	0.008	1.0	NA							-0.020	1.0	0.710
<i>SLC30A5</i>	0.096	1.1	0.592	-0.039	1.0	0.641	0.006	1.0	NA	0.196	1.1	0.013	-0.012	1.0	NA
<i>SLC30A6</i>	0.217	1.2	0.219	0.004	1.0	NA	0.012	1.0	0.855	NA			NA		
<i>SLC30A7</i>	0.216	1.2	0.209	0.012	1.0	0.915	NA								
<i>SLC30A8</i>	<b>0.705</b>	<b>1.6</b>	<b>0.029</b>	-0.031	1.0	0.505				NA			NA		
<i>SLC30A9</i>	0.191	1.1	0.118	0.009	1.0	0.951									
<i>SLC30A10</i>	-0.035	1.0	NA	-0.029	1.0	NA	NA			NA					
<b>ZIP zinc importer gene family</b>															
<i>SLC39A1</i>	0.076	1.1	0.695	0.149	1.1	0.189	NA			NA			NA		
<i>SLC39A2</i>	-0.088	0.9	NA	0.015	1.0	NA									
<i>SLC39A3</i>	-0.028	1.0	0.935	0.085	1.1	0.186	0.222	1.2	0.015	-0.010	1.0	NA	NA		
<i>SLC39A4</i>	0.023	1.0	0.866	0.005	1.2	NA	0.039	1.0	NA	-0.013	1.0	0.866			
<i>SLC39A5</i>	-0.274	0.8	NA	-0.012	1.0	0.881	NA			NA					
<i>SLC39A6</i>	0.063	1.0	0.722	0.006	1.0	0.957							0.187	1.1	0.154
<i>SLC39A7</i>	0.000	1.0	0.982	-0.007	1.0	0.942	-0.005	1.0	0.951	NA			NA		
<i>SLC39A8</i>	0.127	1.1	0.715	0.018	1.0	0.909	0.117	1.1	0.400						
<i>SLC39A9</i>	0.083	1.1	0.690	0.071	1.1	NA	NA			NA					
<i>SLC39A10</i>	0.013	1.0	0.971	-0.048	1.0	0.149									
<i>SLC39A11</i>	-0.344	0.8	0.107	<b>-0.248</b>	<b>0.8</b>	<b>0.002</b>	NA			NA					
<i>SLC39A12</i>	-0.017	1.0	NA	0.007	1.0	NA									
<i>SLC39A13</i>	0.074	1.1	0.611	0.000	1.0	NA	NA			NA					
<i>SLC39A14*</i>	<b>0.585</b>	<b>1.5</b>	<b>0.003</b>	<b>0.473</b>	<b>1.4</b>	<b>0.001</b>									
<b>Transcription factors</b>															
<i>SP1</i>	-0.132	0.9	0.480	0.007	1.0	0.949	NA			NA			NA		
<i>MTF1</i>	-0.008	1.0	0.955	0.015	1.0	0.923									
<i>MTF2</i>	-0.065	1.0	0.782	-0.054	1.0	0.226	NA			NA					
<b>Metallothioneins</b>															
<i>MT1A</i>	0.370	1.3	0.209	0.185	1.1	0.074	NA			NA			NA		
<i>MT1B</i>	NA	NA	NA	-0.025	1.0	NA									
<i>MT1E</i>	0.272	1.2	0.384	<b>0.217</b>	<b>1.2</b>	<b>0.032</b>	-0.017	1.0	0.955	NA			NA		
<i>MT1F*</i>	<b>0.797</b>	<b>1.7</b>	<b>0.004</b>	<b>0.372</b>	<b>1.3</b>	<b>0.012</b>	NA								
<i>MT1G*</i>	<b>0.715</b>	<b>1.6</b>	<b>0.015</b>	<b>0.749</b>	<b>1.7</b>	<b>0.001</b>				0.010	1.0	0.813			
<i>MT1H</i>	0.476	1.4	0.102	<b>0.574</b>	<b>1.5</b>	<b>0.012</b>	NA			NA					
<i>MT1M*</i>	<b>0.589</b>	<b>1.5</b>	<b>0.036</b>	<b>0.385</b>	<b>1.3</b>	<b>0.001</b>									
<i>MT1X</i>	0.350	1.3	0.232	-0.036	1.0	0.865	NA			NA					
<i>MT2A</i>	0.224	1.2	0.507	<b>0.361</b>	<b>1.3</b>	<b>0.004</b>									
<i>MT3</i>	0.450	1.4	NA	-0.077	0.9	0.254	NA			NA					
<i>MT4</i>	NA			-0.015	1.0	NA									

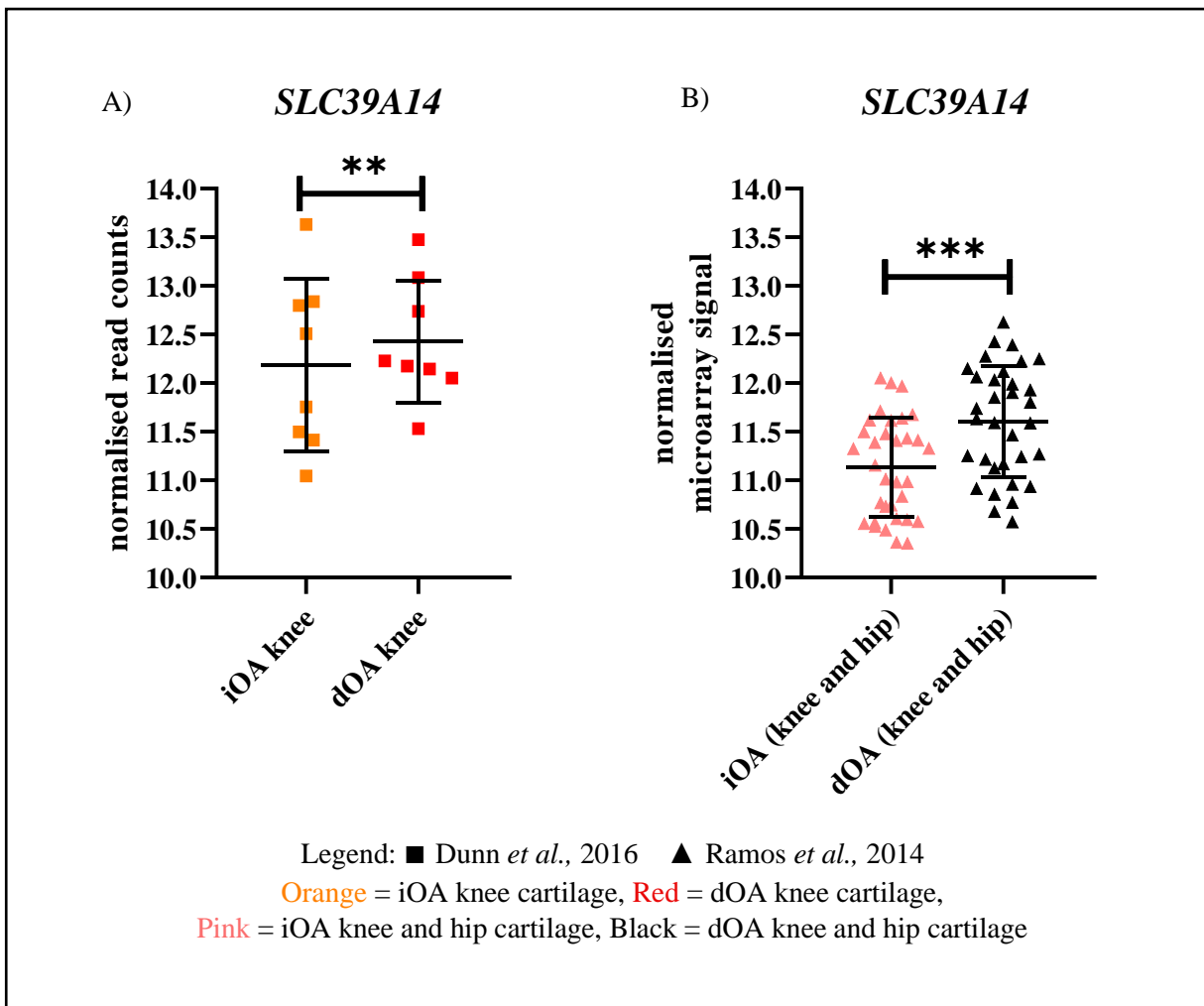


**Figure 3.3 – *SLC39A14* is significantly and differentially expressed in dOA versus iOA knee cartilage of the same knee joint by RNA-Seq (Dunn *et al.*, 2016) and in matched knee or hip OA joints by microarray (Ramos *et al.*, 2014).**

The Ramos *et al.*, 2014 study collected samples of both damaged and intact cartilage from either patient with either knee or hip OA and analysed the gene expression in these groups independent of joint site. Normalised data for *SLC39A14* is expressed as read counts A) or microarray signals B) dependent on the platform used by the research group specified in the legend and were generated by Dr Jamie Soul upon request and are not provided by the SkeletalVis tool. The horizontal lines are the means of the samples with the standard deviation plotted. P values for significantly and differentially expressed genes were calculated in SkeletalVis (Soul *et al.*, 2018b). \*\* p<0.01 \*\*\* p<0.001.

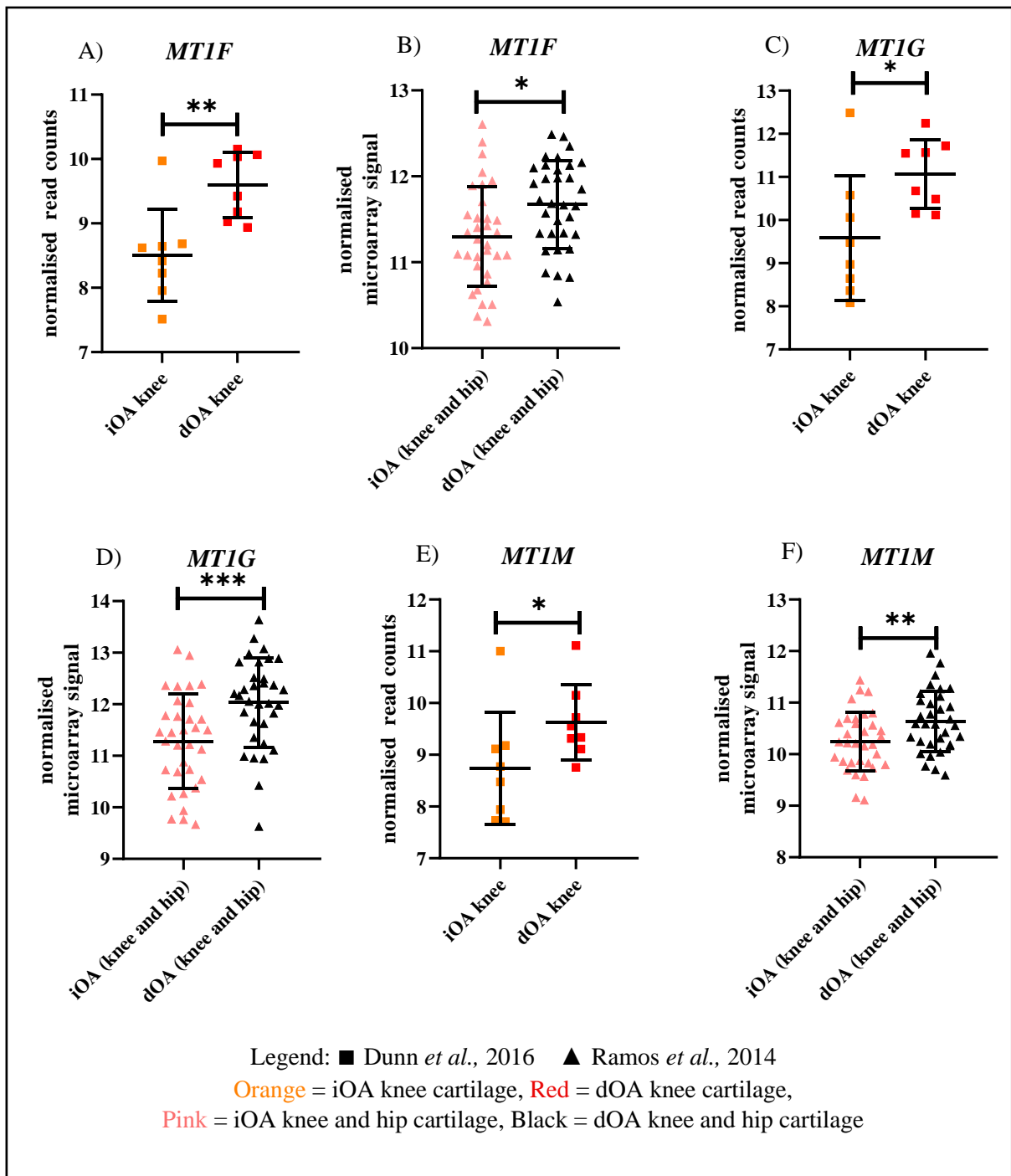


**Figure 3.4 – Metallothioneins significantly and differentially expressed in dOA versus iOA knee cartilage in RNA-Seq (Dunn *et al.*, 2016) and dOA knee and hip joints (Ramos *et al.*, 2014) from different patients.**

The Ramos *et al.*, 2014 study collected samples of both damaged and intact cartilage from either patient with either knee or hip OA and analysed the gene expression in these groups independent of joint site. Normalised data for *MT1F*, *MT1G* and *MT1M* are expressed as read counts (A, C and E) or microarray signals (B, D and F) dependent on the platform used by the research group specified in the legend and were generated by Dr Jamie Soul upon request and are not provided by the SkeletalVis tool. The horizontal lines are the means of the samples with the standard deviation plotted. P values for significantly and differentially expressed genes were calculated in SkeletalVis (Soul *et al.*, 2018b). \*  $p < 0.05$ , \*\*  $p < 0.01$  \*\*\*  $p < 0.001$ .

### **3.6 Influence of IL-1 signalling pathway on zinc homeostasis genes in human and murine chondrocytes**

#### **3.6.1 Human chondrocytes treatment with different IL-1 receptor ligands up to four hours**

In the previous sections, broadly speaking, a dichotomy was observed between upregulated zinc importers and downregulated *MTs* in iOA cartilage versus non-OA cartilage compared to downregulated zinc importers and upregulated *MTs* in dOA cartilage versus iOA cartilage. Together these analyses demonstrate that zinc homeostasis genes are differentially expressed in OA, although only *SLC39A14* was found to change between non-OA and iOA cartilage, and iOA and dOA cartilage, although in different directions. I next wanted to investigate if IL-1 also influenced gene expression of genes involved in zinc homeostasis. Furthermore, the genes *IL-6*, *CXCL8* and *CCL2* were assessed as genes known to be positively regulated by IL-1 cytokines.

I identified a total of three studies where HACs had been exposed to short term 0.05ng/ml IL-1 $\alpha$  and 10ng/ml OSM treatment for one hour and 1.25 hours (Chan *et al.*, 2017) or four hours of IL-1 $\beta$  (Pearson *et al.*, 2016, 1ng/ml; Moazedi-Fuerst *et al.*, 2016, 10ng/ml). Because the IL-1 receptor ligands differed between datasets or the concentration of IL-1 $\beta$  used differed, significantly and differentially expressed genes were determined between the four hour IL-1 $\beta$  datasets (Pearson *et al.*, 2016, 1ng/ml; Moazedi-Fuerst *et al.*, 2016, 10ng/ml) and within the one and 1.25 hour time points of Chan *et al.*, 2017. The gene was considered significantly and differentially expressed if the p value was lower than the FDR  $p < 0.05$  in the same direction for these comparisons. OSM is not an IL-1 receptor ligand but has been used in combination with an IL-1 $\alpha$  transgene in an *in vivo* mouse model and in cultured HACs stimulated with IL-1 $\alpha$  and OSM (Rowan *et al.*, 2003) as a strong inducer of MMP activity and resulting collagen degradation.

More zinc homeostasis genes were differentially expressed after four hours of IL-1 ligand exposure versus untreated cells than IL-1 ligand exposure after one or 1.25 hours versus untreated cells (Table 3.4). There were differences among positive control gene fold change responses for *IL-6*, *CXCL8* or *CCL2* between HACs exposed to 1ng/ml IL-1 $\beta$  and those exposed to 10ng/ml IL-1 $\beta$  after four hours (Figure 3.5). Furthermore, *SLC39A14* was the only zinc importer differentially upregulated (Figure 3.6) 4.2 and 3.6-fold (Table 3.4) after four hours of IL-1 $\beta$  treatment in Pearson *et al.*, 2016 and Moazedi-Fuerst *et al.*, 2016 respectively. Significant (p=0.000 and p=0.011 respectively) ~2-fold differential expression was observed for *MTF1* (Table 3.4, Figure 3.7) in both four hour studies. Among the *MT* genes, *MT1E*, *MT1X* and *MT2A* were significantly (p=0.000) upregulated (Figure 3.8) and parallels with the ipsilateral dOA versus iOA cartilage study could be drawn. There were detectable and significant increased fold changes in *MMP3*, *MMP12* and *MMP13* (Table 3.4) which was present in both Pearson *et al.*, 2016 and Moazedi-Fuerst *et al.*, 2016 four hour IL-1 $\beta$  datasets (Figure 3.9).

**Table 3.4 - SkeletalVis data from three human IL-1-treated chondrocyte datasets treated acutely (1, 1.25 or 4 hours) with IL-1 receptor ligands for genes involved in zinc homeostasis.**

The log<sub>2</sub>-fold change (log<sub>2</sub>FC), fold change (FC) and adjusted p-value (padj) is recorded for each gene entry and the fold change has been formatted across all genes and datasets using a three-colour scheme indicating differential gene downregulation with IL-1 treatment (blue), no change (white), and upregulation with IL-1 treatment (red). Expression data in bold is significantly and differentially expressed with IL-1 for that gene in one dataset. Gene names in bold are significantly and differentially expressed unidirectionally with IL-1 $\alpha$  and OSM for either 1 or 1.25 hours within Chan *et al.*, 2017 or between the four hour IL-1 $\beta$  treatments of Pearson *et al.*, 2016 or Moazedi-Fuerst *et al.*, 2016 studies. Where there were fewer than four probes for a gene on the microarray, NA was used to indicate this. If NA is confined to padj only column, then the p value was not calculated because of insufficient replicates.

Datasets	GSE86578															GSE74220			GSE68428											
References	Chan <i>et al.</i> , 2017															Pearson <i>et al.</i> , 2016			Moazedi-Fuerst <i>et al.</i> , 2016											
Platforms	Illumina HumanHT-12 V4.0 expression beadchip microarray															RNAseq			[HuGene-2_0-st] Affymetrix Human Gene 2.0 ST Array											
N numbers	3 OA knee (50pg/ml IL1 $\alpha$ + 10ng/ml OSM vs control 1 hour or 1.25 hours)															3 OA hip ( 1ng/ml IL1 $\beta$ vs control)			4 OA knee (10ng/ml IL1 $\beta$ untreated vs control)											
Tissue	chondrocytes															chondrocytes			chondrocytes											
Inflammatory and cartilage degrading genes																														
Timepoint	1 hour												1.25 hours						4 hours			4 hours								
	probe 1			probe 2			probe 3			probe 4			probe 1			probe 2			probe 3			probe 4			log2 FC	FC	padj	log2 FC	FC	padj
Gene name	log2 FC	FC	padj	log2 FC	FC	padj	log2 FC	FC	padj	log2 FC	FC	padj	log2 FC	FC	padj	log2 FC	FC	padj	log2 FC	FC	padj	log2 FC	FC	padj	log2 FC	FC	padj			
<i>IL6*</i>	3.337	10.1	0.000	NA			NA			NA			3.481	11.2	0.000	NA			NA			7.904	239.8	0.000	3.492	11.3	0.000			
<i>CXCL8*</i>	2.266	4.8	0.000	1.862	3.6	0.001	NA			NA			2.512	5.7	0.000	1.994	4.0	0.000	NA			7.845	229.9	0.000	7.359	164.1	0.000			
<i>CCL2*</i>	1.530	2.9	0.002	NA			NA			NA			1.641	3.1	0.001	NA			NA			5.013	32.3	0.000	2.120	4.3	0.001			
<i>ADAMTS5</i>	0.665	1.6	0.022	NA			NA			NA			0.456	1.4	0.099	NA			NA			1.205	2.3	0.000	0.442	1.4	0.142			
<i>MMP3*</i>	-0.029	1.0	0.804	NA			NA			NA			-0.166	0.9	0.187	NA			NA			2.390	5.2	0.000	2.992	8.0	0.000			
<i>MMP9</i>	-0.027	1.0	0.881	NA			NA			NA			0.081	1.1	0.681	NA			NA			0.279	1.2	NA	0.039	1.0	0.920			
<i>MMP12*</i>	0.052	1.0	0.929	0.070	1.0	NA	NA			NA			0.190	1.1	0.768	0.121	1.1	NA	NA			3.592	12.1	0.000	3.492	11.3	0.000			
<i>MMP13*</i>	0.545	1.5	0.045	NA			NA			NA			0.173	1.1	0.554	NA			NA			2.731	6.6	0.000	2.773	6.8	0.000			
ZnT zinc exporter gene family																														
<i>SLC30A1</i>	-0.051	1.0	0.778	0.117	1.1	0.647	NA			NA			-0.108	0.9	0.605	-0.060	1.0	0.864	NA			0.291	1.2	0.243	0.558	1.5	0.194			
<i>SLC30A2</i>	0.008	1.0	NA	-0.048	1.0	NA	NA			NA			0.008	1.0	NA	-0.006	1.0	NA	NA			-0.213	0.9	0.827	0.095	1.1	0.631			
<i>SLC30A3</i>	-0.021	1.0	NA	NA			NA			NA			0.071	1.1	NA	NA			NA			0.506	1.4	0.515	0.291	1.2	0.074			
<i>SLC30A4</i>	0.055	1.0	NA	-0.011	1.0	NA	NA			NA			0.018	1.0	NA	0.000	1.0	NA	NA			0.920	1.9	0.000	0.285	1.2	0.361			
<i>SLC30A5</i>	0.017	1.0	0.860	0.362	1.3	0.056	-0.118	0.9	0.498	0.035	1.0	NA	-0.074	1.0	0.471	0.115	1.1	0.587	-0.189	0.9	0.359	-0.034	1.0	NA	0.175	1.1	0.537	-0.059	1.0	0.782
<i>SLC30A6</i>	0.051	1.0	NA	-0.101	0.9	0.343	NA			NA			-0.010	1.0	NA	-0.152	0.9	0.235	NA			0.110	1.1	0.868	-0.120	0.9	0.591			
<i>SLC30A7</i>	0.002	1.0	0.991	NA			NA			NA			0.166	1.1	0.285	NA			NA			0.924	1.9	0.000	0.271	1.2	0.340			
<i>SLC30A8</i>	-0.029	1.0	NA	NA			NA			NA			-0.001	1.0	NA	NA			NA			-0.473	0.7	0.636	0.037	1.0	0.894			
<i>SLC30A9</i>	-0.081	0.9	0.518	NA			NA			NA			-0.025	1.0	0.889	NA			NA			0.167	1.1	0.528	-0.076	0.9	0.825			
<i>SLC30A10</i>	-0.011	1.0	NA	NA			NA			NA			-0.053	1.0	NA	NA			NA			1.405	2.6	0.036	NA	NA	NA			
ZIP zinc importer gene family																														
<i>SLC39A1</i>	-0.178	0.9	0.089	NA			NA			NA			-0.022	1.0	0.876	NA			NA			0.057	1.0	0.882	0.171	1.1	0.588			
<i>SLC39A2</i>	0.009	1.0	NA	NA			NA			NA			0.014	1.0	NA	NA			NA			-0.065	1.0	NA	0.087	1.1	0.829			
<i>SLC39A3</i>	-0.114	0.9	0.199	-0.335	0.8	0.062	-0.065	1.0	NA	-0.065	1.0	0.582	-0.224	0.9	0.045	-0.238	0.8	0.216	-0.066	1.0	NA	-0.019	1.0	0.914	0.125	1.1	0.846	-0.349	0.8	0.289
<i>SLC39A4</i>	0.046	1.0	NA	-0.033	1.0	NA	NA			NA			0.067	1.0	NA	-0.021	1.0	NA	NA			-0.615	0.7	0.460	-0.004	1.0	0.989			
<i>SLC39A5</i>	-0.068	1.0	NA	NA			NA			NA			0.040	1.0	NA	NA			NA			0.193	1.1	NA	0.070	1.0	0.823			
<i>SLC39A6</i>	0.210	1.2	0.244	-0.182	0.9	0.268	NA			NA			-0.053	1.0	0.831	-0.274	0.8	0.167	NA			0.050	1.0	0.920	-0.221	0.9	0.328			
<i>SLC39A7</i>	0.090	1.1	0.343	-0.068	1.0	NA	NA			NA			0.111	1.1	0.324	-0.058	1.0	NA	NA			0.082	1.1	0.883	0.069	1.0	0.777			
<i>SLC39A8</i>	0.680	1.6	0.188	0.139	1.1	0.245	NA			NA			0.169	1.1	0.807	0.083	1.1	0.579	NA			0.317	1.2	0.298	1.117	2.2	0.002			
<i>SLC39A9</i>	-0.294	0.8	0.067	NA			NA			NA			-0.280	0.8	0.115	NA			NA			0.113	1.1	0.762	-0.103	0.9	0.629			
<i>SLC39A10</i>	0.033	1.0	0.803	NA			NA			NA			0.044	1.0	0.784	NA			NA			-0.219	0.9	0.378	-0.372	0.8	0.378			
<i>SLC39A11</i>	-0.194	0.9	0.147	NA			NA			NA			-0.165	0.9	0.287	NA			NA			-0.059	1.0	0.933	-0.270	0.8	0.353			
<i>SLC39A12</i>	0.039	1.0	NA	NA			NA			NA			0.017	1.0	NA	NA			NA			0.081	1.1	NA	0.101	1.1	0.768			
<i>SLC39A13</i>	0.039	1.0	NA	NA			NA			NA			0.023	1.0	NA	NA			NA			-0.144	0.9	0.706	0.041	1.0	0.881			
<i>SLC39A14*</i>	-0.103	0.9	0.584	NA			NA			NA			0.139	1.1	0.546	NA			NA			2.056	4.2	0.000	1.851	3.6	0.000			
Transcription factors																														
<i>SP1</i>	0.057	1.0	0.580	NA			NA			NA			-0.038	1.0	0.784	NA			NA			-0.352	0.8	0.083	-0.146	0.9	0.510			
<i>MTF1*</i>	0.109	1.1	0.436	NA			NA			NA			0.285	1.2	0.099	NA			NA			0.966	2.0	0.000	0.748	1.7	0.011			
<i>MTF2</i>	0.259	1.2	0.076	NA			NA			NA			0.061	1.0	0.729	NA			NA			-0.151	0.9	0.703	-0.312	0.8	0.188			
Metallothioneins																														
<i>MT1A</i>	0.021	1.0	0.860	NA			NA			NA			0.072	1.1	0.577	NA			NA			0.941	1.9	0.175	1.125	2.2	0.019			
<i>MT1B</i>	0.024	1.0	NA	NA			NA			NA			0.015	1.0	NA	NA			NA			0.118	1.1	NA	0.597	1.5	NA			
<i>MT1E*</i>	-0.145	0.9	0.072	0.298	1.2	0.011	NA			NA			0.168	1.1	0.066	0.280	1.2	0.014	NA			1.007	2.0	0.000	1.905	3.7	0.000			
<i>MT1F</i>	-0.221	0.9	0.418	NA			NA			NA			-0.092	0.9	0.805	NA			NA			0.021	1.0	0.995	0.363	1.3	0.542			
<i>MT1G</i>	-0.013	1.0	0.930	NA			NA			NA			0.047	1.0	0.772	NA			NA			0.151	1.1	0.832	0.767	1.7	0.070			
<i>MT1H</i>	-0.049	1.0	0.789	0.583	1.5	0.140	NA			NA			-0.128	0.9	0.541	0.164	1.1	0.747	NA			0.118	1.1	0.959	0.231	1.2	NA			
<i>MT1M</i>	-0.065	1.0	0.791	NA			NA			NA			-0.002	1.0	0.996	NA			NA			1.549	2.9	0.000	0.479	1.4	0.408			
<i>MT1X*</i>	-0.209	0.9	0.109	NA			NA			NA			-0.066	1.0	0.682	NA			NA			1.038	2.1	0.000	1.782	3.4	0.001			
<i>MT2A*</i>	0.019	1.0	0.883	NA			NA			NA			0.141	1.1	0.274	NA			NA			1.670	3.2	0.000	1.195	2.3	0.001			
<i>MT3</i>	0.138	1.1	0.651	NA			NA			NA			0.024	1.0	0.959	NA			NA			0.124	1.1	NA	0.299	1.2	0.512			
<i>MT4</i>	0.096	1.1	NA	NA			NA			NA			0.020	1.0	NA	NA			NA			-0.042	1.0	NA	0.015	1.0	0.969			

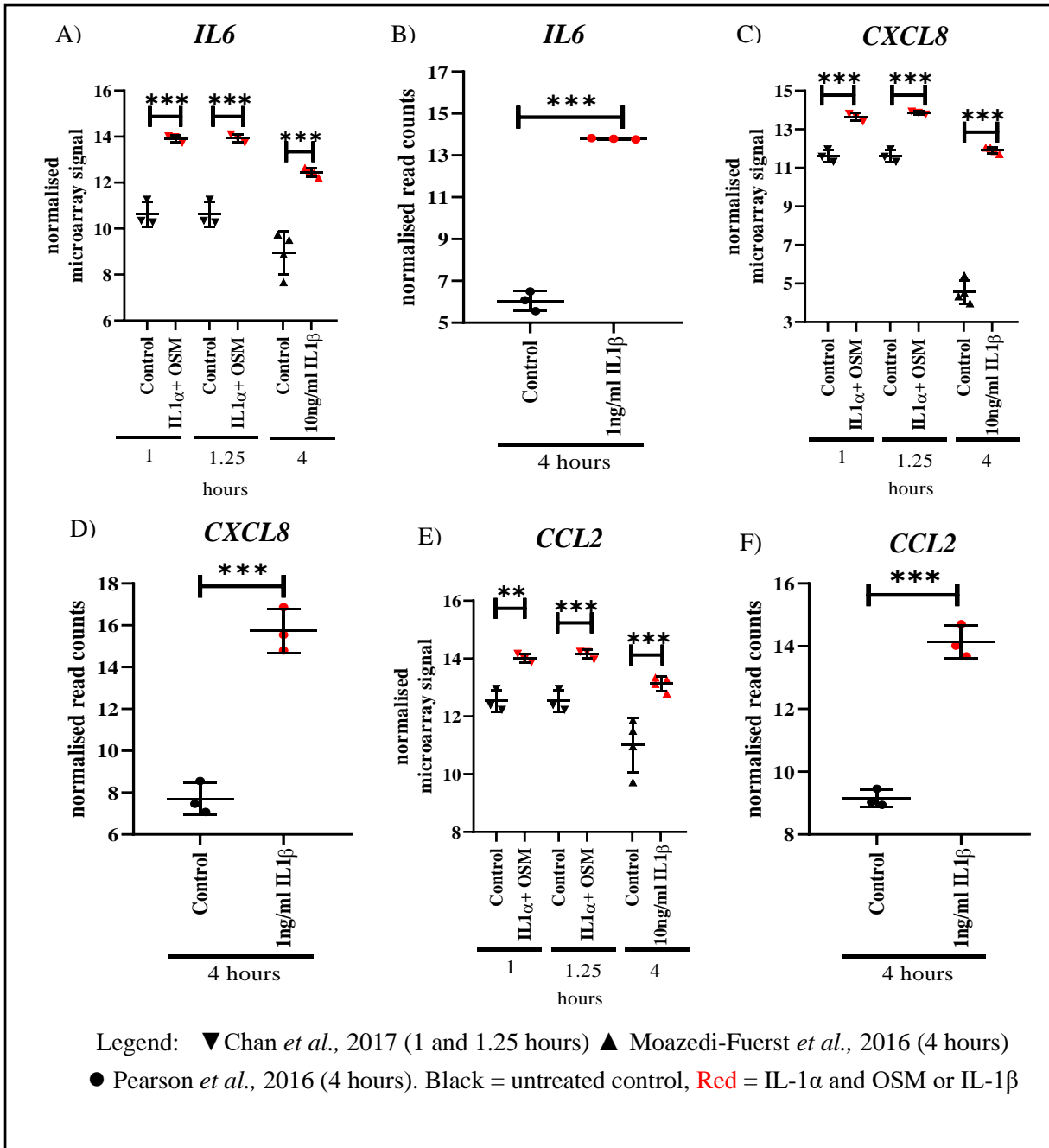


**Figure 3.5 - *IL-6*, *CXCL8* and *CCL2* are differentially expressed in human chondrocytes treated with or without IL-1 for one, 1.25 or four hours in RNA-Seq (Pearson *et al.*, 2016) and microarray (Chan *et al.*, 2017; Moazedi-Fuerst *et al.*, 2016) datasets.**

Normalised data for *IL-6*, *CXCL8* and *CCL2* are expressed as read counts (B, D and F) or microarray signals (A, C and E) dependent on the platform used by the research group specified in the legend and were generated by Dr Jamie Soul upon request and are not provided by the SkeletalVis tool. The horizontal lines are the means of the samples with the standard deviation plotted. P values for significantly and differentially expressed genes were calculated in SkeletalVis (Soul *et al.*, 2018b). \*\*  $p < 0.01$ , \*\*\*  $p < 0.001$ , oncostatin M = OSM.

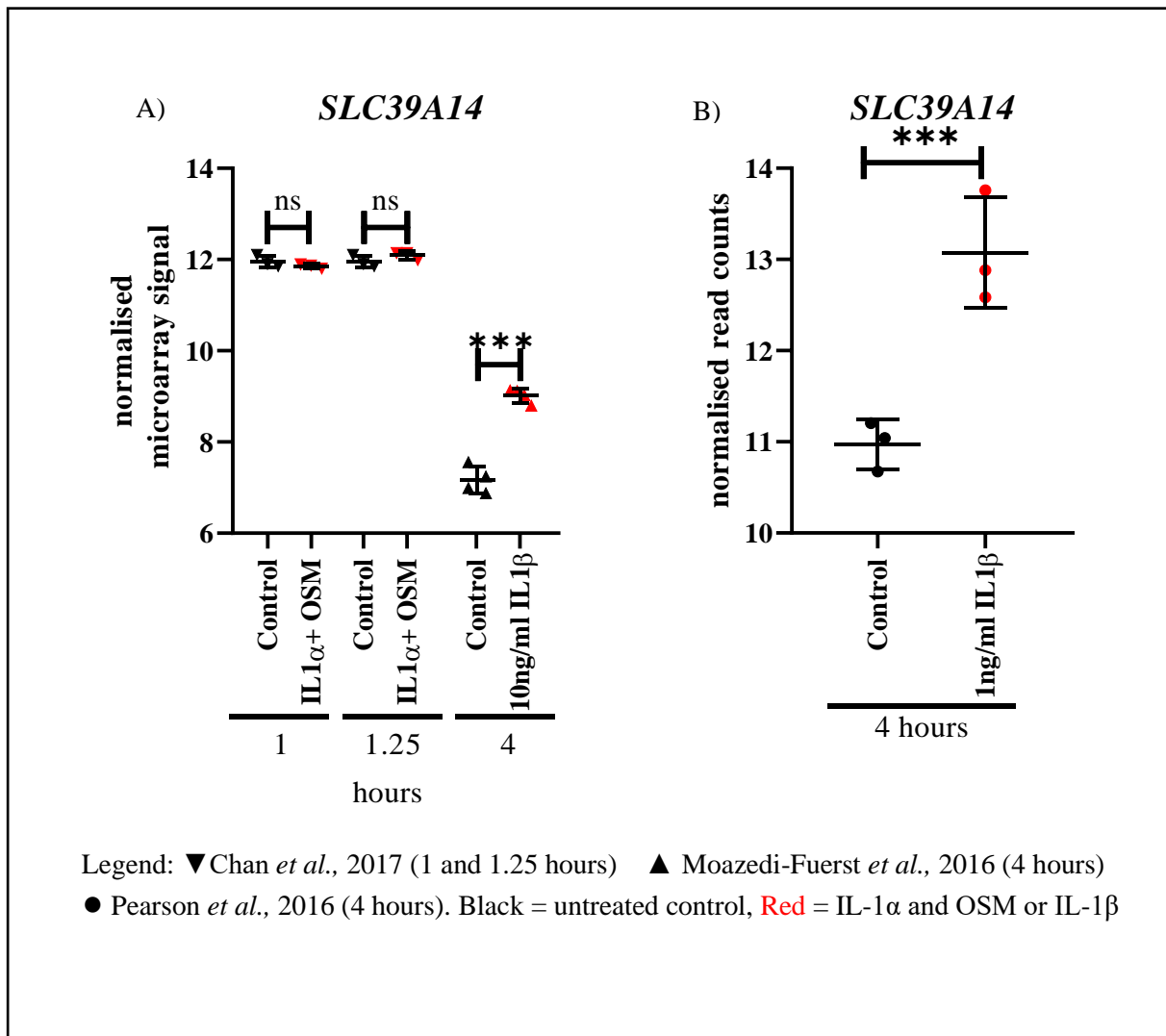


**Figure 3.6 – *SLC39A14* is significantly and differentially expressed in human chondrocytes after four hours IL-1 $\beta$  in microarray (Moazedi-Fuerst *et al.*, 2016) and RNA-Seq (Pearson *et al.*, 2016) datasets.**

Normalised data for *SLC39A14* is expressed as microarray signal A) or read count B) dependent on the platform used by the research group specified in the legend and were generated by Dr Jamie Soul upon request and are not provided by the SkeletalVis tool. The horizontal lines are the means of the samples with the standard deviation plotted. P values for significantly and differentially expressed genes were calculated in SkeletalVis (Soul *et al.*, 2018b). ns = not significant, \*\*\* p<0.001, OSM = oncostatin M.

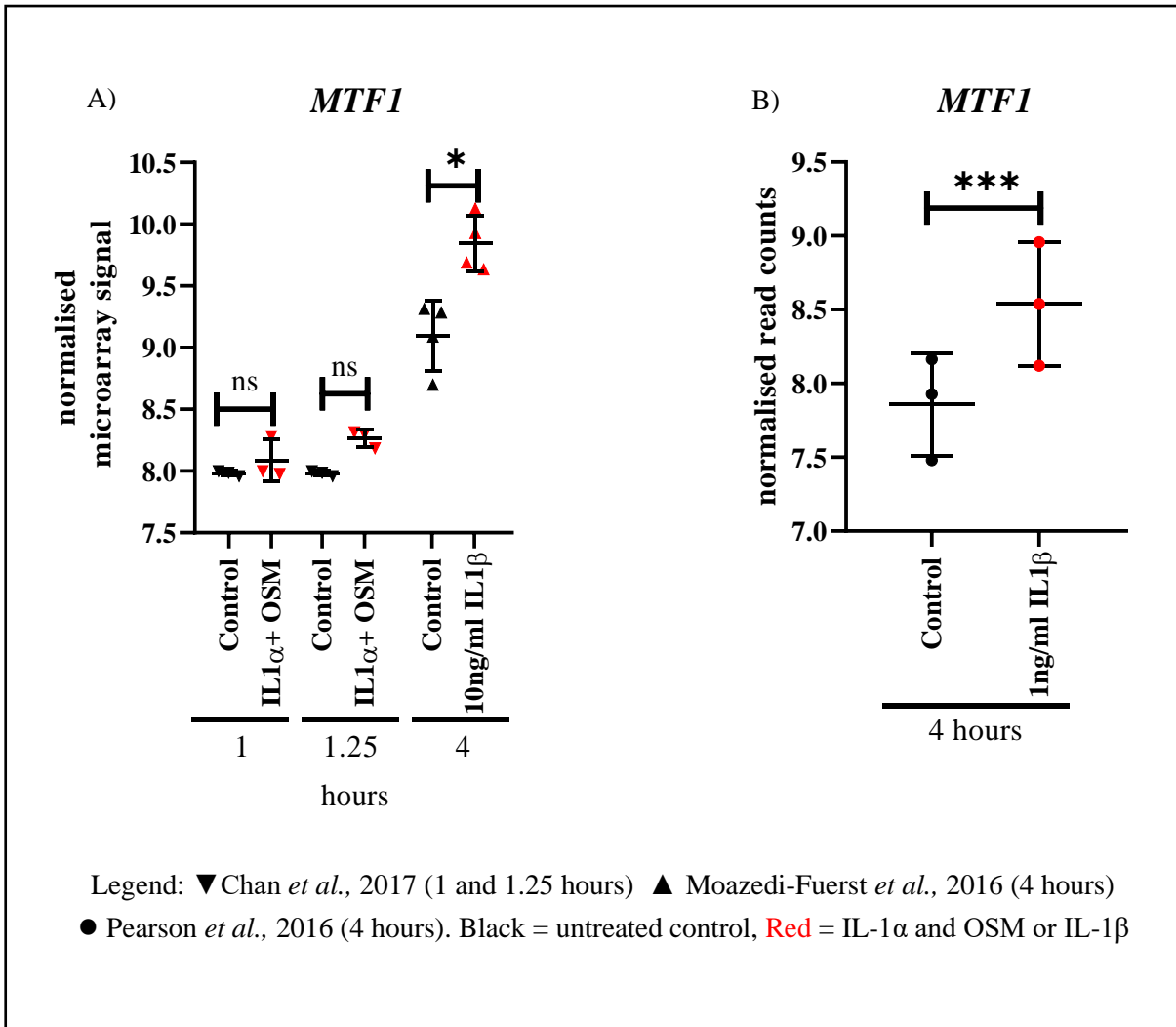


**Figure 3.7 – *MTF1* is significantly and differentially expressed in human chondrocytes after four hours IL-1 $\beta$  in microarray (Moazedi-Fuerst *et al.*, 2016) and RNA-Seq (Pearson *et al.*, 2016) datasets.**

Normalised data for *MTF1* is expressed as read counts A) or microarray signals B) dependent on the platform used by the research group specified in the legend and were generated by Dr Jamie Soul upon request and are not provided by the SkeletalVis tool. The horizontal lines are the means of the samples with the standard deviation plotted. P values for significantly and differentially expressed genes were calculated in SkeletalVis (Soul *et al.*, 2018b). ns = not significant, \* p<0.05, \*\*\* p<0.001, OSM = oncostatin M.

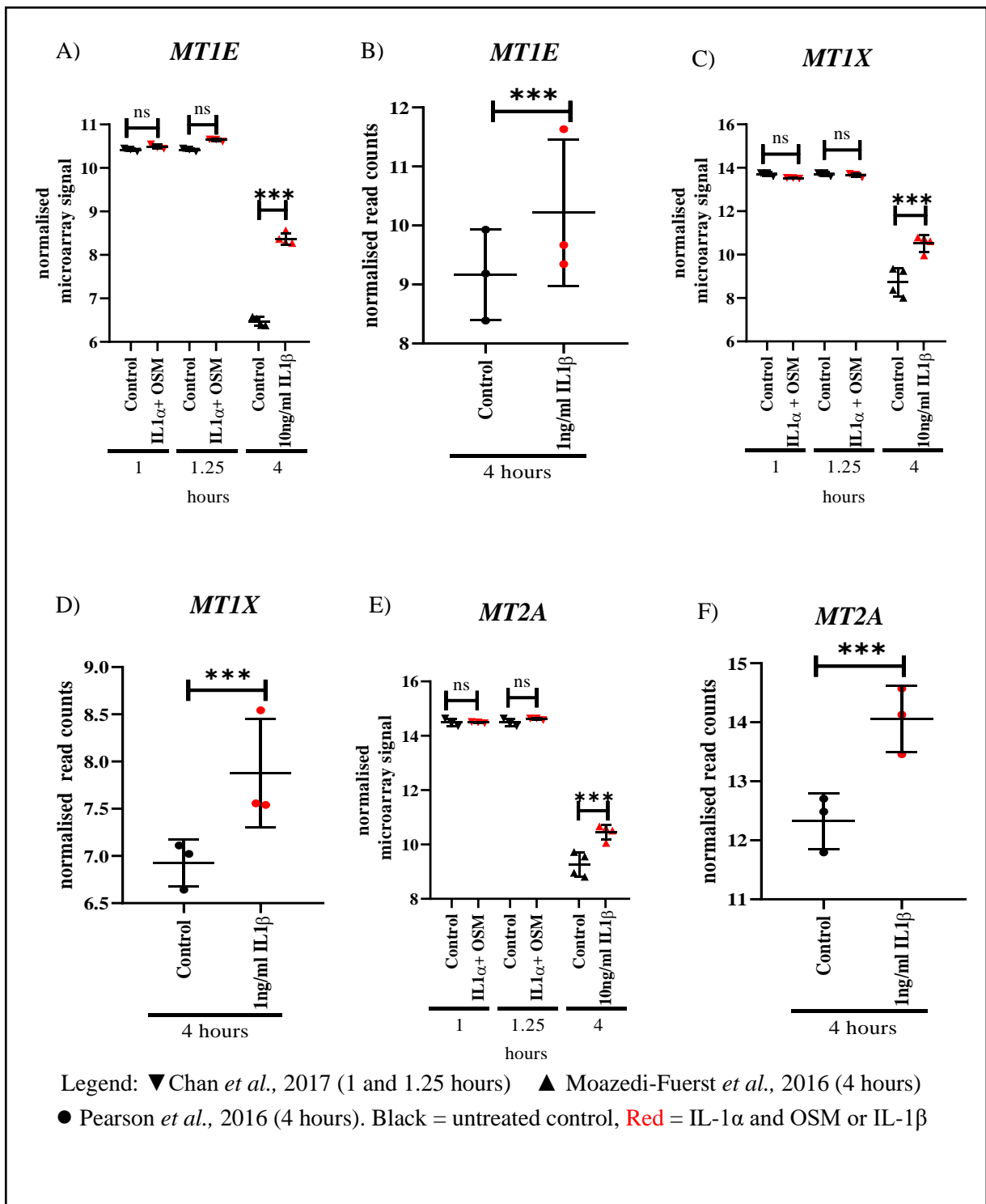


**Figure 3.8 – *MT1E*, *MT1X*, and *MT2A* are significantly and differentially expressed in human chondrocytes after four hours IL-1 $\beta$  in microarray (Moazedi-Fuerst *et al.*, 2016) and RNA-Seq (Pearson *et al.*, 2016) datasets.**

Normalised data for *MT1E*, *MT1X* and *MT2A* are expressed as read counts (B, D and F) or microarray signals (A, C and E) dependent on the platform used by the research group specified in the legend and were generated by Dr Jamie Soul upon request and are not provided by the SkeletalVis tool. The horizontal lines are the means of the samples with the standard deviation plotted. P values for significantly and differentially expressed genes were calculated in SkeletalVis (Soul *et al.*, 2018b). ns = not significant, \*\*\* p<0.001, OSM = oncostatin M.

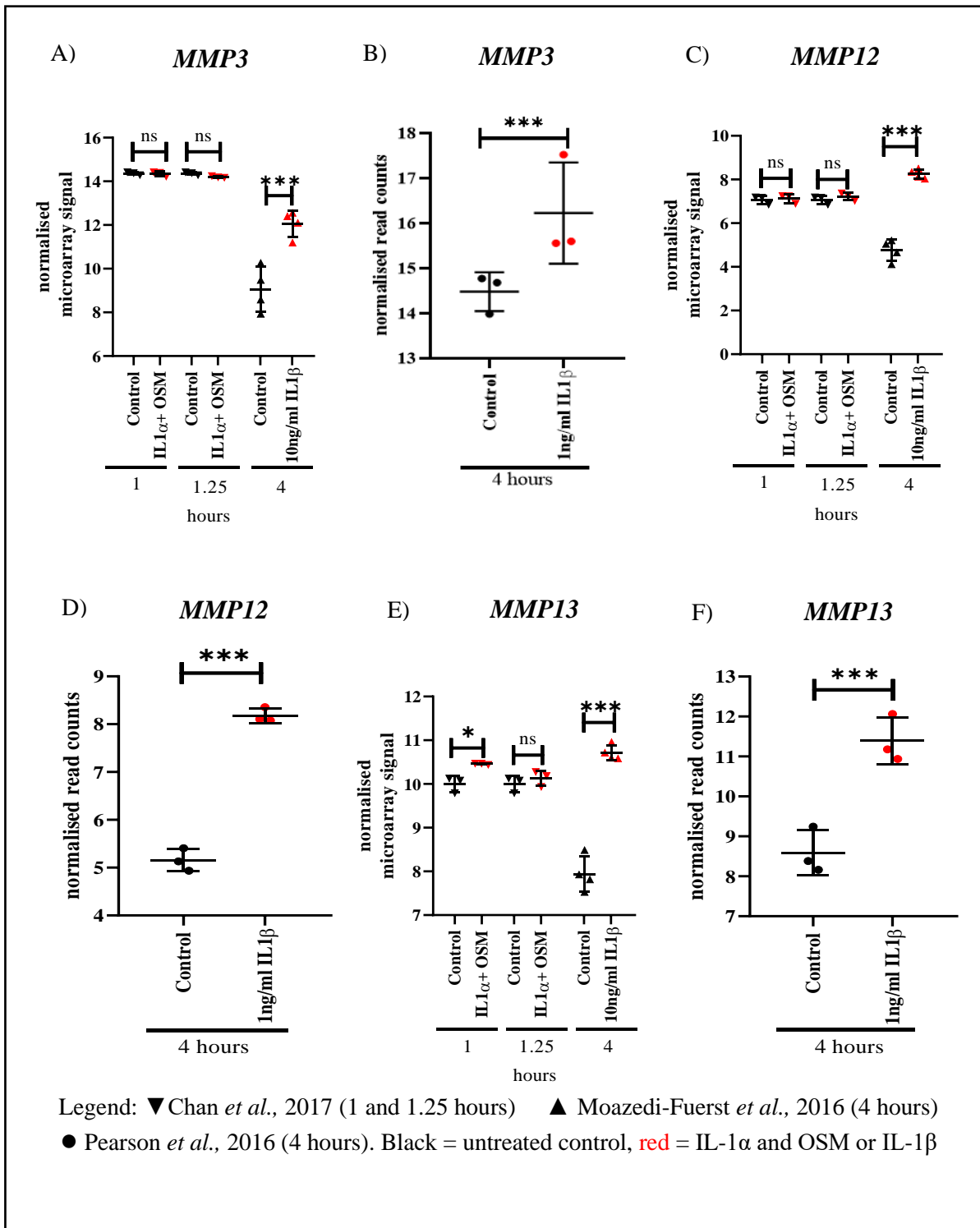


**Figure 3.9 – MMP3, MMP12 and MMP13 are differentially expressed in human chondrocytes after four hours IL-1 $\beta$  in microarray (Moazedi-Fuerst *et al.*, 2016) and RNA-Seq (Pearson *et al.*, 2016) datasets.**

Normalised data for MMP3, MMP12 and MMP13 are expressed as read counts (B, D and F) or microarray signals (A, C and E) dependent on the platform used by the research group specified in the legend and were generated by Dr Jamie Soul upon request and are not provided by the SkeletalVis tool. The horizontal lines are the means of the samples with the standard deviation plotted. P values for significantly and differentially expressed genes were calculated in SkeletalVis (Soul *et al.*, 2018b). not significant = ns, \* p<0.05, \*\*\* p<0.001, oncostatin M = OSM.

### 3.6.2 Treatment of human and mouse chondrocytes with different IL-1 receptor ligands for 24 hours

Next, studies investigating IL-1 treatment of human and mouse chondrocytes for 24 hours were examined (Table 3.5) specifically for zinc homeostasis genes and the IL-1-responsive genes as for section 3.6.1. Genes were only considered significantly and differentially expressed at the FDR  $p < 0.05$  at this time point if significant fold changes were achieved in all studies in the same direction. This analysis comprised three datasets, two human (Comblain *et al.*, 2016, 10pM IL-1 $\beta$ ; Chan *et al.*, 2017, 0.05ng/ml IL-1 $\alpha$  and 10ng/ml OSM) and one murine (unpublished, GSE104793). For clarity, the 24 hour 0.05ng/ml IL-1 $\alpha$  and 10ng/ml OSM treated chondrocytes from Chan *et al.*, 2017 were part of the same experiment using the same stimuli for one and 1.25 hours in section 3.6.1. The human and murine gene names for each gene are indicated in Table 3.5 and an additional column describing fold changes for the murine *Mt* genes (*Mt1* and *Mt2*) is indicated. All the positive control IL-1 responsive genes were significantly and differentially upregulated in all three datasets (Figure 3.10 and Table 3.5). Among the zinc importers, *SLC39A8/Slc39a8* and *SLC39A14/Slc39a14* were upregulated after IL-1 treatment and in the same direction in both species (Figure 3.11). Except for the brain tissue-specific *MT3*, the ubiquitously and squamous cell epithelial localised *MT4*, and *MT2A*, all the other *MT* genes investigated were significantly and differentially upregulated in both human studies (Figure 3.12). Mouse *Mt* genes *Mt1* and *Mt2* were also significantly upregulated 1.9 and 1.7-fold ( $p < 0.000$  and  $p < 0.001$  respectively) and the normalised microarray signals presented in Figure 3.13. *MMP9/Mmp9*, *MMP12/Mmp12*, and *MMP13/Mmp13* were significantly and differentially upregulated in all three datasets (Figure 3.14), only *Mmp3* was specifically upregulated in the mouse (Table 3.5).

**Table 3.5 - SkeletalVis data from two human chondrocyte datasets IL-1-treated 24 hour and one murine IL-1-treated 24 hour chondrocyte dataset for genes involved in zinc homeostasis.**

The log<sub>2</sub>-fold change (log<sub>2</sub>FC), fold change (FC) and adjusted p-value (padj) is recorded for each gene entry and the fold change has been formatted across all genes and datasets using a three colour scheme indicating differential gene downregulation with IL-1 treatment (blue), no change (white), and upregulation with IL-1 treatment (red). Data in bold is significantly and differentially expressed for that gene in at least one dataset and bold gene name indicates differential gene expression in all datasets. Gene names in bold are significantly and differentially expressed unidirectionally with either 10pM IL-1 $\beta$  (Comblain *et al.*, 2016) or IL-1 $\alpha$  and OSM for 24 hours (Chan *et al.*, 2017) or 1ng/ml IL-1 $\beta$  (GSE104793). Human metallothionein genes (*MT1A-MT2A*) and mouse metallothionein genes (*Mt1* and *Mt2*) were considered separately in terms of differential gene expression assessment. Where there were fewer than four probes for a particular gene on the microarray NA was used to indicate this. If NA is confined to padj only column, then the p value was not calculated because of insufficient replicates.

Datasets	GSE75181												GSE86578												GSE104793								
References	Comblain <i>et al.</i> , 2016												Chan <i>et al.</i> , 2017												Unpublished								
Platforms	Illumina HumanHT-12 V4.0 expression beadchip microarray												Illumina HumanHT-12 V4.0 expression beadchip microarray												[MoGene-2.0-st] Affymetrix Mouse Gene 2.0 ST Array [transcript (gene) version]								
N numbers	12 OA knee (10pM IL1 $\beta$ vs control)												3 OA patients knee (50pg/ml IL1 $\alpha$ + 10ng/ml OSM vs control 24 hours)												3 biologicals per group (1ng/ml IL1 $\beta$ vs control)								
Tissue	chondrocytes												chondrocytes												chondrocytes								
<b>Inflammatory and cartilage degrading genes</b>																																	
Timepoint	24 hours												24 hours												24 hours								
Gene name	probe 1			probe 2			probe 3			probe 4			probe 1			probe 2			probe 3			probe 4			log2 FC	FC	padj						
	log2 FC	FC	padj	log2 FC	FC	padj	log2 FC	FC	padj	log2 FC	FC	padj	log2 FC	FC	padj	log2 FC	FC	padj	log2 FC	FC	padj	log2 FC	FC	padj									
<i>IL6/Il6*</i>	<b>6.144</b>	<b>70.7</b>	<b>0.000</b>	NA			NA			NA			<b>3.735</b>	<b>13.0</b>	<b>0.000</b>	NA			NA			NA			<b>6.084</b>	<b>67.9</b>	<b>0.000</b>						
<i>CXCL3/Cxcl3*</i>	<b>6.347</b>	<b>81.4</b>	<b>0.000</b>	6.059	<b>66.7</b>	<b>0.000</b>	NA			NA			<b>3.171</b>	<b>9.0</b>	<b>0.000</b>	<b>2.168</b>	<b>4.5</b>	<b>0.000</b>	NA			NA			NA	NA	NA						
<i>CCL2/Ccl2*</i>	<b>3.212</b>	<b>9.3</b>	<b>0.000</b>	NA			NA			NA			<b>1.620</b>	<b>3.1</b>	<b>0.000</b>	NA			NA			NA			<b>5.929</b>	<b>60.9</b>	<b>0.000</b>						
<i>ADAMTSS/Adamts5</i>	<b>0.364</b>	<b>0.8</b>	<b>0.008</b>	NA			NA			NA			0.267	1.2	0.205	NA			NA			NA			<b>3.446</b>	<b>10.9</b>	<b>0.000</b>						
<i>MMP3/Mmp3</i>	0.039	1.0	0.749	NA			NA			NA			0.047	1.0	0.647	NA			NA			NA			<b>7.206</b>	<b>147.7</b>	<b>0.000</b>						
<i>MMP9/Mmp9*</i>	<b>0.189</b>	<b>1.1</b>	<b>0.006</b>	NA			NA			NA			<b>0.786</b>	<b>1.7</b>	<b>0.000</b>	NA			NA			NA			<b>0.962</b>	<b>1.9</b>	<b>0.032</b>						
<i>MMP12/Mmp12*</i>	<b>0.651</b>	<b>1.6</b>	<b>0.000</b>	NA			NA			NA			<b>1.576</b>	<b>3.0</b>	<b>0.004</b>	<b>0.972</b>	<b>2.0</b>	<b>0.020</b>	NA			NA			NA			<b>1.829</b>	<b>3.6</b>	<b>0.000</b>			
<i>MMP13/Mmp13*</i>	<b>4.028</b>	<b>16.3</b>	<b>0.000</b>	NA			NA			NA			<b>2.401</b>	<b>5.3</b>	<b>0.000</b>	NA			NA			NA			<b>4.483</b>	<b>22.4</b>	<b>0.000</b>						
<b>ZnT zinc importer gene family</b>																																	
<i>SLC30A1/Slc30a1</i>	<b>0.266</b>	<b>1.2</b>	<b>0.004</b>	<b>0.263</b>	<b>1.2</b>	<b>0.000</b>	NA			NA			0.212	1.2	0.175	0.132	1.1	0.585	NA			NA			0.168	1.1	0.147						
<i>SLC30A2/Slc30a2</i>	0.030	1.0	0.180	0.191	1.1	NA	NA			NA			-0.002	1.0	NA	0.163	1.1	NA	NA			NA			-0.007	1.0	0.976						
<i>SLC30A3/Slc30a3</i>	0.025	1.0	0.585	NA			NA			NA			0.090	1.1	0.373	NA			NA			NA			0.032	1.0	0.862						
<i>SLC30A4/Slc30a4</i>	0.032	1.0	NA	-0.004	1.0	NA	NA			NA			-0.008	1.0	NA	-0.003	1.0	NA	NA			NA			<b>0.254</b>	<b>1.2</b>	<b>0.038</b>						
<i>SLC30A5/Slc30a5</i>	<b>0.172</b>	<b>1.1</b>	<b>0.022</b>	<b>0.178</b>	<b>1.1</b>	<b>0.010</b>	<b>0.284</b>	<b>1.2</b>	<b>0.000</b>	0.019	1.0	0.582	<b>0.197</b>	<b>1.1</b>	<b>0.023</b>	<b>0.363</b>	<b>1.3</b>	<b>0.032</b>	0.227	1.2	0.165	0.019	1.0	NA	-0.216	0.9	0.085						
<i>SLC30A6/Slc30a6</i>	-0.046	1.0	0.289	0.032	1.0	0.502	NA			NA			-0.011	1.0	NA	-0.061	1.0	1.066	NA			NA			-0.109	0.9	0.400						
<i>SLC30A7/Slc30a7</i>	<b>0.281</b>	<b>1.2</b>	<b>0.003</b>	NA			NA			NA			<b>0.410</b>	<b>1.3</b>	<b>0.005</b>	NA			NA			NA			-0.128	0.9	0.306						
<i>SLC30A8/Slc30a8</i>	-0.004	1.0	NA	NA			NA			NA			0.046	1.0	NA	NA			NA			NA			0.196	1.1	NA						
<i>SLC30A9/Slc30a9</i>	<b>-0.320</b>	<b>0.8</b>	<b>0.000</b>	NA			NA			NA			-0.178	0.9	0.133	NA			NA			NA			<b>0.355</b>	<b>1.3</b>	<b>0.012</b>						
<i>SLC30A10/Slc30a10</i>	0.001	1.0	0.981	NA			NA			NA			-0.015	1.0	NA	NA			NA			NA			-0.145	0.9	0.683						
<b>ZIP zinc importer gene family</b>																																	
<i>SLC39A1/Slc39a1</i>	<b>-0.340</b>	<b>0.8</b>	<b>0.000</b>	NA			NA			NA			-0.125	0.9	0.174	NA			NA			NA			0.258	1.2	0.077						
<i>SLC39A2/Slc39a2</i>	0.014	1.0	NA	NA			NA			NA			0.050	1.0	NA	NA			NA			NA			-0.084	0.9	0.607						
<i>SLC39A3/Slc39a3</i>	-0.001	1.0	0.993	<b>-0.320</b>	<b>0.8</b>	<b>0.000</b>	-0.029	1.0	0.592	NA			0.004	1.0	0.966	-0.257	<b>0.8</b>	<b>0.095</b>	-0.054	1.0	NA	NA			-0.002	1.0	0.993						
<i>SLC39A4/Slc39a4</i>	-0.014	1.0	NA	-0.009	1.0	NA	-0.027	1.0	0.756	NA			0.047	1.0	NA	-0.077	0.9	NA	-0.153	0.9	0.160	NA			0.061	1.0	0.634						
<i>SLC39A5/Slc39a5</i>	0.008	1.0	0.883	NA			NA			NA			-0.058	1.0	NA	NA			NA			NA			0.063	1.0	0.656						
<i>SLC39A6/Slc39a6</i>	0.032	1.0	0.732	0.018	1.0	0.870	NA			NA			0.234	1.2	0.166	-0.029	1.0	0.868	NA			NA			0.008	1.0	0.959						
<i>SLC39A7/Slc39a7</i>	<b>0.267</b>	<b>1.2</b>	<b>0.000</b>	0.049	1.0	0.368	NA			NA			<b>0.278</b>	<b>1.2</b>	<b>0.008</b>	-0.058	1.0	NA	NA			NA			-0.240	<b>0.8</b>	0.063						
<i>SLC39A8/Slc39a8*</i>	<b>2.306</b>	<b>4.9</b>	<b>0.000</b>	<b>2.715</b>	<b>6.6</b>	<b>0.000</b>	NA			NA			<b>2.226</b>	<b>4.7</b>	<b>0.001</b>	<b>2.093</b>	<b>4.3</b>	<b>0.000</b>	NA			NA			<b>3.398</b>	<b>10.5</b>	<b>0.000</b>						
<i>SLC39A9/Slc39a9</i>	<b>-0.198</b>	<b>0.9</b>	<b>0.002</b>	NA			NA			NA			-0.145	0.9	0.290	NA			NA			NA			-0.149	0.9	0.228						
<i>SLC39A10/Slc39a10</i>	<b>-0.275</b>	<b>0.8</b>	<b>0.000</b>	NA			NA			NA			<b>-0.338</b>	<b>0.8</b>	<b>0.010</b>	NA			NA			NA			<b>1.491</b>	<b>2.8</b>	<b>0.000</b>						
<i>SLC39A11/Slc39a11</i>	0.065	1.0	0.447	NA			NA			NA			0.023	1.0	0.867	NA			NA			NA			-0.304	<b>0.8</b>	0.059						
<i>SLC39A12/Slc39a12</i>	0.040	1.0	NA	NA			NA			NA			0.059	1.0	NA	NA			NA			NA			0.170	1.1	0.242						
<i>SLC39A13/Slc39a13</i>	-0.023	1.0	0.488	NA			NA			NA			0.042	1.0	NA	NA			NA			NA			<b>0.583</b>	<b>1.5</b>	<b>0.003</b>						
<i>SLC39A14/Slc39a14*</i>	<b>2.693</b>	<b>6.5</b>	<b>0.000</b>	NA			NA			NA			<b>1.066</b>	<b>2.1</b>	<b>0.000</b>	NA			NA			NA			<b>1.209</b>	<b>2.3</b>	<b>0.000</b>						
<b>Transcription factors</b>																																	
<i>SF1/Sp1</i>	-0.020	1.0	0.810	NA			NA			NA			0.186	1.1	0.061	NA			NA			NA			0.075	1.1	0.649						
<i>MTF1/Mtf1</i>	<b>0.454</b>	<b>1.4</b>	<b>0.000</b>	NA			NA			NA			<b>0.596</b>	<b>1.5</b>	<b>0.001</b>	NA			NA			NA			0.151	1.1	0.221						
<i>MTF2/Mtf2</i>	0.041	1.0	0.695	NA			NA			NA			0.115	1.1	0.367	NA			NA			NA			<b>0.520</b>	<b>1.4</b>	<b>0.016</b>						
<b>Metallothioneins</b>																																	
<i>MT1A*</i>	<b>1.513</b>	<b>2.9</b>	<b>0.000</b>	NA			NA			NA			<b>0.265</b>	<b>1.2</b>	<b>0.015</b>	NA			NA			NA			NA			NA					
<i>MT1B</i>	0.001	1.0	NA	NA			NA			NA			0.194	1.1	NA	NA			NA			NA			NA			NA					
<i>MT1E*</i>	<b>1.298</b>	<b>2.5</b>	<b>0.000</b>	<b>0.1</b>	<b>1.1</b>	<b>0.003</b>	NA			NA			<b>0.691</b>	<b>1.6</b>	<b>0.000</b>	<b>0.285</b>	<b>1.2</b>	<b>0.004</b>	NA			NA			NA			NA					
<i>MT1F*</i>	<b>1.944</b>	<b>3.8</b>	<b>0.000</b>	NA			NA			NA			<b>0.915</b>	<b>1.9</b>	<b>0.004</b>	NA			NA			NA			NA								
<i>MT1G*</i>	<b>2.731</b>	<b>6.6</b>	<b>0.000</b>	NA			NA			NA			<b>0.544</b>	<b>1.5</b>	<b>0.001</b>	NA			NA			NA			NA								
<i>MT1H*</i>	<b>2.038</b>	<b>4.1</b>	<b>0.000</b>	NA			NA			NA			<b>0.971</b>	<b>2.0</b>	<b>0.000</b>	<b>1.728</b>	<b>3.3</b>	<b>0.001</b>	NA			NA			NA			NA					
<i>MT1M*</i>	<b>1.456</b>	<b>2.7</b>	<b>0.000</b>	NA			NA			NA			<b>1.352</b>	<b>2.6</b>	<b>0.000</b>	NA			NA			NA			NA								
<i>MT1X*</i>	<b>0.897</b>	<b>1.9</b>	<b>0.000</b>	NA			NA			NA			<b>0.420</b>	<b>1.3</b>	<b>0.004</b>	NA			NA			NA			NA								
<i>MT2A</i>	<b>1.729</b>	<b>3.3</b>	<b>0.000</b>	NA			NA			NA			0.125	1.1	0.218	NA			NA			NA			NA								
<i>MT3</i>	0.103	1.1	NA	NA			NA			NA			<b>1.196</b>	<b>2.3</b>	<b>0.001</b>	NA			NA			NA			NA								
<i>MT4</i>	-0.002	1.0	NA	NA			NA			NA			0.016	1.0	NA	NA			NA			NA			NA								
<i>MT1*</i>	NA			NA			NA			NA			NA			NA			NA			NA			NA			NA					
<i>MT2*</i>	NA			NA			NA			NA			NA			NA			NA			NA			NA			<b>0.962</b>	<b>1.9</b>	<b>0.000</b>			
	NA			NA			NA			NA			NA			NA			NA			NA			NA			<b>0.803</b>	<b>1.7</b>	<b>0.001</b>			

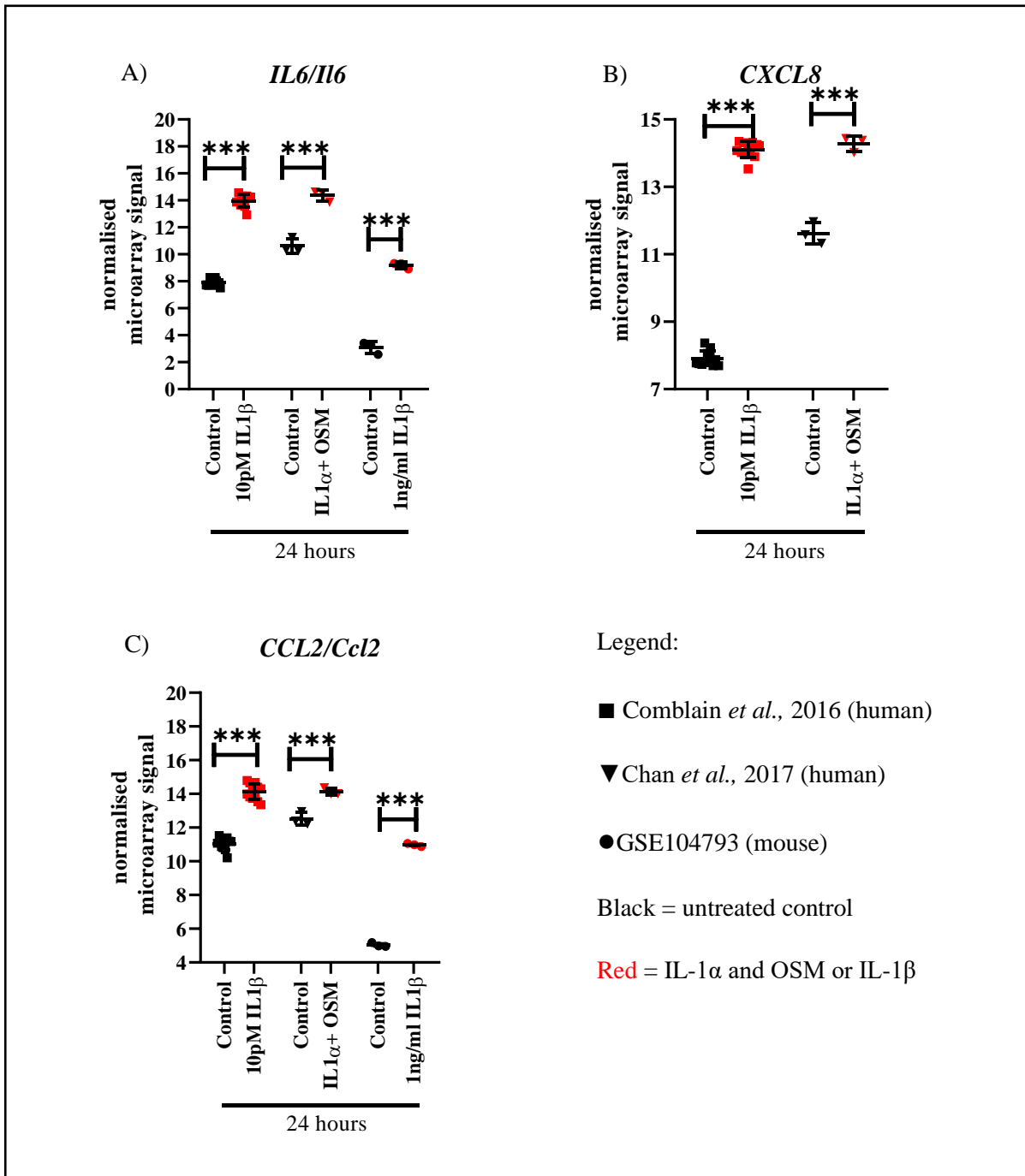


**Figure 3.10 – IL-1 positive control genes (*IL-6/Il-6*, *CXCL8* and *CCL2/Ccl2*) differential expression in human and murine chondrocytes treated  $\pm$  IL-1 for 24 hours.**

Normalised data for *IL-6/Il-6* A), *CXCL8* B) and *CCL2/Ccl2* C) are expressed as microarray signals and were generated by Dr Jamie Soul upon request and are not provided by the SkeletalVis tool. The horizontal lines are the means of the samples with the standard deviation plotted. *Cxcl8* was not included on the Affymetrix array used to assay the mouse chondrocyte transcriptome. P values for significantly and differentially expressed genes were calculated in SkeletalVis (Soul *et al.*, 2018b). \*\*\*  $p < 0.001$ , OSM = oncostatin M.

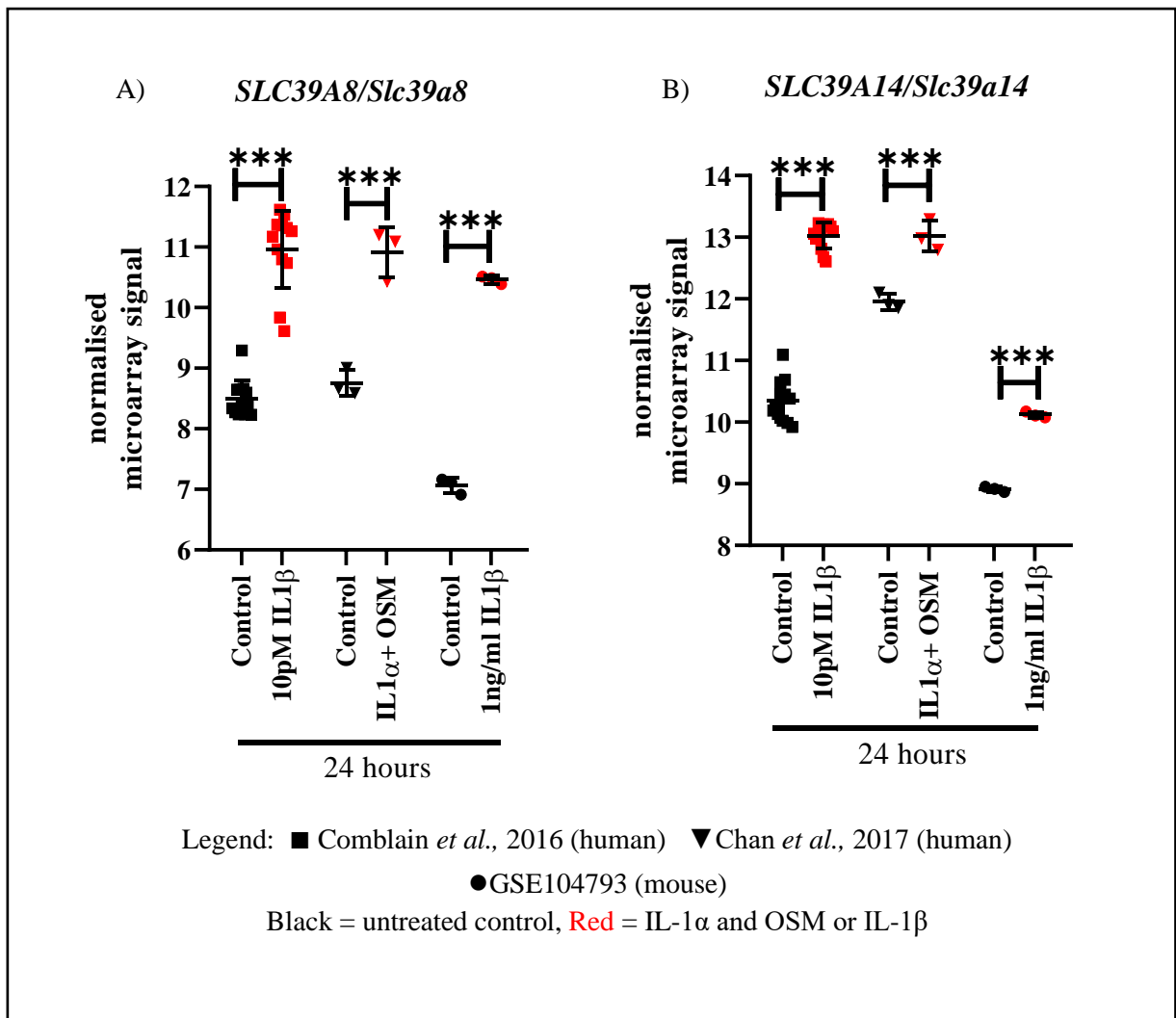


**Figure 3.11 – *SLC39A8/Slc39a8* and *SLC39A14/Slc39a14* are significantly and differentially upregulated in human and murine chondrocytes treated  $\pm$  IL-1 for 24 hours.** Normalised data for *SLC39A8/Slc39a8* A) and *SLC39A14/Slc39a14* B) are expressed as microarray signals and were generated by Dr Jamie Soul upon request and are not provided by the SkeletalVis tool. The horizontal lines are the means of the samples with the standard deviation plotted. P values for significantly and differentially expressed genes were calculated in SkeletalVis (Soul *et al.*, 2018b). \*\*\*  $p < 0.001$ , OSM = oncostatin M.

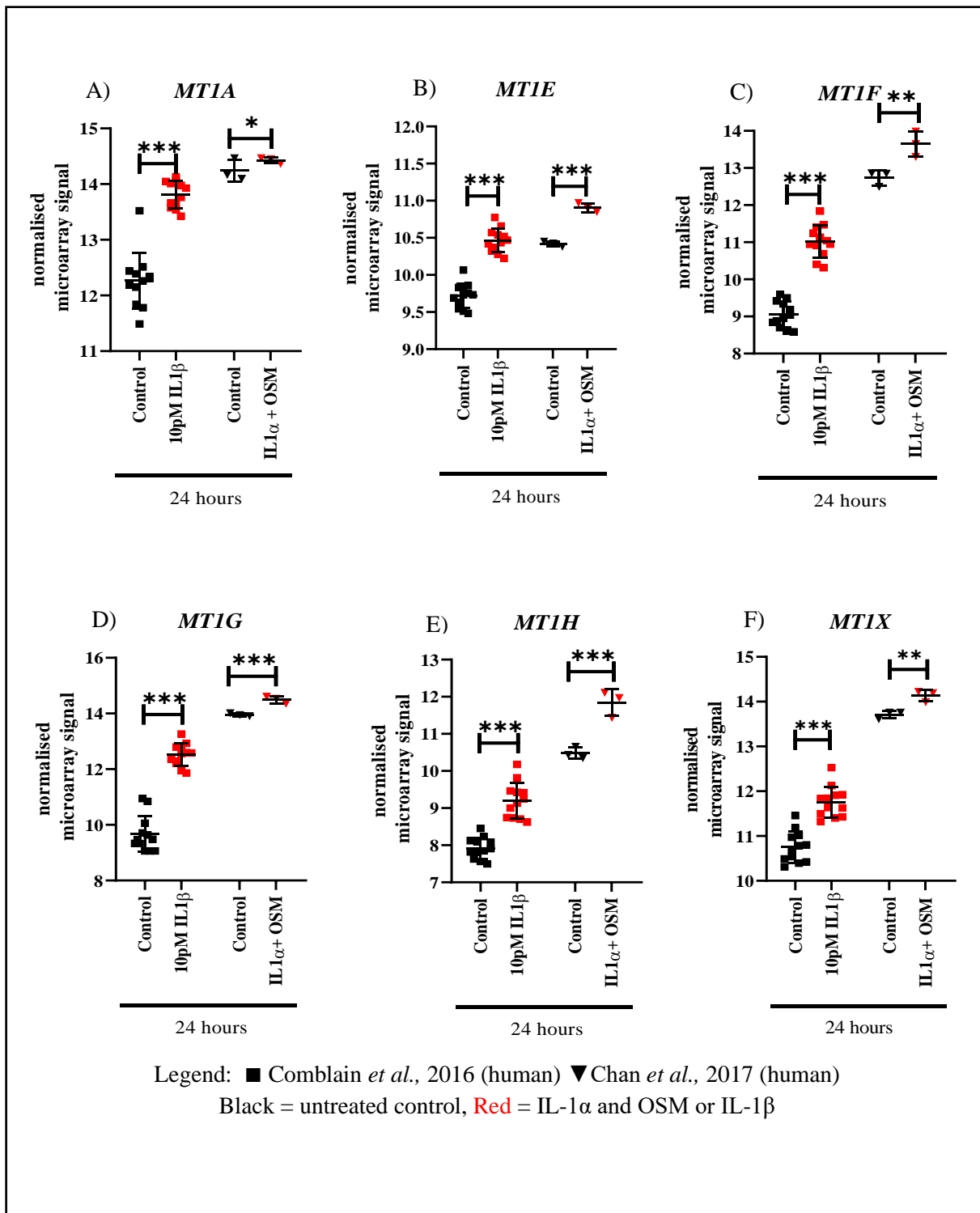


**Figure 3.12 – *MT1A*, *MT1E*, *MT1F*, *MT1G*, *MT1H* and *MT1X* in human chondrocytes treated  $\pm$  IL-1 for 24 hours are significantly and differentially upregulated.**

Normalised data for *MT1A* A), *MT1E* B), *MT1F* C), *MT1G* D), *MT1H* E) and *MT1X* F) are expressed as microarray signals and were generated by Dr Jamie Soul upon request and are not provided by the SkeletalVis tool. The horizontal lines are the means of the samples with the standard deviation plotted. P values for significantly and differentially expressed genes were calculated in SkeletalVis (Soul et al., 2018b). \*  $p < 0.05$ , \*\*  $p < 0.01$ , \*\*\*  $p < 0.001$ , OSM = oncostatin M.

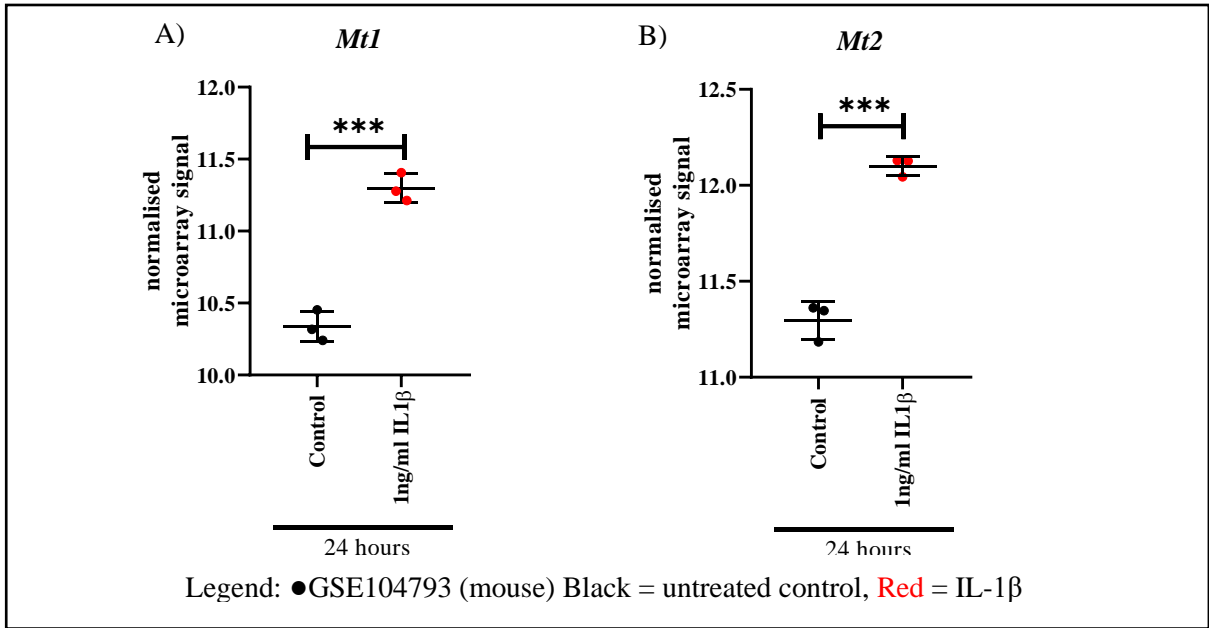


**Figure 3.13 – *Mt1* and *Mt2* are differentially upregulated in murine chondrocytes treated  $\pm$  IL-1 $\beta$  for 24 hours.**

Normalised data for *Mt1* A) and *Mt2* B) is expressed as microarray signals and were generated by Dr Jamie Soul upon request and are not provided by the SkeletalVis tool. The horizontal lines are the means of the samples with the standard deviation plotted. P values for significantly and differentially expressed genes were calculated in SkeletalVis (Soul *et al.*, 2018b). \*\*\* p<0.001.

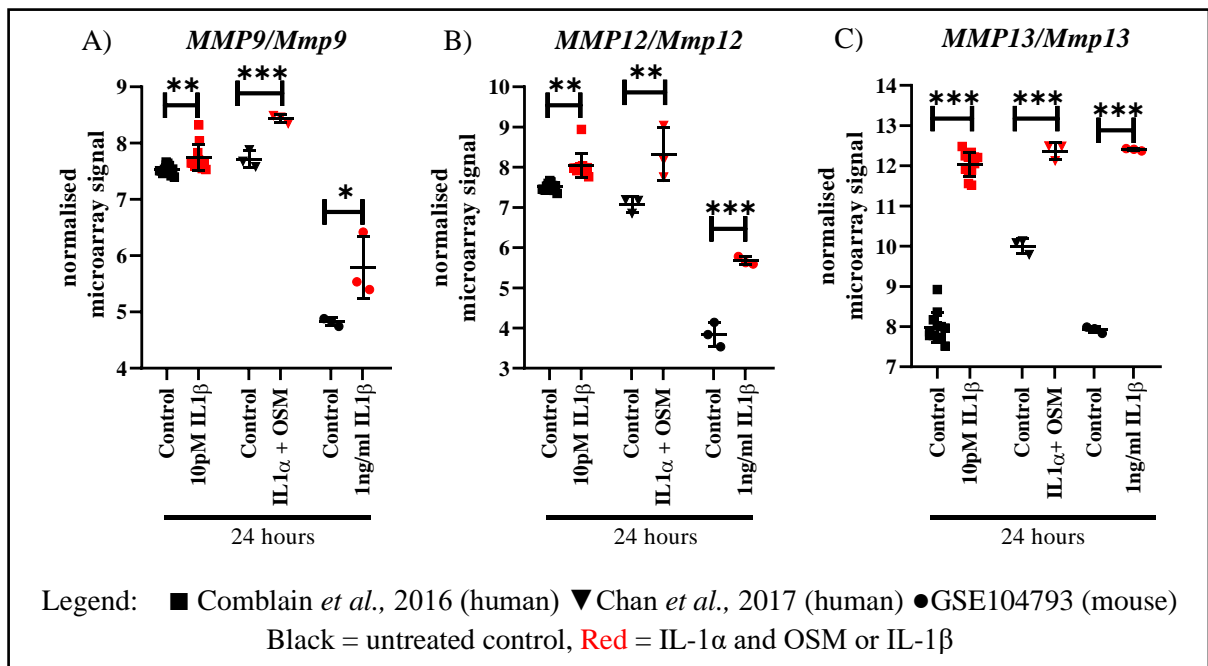


**Figure 3.14 – *MMP9/Mmp9*, *MMP12/Mmp12* and *MMP13/Mmp13* are differentially upregulated in human and murine chondrocytes treated  $\pm$  IL-1 for 24 hours.**

Normalised data for *MMP9/Mmp9* A), *MMP12/Mmp12* B) and *MMP13/Mmp13* C) are expressed as microarray signals and were generated by Dr Jamie Soul upon request and are not provided by the SkeletalVis tool. The horizontal lines are the means of the samples with the standard deviation plotted. P values for significantly and differentially expressed genes were calculated in SkeletalVis (Soul *et al.*, 2018b). \* p<0.05, \*\* p<0.01, \*\*\* p<0.001, OSM=oncostatin M.

### 3.7 Trauma-induced DMM model of OA induction in mice

The zinc-ZIP8-MTF1 axis was characterised in mice (Kim *et al.*, 2014) using a surgically-induced model. I thus explored expression of zinc homeostasis genes in the DMM mouse model of trauma-induced OA in other studies. DMM is a surgically-induced model of OA in mice (Glasson *et al.*, 2007) which involves cutting the medial meniscotibial ligament, subsequently destabilising the medial meniscus, producing OA-lesions three to four weeks later. The control groups normally consist of either unoperated mice or mice in which the ligaments are exposed but not cut, also known as sham surgery. Sometimes research groups perform the sham surgery on the contralateral joint receiving DMM because it reduces total animal number requirements. Herein, two DMM studies were identified (Table 3.6) which focussed on acute (six hours, three and seven days) to more advanced time points (seven, 14 and 42 days) post-surgery. The only zinc transporter that was differentially expressed in DMM-operated whole-joint or cartilage for five out of six time points was *Slc39a14* (Table 3.6 and Figure 3.15).

Datasets	E-GEOD-26475									GSE45793								
References	Burleigh <i>et al.</i> , 2012									Bateman <i>et al.</i> , 2013								
Platforms	A-AFFY-130_Affymetrix GeneChip Mouse Gene 1.0 ST Array [MoGene-1 0-st-v1]									Agilent-014868 Whole Mouse Genome Microarray 4x44K G4122F								
N number	3 mice per treatment group DMM vs Sham									4 mice per treatment group DMM vs Sham								
Tissue	Whole-joint									cartilage								
Timepoints (Days)	0.25			3			7			7			14			42		
<b>Znt zinc exporter gene family</b>																		
Gene name	log2 FC	FC	padj	log2 FC	FC	padj	log2 FC	FC	padj	log2 FC	FC	padj	log2 FC	FC	padj	log2 FC	FC	padj
<i>Slc30a1</i>	-0.107	0.9	0.686	-0.036	1.0	0.970	0.127	1.1	0.548	<b>0.950</b>	<b>1.9</b>	<b>0.045</b>	<b>1.091</b>	<b>2.1</b>	<b>0.004</b>	0.739	1.7	0.052
<i>Slc30a2</i>	0.335	1.3	0.147	0.196	1.1	NA	-0.153	0.9	0.491	0.641	1.6	0.261	0.604	1.5	0.186	0.091	1.1	0.874
<i>Slc30a3</i>	-0.042	1.0	0.899	0.134	1.1	NA	-0.291	0.8	0.170	-0.059	1.0	NA	-0.141	0.9	NA	-0.061	1.0	NA
<i>Slc30a4</i>	-0.229	0.9	0.242	-0.141	0.9	0.764	-0.191	0.9	0.280	<b>1.472</b>	<b>2.8</b>	<b>0.000</b>	<b>0.857</b>	<b>1.8</b>	<b>0.001</b>	<b>1.422</b>	<b>2.7</b>	<b>0.000</b>
<i>Slc30a5</i>	0.049	1.0	0.820	0.032	1.0	0.959	0.143	1.1	0.333	0.552	1.5	0.084	-0.050	1.0	0.873	0.171	1.1	0.557
<i>Slc30a6</i>	0.152	1.1	0.416	0.113	1.1	NA	-0.143	0.9	0.381	0.128	1.1	0.536	<b>0.319</b>	<b>1.2</b>	<b>0.035</b>	0.119	1.1	0.479
<i>Slc30a7</i>	0.061	1.0	0.822	0.202	1.2	0.656	-0.031	1.0	0.896	0.026	1.0	0.913	<b>0.615</b>	<b>1.5</b>	<b>0.000</b>	<b>0.392</b>	<b>1.3</b>	<b>0.010</b>
<i>Slc30a8</i>	-0.175	0.9	NA	0.008	1.0	NA	0.213	1.2	NA	-0.088	0.9	0.701	0.025	1.0	0.898	0.090	1.1	NA
<i>Slc30a9</i>	-0.009	1.0	0.971	0.016	1.0	0.984	-0.130	0.9	0.390	0.381	1.3	0.191	0.411	1.3	0.077	0.057	1.0	0.848
<i>Slc30a10</i>	0.294	1.2	0.229	0.227	1.2	NA	0.080	1.1	0.750	0.226	1.2	NA	0.019	1.0	NA	0.017	1.0	NA
<b>Zip zinc importer gene family</b>																		
<i>Slc39a1</i>	0.235	1.2	0.216	-0.044	1.0	0.948	-0.077	0.9	0.688	0.129	1.1	0.586	<b>0.464</b>	<b>1.4</b>	<b>0.007</b>	<b>0.397</b>	<b>1.3</b>	<b>0.021</b>
<i>Slc39a2</i>	0.199	1.1	0.550	0.110	1.1	NA	0.137	1.1	NA	0.174	1.1	0.431	-0.090	0.9	0.636	-0.126	0.9	0.503
<i>Slc39a3</i>	0.068	1.0	0.793	0.042	1.0	0.955	-0.196	0.9	0.282	0.112	1.1	0.820	-0.410	0.8	0.219	-0.640	0.6	0.052
<i>Slc39a4</i>	-0.214	0.9	0.360	0.164	1.1	NA	-0.078	0.9	NA	-0.889	<b>0.5</b>	<b>0.050</b>	-0.323	0.8	0.404	<b>-0.822</b>	<b>0.6</b>	<b>0.025</b>
<i>Slc39a5</i>	-0.021	1.0	0.932	0.209	1.2	NA	-0.005	1.0	NA	-0.499	<b>0.7</b>	<b>0.005</b>	-0.106	0.9	0.459	-0.080	0.9	0.598
<i>Slc39a6</i>	0.084	1.1	0.721	0.315	1.2	0.336	0.196	1.1	0.264	1.080	<b>2.1</b>	<b>0.004</b>	<b>1.104</b>	<b>2.2</b>	<b>0.000</b>	<b>1.287</b>	<b>2.4</b>	<b>0.000</b>
<i>Slc39a7</i>	0.078	1.1	0.741	0.124	1.1	0.797	-0.171	0.9	0.323	-0.468	<b>0.7</b>	<b>0.036</b>	-0.083	0.9	0.684	<b>-0.649</b>	<b>0.6</b>	<b>0.001</b>
<i>Slc39a8</i>	0.162	1.1	0.388	-0.119	0.9	0.793	-0.080	0.9	0.650	0.302	1.2	0.174	0.269	1.2	0.133	<b>0.466</b>	<b>1.4</b>	<b>0.009</b>
<i>Slc39a9</i>	0.081	1.1	0.668	0.052	1.0	0.912	0.034	1.0	0.848	0.360	1.3	0.271	0.352	1.3	0.177	-0.066	1.0	0.840
<i>Slc39a10</i>	<b>0.652</b>	<b>1.6</b>	<b>0.006</b>	-0.072	1.0	0.923	0.138	1.1	0.542	0.367	1.3	0.356	0.146	1.1	0.677	0.062	1.0	0.874
<i>Slc39a11</i>	-0.025	1.0	0.922	-0.037	1.0	0.953	-0.063	1.0	0.718	-0.154	0.9	0.701	0.194	1.1	0.526	<b>0.801</b>	<b>1.7</b>	<b>0.005</b>
<i>Slc39a12</i>	0.087	1.1	NA	0.143	1.1	NA	0.206	1.2	NA	0.500	1.4	0.358	0.583	1.5	0.172	-0.142	0.9	0.783
<i>Slc39a13</i>	0.152	1.1	0.512	-0.003	1.0	0.998	-0.174	0.9	0.371	0.074	1.1	0.815	0.133	1.1	0.571	<b>-0.377</b>	<b>0.8</b>	<b>0.078</b>
<i>Slc39a14*</i>	<b>1.011</b>	<b>2.0</b>	<b>0.000</b>	<b>0.807</b>	<b>1.7</b>	<b>0.024</b>	<b>0.707</b>	<b>1.6</b>	<b>0.003</b>	<b>1.235</b>	<b>2.4</b>	<b>0.002</b>	<b>1.139</b>	<b>2.2</b>	<b>0.000</b>	0.338	1.3	0.292
<b>Transcription factors</b>																		
<i>Spl</i>	-0.119	0.9	0.484	0.026	1.0	0.968	0.105	1.1	0.473	-0.284	0.8	0.476	-0.381	0.8	0.213	0.207	1.2	0.540
<i>Mtf1</i>	0.135	1.1	0.726	0.163	1.1	0.850	<b>0.585</b>	<b>1.5</b>	<b>0.047</b>	0.114	1.1	0.733	0.168	1.1	0.503	0.213	1.2	0.397
<i>Mtf2</i>	-0.077	0.9	0.799	0.185	1.1	0.730	0.343	1.3	0.106	0.032	1.0	0.909	-0.239	0.8	0.282	-0.114	0.9	0.714
<b>Metallothioneins</b>																		
<i>Mt1</i>	<b>0.843</b>	<b>1.8</b>	<b>0.017</b>	0.732	1.7	0.229	0.603	1.5	0.070	0.432	1.3	0.495	0.756	1.7	0.112	0.008	1.0	0.990
<i>Mt2</i>	<b>1.235</b>	<b>2.4</b>	<b>0.020</b>	1.283	2.4	0.148	0.342	1.3	0.507	0.447	1.4	0.657	1.422	<b>2.7</b>	0.045	-0.098	0.9	0.917

**Table 3.6 – SkeletalVis data from two murine destabilisation of the medial meniscus (DMM) OA datasets for genes involved in zinc homeostasis.**

The log<sub>2</sub>-fold change (log<sub>2</sub>FC), fold change (FC) and adjusted p-value (padj) is recorded for each gene entry and the fold change has been colour-coded across all genes and datasets using a three-colour scheme indicating differential gene downregulation after DMM (blue), no change (white), and upregulation after DMM (red). Data in bold is significantly and differentially expressed for that gene in a specific dataset and time point and gene name with asterisk indicates differential gene expression at more than one time point in both DMM studies. Where NA is confined to padj only column, then the p value was not calculated because of insufficient replicates.

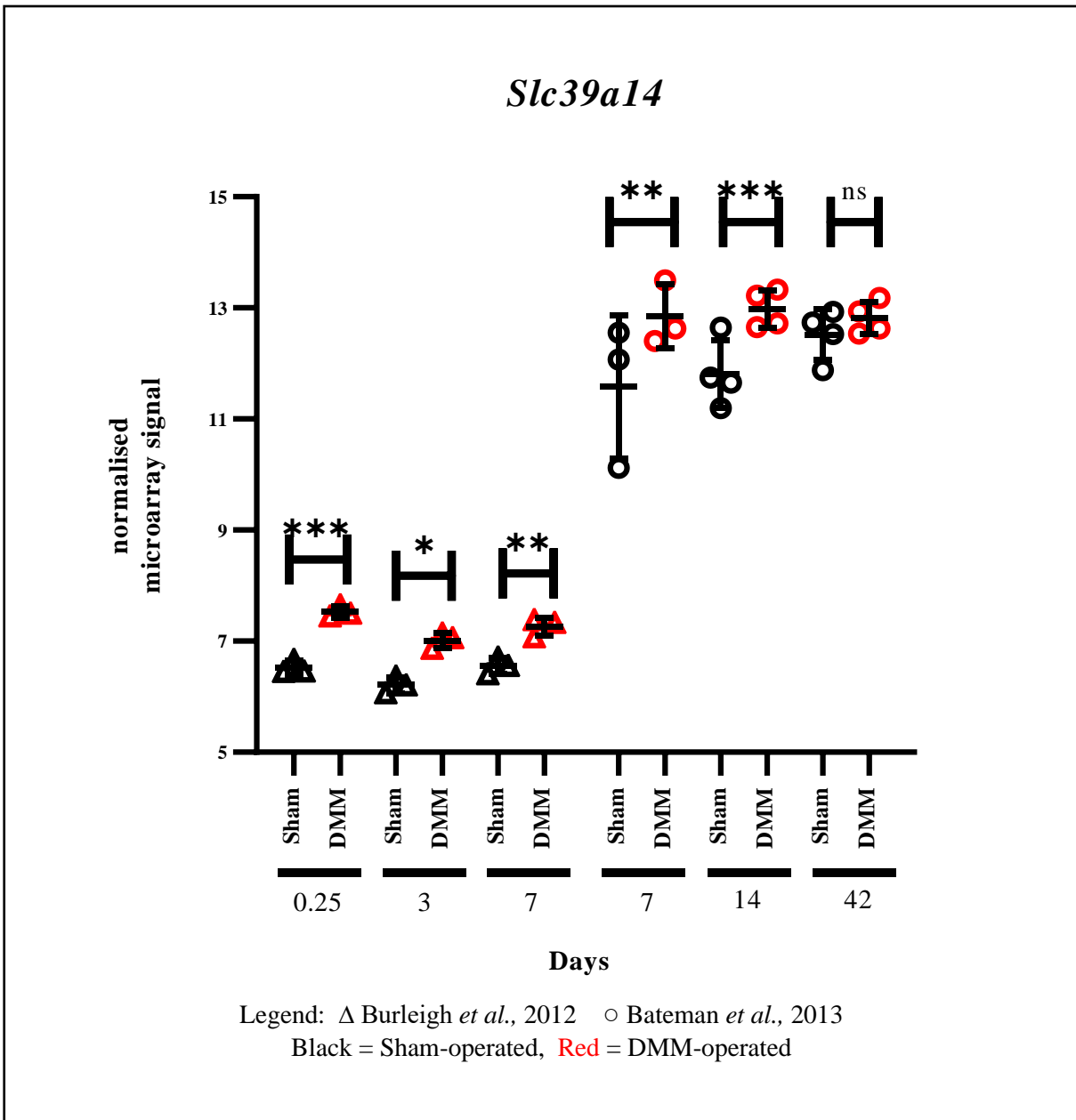


**Figure 3.15 – *Slc39a14* is significantly and differentially overexpressed in cartilage of mice following DMM surgery acutely and up to two weeks.**

Normalised data is expressed as microarray signals and were generated by Dr Jamie Soul upon request and are not provided by the SkeletalVis tool. The horizontal lines are the means of the samples with the standard deviation plotted. P values for significantly and differentially expressed genes were calculated in SkeletalVis (Soul *et al.*, 2018b). n s= non-significant \*  $p < 0.05$ , \*\*  $p < 0.01$ , \*\*\*  $p < 0.001$ , DMM = Destabilisation of the medial meniscus via transection of the medial meniscotibial ligament. Sham = medial meniscotibial ligament exposed but not transected.

### 3.8 Ageing model of OA in mice

Given that *SLC39A14* was upregulated in the DMM mouse model of post-trauma OA, I next examined whether this gene was also dysregulated in the STR/ort mouse, a model for spontaneous OA. This mouse strain is directly derived from a STR/1N mouse strain which was originally created by Strong (Strong, 1944) for the purpose of identifying cancer resistance traits at the site of injection following the administration of carcinogens (Staines *et al.*, 2017). After a period of outbreeding the STR/1N strain was renamed to STR/ort. The STR/ort strain develops OA in several joints including knee, ankle, elbow and temporomandibular joints and is the leading model which mimics the phenotype observed in primary human OA, despite an apparent sexual dimorphism between human and mouse; that male mice develop spontaneous OA more frequently than females. These mice spontaneously develop OA at 18 weeks of age, concomitant with obesity and have elevated levels of IL-1 $\beta$  in articular cartilage in all ages compared to CBA mice (Goldring and Goldring, 2010) and in serum (Chambers *et al.*, 1997). Additionally, a microarray analysis of articular cartilage identified NF- $\kappa$ B as the main modified pathway in STR/ort mice (Poulet *et al.*, 2012). CBA mice are the most appropriate age-matched mouse control, not only because these mice do not develop OA, but because these were one of four parental strains used in the derivation of the STR/ort mouse strain (Staines *et al.*, 2017).

Only one transcriptomic study of the STR/ort mice was present in SkeletalVis at the time of consultation of the database. Gene expression in cartilage was assessed pre-OA onset (eight weeks), at onset of OA (18 weeks) and advanced OA (40 weeks). Several genes were dysregulated at time points when OA had developed but there were no differences between the two mouse strains at eight weeks (Table 3.7). *Slc30a9* and *Slc30a10* of the zinc exporters were downregulated and *Slc39a14* of the zinc importers was upregulated. Interestingly, *Slc39a8* was the most significantly ( $p=0.012$ ) downregulated zinc importer at 18 weeks and although significance threshold was just missed ( $p=0.053$  and  $p=0.06$ ) this trend was observed as early as 8 weeks and at the latest time point of 40 weeks (Table 3.7).

**Table 3.7 – SkeletalVis data from a single study of a spontaneous OA ageing mouse model using STR/ort mice.**

The log<sub>2</sub>-fold change (log<sub>2</sub>FC), fold change (FC) and adjusted p-value (padj) is recorded for each gene entry and the fold change has been colour-coded across all genes and datasets using a three colour scheme indicating differential gene downregulation in STR/Ort strain (blue), no change (white), and upregulation in STR/Ort strain (red). Data in bold is significantly and differentially expressed for that gene at a time point and bold gene name indicates differential gene expression at 18 and 40 weeks. Where NA is confined to padj only column, then the p value was not calculated because of insufficient replicates.

Dataset	GSE33754								
Reference	Poulet <i>et al.</i> , 2012								
Platform	[MoGene-1_0-st] Affymetrix Mouse Gene 1.0 ST Array [transcript								
N number	4 animals per group STR/Ort OA prone vs CBA mice								
Tissue	cartilage								
Timepoints (weeks)	8			18			40		
Gene name	log <sub>2</sub> FC	FC	padj	log <sub>2</sub> FC	FC	padj	log <sub>2</sub> FC	FC	padj
<i>Slc30a</i> zinc exporter gene family									
<i>Slc30a1</i>	-0.105	0.9	0.559	-0.193	0.9	0.102	-0.046	1.0	0.745
<i>Slc30a2</i>	0.097	1.1	0.646	0.132	1.1	0.352	-0.016	1.0	0.931
<i>Slc30a3</i>	0.106	1.1	0.506	-0.053	1.0	0.692	-0.075	0.9	0.526
<i>Slc30a4</i>	0.185	1.1	0.524	0.192	1.1	0.355	0.247	1.2	0.206
<i>Slc30a5</i>	-0.036	1.0	0.866	-0.031	1.0	0.836	0.075	1.1	0.530
<i>Slc30a6</i>	0.000	1.0	0.998	0.026	1.0	0.885	0.064	1.0	0.659
<i>Slc30a7</i>	0.056	1.0	0.756	0.147	1.1	0.170	0.184	1.1	0.084
<i>Slc30a8</i>	0.089	1.1	0.535	-0.034	1.0	0.789	0.035	1.0	NA
<b><i>Slc30a9*</i></b>	-0.296	0.8	0.239	<b>-0.488</b>	<b>0.7</b>	<b>0.009</b>	-0.320	0.8	0.089
<b><i>Slc30a10*</i></b>	-0.350	0.8	0.052	<b>-0.397</b>	<b>0.8</b>	<b>0.005</b>	<b>-0.441</b>	<b>0.7</b>	<b>0.003</b>
<i>Slc39a</i> zinc importer gene family									
<i>Slc39a1</i>	0.205	1.2	0.231	0.201	1.1	0.114	0.188	1.1	0.143
<i>Slc39a2</i>	-0.115	0.9	0.559	0.009	1.0	0.967	0.015	1.0	0.932
<i>Slc39a3</i>	0.008	1.0	0.975	-0.007	1.0	0.972	-0.081	0.9	0.515
<i>Slc39a4</i>	-0.095	0.9	0.628	-0.047	1.0	0.778	-0.154	0.9	0.223
<i>Slc39a5</i>	-0.044	1.0	0.849	0.105	1.1	0.431	0.076	1.1	0.578
<i>Slc39a6</i>	0.043	1.0	0.876	0.095	1.1	0.564	-0.021	1.0	0.910
<i>Slc39a7</i>	0.050	1.0	0.809	0.094	1.1	0.459	0.169	1.1	0.143
<b><i>Slc39a8*</i></b>	-0.379	0.8	0.053	<b>-0.380</b>	<b>0.8</b>	<b>0.012</b>	-0.286	0.8	0.060
<i>Slc39a9</i>	0.064	1.0	0.664	0.090	1.1	0.366	0.025	1.0	0.833
<i>Slc39a10</i>	0.072	1.1	0.708	0.008	1.0	0.969	-0.137	0.9	0.254
<i>Slc39a11</i>	0.006	1.0	0.988	0.118	1.1	0.493	0.162	1.1	0.309
<i>Slc39a12</i>	-0.189	0.9	0.249	-0.163	0.9	0.184	-0.024	1.0	NA
<b><i>Slc39a13*</i></b>	0.036	1.0	0.904	0.201	1.1	0.172	<b>0.331</b>	<b>1.3</b>	<b>0.025</b>
<b><i>Slc39a14*</i></b>	-0.001	1.0	0.998	<b>0.933</b>	<b>1.9</b>	<b>0.000</b>	<b>0.772</b>	<b>1.7</b>	<b>0.000</b>
Transcription factors									
<i>Sp1</i>	-0.051	1.0	0.816	-0.144	0.9	0.246	-0.097	0.9	0.453
<i>Mtf1</i>	0.010	1.0	0.972	0.003	1.0	0.990	0.002	1.0	0.991
<i>Mtf2</i>	-0.159	0.9	0.17	-0.103	0.9	0.26	0.024	1.0	0.83
Metallothioneins									
<b><i>Mt1*</i></b>	-0.468	0.7	0.205	<b>0.670</b>	<b>1.6</b>	<b>0.015</b>	0.144	1.1	0.657
<b><i>Mt2*</i></b>	-0.366	0.8	0.179	<b>0.525</b>	<b>1.4</b>	<b>0.011</b>	0.194	1.1	0.369

### 3.9 Summary of SkeletalVis analysis on zinc homeostasis genes

In summary, the most consistently and significantly altered zinc importer between cartilage and chondrocytes was *SLC39A14*. Except for the intact OA cartilage versus non-OA control cartilage comparison, *SLC39A14* was upregulated in damaged OA cartilage, in STR/ort murine cartilage, and in human and murine chondrocytes treated with IL-1 receptor ligands for four and 24 hours. *SLC39A8* was not differentially expressed in human cartilage but was upregulated in chondrocytes by IL-1 receptor ligands at 24 hours. *SLC39A8* was downregulated in the Str/Ort mouse cartilage at 18 weeks when OA manifests spontaneously in this OA model. Though no two mouse models for OA are comparable, this result contradicts the spontaneous OA at 12 months in mice constitutively expressing *Slc39a8* in a cartilage-specific manner which at 10-12 weeks old also develop worse cartilage fibrillation six weeks after DMM (Kim *et al.*, 2014). Potentially *SLC39A14* and not *SLC39A8* facilitates zinc entry from the extracellular space in human cartilage. *MTF1* was not significantly altered in cartilage but only in chondrocytes treated with IL-1 for four hours. *MMP9/Mmp9*, *MMP12/Mmp12* and *MMP13/Mmp13* were upregulated after four and 24 hours of IL-1-treatment in human and murine chondrocytes, but also *Mmp3* only at four hours in IL-1-treated murine chondrocytes. *ADAM-TS5/Adam-ts5* was not significantly altered in IL-1-treated human or murine chondrocytes. *MT1A* and *MT1X* were suppressed in intact OA cartilage when compared to non-OA cartilage but other *MT* members *MT1F*, *MT1G* and *MT1M* (Table 3.8) were upregulated in damaged OA cartilage compared to preserved OA cartilage. These same *MT* genes and other family members were also upregulated in IL-1 treated human chondrocytes treated for four or 24 hours.

**Table 3.8 – Summary of zinc homeostasis genes significantly and differentially expressed in iOA or dOA cartilage, IL-1-treated chondrocytes, DMM or STR/ort mice.**

The table highlights only those genes which were significantly expressed (green cells) while the coloured arrows relate the direction of the change. N/A indicates a mouse gene not expressed in humans.

Gene	human cartilage		chondrocytes		mouse cartilage	
	iOA versus non-OA	dOA versus iOA	IL1 vs control		DMM	STR/ort
			human	human and/or mouse		
<i>SLC30A2/Slc30a2</i>	↓					
<i>SLC30A9/Slc30a9</i>						↓
<i>SLC30A10/Slc30a10</i>						↓
<i>SLC39A3/Slc39a3</i>	↑					
<i>SLC39A7/Slc39a7</i>	↑					
<i>SLC39A8/Slc39a8</i>				↑		↓
<i>SLC39A14/Slc39a14</i>	↓	↑	↑	↑	↑	↑
<i>MTF1/Mtf1</i>			↑			
<i>MT1A</i>	↓			↑		
<i>MT1E</i>			↑	↑		
<i>MT1F</i>		↑		↑		
<i>MT1G</i>		↑		↑		
<i>MT1H</i>				↑		
<i>MT1M</i>		↑		↑		
<i>MT1X</i>	↓		↑	↑		
<i>MT2A</i>			↑			
<i>Mt1</i>	N/A	N/A	N/A	↑		
<i>Mt2</i>	N/A	N/A	N/A	↑		

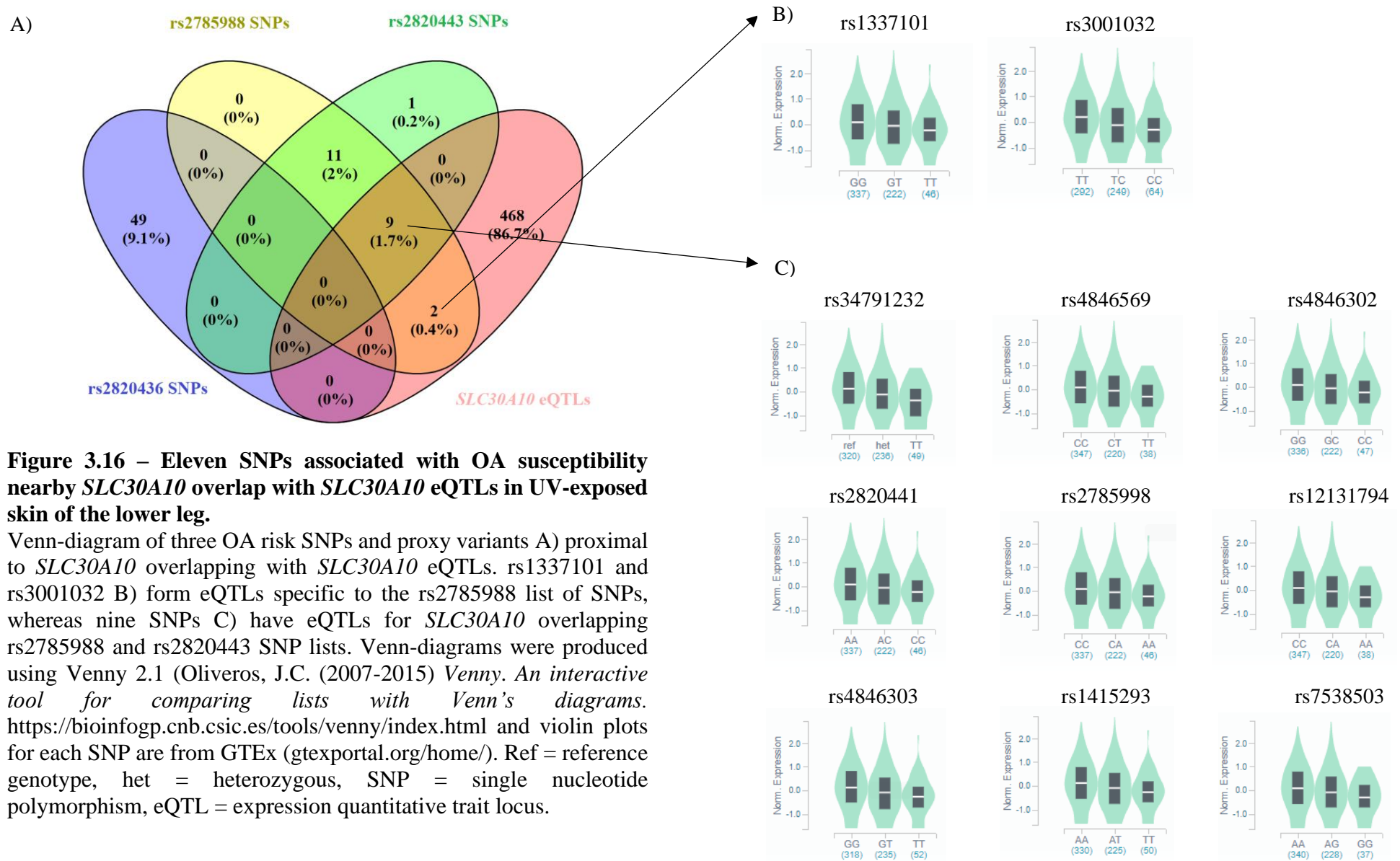
### 3.10 Do human genetic studies implicate zinc homeostasis in OA pathogenesis?

GWAS of OA cartilage or a surrogate measure of decreased cartilage thickness, mjsw, have enabled the identification of single nucleotide polymorphisms (SNPs) some of which map near zinc transporters (Castano-Betancourt *et al.*, 2016; Stykarsdottir *et al.*, 2018; Zengini *et al.*, 2018; Tachmazidou *et al.*, 2019). These five OA or mjsw risk SNPs map nearby or within the *SLC30A10*, *SLC30A5* or *SLC39A8* genes and summary information for the five SNPs is shown in Table 2.2.

The SNPs identified through GWAS studies are not necessarily the functional SNP associated with the phenotype. This is because the genotyping platforms are designed for cost-effectiveness and exploit LD to minimise the total number of SNPs that need to be genotyped per individual, whilst maintaining SNP coverage in the population under investigation. LD describes the degree to which an allele of one SNP is inherited/correlates with an allele of another SNP within a population (Bush and Moore, 2012). These LD blocks occur on the same chromosome and are sites of limited recombination and genotyping marker risk alleles of SNPs can reliably predict alleles of other SNPs from the same LD block. Therefore, the presence of LD creates two possible outcomes from GWAS: either the genotyped SNP is the functional variant and occurs significantly more frequently in case control GWAS, or more likely, the genotyped SNP is just a significantly associated sentinel SNP. Only functional genetic experiments can elucidate the functional SNP within an LD block.

Usually, risk alleles for common complex disease such as OA act by subtly altering the expression of nearby genes. However, the target genes of these risk variants are currently unknown. When there is a correlation between gene expression and a SNP stratified by genotype this is known as an expression quantitative trait locus (eQTL). The online database GTEx ([gtexportal.org/home/](http://gtexportal.org/home/)) has matched genotype gene expression data in nearly 1000 individuals from 54 non-diseased tissue sites (release version eight), the most relevant tissue to OA in this dataset being skeletal muscle. To determine SNPs in LD with the five SNPs in Table 2.2 the website LDlink (<https://ldlink.nci.nih.gov>), a repository of genotype data for the 1000 Genomes Project, was used to investigate each SNP in LD using the  $r^2$  correlation cut-off 0.8 in samples from five European populations. These were northern and western Europeans residing in Utah, Italian Tuscans, Finns, British (from England and Scotland) and Iberian people of Spain. I was interested in comparing the SNP lists mapping to the three zinc transporters identified with LDlink with the eQTLs in GTEx to identify overlapping SNPs with eQTLs for these zinc transporters. These are illustrated in Figures 3.16 and 3.17 as Venn diagrams or violin plots.

There were 21 SNPs in LD ( $r^2 \geq 0.8$ ) with the sentinel SNP rs2785988 and 20 SNPs in LD ( $r^2 \geq 0.8$ ) with the sentinel SNP rs2820443. For the OA hip risk variant rs2785988, mapping to near *SLC30A10*, 11 of 21 SNPs in LD ( $r^2$  0.81-0.97) overlapped with *SLC30A10* eQTLs in UV-exposed skin (Figure 3.16A). Nine of these eleven SNPs shared an eQTL for *SLC30A10* and were also in LD ( $r^2 \geq 0.83$ -0.96) with the OA hip and/or knee risk variant rs2820443. In every instance, possession of the minor allele resulted in reduced *SLC30A10* gene expression compared to major allele possession (Figure 3.16B and C). There were 48 SNPs in LD ( $r^2 \geq 0.8$ ) with the hospital diagnosed OA associated SNP rs2820436 that also maps to the *SLC30A10* locus, but none of these overlapped with the 479 SNPs that formed an eQTL with *SLC30A10* in GTEx. For the hip mjsw associated SNP rs10471753, which maps near to *SLC30A5* there were 32 SNPs in LD ( $r^2 \geq 0.8$ ), but none of these overlapped with the 263 SNPs that formed an eQTL with *SLC30A5* in various tissues (Figure 3.17A). The rare OA associated SNP rs13107325 maps to exon eight of *SLC39A8* and is predicted to change the amino acid sequence. There were three SNPs in LD with this SNP ( $r^2 \geq 0.8$ ), but none of these overlapped with the 370 *SLC39A8* eQTL SNPs in GTEx (Figure 3.17B).



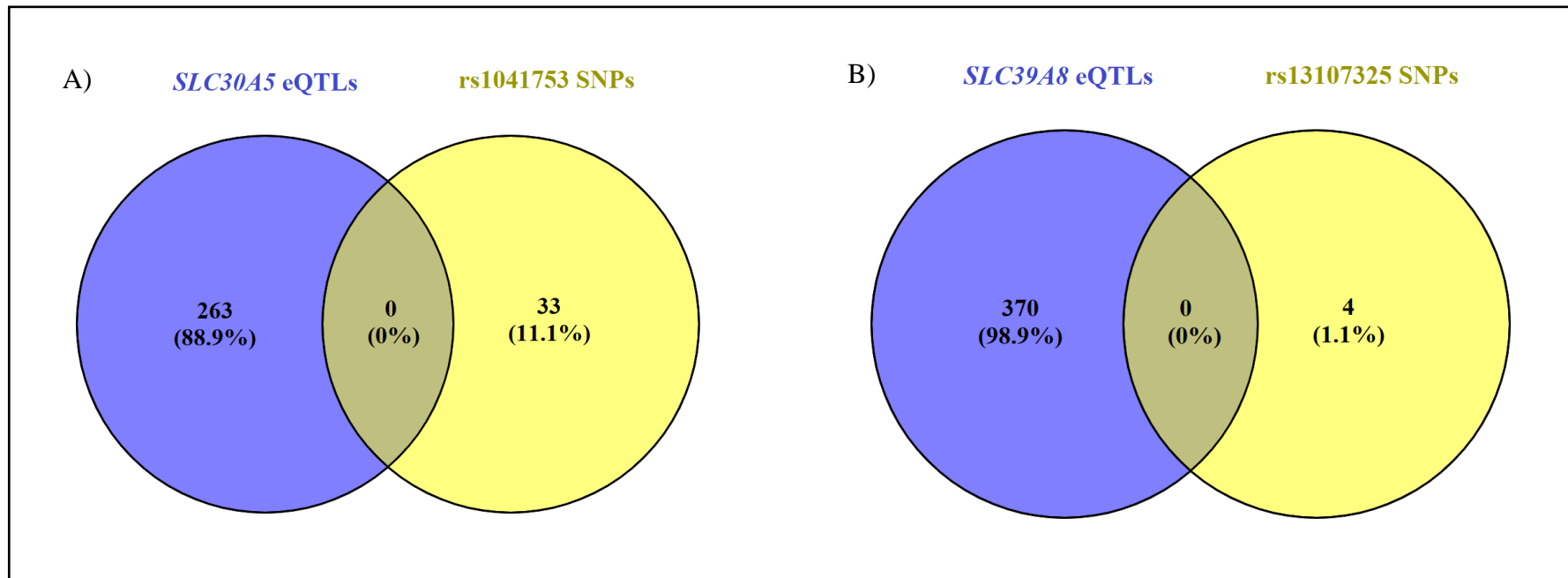


**Figure 3.17 - SNPs in LD with rs10471753 do not overlap with eQTLs for *SLC30A5* A) and SNPs in LD with rs13107325 do not overlap with eQTLs for *SLC39A8* in GTEx B).**

Venn-diagrams were produced using Venny 2.1 (Oliveros, J.C. (2007-2015) *Venny. An interactive tool for comparing lists with Venn's diagrams.* <https://bioinfogp.cnb.csic.es/tools/venny/index.html>. SNP = single nucleotide polymorphism.

### **3.11 Utilising existing RNA-Seq hip and knee OA cartilage data to identify zinc homeostasis genes for laboratory-based analyses**

Transcripts per million (TPM) RNA-Seq data from the knee OA ipsilateral cartilage (Dunn *et al.*, 2016) and hip cartilage (Ajekigbe *et al.*, 2019) studies were provided by Dr. Kathleen Cheung, Newcastle University, Faculty of Medical Sciences. Genes with TPM values >4 were considered expressed in cartilage and with this understanding I proceeded to design qPCR assays for each of the genes in Table 3.9. *SLC30A2* and *SLC30A3* zinc transporter qPCR assays expressed solely in hip based on the RNA-Seq data (Table 3.9) were measured in laboratory experiments with HACs derived from knee cartilage to confirm absence of gene expression. Every gene in this panel was initially investigated in SW1353 chondrosarcoma and T/C-28a2 rib chondrocytes and the list was later condensed if a gene was consistently not detectable in these cell lines.

**Table 3.9– List of zinc homeostasis and inflammation-associated genes investigated for appreciable cartilage tissue expression (TPM) in two RNA-Seq datasets of hip and knee respectively.**

Genes with TPM values of  $\geq$  four (bold) in hip or knee cartilage were chosen for analysis, with qPCR assays designed with the Roche Probe Library assay design tool [https://lifescience.roche.com/en\\_gb/brands/universal-probe-library.html#assay-design-center](https://lifescience.roche.com/en_gb/brands/universal-probe-library.html#assay-design-center). *CXCL8* was investigated regardless of these TPM values. NOF = Neck of femur.

Gene	Ajekigbe, Cheung <i>et al.</i> , 2019		Dunn <i>et al.</i> , 2016	
	Hip OA cartilage (n=10)	NOF cartilage (n=6)	Knee OA cartilage	
			iOA (n=8)	dOA (n=8)
<b><i>IL6</i></b>	0.07	9.69	0.15	0.67
<i>CXCL8</i>	0.21	1.50	0.46	2.29
<b><i>CCL2</i></b>	2.72	27.18	16.28	16.52
<b><i>SLC30A1</i></b>	9.46	8.53	13.00	23.51
<b><i>SLC30A2</i></b>	8.64	8.34	0.62	0.58
<b><i>SLC30A3</i></b>	4.37	3.68	0.01	0.01
<i>SLC30A4</i>	2.89	2.33	3.30	3.75
<b><i>SLC30A5</i></b>	21.67	14.86	33.89	36.19
<b><i>SLC30A6</i></b>	10.32	7.67	13.86	15.68
<b><i>SLC30A7</i></b>	5.04	4.71	6.00	6.61
<i>SLC30A8</i>	0.27	0.10	0.07	0.27
<b><i>SLC30A9</i></b>	22.29	16.72	34.32	37.25
<i>SLC30A10</i>	0.47	0.36	0.02	0.00
<b><i>SLC39A1</i></b>	88.68	101.51	86.97	85.61
<i>SLC39A2</i>	0.11	0.05	0.07	0.05
<b><i>SLC39A3</i></b>	16.19	9.21	14.71	14.24
<b><i>SLC39A4</i></b>	23.61	14.43	12.06	11.13
<i>SLC39A5</i>	0.85	0.63	0.17	0.06
<b><i>SLC39A6</i></b>	112.23	64.30	95.24	97.32
<b><i>SLC39A7</i></b>	196.58	114.04	232.82	211.54
<b><i>SLC39A8</i></b>	72.99	71.07	97.10	108.88
<b><i>SLC39A9</i></b>	40.57	31.12	35.70	36.44
<b><i>SLC39A10</i></b>	5.89	4.13	5.58	5.34
<b><i>SLC39A11</i></b>	17.14	7.78	14.43	10.56
<i>SLC39A12</i>	0.03	0.02	0.01	0.00
<b><i>SLC39A13</i></b>	74.82	32.92	59.17	57.65
<b><i>SLC39A14</i></b>	459.60	1976.02	239.09	353.44
<b><i>MTF1</i></b>	4.38	3.74	3.07	2.93
<b><i>MT1A</i></b>	8.88	22.41	12.23	16.74
<b><i>MT1E</i></b>	470.32	911.92	537.73	717.29
<b><i>MT1F</i></b>	66.13	65.38	49.62	91.40
<b><i>MT1G</i></b>	212.15	861.99	161.53	397.51
<b><i>MT1H</i></b>	31.28	78.19	14.03	33.13
<b><i>MT1M</i></b>	31.42	91.78	56.00	93.20
<b><i>MT1X</i></b>	1398.17	3419.96	1486.97	1855.35
<b><i>MT2A</i></b>	1161.41	6569.69	1073.51	1292.62
<b><i>MMP13</i></b>	24.58	4.98	29.68	50.84
<b><i>ADAMTSS</i></b>	3.97	22.87	3.74	6.83

### 3.12 Chapter summary

In this chapter I have utilised the transcriptomics database SkeletalVis to identify differentially expressed genes pertinent to zinc homeostasis in different human and murine cartilage and chondrocyte datasets. In iOA cartilage, *SLC39A8* was not dysregulated but the zinc importers *SLC39A3* and *SLC39A7* were upregulated and the zinc exporter *SLC30A2* and importer *SLC39A14* downregulated, suggesting zinc homeostasis may be disrupted. *SLC39A8* was differentially upregulated in human and mouse chondrocytes treated with different concentrations of IL-1 receptor ligands and despite the STR/ort mice having elevated IL-1 $\beta$  in articular cartilage, *Slc39a8* was downregulated at OA-onset (18 weeks). Except for iOA cartilage, where it was downregulated, *SLC39A14* was consistently differentially upregulated in every other cartilage or chondrocyte dataset. The zinc-sensing transcription factor *MTF1* was upregulated in human chondrocytes after 4 hours and 24 hours of IL-1 treatment but not after 24 hours in murine chondrocytes. *MT1A* and *MT1X* were significantly downregulated in the iOA cartilage compared to non-OA. When dOA was compared against iOA cartilage *MT1F*, *MT1G* and *MT1M* were upregulated in damaged cartilage. Several *MT* genes were also upregulated after IL-1 treatment, with a greater number upregulated after 24 hours than for four hours, possibly reflecting the protective response to greater oxidative stress. This analysis strongly suggests, in addition to the IL-1-mediated differential upregulation of *SLC39A8*, that *SLC39A14* is relevant for dysregulated zinc homeostasis in chondrocytes.

To determine if the zinc homeostasis was associated with genetic risk for OA, I correlated the genotype at OA or minimal joint space risk variants at three loci with expression of the nearby *SLC30A10*, *SLC30A5* and *SLC39A8* genes using the GTEx project eQTL data. The SNP eQTL correlation analysis identified a total of 11 SNP *SLC30A10* eQTL correlations among the 69 SNPs in LD with the marker SNPs rs2820436, rs2785988 and rs2820443. The observed eQTL was always present in the same tissue; UV-exposed skin of the lower leg. Unfortunately, GTEx only has expression data for skeletal muscle and not other musculoskeletal tissues such as cartilage and bone so it is not possible to determine if these OA SNPs also drive eQTLs of these genes in tissues relevant to OA. However, a recent preprint (Steinberg *et al.*, 2019) identified 1891 cis-eQTLs (defined as occurring one megabase either direction of the transcription start site of target gene) genome wide from an imputed 10.25 million autosomal SNPs between low-grade and high-grade osteoarthritic cartilage of up to 115 patients. It will be interesting, once the data has been peer reviewed and this list of eQTL SNPs for cartilage become available to compare the results with the 11 SNPs identified.

## Chapter 4: ESTABLISHING ACTIVITY OF THE ZINC-ZIP8-MTF1 AXIS IN HACs

### 4.1 Introduction

Having confirmed zinc homeostasis genes were upregulated in human cartilage and chondrocytes treated with IL-1 ligands from published transcriptomic datasets, I investigated zinc homeostasis genes in knee OA human articular chondrocytes (HACs) cultured *in vitro* for one (16 donors) or two passages (six of 16 donors) with or without IL-1 $\alpha$ . Of the six HAC donors cultured beyond one passage with IL-1 $\alpha$ , only two of these donors were used for gene expression assessment in later passages because of issues with nucleic acid extraction or a problem with the cDNA synthesis. The HACs were cultured for one passage (7-20 days) immediately post extraction, then split and treated for the first (10-13 days) and second passages (12-15 days) with 0.1ng/ml IL-1 $\alpha$  after which the cells were passaged a final time without IL-1 $\alpha$  (11-14 days). Cells were collected for gene expression, intracellular zinc quantification or medium for extracellular zinc quantification.

### 4.2 Aims

The aims of this chapter are to address each result in the proposed order of zinc-ZIP8-MTF1 activation in HACs. These include:

- Initially determine whether IL-1 $\alpha$  is as capable as IL-1 $\beta$  in the activation of IL-1 positive control genes (*IL-6*, *CXCL8* and *CCL2*), *SLC39A8* and *SLC39A14*.
- Determine the effect of IL-1 stimulation of HACs over multiple passages on cell numbers, positive control, *SLC39A8* and *SLC39A14* gene expression.
- Examine gene expression of proliferation markers *MKI67*, *TOP2A* and *TPX2* or senescent markers *PARP2*, *CAMK2G* and *CDKN1A* by qPCR in HAC culture time course.
- Investigate if IL-1 treatment for one passage activates the zinc-ZIP8-MTF1 axis described in mouse chondrocytes specifically examining:
  - Zinc transporters' expression
  - Intracellular and extracellular zinc levels
  - *MTF1* gene expression and localisation
  - *MT* gene expression
  - Cartilage matrix-degrading gene expression

#### ***4.3.1 Do IL-1 $\alpha$ and IL-1 $\beta$ stimulate the same gene expression changes in human OA chondrocytes for a defined gene panel?***

Kim *et al.*, 2014 demonstrated that after 24 hours of IL-1 $\beta$  exposure, healthy murine knee chondrocytes upregulate genes associated with the zinc-ZIP8-MTF1 axis. I wanted to investigate if this signalling pathway is also activated by IL-1 in human OA knee chondrocytes. IL-1 $\alpha$  was readily available to our research group and so I chose to use this for *in vitro* experiments after firstly determining if IL-1 $\alpha$  and IL-1 $\beta$  could elicit similar gene expression responses in chondrocytes. IL-1 $\alpha$  binds the same IL-1 receptor as IL-1 $\beta$  with greater affinity (0.1-0.3nM for IL-1 $\alpha$  versus 0.5-1nM for IL-1 $\beta$ ) (Dinareello, 2003). HACs extracted from intact OA knee cartilage from two donors undergoing total joint replacement surgery were treated  $\pm$  0.1ng/ml IL-1 $\alpha$  or 1ng/ml IL-1 $\beta$  for 10 or 12 days respectively. The expression levels of the IL-1 responsive positive control genes *IL-6*, *CXCL8* and *CCL2* were measured by qPCR analysis (Figure 4.1), as were *SLC39A8* and *SLC39A14*. Statistical analysis of this data was not possible to conduct with just two donors, but IL-1 $\alpha$  treatment did induce similar fold change differential gene expression responses within the same individual across IL-1 $\alpha$  or IL-1 $\beta$  treatments. However, the magnitude of the response differed between donors because of a difference in baseline expression in control samples. This result indicated, other than the requirement of an additional HAC donor, that IL-1 $\alpha$  was as capable of activation of the IL-1 signalling pathway as IL-1 $\beta$  in HACs and so IL-1 $\alpha$  was used for all subsequent experiments described in this chapter.

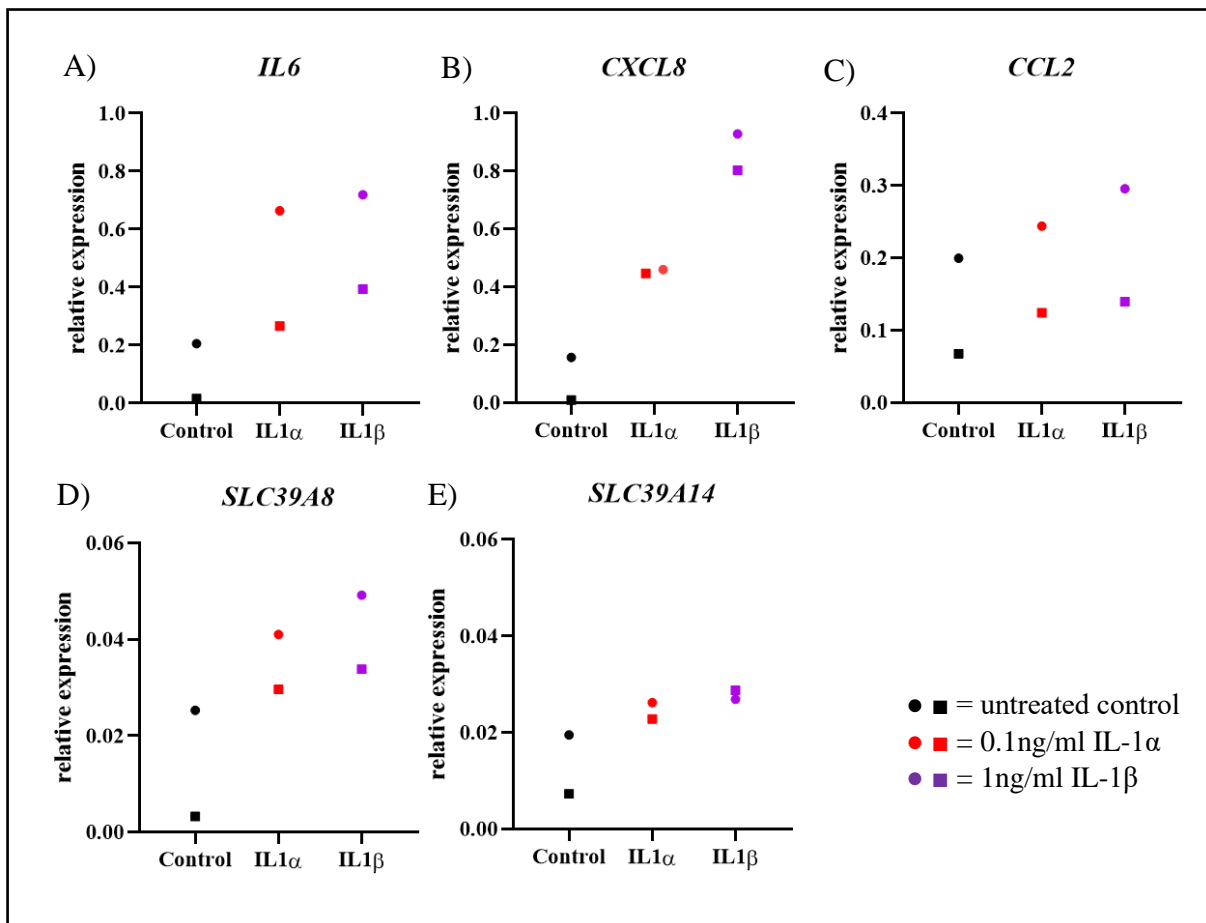


**Figure 4.1 – Comparison of IL-1 $\alpha$  or IL-1 $\beta$ -inducible positive control genes after one passage in two HAC donors.**

HACs from two donors (squares, donor 18 and circles, donor 19) were treated with or without 0.1ng/ml IL-1 $\alpha$  or 1ng/ml IL-1 $\beta$  for 12 and 10 days respectively. Gene expression for *IL-6* A), *CXCL8* B), *CCL2* C), *SLC39A8* D) and *SLC39A14* E) was measured. Data is normalised to housekeeper genes *18S*, *GAPDH* and *HPRT1*. Dots represent the mean gene expression in technical triplicate.

### 4.3.2 IL-1 $\alpha$ -mediated HAC qPCR expression responses

#### 4.3.2.1 IL-1 $\alpha$ reduces HAC cell number for one or more passages with consequences for cellular proliferation but not senescence marker gene expression

There was a significant reduction ( $p < 0.0001$ ) in the total number of HACs counted at passage end P2 in IL-1 $\alpha$  treated flasks compared to control flasks and when IL-1 $\alpha$  was removed at the beginning of P4 ( $p = 0.0387$ ) after a paired t test (Figure 4.2). This demonstrates that IL-1 $\alpha$  inhibitory effect on cell number persisted many days after which the stimulus was removed.

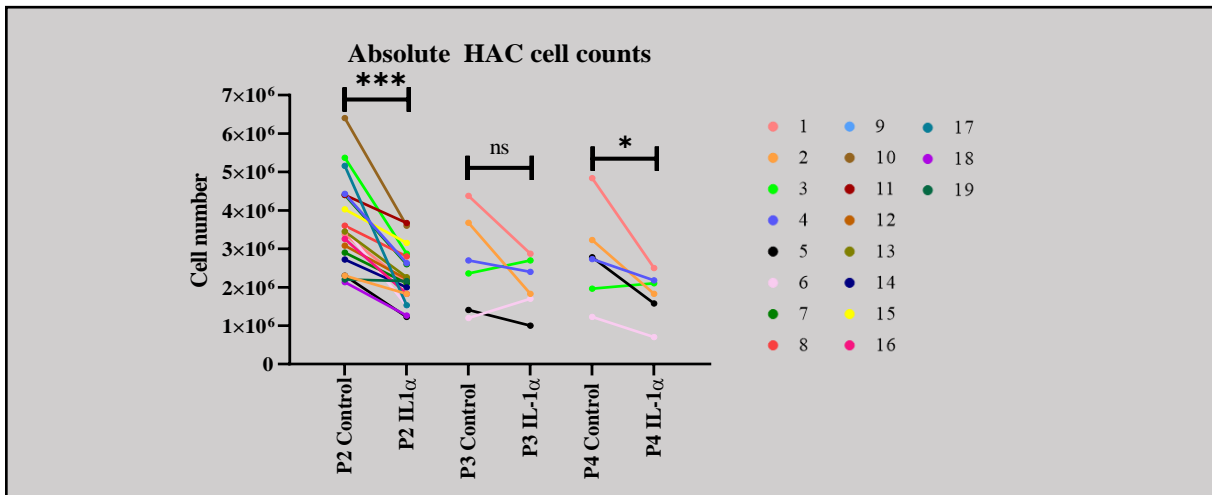


**Figure 4.2 – Dot plots of matched HAC donor cell counts in IL-1 $\alpha$ -treated or untreated control flasks treated consecutively for two passages and a final passage without IL-1 $\alpha$ .** HACs from 19 donors were cultured for one passage (10-13 days) with or without 0.1ng/ml IL-1 $\alpha$ . Six of these 19 HACs were cultured  $\pm$  IL-1 $\alpha$  for passage three (12-15 days) and without IL-1 $\alpha$  for passage four (11-14 days) respectively. Sixteen of 19 HAC donors passaged once in the presence of IL-1 $\alpha$  and two of these 16 donors were used for qPCR analysis at passages three (P3) and four (P4). Each colour is a different HAC donor, matched across IL-1 $\alpha$  treatment over time. Analysis used was paired t-test, \* $p < 0.05$ , \*\*\*  $p < 0.001$ . ns = non-significant.

Having determined that total cell numbers were reduced after a single passage with IL-1 $\alpha$ , I next investigated the relationship between proliferation and senescence gene expression in these samples. I ordered validated proliferation marker qPCR primers assays for *MKI67*, *TOP2A*, and *TPX2*, having identified these genes as prognostic markers for mantle cell lymphoma patient stratification in clinical trials (Brizova *et al.*, 2010), but also as reliable markers generally. Ki-67, the protein derived from the *MKI67* gene, has been used in prognostic studies in cancer research for decades and can only be detected in active phases of the cell cycle (interphase and mitosis), emphasising its use in clinical testing and for monitoring responses to chemotherapeutic agents (Scholzen and Gerdes, 2000). One role of Ki-67 is to maintain chromosome positioning to the nucleolus pre mitosis at G2 checkpoint in interphase (Booth *et al.*, 2014; Sobecki *et al.*, 2016; Matheson and Kaufman, 2017). This is mediated through Ki-67 interaction with the perichromosomal layer, a proteinaceous sheath coating individual chromosomes, which if disturbed is associated with asymmetric distribution in daughter cells and aggregation of mitotic chromosomes (Sun and Kaufman, 2018). *TOP2A* encodes DNA topoisomerase 2-alpha which can create and repair DNA double strand breaks as a relief from torsional stress in the process of chromosome condensing (Cuvier and Hirano, 2003) and has a role in sister chromatid separation in meiosis. *TPX2* encodes TPX2, a microtubule-associated protein that is required for mitotic spindle assembly (Wadsworth, 2015).

To identify senescence markers, I used data from Jennifer Scott's Thesis, a former PhD student of Professor David Young, Newcastle University, Faculty of Medical Science. She compared gene expression of senescence-associated genes in two pairs of groups, senescent fibroblasts against mitotically active fibroblasts and OA cartilage against non-OA NOF cartilage. The genes initially selected based on a significant p value of 0.003 from Mann-Whitney U t-testing of the fibroblast data were *CDKN2A*, *CAMK2G* and *PARP2*. However, *CDKN1A* (p value=0.0003) a related cyclin dependent kinase was investigated instead of *CDKN2A* in my HAC samples because the *CDKN2A* primers did not validate.

The proliferation markers were all found significantly (*MKI67* p<0.0001, *TOP2A* p=0.0054 and *TPX2* p=0.0072) reduced by paired t-testing after one passage with IL-1 $\alpha$  in 14 of the 16 HAC donors in which these genes were measured (Figure 4.3A-C). The Ct values for *MKI67* in control and IL-1 $\alpha$ -treated samples from HAC donor three were not detected. Senescence-associated gene expression markers were non-significantly expressed after IL-1 $\alpha$  in the eight HAC donors in which the genes were measured (Figure 4.3D-F).

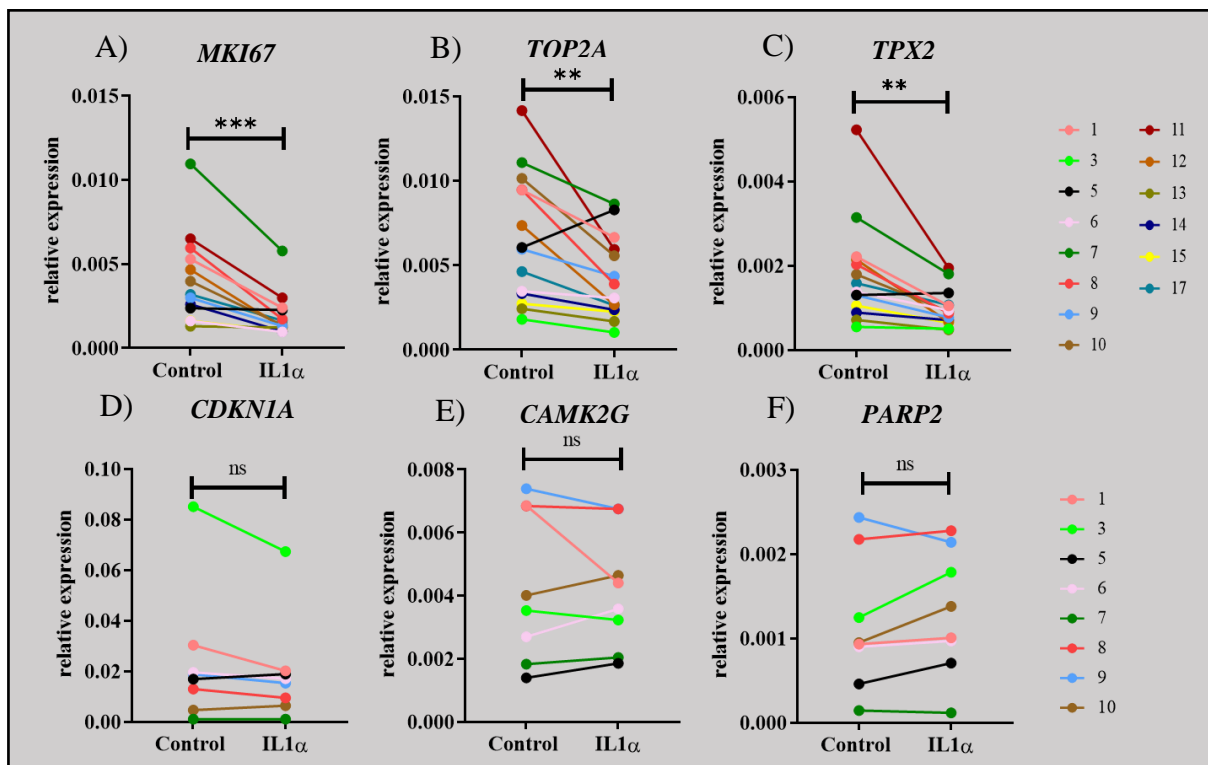


**Figure 4.3- Proliferation (*MKI67*, *TOP2A* and *TPX2*) and senescence-associated (*CDKN1A*, *CAMK2G*, and *PARP2*) gene expression after one passage of IL-1 $\alpha$ .**

HACs from 16 donors were treated with or without 0.1ng/ml IL-1 $\alpha$  for one passage (10 to 13 days) before proliferation (A-C) and senescence-associated genes (D-F) were measured in 14 and eight HAC donors respectively. Dots are the mean gene expression from a single flask in technical triplicate. Connecting lines are matched HAC donor normalised gene expression responses to IL-1 $\alpha$  treatment and data is normalised to housekeeper genes *18S*, *GAPDH*, and *HPRT1*. Data was analysed with a paired t-test. ns = non-significant, \*\* p<0.01, \*\*\* p<0.001.

#### 4.3.2.2 Positive control genes *IL-6*, *CXCL8* and *CCL2*

OA knee HACs from a total of 16 donors were treated with or without 0.1ng/ml IL-1 $\alpha$  for one passage (10-13 days) and gene expression measured by qPCR. To confirm all HACs responded to IL-1 $\alpha$  the expression of the IL-1 responsive genes *IL-6* (Figure 4.4A), *CXCL8* (Figure 4.4B) and *CCL2* (Figure 4.4C) were assessed. These genes were significantly ( $p < 0.001$ ) upregulated (19.6, 32.6 and two-fold respectively) after paired (*IL6* and *CCL2*) or Wilcoxon t-tests (*CXCL8*) in IL-1 $\alpha$  treated HACs compared to untreated HACs from the same donor (referred to as control HACs). The *CCL2* fold induction compared to control was only moderate in comparison to *IL-6* and *CXCL8*, yet still significant (Figure 4.4C). This same data is presented as a log<sub>2</sub>-fold change heatmap clearly illustrating between donor gene expression variation and markedly higher expression levels of *IL-6* and *CXCL8* compared to *CCL2* after IL-1 $\alpha$  exposure (Figure 4.4D).

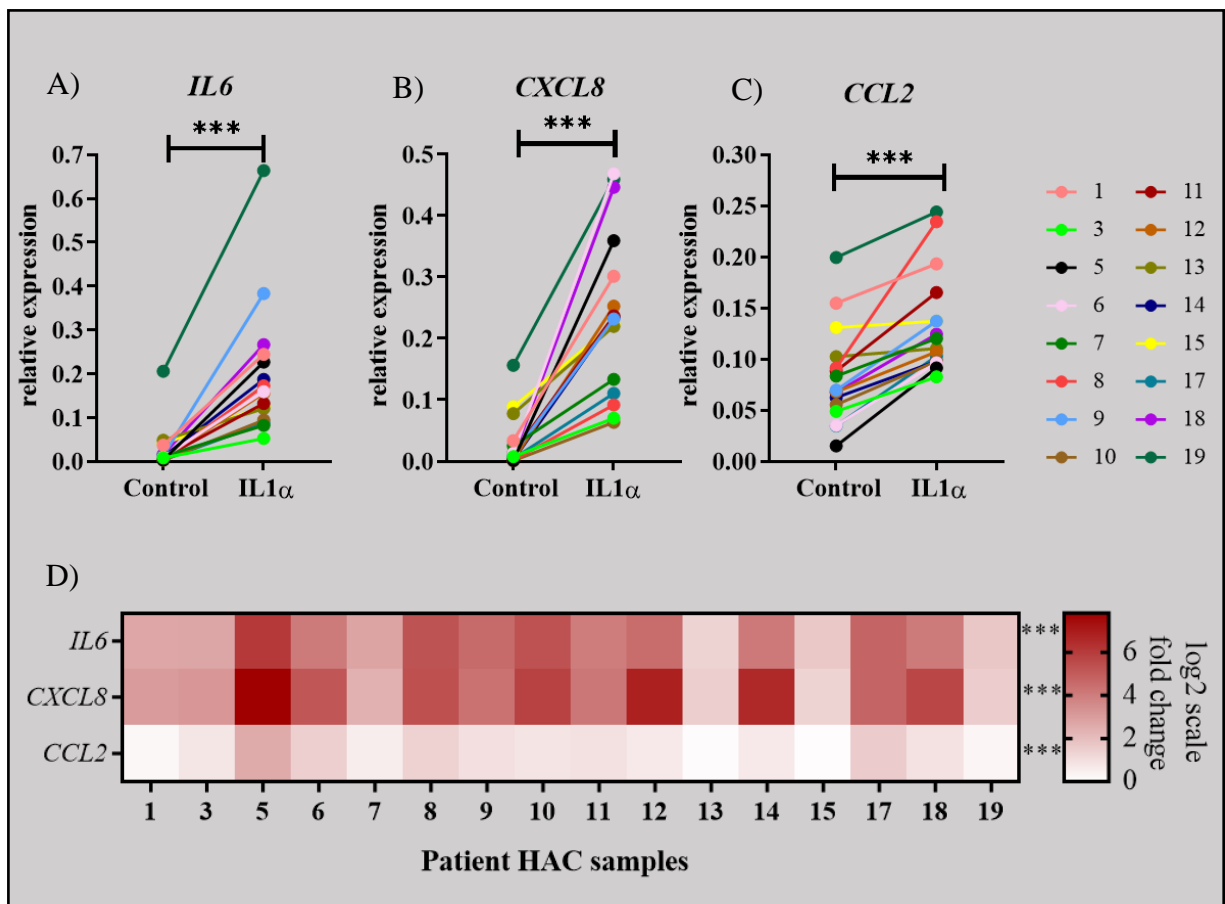


**Figure 4.4 – *IL-6*, *CXCL8*, and *CCL2* are all significantly upregulated by IL-1 $\alpha$  in HACs.** HACs were treated with or without 0.1ng/ml IL-1 $\alpha$  for 10-13 days and connecting coloured lines for *IL-6* A), *CXCL8* B) and *CCL2* C) are matched HAC donor normalised gene expression responses. Data is normalised to housekeeper genes *18S*, *GAPDH*, and *HPRT1*. Log<sub>2</sub>-fold expression data of same data for all 16 HAC donors illustrated as heatmap D). Normalised or log<sub>2</sub> transformed data was analysed with a paired t-test. *CXCL8* was analysed by Wilcoxon t-test, \*\*\*  $p < 0.001$ .

To summarise, IL-1 $\alpha$  treatment of HACs for one passage led to decreased cell counts and gene expression reduction of all proliferation-associated gene markers. There was no evidence that HACs were senescent after IL-1 $\alpha$  treatment for one passage. An explanation for the reduction in cell number and proliferation markers might be a consequence of arrested cell cycle but was not investigated further.

#### ***4.3.2.3 SLC39A8 and SLC39A14 are upregulated in response to IL-1 $\alpha$ in human OA knee chondrocytes***

I next determined if zinc transporter genes are dysregulated by IL-1 $\alpha$  for one passage by analysing mRNA expression of genes encoding five zinc exporters and 11 zinc importers, including *SLC39A8* and *SLC39A14* (Figure 4.5A and B). Of the zinc transporters only *SLC39A8* and *SLC39A14* were significantly upregulated (5.5 and 2.9-fold,  $p < 0.0001$ ) in all sixteen HAC donors and *SLC30A7* was downregulated (0.7-fold,  $p = 0.0085$ ) in HACs from donors 1, 3, 5-10 (Figure 4.5C). None of the other zinc transporter genes assayed showed consistent responses to IL-1 $\alpha$  across the first eight donors (Figure 4.5D) which partly explains why the zinc transporters, except for *SLC39A8* and *SLC39A14*, were not explored in donors 11-19, time and expense being a secondary factor.

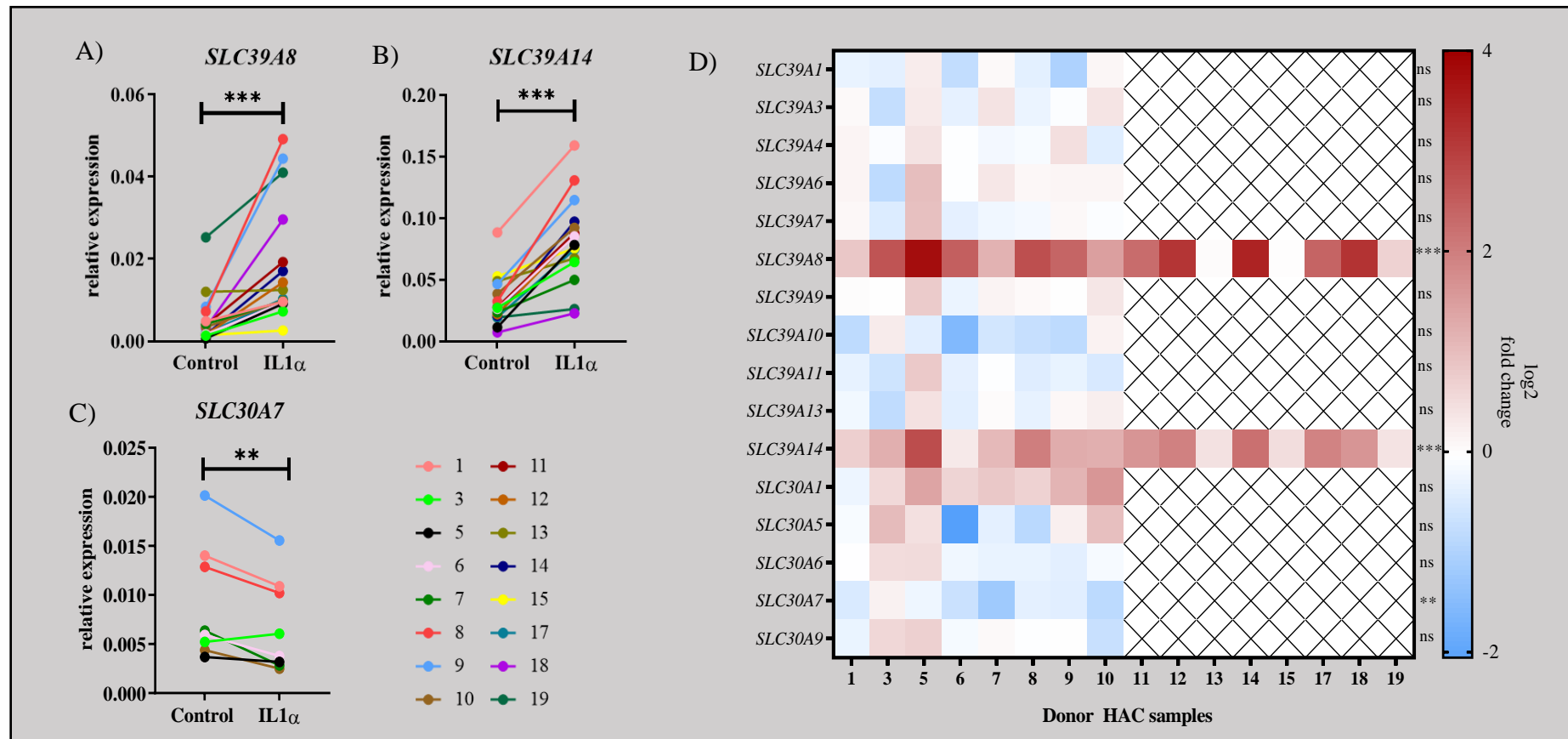


**Figure 4.5 – Zinc transporters that are significantly and differentially expressed after IL-1 $\alpha$  treatment of HACs for one passage.**

HACs from 16 donors were treated with or without 0.1ng/ml IL-1 $\alpha$  for one passage and connecting coloured lines for *SLC39A8* A), *SLC39A14* B) and *SLC30A7* C) are matched HAC donor normalised gene expression responses. Data is normalised to housekeeper genes *18S*, *GAPDH*, and *HPRT1*. Log<sub>2</sub>-fold change expression data for all 16 HAC donors illustrated as heatmap D). Red, white and blue boxes represent genes upregulated, unchanged or downregulated by IL-1 $\alpha$  respectively. A cross indicates the gene was not measured in a sample. HAC donor 16 was omitted from the qPCR analysis because  $C_t$  replicate values of housekeepers deviated >1. Data satisfying a D'Agostino-Pearson omnibus k2 normality test prior to or after log<sub>2</sub> transformation was analysed with a paired t-test, otherwise a Wilcoxon t-test was used. \*\* p<0.01, \*\*\* p<0.001. ns = non-significant.

Next, I explored the effects of continued IL-1 $\alpha$  exposure on *SLC39A8* and *SLC39A14* gene expression specifically for another passage before its removal at passage four in two HAC donors which is displayed in Figure 4.6 as a heatmap. The log 2-fold change expression of *SLC39A8* and *SLC39A14* was lower after the second passage with IL-1 $\alpha$  (P3) than the first passage (P2) but was still approximately four-fold higher than control flasks at P3. IL-1 $\alpha$  removal at P4 led to a 50% and 30% reduction in *SLC39A8* fold change expression and a 57% and 68% reduction in *SLC39A14* fold change expression when compared to IL-1 $\alpha$ -treated flasks at P3 for donor five and six respectively (Figure 4.6). These measurements were not statistically validated given that the required minimum of at least three HAC donors samples treated with IL-1 $\alpha$  beyond one passage was not obtained.

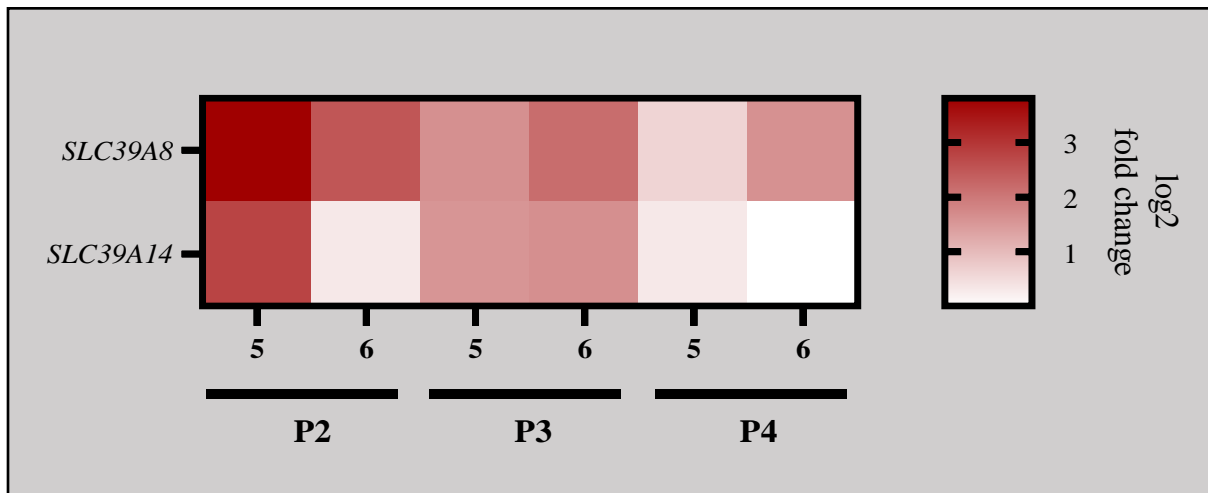


**Figure 4.6 – Heatmap of *SLC39A8* and *SLC39A14* log<sub>2</sub>-fold change gene expression after IL-1 $\alpha$  treatment (P2 and P3) and without IL-1 $\alpha$  (P4) in two HAC donors.**

HAC donors five and six were treated with 0.1ng/ml IL-1 $\alpha$  for 12 days for P2 and 14 and 12 days respectively for P3. IL-1 $\alpha$  was removed at the beginning of the fourth passage, the cells collected after 14 and 11 days respectively and *SLC39A8* and *SLC39A14* measured by qPCR. Data is normalised to housekeeper genes *18S*, *GAPDH*, and *HPRT1* and expressed as log<sub>2</sub>-fold changes relative to control flasks at the same passage. Red and white boxes represent a spectrum of upregulated to unchanged genes after IL-1 $\alpha$  respectively. P2-4 = passages two, three and four.

### ***4.3.3 Do intracellular zinc levels in OA knee HACs change after IL-1 $\alpha$ treatment?***

#### ***4.3.3.1 Non-specificity of zinc spectrophotometry kit in a cell-free experiment testing biologically relevant metal ions***

As observed in murine chondrocytes, *SLC39A8* and *SLC39A14* are upregulated after exposure to IL-1 $\alpha$  in human chondrocytes (section 3.6.2). The next step in evaluating the zinc-ZIP8-MTF1 axis in chondrocytes was to determine whether IL-1 $\alpha$  would alter cytoplasmic zinc concentrations following one passage of IL-1 $\alpha$  treatment. Although a change in intracellular zinc concentration would not determine which specific zinc transporters proteins mediate any change, it would provide indirect evidence of zinc transporter activity.

The gold-standard methodologies for zinc concentration assessment from biological samples include flame atomic absorption spectroscopy (Hare *et al.*, 2015) and fluorescently labelled probes which work according to the principal of Förster resonance energy transfer. The instrumentation for these methods were not available and not pursued to conduct this research. Thus, a spectrophotometric assay from Sigma was alternatively used. A full description explaining the chemistry in the kit was not available from the manufacturer (for intellectual property reasons) but what was discerned was that the chemistry was modified from a paper published by Homsher and Zak (Homsher and Zak, 1985) in which zinc was measured from serum but has since been adapted to measure zinc in a range of biological samples.

To test whether the kit was specific to zinc ions or could detect other metal ions by influencing the absorbance measured, a cell-free experiment with metal solutions was prepared. 4 $\mu$ M zinc  $\pm$  4 $\mu$ M iron sulphate heptahydrate (Fe<sub>2</sub>SO<sub>4</sub>.7H<sub>2</sub>O), 4 $\mu$ M copper sulphate hexahydrate (Cu<sub>2</sub>SO<sub>4</sub>6H<sub>2</sub>O), 4 $\mu$ M calcium chloride (CaCl<sub>2</sub>) or 4 $\mu$ M magnesium chloride (MgCl<sub>2</sub>) were tested. For biological samples, it is recommended to use trichloroacetic acid (TCA) as a protein precipitant removing protein-bound zinc which does not represent the zinc pool available for signalling. It is important to note the zinc concentrations described in the cell-based experiments may represent a fraction of the total free zinc pool available to the cell as the precipitated negatively charged proteins may leach zinc ions from the solution because of electrostatic forces of attraction.

As TCA addition to the biological samples was necessary, these metal ion preparations were thus made  $\pm$  TCA in singlicate, and the zinc standard was prepared in the same way. The absorbances should be similar whether TCA is included or not, as there was no source of protein in the cell-free metal salt solutions. TCA was included in these experiments as a protein precipitant removing protein-bound zinc which does not represent the zinc pool available for signalling.

As can be observed in Figure 4.7, TCA did not influence the line of best fit of the standard curves (Figure 4.7A) and thus the zinc quantified in the metal ion solutions was close to the predicted  $4\mu\text{M}$  metal ion input (Figure 4.7B). However, there was a 1.5-fold increase in zinc concentration when  $\text{Fe}_2\text{SO}_4 \cdot 7\text{H}_2\text{O}$  and zinc were combined compared to zinc alone irrespective of TCA inclusion or not. No other metal ion in the experiment influenced the zinc concentration to the same extent. This result may suggest that the chemistry of the kit fails to mask iron ions from the pyridyl azo ligand contributing to this increase, but the result may also be random as samples and standards were only measured in singlicate and the experiment was unrepeated so statistical analysis was impossible. TCA was subsequently always included in the standard curves of future test plates.

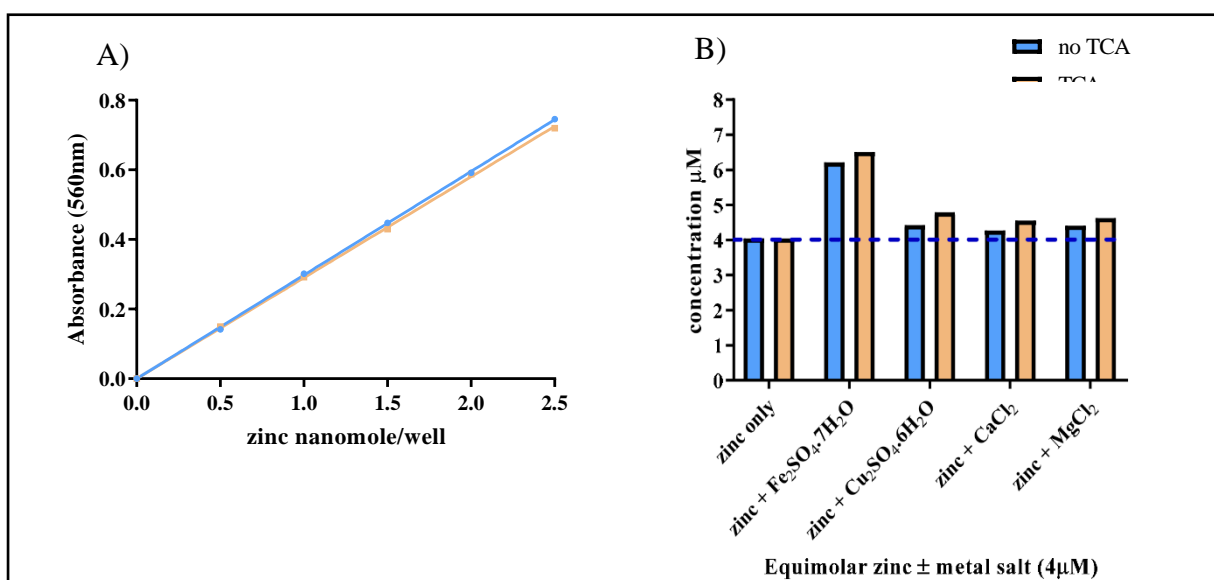


**Figure 4.7 – Cell-free zinc assay measurements  $\pm$  TCA inclusion using MAK032 zinc assay kit.**

Zinc standard curves with (orange) and without TCA (blue) from which the sample concentration was calculated A). The resulting molar concentrations calculated from  $4\mu\text{M}$  preparations of  $\text{ZnCl}_2$  only or in combination with  $4\mu\text{M}$  other metal salts B). Zinc standards and samples for this experiment were singlicate measurements.

#### ***4.3.3.2 Attempted correction for iron influence on metal ion absorbance using 2,2'-bipyridine***

Given that iron ions interfere with the absorbance measurement, and the subsequently derived zinc concentration, the iron-specific inhibitor 2,2'-bipyridine was tested. Fritz Blau discovered 2,2'-bipyridine in 1888 in the dry distillation of copper (II) pyridine-2-carboxylate (Blau, 1888). It is an organic uncharged compound that chelates iron in a 3:1 stoichiometry (Constable and Housecroft, 2019). Final 1.82 $\mu$ M solutions of ZnCl<sub>2</sub>, Fe<sub>2</sub>SO<sub>4</sub>·7H<sub>2</sub>O or both ZnCl<sub>2</sub> and Fe<sub>2</sub>SO<sub>4</sub>·7H<sub>2</sub>O were prepared in water with or without 2,2'-bipyridine at 45, 227, and 450 $\mu$ M concentrations. Figures 4.8A and B show the unadjusted and adjusted metal ion concentrations, having further subtracted the average absorbance of the iron only solutions from the raw absorbances for Fe<sub>2</sub>SO<sub>4</sub>·7H<sub>2</sub>O only and ZnCl<sub>2</sub> and Fe<sub>2</sub>SO<sub>4</sub>·7H<sub>2</sub>O combined (Figure 4.8B). As shown in Figure 4.8A, this experiment confirmed that the zinc ion concentration calculated was equivalent to the defined input concentration. 1.82 $\mu$ M ZnCl<sub>2</sub> and Fe<sub>2</sub>SO<sub>4</sub>·7H<sub>2</sub>O gave consistently greater  $\mu$ M concentrations compared to ZnCl<sub>2</sub> only, suggesting that this kit is not as specific as was originally marketed. Furthermore, 2,2'-bipyridine was not behaving as an iron inhibitor and though statistics was not possible, there was a dose-dependent trend in increasing absorbance and subsequent concentration calculated with increasing amounts of 2,2'-bipyridine added. Having accounted for the iron contribution (Figure 4.8B) in the analysis, the combined ZnCl<sub>2</sub> and Fe<sub>2</sub>SO<sub>4</sub>·7H<sub>2</sub>O solution did not completely return to 1.82 $\mu$ M in the absence or presence of inhibitor, suggesting the signals generated from each metal component are not simply additive.

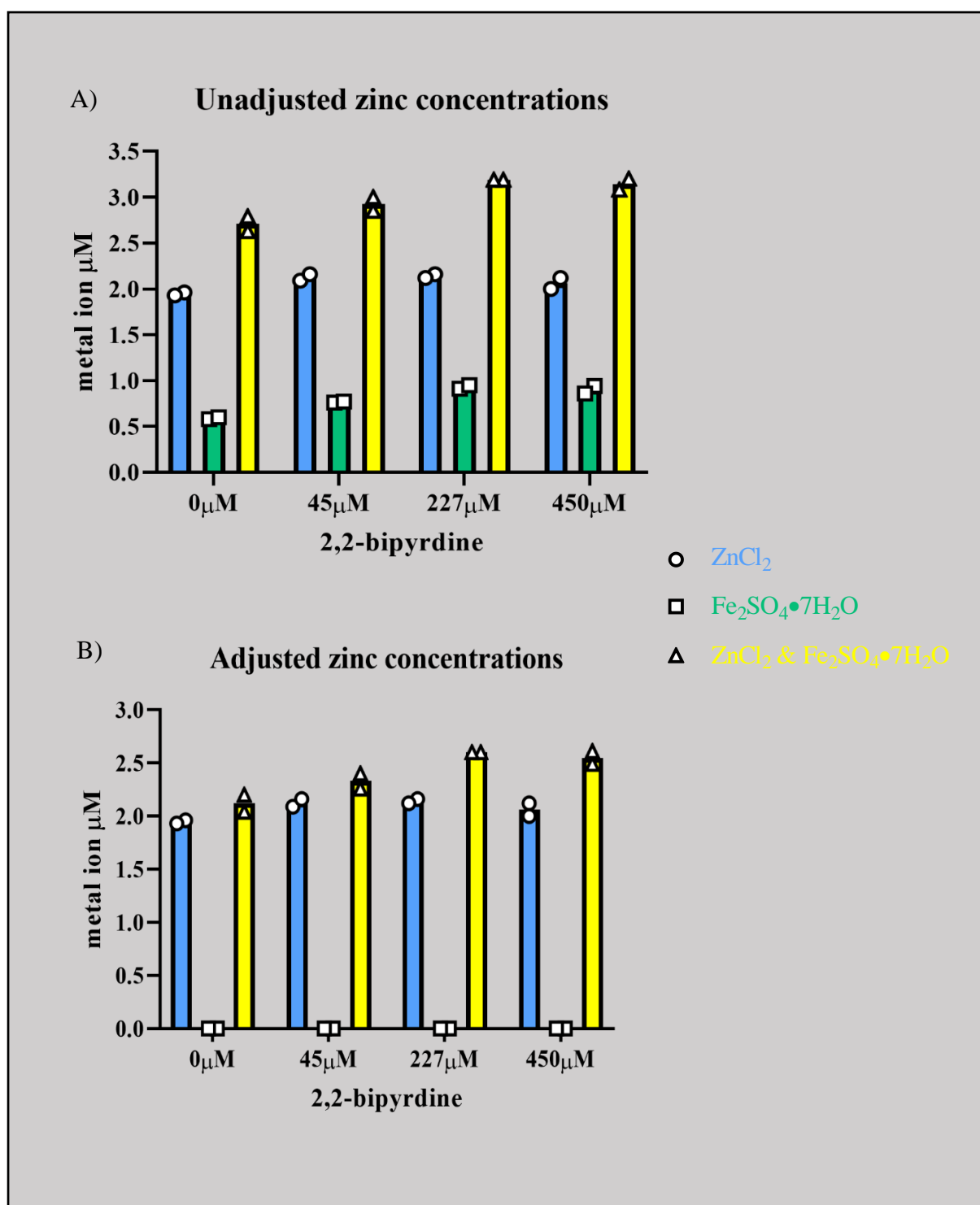


**Figure 4.8 – Attempted iron chelation in cell-free metal salt solutions using the iron chelator 2,2'-bipyridine.**

The zinc micromolar concentrations were calculated as before for each mean absorbance generated from each cell-free metal salt (ZnCl<sub>2</sub> or Fe<sub>2</sub>SO<sub>4</sub>·7H<sub>2</sub>O) or combination of metal salts. The iron ion absorbance influence A) was subtracted from the average absorbance from wells containing both metal salts to give the results in B). The bars represent the mean micromolar concentration and the dots are the technical duplicate measurements.

#### 4.3.3.3 Zinc is specifically upregulated in IL-1 $\alpha$ -treated HACs but not downregulated in matched IL-1 $\alpha$ spent cultured HAC medium

Despite the non-specificity of the MAK032 kit for zinc ions, and the inability to remove iron ions from the solution and the final measurement, I proceeded to measure metal ion content using the MAK032 kit in matched HAC supernatant and lysed cells passed once with or without IL-1 $\alpha$ .

Initially, IL-1 $\alpha$ -treated spent medium alone was tested from a single HAC donor (Figure 4.9) with or without 7% TCA and the experiment conducted as described in chapter 2.7. The effect of TCA inclusion in the sample reduced the total metal ion content by approximately 50% compared to TCA absent preparations, which was consistent with TCAs role as a protein precipitant. Thus, with the possibility of free zinc leaching, in addition to the interference of iron ions, the measure of free zinc with this kit may only represent a small fraction of the total.

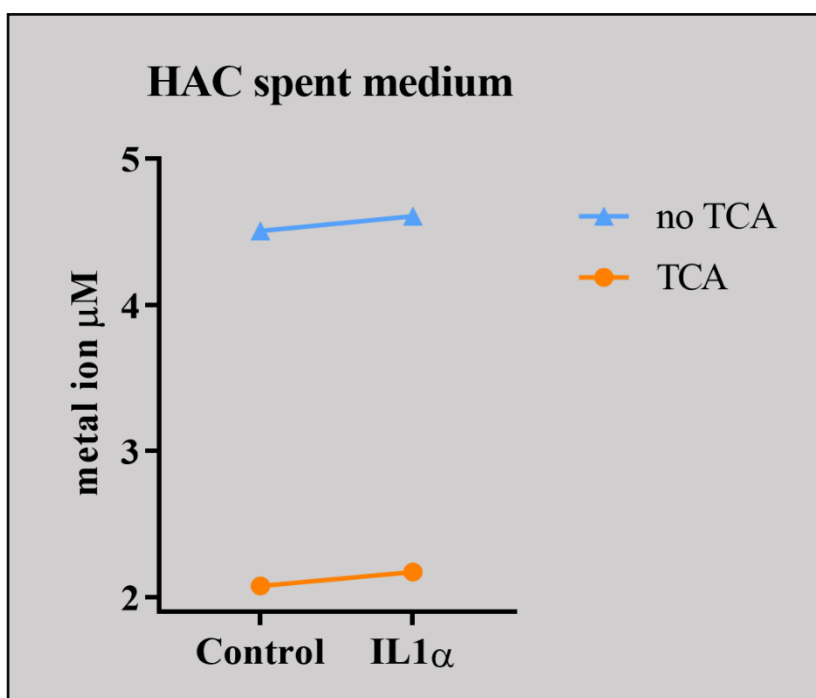


**Figure 4.9 – TCA use in untreated or IL1- $\alpha$ -treated HAC medium led to ~ two-fold total metal ion concentration reduction.**

Medium of one cultured HAC donor was mixed  $\pm$  TCA and the metal ion content of the sample determined with the MAK032 kit. The connecting lines are samples matched by TCA inclusion or not, and the dots are means of samples measured in technical duplicate.

Next, the levels of zinc and/or iron in paired IL-1 $\alpha$  treated HAC cell lysate and spent cultured medium for seven HAC donors (donors 11-17) was quantified. A significant upregulation (2.26-fold  $p=0.0004$ ) of intracellular metal ions in cells treated with IL-1 $\alpha$  for one passage (10-11 days) was observed (Figure 4.10A). There was no change in metal ion concentration with IL-1 $\alpha$  in the seven matched spent medium samples (Figure 4.10B) and metal ion content in media controls gave similar absorbance values to spent medium samples (not shown). An additional six HAC donor spent medium samples (Figure 4.10C) confirmed IL-1 $\alpha$  did not alter zinc concentration in the spent medium.

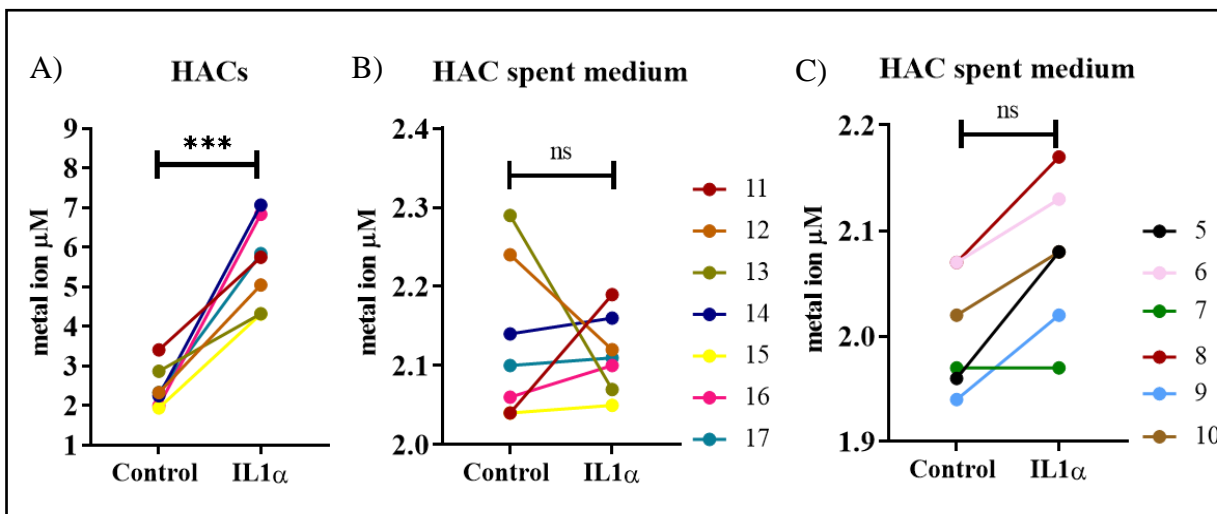


**Figure 4.10 – Metal ion content is significantly upregulated in matched HAC lysates but not HAC spent medium  $\pm$  IL-1 $\alpha$  treatment for one passage.**

In the same experiment, cell lysate A) and spent media samples B) from HAC donors 11-17 were treated with TCA and metal ion content determined. Each HAC donor is colour-coded and connecting lines illustrate the change in metal ion micromolar concentration after IL-1 $\alpha$  treatment for one passage. Additional unmatched HAC spent medium samples from a separate experiment were combined to highlight all HAC samples in which zinc was quantified C). The dots are means of samples measured in technical duplicate and there are no error bars for clarity. The data was analysed with a paired t-test. \*\*\* $<0.001$ , ns = non-significant.

Taken together, these data suggest intracellular metal ion concentration increases in HACs derived from donor OA knee cartilage in response to IL-1 $\alpha$ . The concentrations measured here reflect at least a combination of endogenous zinc and iron ions that may be present in the samples and so I cannot determine if this IL-1 $\alpha$ -stimulated increased ion content is due to increased intracellular zinc, iron or a combination of both. The fact that there were no significant changes in the spent medium of IL-1 $\alpha$  cultured HACs may reflect the reduced assay sensitivity in resolving metal ion exchange between the cell and its extracellular environment where metal ions are already in excess.

#### 4.3.4 *MTF1* mRNA expression levels are unchanged following IL-1 $\alpha$ treatment in HACs

As there was evidence of increased intracellular levels of metal ions after IL-1 $\alpha$  in HACs, I investigated if transcriptomic levels of *MTF1* also changed following IL-1 $\alpha$  treatment. *MTF1* is primarily upregulated following heavy metal exposure but is also known to alter its activity in response to oxidative stress and hypoxia (Kim *et al.*, 2014). To test whether there was a transcriptomic response to the elevated zinc concentrations determined in 4.3.3.3, *MTF1* gene expression was assessed in HACs treated with 0.1ng/ml IL-1 $\alpha$  for one passage in eight HAC donors (donors 1, 3, 5-10). As can be observed in Figure 4.11 *MTF1* expression was not significantly altered following IL-1 $\alpha$  treatment in HACs. No change in *MTF1* transcript was also reported by Kim *et al.*, 2014 in murine chondrocytes treated with or without Ad-ZIP8 but was also associated with increased intracellular zinc as observed in HACs here (4.3.3.3).

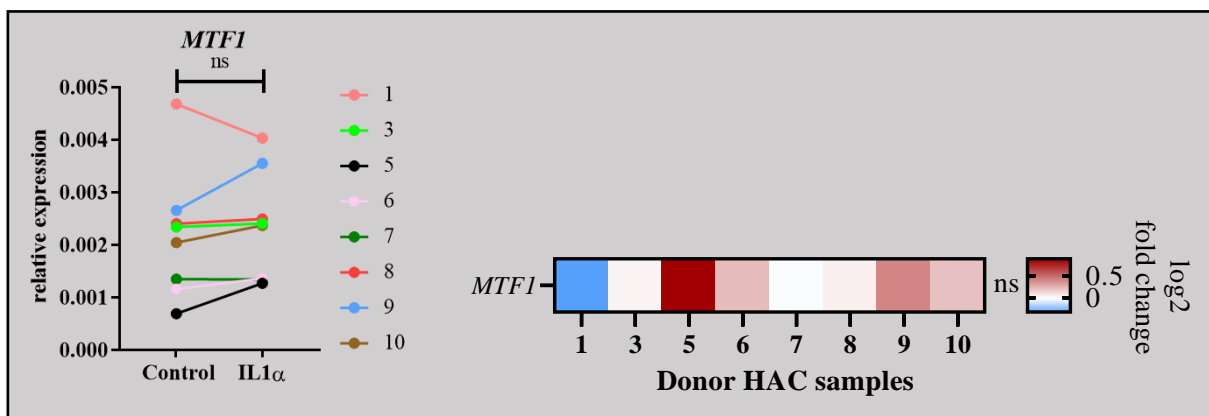


**Figure 4.11 – *MTF1* transcript is not significantly and differentially altered after IL-1 $\alpha$  treatment of HACs for one passage.**

HACs from eight donors were treated  $\pm$  0.1ng/ml IL-1 $\alpha$  for one passage and connecting coloured lines highlight directional changes in gene expression for each HAC donor A). Data is normalised to housekeeper genes *18S*, *GAPDH*, and *HPRT1*. Log<sub>2</sub>-fold change *MTF1* expression data is plotted as a heatmap B). Red, white and blue boxes represent *MTF1* upregulation, no change or downregulation with IL-1 $\alpha$  respectively. Data was analysed with a paired t-test. ns = non-significant.

### **4.3.5 Does *IL-1 $\alpha$* trigger nuclear translocation of MTF1 in OA knee HACs?**

#### **4.3.5.1 Screening HAC nuclear, cytoplasmic and whole protein lysates with N-terminal targeting MTF1 antibody**

To determine if MTF1 undergoes nuclear translocation in response to IL-1 treatment in HACs as has been reported in mouse chondrocytes, western blot analysis was performed on nuclear, cytoplasmic and whole protein fractions from two HAC donors. These lysates (Figures 4.12 and 4.13) were extracted by Dr. Adrian Falconer, Newcastle University, Faculty of Medical Sciences and the nuclear and cytoplasmic proteins were extracted using the same methods described in 2.10.1 and 2.10.2 without the additional PBS washes before nuclei lysis. The first donor's chondrocytes are untreated lysates (Figure 4.12) and the second donor's chondrocytes were treated with 0.05ng/ml IL-1 $\alpha$  and 10ng/ml oncostatin M (OSM) for six hours (Figure 4.13).

MTF1 has a predicted molecular weight of 81kDa according to the Human Protein Atlas (HPA, <https://www.proteinatlas.org/ENSG00000188786-MTF1/antibody>), from which the N-terminal MTF1 antibody was first trialled. This antibody targets an epitope region of 69 amino acids (N<sub>69</sub>70-138C<sub>615</sub>) in the N-terminal region. Surprisingly, most manufacturers of MTF1 antibodies only trial their antibodies on recombinant protein derived from overexpressed MTF1 in cell lines like HEK293 cells, so with this in mind I proceeded. This antibody was selected based on its reactivity to human MTF1, whereas the MTF1 antibody used by Kim *et al.*, 2014 (NBP1-86380) was only tested in murine chondrocytes and has dual reactivity with human MTF1. NBP1-86380 MTF1 antibody was on back order for six months so it was necessary to conduct preliminary western blots with HPA MTF1 polyclonal antibody.

In this first experiment (Figure 4.12) using untreated nuclear and cytoplasmic HAC protein, a band was observed at 35kDa and potentially a second band at 40kDa in both fractions probed with N-terminal MTF1 antibody. As these lysates had been prepared and handled by another researcher in the group, I could not attribute these bands as potential cleavage products due to protease activity or whether the antibody was just non-specific. The purity of the lysate fractions was investigated by GAPDH and Histone 2A probing. This was necessary for any further use of the lysates in MTF1 translocation assessment. There was evidence of contamination of the nuclear lysate with cytoplasmic protein lysate because a 37kDa band for GAPDH was present (Figure 4.12). Any reciprocal contamination of nuclear protein in the cytoplasmic lysate was undetermined using Histone 2A as a marker (not shown).

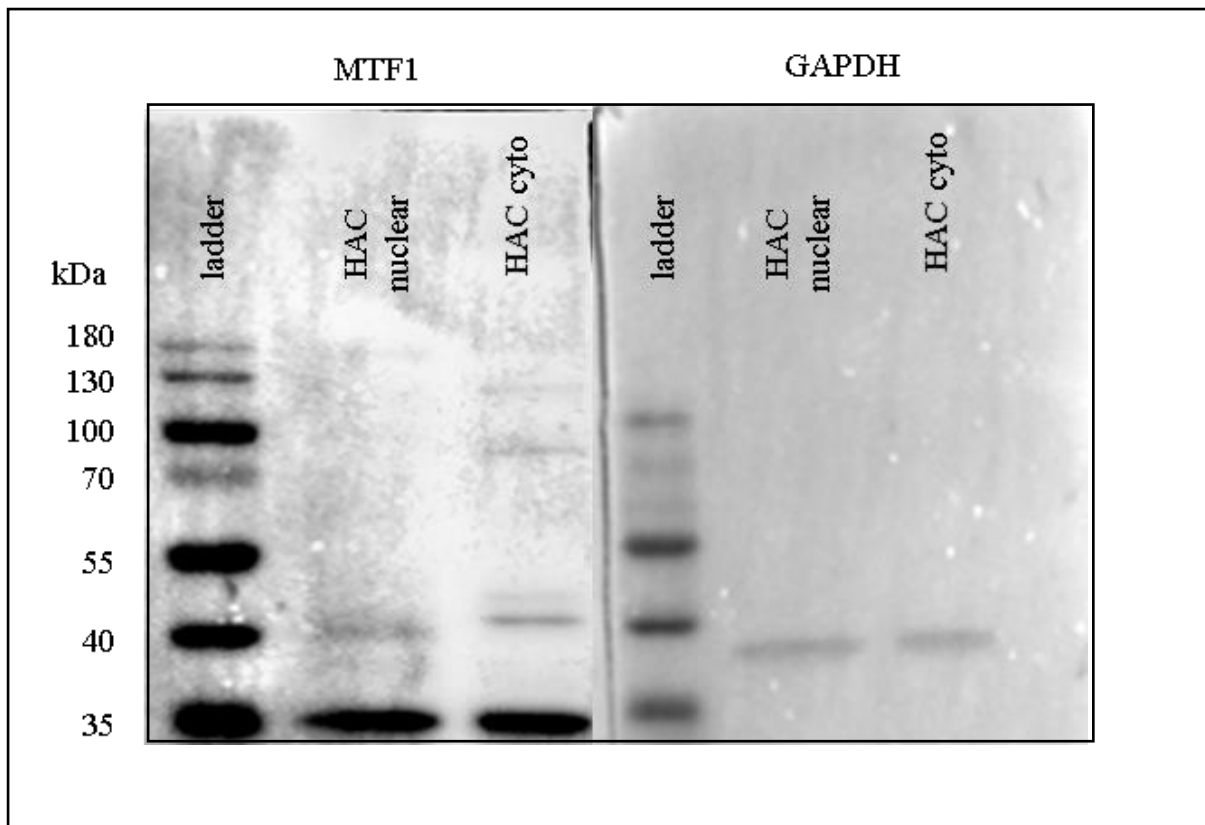


**Figure 4.12 – N-terminal MTF1 antibody detects multiple bands in 10µg untreated HAC nuclear and cytoplasmic lysates and GAPDH cytoplasmic protein marker found in both fractions.**

Consecutively, from left to right, lanes contain PageRuler prestained ladder, untreated HAC nuclear and cytoplasmic (cyto) lysate. Blot was probed with either N-terminal MTF1 antibody overnight or GAPDH antibody for one hour.

#### **4.3.5.2 Comparison of N and C-terminal targeting MTF1 antibodies in HAC lysates stimulated for six hours with or without IL-1 $\alpha$ and OSM**

Next, the same N-terminal MTF1 antibody and an additional C-terminal MTF1 antibody (Santa Cruz, 365090) was tested in the IL-1 $\alpha$  and OSM six hour treated HAC lysates. As a positive control for the antibodies, the MTF1 overexpression lysate (Origene, LC401804) was loaded alongside the HAC lysates. This was in order to clarify the discrepancy between expected and observed protein size of MTF1. The C-terminal MTF1 antibody binds a 299 amino acid sequence in position N<sub>453</sub>-C<sub>753</sub>.

Having stained the PVDF membrane with ponceau red, the transferred proteins could be observed, albeit weakly, and there were two major protein bands in the overexpressed MTF1 lysate lane (Figure 4.13A). Both antibodies detected two bands of ~55kDa and ~25kDa in the lane containing the overexpressed MTF1 lysate, although this was smaller than the predicted size of MTF1. Despite using two separate antibodies, one raised towards the N terminal and the other against the C-terminal end of MTF1, neither antibody detected protein bands of the same size as that observed in the overexpressed MTF1 lysate lane in the HAC protein lysates. The C-terminal MTF1 antibody detected no bands in any of the nuclear, cytoplasmic or whole protein HAC lysates (Figure 4.13B) whereas N-terminal MTF1 antibody detected ~30kDa band of equal intensity in each sample (Figure 4.13C). It should be noted that the same N-terminal MTF1 antibody used in Figure 4.12 gave a band of 35kDa in these samples. As the 55kDa and 25kDa bands observed in the overexpressed MTF1 lysate lane total the 81kDa predicted size of MTF1, these bands may represent MTF1 cleavage products.

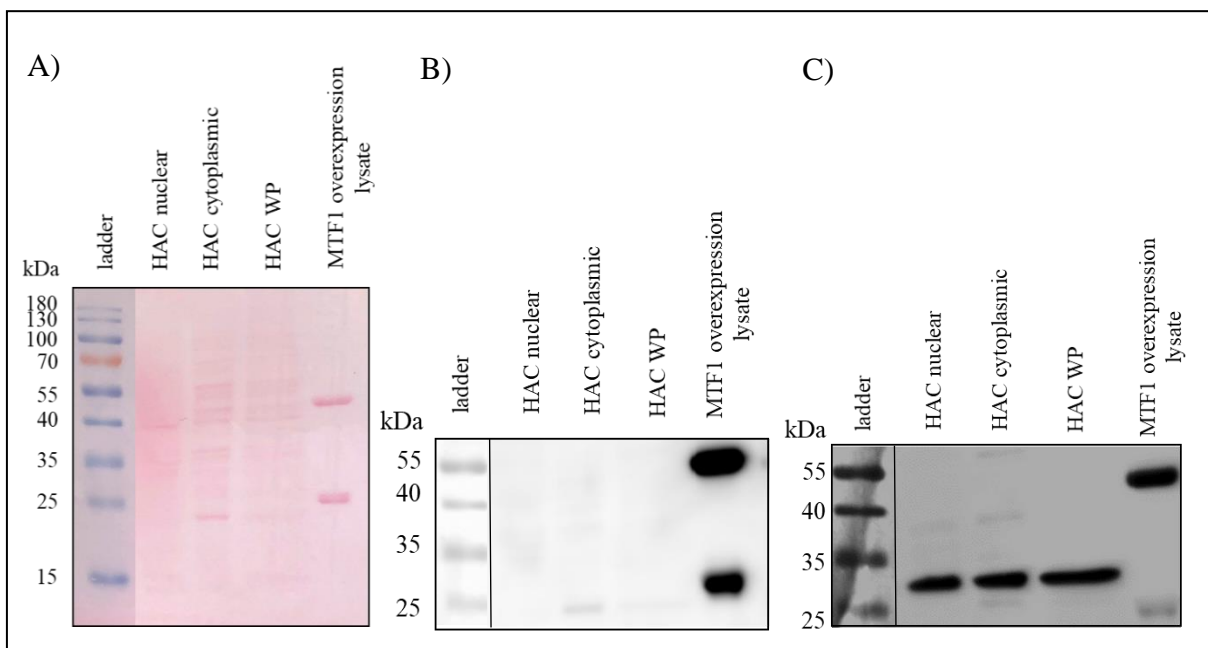


**Figure 4.13 – Western blots using C and N-terminal MTF1 antibodies in six-hour IL-1 $\alpha$  and oncostatin M-treated HAC nuclear, cytoplasmic and whole protein lysates and overexpressed MTF1 lysate.**

Consecutively, from left to right, lanes contain PageRuler prestained ladder, 10 $\mu$ g IL-1 $\alpha$  and OSM six hour-treated HAC nuclear and cytoplasmic lysate and MTF1 overexpression lysate (Origene, LC401804). Ponceau red staining of the proteins after wet transfer A) then the blot was probed with the C-terminal MTF1 antibody B) before the same blot was re-probed overnight with N-terminal MTF1 antibody C). WP= whole protein kDa = kilodaltons.

The possibility of MTF1 protein cleavage was explored by analysing potential protease-mediated cleavage sites using the database PROSPER ([prosper.erc.monash.edu.au](http://prosper.erc.monash.edu.au)). This database provided potential cleavage sites targeted by aspartic, cysteine, serine, and metalloproteinases or more than one of these families (Figure 4.14A). The amino acid sequence provided to PROSPER was the MTF1 sequence with the c-myc-FLAG tag (EQKLISEEDLAANDILDYKDDDDKV) at the end. In Figure 4.14B that same sequence shows the binding sites for the N-terminal (blue) and C-terminal (green) MTF1 antibodies. Using these sequences as input for a multiple sequence alignment using the basic local alignment search tool ([blast.ncbi.nlm.nih.gov/Blast.cgi](http://blast.ncbi.nlm.nih.gov/Blast.cgi)) returned a 50% alignment for a 10 amino acid sequence with the comparable amino acids highlighted in yellow in each sequence (Figure 4.14B).

Using the PeptideCutter tool in ExPASy ([web.expasy.org/peptide\\_cutter](http://web.expasy.org/peptide_cutter)) and cross referencing the potential cleavage sites identified with PROSPER in MTF1 (Figure 4.14A), I determined the cleavage site which gave protein fragments approximating that which was observed in the western blot positive control lanes. Cleavage of the alanine at position 511 (highlighted in bold in Figure 4.14B) gave peptide sequences of size 55.8kDa and 25.2kDa. This cleavage by a member of the metalloproteinase family may explain the results observed with the MTF1 overexpressed lysate, but is somewhat complicated by the fact that EDTA, a known inhibitor of metalloproteinases, was used in the extraction of the MTF1 overexpression lysate by the manufacturer.

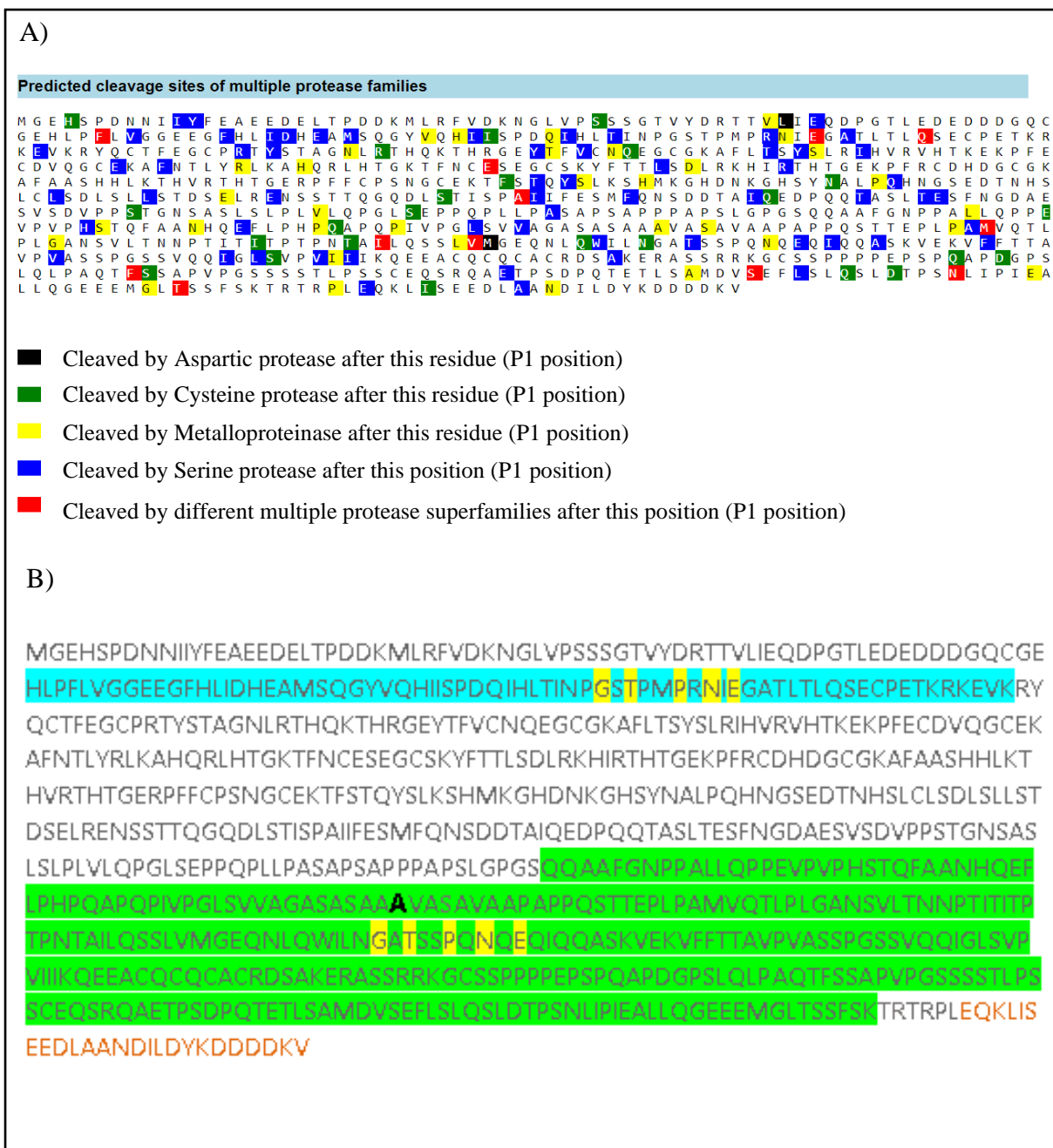


**Figure 4.14 – Predicted cleavage sites of multiple protease families for the human protein MTF1 using the database PROSPER.**

The amino acid sequence of human MTF1 with the c-myc-FLAG residue (EQKLISEEDLAANDILDYKDDDDKV) was passed to PROSPER and potential cleavage sites for different protease families calculated A). The amino acids corresponding to the epitopes of the N-terminal MTF1 antibody (blue) and C-terminal MTF1 antibody (green) were analysed using BLAST for alignment and these amino acids are highlighted in yellow B). The c-myc-FLAG tag is highlighted at the end of the sequence in orange. The alanine amino acid highlighted in bold is a predicted cleavage site for metalloproteinases, the resulting fragments of which generate approximately 55 and 25kDa sized bands.

As both antibodies bind at opposite ends of the protein with insufficient amino acid sequence overlap for antibody binding outside its normal epitopic region, it is probable that after reprobing the blot with the N-terminal MTF1 antibody the smaller and fainter ~25kDa band was the result of residual binding of the primary C-terminal antibody. This theory is consistent with the fact that if cleavage were to occur at position 511 (Figure 4.14B, alanine in bold), then the C-terminal MTF1 antibody could bind both fragments, whereas the N-terminal MTF1 antibody will only bind the ~55kDa fragment.

Based on this western blot analysis, I concluded that both the N and C-terminal targeting anti-MTF1 antibodies were unable to detect MTF1 endogenously in HACs. As HACs are not easily transfected, I could not overexpress a tagged version of the protein in these cells to investigate MTF1 at the protein level further. I thus chose to examine genes reported in mice chondrocytes to be downstream and dependent on MTF1 activity in the zinc-ZIP8-MTF1 pathway.

#### **4.3.6 Metallothioneins are upregulated following IL-1 $\alpha$ stimulation for one passage in HACs**

Despite not detecting transcriptional changes to *MTF1* levels after IL-1 $\alpha$  exposure and unable to assess MTF1 protein levels and subcellular localisation due to antibody issues, the expression of the MTF1-regulated *MT* genes was assessed. Of the eight *MT* genes examined in IL-1 $\alpha$  treated HACs, *MT1A*, *MT1F*, *MT1G*, *MT1H* and *MT2A* were significantly upregulated (Figure 4.15A-E). For *MT1A* and *MT1G*, this upregulation was observed in the majority of HAC donors, except for HAC donor three which broadly inhibited *MT* expression after one passage of IL-1 $\alpha$ . *MT1G* was increased more than 16-fold in 25% of donors. *MT1F*, *MT1H* and *MT2A* were significantly upregulated (p=0.027, p=0.0078 and p=0.0257 respectively), in all eight HAC samples in which the gene was measured. *MT1E* and *MT1X* gene expression was not significantly different after IL-1 $\alpha$  treatment. A heatmap of log<sub>2</sub>-fold change differential gene expression of all the *MTs* measured by qPCR after one passage with IL-1 $\alpha$  is shown in Figure 4.15F.

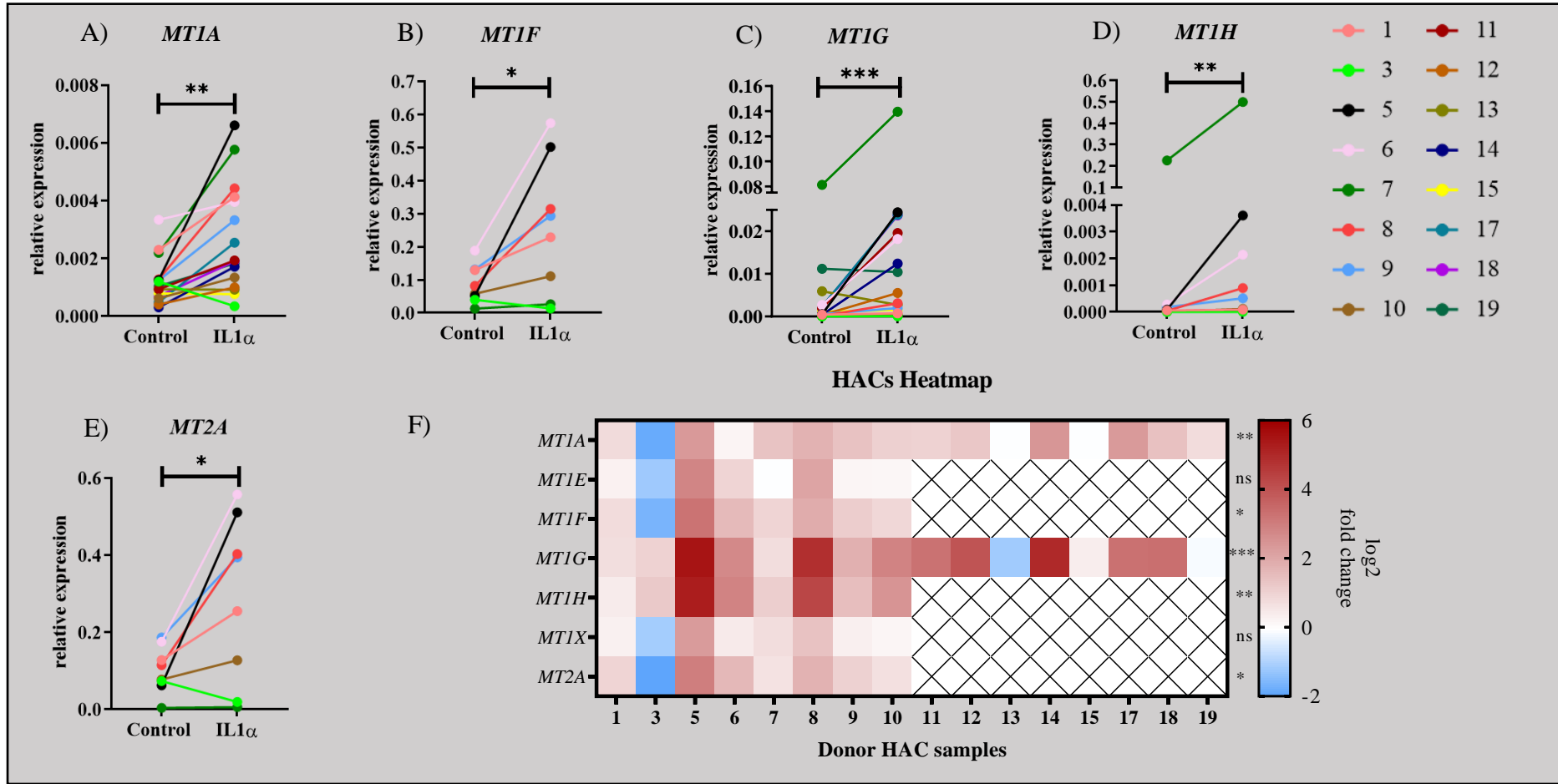


**Figure 4.15 – Metallothioneins including *MT1A*, *MT1F*, *MT1G*, *MT1H* and *MT2A* are all significantly and differentially upregulated after IL-1 $\alpha$  treatment in HAC donors.**

HACs from 16 donors were treated  $\pm$  0.1ng/ml IL-1 $\alpha$  for one passage and connecting coloured lines for *MT1A* A), *MT1F* B), *MT1G* C), *MT1H* D), *MT2A* E) and are matched HAC donor normalised gene expression responses. Data is normalised to housekeeper genes *I8S*, *GAPDH*, and *HPRT1*. Log<sub>2</sub>-fold change expression data for all 16 HAC donors illustrated as heatmap F). Red, white and blue boxes represent genes upregulated, unchanged or downregulated with IL-1 $\alpha$  respectively. A cross indicates the gene was not measured in the sample. Normalised data was analysed with a paired t-test, only *MT1H* was analysed with Wilcoxon t-test. \*p<0.05, \*\*p<0.01 and \*\*\* p<0.001 ns = non-significant.



#### 4.3.7 Cartilage matrix-degrading gene expression

To understand if IL-1 $\alpha$  treatment for one passage in HACs impacted on cartilage matrix-degrading enzymes, *ADAM-TS5* and *MMP13* expression were measured. *ADAM-TS5* was selected because it binds and cleaves at the OA-associated aggrecan cleavage site (Glu 373/Ala 374). It was also shown that in mice lacking the catalytic domain (exon three) of *ADAM-TS5* and had undergone DMM surgery, TEGE<sup>373</sup> fragments were absent from articular cartilage (Glasson *et al.*, 2005). This highlights *ADAM-TS5*'s role as a critical protease contributing to aggrecan loss with consequential type II collagen breakdown mediated by MMPs at later stages. *MMP13* rather than *MMP1* was prioritised for gene expression assessment because the former MMP is associated with type II collagen degradation derived from OA chondrocytes, whereas the latter enzyme derives from synovial fibroblasts and *MMP1* collagenolytic activity is more strongly associated in RA than OA (Chan *et al.*, 2017). *ADAM-TS5* (Figure 4.16A) was significantly upregulated (1.3-fold,  $p=0.0222$ ) but *MMP13* (Figure 4.16B) was not significantly and differentially expressed after IL-1 $\alpha$  treatment for one passage. HAC donor five had the largest fold upregulation (2.4 and 2.8-fold) for *ADAM-TS5* and *MMP13* respectively and HAC donor three *MMP13* differential gene expression was inhibited by 61% after IL-1 $\alpha$  treatment (Figure 4.16C).

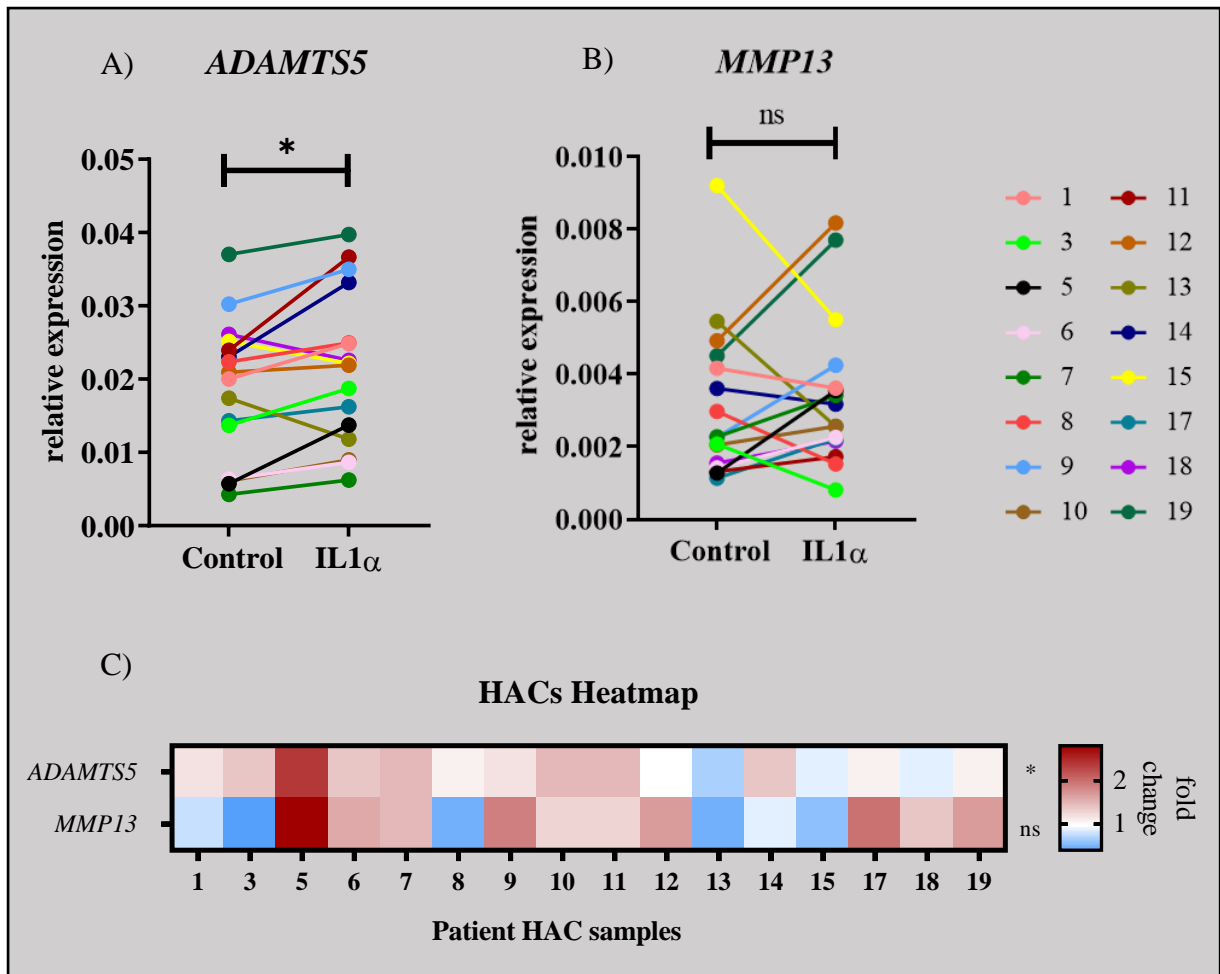


**Figure 4.16 – ADAM-TS5 and MMP13 are not significantly and differentially expressed after IL-1 $\alpha$  treatment.**

HACs from 16 donors were treated with or without 0.1ng/ml IL-1 $\alpha$  for one passage and connecting coloured lines for ADAM-TS5 A) and MMP13 B) are matched HAC donor normalised gene expression responses. Data is normalised to housekeeper genes *18S*, *GAPDH*, and *HPRT1*. Fold change expression data for all 16 HAC donors illustrated as heatmap C). Red, white and blue boxes represent genes upregulated, unchanged or downregulated with IL-1 $\alpha$  respectively. Data satisfying a D'Agostino-Pearson omnibus k2 normality test prior to or after log2 transformation was analysed with a paired t-test, \* p<0.05 ns = non-significant.

#### 4.4 Chapter summary

The data presented provides compelling and reproducible evidence for *SLC39A8* and *SLC39A14* upregulation in IL-1 $\alpha$ -treated HACs. This cohort of 16 HAC donors recapitulated the *SLC39A8* and *SLC39A14* expression patterns identified in published HAC transcriptomic datasets in SkeletalVis. The pro-inflammatory gene expression response in HACs after IL-1 $\alpha$  mimicked a previous cell culture study using IL-1 $\beta$  in SW1353 cells and HACs, whereby bioinformatics analysis revealed the transcription factor, NF $\kappa$ B, as one of the main transcription factors mediating downstream action of IL-1 (Gebauer *et al.*, 2005). As NF $\kappa$ B is involved in regulating pro-inflammatory gene expression, it follows that the pro-inflammatory genes *IL-6*, *CXCL8* and *CCL2* were upregulated in HACs. Gebauer *et al.*, 2005 also stated the most common gene signature overlap between the SW1353 cell line and HACs was the expression of catabolic matrix genes, with very little overlap elsewhere. *ADAM-TS5* but not *MMP13* was upregulated by IL-1 $\alpha$  in this instance which only partially reflected the observations of Gebauer *et al.*, 2005 in their HAC samples. This may be because of the time the cells were in culture before treatment, treatment duration itself, or because serum starvation was not performed.

Several *MTs* were differentially upregulated following IL-1 $\alpha$  stimulation. However, it is unclear whether these and matrix-degrading gene expression changes are dependent on NF $\kappa$ B, MTF1 or both. As there were no observed MTF1 transcriptional changes, there is still the possibility that MTF1 protein activity is changing in chondrocytes exposed to IL-1 $\alpha$ . A summary schematic for the zinc-ZIP8-MTF1 axis activity in HACs is presented in Figure 4.17. A new strategy to detect tagged overexpressed MTF1 protein in chondrocyte cell lines was adopted and is described in chapters five and six.

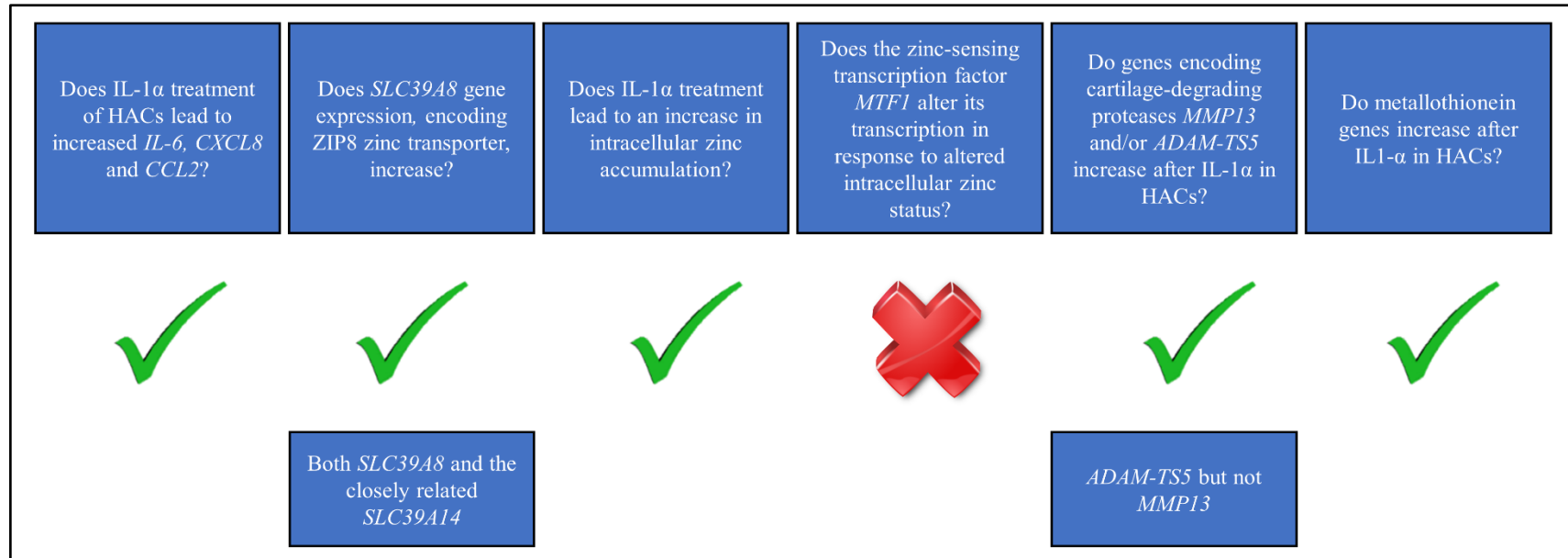


**Figure 4.17 – Summary of zinc-ZIP8-MTF1 axis exploration in HACs.**

## Chapter 5: INVESTIGATING THE ZINC-ZIP8-MTF1 AXIS IN T/C-28A2 RIB CHONDROCYTES

### 5.1 Introduction

Having explored zinc homeostasis genes in HACs from OA knee cartilage, the investigation of MTF1 activity and localisation following IL-1 $\alpha$  stimulation could no longer be advanced using HACs alone. Chondrocyte cell lines, such as T/C-28a2 cells, were established to overcome the limitations of culturing HACs; primarily that once extracted from the cartilage, HACs are slow to proliferate, and dedifferentiate over time losing the characteristic chondrocyte gene expression profile (Goldring *et al.*, 1994a) e.g. loss of *COL2A1* and *SOX9*.

This chapter explores the zinc-ZIP8-MTF1 axis in TC/-28a2 cells. The T/C-28a2 cell line was derived from discarded rib cartilage of a 15-year-old human female undergoing pectus excavatum surgery through transfection of the chondrocytes with the SV40 large T antigen inserted in the retroviral neomycin-resistant pZipNeoSV (X) vector. This vector contains the neomycin-resistance gene and was selected for over many months with G418 antibiotic. The cells were further expanded in suspension culture on agarose-coated plates, which resulted in the morphological stability of the 'polygonal cobblestone' chondrocyte appearance originally observed with transfection. The C-28/I2 line was created as one of over 40 clonal lines following clonal expansion of the T/C-28a2 cell line. T/C-28a4 cells were derived from transfection of a five-year-old's costal chondrocytes with the origin-defective SV40 plasmid using the polybrene/DMSO method. T/C-28a2 and T/C-28a4 cells express collagen types II, IX and XI and proteoglycans aggrecan, link protein, biglycan and decorin optimally in a serum-free defined medium containing 1% Nutridoma SP (Finger *et al.*, 2003). 5pM IL-1 treatment of these cells with or without 10 $\mu$ g/ml cycloheximide promoted *COL2A1* and *MMP1* expression from 1-6 hours in both lines but inhibited *COL2A1* at 24 hours specifically in T/C-28a2 cells. IL-1 + cycloheximide more notably reduced *MMP1* in T/C-28a4 than in T/C-28a2 but this was because *MMP1* was constitutively higher in T/C-28a2 cells following a medium change at time zero, 24 hours after serum-free medium culture. Cycloheximide partially recovered *COL2A1* expression when stimulated with IL-1 compared to IL-1 alone at 24 hours in T/C-28a2 cells (Goldring *et al.*, 1994a). This collagen gene expression recovery was consistent with previous results in non-immortalised human chondrocytes where the IL-1-mediated *COL2A1* gene downregulation was not a consequence of decreased  $\alpha 1$  (II) procollagen mRNA stability but was suggested that cycloheximide blocks an IL-1-induced repressor factor for  $\alpha 1$  (II) procollagen gene transcription (Goldring *et al.*, 1994b).

Interestingly, when the medium was not changed prior to stimulation and after a 24 hour period of serum-free medium culture, the constitutive levels of *MMP1* in T/C2-8a2 were lower, such that the inhibitory effect of cycloheximide on *MMP1* expression was more dramatic. At 24 hours there was no recovery of *COL2A1* by cycloheximide in the presence of IL-1 $\alpha$  and *COL2A1* levels were lower than IL-1 alone (Goldring *et al.*, 1994a). The C-28/I2 line expressed the greatest levels of catabolic matrix genes compared to the T/C-28a2 and T/C-28a4 lines, yet all had comparable *SOX9* expression (Finger *et al.*, 2003). At first glance the C-28/I2 cells might be prioritised for use in this research project to understand how IL-1 correlates with changes in zinc homeostasis genes and ultimately cartilage matrix-degrading genes. However, the TC28/I2 line proliferates at a reduced rate compared to T/C-28a2 cells and thus in the interests of conducting *in vitro* experiments in a timely manner T/C-28a2 cells were used. T/C-28a2 cells can be cultured to confluency in a shorter duration and are also amenable to transfection. In the next sections, IL-1 and/or ZnCl<sub>2</sub> were used as stimuli on T/C-28a2 cells or stably luciferase expressing T/C-28a2 cells and addressing the activation of each component of the zinc-ZIP8-MTF1 axis will be discussed.

## 5.2 Aims

This chapter aims to address the consequence of IL-1 $\alpha$  stimulation on the expression of zinc homeostasis genes and subsequent impact on cartilage matrix-degrading gene expression in T/C-28a2 cells. This was achieved with the following experimental objectives:

- Establish an IL-1 $\alpha$  concentration for use in T/C-28a2 cells that obviates toxicity and elicits an IL-1 positive gene expression (*IL-6* and *CXCL8*) response.
- Determine if IL-1 $\alpha$  and IL-1 $\beta$  elicit the same response in T/C-28a2 cells as they do in HACs by quantifying the expression of IL-1 positive control genes (*IL-6*, *CXCL8* and *CCL2*) and selected zinc transporters.
- Investigate if IL-1 and/or ZnCl<sub>2</sub> treatment for one or more passages activates the zinc-ZIP8-MTF1 axis described in mouse chondrocytes, specifically examining:
  - Zinc transporters' gene expression
  - Intracellular and extracellular zinc levels
  - *MTF1* gene expression, localisation and activity
  - *MT* expression
  - Cartilage matrix-degrading gene expression

### 5.3.1 *IL-1 $\alpha$* concentration evaluation for T/C-28a2 cells

The optimal *IL-1 $\alpha$*  concentration to use with T/C-28a2 cells had not been determined in the lab and this cytokine is less frequently used in the literature compared to *IL-1 $\beta$* . *IL-1 $\alpha$*  was evaluated at three concentrations (0.1, 0.25 and 0.5ng/ml) in T/C-28a2 cells based on the concentrations previously optimised in HACs (0.1ng/ml) and SW1353 chondrosarcoma cells (0.5ng/ml). These concentrations were 1111 and 5555-fold more than the 5pM *IL-1 $\beta$*  used in the original characterisation of the T/C-28a2 line derived by Goldring *et al.*, 1994. The aim was to determine which concentration would induce *IL-6* or *CXCL8* positive control genes successfully and whether changes to the genes were observed after *IL-1 $\alpha$*  removal. The cells were treated with *IL-1 $\alpha$*  for three consecutive passages (each lasting 72 hours) with cells collected at the end of each passage. *IL-1 $\alpha$*  was removed at day 12 and cultured for a further passage with the cells collected on day 15. Only one biological was set up per concentration per time point so statistics was not possible and only a description of the trends in the data are provided (Figure 5.1A and B). There was an apparent effect of *IL-1 $\alpha$*  on *IL-6* and *CXCL8* gene expression with more apparent concentration dependent effects of *IL-1 $\alpha$*  on *CXCL8* at day six and nine. Both genes showed concentration-dependent gene expression reduction after *IL-1 $\alpha$*  removal at the beginning of the fourth passage. The *IL-1 $\alpha$*  concentration selected for all future experiments was 0.25ng/ml because the cells appeared viable at this concentration and removal of 0.5ng/ml *IL-1 $\alpha$*  at day 12 did not result in reduced gene expression measured at day 15, unlike 0.25ng/ml. For all *IL-1 $\alpha$*  T/C-28a2 experiments the genes *IL-6*, *CXCL8* and *CCL2* were assessed to confirm the cells were responsive to *IL-1 $\alpha$* .

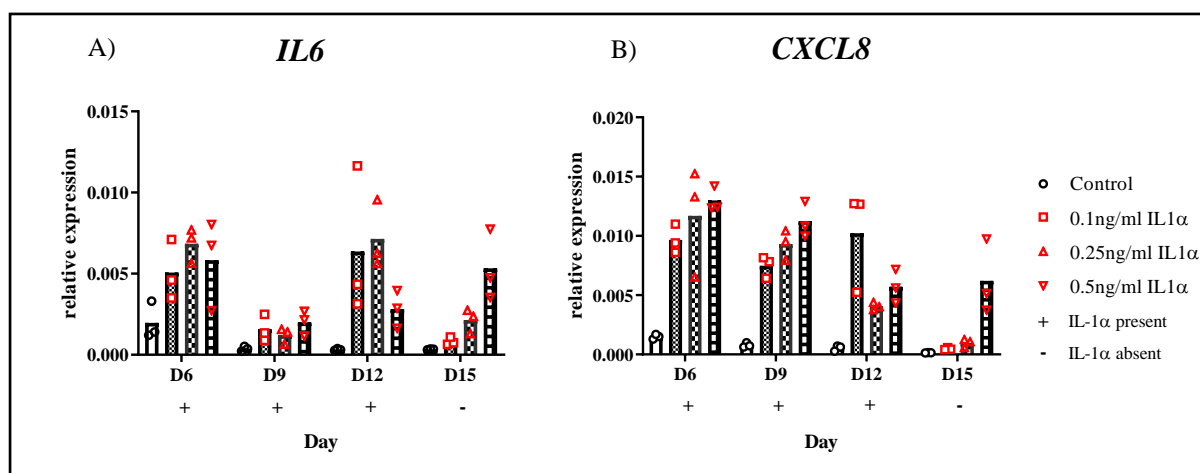


**Figure 5.1 – *IL-6* and *CXCL8* gene expression in T/C-28a2 cells treated  $\pm$  *IL-1 $\alpha$*  for three passages and its removal for the fourth passage.**

Three concentrations of *IL-1 $\alpha$*  were tested to address *IL-6* A) and *CXCL8* B) normalised gene expression by qPCR. Data is normalised to housekeepers *18S*, *GAPDH* and *HPRT1*. The bars represent the mean of three qPCR technical replicates for each of the three flasks per condition.

### 5.3.2 Do T/C-28a2 cells respond in the same manner to IL-1 $\alpha$ as IL-1 $\beta$ ?

IL-1 $\alpha$  and IL-1 $\beta$  signal through the same receptor with IL-1 $\alpha$  having ~10-fold higher affinity for IL-1R1 (Chin *et al.*, 1988). Both cytokines trigger similar gene expression responses in HACs as observed in section 4.3.1. I thus investigated whether T/C-28a2 cells also respond in an identical manner to both IL-1 $\alpha$  and IL-1 $\beta$ . One experiment was conducted comparing T/C-28a2 cells treated for 72 hours with 0.25ng/ml IL-1 $\alpha$  or 2.5ng/ml IL-1 $\beta$  and the genes *IL-6*, *CXCL8*, *CCL2* were quantified by qPCR (Figure 5.2A-C). All three genes were significantly upregulated by IL-1 $\alpha$  (8-fold p=0.019, 23-fold p=0.0041, and 15-fold p=0.0027 compared to control respectively). All three genes were also upregulated significantly by IL-1 $\beta$  (10-fold p=0.0012, 43-fold p=0.0007 and 17-fold p=0.0098 compared to control respectively). This result indicated that IL-1 $\alpha$  and IL-1 $\beta$  responses were indistinguishable with the exception of *CXCL8* (p=0.0121). Furthermore, IL-1 $\alpha$  is more potent than IL-1 $\beta$  as it induces similar gene expression changes as IL-1 $\beta$  but at 10-fold lower concentration.

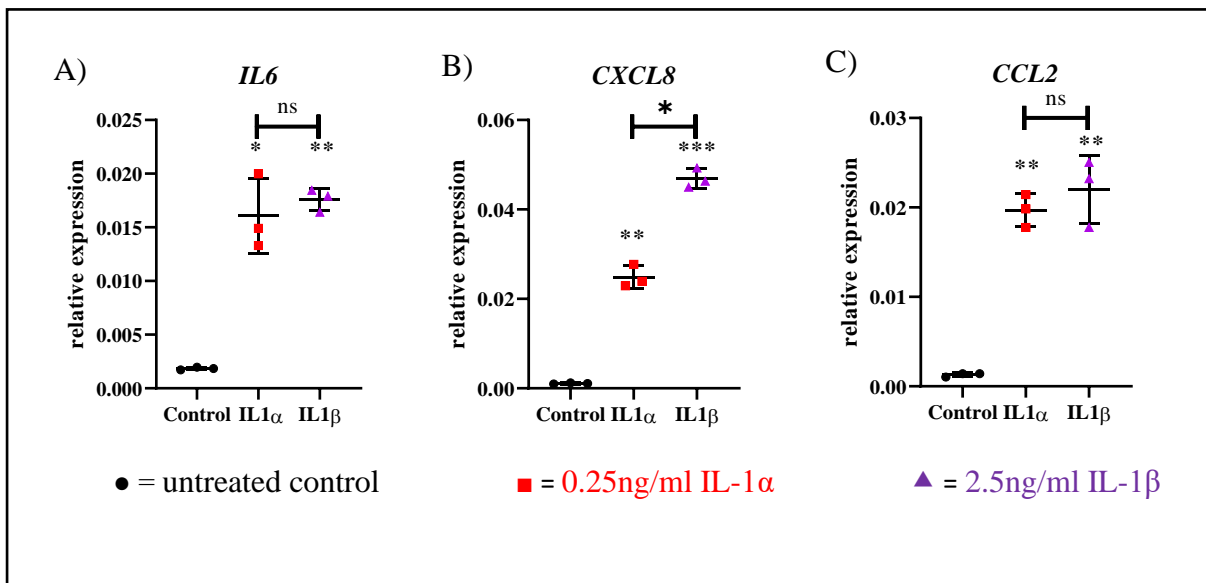


**Figure 5.2 – Normalised *IL-6*, *CXCL8* and *CCL2* gene expression responses in T/C-28a2 cells treated  $\pm$  IL-1 $\alpha$  or IL-1 $\beta$ .**

Four hours after seeding, T/C-28a2 cells were treated with or without 0.25ng/ml IL-1 $\alpha$  or 2.5ng/ml IL-1 $\beta$  for one passage (72 hours) and the genes *IL-6* A), *CXCL8* B) and *CCL2* C) quantified by qPCR. Data is normalised to housekeepers *18S*, *GAPDH* and *HPRT1*. Data satisfying a Shapiro Wilk normality test prior to or after log<sub>2</sub> transformation was analysed with a paired t-test comparing treatments against control or IL-1 $\alpha$  against IL-1 $\beta$ . Symbols represent the mean of three qPCR technical replicates for each of the three flasks per condition and error bars are the standard deviation. Horizontal lines are the group mean. ns = non-significant p>0.05.

### 5.3.3 *SLC39A14* but not *SLC39A8* is upregulated after one passage with *IL-1 $\alpha$*

Next, the zinc transporter genes' expression was assessed in T/C-28a2 cells treated for one passage lasting 72 hours with 0.25ng/ml *IL-1 $\alpha$* . A total of six experiments and cDNA from up to 16 flasks per condition (untreated or *IL-1 $\alpha$* -treated) for a 72 hour passage was analysed. Using RNA-Seq data from Table 3.9 (Chapter 3) the human zinc transporters expressed in cartilage were determined using a TPM threshold >4. Transporters absent from the subsequent figures were not expressed in OA cartilage. After 72 hours of *IL-1 $\alpha$*  exposure, *SLC39A13* and *SLC39A14* were significantly upregulated 1.2-fold (p=0.0028) and 2.2-fold (p=0.0001) respectively, with *SLC39A8* not showing a significant change in expression in any experiment (Figure 5.3 A-C). *Slc39a8* is upregulated in mouse chondrocytes after *IL-1 $\beta$*  exposure, and so I next investigated if *IL-1 $\beta$*  treatment led to *Slc39a8* upregulation in the T/C-28a2 human chondrocytes. *SLC39A8* showed no change in expression in chondrocytes treated with either cytokine compared to untreated cells (Figure 5.3D), whereas *SLC39A14* was upregulated 2.4-fold (p=0.0006) and 2.5-fold (p=0.004) after 72 hours of *IL-1 $\alpha$*  and *IL-1 $\beta$*  treatment respectively (Figure 5.3E). Differences between *IL-1* ligands for either *SLC39A8* or *SLC39A14* gene expression were negligible.

Two experiments totalling 3-5 biological replicates in which all zinc transporters were assessed after IL-1 $\alpha$  exposure for 24, 72 (P1), 144 (P2) and 216 (P3) hours and its removal from T/C-28a2 cells for a final 72 hour passage (288 hour, P4) was conducted. No significant difference between IL-1 $\alpha$  and control treatments for *SLC39A8* expression was observed (Figure 5.4A). *SLC39A13* was significantly upregulated (1.2-fold, p=0.0028) at P1. *SLC39A14* expression remained non-significantly elevated after 144 (1.9-fold, Figure 5.4B) and 216 hours (P3, 1.7-fold, Figure 5.4B) and although zinc transporter gene downregulation following IL-1 $\alpha$  removal was not evident when compared to untreated cells from the same passage, the effect of downregulation was evident when compared to P1 (Figure 5.4B and C). Among zinc exporters, *SLC30A3* was significantly downregulated (0.8-fold, p=0.0197) at 24 hours and although not significant *SLC30A5* was also among the most prominently downregulated zinc transporters compared to control at each passage as summarised in a fold change heatmap (Figure 5.4C).

Next, the effect of zinc  $\pm$  IL-1 $\alpha$  on *SLC39A8* and *SLC39A14* expression was examined. This was a single experiment performed in biological triplicate and the concentration of ZnCl<sub>2</sub> used (100 $\mu$ M) in this experiment was selected from Kim *et al.*, 2014. None of the treatments induced a *SLC39A8* expression profile in T/C-28a2 cells that was different to control after 72 hours (Figure 5.4D). *SLC39A14* was significantly upregulated (2-fold, p=0.0046) following IL-1 $\alpha$  treatment for 72 hours and was also significantly upregulated (2.2-fold, p=0.0028) in the combined IL-1 $\alpha$  + ZnCl<sub>2</sub> treatment, though this appears to be driven by the IL-1 $\alpha$  and not the ZnCl<sub>2</sub>. No conclusion about the effect of ZnCl<sub>2</sub> on *SLC39A8* or *SLC39A14* gene expression (Figure 5.4D and E) was possible because one of the triplicate ZnCl<sub>2</sub>-treated flasks became infected. The fold changes of all genes measured in flasks treated with 0.25ng/ml IL-1 $\alpha$  for 72 hours is presented in Appendix E and the equivalent relative gene expression graphs for all zinc transporters measured at either 72 hours or in the context of the complete time course are in Figures 5.5-5.8.

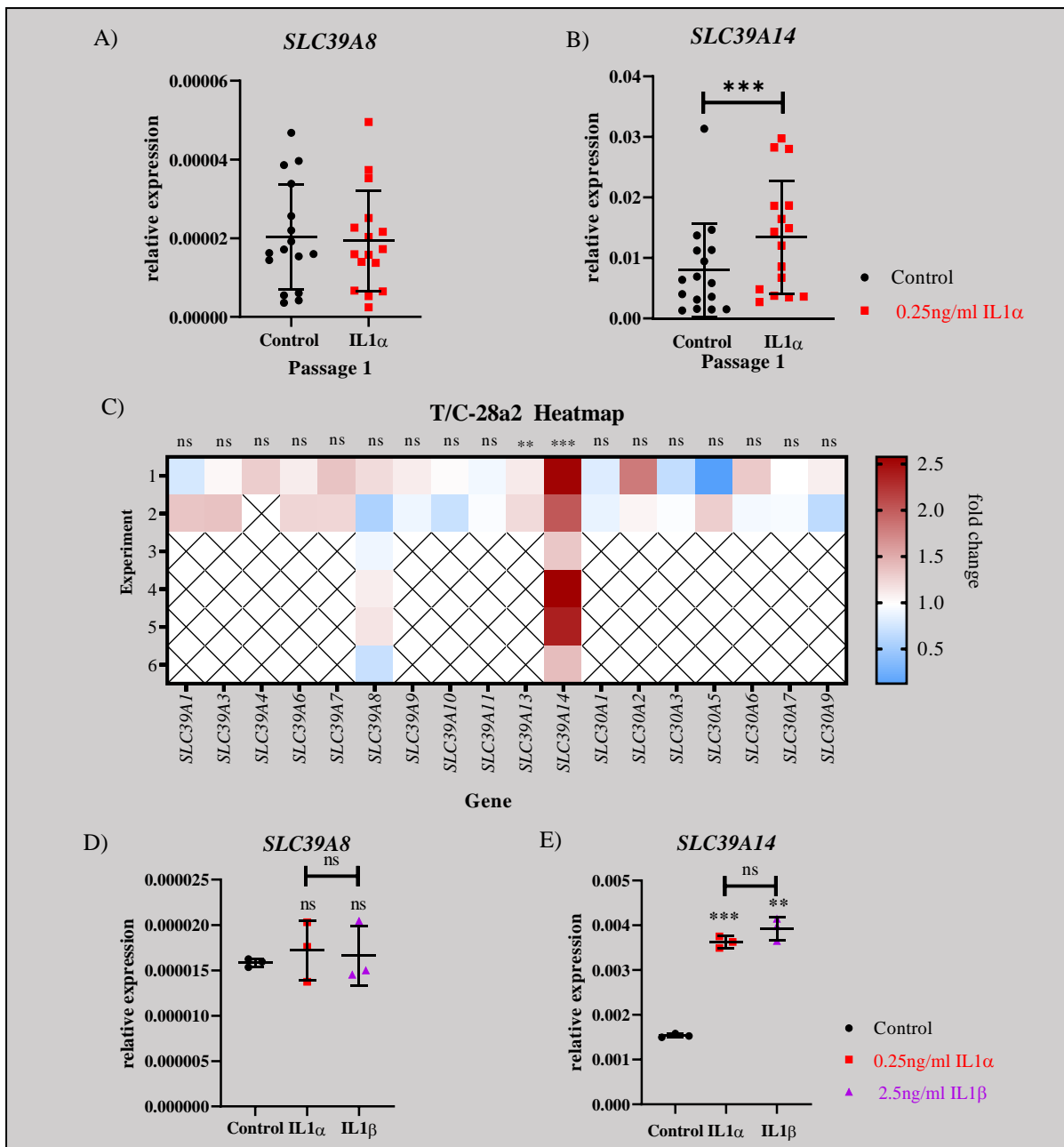


**Figure 5.3– *SLC39A14*, not *SLC39A8* is significantly upregulated by IL-1 $\alpha$  in T/C-28a2 cells after 72 hours in six experiments and is also significantly different from control after IL-1 $\beta$  treatment.**

Relative gene expression of *SLC39A8* A) and *SLC39A14* B) genes normalised to housekeeper genes *18S*, *GAPDH* and *HPRT1*. Heatmap summarising IL-1 $\alpha$ -mediated zinc transporter gene expression fold changes relative to controls after one passage lasting 72 hours C). Red indicates differential fold change upregulation with IL-1 $\alpha$ , and blue represents differentially downregulated fold change with IL-1 $\alpha$ . Genes marked with a cross were not measured in these samples. Relative gene expression of *SLC39A8* D) and *SLC39A14* E) of IL-1 $\alpha$  or IL-1 $\beta$ -treated T/C-28a2 cells treated in biological triplicate for 72 hours. Symbols represent mean of three qPCR technical replicates for each flask per condition from every biological replicate across one (D and E) or six (A, B and C) experiments. Horizontal lines are the group mean and error bars are standard deviation. Data satisfying either a D’Agostino-Pearson omnibus k2 (*SLC39A8* and *SLC39A14*) or a Shapiro Wilk normality test prior to or after log2 transformation was analysed with a paired t-test. \*\* p<0.01, \*\*\* p<0.001 ns = non-significant p >0.05.

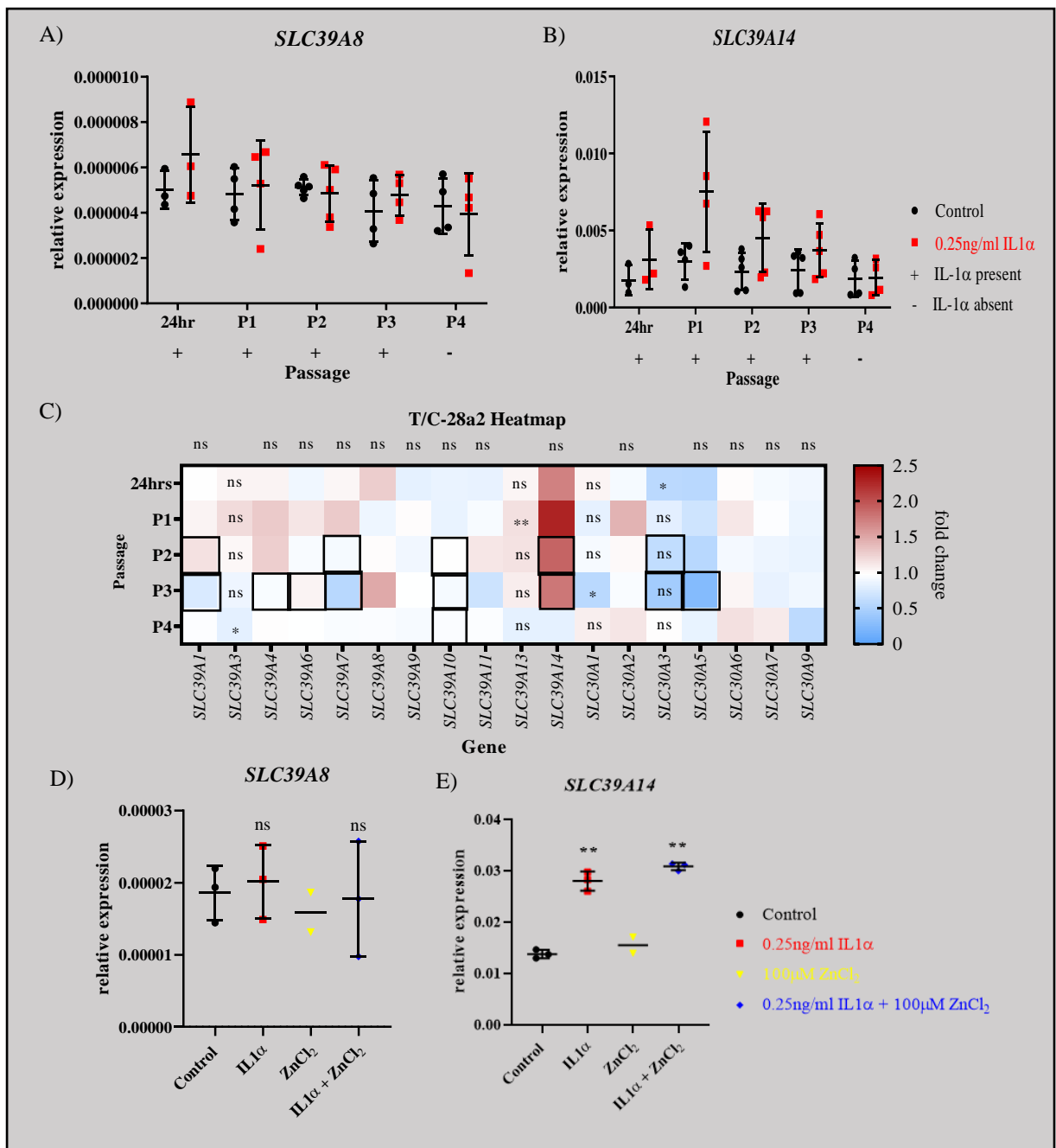


**Figure 5.4– Long-term exposure of T/C-28a2 cells to IL-1 $\alpha$  does not lead to sustained and elevated *SLC39A8* or *SLC39A14* expression compared to control, nor does ZnCl<sub>2</sub> influence *SLC39A8* or *SLC39A14* expression.**

Relative gene expression of *SLC39A8* A) and *SLC39A14* B) genes normalised to housekeeper genes *18S*, *GAPDH* and *HPRT1*. Heatmap summarising IL-1 $\alpha$ -mediated zinc transporter gene expression fold changes relative to controls after three passages with IL-1 $\alpha$  present and one passage without IL-1 $\alpha$  C). Red indicates differential fold change upregulation with IL-1 $\alpha$ , and blue represents differentially downregulated fold change with IL-1 $\alpha$ . Relative gene expression of *SLC39A8* D) and *SLC39A14* E) of IL- $\alpha$ , ZnCl<sub>2</sub> or both IL-1 $\alpha$  + ZnCl<sub>2</sub> treatments of T/C-28a2 cells in biological triplicate for 72 hours. Symbols represent mean of three qPCR technical replicates for each flask per condition from every biological replicate across one (D and E) or two experiments (A, B and C). Horizontal lines are the group mean and error bars are standard deviation. Data satisfying a Shapiro Wilk normality test prior to or after log<sub>2</sub> transformation was analysed with a paired t-test, otherwise a Wilcoxon t-test was used (highlighted squares in C). Data in D and E was analysed by paired t-test. \* p<0.05, \*\* p<0.01, ns = non-significant p >0.05.

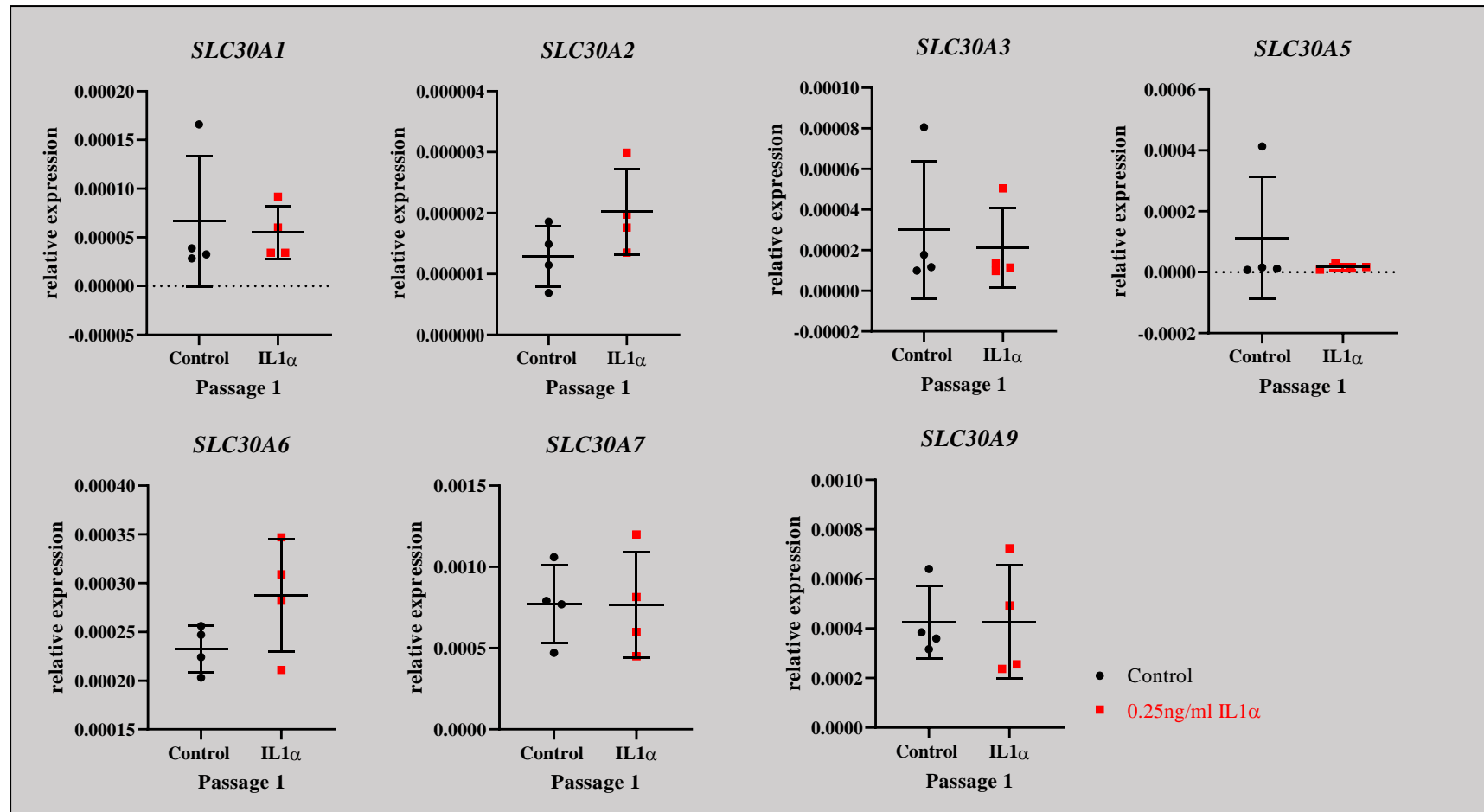


**Figure 5.5– Zinc exporter gene expression in T/C-28a2 cells treated  $\pm$  IL-1 $\alpha$  for 72 hours.**

Zinc exporters were all initially assessed in cDNA from preliminary T/C-28a2 cell experiments where 0.25ng/ml IL-1 $\alpha$  exposure was maintained for 24, 72, 144, and 216 hours and its removal for cell recovery for a further 72 hours totalling 288 hours of culture. Only the 72 hour data is presented here and data satisfying a Shapiro Wilk normality test prior to or after log<sub>2</sub> transformation was analysed with a paired t-test. Symbols represent the mean of three qPCR technical replicates for each flask from two experiments and the mean relative expression is normalised to housekeepers *18S*, *GAPDH* and *HPRT1*. Horizontal lines are the group mean and error bars are the standard deviation.

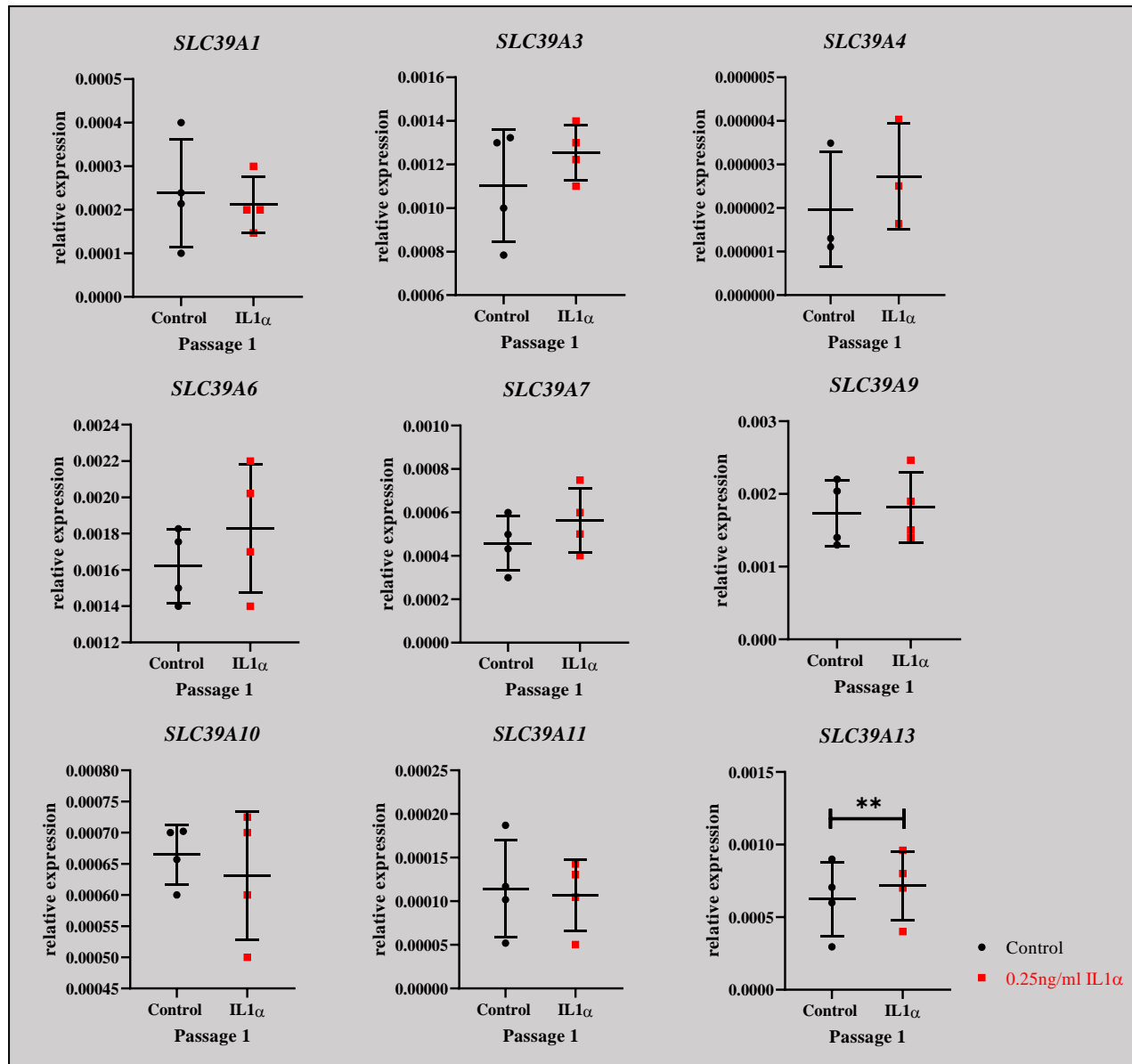


**Figure 5.6– Zinc importer gene expression in T/C-28a2 cells treated  $\pm$  IL-1 $\alpha$  for 72 hours.**

Zinc importers were all initially assessed in cDNA from preliminary T/C-28a2 cell experiments where 0.25ng/ml IL-1 $\alpha$  exposure was maintained for 24, 72, 144, and 216 hours and its removal for cell recovery for a further 72 hours totalling 288 hours of culture. Only the 72 hour data is presented here and data satisfying a Shapiro Wilk normality test prior to or after log<sub>2</sub> transformation was analysed with a paired t-test. Symbols represent the mean of three qPCR technical replicates for every flask from two experiments and the mean relative expression is normalised to housekeepers *18S*, *GAPDH*, *HPRT1*. Horizontal lines are the group mean and error bars are the standard deviation.

\*\* p<0.01

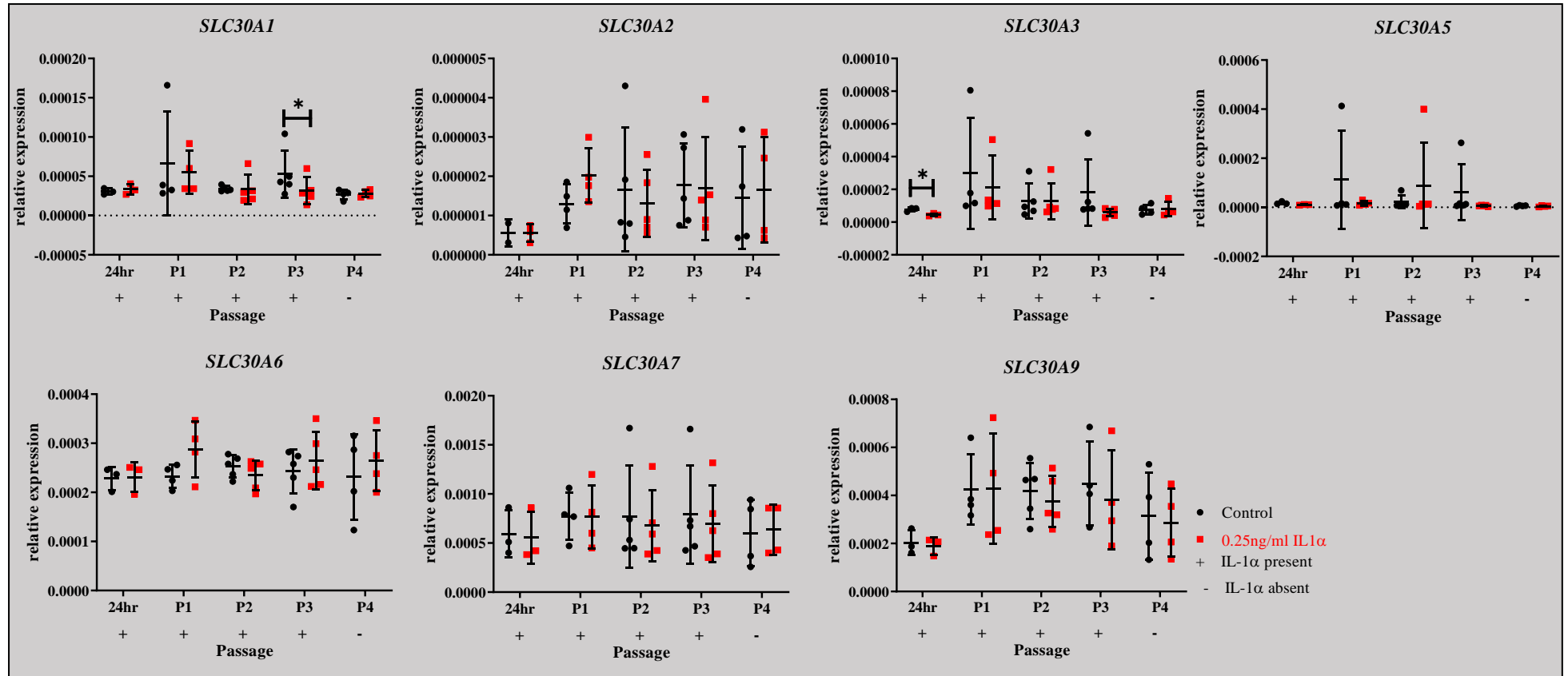


**Figure 5.7- Zinc exporter gene expression in T/C-28a2 cells treated  $\pm$  IL-1 $\alpha$  for consecutive passages up to 216 hours (P3) and cell recovery for 72 hours (P4).**

P1 data presented here is the same as Figure 5.5 but with the added context of the remaining passages of the time course for the two experiments. The experiment was repeated with three biological replicates per condition per passage totalling 60 samples. However, due to RNA degradation during extraction only three to five biological replicates (42 samples) were available for analysis by either paired or Wilcoxon's t-test. Normalised data satisfying a Shapiro Wilk normality test prior to or after log<sub>2</sub> transformation was analysed with a paired t-test. Where the data was not normal a Wilcoxon t-test of the normalised data was conducted (P2 -*SLC30A3*; P3 - *SLC30A3* and *SLC30A5*). Symbols represent mean of three qPCR technical replicates for every flask from two experiments and the mean relative expression is normalised to housekeepers *18S*, *GAPDH* and *HPRT1*. Horizontal lines are the group mean and error bars are the standard deviation. \* p<0.05

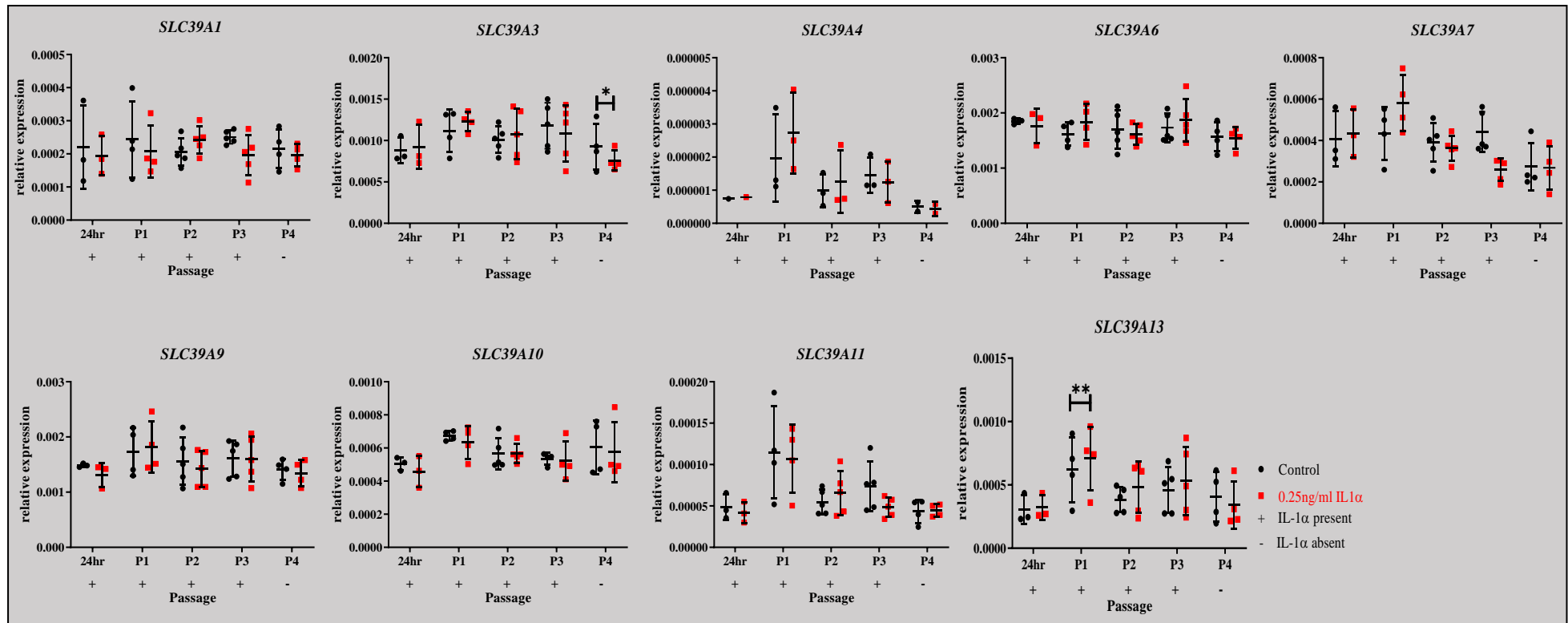


**Figure 5.8– Zinc importer gene expression in T/C-28a2 cells treated  $\pm$  IL-1 $\alpha$  for consecutive passages up to 216 hours (P3) and cell recovery for 72 hours (P4).**

P1 data presented here is the same as Figure 5.6 but with the added context of the remaining passages of the time course for the two experiments. The experiment was repeated with three biological replicates per condition per passage totalling 60 samples. However, due to RNA degradation during extraction only three to five biological replicates (42 samples) were available for analysis by paired t-test. Normalised data satisfying a Shapiro Wilk normality test prior to or after log<sub>2</sub> transformation was analysed with a paired t-test. Where the data was not normal a Wilcoxon t-test of the normalised data was conducted (P2 -*SLC39A1*, 7, 10 and 13; P3 – as before and additionally *SLC39A4* and 6; P4 – *SLC39A10*). Symbols represent mean of three qPCR technical replicates for every flask from two experiments and the mean relative expression is normalised to housekeepers *18S*, *GAPDH* and *HPRT1*. Horizontal lines are the group mean and error bars are the standard deviation. \*\* p<0.01

### 5.3.4 What effect does IL-1 $\alpha$ treatment have on T/C-28a2 intracellular and extracellular zinc levels?

In murine chondrocytes, IL-1 induced upregulation of *Slc39a8* which led to an increase in intracellular zinc levels (Kim *et al.*, 2014). Although *SLC39A8* was not upregulated in T/C-28a2 cells in response to IL-1 $\alpha$ , the related zinc importer gene *SLC39A14* was upregulated. Thus, the MAK032 kit was used to investigate whether the metal ion concentration intracellularly or in spent medium was influenced by 0.25ng/ml IL-1 $\alpha$  exposure to T/C-28a2 cells treated for 72 hours. As shown in Chapter 4, this kit is not specific to zinc and can also detect Fe<sup>2+</sup>. Thus, the concentrations measured represent zinc and iron combined. Unlike HACs (Chapter 4, Figure 4.10), the metal ion concentration in T/C-28a2 cells or in spent medium was not significantly altered by 0.25ng/ml IL-1 $\alpha$  exposure after two experiments carried out in biological duplicate and triplicate respectively (Figure 5.9).

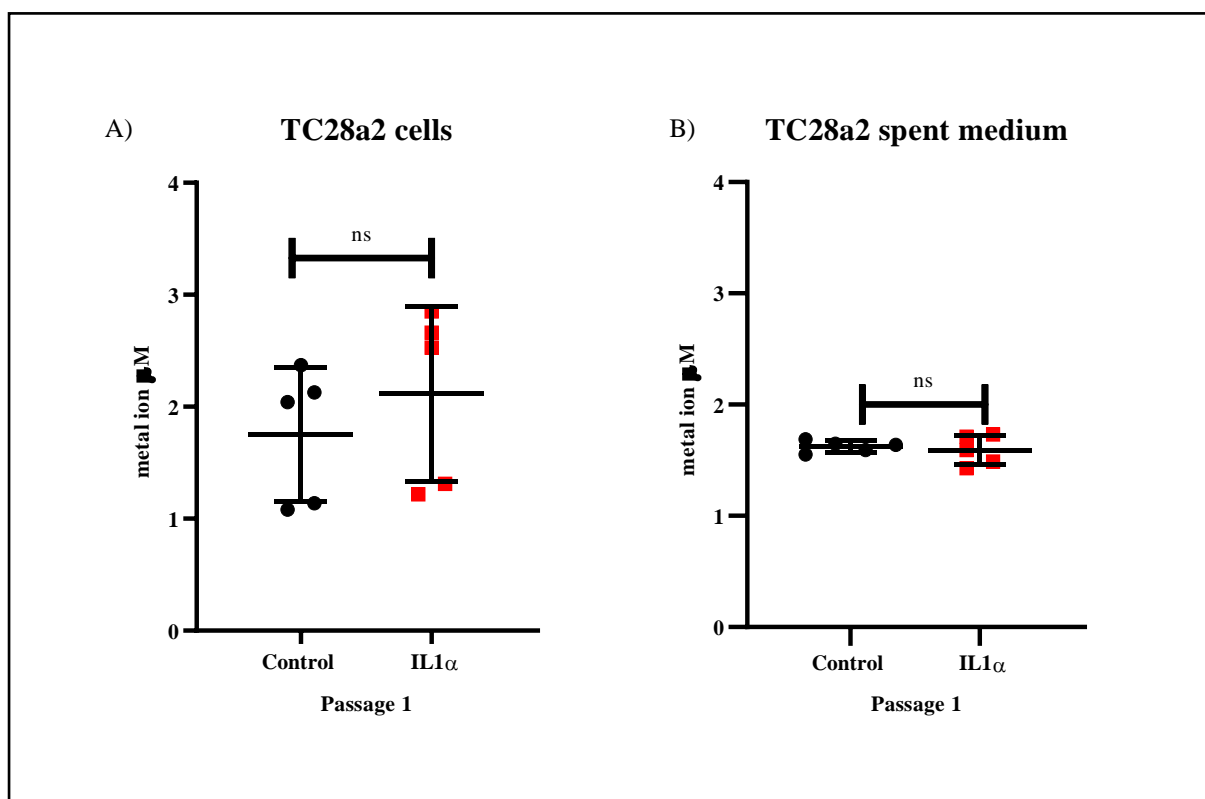


**Figure 5.9–Metal ion content determined using a spectrophotometric method in T/C-28a2 cells and spent medium  $\pm$  IL-1 $\alpha$  was not significantly different.**

T/C-28a2 cells were treated in biological duplicate or triplicate  $\pm$  0.25ng/ml IL-1 $\alpha$  for one passage (72 hours) in monolayer culture for a total of two experiments. The cells A) and matched spent medium B) were collected and metal ion content measured using the MAK032 spectrophotometric kit. Symbols represent means of duplicate measurements of control (black) or IL-1 $\alpha$ -treated (red) cell pellets or spent medium and horizontal line is the group mean and the error bars are standard deviation. The data was analysed with a paired t-test. ns = non-significant.

### 5.3.5 Is *MTF1* gene expression upregulated in response to *IL-1 $\alpha$* in T/C-28a2 cells?

Although the spectrophotometric experiment indicated the intracellular zinc levels were unchanged in T/C-28a2 cells after 72 hours of *IL-1 $\alpha$*  treatment, I next investigated if expression of the zinc sensing transcription factor *MTF1* was upregulated in these cells. As the metal ion concentration was unchanged by *IL-1 $\alpha$* , after 72 hours it was perhaps unsurprising to find the *MTF1* transcript was also not significantly different at 72 hours or at any time point tested (Figure 5.10).

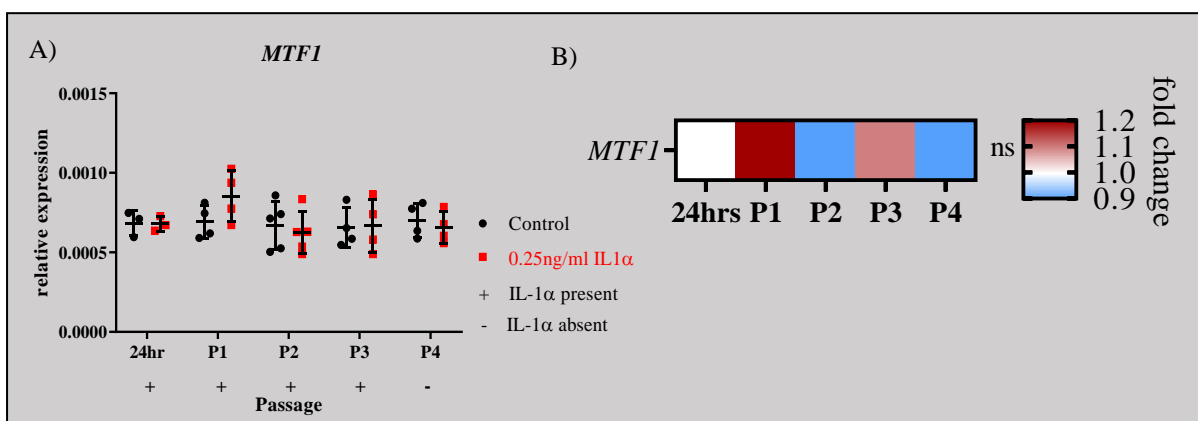


**Figure 5.10–*MTF1* relative expression and fold change in T/C-28a2 cells treated  $\pm$  *IL-1 $\alpha$* .** *MTF1* expression A) was assessed in cDNA from preliminary T/C-28a2 cell experiments where *IL-1 $\alpha$*  exposure was maintained for 24, 72 (P1), 144 (P2), and 216 (P3) hours and its removal for cell recovery for a further 72 hours totalling 288 (P4) hours of culture. Summary heatmap of *MTF1* expression fold change relative to untreated control B). Red indicates differential fold change upregulation with *IL-1 $\alpha$* , and blue represents differentially downregulated fold change with *IL-1 $\alpha$* . Symbols represent mean of three qPCR technical replicates for every flask from two experiments and the mean relative expression normalised to housekeepers *18S*, *GAPDH*, *HPRT1*. Horizontal lines are the group mean and error bars are the standard deviation. Normalised data was assessed for normality by Shapiro Wilk test and a paired t-test carried out at each time point  $p > 0.05$ .

### 5.3.6 How do C and N-terminal MTF1 antibodies perform in western blots using untreated T/C-28a2 nuclear and whole protein lysates?

T/C-28a2 nuclear and whole protein lysates, provided by a colleague whose experiments did not make use of cytoplasmic lysate, were used in these experiments rather than all three fractions. The efficacy of the C and N-terminal MTF1 antibodies in lysates prepared from untreated T/C-28a2 cells was assessed. Neither MTF1 antibodies detected a protein of 81kDa (the expected weight of MTF1 full length protein) in the T/C-28a2 lysates (Figure 5.11). Instead, multiple bands were observed on the same blot probed sequentially with the different MTF1 antibodies. The same bands for the overexpressed MTF1 lysate control were observed with both the C and N terminal MTF1 antibodies as observed in HACs (section 4.3.5.2), because these T/C-28a2 samples were loaded as part of a larger gel containing HACs, T/C-28a2 and SW1353 lysates but Figure 5.11 has been cropped to address each cell type separately. The full blot is available in appendix G. MTF1 could not be detected in T/C-28a2 cells by western blot with either antibodies that detect different parts of the protein, let alone could be used to address translocation in the T/C-28a2 cell line.

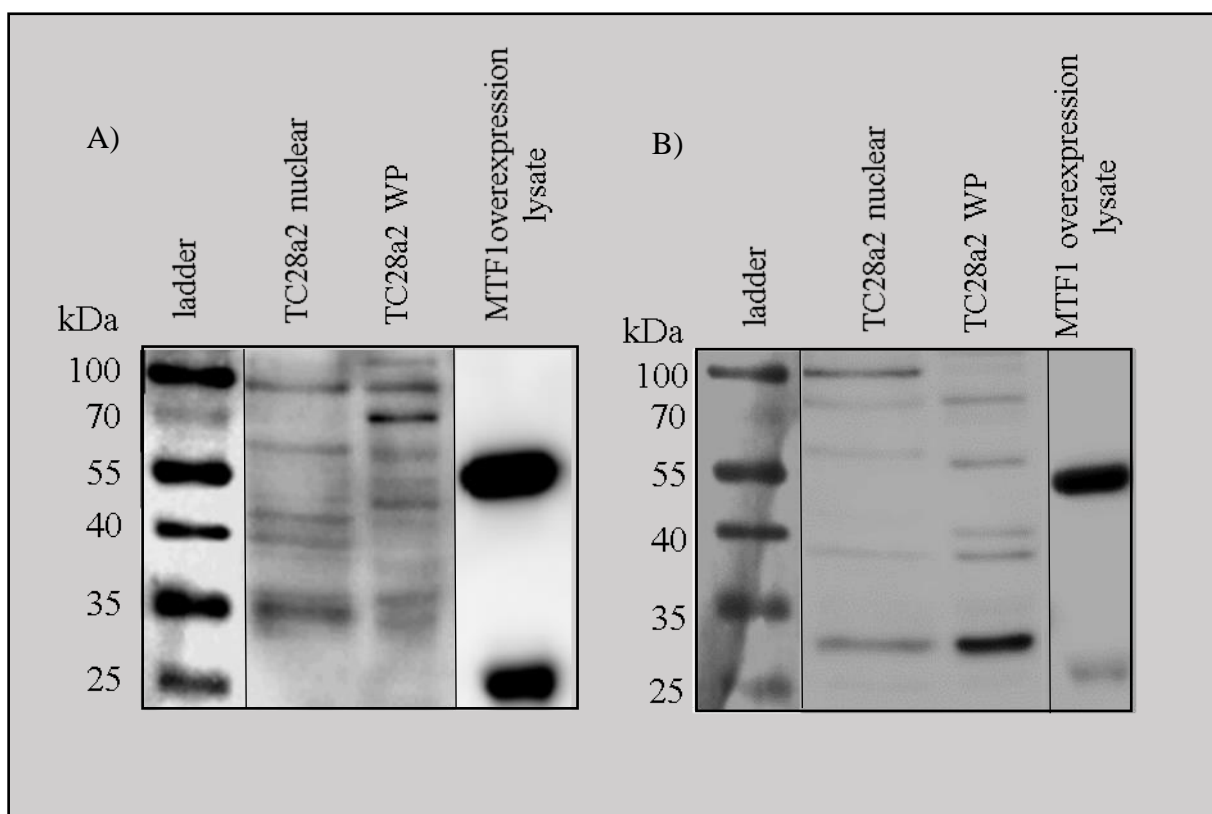


**Figure 5.11– Western blot comparing C and N-terminal MTF1 antibody consecutively on untreated T/C-28a2 nuclear and cytoplasmic lysates.** The blot was probed with the C-terminal MTF1 antibody A) and after visualisation, the same blot was re-probed with N-terminal MTF1 antibody B). Overexpressed MTF1 lysate was purchased from Origene (LC401804). WP = whole protein, kDa = kilodaltons.

### **5.3.7 What are the effects of IL-1 $\alpha$ and/or ZnCl<sub>2</sub> treatment on MTF1 activity?**

MTF1 activity could not be measured in HACs, but as T/C-28a2 cells are easily transfected, MTF1 activity can be studied using reporter assays in this cell line. To test whether MTF1 activity changed after exposure to 0.25ng/ml IL-1 $\alpha$  or 2.5ng/ml IL-1 $\beta$  for 24 hours, a luciferase reporter assay for MTF1 was carried out. As a positive control, cells were treated with ZnCl<sub>2</sub> alone or  $\pm$  IL-1 $\alpha$  to increase intracellular zinc levels and stimulate the zinc homeostatic response. The reporter plasmid, pGL4.40 luciferase, encodes the firefly luciferase protein under the control of a minimal promoter and contains five copies of a 5' MRE immediately upstream of a minimal promoter (Appendix A). The MRE is a sequence (TGCNCRC) specifically recognised and bound by MTF1 that is found in the promoter of MTF1 target genes (Giedroc *et al.*, 2001). The MRE pGL4.40 plasmid or cloned empty control pGL4.40 plasmid were co-transfected separately with renilla luciferase into T/C-28a2 cells for 24 hours, media removed and then replaced with media containing different IL-1 cytokines and/or ZnCl<sub>2</sub> for a further 24 hours. Cells were then lysed and luciferase and renilla activity measured. After normalisation of the raw luciferase signal against the renilla luciferase signal the amount of light production is proportional to MTF1 binding at the MRE, a readout of MTF1 transcription factor activity.

Initial examination of the normalised firefly:renilla data from T/C-28a2 cells transfected with the empty control pGL4.40 plasmid demonstrated that the different stimuli had a significant effect on firefly:renilla luciferase ratios. This indicates that the treatments affect the activity of the minimal promoter in T/C-28a2 cells transfected with the empty control pGL4.40 plasmid (Figure 5.12A). MRE to control luciferase ratios above one thus indicates increased MTF1 activity (Figure 5.12B) and those below one indicates repressed activity. The normalised luciferase activity of the MRE plasmid was further normalised to the empty control pGL4.40 plasmid data for each respective stimulus to account for the effect stimulation had on basal luciferase activity in Figure 5.12A. The experiment was completed a total of four times with six sextuplicate wells per condition.

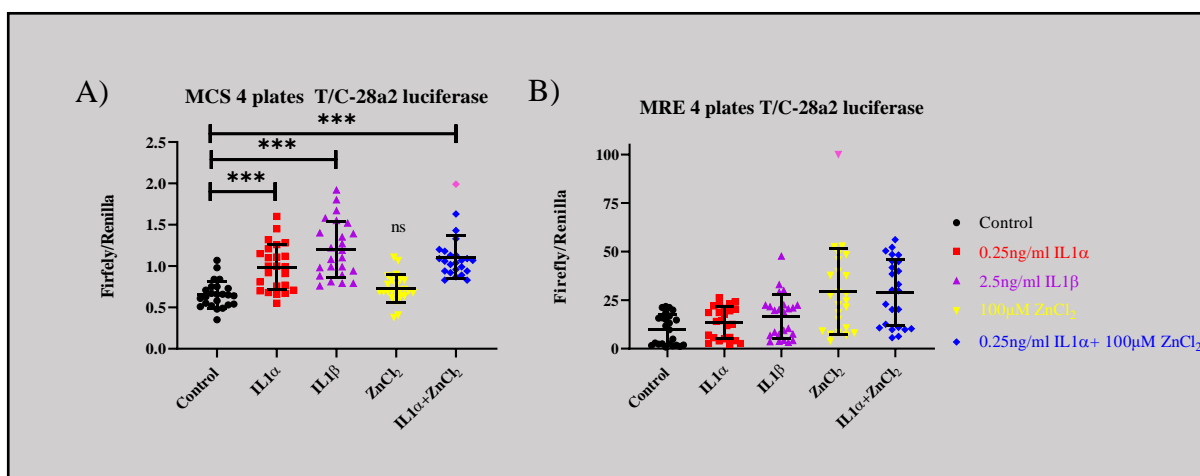


**Figure 5.12 – Raw firefly:renilla ratios from T/C-28a2 cells transiently transfected with empty control pGL4.40 and renilla luciferase or MRE pGL4.40 plasmid and renilla luciferase.**

T/C-28a2 cells transiently transfected with the empty control pGL4.40 plasmid and renilla luciferase A) and T/C-28a2 cells transiently transfected with the MRE pGL4.40 plasmid and renilla luciferase B). Cells were transfected for 24 hours followed by a further 24 hour exposure to medium only or 0.25ng/ml IL-1 $\alpha$ , 2.5ng/ml IL-1 $\beta$ , 100 $\mu$ M ZnCl $_2$  or 0.25ng/ml IL-1 $\alpha$  + 100 $\mu$ M ZnCl $_2$  before luciferase activity was measured. Each coloured symbol is a different treatment with all six technical replicates from four experiments totalling 24 replicate values. The firefly luciferase data has been normalised to the renilla luciferase to account for any variation in transfection efficiency. The firefly:renilla ratios were analysed for normality by D'Agostino-Pearson omnibus k2 test ( $n > 8$ ) and either an unpaired t-test with Welch's correction or Mann-Whitney t-test (IL-1 $\alpha$  + ZnCl $_2$  vs control) was conducted. Outliers in the dataset are highlighted in pink and were determined by addition or subtraction of 1.5 times the interquartile range of the 75<sup>th</sup> or 25<sup>th</sup> percentile respectively. \*\*\*  $p < 0.001$  ns = non-significant.

In the cells transfected with the pGL4.40 plasmid, 0.25ng/ml IL-1 $\alpha$  or 2.5ng/ml IL-1 $\beta$  treatment for 24 hours resulted in non-significant changes in luciferase activity. This indicates that MTF1 activity in T/C-28a2 chondrocytes is not altered after 24 hours exposure to either IL-1 $\alpha$  or IL-1 $\beta$ . However, the positive control 100 $\mu$ M ZnCl<sub>2</sub> and 0.25ng/ml IL-1 $\alpha$  + 100 $\mu$ M ZnCl<sub>2</sub> stimulus significantly increased luciferase activity, confirming that the reporter assay was able to detect increased MTF1 activity in response to increased cellular levels of zinc. ZnCl<sub>2</sub> treated cells had higher activity than ZnCl<sub>2</sub> + IL-1 $\alpha$ , although the difference in luciferase activity between these two stimuli were not significant from one another (Figure 5.13, 2.4 and 1.8-fold respectively). This analysis indicated that ZnCl<sub>2</sub> was indeed increasing MTF1 activity as measured using the MRE luciferase reporter plasmid. There was evident variation of the 24 measurements within groups, often whole plates grouping separately from other plates with the same treatment.

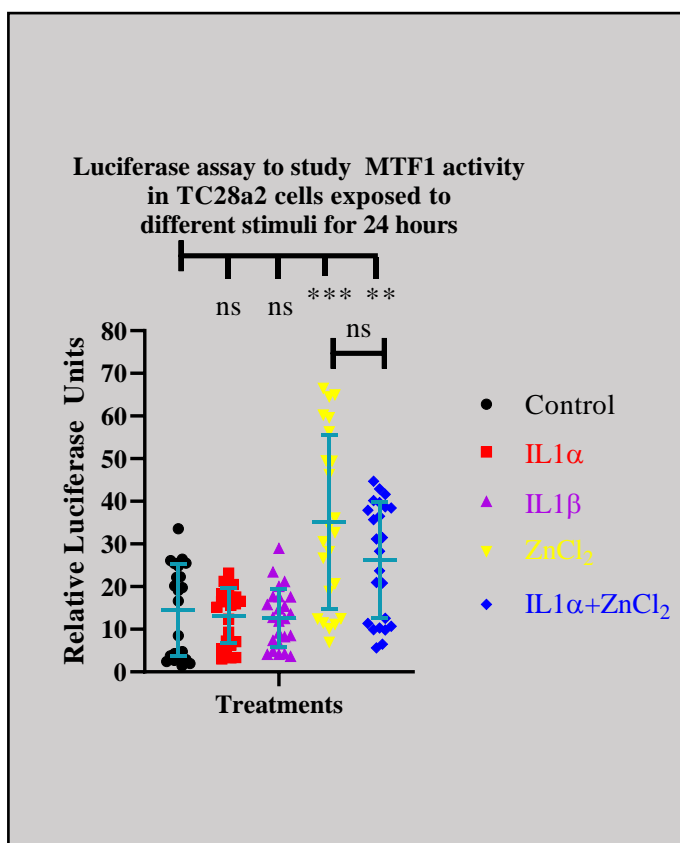


**Figure 5.13- Luciferase reporter assay measuring MTF1 activity in T/C-28a2 cells treated  $\pm$  IL-1 $\alpha$ , IL-1 $\beta$ , ZnCl<sub>2</sub> or IL-1 $\alpha$  + ZnCl<sub>2</sub> for 24 hours.**

T/C-28a2 cells seeded and incubated for 24 hours were transfected for an additional 24 hours with either empty control or MRE pGL4.40 plasmid then treated in technical sextuplicate  $\pm$  0.25ng/ml IL-1 $\alpha$  (red), 2.5ng/ml IL-1 $\beta$  (purple), 100 $\mu$ M ZnCl<sub>2</sub> (yellow) or 0.25ng/ml IL-1 $\alpha$  + 100 $\mu$ M ZnCl<sub>2</sub> (blue) for a further 24 hours. The experiment was repeated a further three times. Symbols represent each of 23-24 measurements (after outlier removal) for each treatment across four experiments. Horizontal bars show the mean of each condition and the error bars are standard deviation. Statistical analysis is Mann-Whitney t-test \*\*\* p<0.001, ns = non-significant.

Due to the difficulties in detecting MTF1 protein in T/C-28a2 cells by western blot I had planned to conduct further MTF1 western blots by assessing the effect of IL-1 $\alpha$  and/or ZnCl<sub>2</sub> treatment in these cells having overexpressed MTF1 via transfection of the MTF1 plasmid and selected with the antibiotic G418. However, this approach was not possible because the MTF1 plasmid could not be selected in T/C-28a2 cells, as the SV40 large T antigen construct used in the derivation of the T/C-28a2 cell line were already resistant to G418 (Goldring *et al.*, 1994a). Thus, the pGL4.40 luciferase T/C-28a2 overexpressing line was created (chapter 2, section 2.9) in which the cells could be reliably transiently transfected with MTF1 plasmid before treatment for 72 hours and genes of interest measured.

Before the transfected cell line could be used for additional transient transfections with the MTF1 plasmid, overexpression of stably expressed luciferase in the T/C-28a2 cells needed to be addressed. This was achieved by qPCR using two distinct luciferase assays located in the open reading frame of the plasmid (LUC2\_ORF1 and LUC2\_ORF2) and through normalisation against *GAPDH* only (Appendix A). This was to determine whether the NotI-digested linear or circular pGL4.40 plasmid transfections and hygromycin B selection had been successful and which cell line (linear or circular) would be used for transient MTF1 overexpression experiments. *Luciferase* mRNA levels were detected at 1000-fold higher in the NotI-digested linear pGL4.40 luciferase T/C-28a2 line (Figure 5.14A) compared to untransfected T/C-28a2 cells that do not contain the pGL4.40 plasmid and have a background C<sub>t</sub> average of 36.5. *Luciferase* mRNA was observed for the circular pGL4.40 luciferase T/C-28a2 line 500 times higher than the untransfected line but ~2-fold lower than the linear line. Furthermore, *luciferase* detection with assay two gave a 24-fold and 8-fold increase in NotI-digested linear and circularly transfected lines respectively (Figure 5.14B) compared to untransfected T/C-28a2 cells (C<sub>t</sub> average 30.4). The discrepancy in fold changes between these two assays, despite being designed to the same plasmid may be explained by greater variation in the qPCR technical triplicate of assay one which contributed to a 64-fold higher baseline measurement of the untransfected T/C-28a2 cells with assay two compared to assay one. The NotI-digested linear pGL4.40 luciferase T/C-28a2 line and the assay one primers were selected for further experimentation for future qPCR detection of *luciferase*.

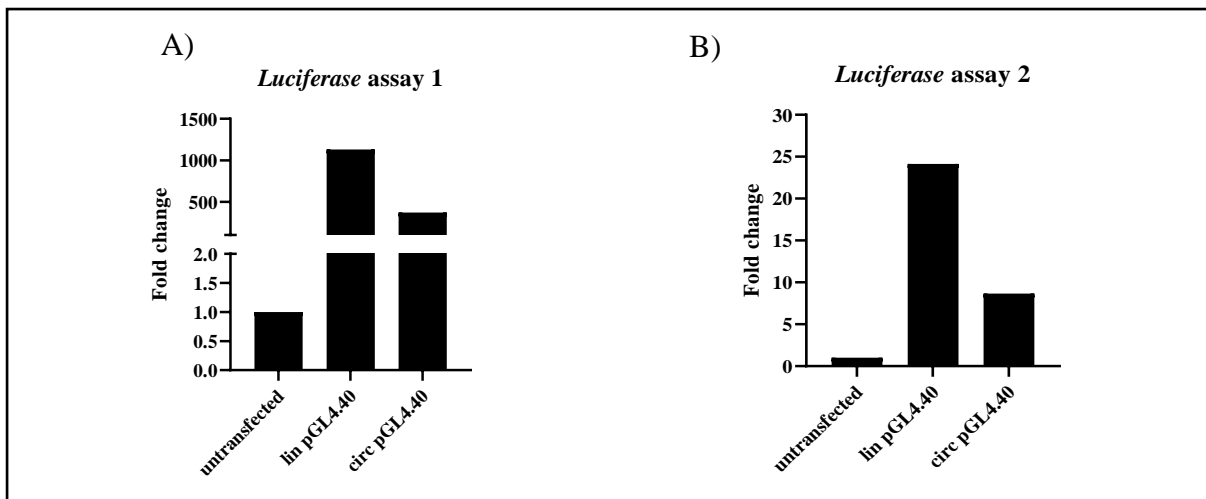


**Figure 5.14– Assessment of *luciferase* gene expression in stably selected NotI-digested linear or circular transfected pGL4.40 *luciferase* overexpressing T/C-28a2 cell line.**

Two qPCR *luciferase* assays (A and B) were utilised to measure *luciferase* gene expression. T/C-28a2 cells were transfected or not with either NotI-digested linear plasmid or native pGL4.40 plasmid for 24 hours. Cells were cultured and expanded progressively from 6 well plates to T25 to T75cm<sup>2</sup> flasks and the transfected cells selected with 50µg/ml hygromycin B until cells were collected after 13 days. Bars represent means of the technical triplicate from the qPCR. Lin = NotI-digested linear plasmid, circ= circular native pGL4.40 plasmid.

Luciferase expressing T/C-28a2 cells were transiently transfected with MTF1 plasmid and after 24 hours, the media replaced ± 0.25ng/ml IL-1α, 100µM ZnCl<sub>2</sub> or 0.25ng/ml IL-1α + 100µM ZnCl<sub>2</sub> for 72 hours. MTF1 transient overexpression was confirmed using the same qPCR primers for *MTF1* as used for expression analysis in HACs (section 4.3.4). These primers amplify both endogenous *MTF1* and that transcribed from the *MTF1* plasmid. In this instance statistics were not possible as only eight flasks rather than 24 were manageable at any one time. This experiment was conducted once towards the end of my PhD. Therefore, the data in Figure 5.15 represents the mean of the technical measurements from the qPCR from a single flask and no statistics could be performed. In pGL4.40 luciferase expressing T/C-28a2 cells, unstimulated *MTF1* levels were increased 1.63-fold in non-stimulated *MTF1* transiently overexpressing cells compared to the unstimulated mock-transfected (lipofectamine2000 only) cells (Figure 5.15, columns one and five). The results suggest that *MTF1* gene expression was inhibited in pGL4.40 luciferase expressing T/C-28a2 cells mock-transfected with lipofectamine2000 and treated with IL-1α (0.64-fold) or IL-1α + ZnCl<sub>2</sub> (0.79-fold) treatment compared to lipofectamine2000 control cells (Figure 5.15). However, transient overexpression of *MTF1* in this cell line after treatment rescued the *MTF1* gene expression, though treatment differences (of any kind) were negligible from control.

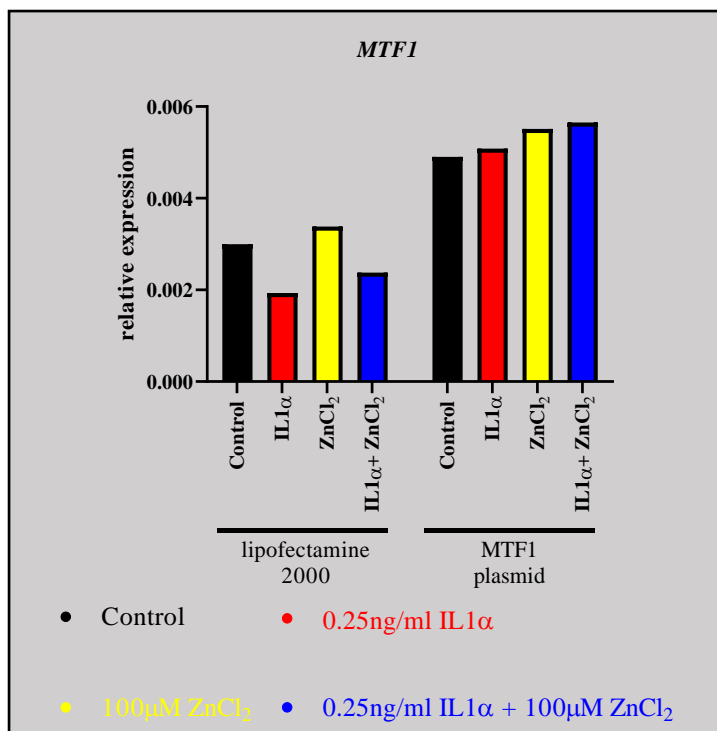


**Figure 5.15- Normalised *MTF1* gene expression in NotI-digested linear pGL4.40 luciferase overexpressing T/C-28a2 cells transiently transfected for 24 hours  $\pm$  MTF1 plasmid then treated  $\pm$  IL-1 $\alpha$  and/or ZnCl $_2$  for 72 hours.**

Cells were treated with IL-1 $\alpha$  (red), ZnCl $_2$  (yellow) or both IL-1 $\alpha$  + ZnCl $_2$  (blue). Data is normalised to housekeepers *18S*, *GAPDH* and *HPRT1*. Each bar represents the average normalised expression of the technical qPCR triplicate.

As the T/C-28a2 luciferase assay data represents the effect of stimuli exposure for 24 hours rather than the 72 hours at which target genes were measured by qPCR, an experiment to test MTF1 activity was devised using the pGL4.40 luciferase T/C-28a2 cell line. These cells were subject to the same stimuli for 72 hours, 24 hours after transient transfection with MTF1 plasmid and the gene expression of *luciferase* measured as an indicator of MTF1 activity. As this experiment required mock transfections with lipofectamine 2000 with or without MTF1 plasmid of multiple flasks, the experiment was conducted just once. Therefore, the data in Figure 5.15 represents the mean of the technical measurements from the qPCR from a single flask and no statistics could be performed. As had previously been observed upon transient transfection of cells with the luciferase construct (Figure 5.13), stimulation with ZnCl $_2$  alone or in combination with IL-1 $\alpha$  increased basal MTF1 activity compared to unstimulated and IL-1 $\alpha$  treated luciferase stable cells (Figure 5.16). Stimulation with ZnCl $_2$  also increased MTF1 activity in cells that transiently overexpressed MTF1 compared to unstimulated MTF1 overexpressing cells. Although transient transfection of MTF1 plasmid into luciferase overexpressing T/C-28a2 cells, increased overall *MTF1* transcript levels independently of stimulation (Figure 5.15), this was not accompanied by changes in MTF1 activity across any of the treatments (Figure 5.16) in this single experiment.

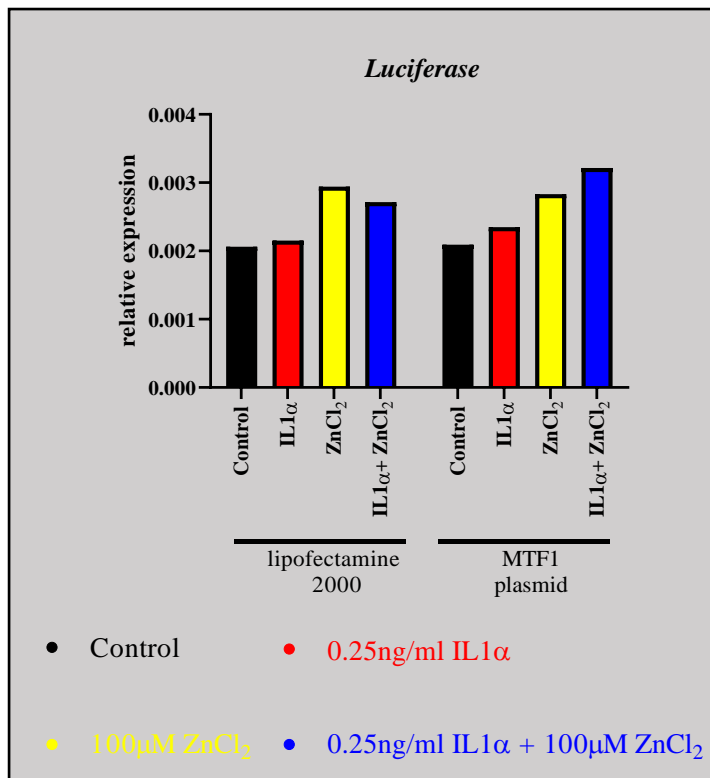


**Figure 5.16– Normalised *Luciferase* gene expression in NotI-digested linear pGL4.40 luciferase T/C-28a2 cells transiently transfected for 24 hours  $\pm$  MTF1 plasmid then treated  $\pm$  IL-1 $\alpha$  alone and/or ZnCl $_2$  for 72 hours.** pGL4.40 luciferase T/C-28a2 cells were transfected with or without MTF1 plasmid for 24 hours before treatment with IL-1 $\alpha$  (red), ZnCl $_2$  (yellow) or IL-1 $\alpha$  + ZnCl $_2$  (blue) for 72 hours. Data is normalised to housekeepers *18S*, *GAPDH* and *HPRT1*. Each bar represents the average normalised expression of the technical qPCR triplicate.

### 5.3.8 Does IL-1 $\alpha$ upregulate metallothionein gene expression in T/C-28a2 cells?

*MT1A* and *MT1G* were next studied to investigate if IL-1 $\alpha$  induced *MT* expression which would be indirect evidence for increased MTF1 activity and is a potential mechanism to buffer against potential alterations to intracellular zinc ion concentrations. The selection of *MT1A* and *MT1G* from the eight *MT* genes qPCR assays that had been designed against was based on Rushton *et al.*, 2015 work identifying these genes alongside inflammatory genes as highly expressed in a subcluster of OA hip cartilage patients with differential patterns in DNA methylation. This decision was representative for the *MT* expression change elicited by IL-1 $\alpha$  in HACs (4.3.6). These two genes were also measured in SW1353 cells in the next chapter. 0.25ng/ml IL-1 $\alpha$  treatment of T/C-28a2 cells for 72 hours resulted in *MT1A* (3.9-fold,  $p < 0.0001$ ) but not *MT1G* upregulation (1.7-fold,  $p = 0.0076$ ) in Figures 5.17A and B. Each symbol in the dot plots is an individual biological replicate for control or IL-1 $\alpha$ -treated flasks for six experiments. A summary heatmap for the fold changes averaged over the biological replicates from each of six experiments is presented in Figure 5.17C.

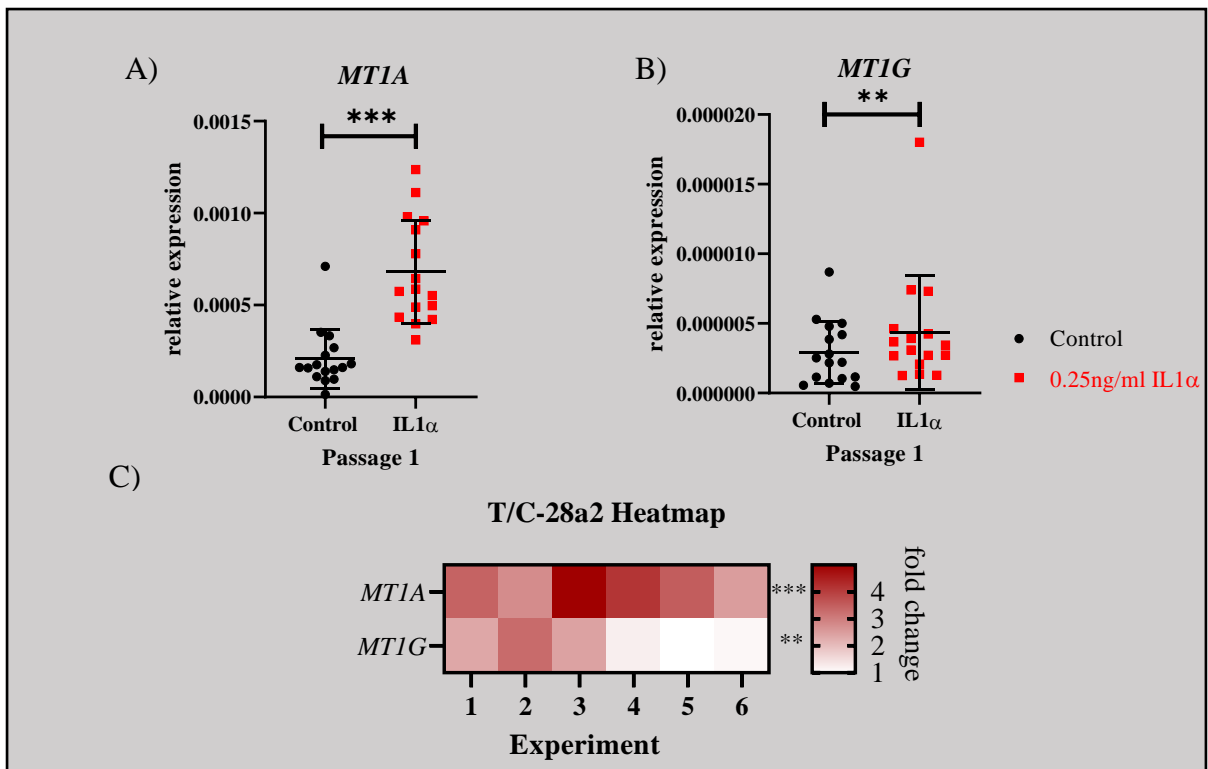


**Figure 5.17 – *MTIA* and *MTIG* are significantly upregulated by IL-1 $\alpha$  in T/C-28a2 cells after a 72 hour passage.**

The relative gene expression changes for *MTIA* A) and *MTIG* B) are normalised to housekeeper genes *18S*, *GAPDH* and *HPRT1* after 72 hours of treatment with 0.25ng/ml IL-1 $\alpha$ . Heatmap summarising IL-1 $\alpha$ -mediated *MT* gene expression fold changes relative to controls after 72 hours C). Red indicates differential fold change upregulation by IL-1 $\alpha$ , and white represents no change with IL-1 $\alpha$ . Symbols represent the mean of three qPCR technical replicates for each flask from every biological replicate for six experiments. Horizontal lines are the group mean and error bars are the standard deviation. *MTIA* and *MTIG* were analysed by Wilcoxon and paired t-tests respectively \*\* p<0.01, \*\*\* p <0.0001.

The T/C-28a2 time course with IL-1 $\alpha$  was carried out in two experiments and cDNA was made from 3-5 biological replicates per condition per time point. Only *MTIA* was significantly upregulated (2.5-fold p<0.0001) after 96 hours of IL-1 $\alpha$  treatment but no difference between control and treatment was observed for *MTIG* (Figure 5.18A and B). The fold changes of IL-1 $\alpha$  compared to control summarised for both experiments at each passage is presented in the heatmap in Figure 5.18C. Next, an experiment was conducted to compare ZnCl<sub>2</sub> with IL-1 $\alpha$ -mediated *MT* responses as a positive control for *MT* induction. While there was an observed upregulation with ZnCl<sub>2</sub>, statistical comparison for this treatment could not be performed because one biological replicate in the triplicate condition became infected. IL-1 $\alpha$  treatment with or without ZnCl<sub>2</sub> resulted in significant *MTIA* upregulation at 72 hours (6.1-fold p=0.0474, 3.7-fold p=0.015 respectively) but only *MTIG* was significant (16.7-fold p=0.012) after combined treatment, suggesting ZnCl<sub>2</sub> drives this *MTs* gene expression specifically (Figure 5.18D and E).

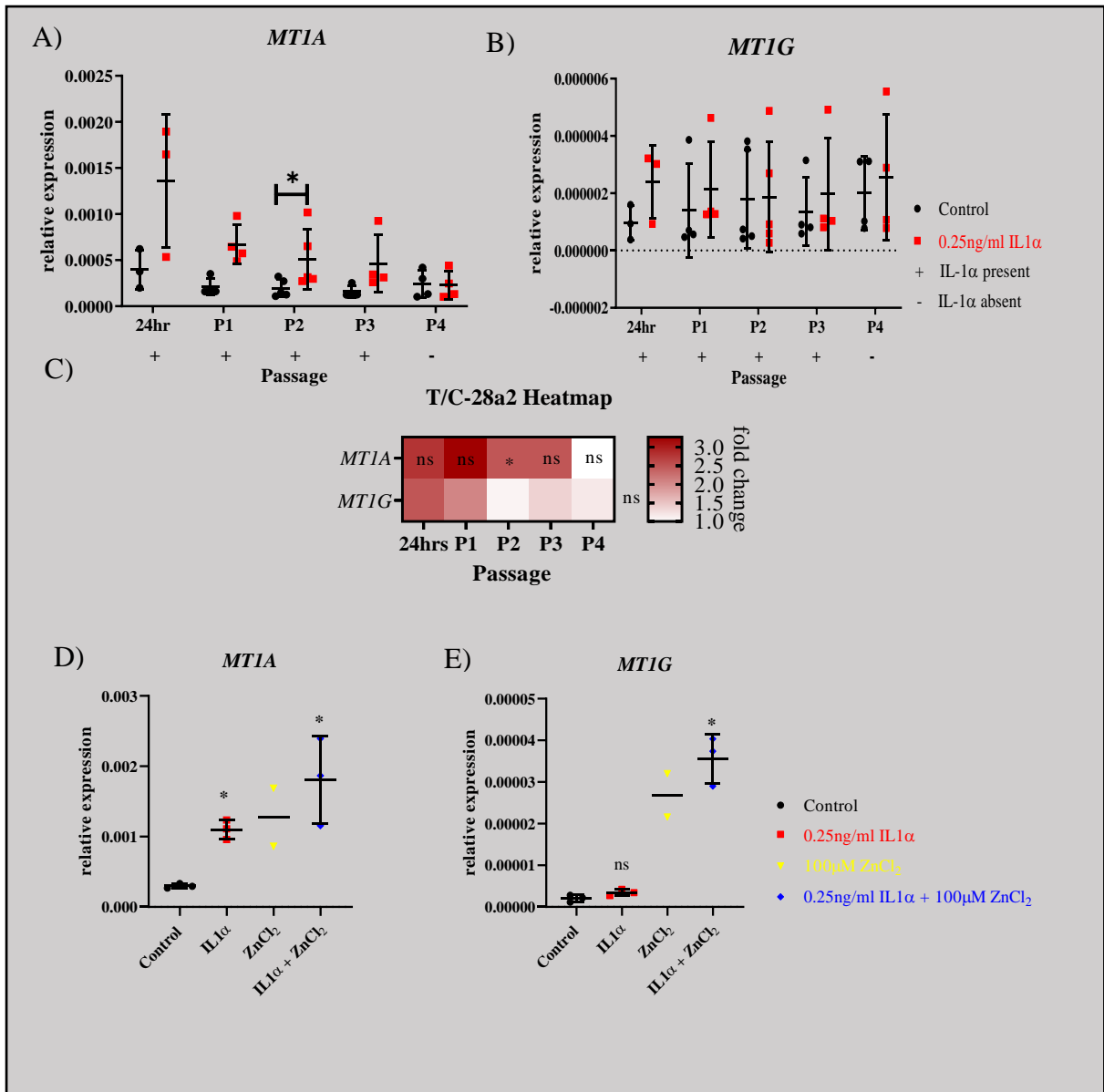


**Figure 5.18 – *MTIA* was significantly upregulated by IL-1 $\alpha$  at multiple timepoints or not at all for *MTIG* and effects of ZnCl<sub>2</sub> treatment alone were undetermined.**

Relative gene expression of *MTIA* A) and *MTIG* B) genes normalised to housekeeper genes *18S*, *GAPDH* and *HPRT1*. Heatmap summarising IL-1 $\alpha$ -mediated *MT* gene expression fold changes relative to controls after three passages with IL-1 $\alpha$  present and one passage without IL-1 $\alpha$  C). Red indicates differential fold change upregulation with IL-1 $\alpha$ , and white represents no change with IL-1 $\alpha$ . Relative gene expression of *MTIA* D) and *MTIG* E) genes following IL- $\alpha$ , ZnCl<sub>2</sub> or both IL-1 $\alpha$  + ZnCl<sub>2</sub> treatments of T/C-28a2 cells in biological triplicate for 72 hours. Symbols represent mean of three qPCR technical replicates for each flask from every biological replicate across one (D and E) or two experiments (A, B and C). Horizontal lines are the group mean and error bars are standard deviation. Normalised data satisfying a Shapiro Wilk normality test prior to or after log<sub>2</sub> transformation was analysed with a paired t-test, otherwise a Wilcoxon t-test was used. Normalised data in D) and E) was analysed by paired t-test ns = non-significant \* p < 0.05.

### 5.3.9 Does cartilage matrix-degrading gene expression change in response to IL-1 $\alpha$ and/or ZnCl<sub>2</sub> stimulation in T/C-28a2 cells?

The effect of IL-1 $\alpha$  on cartilage matrix-degrading gene expression in T/C-28a2 cells was assessed next and in a later experiment ZnCl<sub>2</sub> was used alongside IL-1 $\alpha$  as a positive control testing activation of the zinc-ZIP8-MTF1 axis. *ADAM-TS5* and *MMP13* were both significantly upregulated 1.8 (p=0.0002) and 2.5-fold (p<0.0001) respectively after IL-1 $\alpha$  treatment for 72 hours (Figure 5.19A and B). Figure 5.19C is a heatmap highlighting the interexperimental differences in *ADAM-TS5* and *MMP13* fold change after IL-1 $\alpha$ . Only *ADAM-TS5* expression was maintained at 1.8-fold beyond 72 hours until 96 hours (Figure 5.20A-C). The effect of ZnCl<sub>2</sub> treatment could not be properly ascertained (Figure 5.20D and E).

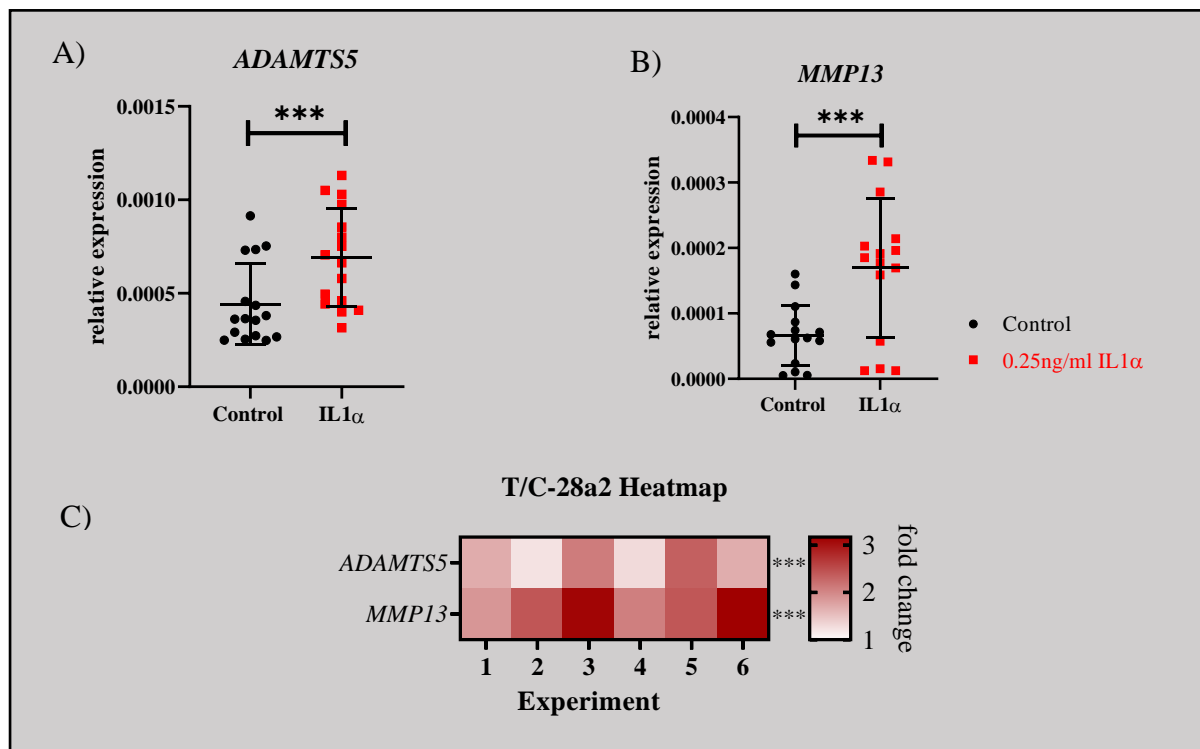


**Figure 5.19 – *ADAM-TS5* and *MMP13* are significantly upregulated by IL-1 $\alpha$  in T/C-28a2 cells after a 72 hour passage.**

The relative gene expression changes for *ADAM-TS5* A) and *MMP13* B) normalised to housekeeper genes *18S*, *GAPDH* and *HPRT1* after 72 hours of treatment with 0.25ng/ml IL-1 $\alpha$ . Heatmap summarising IL-1 $\alpha$ -mediated matrix-degrading enzymes gene expression fold changes relative to controls after 72 hours C). Red indicates differential fold change upregulation with IL-1 $\alpha$ , and white represents no change with IL-1 $\alpha$ . Symbols represent the mean of three qPCR technical replicates for each flask from every biological replicate for six experiments. Horizontal lines are the group mean and error bars are the standard deviation. Normalised data satisfying a D’Agostino-Pearson omnibus k2 normality test prior to or after log<sub>2</sub> transformation was analysed with a paired t-test, \*\*\* p <0.0001.

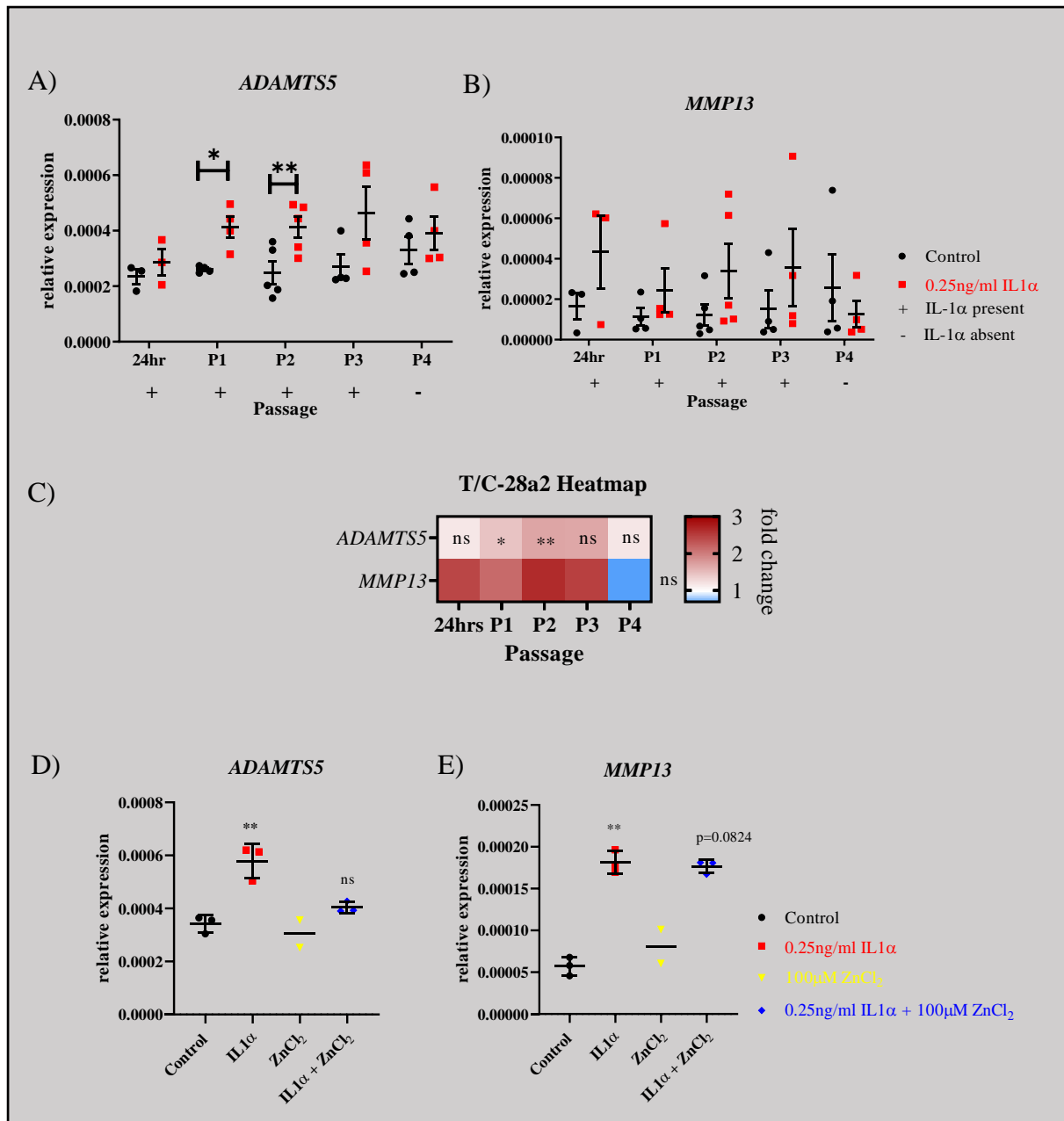


**Figure 5.20 – ADAM-TS5 was significantly upregulated by IL-1α at multiple timepoints of a time course experiment or not at all for MMP13. Effects of ZnCl<sub>2</sub> treatment alone were undetermined.**

Relative gene expression of ADAM-TS5 A) and MMP13 B) normalised to housekeeper genes *18S*, *GAPDH* and *HPRT1*. Heatmap summarising IL-1α-mediated *MT* gene expression fold changes relative to controls after three passages with IL-1α present and one passage without IL-1α C). Red indicates differential fold change upregulation with IL-1α, white represents no change and blue is downregulation with IL-1α. Relative gene expression of ADAM-TS5 D) and MMP13 E) genes from IL-α, ZnCl<sub>2</sub> or both IL-1α + ZnCl<sub>2</sub> treatments of T/C-28a2 cells in biological triplicate for 72 hours. Symbols represent mean of three qPCR technical replicates for each flask from every biological replicate across one (D and E) or two experiments (A, B and C). Horizontal lines are the group mean and error bars are standard deviation. Normalised data satisfying a Shapiro Wilk normality test prior to or after log<sub>2</sub> transformation was analysed with a paired t-test, otherwise a Wilcoxon t-test was used, \* p<0.05 \*\* p<0.01. ns = non-significant.

## 5.4 Chapter summary

There is no evidence that the zinc-ZIP8-MTF1 axis is active in T/C-28a2 cells. IL-1 $\alpha$  stimulates cartilage matrix-degrading gene expression in T/C-28a2 cells, which can occur independently of proteins associated with the zinc-ZIP8-MTF1 axis and although statistical comparison between ZnCl<sub>2</sub> and control was not possible due to the loss of a biological sample due to contamination, ZnCl<sub>2</sub> was clearly not as effective as IL-1 $\alpha$  in upregulating matrix-degrading genes. A summary schematic for the zinc-ZIP8-MTF1 axis activity in T/C-28a2 cells is presented in Figure 5.21. As no direct assessment of MTF1 dependence on the IL-1-mediated expression of cartilage matrix-degrading genes was performed, the relationship between them remains undetermined. The dependency of MTF1 in IL-1 $\alpha$ -stimulated cartilage matrix-degrading gene expression needed to be addressed using siRNA against *MTF1* or against *SLC39A14* to definitively implicate zinc-ZIP8-MTF1 axis involvement.

Does <i>SLC39A8</i> gene expression, encoding ZIP8 zinc transporter, increase?	Does IL-1 $\alpha$ treatment lead to an increase in intracellular zinc accumulation?	Does the zinc-sensing transcription factor <i>MTF1</i> alter its transcription in response to altered intracellular zinc status?	Do genes encoding cartilage-degrading proteases <i>MMP13</i> and <i>ADAM-TS5</i> increase after IL-1 $\alpha$ in T/C-28a2 cells?	Do metallothionein genes increase after IL-1 $\alpha$ in T/C-28a2 cells?
				
<i>SLC39A13</i> and <i>14</i> not <i>SLC39A8</i>				<i>MT1A</i> not <i>MT1G</i>

**Figure 5.21- Summary of zinc-ZIP8-MTF1 axis exploration in T/C-28a2 cells.**

## Chapter 6: INVESTIGATING THE ZINC-ZIP8-MTF1 AXIS IN SW1353 CHONDROCYTES

### 6.1 Introduction

Despite a role for IL-1 $\alpha$ -mediated *ADAM-TS5* and *MMP13* gene upregulation in T/C-28a2 cells and selective upregulation of *SLC39A14* (and not *SLC39A8*), there was no evidence of intracellular zinc accumulation by any mechanism nor changes to *MTF1* gene expression in T/C-28a2 cells. In addition, MTF1 went undetected by western blot, meaning any association of MTF1 (and hence zinc-ZIP8-MTF1 axis) to the observed upregulation of genes encoding cartilage matrix-degrading enzymes (*ADAM-TS5* and *MMP13*) in T/C-28a2 cells was unattributable. Therefore, the SW1353 cell line was acquired to address the same questions pertaining to IL-1 $\alpha$ -mediated zinc-ZIP8-MTF1 activation that was not entirely achieved in the T/C-28a2 cell investigation.

SW1353 cells are a chondrosarcoma cancer derived from a 72-year-old primary bone cancer of the humerus. The SW1353 cell line has historically been used in conjunction with primary HACs not only for their preferential proliferative capacity but because of metalloproteinase (*MMP1*, *MMP3* and *MMP13*) transcriptomic overlap with HACs after IL-1 treatment (Gebauer *et al.*, 2005). Furthermore, SW1353 cells were used to address MTF1 overexpression which was not possible in either HACs or T/C-28a2 cells and the overexpression lines generated were characterised for MTF1 activity and localisation. On this basis, and from complementary evidence from murine chondrocytes and cartilage that the zinc-ZIP8-MTF1 axis induces cartilage matrix-degrading enzyme activity, the following chapter aims were addressed.

## 6.2 Aims

This chapter aims to address the consequence of IL-1 $\alpha$  stimulation on the expression of zinc homeostasis genes and subsequent impact on cartilage matrix-degrading gene expression in SW1353 cells. This was achieved with the following experimental objectives:

- Determine if IL-1 $\alpha$  and IL-1 $\beta$  elicit the same response as T/C-28a2 cells and HACs by quantifying the expression of IL-1 positive control genes (*IL-6*, *CXCL8* and *CCL2*) and selected zinc transporters.
- Investigate if IL-1 and/or ZnCl<sub>2</sub> treatment for one or more passages activates the zinc-ZIP8-MTF1 axis described in mouse chondrocytes, specifically examining:
  - Zinc transporters' gene expression
  - Intracellular and extracellular zinc levels
  - *MTF1* gene expression, localisation and activity
  - *MTs* expression
  - Cartilage matrix-degrading gene expression

### 6.3.1 Do *IL-1α* and *IL-1β* stimulate the same gene expression changes in SW1353 cells?

The first investigation conducted with the SW1353 cells was akin to the comparisons made in HACs (4.3.1) and T/C-28a2 cells (5.3.2), whereby *IL-1α* and *IL-1β* were considered in parallel for gene expression responses. One experiment was conducted comparing SW1353 cells treated for 72 hours with 0.5ng/ml *IL-1α* or 5ng/ml *IL-1β* and the genes *IL-6*, *CXCL8* and *CCL2*, were quantified by qPCR (Figure 6.1A-C), the concentration differences reflecting the differences in *IL-1R1* affinity for each ligand. All three genes were upregulated by *IL-1α*, 92, 127 and 89-fold compared to control respectively. All three genes were also upregulated by *IL-1β*, by 261, 269 and 128-fold compared to control respectively. The mean housekeeper expression for one of the untreated biological controls differed by greater than one unit from the other two biologicals, so no statistics comparing untreated control with *IL-1* cytokines could be performed. Comparison of the *IL-1α* and *IL-1β* responses by paired t-test highlighted differences in inflammation-associated gene expression response (Figure 6.1). However, *IL-1α* was selected as the cytokine to test zinc homeostasis in the wider family of zinc transporters and MTs, consistent with investigations in previous chapters.

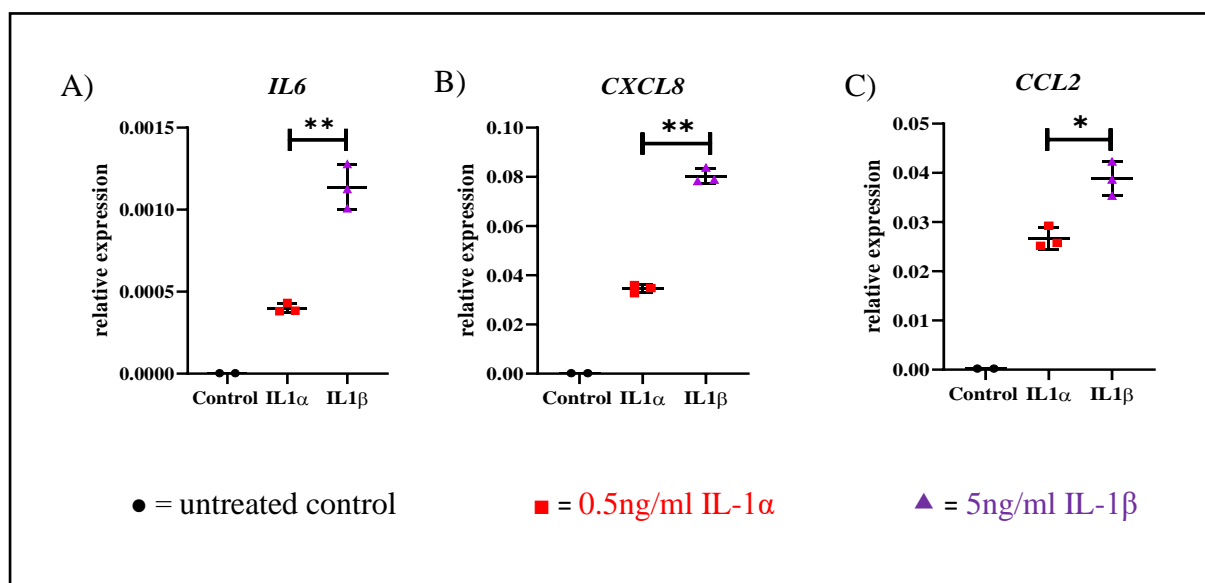


**Figure 6.1 – Normalised *IL-6*, *CXCL8*, *CCL2* gene expression responses in SW1353 cells treated ± *IL-1α* or *IL-1β*.**

Four hours after seeding, SW1353 cells were treated with or without 0.5ng/ml *IL-1α* or 5ng/ml *IL-1β* for one passage (72 hours) and the genes *IL-6* A), *CXCL8* B) and *CCL2* C) quantified by qPCR. Data is normalised to housekeepers *18S*, *GAPDH* and *HPRT1*. Statistic is paired t-test comparing *IL-1α* treatment against *IL-1β*. Symbols represent the mean of three qPCR technical replicates for each of the three flasks per condition and error bars are the standard deviation. Horizontal lines are the group mean. \*  $p < 0.05$  \*\*  $p < 0.01$

### **6.3.2 Are zinc homeostasis genes upregulated in SW1353 cells after stimulation with or without IL-1 $\alpha$ and/or ZnCl $_2$ treatment?**

To understand how zinc transporter gene expression was regulated by IL-1 $\alpha$  long-term, SW1353 cells were exposed to IL-1 $\alpha$  for between 24 and 216 hours. The experiments in which SW1353 cells were treated with or without IL-1 $\alpha$  for one passage (72 hours) were repeated three times in total by myself. In addition, four additional cDNA samples per condition were also available for analysis for the 72 hour time point from a time course experiment performed in duplicate by Dr Louise Reynard. In this time course experiment, SW1353 cells were exposed to IL-1 $\alpha$  for 216 hours across three consecutive 72 hour passages before its removal for the final fourth 72 hour passage. In a single experiment the SW1353 cells were treated in biological duplicate with or without 0.5ng/ml IL-1 $\alpha$ , 100 $\mu$ M ZnCl $_2$  or both 0.5ng/ml IL-1 $\alpha$  + 100 $\mu$ M ZnCl $_2$  for 72 hours.

#### **6.3.2.1 SLC39A8 and SLC39A14 are upregulated after one passage with IL-1 $\alpha$**

After confirming that IL-1 $\alpha$  responsive positive control genes are upregulated in SW1353 cells after IL-1 $\alpha$  treatment, the zinc transporters were assessed in SW1353 cells treated for one passage lasting 72 hours with 0.5ng/ml IL-1 $\alpha$ . A total of five experiments and cDNA from 12 flasks per condition (untreated and IL-1 $\alpha$ -treated) for a 72 hour passage was analysed and cDNA synthesised by Dr. Louise Reynard in the dot plots have solid borders. Using RNA-Seq data from Table 3.9 (Chapter three) the human zinc transporters expressed in cartilage were determined using a TPM threshold >4. Transporters absent from Figure 6.2C were not expressed in OA cartilage. The genes that were most significantly upregulated after 72 hours were *SLC39A8* (2-fold,  $p < 0.0001$ ) and *SLC39A14* (3.1-fold,  $p < 0.0001$ ) respectively (Figure 6.2A and B) with *SLC39A6* (1.2-fold,  $p = 0.0268$ ), *7* (1.2-fold,  $p = 0.0152$ ), *10* (0.8-fold,  $p = 0.0202$ ) and *SLC30A7* (1.2-fold,  $p = 0.075$ ) also significantly different after IL-1 $\alpha$  treatment (Appendix F). Only *SLC39A8* and *SLC39A14* were investigated beyond experiments one and two because they were the only prominently upregulated genes after 72 hours (Figure 6.2C). In the experiment comparing cytokine treatments against untreated control on SW1353 for 72 hours, IL-1 $\alpha$  and IL-1 $\beta$  upregulated *SLC39A8* 1.8 and 2.8-fold respectively (Figure 6.2D). *SLC39A14* was upregulated by IL-1 $\alpha$  and IL-1 $\beta$  3.2 and 4.7-fold respectively (Figure 6.2E) and neither *SLC39A8* nor *SLC39A14* was significantly different from each other for either IL-1 ligand.

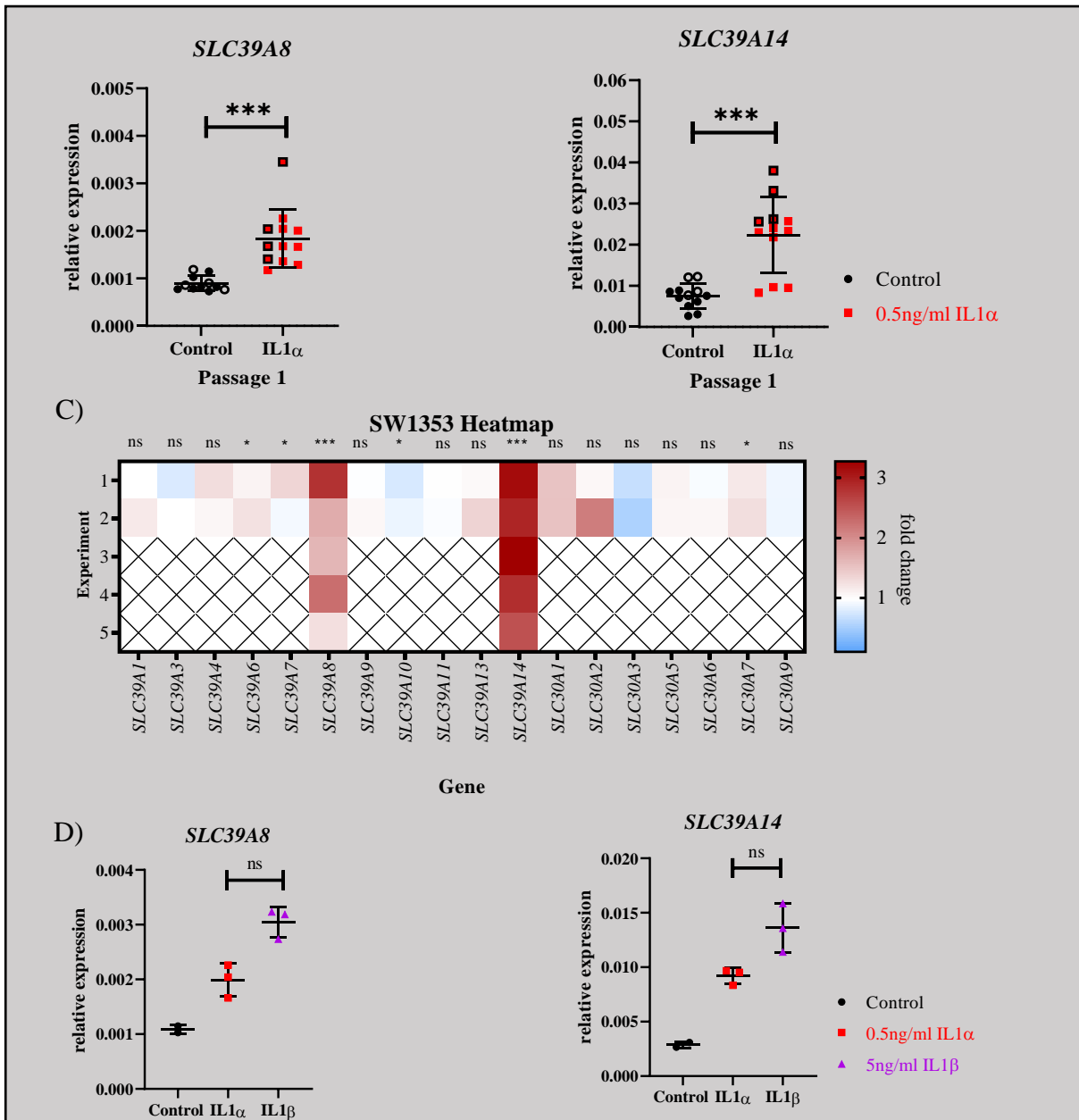


**Figure 6.2 – *SLC39A8* and *SLC39A14* are among the most significantly upregulated zinc transporters after IL-1 $\alpha$  in SW1353 cells after 72 hours in five experiments.**

Relative gene expression of *SLC39A8* A) and *SLC39A14* B) is normalised to housekeeper genes *18S*, *GAPDH* and *HPRT1*. Heatmap summarising IL-1 $\alpha$ -mediated zinc transporter gene expression fold changes relative to controls after one passage lasting 72 hours C). Red indicates differential fold change upregulation with IL-1 $\alpha$ , and blue represents differentially downregulated fold change with IL-1 $\alpha$ . Genes marked with a cross were not measured in these samples. Relative gene expression of *SLC39A8* D) and *SLC39A14* E) of IL-1 $\alpha$  or IL-1 $\beta$ -treated SW1353 cells treated in biological triplicate for 72 hours. Symbols represent mean of three qPCR technical replicates for each flask from every biological replicate across one (D and E) or five (A, B and C) experiments. Unfilled circular dots and solid-bordered square symbols (A and B) are Dr Reynard's cDNA samples. Horizontal lines are the group mean and error bars are standard deviation. Data satisfying either a D'Agostino-Pearson omnibus k2 (*SLC39A8* and *SLC39A14*) or a Shapiro Wilk normality test prior to or after log<sub>2</sub> transformation was analysed with a paired t-test. \* p<0.05 \*\*\* p<0.001, ns = non-significant p >0.05.

Two experiments totalling four biological replicates per treatment per time point in which all zinc transporters were assessed after IL-1 $\alpha$  exposure for 24, 72 (P1), 144 (P2) and 216 (P3) hours and its removal from SW1353 cells for a final 72 hour passage (288 hour, P4) were conducted. *SLC39A8* and *SLC39A14* gene expression was elevated after IL-1 $\alpha$  treatment after 72 hours (2.3-fold, p = 0.0494; 3.1-fold, p = 0.0017 respectively). Additionally, *SLC39A8* was significantly upregulated after 216 hours (1.9-fold, p = 0.0453) (Figure 6.3A-C). ZnCl<sub>2</sub> treatment alone or in the presence of IL-1 $\alpha$  did not influence *SLC39A8* or *SLC39A14* gene expression after 72 hours and the regulation of these genes in the combined treatment was driven solely by IL-1 $\alpha$  (Figure 6.3D and E). This was logical given that ZnCl<sub>2</sub> has not previously been described by Kim and colleagues as a positive feedback regulator of zinc importer gene expression. The fold changes of all genes measured in flasks treated with 0.5ng/ml IL-1 $\alpha$  for 72 hours is presented in appendix F and the equivalent relative gene expression graphs for all transporters are in Figures 6.4-6.7.

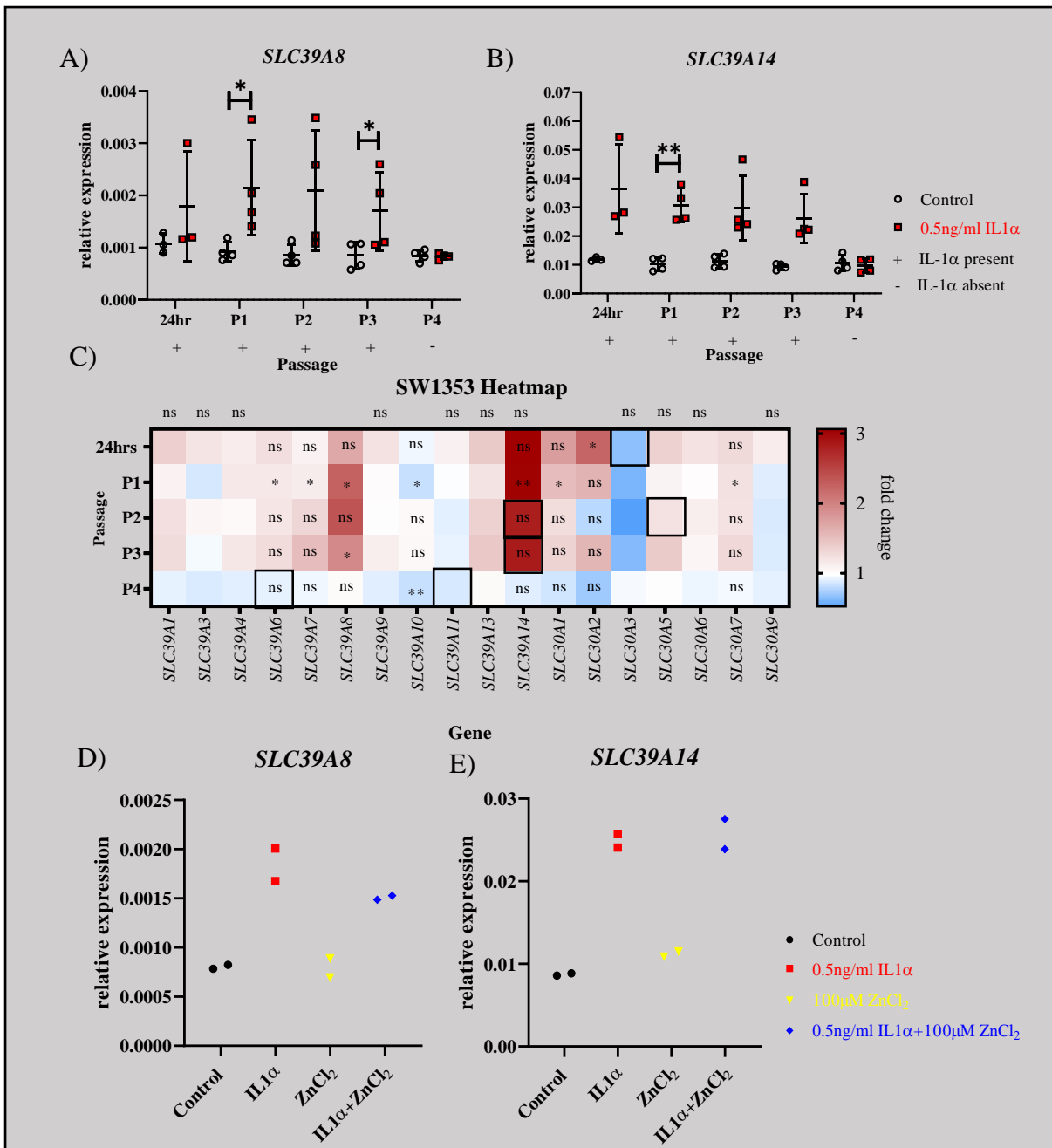


**Figure 6.3 – *SLC39A8*, not *SLC39A14* expression was not sustained beyond P1 by IL-1α in SW1353 time course and ZnCl<sub>2</sub> does not influence *SLC39A8* or *SLC39A14* expression.** Relative gene expression of *SLC39A8* A) and *SLC39A14* B) is normalised to housekeeper genes *18S*, *GAPDH* and *HPRT1*. Heatmap summarising IL-1α-mediated zinc transporter gene expression fold changes relative to controls after three passages with IL-1α present and one passage without IL-1α C). Red indicates differential fold change upregulation with IL-1α, and blue represents differentially downregulated fold change with IL-1α. and are Relative gene expression of *SLC39A8* D) and *SLC39A14* E) from IL-α, ZnCl<sub>2</sub> or both treatments of SW1353 cells treated in biological duplicate for 72 hours. Symbols represent mean of three qPCR technical replicates for each flask per condition from every biological replicate across one (D and E) or two experiments (A, B and C). Horizontal lines are the group mean and error bars are standard deviation. Normalised data satisfying a Shapiro Wilk normality test prior to or after log<sub>2</sub> transformation was analysed with a paired t-test, otherwise a Wilcoxon t-test was used (highlighted squares in C), \* p<0.05 \*\* p<0.01 ns = non-significant p >0.05.

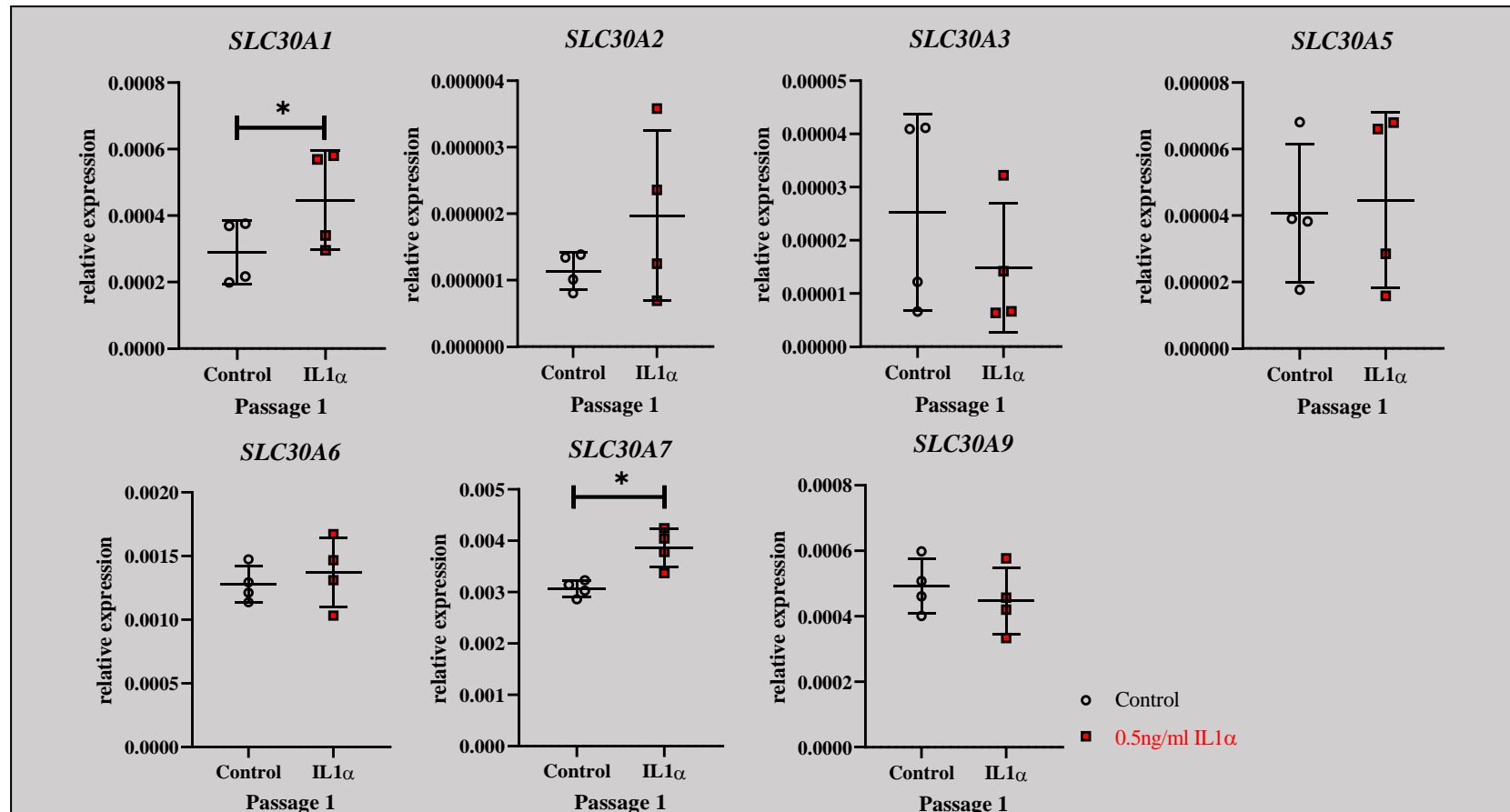


**Figure 6.4 - Zinc exporter gene expression in SW1353 cells treated  $\pm$  IL-1 $\alpha$  for 72 hours.**

Zinc exporters were all initially assessed in cDNA from SW1353 cell experiments where 0.5ng/ml IL-1 $\alpha$  exposure was maintained for 24, 72, 144, and 216 hours and its removal for cell recovery for a further 72 hours totalling 288 hours of culture. Only the 72 hour data is presented and data satisfying a Shapiro Wilk normality test prior to or after log<sub>2</sub> transformation was analysed with a paired t-test. Symbols represent the mean of three qPCR technical replicates for each flask per condition from two experiments and the relative expression normalised to housekeepers *18S*, *GAPDH* and *HPRT1*. Horizontal lines are the group mean and error bars are the standard deviation. \* p<0.05

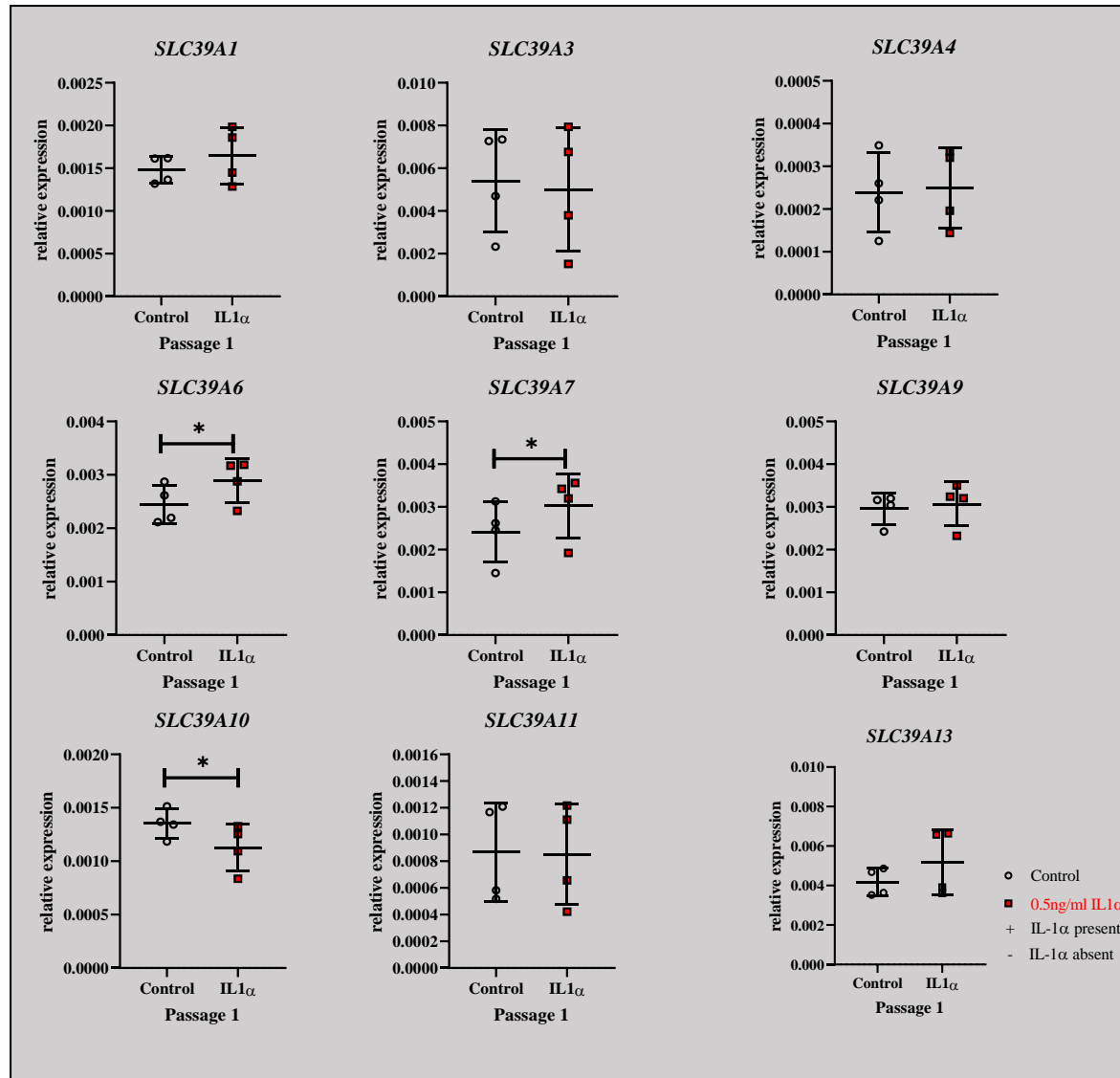


**Figure 6.5- Zinc importer gene expression in SW1353 cells treated  $\pm$  IL-1 $\alpha$  for 72 hours.**

Zinc importers were all initially assessed in cDNA from preliminary SW1353 cell experiments where 0.5ng/ml IL-1 $\alpha$  exposure was maintained for 24, 72, 144, and 216 hours and its removal for cell recovery for a further 72 hours totalling 288 hours of culture. Only the 72 hour data is and data satisfying a Shapiro Wilk normality test prior to or after log2 transformation was analysed with a paired t-test. Symbols represent the mean of three qPCR technical replicates for every flask per condition from two experiments and the mean relative expression normalised to housekeepers *18S*, *GAPDH*, *HPRT1*. Horizontal lines are the group mean and the error bars are the standard deviation. \* p<0.05

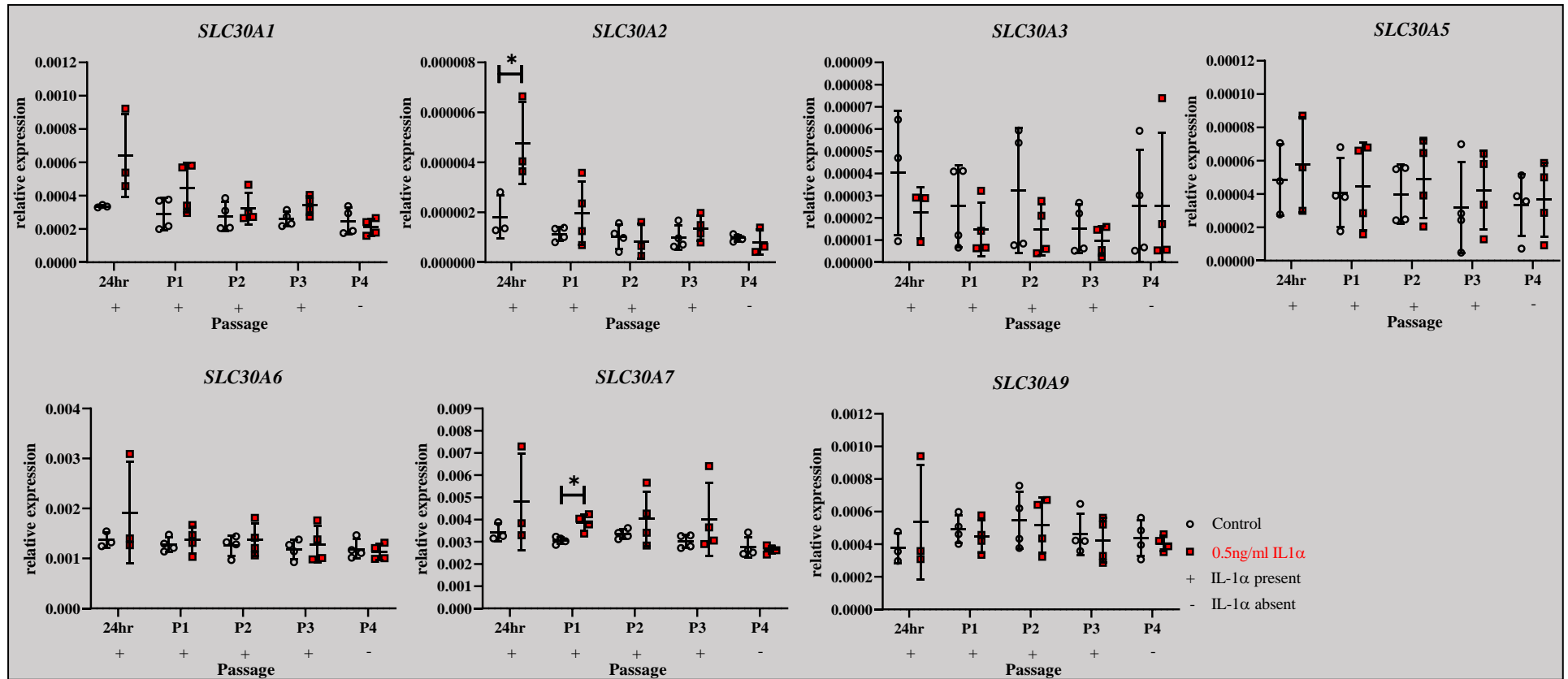


**Figure 6.6 - Zinc exporter gene expression in SW1353 cells treated  $\pm$  IL-1 $\alpha$  for consecutive passages up to 216 hours (P3) and cell recovery for 72 hours (P4).**

P1 data presented here is the same as Figure 6.4 but with the added context of the remaining passages of the time course for the two experiments. The experiment was repeated with two biological replicates per condition per passage, except for 24 hours, totalling 38 samples. Normalised data satisfying a Shapiro Wilk normality test prior to or after log<sub>2</sub> transformation was analysed with a paired t-test. Where the data was not normal a Wilcoxon t-test of the normalised data was conducted (24hr – *SLC30A3*, P2 – *SLC30A5*). Symbols represent mean of three qPCR technical replicates for every flask from two experiments and the mean relative expression normalised to housekeepers *18S*, *GAPDH* and *HPRT1*. Horizontal lines are the group mean and error bars are the standard deviation. \* p<0.05

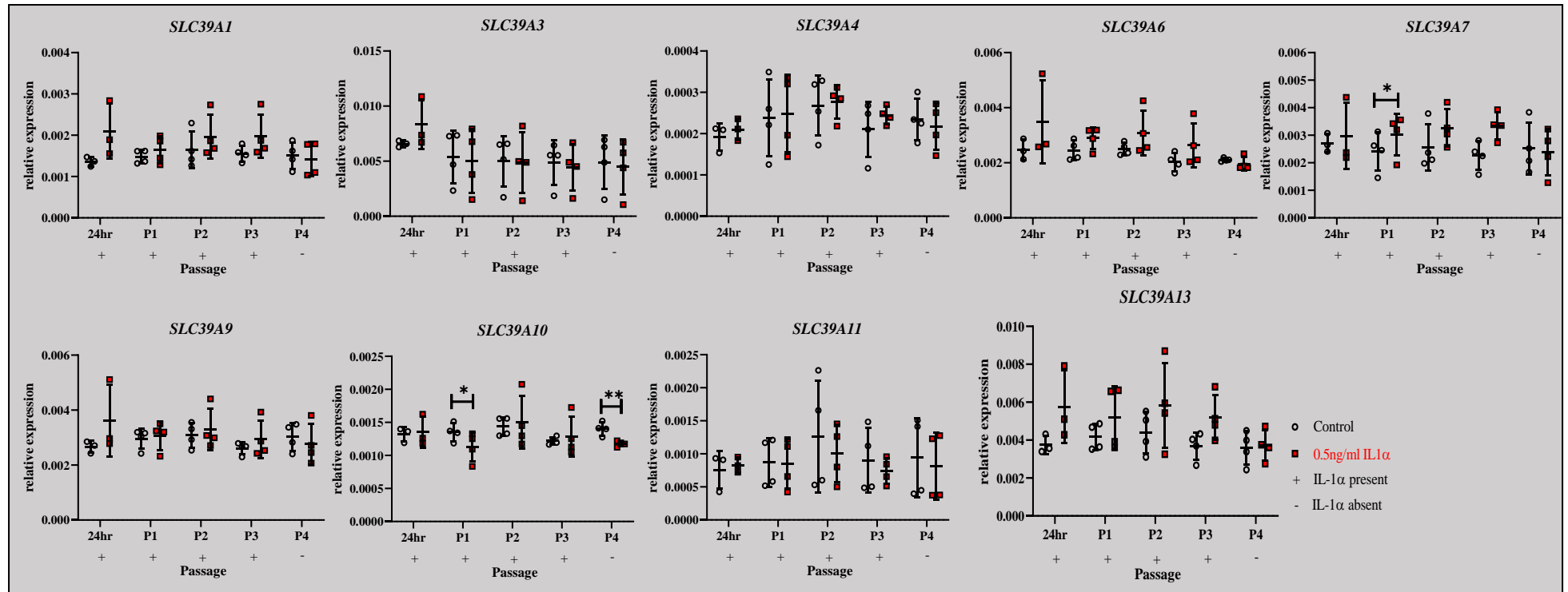


**Figure 6.7 - Zinc importer gene expression in SW1353 cells treated  $\pm$  IL-1 $\alpha$  for consecutive passages up to 216 hours (P3) and cell recovery for 72 hours (P4).**

P1 data presented here is the same as Figure 6.5 but with the added context of the remaining passages of the time course for the two experiments. The experiment was repeated with two biological replicates per condition per passage, except for 24 hours, totalling 38 samples. Normalised data satisfying a Shapiro Wilk normality test prior to or after log<sub>2</sub> transformation was analysed with a paired t-test. Where the data was not normal a Wilcoxon t-test of the normalised data was conducted (P4 – *SLC39A6* and *SLC39A11*). Symbols represent mean of three qPCR technical replicates for every flask from two experiments and the mean relative expression normalised to housekeepers *18S*, *GAPDH* and *HPRT1*. The zinc exporters' gene expression for samples from IL-1 $\alpha$ -treated flasks were not significantly different from control at any passage in the time course  $p > 0.05$ . Horizontal lines are the group mean and error bars are the standard deviation. \*  $p < 0.05$

### 6.3.3 What effect does IL-1 $\alpha$ treatment have on SW1353 intracellular and extracellular zinc levels?

As mRNA expression of *SLC39A8* and *SLC30A14*, encoding the zinc importer proteins ZIP8 and ZIP14 respectively, were upregulated after 72 hours exposure to IL-1 $\alpha$  in SW1353 cells, I next wanted to see if this was accompanied by changes in intracellular zinc levels. The MAK032 kit was used to measure the metal ion concentration intracellularly or in spent medium of the SW1353 cells treated with or without 0.5ng/ml IL-1 $\alpha$  for 72 hours. As demonstrated in 4.3.3.1, this kit detects both zinc and iron ions and so any changes seen in levels after IL-1 $\alpha$  treatment may be due to zinc and/or iron. The zinc and iron metal ion concentration in cells or spent medium was not significantly altered by 72 hours of 0.5ng/ml IL-1 $\alpha$  exposure (Figure 6.8). The standard deviation within groups (control and IL-1 $\alpha$ ) was greater in the cell pellets than the spent medium. The concentrations measured in spent medium samples reflected the zinc sulfate concentration (1.5 $\mu$ M) supplemented in DMEM F-12 medium (Fischer Scientific, 11320074).

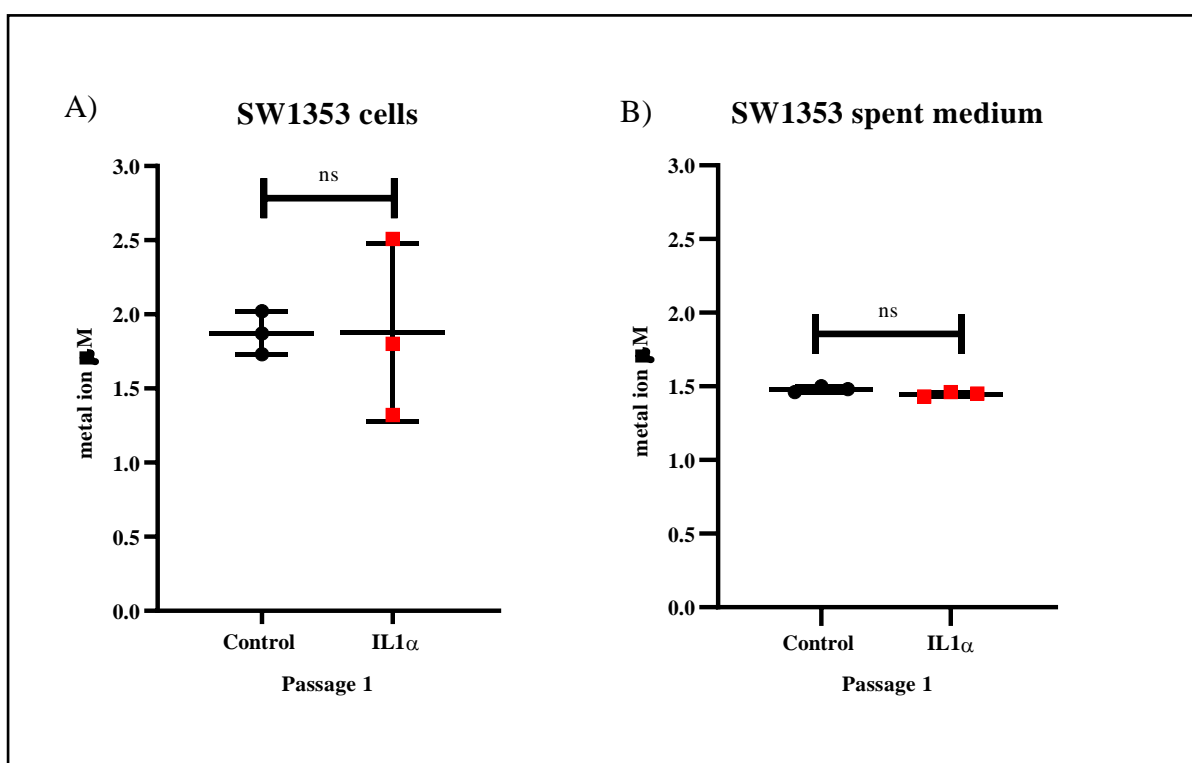


**Figure 6.8 – Metal ion content determined using a spectrophotometric method in SW1353 cells and spent medium treated  $\pm$  IL-1 $\alpha$  was not significantly different.**

SW1353 cells were treated in biological triplicate  $\pm$ 0.5ng/ml IL-1 $\alpha$  for one passage (72 hours) in monolayer culture. The cells A) and matched spent medium B) were collected, and metal ion content measured using the MAK032 spectrophotometric kit. Symbols represent means of duplicate measurements of control (black) or IL-1 $\alpha$ -treated (red) cell pellets or spent medium biological samples from a single experiment and horizontal line is the group mean and the error bars are the standard deviation. Data was analysed with a paired t-test ns = non-significant.

### 6.3.4 Is *MTF1* gene expression upregulated in response to *IL-1 $\alpha$* in SW1353 cells?

In mouse chondrocytes, *IL-1 $\beta$*  stimulation is accompanied by increased intracellular zinc levels after 24 hours. This in turn triggers nuclear translocation and increased activity of the zinc sensing transcription factor *MTF1*. This then upregulates the expression of target genes, including the *MTs*, resulting in a negative feedback loop that restores zinc levels to normal. Although intracellular zinc levels are not upregulated after one passage of *IL-1 $\alpha$*  stimulation in SW1353 human chondrosarcoma cells, this may be because the negative feedback loop mediated by *MT* has already returned zinc levels to normal by a 72 hour time point.

The *MTF1* transcript was next assessed after SW1353 cells had been stimulated with *IL-1 $\alpha$*  for 24 to 216 hours to determine a relationship between intracellular zinc status of the SW1353 cell and a positive feedback on *MTF1* transcript dependency. As the metal ion concentration was unchanged by *IL-1 $\alpha$* , it was surprising to find the *MTF1* transcript was significantly different (1.3-fold  $p=0.0464$ ) between control and stimulated cells at P1 (Figure 6.9). This effect was not sustained at later passages with *IL-1 $\alpha$*  present.

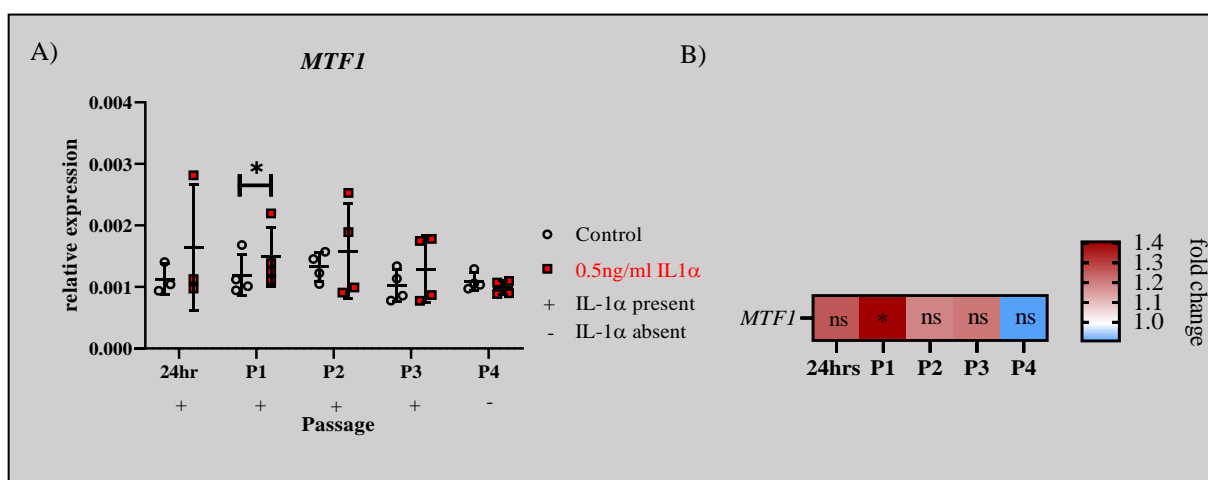


**Figure 6.9 –*MTF1* expression significantly elevated at P1 in SW1353 cells treated  $\pm$  *IL-1 $\alpha$* .** *MTF1* expression was assessed in SW1353 cDNA from Dr. Reynard's two experiments where 0.5ng/ml *IL-1 $\alpha$*  exposure was maintained for 24, 72 (P1), 144 (P2), and 216 (P3) hours and its removal for cell recovery for a further 72 hours totalling 288 (P4) hours of culture A). Normalised data satisfying a Shapiro Wilk normality test prior to or after log2 transformation was analysed with a paired t-test, otherwise Wilcoxon t-test (P4) was used. Symbols represent the mean of three qPCR technical replicates for every flask from two experiments and the mean relative expression normalized to housekeepers *18S*, *GAPDH* and *HPRT1*. Horizontal lines are the group mean and error bars are the standard deviation. Summary heatmap of *MTF1* expression fold change relative to untreated control B). Red indicates differential fold change upregulation with *IL-1 $\alpha$* , and blue represents differentially downregulated fold change of a gene with *IL-1 $\alpha$* . \*  $p<0.05$  ns = non-significant.

### **6.3.5 Does *IL-1 $\alpha$* stimulation trigger *MTF1* nuclear translocation in SW1353 cells?**

#### **6.3.5.1 Optimising the nuclear and cytoplasmic fraction extractions for western blot analysis**

Having determined that *MTF1* gene expression was unchanged by *IL-1 $\alpha$* , the next assessment was if *MTF1* protein location changed between cytoplasmic and nuclear fractions after *IL-1 $\alpha$*  treatment, indicating a potential response for *MTF1*-driven target gene expression responses. In previous western blots (4.3.5.1) there was cytoplasmic GAPDH protein carryover in the nuclear HAC fraction in the samples extracted by Dr. Adrian Falconer, so an additional PBS wash was added after the extraction of the cytoplasmic fraction prior to nuclear lysis in order to address this. Two different cytoplasmic proteins (calnexin and GAPDH) were detected and contrasted with the nuclear protein lamin A/C (Figure 6.10) highlighting that the resulting additional wash step in the methodology led to improved, though not total elimination of the cytoplasmic protein carryover into the nuclear fraction. The untreated 24 and 72 hour SW1353 nuclear protein lysates were pure and the extraction protocol remained the same with the additional PBS wash step for all future western blots comparing *MTF1* protein localisation between cytosolic and nuclear fractions.

### **6.3.5.2 Detection of MTF1 protein in untreated SW1353 lysates using N and C-terminal targeting antibodies**

Next, having improved the extraction methodology for protein fractions, I assessed the subcellular location of MTF1 using the N-terminal and C-terminal MTF1 antibodies in the 72 hour SW1353 lysate preparations from 6.3.5.1. As a positive control whole cell protein lysate from HEK293 cells in which MTF1 was overexpressed was used. The MTF1 protein is predicted to be 81kDa, however, the C-terminal antibody recognises two bands of 55 and 25kDa in the HEK293 MTF1 overexpression lysate and no proteins of the expected size in either the nuclear or cytoplasmic fraction from SW1353 cells (Figure 6.11A) Bands detected with the C-terminal MTF1 antibody in Figure 6.11A do not resemble the banding patterns on the product datasheet from Santa Cruz, though this manufacturer's datasheet only shows overexpressed MTF1 from HEK293 cells and not endogenous protein from other human cells. There was a band observed in the 72 hour nuclear lysate greater than 70kDa, though this did not correspond to the bands observed in the overexpressed MTF1 lysate lane so could not be MTF1 (Figure 6.11A). The N-terminal MTF1 antibody also detects two bands in the HEK293 overexpression lysate (Figure 6.11B), and these bands are the same as those recognised by the C-terminal antibody in Figure 6.11A. The N-terminal MTF1 antibody recognises proteins of the same size as those detected in HACs (4.3.5.2), T/C-28a2 cells (5.3.6) and in SW1353 nuclear and cytoplasmic lysates. However, the protein bands recognised in SW1353 lysates were completely different sizes compared to the overexpressed MTF1 lysate, again suggesting this antibody did not recognise MTF1.

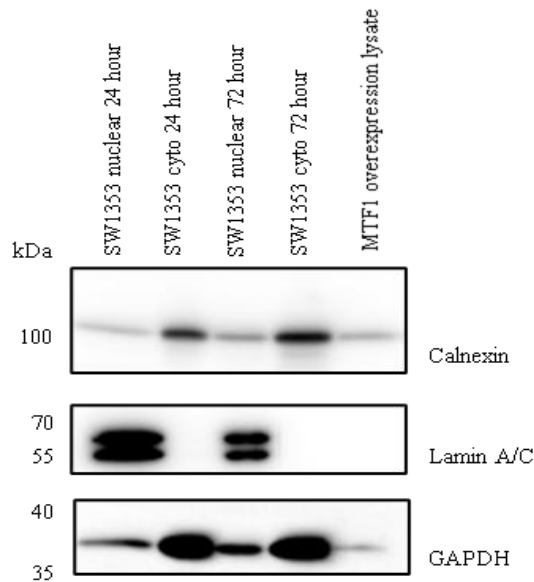


**Figure 6.10 – Optimisation of untreated SW1353 nuclear and cytoplasmic proteins extracted 24 and 72 hours after plating with the NE-PER kit with an additional PBS wash.** Five micrograms of nuclear or cytoplasmic (cyto) protein was loaded in each well and the proteins separated by gel electrophoresis. The blot was probed with 50ng/ml anti-Calnexin, 1µg/ml anti-lamin AC or 0.025µg/ml of anti-GAPDH antibodies. Overexpressed MTF1 lysate was purchased from Origene (LC401804). kDa = kilodaltons.

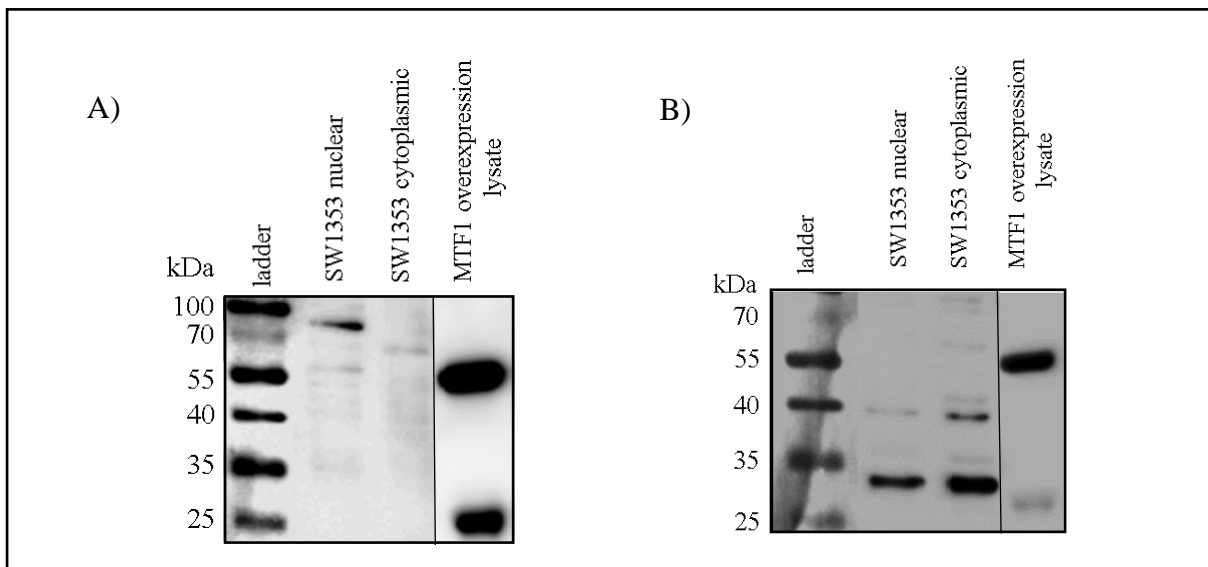


**Figure 6.11 – Western blot comparing C and N-terminal MTF1 antibody consecutively on untreated SW1353 nuclear and cytoplasmic lysates collected 72 hours after seeding.** Three micrograms of SW1353 nuclear and cytoplasmic protein and 10µg overexpressed MTF1 lysate on blot. The blot was first probed with 2µg/ml C-terminal MTF1 antibody A) and after visualising the blot, the same blot was reprobed with 0.4µg/ml N-terminal MTF1 antibody B). Overexpressed MTF1 lysate was purchased from Origene (LC401804). kDa = kilodaltons.

A final attempt at detecting endogenous MTF1 by western blot analysis with the N and C-terminal antibodies in SW1353 cells was undertaken in a new experiment in which SW1353 cells were treated with or without 0.5ng/ml IL-1 $\alpha$ , 100 $\mu$ M ZnCl<sub>2</sub> or 0.5ng/ml IL-1 $\alpha$  + 100 $\mu$ M ZnCl<sub>2</sub> for 24 or 72 hours. At this point, I ran out of the HEK293 MTF1 overexpression lysate positive control, and so I made my own by transiently transfecting SW1353 cells for 24 hours with the MTF1 plasmid and the extracted lysate from these cells used as a positive control.

The nuclear and cytoplasmic lysates prepared from these cells were electrophoresed and blotted separately from each other and then probed for MTF1 with either the N or C-terminal MTF1 antibodies and the GAPDH loading control. As can be seen in Figures 6.12A and 6.12B the transfection of the cells with the MTF1 plasmid was unsuccessful as no MTF1 protein was detected with either antibody. Despite knowing that the additional PBS wash did not entirely eliminate cytoplasmic protein carryover in the subsequent nuclear protein extraction (Figure 6.10) the GAPDH antibody showed there was uniform loading in the nuclear lysate blot (Figure 6.12A). However, the residual GAPDH detected in the 24 hour untreated control nuclear lysate was the lowest among the other nuclear lysate samples (Figure 6.12A, lane 1) and GAPDH was not detected in the corresponding cytoplasmic lysate from the same sample (Figure 6.12B, lane 1). There was no distinguishing difference in the bands observed with N-terminal MTF1 antibody between nuclear or cytoplasmic lysates with or without treatments. Although a protein of the expected size of MTF1 was not detected with either antibody in SW1353 cells it was an interesting observation nonetheless that probing the nuclear lysate blot (Figure 6.12A) with the C-terminal MTF1 antibody gave a single band in untreated and IL-1 $\alpha$ -treated lysates but none of the lysates treated with ZnCl<sub>2</sub>. This experiment was only performed once so would need repeating to confirm that this band is not present in ZnCl<sub>2</sub> treated cells. No band was detected with C-terminal MTF1 antibody in Figure 6.12B.

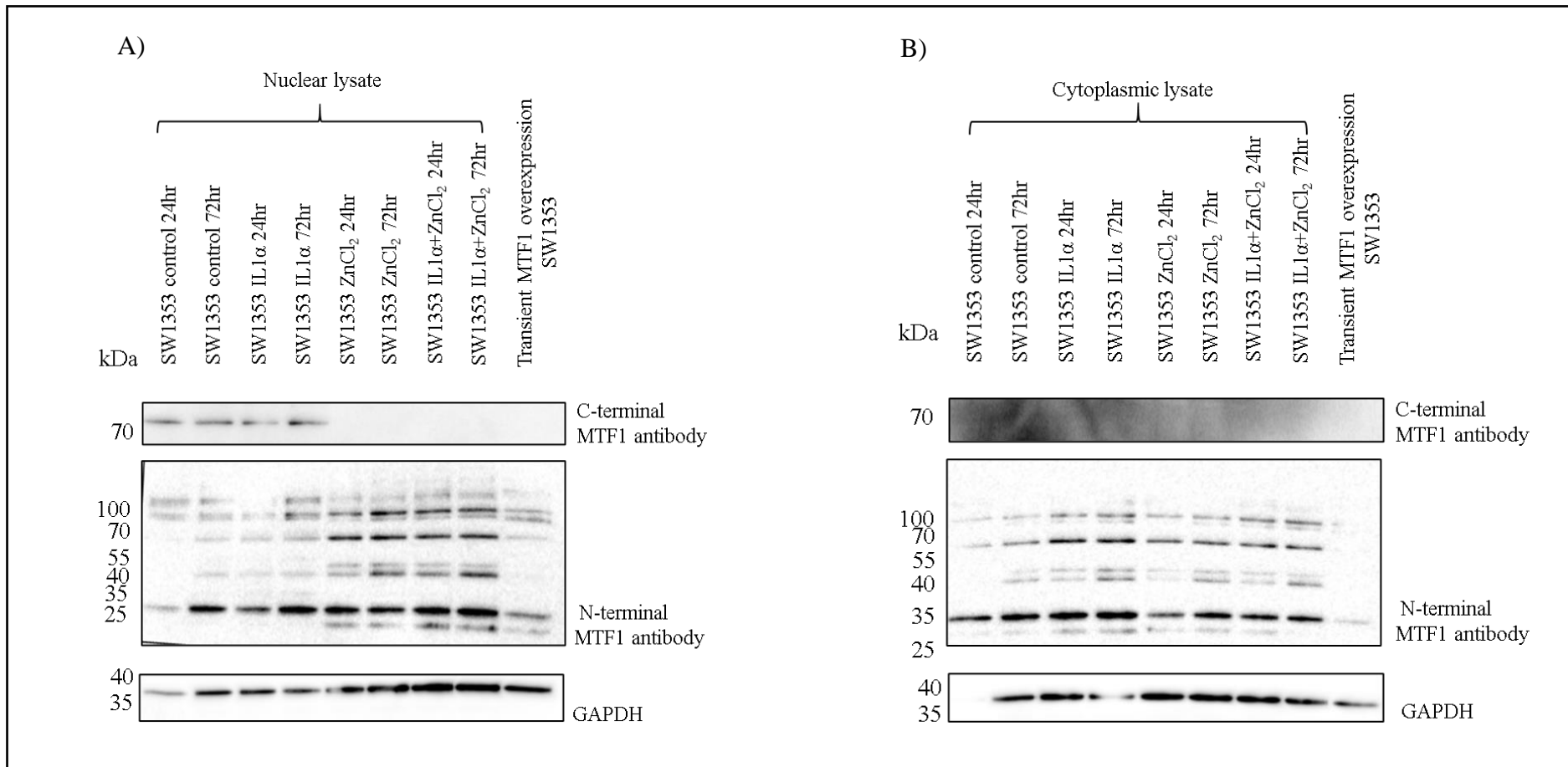


**Figure 6.12 – Twenty-four and 72 hour-treated SW1353 nuclear or cytoplasmic lysates probed consecutively on separate blots with C and N-terminal MTF1 antibody.**

Twenty micrograms of nuclear A) or cytoplasmic lysates B) from 24 or 72 hour untreated (control), 0.5ng/ml IL-1 $\alpha$ , 100 $\mu$ M ZnCl<sub>2</sub> or 0.5ng/ml IL-1 $\alpha$  + 100 $\mu$ M ZnCl<sub>2</sub> SW1353 cells were analysed on separate blots using C and N-terminal MTF1 antibodies respectively. A positive control of whole-protein lysate from SW1353 cells transiently transfected with MTF1 expression plasmid was included. The loading control was GAPDH antibody. kDa = kilodaltons.

### 6.3.5.3 Overexpression of *c-myc-FLAG-tagged MTF1* in SW1353 cells

Due to previous unsuccessful attempts to detect MTF1 in HACs, T/C-28a2 and now SW1353 cells using commercially available C and N-terminal anti-MTF1 antibodies, a new approach was adopted. SW1353 cells were transfected with a plasmid containing the MTF1 open reading frame together with a c-myc and FLAG tag. This plasmid thus encodes the MTF1 protein fused to both a c-myc and FLAG tag and should result in overexpression of a protein that can be detected by both anti-c-myc and anti-FLAG antibodies. The transfection of SW1353 cells with short hairpin RNA plasmid containing GFP was detectable 24 hours following transfection (Figure 6.13) and thus using FuGENE reagent and plasmids incorrectly was likely the cause of the failed transfection used as a positive control in Figure 6.12.

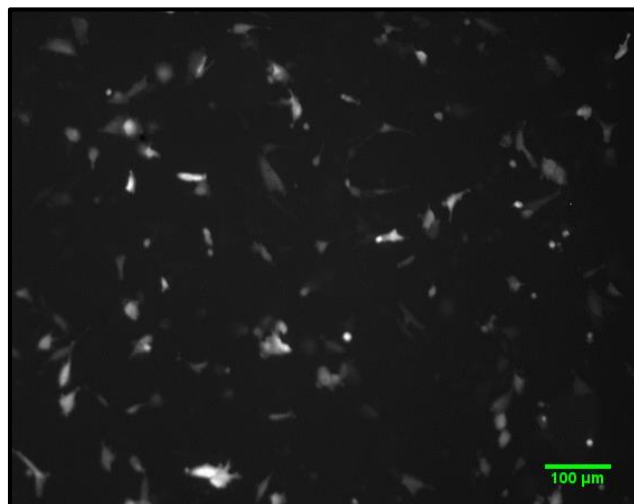


**Figure 6.13 – SW1353 cells expressing GFP 24 hours after transfection with short hairpin RNA encoding GFP.**

SW1353 cells were seeded at  $0.5 \times 10^6$  cells in a 10cm dish for 24 hours. The next day at approximately 50% confluency the cells were transfected with 5.6 $\mu$ g of a short hairpin RNA vector which expresses GFP in 16.8 $\mu$ l of FuGENE transfection reagent and the cells cultured at 37°C for 48 hours in DMEM without serum. The image was taken 24 hours after transfection with an Axiovert fluorescence microscope using the x4 objective. Scale bar is 100 $\mu$ m.

SW1353 cells were transfected with the MTF1 plasmid and protein collected after 48 hours (Figure 6.14 A and B, left well). As a negative control for both the c-myc and FLAG antibodies, protein was also collected from SW1353 cells transfected with a GFP plasmid for 48 hours (Figure 6.14 A and B, middle well). Dr Matt Barter (Newcastle University) provided protein lysate from SW1353 cells transduced with a Cas9-FLAG plasmid to use as a positive control for the anti-FLAG antibody (Figure 6.14 A and B, right well). These lysates were subject to western blot analysis and the blot was probed with the FLAG antibody (CST, 2368, Figure 6.14A) or the anti-c-myc antibody (Figure 6.14B). The anti-FLAG antibody detected the FLAG-tagged Cas9 at the predicted molecular weight of 160kDa but multiple bands were detected in the SW1353 transiently transfected with MTF1 plasmid for 48 hours (Figure 6.14A), none of which were the same size as the predicted 84kDa c-myc-FLAG-tagged MTF1 protein. However, a band of ~130kDa was detected with the FLAG antibody in cells transfected with the MTF1 plasmid, and this band was not present in either of the two control samples. Two protein bands were observed at ~35kDa in all the samples with the anti-FLAG antibody (Figure 6.14A), including the middle lane containing lysate from cells transfected with the GFP expression plasmid, indicating that these bands were non-specific (Figure 6.14A). For the blot that was probed with c-myc antibody (Figure 6.14B) the same banding pattern was present in every sample. Furthermore, no protein was detected at the predicted size of the c-myc-FLAG-tagged MTF1 protein. Together this indicates that the anti-c-myc antibody could not discriminate between positive or negative controls and so was unsuitable for use in reliable MTF1 overexpression detection.

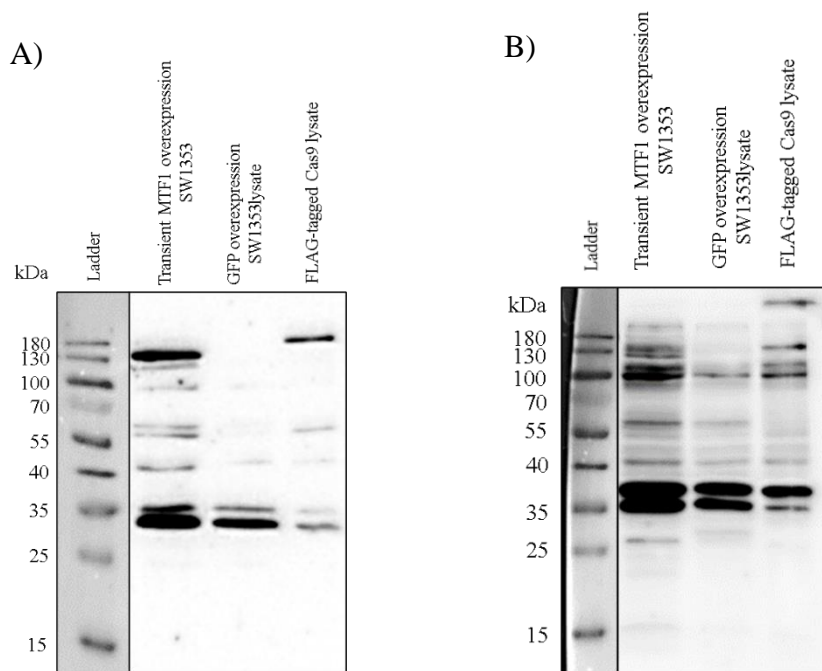


**Figure 6.14 – Western blots for MTF1 detection in transiently MTF1 overexpressing SW1353 cell lysates using FLAG or c-myc antibodies respectively.**

SW1353 cells were transfected with either MTF1 or GFP expression plasmids for 48 hours before extraction of whole protein lysates. Cas9 FLAG-tagged lysate was provided by Dr. Matt Barter. The first blot contains 20 $\mu$ g of protein and was probed with 42ng/ml FLAG antibody A) and the second blot contains 20 $\mu$ g protein and was probed with 1 $\mu$ g/ml c-myc antibody B). kDa = kilodaltons.

Although the FLAG antibody detected both the Cas9-FLAG protein and a 130kDa protein specifically in the c-myc-FLAG-tagged MTF1 protein lysate, it was unclear if the latter protein was in fact the tagged MTF1 protein. To investigate this further, two other anti-FLAG monoclonal antibodies purchased from Origene (TA50011-100 and TA180144) were tested. Neither of these monoclonal antibodies could detect the 160kDa Cas9-FLAG fusion protein. As an example, Figure 6.15A highlights the inability of Origene’s TA50011-100 FLAG antibody to detect 160kDa Cas9-FLAG (Figure 6.15A) in comparison to CST’s FLAG antibody (Figure 6.15B). The gel electrophoresis and transfer of these Cas9-FLAG samples to PVDF was conducted by Dr. Matt Barter and the blot was provided as a spare. All lanes of protein lysate contained different guide RNA combinations targeting exon one of *SOX9*, but in this instance only the efficacy of the FLAG antibodies was being assessed and the results were uniform between the samples (Figure 6.15). The FLAG antibody (CST, 2368) was used for future SW1353 western blots, despite the disparity between the band(s) observed (Figure 6.14) and the 84kDa c-myc-FLAG-tagged MTF1 protein.

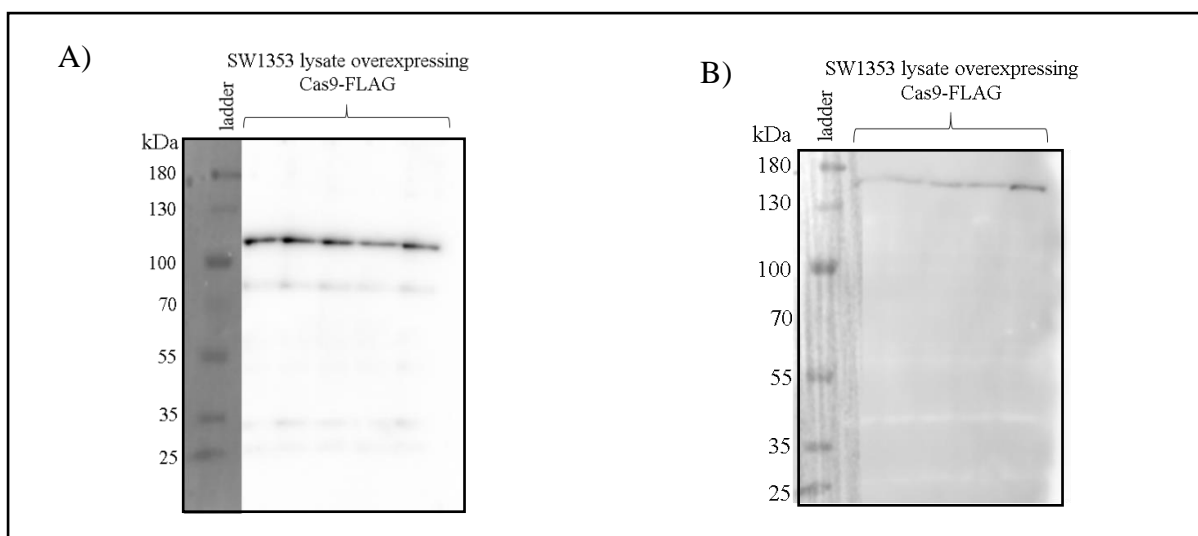


**Figure 6.15 – Western blot comparing commercially available anti-FLAG tag antibodies in SW1353 lysates overexpressing Cas9-FLAG fusion protein.**

The blot was probed with 0.5 $\mu$ g/ml FLAG antibody (TA50011-100) A) and then reprobed with 42ng/ml FLAG antibody (CST, 2368) B). The amount of protein on the blot is unknown as the blot itself was provided unprobed by Dr. Matt Barter and highlights the difference in antibody quality from different manufacturers. kDa = kilodaltons.

### 6.3.6 Production of an MTF1 overexpressing SW1353 cell line

To overcome the difficulties in examining the effect of IL- $\alpha$  on detecting endogenous MTF1 localisation using commercially available antibodies, I decided to make SW1353 cells that stably expressed the MTF1-MYC-FLAG fusion protein. Stable MTF1 overexpression and selection with G418 antibiotic was achieved through transfection of both AgeI-digested linear MTF1 expression plasmid and circular forms into the SW1353 cell line. Analysis of the RNA extracted from these lines in comparison to untransfected SW1353 cells revealed that overexpression of MTF1 was successful (Figure 6.16). The combined endogenous and plasmid encoding MTF1 mRNA was quantified using three separate assays to different regions of the MTF1 open reading frame (Figure 6.16 A-C and Appendix B). A fourth assay was designed to span the MYC-FLAG encoding sequence and thus only detects fusion transcripts originating from the MTF1 plasmid (Figure 6.16D). In all assays, the linear form of the transfected MTF1 plasmid led to between 1.6 and 2.1-fold greater expression over cells transfected with the circular MTF1 plasmid, with transfected cells having 4-12 times higher MTF1 expression than untransfected cells.

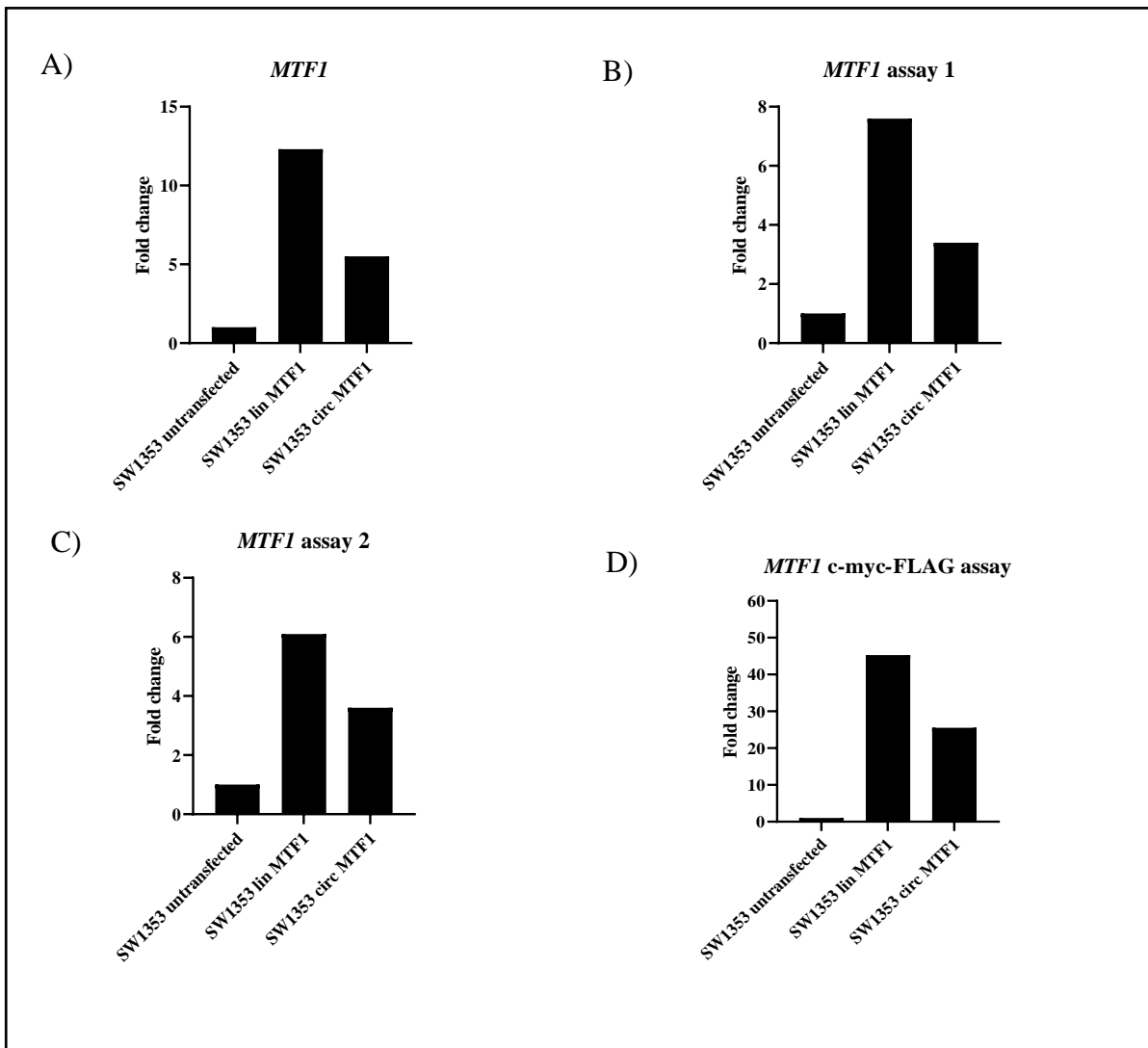


**Figure 6.16 – *MTF1* gene expression in *MTF1* overexpressing SW133 cells as fold change relative to untransfected SW1353 cells.**

The primers flanking intron five of *MTF1* transcript were identical to *MTF1* primers for qPCR data presented previously A). *MTF1* qPCR assays designed to either the open reading frame of the *MTF1* plasmid (B-C; detect endogenous and plasmid encoded transcript) or the region spanning the *MTF1*-FLAG sequence D). Bars represent means of the technical triplicate from the qPCR. Lin = linear-transfected, circ = circular-transfected.

### 6.3.6.1 MTF1 overexpression confirmation by western blot

The detection of stable MTF1 protein overexpression in SW1353 cells was determined with the FLAG antibody from CST (Figure 6.17). The band observed at 130kDa is present in both cell lines transfected with the AgeI-digested linear and circular MTF1 plasmid but is absent in the untransfected SW1353 cells. The 130kDa band was also observed with this antibody previously when the MTF1 plasmid was transiently overexpressed in SW1353 cells (Figure 6.14A). I therefore took this band to represent overexpressed MTF1 fusion protein, despite the size discrepancy between predicted 84kDa and ~130kDa observed.

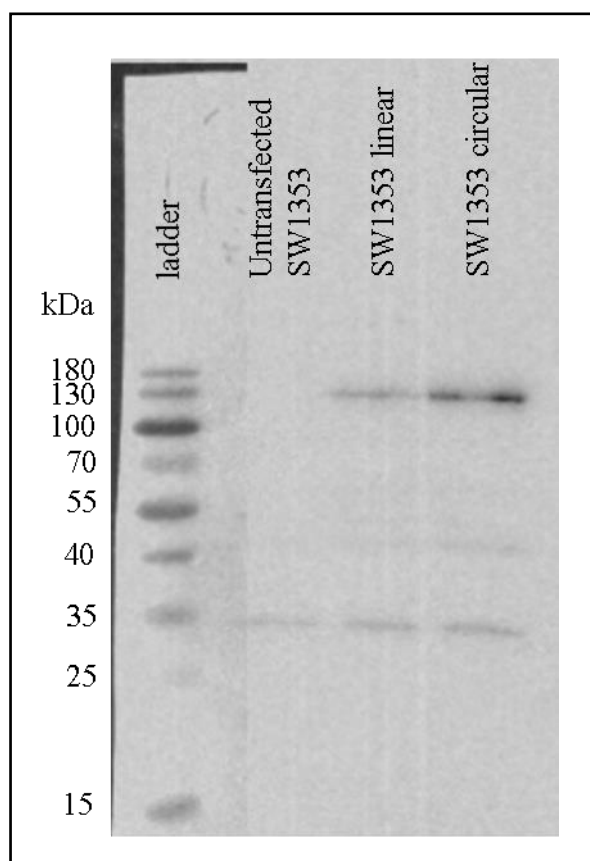


**Figure 6.17 – MTF1 protein overexpression confirmation in SW1353 cells transfected and selected with 1mg/ml G418 generating the MTF1 overexpression cell lines.**

Ten micrograms of protein were loaded on each lane and the blot was probed with 42ng/ml FLAG antibody. kDa = kilodaltons. Linear = AgeI-digested linear overexpressing MTF1 SW1353 cells, circular = undigested MTF1 overexpressing SW1353 cells.

### **6.3.6.2 Do *IL-1 $\alpha$* and/or zinc stimulate MTF1 nuclear translocation?**

Having generated a stable MTF1 overexpressing SW1353 cell line in which I believed the protein could reliably be detected using the FLAG antibody, I used this cell line to address MTF1 subcellular localisation. Cells were treated with or without 0.5ng/ml IL-1 $\alpha$ , 100 $\mu$ M ZnCl<sub>2</sub> or 0.5ng/ml IL-1 $\alpha$  + 100 $\mu$ M ZnCl<sub>2</sub> for either 24 or 72 hours and the nuclear and cytoplasmic lysates collected at each time point. As a positive control for these western blots I transfected HEK293 cells with MTF1 plasmid and collected the whole protein lysate.

Experiments were grouped by time point such that cells were seeded in technical duplicate for each treatment and the experiment was repeated three times for a total of six western blots per time point. Figures 6.18 and 6.19 illustrate two of six representative western blots per time point where each blot are biological replicates from the same experiment. The remaining western blots are in Appendices H and I. The 130kDa putative MTF1-MYC-FLAG fusion protein was detected by the anti-FLAG antibody in all blots, with a protein of the same size also detected in the HEK293 lysate positive control made in-house. Furthermore, the nuclear and cytoplasmic loading controls for each fraction confirmed the purity of these fractions. Also of note in Figures 6.18 and 6.19 is that MTF1 is located predominantly in the cytoplasm after 24 hours irrespective of treatment and that it migrates to the nucleus by 72 hours, reflecting the translocation behaviour of MTF1. All six western blots per timepoint were subject to densitometry analysis, with the intensity of the MTF1-MYC-FLAG fusion protein plotted relative to the respective GAPDH cytoplasmic or lamin A/C nuclear control (Figure 6.20). The additional 55kDa band observed in the 72 hour lamin A/C blots to greater or lesser extents was an artefact and because this was non-specific, was not included in the densitometric analysis.



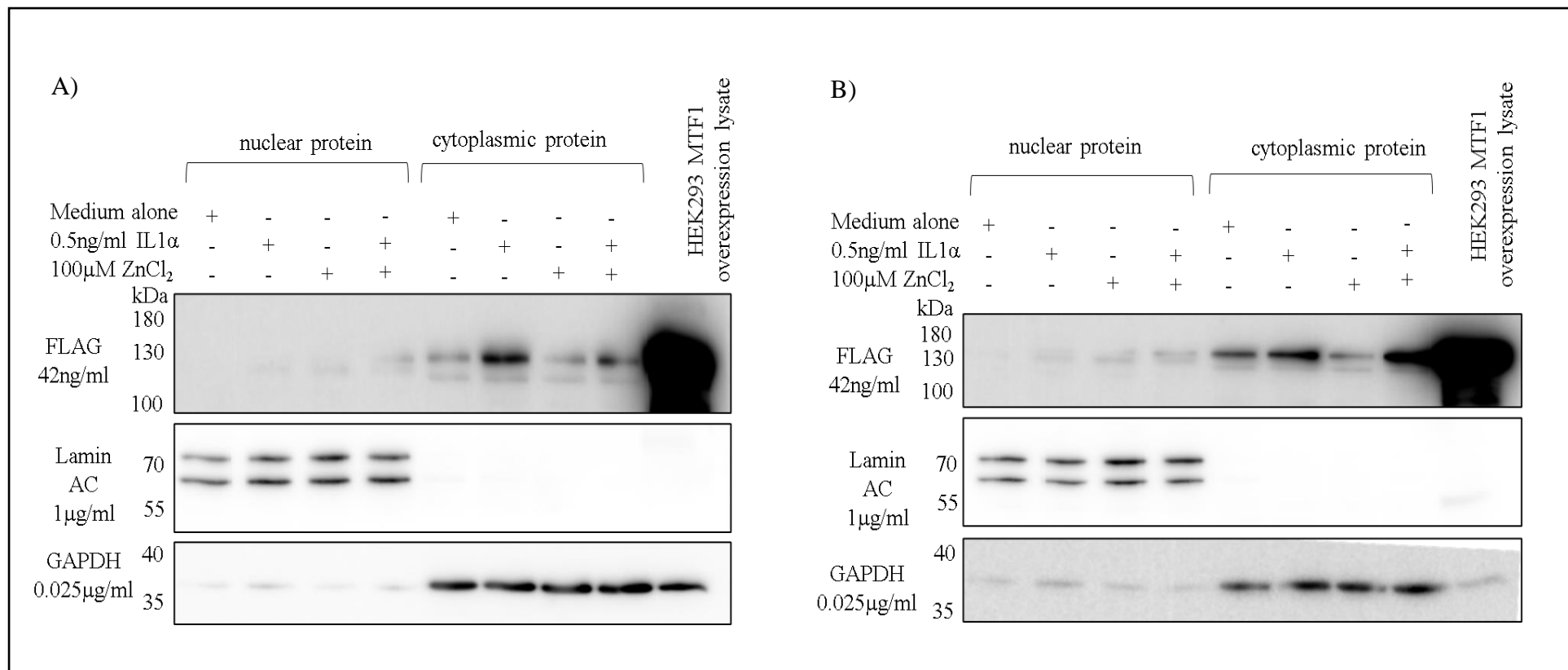


**Figure 6.18 – Western blots highlighting biological replicates from one of three representative experiments for AgeI-digested linear MTF1 overexpressing SW1353 cells in nuclear and cytoplasmic lysates  $\pm$  treatment for 24 hours.**

SW1353 cells overexpressing MTF1 were treated with or without 0.5ng/ml IL-1 $\alpha$ , 100 $\mu$ M ZnCl $_2$  or 0.5ng/ml IL-1 $\alpha$  + 100 $\mu$ M ZnCl $_2$  for 24 hours in duplicate for a total of three experiments and the nuclear and cytoplasmic lysates from each replicate condition collected. Western analysis was performed for all six repeats, with A) and B) being two representative western blots. 10 $\mu$ g of protein was probed with FLAG (CST, 2368), Lamin AC or GAPDH antibodies with the respective cut sections of the blot according to the expected molecular weight of MTF1 or loading control proteins. The positive control was also 10 $\mu$ g of MTF1 overexpression lysate derived from HEK293 cells transfected with MTF1 expression plasmid in-house. kDa = kilodaltons.

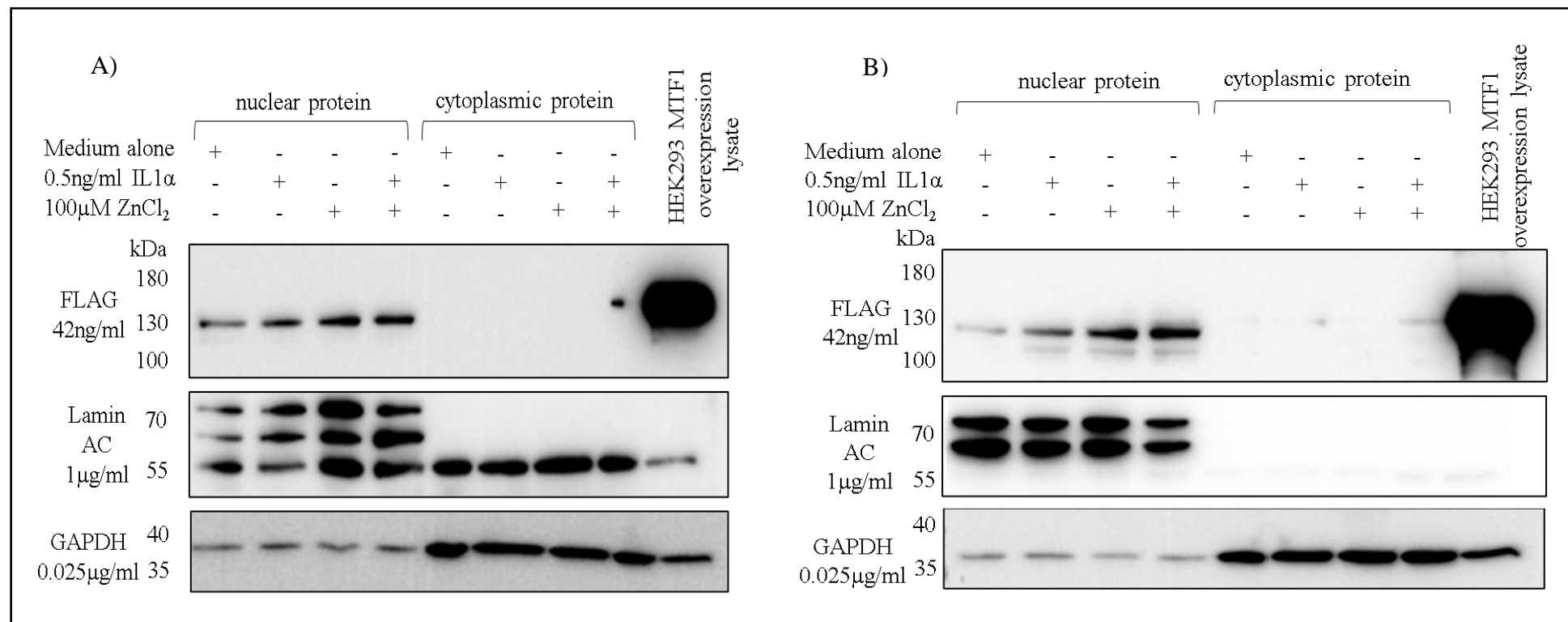


**Figure 6.19 – Western blots highlighting biological replicate from one of three representative experiments for AgeI-digested linear MTF1 overexpressing SW1353 cells in nuclear and cytoplasmic lysates  $\pm$  treatment for 72 hours.**

SW1353 cells overexpressing MTF1 were treated with or without 0.5ng/ml IL-1 $\alpha$ , 100 $\mu$ M ZnCl<sub>2</sub> or 0.5ng/ml IL-1 $\alpha$  + 100 $\mu$ M ZnCl<sub>2</sub> for 72 hours in duplicate for a total of three experiments and the nuclear and cytoplasmic lysates from each replicate condition collected. Western analysis was performed for all six repeats, with A) and B) being two representative western blots. 10 $\mu$ g of protein was probed with FLAG (CST, 2368), Lamin AC or GAPDH antibodies with the respective cut sections of the blot according to the expected molecular weight of MTF1 or loading control proteins. The positive control was also 10 $\mu$ g of MTF1 overexpression lysate derived from HEK293 cells transfected with MTF1 expression plasmid in-house. kDa = kilodaltons.

The densitometry data has been colour coded for the experiments grouping the biological replicates with similar colour schemes. The analysis of the 24 hour western blots confirms that the MTF1 protein was present at greater levels in the cytoplasm compared to the nucleus and that IL-1 $\alpha$  treatment alone or in the presence of ZnCl<sub>2</sub> was associated with significantly higher cytoplasmic levels ( $p=0.0313$ ) compared to the control (Figure 6.20A, appendix H). ZnCl<sub>2</sub> alone led to comparable cytoplasmic MTF1 levels as the control. The MTF1-MYC-FLAG fusion protein was only detected in the nuclear fraction at 72 hours (Figure 6.20B, appendix I) and semi-quantitative densitometry confirmed MTF1 levels are higher in the nucleus than cytoplasm at this time point when MTF1 was normalised to the relevant control protein. There was a large amount of variation in MTF1:lamin AC densitometry values for the nuclear fraction at the 72 hour time point, and no clear differences between the control or treated cells were observed (Figure 6.20B).

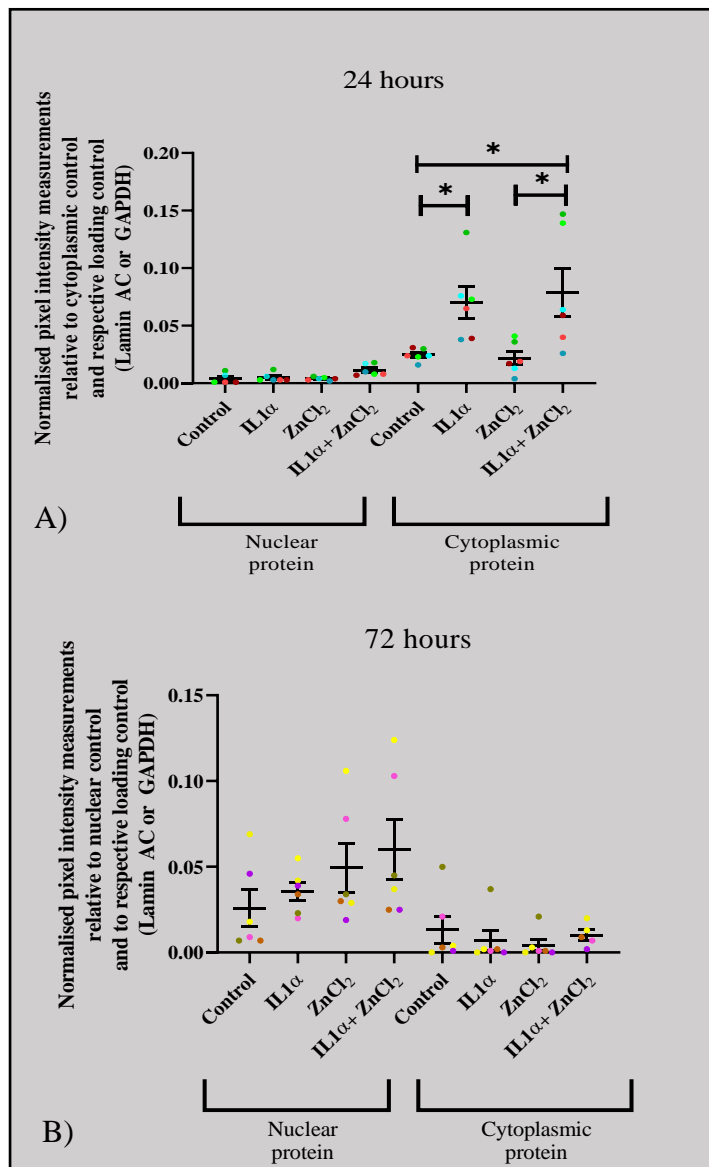


**Figure 6.20 - Densitometry analysis of western blots determining MTF1 translocation between cytoplasmic and nuclear compartments 24 A) or 72 hours B) after treatment.**

SW1353 cells overexpressing the MTF1 c-myc-FLAG tagged protein were treated  $\pm$  0.5ng/ml IL-1 $\alpha$ , 100 $\mu$ M ZnCl<sub>2</sub> or 0.5ng/ml IL-1 $\alpha$  + 100 $\mu$ M ZnCl<sub>2</sub> for 24 A) or 72 hours B). Six western blots were conducted per time point and each condition per experiment was in biological duplicate which is colour coded in pairs. Pixel intensity measurements for FLAG bands were normalised to cytoplasmic control FLAG band at 24 hours or nuclear control FLAG band at 72 hours. This was then divided by the respective loading control for cytoplasmic (GAPDH) or nuclear (lamin AC) proteins. Background intensity was accounted for per lane of sample in every measurement calculated. Effect of treatments in relevant protein fraction was compared to control by Wilcoxon t-test. \*  $p<0.05$ .

In summary, these western blots demonstrated that MTF1 translocated from the cytoplasm to the nucleus between 24 and 72 hours independently of IL-1 $\alpha$  and/or ZnCl<sub>2</sub> stimulation. Furthermore, IL-1 $\alpha$  was associated with increased cytoplasmic MTF1 levels at 24 hours potentially suggesting that at this time point the cell is loading the cytoplasm with excess MTF1 prior to translocation to later target MTF1-specific genes in response to IL-1 $\alpha$ . Given that the loading controls have been included in the densitometry analysis to account for uniform loading, the 72 hour blots would suggest that there may have been an issue with loading as the biological replicate samples, for the nuclear protein at least, are more variable. It is not as clear in the 72 hour western blots if treatment had an effect on MTF1 levels when compared against the nuclear control and I cannot compare the same treatment between compartments in this instance because the MTF1 nuclear control is both variable and at a higher level than the MTF1 cytoplasmic control.

### **6.3.6.3 *Detecting endogenous and plasmid-encoded MTF1 using immunocytochemistry***

qPCR and the western blot analysis of the MTF1-MYC-FLAG SW1353 cell line indicated that this fusion gene was being transcribed and translated. Although both anti-MTF1 antibodies used for western blot analysis were unable to detect the endogenous MTF1 antibody, nor the MTF1-MYC-FLAG fusion protein by western blot analysis, immunocytochemistry was conducted with these antibodies in attempts to visualise MTF1 endogenously, after transient transfection or in AgeI-digested linear MTF1 overexpressing SW1353 cells. The ICC results of the initial experiment from 2.12.1 indicated that SW1353 cells transiently transfected with 1 $\mu$ g of MTF1 plasmid for 48 hours do not express MTF1 with a high efficiency. Nuclear localisation was 15.7 and 17.9% with single stains using c-myc and C-terminal MTF1 antibodies respectively (Figure 6.21), however there were so few cells after the staining protocol due to a technical fault during PBS washing of the chamber slides that this is a likely underestimate of the actual transfection efficiency. Another explanation for the poor transfection efficiency was the ineffective permeabilisation where I accidentally used 0.2 instead of 0.5% Triton X-100. Therefore, ICC was conducted again for another chamber slide experiment in which MTF1 detection was attempted in untransfected, transiently transfected or in G418-selected AgeI-digested linear MTF1 plasmid expressing SW1353 cells (Figure 6.22). Additionally, as a control for the transfection, I sourced HEK293 cells which are easily transfectable.

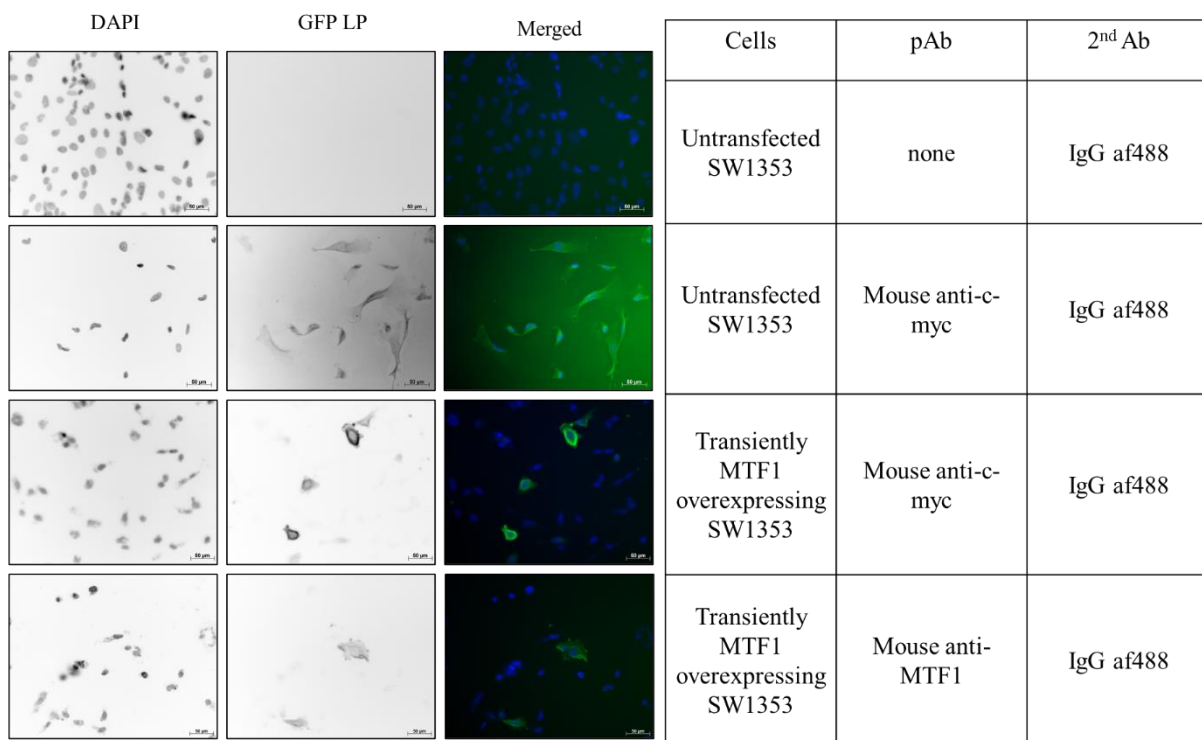


**Figure 6.21 – ICC of untransfected or transiently transfected SW1353 cells with MTF1 plasmid and stained ± anti-c-myc or anti-MTF1 antibodies.**

Cells were stained ± C-terminal MTF1 or c-myc antibodies and the secondary goat anti-mouse IgG af488 fluorophore. There was incomplete permeabilisation and fewer cells than expected after staining in this experiment due to technical errors which partly explains the low nuclear localisation efficiencies 15.7 and 17.9% for c-myc and C-terminal MTF1 antibodies. Different staining patterns were observed with the c-myc antibody before and after transient MTF1 plasmid transfection. Images presented are representative for the whole well among 3-4 images taken per well per field of view. The magnification is x20 and the scale bars are 50µm. GFP LP = green fluorescent protein long-pass filter. pAB = primary antibody, 2<sup>nd</sup> Ab = secondary antibody.



Figure 6.22A demonstrates that endogenous MTF1 in untransfected SW1353 cells was not detectable with the C-terminal anti-MTF1 antibody (Santa Cruz, 365090). MTF1 was present in HEK293 cells transfected with MTF1 plasmid, yet untransfected SW1353 cells and SW1353 cells stably overexpressing linear MTF1-MYC-FLAG protein were very weakly staining or absent for MTF1 with the same antibody (Figure 6.22A). During the preparation of the FuGENE, serum-free medium and MTF1 plasmid mix I unfortunately added excess FuGENE reagent such that a 4.8:1 ratio rather than 3:1 ratio of FuGENE per  $\mu\text{g}$  plasmid was incorporated. Thus there may have been some cytotoxicity to the cells receiving MTF1 plasmid. Despite this, perhaps the difference in staining between cell lines is a reflection of the ease with which HEK293 cells can be transfected. For the same experiment in which the FLAG-tagged region of MTF1 was examined with the FLAG antibody (CST 2368), MTF1 was observed in all the transfected cells in a diffuse cytoplasmic manner (Figure 6.22B). However, staining was observed in the untransfected SW1353 cells, suggesting that this antibody binds non-specifically as FLAG is not an endogenous peptide in cells. Linear MTF1 overexpressing SW1353 cells were not stained with the goat anti-rabbit IgG af594 antibody without a primary antibody to definitively test for non-specificity of the secondary antibody and the concentration used in all wells was accidentally 2.5 times greater than the manufacturer's recommendation ( $10\mu\text{g/ml}$  instead of  $4\mu\text{g/ml}$ ).

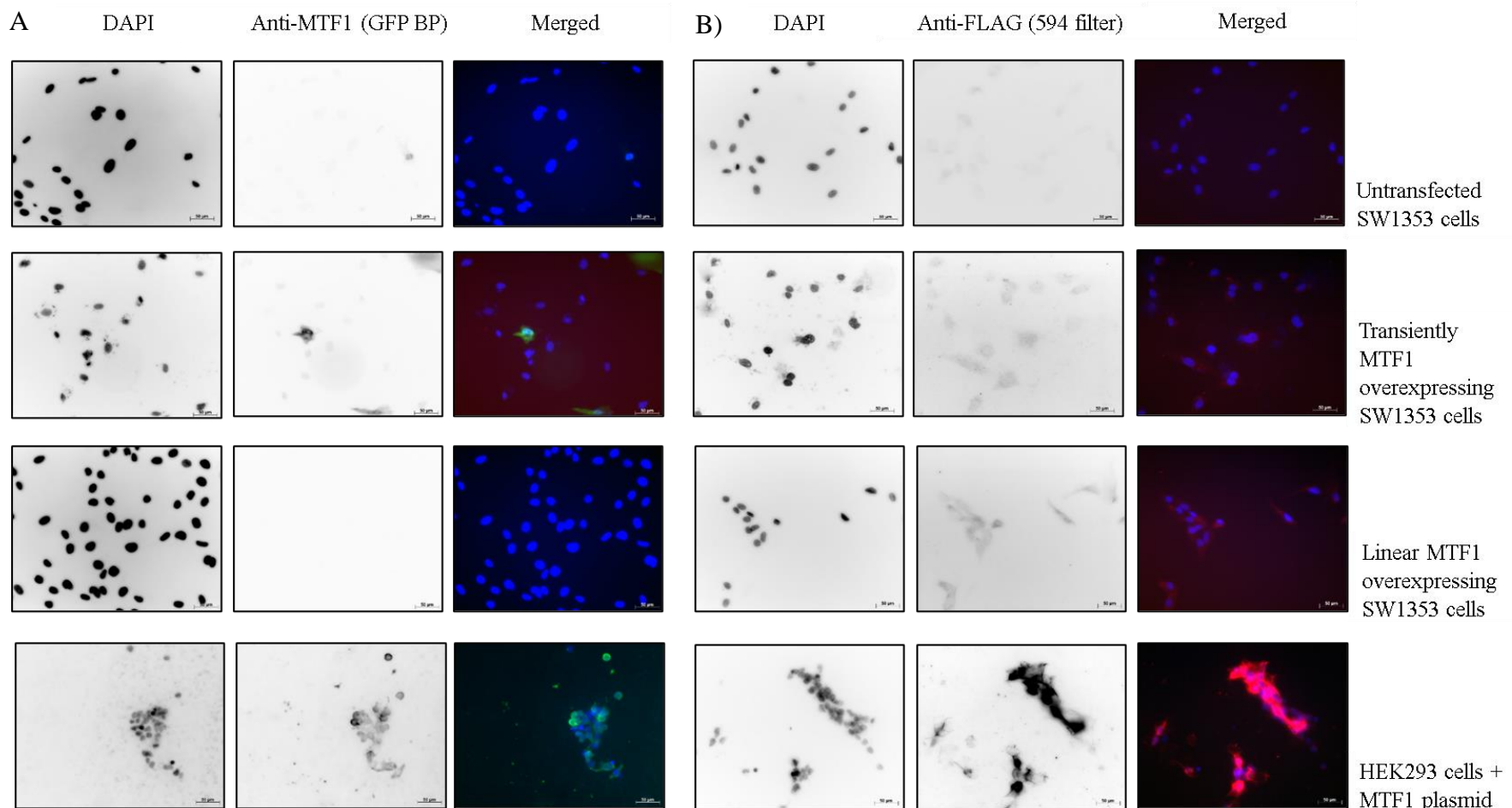


**Figure 6.22 – ICC experiment using two strategies to detect MTF1 protein with C-terminal MTF1 antibody A) or FLAG antibody B).**

MTF1 expression in SW1353 cells was assessed endogenously in untransfected cells, in SW1353 and HEK293 cells transiently transfected with 1 $\mu$ g of MTF1 plasmid for 48 hours and in stably linear MTF1 overexpressing SW1353 cells. Camera exposure times were 1637 and 136 milliseconds for the GFP-bandpass (BP) A) and the 594 filter B) respectively. Scale bar is 50 $\mu$ m and images were taken at x20 magnification.

The last experiment attempted with two chamber slides addressed MTF1 translocation after 0.5ng/ml IL1 $\alpha$ , 100 $\mu$ M ZnCl<sub>2</sub>, or 0.5ng/ml IL1 $\alpha$  + 100 $\mu$ M ZnCl<sub>2</sub> treatment for 24 or 72 hours respectively. The cells used were the stable MTF1 overexpressing SW1353 cells that were also used in the cellular fraction western blot analysis (6.3.6.2). The anti-FLAG antibody was used to stain the wells of one chamber slide (results not shown), and the other chamber slide costained with anti-FLAG and anti beta-actin antibodies (Figure 6.23 A and B). The concept behind costaining in this manner would in theory make counting true MTF1 nuclear staining easier by excluding cells with a FLAG staining pattern overlapping beta-actin which is strictly cytoplasmic in location. The beta-actin (GFP BP channel) and cytoplasmic MTF1 (594 filter channel) staining pattern was overlapping and near identical to the extent that inclusion of an alternative cytoplasmic protein costain was obsolete (Figure 6.23 A and B). However, the costaining was particularly effective in differentiating nuclear anti-FLAG MTF1 from cytoplasmic staining in the IL-1 $\alpha$  with or without ZnCl<sub>2</sub> conditions (Figure 6.23B, rows two and four). When the percentage nuclear cells was calculated the variation from the three fields of view per well per condition was so large that no meaningful conclusion could be made about the effect of treatment on translocation (Figure 6.24). In this experiment the specificity of the primary antibodies was tested by omission of the primary anti-FLAG and anti-beta-actin antibodies during the ICC staining procedure and no staining was observed in either channel (not shown).

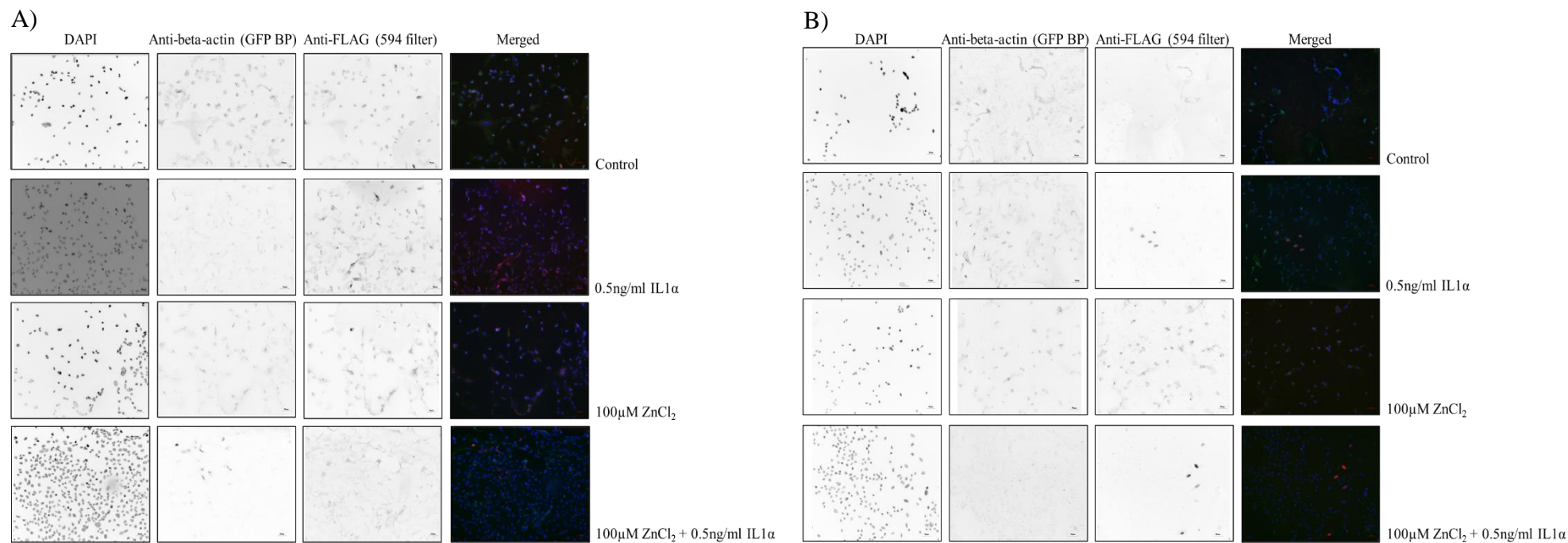


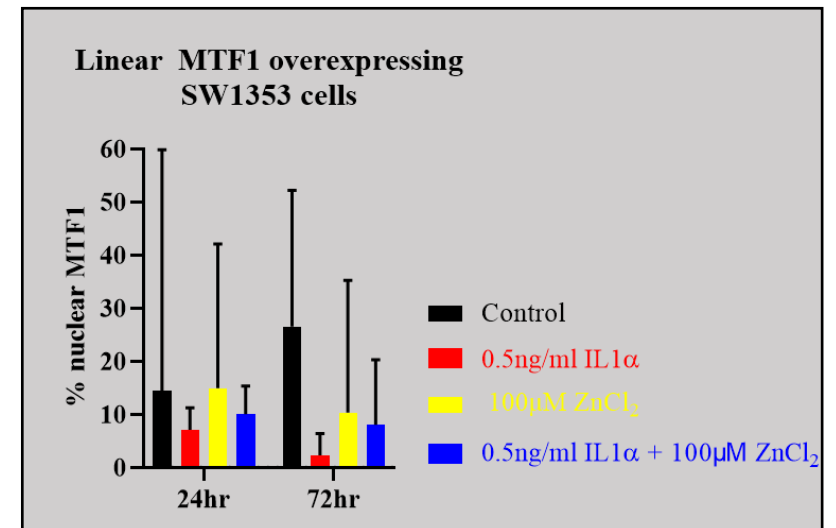
**Figure 6.23- ICC costaining with anti-MTF1 (GFP BP filter) and anti-FLAG (594 filter) antibodies of linear MTF1 overexpressing SW1353 cells treated for 24 A) or 72 hours B)  $\pm$  IL-1 $\alpha$  and/or ZnCl $_2$ .**

Cells were seeded at  $7.5 \times 10^3$  cells/well for four hours before half the chamber slide medium was replaced with medium containing 0.5ng/ml IL-1 $\alpha$ , 100 $\mu$ M ZnCl $_2$ , or 0.5ng/ml IL-1 $\alpha$  + 100 $\mu$ M ZnCl $_2$  B). Forty-eight hours afterwards the medium was removed from the other four wells and replaced with the same treatments for 24 hours A). Images presented are representative for the whole well among 3-4 images taken per well per field of view. Camera exposure times were 58 and 204 milliseconds for the GFP-band pass (BP) and the 594 filter respectively. The magnification is x10 and the scale bars are 50 $\mu$ m.

	well, field of view	Control			0.5ng/ml IL1 $\alpha$			100 $\mu$ M ZnCl $_2$			0.5ng/ml IL1 $\alpha$ + 100 $\mu$ M ZnCl $_2$		
		counts MTF1 + nuclei alone	total cells expressing MTF1 in the cytoplasm	% nuclear	counts MTF1 + nuclei alone	total cells expressing MTF1 in the cytoplasm	% nuclear	counts MTF1 + nuclei alone	total cells expressing MTF1 in the cytoplasm	% nuclear	counts MTF1 + nuclei alone	total cells expressing MTF1 in the cytoplasm	% nuclear
24hr	1.1	1	80	1.2	21	507	4.0	30	395	7.1	25	296	7.8
	1.2	12	272	4.2	19	201	8.6	31	180	14.7	32	157	16.9
	1.3	48	11	81.4	31	224	12.2	46	34	57.5	19	231	7.6
<b>TOTAL</b>		13	352		71	932		61	575		44	527	
% nuclear	outliers included			14.4			7.1			14.9			10
	outliers excluded			3.6			N.A			9.6			7.7
72hr	1.1	52	108	32.5	0	321	0.0	5	362	1.4	7	159	4.2
	1.2	17	8	68.0	5	182	2.7	4	79	4.8	11	168	6.1
	1.3	43	195	18.1	9	104	8.0	48	56	46.2	14	39	26.4
<b>TOTAL</b>		95	303		14	607		9	441		18	327	
% nuclear	outliers included			26.5			2.3			10.3			8.0
	outliers excluded			23.9			N.A			2.0			5.2

**Figure 6.24 - Manual cell counts from an ICC experiment using linear MTF1 overexpressing SW1353 cells treated  $\pm$  IL-1 $\alpha$  and/or ZnCl $_2$  for 24 or 72 hours testing anti-FLAG and anti-beta-actin antibody costaining.**

A) For each of three fields of view per well per condition the percentage nuclear MTF1 expression was calculated with and without outliers (highlighted in red). B) The data from A) plotted as a bar chart with the bars representing the data including outliers (where present) and the error bars is standard deviation.



### 6.3.7 What are the effects of IL-1 $\alpha$ and/or ZnCl<sub>2</sub> treatment on MTF1 activity?

MTF1 activity could not be measured in HACs, but as SW1353 cells are easily transfected, MTF1 activity can be studied using reporter assays in this cell line. To test whether MTF1 activity changed after the introduction of 0.5ng/ml IL-1 $\alpha$  or 5ng/ml IL-1 $\beta$  treatments over a 24 hour incubation period, a luciferase reporter assay for MTF1 was carried out. As a positive control, cells were treated with ZnCl<sub>2</sub> with or without IL-1 $\alpha$  to increase intracellular zinc levels and stimulate the zinc homeostatic response. The reporter plasmid MRE pGL4.40 plasmid encodes the firefly luciferase protein under the control of a minimal promoter and contains five copies of a 5' MRE immediately upstream of a minimal promoter (Appendix A). The MRE is a sequence (TGCNCRC) specifically recognised and bound by MTF1 that is found in the promoter of MTF1 target genes. The MRE pGL4.40 plasmid or cloned empty control pGL4.40 plasmid were co-transfected separately with renilla luciferase into SW1353 cells for 24 hours, media removed and then replaced with media containing different IL-1 cytokines and/or ZnCl<sub>2</sub> for a further 24 hours. Cells were lysed and the luciferase and renilla levels quantified with the raw firefly luciferase signal normalised against the renilla luciferase signal. The normalised luciferase activity is proportional to MTF1 activity.

Initial examination of the normalised firefly:renilla data from SW1353 cells transfected with the empty control pGL4.40 luciferase plasmid demonstrated that the mean luciferase signal was not significantly different between treatments (Figure 6.25). Despite this, the normalised firefly:renilla data for the SW1353 cells transfected with the MRE pGL4.40 plasmid were divided by the normalised firefly:renilla data of the SW1353 cells transfected with the empty control pGL4.40 plasmid for each respective stimulus (Figure 6.26).

Both IL-1 cytokines significantly reduced luciferase activity (IL-1 $\alpha$  p = 0.0114, IL-1 $\beta$  p <0.0001), by 13 and 25% compared to the control respectively (Figure 6.26). ZnCl<sub>2</sub> alone or in combination with IL-1 $\alpha$  was associated with a 38% (p<0.0001) and 21% (p<0.0001) mean increase in luciferase activity compared to the control (Figure 6.26). The results of this luciferase reporter assay indicates that ZnCl<sub>2</sub> does indeed stimulate increased MTF1 activity. This result was consistent with the effect that ZnCl<sub>2</sub> had on MTF1 activity at the same concentration tested in mouse chondrocytes (Kim *et al.*, 2014).

I next wanted to compare MTF1 activity between normal SW1353 cells and those stably overexpressing MTF1, and so both cell lines were transiently transfected with either empty control pGL4.40 or MRE pGL4.40 plasmid in the same 96 well plate format. This would allow a treatment comparison between cells with endogenous MTF1 or endogenous and overexpressed MTF1 over a 24 hour period. Unlike results where firefly:renilla ratios in cells transfected with the empty control pGL4.40 plasmid were unaffected by treatment (Figure 6.25), there was variation observed between plates (Figure 6.27) independent of both the luciferase plasmid and the cell line used (SW1353 Figure 6.27A and B; linear MTF1 overexpressing SW1353, Figure 6.27C and D). Fortunately, this pattern was roughly consistent for the same cell line treated with the MRE pGL4.40 plasmid (Figure 6.27B versus 6.27A; 6.27D versus 6.27C) which was justification for the normalisation of the MRE pGL4.40 firefly:renilla ratio to the empty control pGL4.40 firefly:renilla ratio for each treatment. The experiment was completed a total of four times with six sextuplicate wells per condition (Figure 6.28). Although the levels of MTF1 are higher in the MTF1-MYC-FLAG cells than normal SW1353 cells, comparable levels of luciferase activity were observed in untreated and IL-1 $\alpha$  conditions. The luciferase (and thus MTF1) activity was higher in the overexpressing cell line compared to normal SW1353 cells after ZnCl<sub>2</sub> stimulation alone (1.3-fold, p=0.0009) or in combination with IL-1 $\alpha$  (2.3-fold, p<0.0001) in Figure 6.28.

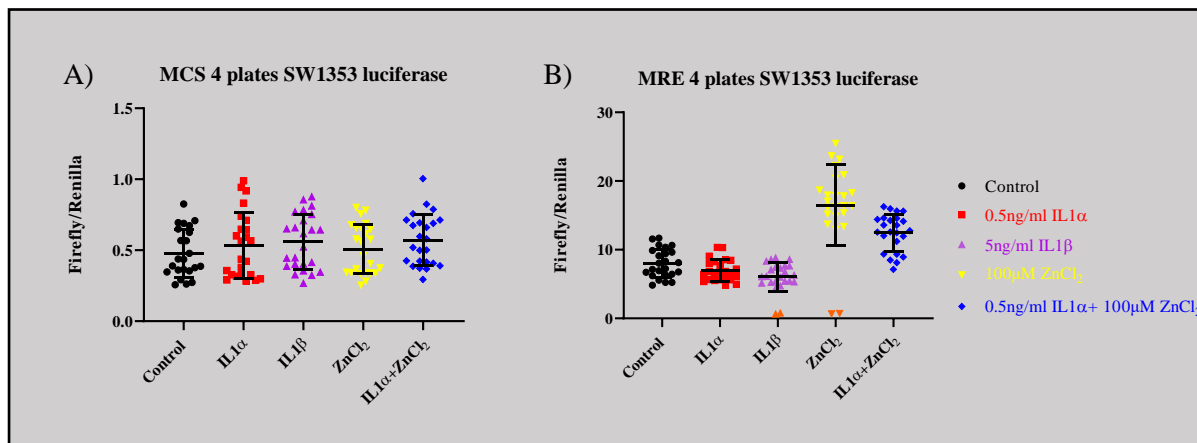


**Figure 6.25 - Raw firefly:renilla ratios from SW1353 cells transiently transfected with empty control pGL4.40 and renilla luciferase or MRE pGL4.40 plasmid and renilla luciferase.**

SW1353 cells transiently transfected with the empty control pGL4.40 plasmid and renilla luciferase A) and SW1353 cells transiently transfected with the MRE pGL4.40 plasmid and renilla luciferase B). Cells were transfected for 24 hours followed by a further 24 hour exposure to medium only or 0.5ng/ml IL-1 $\alpha$ , 5ng/ml IL-1 $\beta$ , 100 $\mu$ M ZnCl<sub>2</sub> or 0.5ng/ml IL-1 $\alpha$  + 100 $\mu$ M ZnCl<sub>2</sub> before luciferase activity was measured. Each coloured symbol is a different treatment with all six technical replicates from four experiments totalling 24 replicate values. Horizontal lines and error bars are the mean and standard deviation respectively. The firefly luciferase data has been normalised to the renilla luciferase to account for any variation in transfection efficiency. Outliers are highlighted in orange.

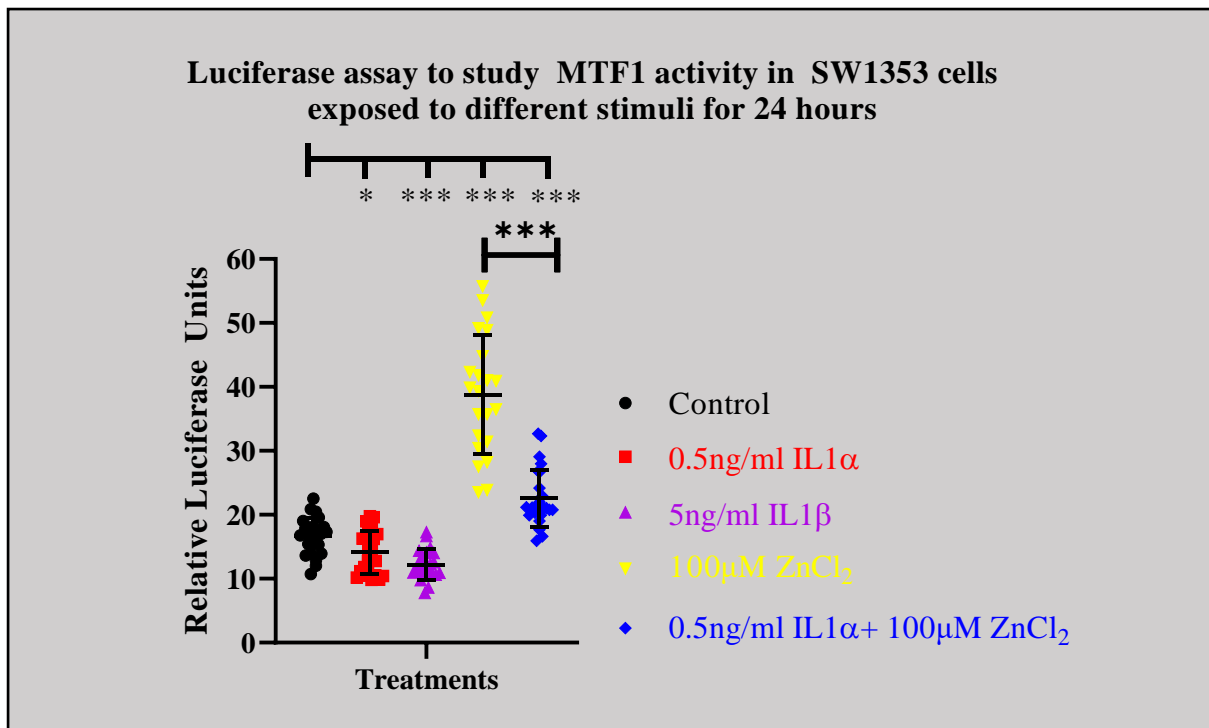


**Figure 6.26 – Luciferase reporter assay measuring MTF1 activity in SW1353 cells treated  $\pm$  IL-1 $\alpha$ , IL-1 $\beta$ , ZnCl $_2$  or IL-1 $\alpha$  + ZnCl $_2$  for 24 hours.**

SW1353 cells seeded and incubated for 24 hours were transfected for an additional 24 hours with either empty or MRE pGL4.40 plasmid then treated in technical sextuplicate with or without IL-1 $\alpha$  (red), IL-1 $\beta$  (purple), ZnCl $_2$  (yellow) or IL-1 $\alpha$  + ZnCl $_2$  (blue) for a further 24 hours. A total of four experiments were conducted. Symbols represent each of 23-24 measurements (after outlier removal) for each treatment across four experiments. The firefly:renilla ratios were analysed for normality by D'Agostino-Pearson omnibus k2 test ( $n > 8$ ) and an unpaired t-test with Welch's correction was conducted or Mann Whitney t-test (IL-1 $\alpha$  vs control). Horizontal lines and error bars are the mean and standard deviation respectively. \*  $p < 0.05$ , \*\*\*  $p < 0.001$ .

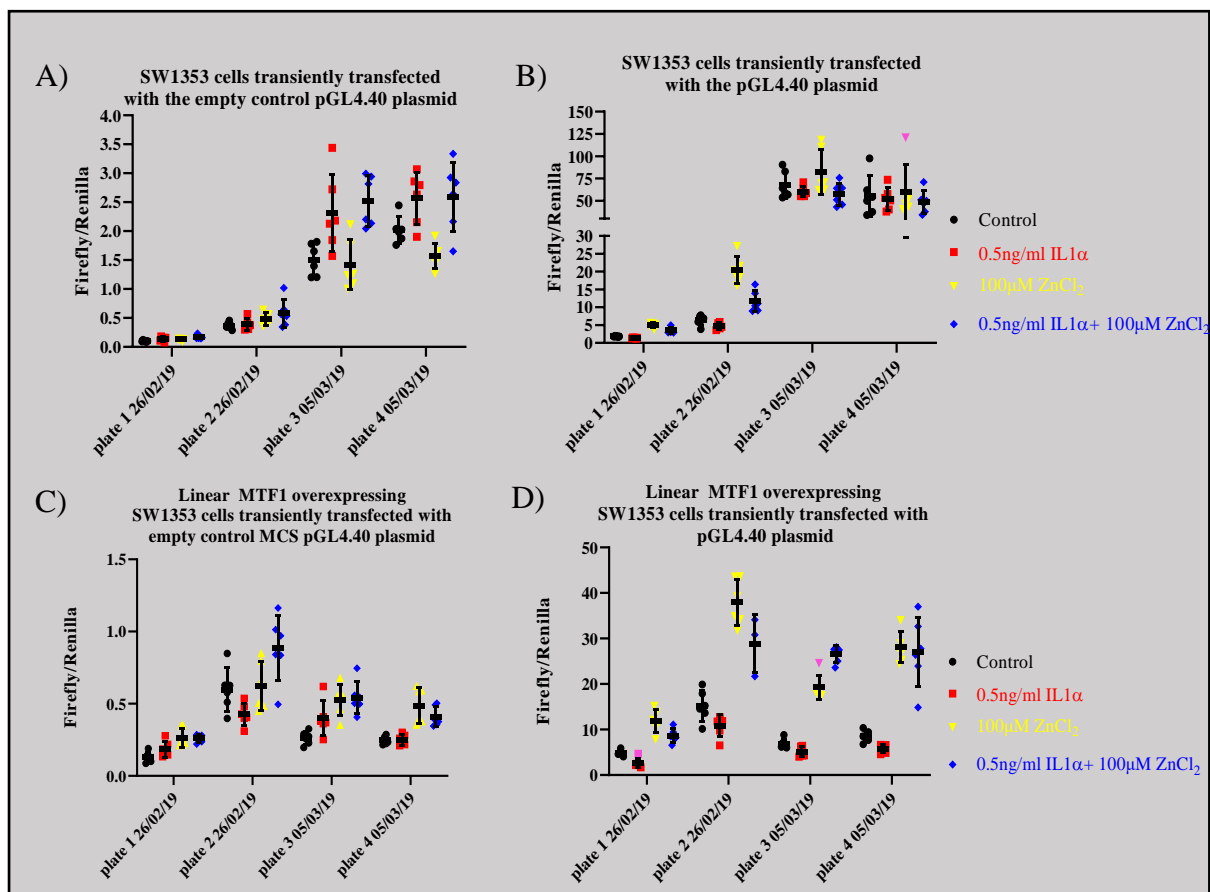


**Figure 6.27 – Raw firefly:renilla ratios from SW1353 cells or linear MTF1 overexpressing SW1353 cells transiently transfected with empty control pGL4.40 and renilla luciferase or pGL4.40 plasmid and renilla luciferase.**

Each graph is the firefly:renilla luciferase data for SW1353 (A and B) or linear MTF1 overexpressing SW1353 cells (C and D) transiently transfected  $\pm$  pGL4.40 plasmid or empty control pGL4.40 plasmid and renilla luciferase for 24 hours. Cells were treated  $\pm$  medium containing IL-1 $\alpha$  and/or ZnCl $_2$  for another 24 hours before the luciferase activity was measured. Each experiment is presented as the plate it was assayed on to determine the variation between the empty control pGL4.40 and pGL4.40 plasmid-treated cells over time and each coloured symbol is a different treatment. Symbols coloured pink are outliers for that sextuplicate measurement determined by addition or subtraction of 1.5 times the interquartile range of the 75<sup>th</sup> or 25<sup>th</sup> percentile respectively. Horizontal lines and error bars are the mean and standard deviation respectively.

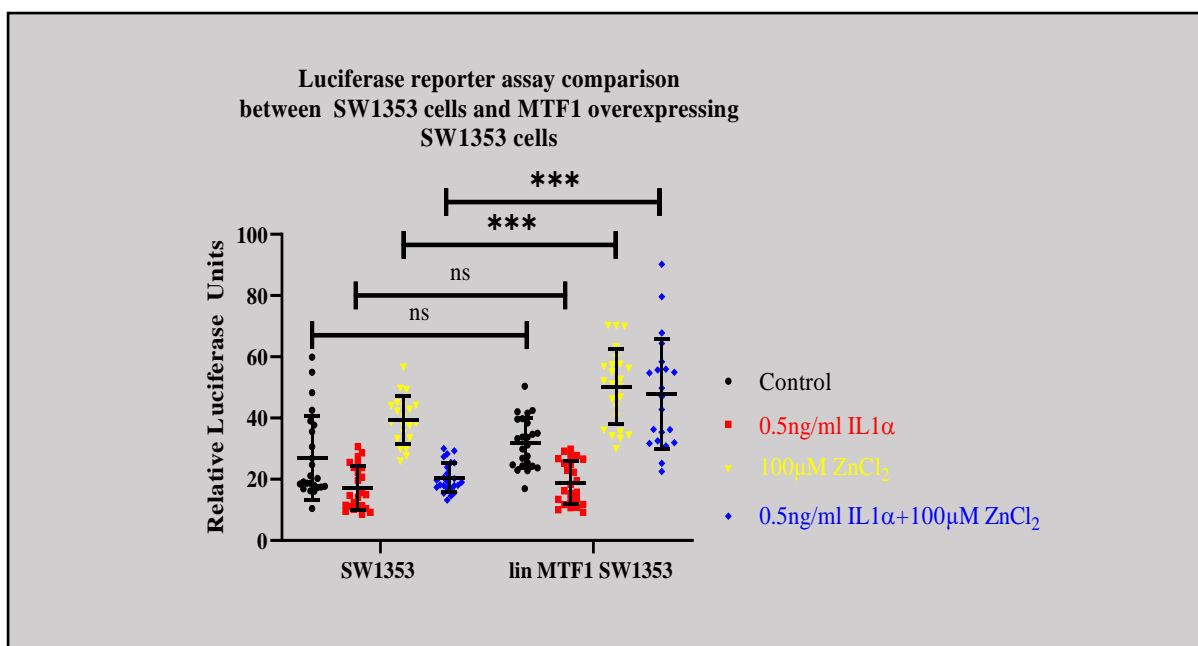


**Figure 6.28 – Luciferase reporter assay comparing SW1353 cells against MTF1 overexpressing SW1353 cells ± IL-1α alone and/or ZnCl<sub>2</sub> for 24 hours.**

SW1353 cells or SW1353 cells overexpressing MTF1 were seeded and incubated for 24 hours and both lines were transfected for an additional 24 hours with either empty or MRE pGL4.40 plasmid then treated in technical sextuplicate with or without IL-1α (red), ZnCl<sub>2</sub> (yellow) or IL-1α + ZnCl<sub>2</sub> (blue) for a further 24 hours. A total of four experiments were conducted. Symbols represent each of 23-24 measurements (after outlier removal) for each treatment across four experiments. Horizontal bars show the mean of each condition and the error bars are standard deviation. Statistical analysis is unpaired t-test with Welch's correction for all pairings except IL-1α which was analysed by Mann-Whitney t test. \*\*\* p<0.001, ns = non-significant.

The nuclear and cytoplasmic western blots in section 6.3.6.2 demonstrated that MTF1 subcellular localisation was different between the 24 and 72 hour time points. The transcriptional activity of the MTF1 protein may therefore be different between these time points. It is not possible to stimulate cells transiently transfected with the luciferase plasmids for 72 hours, and so the stable pGL4.40 luciferase SW1353 cell line was created (section 2.9). Instead of quantifying luciferase activity using a luminometer, the stable pGL4.40 luciferase SW1353 line had MTF1 activity assessed through qPCR measurement of *luciferase* mRNA levels. This was achieved by qPCR using two distinct luciferase assay regions of the open reading frame of the plasmid (LUC2\_ORF1 and LUC2\_ORF2) and through normalisation against the *GAPDH* housekeeping gene only. The *luciferase* mRNA was detected at 7000-fold higher level in the pGL4.40 transfected cell line compared to untransfected SW1353 cells (which do not contain the *luciferase* gene) using luciferase qPCR assay one (Figure 6.29A). Luciferase qPCR assay two achieved a 165-fold increase in *luciferase* in pGL4.40 transfected cells (Figure 6.29B) compared to untransfected SW1353 cells.

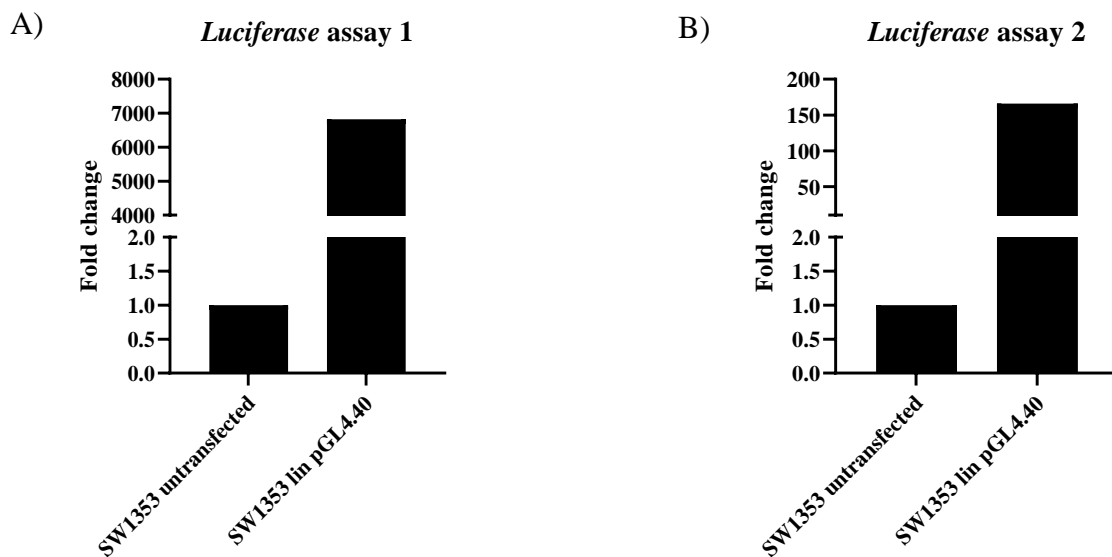


**Figure 6.29 – Assessment of *luciferase* gene expression in stably selected NotI-digested linear transfected pGL4.40 luciferase-overexpressing SW1353 cell line.**

Two qPCR *luciferase* assays (A and B) were utilised to measure *luciferase* gene expression. SW1353 cells were transfected ± NotI-digested linear plasmid or native MRE pGL4.40 plasmid for 24 hours. Cells were expanded from 6 well plates to T25 to T75cm<sup>2</sup> flasks in the presence of 200µg/ml hygromycin B until linear transfected cells were collected. Circular transfected cells were disposed of due to an infection. Bars are the mean of the technical replicate from the qPCR. Lin = AgeI-digested linear MTF1 overexpressing SW1353 cells.

The stable MRE pGL4.40 luciferase expressing SW1353 cells were transiently transfected for 24 hours with the MTF1 plasmid and then the medium removed and replaced with or without 0.5ng/ml IL-1 $\alpha$ , 100 $\mu$ M ZnCl $_2$ , or 0.5ng/ml IL-1 $\alpha$  + 100 $\mu$ M ZnCl $_2$  for 72 hours. As a negative control, cells were mock transfected with FuGENE only. This experiment was only conducted once, with only one T75cm $^2$  flask per condition, and so statistics was not possible. *MTF1* expression was quantified by qPCR using the same primers used in HACs and T/C-28a2 cells. *MTF1* expression was similar for all four conditions in the mock transfected SW1353 MRE pGL4.40 luciferase cell line (Figure 6.30). However, transient transfection of the MTF1 plasmid into the MRE pGL4.40 luciferase expressing SW1353 cells was associated with higher baseline *MTF1* transcript levels by ~500-fold. *MTF1* expression was reduced 0.64-fold in the 0.5ng/ml IL-1 $\alpha$  treated flasks transfected with MTF1 plasmid compared to the untreated transfected control, though this is based on a single flask and so this result should not be overinterpreted.

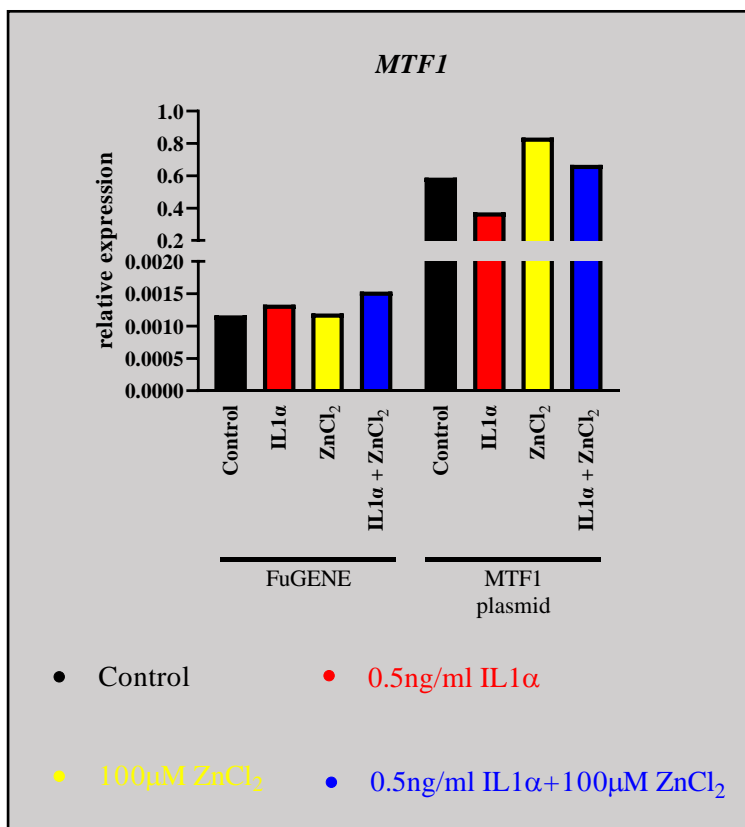


**Figure 6.30 – Normalised *MTF1* gene expression in pGL4.40 luciferase overexpressing SW1353 cells transiently transfected  $\pm$  MTF1 plasmid for 24 hours then treated  $\pm$  IL-1 $\alpha$  alone and/or ZnCl $_2$  for 72 hours.** pGL4.40 luciferase overexpressing SW1353 cells were transfected  $\pm$  MTF1 plasmid for 24 hours before treatment with IL-1 $\alpha$  (red), ZnCl $_2$  (yellow) or IL-1 $\alpha$  + ZnCl $_2$  (blue) for 72 hours. Data is normalised to housekeepers *18S*, *GAPDH* and *HPRT1*. Each bar represents the average normalised expression of the technical qPCR triplicate.

The previous experiments confirmed that the luciferase cell line expresses the *luciferase* gene, and that these cells can be successfully transiently transfected with the MTF1 overexpression construct. Next, luciferase levels (as a readout of MTF1 activity) were measured in the luciferase stable cell line after they were subject to the same stimuli for 72 hours, 24 hours after transient transfection with MTF1 plasmid. Again as this experiment was only performed once in a single T75cm<sup>2</sup> flask per condition, the data in Figure 6.31 represents the mean expression value from three qPCR technical measurements from the same cDNA sample and no statistics could be performed. MTF1 transiently overexpressing cells stimulated for 72 hours with ZnCl<sub>2</sub> alone or in combination with IL-1 $\alpha$  had higher *luciferase* levels (and thus MTF1 activity) than unstimulated or IL-1 $\alpha$ -only stimulated MTF1 overexpressing cells (Figure 6.31). However, these are merely observations from a single T75cm<sup>2</sup> flask and for meaningful interpretation this experiment ideally would have been repeated so that there was at least three biological replicates for statistical analysis.

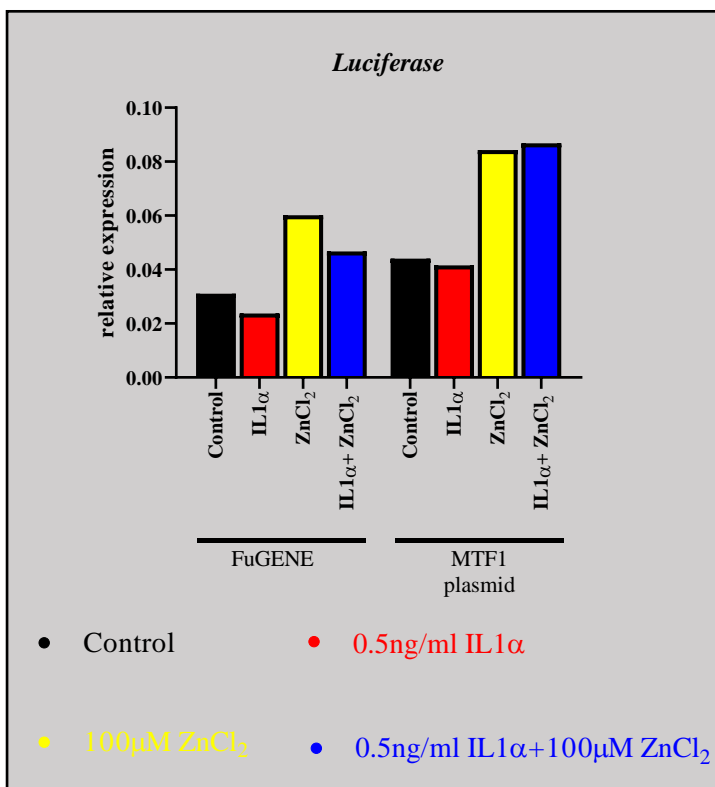


**Figure 6.31 – Normalised *luciferase* gene expression in pGL4.40 luciferase overexpressing SW1353 cells transiently transfected  $\pm$  MTF1 plasmid for 24 hours then treated  $\pm$  IL-1 $\alpha$  alone and/or ZnCl<sub>2</sub> for 72 hours.**

pGL4.40 luciferase overexpressing SW1353 cells were transfected  $\pm$  MTF1 plasmid for 24 hours before treatment with IL-1 $\alpha$  (red), ZnCl<sub>2</sub> (yellow) or IL-1 $\alpha$  + ZnCl<sub>2</sub> (blue) for 72 hours. Data is normalised to housekeepers *18S*, *GAPDH* and *HPRT1*. Each bar represents the average normalised expression of the technical qPCR triplicate.

### 6.3.8 Does metallothionein gene expression change in response to IL-1 $\alpha$ stimulation in SW1353 cells?

*MT1A* and *MT1G* were next studied to investigate if IL-1 $\alpha$  induced *MT* expression which would be indirect evidence for increased MTF1 activity and is a potential mechanism to buffer against potential alterations to intracellular zinc ion concentrations. The selection of *MT1A* and *MT1G* from the eight *MT* genes qPCR assays that had been designed against was based on Rushton *et al.*, 2015 work identifying these genes alongside inflammatory genes as highly expressed in a subcluster of OA hip cartilage patients with differential patterns in DNA methylation. This decision was representative for the *MT* expression change elicited by IL-1 $\alpha$  in HACs (4.3.6). Treatment of SW1353 cells with 0.5ng/ml IL-1 $\alpha$  for 72 hours resulted in significant upregulation of both *MT1A* and *MT1G* (2.5-fold, p=0.0019 and 4.6-fold, p=0.001 respectively) (Figure 6.32A and B). The heatmap in Figure 6.32C summarises the *MT1A* and *MT1G* gene expression fold change from IL-1 $\alpha$ -treated flasks compared to control for the same experiment and compares fold changes across all five experiments. While *MT1A* fold change was similar across all experiments, *MT1G* fold change was highest (8.6 and 6.9-fold upregulated) in the first two experiments which were the cDNAs provided by Dr. Reynard (Appendix F).

Two experiments totalling three to four biological replicates per treatment per time point in which both *MT1A* and *MT1G* expression was assessed after IL-1 $\alpha$  exposure for 24, 72 (P1), 144 (P2) and 216 (P3) hours and its removal from SW1353 cells for a final 72 hour passage (288 hour, P4) was conducted. There was no significant difference in *MT1A* expression between IL-1 $\alpha$  and control in passages containing IL-1 $\alpha$  nor when IL-1 $\alpha$  was removed for a final 72 hours (Figure 6.33A). *MT1G* was significantly upregulated (7.7-fold, p=0.0117) after 72 hours but not at any other time point. The fold changes of IL-1 $\alpha$  compared to control summarised for both experiments at each passage is presented in the heatmap in Figure 6.33C. Next, an experiment was conducted to compare ZnCl<sub>2</sub> with IL-1 $\alpha$ -mediated *MT* responses as a positive control for *MT* induction. Though this experiment was only conducted once with two biological replicates without statistical analysis, IL-1 $\alpha$  appeared to promote *MT1A* upregulation (Figure 6.33D), whereas ZnCl<sub>2</sub> might lead to *MT1G* upregulation (Figure 6.33E).

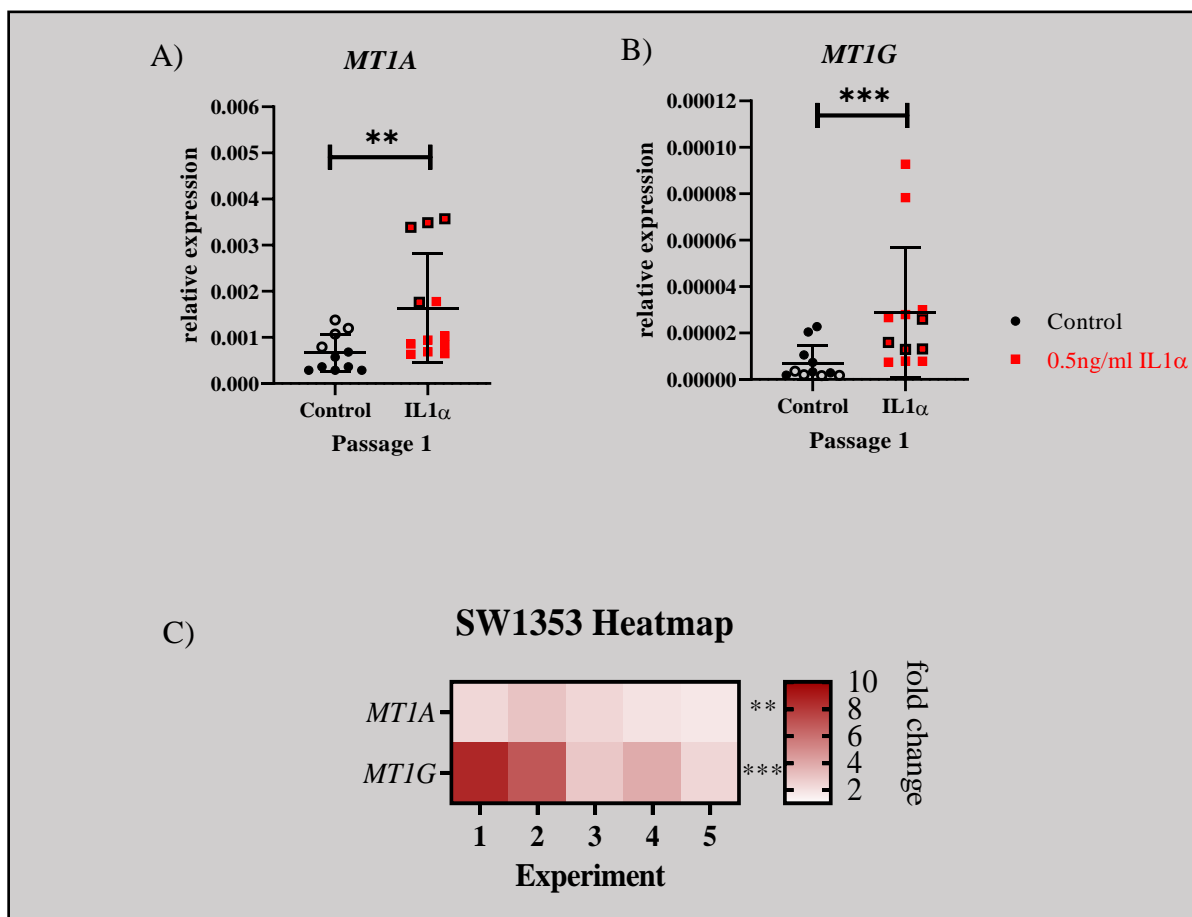


**Figure 6.32 – *MTIA* and *MTIG* gene expression is significantly upregulated by IL-1 $\alpha$  after a 72 hour passage in SW1353 cells.**

The relative gene expression changes for *MTIA* A) and *MTIG* B) were normalised to housekeeper genes *18S*, *GAPDH* and *HPRT1* after 72 hours of treatment with 0.5ng/ml IL-1 $\alpha$ . Heatmap summarising IL-1 $\alpha$ -mediated *MT* gene expression fold changes relative to controls after one passage lasting 72 hours for each of five experiments C). Red indicates differential fold change upregulation with IL-1 $\alpha$ , and white represents no change with IL-1 $\alpha$ . Normalised data satisfying a D'Agostino-Pearson omnibus k2 normality (*MTIA*) test was analysed with a paired t-test, and *MTIG* analysed by Wilcoxon t-test. Symbols represent the mean of three qPCR technical replicates for each flask from every biological replicate from five experiments. Unfilled circular dots and solid-bordered square symbols (A and B) are Dr Reynard's cDNA samples. Horizontal lines are the group mean and error bars are standard deviation. \*\* p<0.01 \*\*\* p<0.0001.

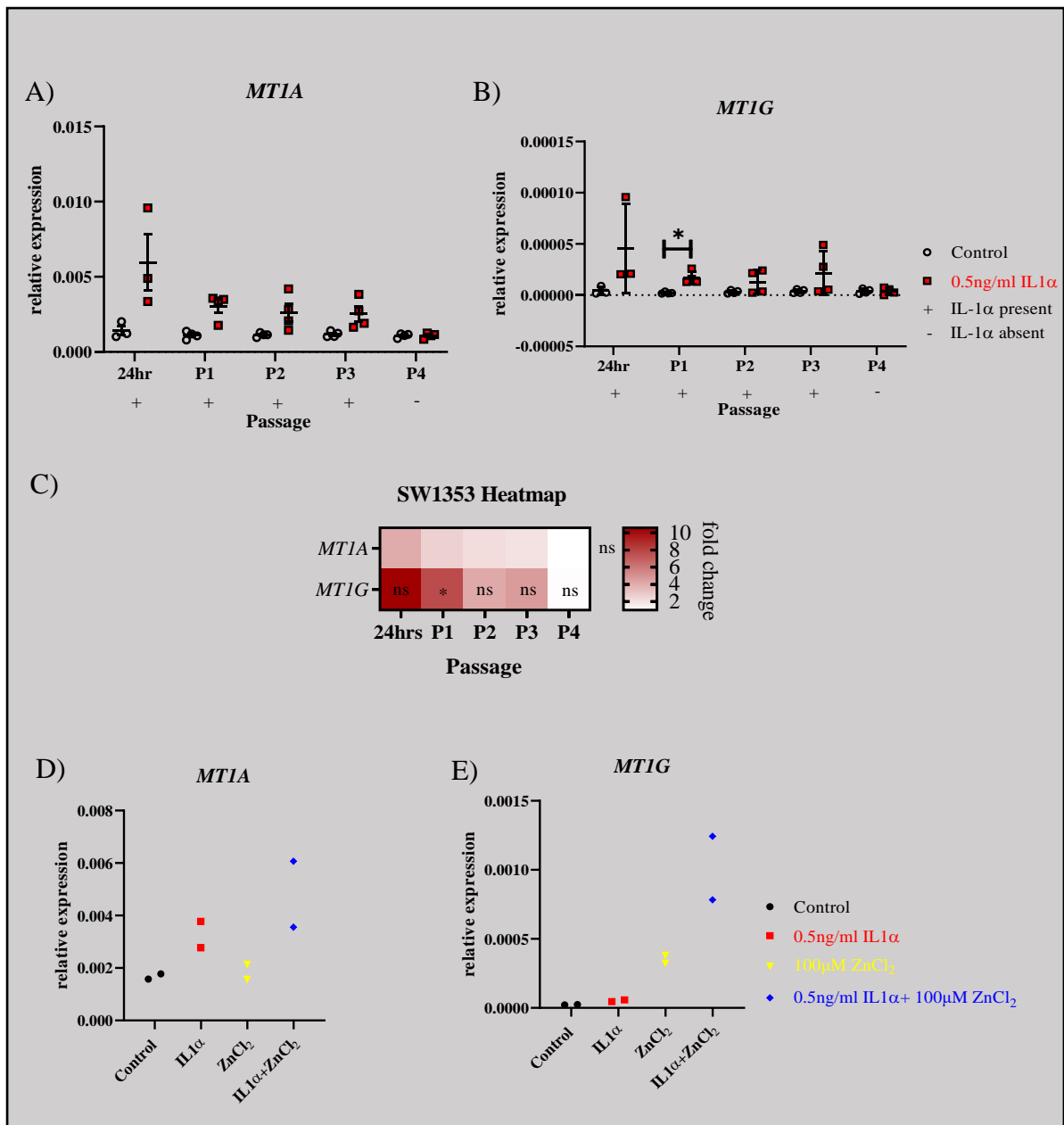


**Figure 6.33 - *MTIG* and not *MTIA* was upregulated after P1 in IL-1 $\alpha$  time course experiments and effects of ZnCl<sub>2</sub> treatment alone or with IL-1 $\alpha$  on *MTIA* and *MTIG* expression were undetermined in SW1353 cells.**

The relative gene expression of *MTIA* A) and *MTIG* B) normalised to housekeeper genes *18S*, *GAPDH* and *HPRT1*. Heatmap summarising IL-1 $\alpha$ -mediated *MT* gene expression fold changes relative to controls after three passages with IL-1 $\alpha$  present and one passage without IL-1 $\alpha$  C). Red indicates differential fold change upregulation with IL-1 $\alpha$ , and white represents no change with IL-1 $\alpha$ . The relative gene expression of *MTIA* and *MTIG* genes following IL- $\alpha$ , ZnCl<sub>2</sub> or both treatments of SW1353 cells treated in biological duplicate for 72 hours (D and E respectively). Normalised data satisfying a Shapiro Wilk normality test prior to or after log<sub>2</sub> transformation was analysed with a paired t-test. Where the data was not normal a Wilcoxon t-test of the normalised data was conducted (24 hour – *MTIG*, P1 – *MTIA*). Symbols represent mean of three qPCR technical replicates for each flask from every biological replicate across one (D and E) or two experiments (A, B and C). Horizontal lines are the group mean and error bars are standard deviation. \* p<0.05 ns = non-significant.

### 6.3.9 Does cartilage matrix-degrading gene expression change in response to IL-1 $\alpha$ and ZnCl<sub>2</sub> stimulation in SW1353 cells?

The effect of IL-1 $\alpha$  on cartilage matrix-degrading gene expression in SW1353 cells was assessed next and in a later experiment ZnCl<sub>2</sub> was used alongside IL-1 $\alpha$  as a positive control testing activation of the zinc-ZIP8-MTF1 axis. *MMP13* expression was significantly upregulated 30.1-fold (p=0.001) after 72 hours following IL-1 $\alpha$  treatment (Figure 6.34A), though this increase was more prominent in cDNAs derived from Dr Reynard's two experiments than my own. *ADAM-TS5* gene expression on the other hand was extremely low (average Ct <35) both in my own SW1353 cDNA samples and those from Dr. Reynard's experiments, and was low independent of treatment. Thus, for some samples either an entire technical triplicate failed detection or even loss of one replicate meant an average could not be calculated and both outcomes meant that reliable data was not generated for this gene across all experiments (Figure 6.34B). The heatmap in Figure 6.34C illustrates the log<sub>2</sub> fold *MMP13* and *ADAM-TS5* gene expression changes for IL-1 $\alpha$ -treated flasks compared to controls for five experiments.

Two experiments totalling four biological replicates per treatment per time point in which both *MMP13* and *ADAM-TS5* expression was assessed after IL-1 $\alpha$  exposure for 24, 72 (P1), 144 (P2) and 216 (P3) hours and its removal from SW1353 cells for a final 72 hour passage (288 hour, P4) was conducted. *ADAM-TS5* expression (Figure 6.35A) between IL-1 $\alpha$  and control in P3 was significantly downregulated (0.4-fold, p = 0.013) and *MMP13* expression (Figure 6.36B) was significantly different from control at P4 (1.2-fold p = 0.0405). The log<sub>2</sub>-fold change of *MMP13* and *ADAM-TS5* gene expression for IL-1 $\alpha$ -treated flasks compared to controls for both experiments at each time point is presented as a heatmap but no significant differences were observed (Figure 6.35C). Finally, one experiment was conducted with two flasks per condition in which ZnCl<sub>2</sub> was included with or without IL-1 $\alpha$  to determine the role of zinc in cartilage matrix-degrading gene expression regulation. As this experiment was not repeated, statistics could not be conducted, however it was very clear from the data that ZnCl<sub>2</sub> did not influence the expression of either *ADAM-TS5* or *MMP13* and that IL-1 $\alpha$  provided the stimulus for upregulation in the combined treatment (Figure 6.35D). *ADAM-TS5* was not measured in the experiment with ZnCl<sub>2</sub> due to the consistently high Cts measured previously which had taught me from prior experiments that calculating Ct means was a problem especially if one or more measurements from the technical triplicate failed to amplify.

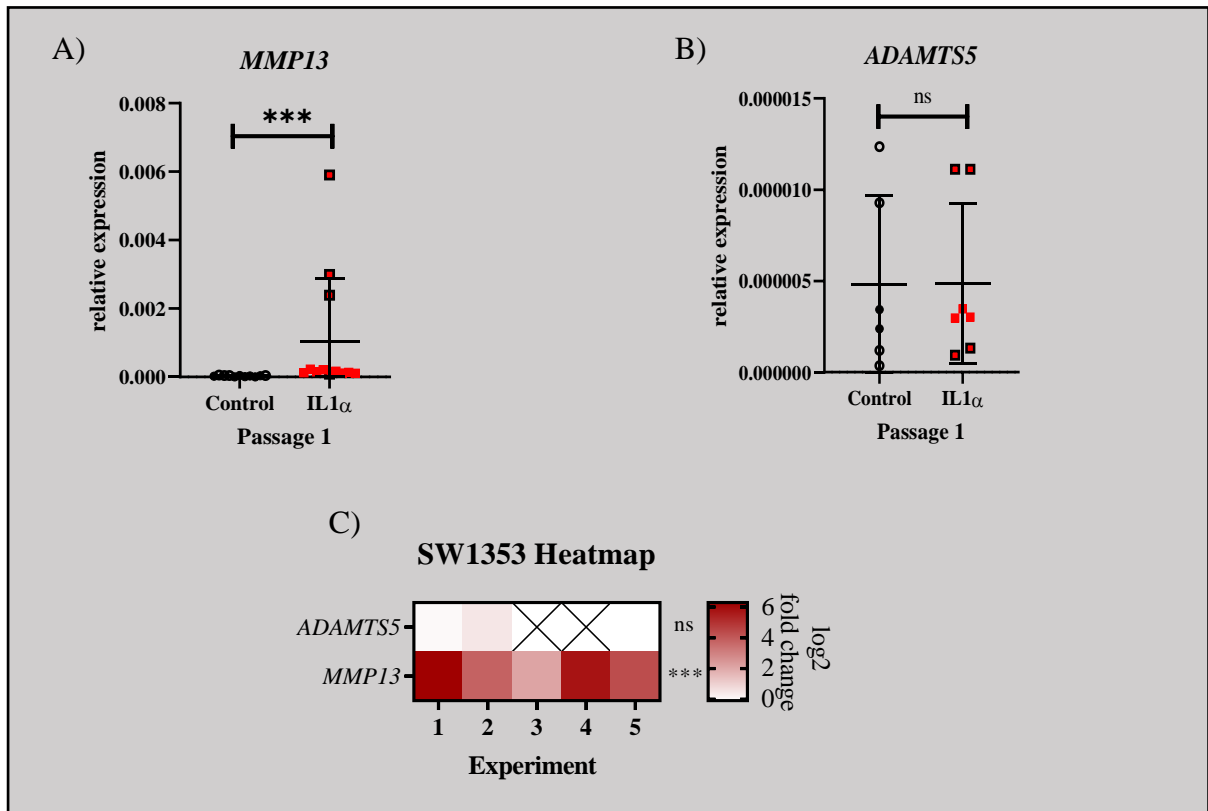


**Figure 6.34 – *MMP13*, but not *ADAM-TS5* is significantly upregulated by IL-1 $\alpha$  after a 72 hour passage in SW1353 cells.**

The relative gene expression changes for *MMP13* A) and *ADAM-TS5* B) normalised to housekeeper genes *18S*, *GAPDH* and *HPRT1* after 72 hours of treatment with 0.5ng/ml IL-1 $\alpha$ . Heatmap summarising IL-1 $\alpha$ -mediated *ADAM-TS5* and *MMP13* gene expression fold changes relative to controls after one passage lasting 72 hours for each of five experiments C). Red indicates differential fold change upregulation with IL-1 $\alpha$ , and white represents no change with IL-1 $\alpha$ . Normalised data or log<sub>2</sub> transformed data satisfying a D’Agostino-Pearson omnibus k<sub>2</sub> normality test was analysed with a paired t-test. Symbols represent the mean of three qPCR technical replicates for each flask from every biological replicate from five (A) or three (B) experiments respectively. Horizontal lines are the group mean and error bars are standard deviation. Unfilled circular dots and solid-bordered square symbols (A and B) are Dr Reynard’s cDNA samples. \*\*\* p =0.001, ns = non-significant.

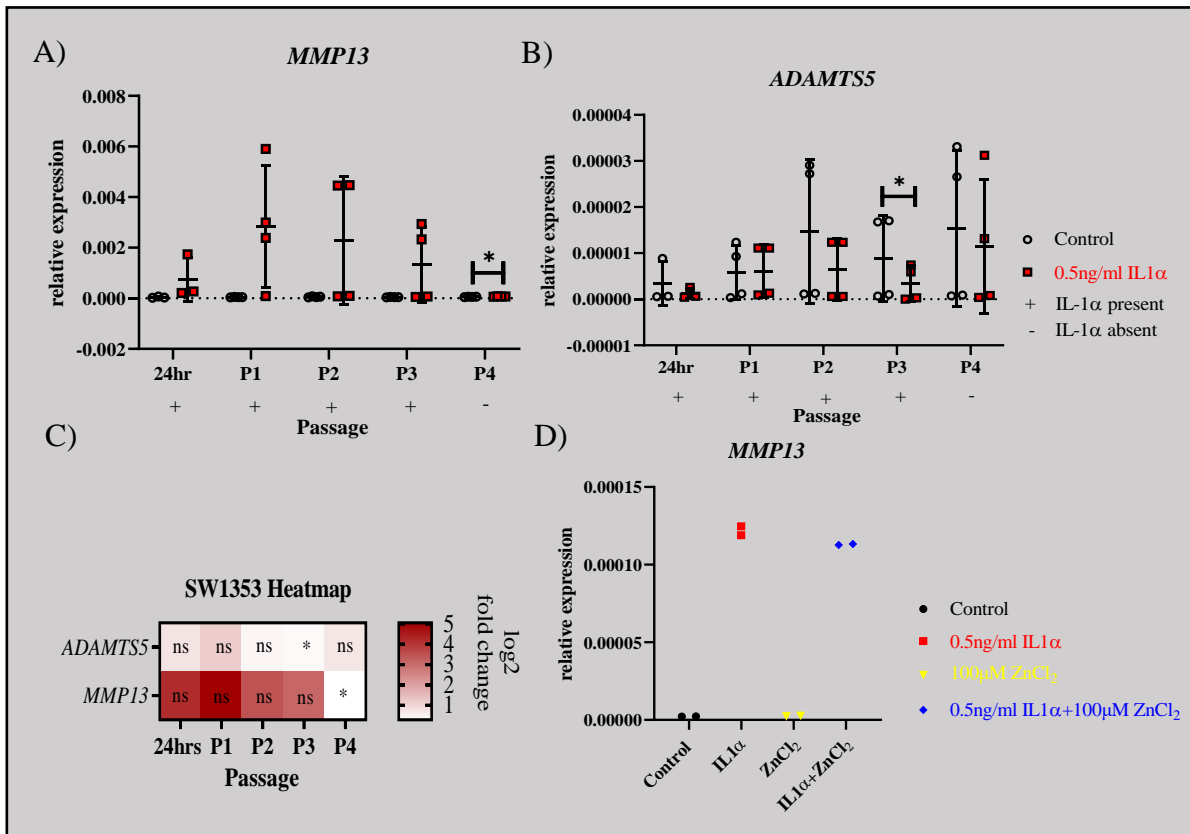


**Figure 6.35 - *MMP13* and *ADAM-TS5* were not upregulated in IL-1 $\alpha$  time course experiments and effects of ZnCl<sub>2</sub> treatment alone or with IL-1 $\alpha$  on matrix-degrading gene expression were undetermined in SW1353 cells.**

A) and B) is relative gene expression of *MT1A* and *MT1G* genes normalised to housekeeper genes *18S*, *GAPDH* and *HPRT1*. C) Heatmap summarising IL-1 $\alpha$ -mediated cartilage matrix-degrading gene expression log<sub>2</sub> fold changes relative to controls after three passages with IL-1 $\alpha$  present and one passage without IL-1 $\alpha$ . Red indicates differential fold change upregulation with IL-1 $\alpha$ , and white represents no change with IL-1 $\alpha$ . D) is the relative gene expression of *MMP13* following IL- $\alpha$ , ZnCl<sub>2</sub> or both treatments of SW1353 cells treated in biological duplicate for 72 hours. Normalised data satisfying a Shapiro Wilk normality test prior to or after log<sub>2</sub> transformation was analysed with a paired t-test. Where the data was not normal a Wilcoxon t-test of the normalised data was conducted (P2 – *ADAM-TS5* and *MMP13*). Symbols represent the mean of three qPCR technical replicates for each flask from every biological replicate across one (D and E) or two experiments (A, B and C) and bars are the mean relative expression per group. Horizontal lines are the group mean and error bars are the standard deviation. \* p<0.05, ns = non-significant.



## 6.4 Chapter summary

While there was evidence that IL-1 $\alpha$  treatment of SW1353 cells activated transcription of classic pro-inflammatory genes and both *SLC39A8* and *SLC39A14* zinc transporters, this did not translate to classical activation of the zinc-ZIP8-MTF1 axis. For example, metal ion assessment after IL-1 $\alpha$  treatment using the MAK032 zinc assay kit resulted in no detectable change in intracellular ion content. However, there was transcriptional feedback on the *MTF1* gene (1.3-fold p=0.0464), but this did not translate to increased MTF1 activity determined by luciferase reporter assay. In fact, IL-1 $\alpha$  was consistently repressing transcription of the luciferase reporter both when MTF1 was present at endogenous levels and when MTF1 was overexpressed. I was confident the luciferase reporter assay worked as expected as ZnCl<sub>2</sub> positive control resulted in significant *luciferase* activity. Despite the challenges of MTF1 protein detection in SW1353 cells, use of c-myc-FLAG-tagged MTF1 in MTF1 overexpressing SW1353 cells did provide evidence of MTF1 trafficking between cytoplasmic and nuclear compartments based on western blot data, though it was not clear that any treatment further influenced the protein cytoplasmic levels at 72 hours. As *MTs* are inducible in response to multiple physiological stimuli and have different response elements in their promoter sequences controlling transcription (Davis and Cousins, 2000), it is plausible that IL-1-mediated *MT* gene transcription occurs through MTF1-independent transcription factor recruitment. A summary schematic for the zinc-ZIP8-MTF1 axis activity in SW1353 cells is presented in Figure 6.36.

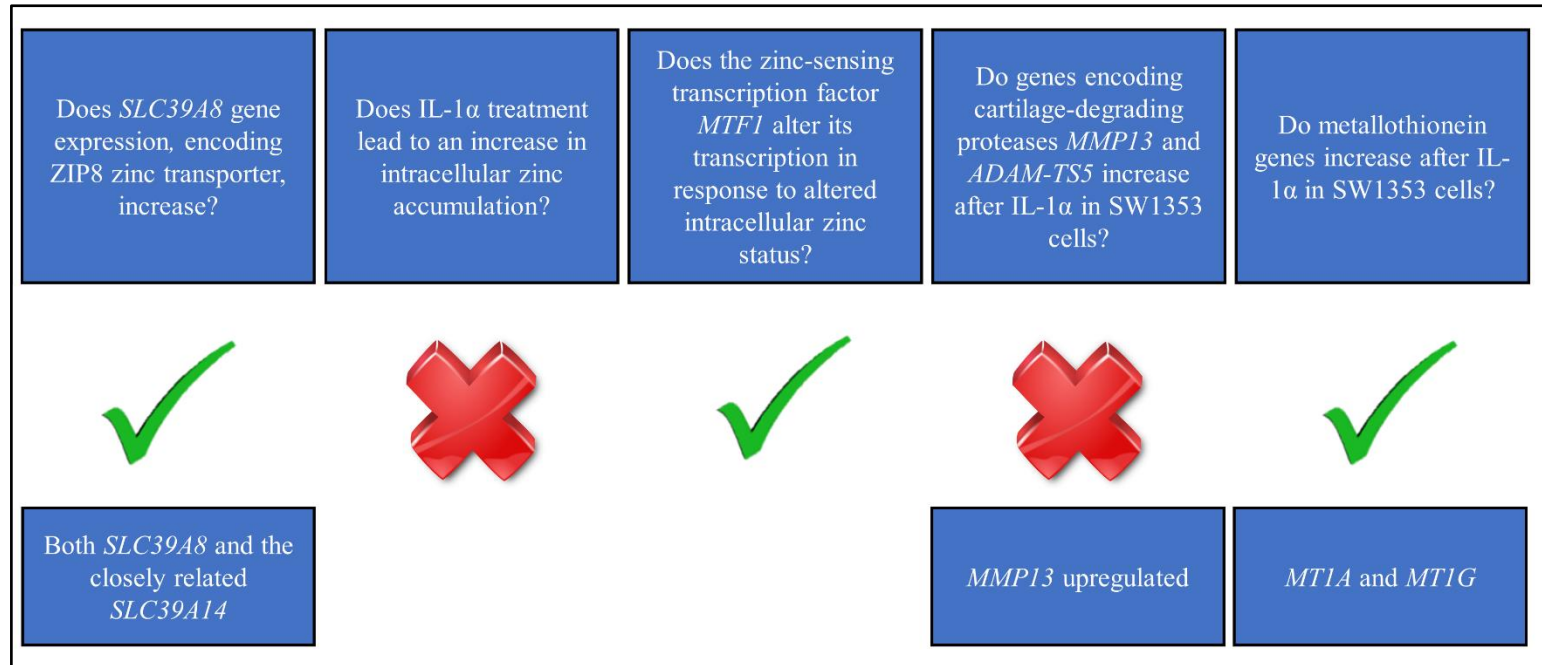


**Figure 6.36 – Summary of zinc-ZIP8-MTF1 axis exploration in SW1353 cells.**

## Chapter 7. DISCUSSION

The aim of this research was to determine whether zinc homeostasis is disrupted in human OA chondrocytes and whether this contributes to disease pathogenesis. Although the role of zinc homeostasis in OA pathogenesis has not been studied in human chondrocytes, several lines of evidence suggest that it may play a role in disease. Firstly, the zinc-ZIP8-MTF1 signalling axis, acts as a facilitator of OA pathogenesis following joint trauma. This pathway was discovered in murine chondrocytes that were exposed to IL-1 *in-vitro* and confirmed using several ZIP8 and MTF1 overexpression and deletion mouse models (Kim *et al.*, 2014). Several genes in this pathway are modified in terms of cartilage DNA methylation and gene expression in a subgroup of OA hip patients (Rushton *et al.*, 2015). Furthermore, recent GWAS for OA and related endophenotypes have identified three different risk loci that map to or encompass zinc transporter genes (Castano-Betancourt *et al.*, 2016; Styrkarsdottir *et al.*, 2018; Zengini *et al.*, 2018; Tachmazidou *et al.*, 2019). Together, these data suggest that altered zinc homeostasis may contribute to OA pathogenesis, at least in a subgroup of patients.

The potential role of zinc in OA was initially investigated in chapter three using existing human and murine OA cartilage and chondrocyte gene expression datasets available on the SkeletalVis tool (Soul *et al.*, 2018b). In addition to looking at genes involved in the zinc-ZIP8-MTF1 pathway, I broadened the search criteria to account for the diversity of zinc transporters and MTs associated with the mammalian genome. The principal discovery from the transcriptomics analysis was that among the zinc transporters, *SLC39A14* was the most consistently differentially expressed and was upregulated in ipsilateral damaged OA cartilage and IL-1 treated chondrocytes of human and murine origin. *SLC39A14* was downregulated in intact OA cartilage and *SLC39A8* was also downregulated in a transgenic mouse that spontaneously develops OA at 18 weeks which contradicts the role for ZIP8-mediated zinc entry and cartilage erosion identified by Kim *et al.*, 2014. These results support the possibility that *SLC39A14* is a principal zinc importer in human chondrocytes exposed to IL-1, but that *SLC39A14* facilitates zinc entry, only once the cartilage becomes damaged. Several *MTI* isoforms were also upregulated in the damaged human cartilage and IL-1-treated chondrocytes, so this may be a response to the damage by protecting chondrocytes from further apoptosis (Kim *et al.*, 2014; Won *et al.*, 2016) or may just correlate with the damage.

Chapter three also investigated if the OA and mjsw SNPs impacted on expression of nearby zinc transporter genes using the databases LDlink (<https://ldlink.nci.nih.gov/?tab=home>) and GTEx ([gtexportal.org/home/](https://gtexportal.org/home/)). Matched expression and genotype data from hundreds of individuals from 54 different healthy tissue types was available in GTEx. This was used to determine if SNPs identified through recent OA and mjsw GWAS meta-analyses are associated with eQTLs of nearby zinc transporters *SLC30A5* (rs1041753 mjsw), *SLC30A10* (rs2820436, rs2785988, rs2820433 all OA-associated) and *SLC39A8* (rs13107425 OA-associated).

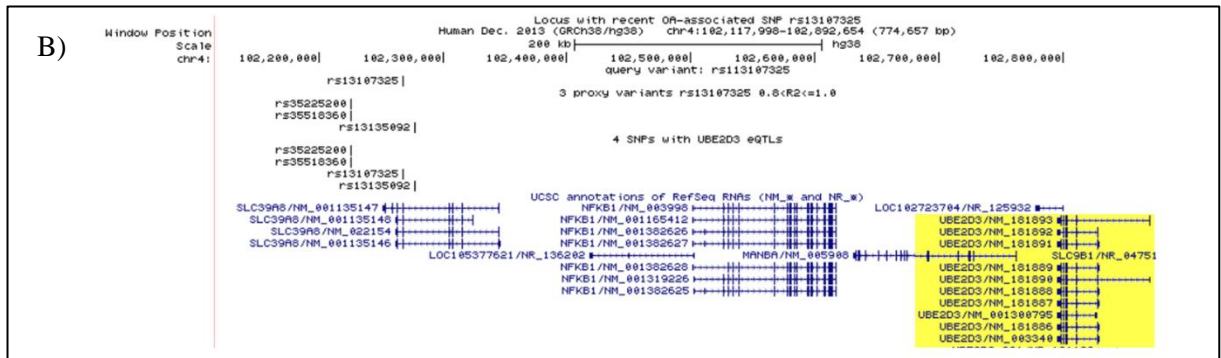
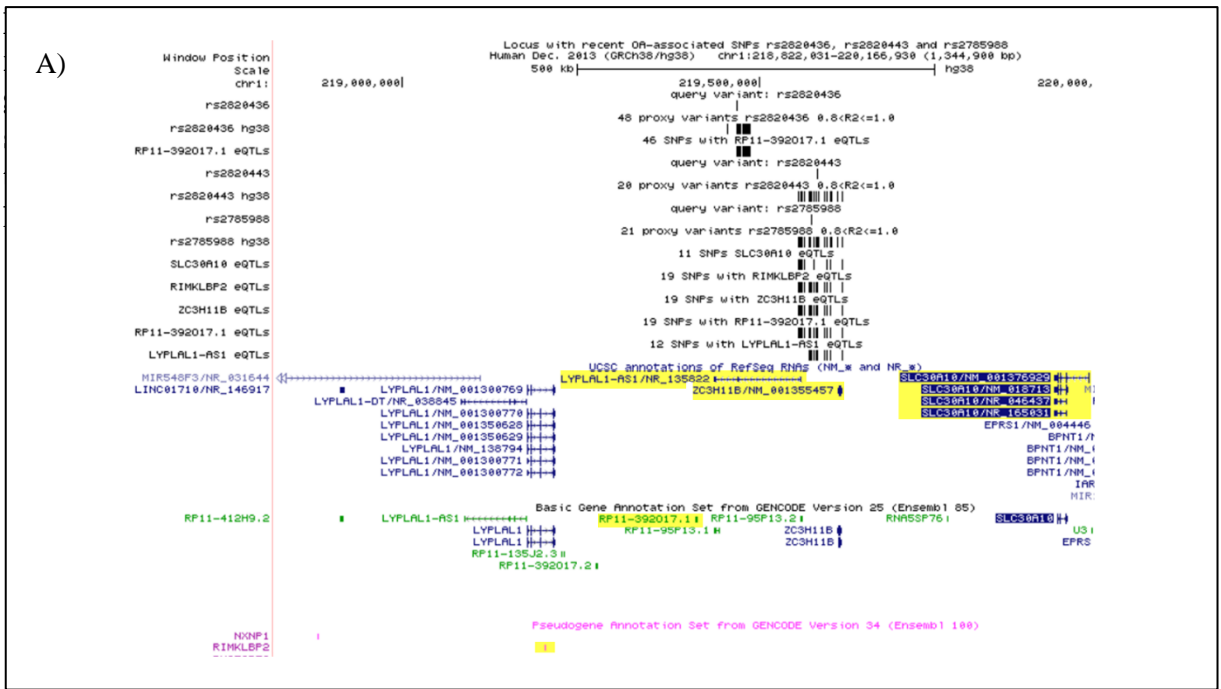
Four hundred and seventy-nine unique eQTLs for *SLC30A10* were identified in multiple tissues on GTEx, 11 of which were associated with SNPs at either rs2820443 (nine SNPs) or rs2785988 (two SNPs) loci. There were no *SLC30A10* eQTLs identified for the list of SNPs in LD with rs2820436, nor were any SNPs identified with eQTLs for *SLC30A5* or *SLC39A8* using rs1041753 and rs13107425 lists respectively. Thus, the 11 SNPs with *SLC30A10* eQTLs in UV-exposed skin of the lower leg cannot be assumed to translate to skeletal tissues because of the tissue-specific nature of eQTLs.

Additional eQTLs unrelated to the homeostasis of zinc but in LD with the OA or mjsw-associated risk SNPs were identified in GTEx (Table 8.1). These were not discussed in the chapter three results because the relevance of these genes to zinc homeostasis is unknown. For each SNP and its associated proxy variants, either single or multiple eQTLs in one or more tissues were identified, often with eQTLs overlapping the OA-GWAS SNPs identified at chromosome one nearby *SLC30A10* (Table 8.1, Figure 8.1A). This was because SNPs rs2820443 and rs2785988 were in high LD with each other ( $r^2=0.98$ ) but rs2820436 was not in high LD ( $r^2=0.45$ ) with either of these SNPs. The number of SNPs associated with each eQTL which overlap with the sentinel SNP and its proxy variants is shown in brackets and if the sentinel SNP was among the identified eQTLs an asterisk indicates this (Table 8.1). Furthermore, the eQTL was stratified by the tissue it was identified in from GTEx, for example 46 of 49 SNPs in LD with the sentinel SNP rs2820436 had an eQTL for *RP11-392O17.1* of which 18 were found to be operational in the transverse colon. This analysis does not go further to address the direction of gene expression influenced by the SNPs associated with the eQTL, but as eQTLs are tissue-specific it would not make sense to do this until skeletal tissues become available to study. The SNPs and eQTLs for OA (nearby *SLC39A8*) or mjsw (*SLC30A5*)-associated risk are presented as uploaded tracks in the UCSC browser in Figures 8.1B and 8.2.

**Table 8.1 – eQTLs for recently identified OA or hip mjsw-associated risk in proximity to zinc transporters.**

Of the five OA or hip mjsw-risk variants recently identified, only rs2820443 and rs2785988 had an eQTL with their proximal zinc transporter (in this instance *SLC30A10* marked by an asterisk) in addition to a further 10 and 11 proxy variants in LD ( $r^2 \geq 0.8$ ) with each sentinel SNP respectively. Otherwise, seven genes had eQTLs for one or more of the five risk SNPs and the number of proxy variants with eQTLs for that gene and in which tissues are indicated in brackets.

GWAS SNP + (no. LD proxy variants $R^2 = 0.8$ )	Reference	Clinical endophenotype	Proximal zinc transporter	eQTL-associated gene(s) on GTEx (no. LD proxy variants)	Tissue(s) associated with eQTL (no. SNPs in LD ( $R^2 = 0.8$ ) with SNP in column 1)
rs2820436 (48)	Zengini, E <i>et al.</i> , 2018	OA (across any joint site)	<i>SLC30A10</i> *	<i>RP11-392O17.1</i> * (46)	UV-exposed skin lower leg * (46)
					no UV exposed suprapubic skin * (46)
					kidney cortex * (46)
					Adipose subcutaneous * (45)
					Adrenal gland * (46)
rs2820443 (20)	Tachmazidou, I. <i>et al.</i> , 2019	OA (knee and hip)	<i>SLC30A10</i> *	<i>RP11-392O17.1</i> * (18)	Transverse colon * (18)
					UV-exposed skin lower leg * (10)
					<i>SLC30A10</i> (10)
					Testis * (18)
					<i>ZC3H11B</i> * (18)
					Artery-Aorta * (12)
					<i>LYPLALI-AS1</i> * (12)
					UV-exposed skin lower leg * (18)
					no UV exposed suprapubic skin * (18)
					Adrenal gland (7)
rs2785988 (21)	Styrkarsdottir, U. <i>et al.</i> , 2018	OA (hip)	<i>SLC30A10</i> *	<i>RP11-392O17.1</i> * (19)	Kidney cortex (6)
					Adipose subcutaneous (6)
					<i>RIMKLBP2</i> * (18)
					Adipose-subcutaneous * (18)
					<i>SLC30A10</i> (11)
					UV-exposed skin lower leg * (11)
					<i>ZC3H11B</i> * (19)
					Testis * (19)
					<i>LYPLALI-AS1</i> * (12)
					Artery-Aorta * (12)
rs13107325 (3)	Tachmazidou, I. <i>et al.</i> , 2019	OA	<i>SLC39A8</i>	<i>UBE2D3</i> * (4)	UV-exposed skin lower leg * (19)
					no UV exposed suprapubic skin * (19)
					Adrenal gland (8)
					Kidney cortex (7)
					Adipose subcutaneous (7)
rs10471753 (32)	Castaño-Betancourt, M.C. <i>et al.</i> , 2016	Hip minimal joint space width	<i>SLC30A5</i>	<i>CTC-537E7.2</i> * (29)	Adipose subcutaneous * (19)
					Testis * (29)
					minor salivary gland * (26)
				<i>MARVELD2</i> (2)	Prostate (21)
					oesophagus (3)
					Testis (2)
					minor salivary gland (2)
prostate (2)					
oesophagus (2)					



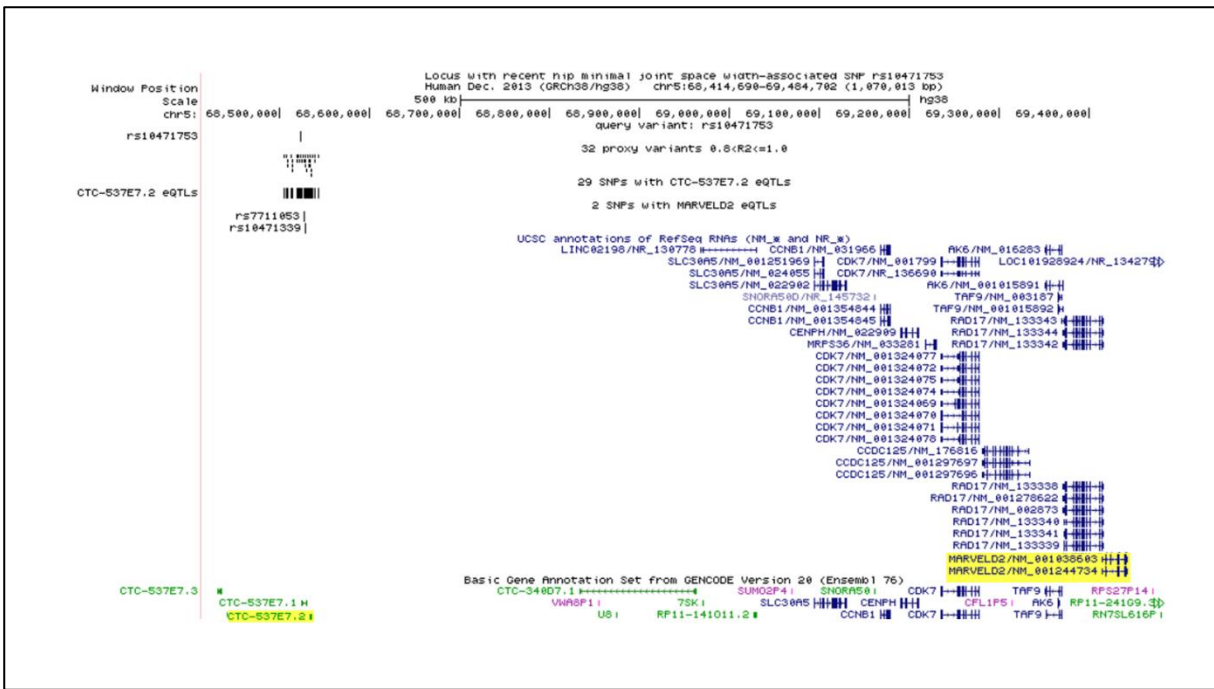


**Figure 8.2 – Visualisation of the hip mjsw-associated risk SNP rs10471753 nearby *SLC30A5* using the UCSC genome browser.**

Uploaded tracks for the genomic coordinates of rs10471753, proxy variants in LD ( $r^2 \geq 0.8$ ) with rs10471753, and the SNPs for which the named eQTL were described are presented. The gene sequences for the region shown are in blue and the highlighted yellow genes and long intergenic non-coding RNAs are the eQTLs.

Next, I decided to use specific datasets in SkeletalVis to explore the expression of these genes for which eQTLs had been identified in GTEx. The data in Table 8.2 provides information about the expression of the genes in OA hip and knee cartilage or in IL-1 $\beta$ -treated HACs from OA hip in relation to the five GWAS SNPs. Data in bold is where a fold change and significant p value was recorded from SkeletalVis and either TPM, normalised microarray signals or read counts are shown dependent on the platform (microarray or RNA-Seq) used by the researchers. The three long non-coding RNAs (lncRNA) *RP11-392O17.1*, *LYPLALI-AS1*, and *CTC-537E7.2* were not identified in any of the knee and hip transcriptomic datasets nor in the study by Pearson *et al.*, 2016, which was conducted to identify differentially expressed lncRNA in hip OA chondrocytes. However, *RIMKLBP2* was significantly downregulated (0.32-fold, p=0.001873) in IL-1 $\beta$ -treated HACs compared to untreated controls, though this was classified as a pseudogene and its role in OA is not known. The most compelling gene with which an eQTL was associated with SNPs in LD and including rs13107325 was *UBE2D3*, which was significantly downregulated in the hip and knee cartilage datasets, except for the ipsilateral knee OA cartilage analysis by Dunn *et al.*, 2016 (Table 8.2). *UBE2D3* encodes ubiquitin-conjugating enzyme E2 D3 which can interact with E3 ligases which catalyse the ubiquitination of target protein substrates. I do not know what the protein targets of UBE2D3 are in cartilage nor if possession of the rs13107325 risk allele confers further reduced *UBE2D3* expression in OA cartilage. What the functional consequence is for the presumably reduced ubiquitination of UBE2D3 targets in cartilage tissue should be followed up.

**Table 8.2 – Gene expression information for each eQTL associated with SNPs in proximity to zinc transporters in hip and knee OA cartilage and hip OA chondrocytes.** Details of the samples for each RNA-Seq or microarray are provided in the column headings and either TPM (transcripts per million), fold changes and p-values, normalised microarray signals or normalised read counts for the data are provided. All data was sourced from SkeletalVis, apart from the TPM data for the Ajekigbe *et al.*, 2019 study which had already been provided to me by our bioinformatician, Dr. Kathleen Cheung.

Locus	OA or MJSW-associated SNPs	eQTL gene(s)	gene biotype	Ajekigbe <i>et al.</i> , 2019		Dunn <i>et al.</i> , 2016		Fisch <i>et al.</i> , 2018		Soul <i>et al.</i> , 2018		Xu <i>et al.</i> , 2012		Pearson <i>et al.</i> , 2016											
				Hip OA cartilage (n=10)	NOF cartilage (n=6)	Knee dOA cartilage (n=8)	Knee iOA cartilage (n=8)	Knee iOA cartilage (n=20)	Knee non-OA cartilage (n=18)	Knee iOA cartilage (n=60)	Knee non-OA cartilage (n=10)	Hip iOA cartilage (n=12)	NOF cartilage (n=13)	IL1-β treated chondrocytes (4 hours, n=3 donors)	Untreated chondrocytes (4 hours, n=3 donors)										
Chr1	rs2820436, rs2820443, rs2785988	<i>RP11-332D17.1</i>	lincRNA	TPM		NA	NA	NA	NA	NA	NA	NA	NA	NA											
	rs2820443, rs2785988	<i>LYPLAL1-AS1</i>	lincRNA	TPM		NA	NA	NA	NA	NA	NA	NA	NA	NA											
	rs2820443, rs2785988	<i>FAMK1LBP2</i>	pseudogene	1.37	1.42	NA	NA	NA	NA	NA	NA	FC IL-1β vs untreated	adj. p value												
	rs2820443, rs2785988	<i>ZC3H1B</i>	protein-coding	FC (OA vs NOF)	adj. p value	NA	NA	NA	NA	NA	NA	0.32	1.87E-03												
				TPM								normalised read counts	NA												
				0.17	0.13								FC IL-1β vs untreated	adj. p value											
				1.05	0.979																				
Chr4	rs13107325	<i>UBE2D3</i>	protein-coding	FC (OA vs NOF)	adj. p value	UBE2D3 probe 1	FC (dOA vs iOA)	adj. p value	FC (iOA vs non-OA)	adj. p value	FC (iOA vs non-OA)	adj. p value	UBE2D3 probe 1	FC (iOA vs non-OA)	adj. p value	FC IL-1β vs untreated	adj. p value								
				0.57	2.0569E-15													0.67	7.11E-04	0.64	2.58E-10	1.00	NA		
				TPM														normalised read counts		normalised read counts		UBE2D3 probe 2	0.99	NA	
				157.70	246.40													6.76	7.42	10.26	10.82	UBE2D3 probe 3	0.70	3.6E-08	
												UBE2D3 probe 4	0.51	7.8E-11											
				normalised microarray signals									9.28	9.57											
Chr5	rs10471753	<i>MARVELD2</i>	protein-coding	TPM		<i>MARVELD2</i> probe 1	FC (dOA vs iOA)	adj. p value	FC (iOA vs non-OA)	adj. p value	FC (iOA vs non-OA)	adj. p value	<i>MARVELD2</i> probe 1	FC (iOA vs non-OA)	adj. p value	FC IL-1β vs untreated	adj. p value								
				0.00	0.00													NA	NA	NA	NA	NA	NA		
				1.51	0.270													1.17	0.649	0.67	0.233	1.23	0.8608	1.05	NA
				0.77	0.506													0.90	0.873	0.93	0.769	1.06	0.9112	1.00	NA
												<i>MARVELD2</i> probe 2	0.98	0.497	1.14	0.748									
												<i>MARVELD2</i> probe 3													

The *in silico* transcriptomic analysis in chapter three indicated that genes involved in zinc homeostasis are dysregulated in human OA tissue and in cultured HACs after responses to IL-1. I therefore investigated this *in vitro* in chapters four through six, focussing on analysing the zinc-ZIP8-MTF1 pathway in end-stage knee OA chondrocytes (chapter four) and in the human chondrogenic T/C-28a2 cell line (chapter five) and SW1353 human chondrosarcoma cell line (chapter six). The aim of these chapters was to understand if IL-1 ligands (principally IL-1 $\alpha$  but also a few experiments with IL-1 $\beta$ ) altered zinc homeostasis gene expression and what the downstream consequence of this was on expression of cartilage matrix-degrading genes in human chondrocytes as has been reported in murine chondrocytes (Kim *et al.*, 2014). The IL-1-responsive positive control genes *IL-6*, *CXCL8* and *CCL2* were universally upregulated by IL-1 $\alpha$  across HACs and cell lines and IL-1 $\alpha$  elicited a similar gene expression response profile as IL-1 $\beta$  when used at a concentration ten times lower than IL-1 $\beta$ . These genes' upregulation in response to IL-1 is not a novel finding but was an indicator that cells were responding to the stimulus in a predictable manner. In HACs, IL-1 $\alpha$  exposure for one passage was associated with reduced HAC cell numbers compared to untreated HACs from the same donor, with reduced expression of the proliferation genes *MKI67*, *TOP2A* and *TPX2* following IL-1 $\alpha$  stimulation. However, based on cell counts, there was no differences in cell number between SW1353 and T/C-28a2 cells treated with and without IL-1 $\alpha$ , indicating that the inhibitory effect of IL-1 $\alpha$  on proliferation was restricted to HACs.

Assessment of zinc transporter gene expression after one passage of IL-1 $\alpha$  treatment in HACs revealed *SLC39A8* and *SLC39A14* to be the most prominently upregulated of all the zinc transporters, consistent with the *in silico* SkeletalVis results. However, *SLC39A14* was specifically upregulated for T/C-28a2 cells whereas *SLC39A8* and *SLC39A14* was upregulated in SW1353 cells. *SLC39A8* upregulation was similarly observed in hip OA cartilage (Rushton *et al.*, 2015) but *SLC39A14* upregulation reported here is a novel finding. The differences in zinc transporter expression between primary HACs and cell lines in response to IL-1 may reflect differing zinc homeostasis requirements dependent on the needs of the tissue from which the chondrocyte originates. For example, T/C-28a2 rib chondrocytes and SW1353 chondrosarcoma of the humerus differ from knee-derived HACs which may have a unique zinc transporter expression profile in response to mechanical stress-induced IL1 $\alpha$  release following chondrocyte cell death.

Only HACs had elevated intracellular metal ion content after one passage with IL-1 $\alpha$  with no increase observed for T/C-28a2 or SW1353 cells. I am cautious when describing the resulting metal ion increases for HACs as solely attributable by zinc because I demonstrated the chemistry and resulting absorbance could be influenced by iron ions in cell-free experiments. The iron chelator, 2,2'-bipyridine, was unable to reduce this influence in additional cell-free experiments using the MAK032 zinc assay kit. Overall, there was no consensus that IL-1 $\alpha$  stimulation resulted in measurable changes in intracellular zinc content with the spectrophotometry kit employed.

In murine chondrocytes, IL-1 stimulated upregulation of *Slc39a8* expression and increased intracellular zinc leads to increased nuclear translocation and activation of MTF1 transcription factor, although expression of the gene is unchanged (Kim *et al.*, 2014). The expression, subcellular localisation and activity of MTF1 was thus measured after IL-1 $\alpha$  treatment in human chondrocytes using a combination of qPCR, western blot and luciferase reporter assays. There was no evidence that *MTF1* gene expression was altered in response to IL-1 $\alpha$  in HACs, but *MTF1* was significantly upregulated (1.3-fold p=0.0464) in SW1353 cells after IL-1 $\alpha$ . *MTF1* expression was shown to increase after four hours in the IL-1 $\beta$  transcriptomic datasets (Moazedi-Fuerst *et al.*, 2016; Pearson *et al.*, 2016). Perhaps the disparity between the cell lines and HACs might be explained by the difference in the time after IL-1 exposure at which *MTF1* expression was measured. In this thesis, *MTF1* was measured in HACs after 10-13 days of IL-1 $\alpha$  and in T/C-28a2 and SW1353 cell lines after 72 hours with IL-1 $\alpha$ , so was not comparable. Furthermore, all HAC samples were cultured to confluency for a variable 7-20 days (dependent on the donor) prior to the passage with IL-1 $\alpha$ , suggesting that in addition to differing duration of IL-1 $\alpha$  exposure, HAC dedifferentiation is likely to have occurred which could further contribute to this or indeed any gene expression difference. This observation that *MTF1* gene expression was for the most part unchanged after IL-1 $\alpha$  was not entirely unexpected because Kim *et al.*, 2014 also did not see changes in *Mtf1* gene or protein expression when murine chondrocytes were transduced with Ad-ZIP8 for 2 hours and incubated for 24 hours. Although the mechanism by which *SLC39A8* was overexpressed differs for our approaches (Ad-ZIP8 versus IL-1), the observation that *Mtf1* did not change was consistent, at least in HACs and T/C-28a2 cells.

In murine chondrocytes, IL-1 induced *Slc39a8* overexpression and increased cytoplasmic zinc levels. IL-1 is associated with increased nuclear localisation of MTF1 transcription factor. I thus investigated if IL-1 also triggers MTF1 nuclear translocation in human chondrocytes. Unfortunately, the antibody used by Kim *et al.*, 2014 was no longer available, and so I used two different commercially available antibodies against MTF1. Despite my concerted best efforts, I was unable to detect endogenous MTF1 protein by western blot in HACs having trialled both commercial N and C-terminal antibodies. The size of MTF1 quoted by the manufacturers did not match with protein bands observed in western blots during their validation procedure. These antibodies did not detect an endogenous protein of the correct size in either HACs or the cell lines but were able to detect a band in MTF1 overexpressed lysate derived from HEK293 cells, albeit one larger than the expected size. The MTF1 overexpression lysate (LC401804) which was used as a positive control consistently presented with two bands with the C-terminal antibody. I believe a cleavage of the protein had occurred within the C-terminal epitope where a potential metalloproteinase cleavage of an alanine at position 511 generated bands of the observed size. Despite the protease inhibitor cocktails and RIPA buffer prepared for whole protein extraction not containing EDTA (a metalloproteinase inhibitor) the lysate was prepared from HEK293 with RIPA containing EDTA by the manufacturer, so I am unable to explain this observation.

Fortunately, the use of the c-myc-FLAG-tagged MTF1 plasmid and the FLAG antibody enabled detection of overexpressed MTF1 in the SW1353 cell line. Furthermore, overexpressing c-myc-FLAG-tagged MTF1 in HEK293 in-house resulted in the same band observed between positive control and samples of AgeI-digested linear MTF1 overexpressing SW1353 cells. The shuttling of MTF1 was confirmed by western blot as MTF1 was present in the cytoplasm of MTF1 overexpressing SW1353 cells 24 hours after treatment and in the nucleus at 72 hours. IL-1 $\alpha$  alone or with ZnCl<sub>2</sub> increased cytoplasmic MTF1 content but not ZnCl<sub>2</sub> alone. There was no clear effect of treatment on the enrichment of nuclear MTF1 content at 72 hours.

As well as increased nuclear translocation, Kim *et al.*, 2014 saw greater transcriptional activity of MTF1 after Ad-ZIP8 transduction or metal chloride treatment by luciferase reporter assay. Therefore, I began an investigation into whether IL-1 $\alpha$  might alter MTF1 protein activity using a pGL4.40 luciferase reporter construct containing five MRE consensus sites assay in T/C-28a2 and SW1353 cells.

There was no significant increase in MTF1 transcriptional activity after IL-1 $\alpha$  treatment detected by luciferase reporter assay in T/C-28a2 cells. However, ZnCl<sub>2</sub> treatment triggered increased MTF1 transcriptional activity, presumably via the known mechanism of zinc-induced MTF1 recruitment to MREs of target genes, in this case driving the expression of the reporter gene *luciferase*. This indicates that the MRE luciferase assay was working as expected. The combined treatment of IL-1 $\alpha$  + ZnCl<sub>2</sub> also produced greater MTF1 transcriptional activity than IL-1 $\alpha$  alone or after no treatment but less so than ZnCl<sub>2</sub> alone. An inhibitory effect of IL-1 $\alpha$  on MTF1 transcriptional activity was observed in SW1353 cells treated with IL-1 $\alpha$  or IL-1 $\beta$  for 24 hours using the same luciferase assay and this effect persisted in luciferase assays using SW1353 cells stably overexpressing MTF1. This finding was unexpected and may suggest MTF1 association at the MRE sites in the pGL4.40 luciferase reporter was altered, though this was not investigated. It was undetermined whether stable luciferase overexpressing cell lines transiently transfected with MTF1 plasmid and treated with IL-1 $\alpha$  and/or ZnCl<sub>2</sub> for 72 hours resulted in increased MTF1 transcriptional activity by measuring *luciferase* gene expression. This was because the experiment was conducted once with each cell line so statistics was not possible.

MTs are MTF1 target genes and have shown to have pleiotropic effects in cartilage of mice *in vivo*. For example, *Mt1* and *Mt2* is upregulated following Ad-ZIP8 or Ad-MTF1 upregulation and double *Mt* knockout results in worse OA cartilage lesions after DMM surgery compared to wild type DMM operated mice and compared to *Mt1/2* double knockout sham-operated mice. Furthermore, the cartilage lesions were associated with increased chondrocyte apoptosis but not in increased *Mmp* gene expression. Thus, MTs are chondroprotective, at least up to a limit, whereby *Mt2* but not *Mt1* aberrant overexpression causes worse OA cartilage lesions independently of the zinc-ZIP8-MTF1 axis (Won *et al.*, 2016). Thus, I wanted to investigate if IL-1 $\alpha$  affected *MT* expression in HACs and cell lines. *MT1* isoforms, *MT1A* and *MT1G*, were upregulated in both HACs and SW1353 cells but *MT1A* alone was increased in T/C-28a2 cells consistent with the SkeletalVis findings. The expression of the other *MT1* isoforms were not reliably detected across samples from HACs and cell lines, despite successful primer validation. *MT1A* and *MT1G* were measured consistently between the HACs and cell lines and were focussed on because these genes were significantly expressed in a subcluster of OA hip cartilage from patients with differential promoter methylation compared to hip cluster one and NOF cartilage (Rushton *et al.*, 2015). As alluded to in the chapter five summary, the degree to which *MT1A* and *MT1G* upregulation was dependent on *MTF1* was not investigated by siRNA-mediated knockdown of *MTF1* experiments because of time limitations. This experiment may have provided evidence for crosstalk between the IL-1 $\alpha$  and zinc-ZIP8-MTF1 signalling pathways and a novel hypothesis may be that knockdown of *MTF1* would have had consequences for *MT* gene expression and subsequent heavy metal detoxification and oxidative stress management. However, given that MTF1 transcriptional activity was not increased by IL1 treatment in either cell line where activity could be measured using the MRE luciferase reporter assay, this suggest that the IL-1-induced upregulation of *MT1A* is independent of MTF1.

In murine chondrocytes, *Mmp13* and *Adam-ts5* are upregulated when ZIP8 and/or MTF1 is overexpressed. This upregulation is thought to be responsible for the increased cartilage degradation observed in Ad-MTF1 and Ad-ZIP8 mice compared to control mice that occurs after surgical induction of OA. However, it is unclear if these genes contain MRE elements in the control regions and are thus direct targets of the MTF1 transcription factor, or if MTF1-related upregulation is an indirect effect. In human chondrocytes and chondrocyte cell lines, upregulation of *ADAM-TS5* and *MMP13* by IL-1 $\alpha$  was by no means consistent across the different cell types investigated. I have already mentioned how treatment duration and dedifferentiation may have contributed to differences in gene expression, but another contributing factor could be that HACs or cell lines were not cultured in serum-free medium prior to stimulation with IL-1 nor throughout the culture period with IL-1 $\alpha$ .

Evidence for crosstalk between the IL-1 $\alpha$  and zinc-ZIP8-MTF1 signalling pathways has been illustrated in immune cells where NF- $\kappa$ B-regulated *SLC39A8* gene expression increases labile intracellular zinc which feeds back negatively on I $\kappa$ B kinase complex (IKK) preventing I $\kappa$ B phosphorylation and further activation of the NF- $\kappa$ B pathway (Liu *et al.*, 2013). This negative feedback loop, if present in chondrocytes, may be an attempt to offset the pro-inflammatory, ROS-inducing and cartilage matrix-degrading effects of NF- $\kappa$ B and for the requirement of ZIP8-mediated zinc antioxidative action. Huang *et al.*, 2018 demonstrated the antioxidative properties of zinc in protecting rats from monosodium iodoacetate (MIA)-mediated cartilage destruction and mimicked the protective effects when co-administered with MIA in SW1353 chondrosarcoma (Huang *et al.*, 2018). For example, serum taken from rats receiving MIA and zinc had decreased pro-inflammatory and cartilage matrix-degrading gene expression while simultaneously increasing anti-inflammatory *IL-10* and the antioxidant GSH compared to mice receiving MIA alone.

In conclusion, the data I have generated does not suggest that IL-1 $\alpha$ -mediated activation of zinc-ZIP8-MTF1 signalling results in cartilage matrix-degrading gene expression in chondrocytes. As the experiments were designed to address IL-1 $\alpha$ -mediated activation of the pathway, the overlap, or not as may be the case, between NF- $\kappa$ B or MTF1-driven responses on cartilage matrix-degrading gene expression was unanswered. IL-1 $\alpha$ -mediated *SLC39A8* and *SLC39A14* overexpression had functional consequences in terms of elevated intracellular zinc ions in HACs but further research exploring which response, pro-catabolic or chondroprotective antioxidative free-radical scavenging and metal sequestration, following zinc increase is required to define the zinc-ZIP8-MTF1 axis contribution to human OA pathogenesis. The SkeletalVis transcriptomic analysis indicates that various proteins involved in zinc homeostasis are dysregulated in OA cartilage, and that more work addressing the functional impact of the five GWAS OA and hip mjsw risk SNPs on zinc transporter gene expression, or indeed expression of genes with eQTLs for the five SNPs, is required. There remain many questions on the role of zinc in OA which should be further explored.

## Chapter 8. BIBLIOGRAPHY

Ajekigbe, B., Cheung, K., Xu, Y., Skelton, A.J., Panagiotopoulos, A., Soul, J., Hardingham, T.E., Deehan, D.J., Barter, M.J. and Young, D.A. (2019) 'Identification of long non-coding RNAs expressed in knee and hip osteoarthritic cartilage', *Osteoarthritis Cartilage*, 27(4), pp. 694-702.

Andreini, C., Banci, L., Bertini, I. and Rosato, A. (2006) 'Counting the zinc-proteins encoded in the human genome', *J Proteome Res*, 5(1), pp. 196-201.

Apte, S.S. (2009) 'A disintegrin-like and metalloprotease (reprolysin-type) with thrombospondin type 1 motif (ADAMTS) superfamily: functions and mechanisms', *J Biol Chem*, 284(46), pp. 31493-7.

Archer, C.W., Dowthwaite, G.P. and Francis-West, P. (2003) 'Development of synovial joints', *Birth Defects Res C Embryo Today*, 69(2), pp. 144-55.

Artells, E., Palacios, Ò., Capdevila, M. and Atrian, S. (2013) 'Mammalian MT1 and MT2 metallothioneins differ in their metal binding abilities', *Metallomics*, 5(10), pp. 1397-410.

Arthritis Research UK (2013) *Osteoarthritis in general practice*. Chesterfield: Keele University UK, A.R. [Online]. Available at: <https://www.versusarthritis.org/media/2115/osteoarthritis-in-general-practice.pdf>.

ATCC SW 1353 [SW 1353, SW1-353] (ATCC HTB-94) [Internet]. Available at: [https://www.lgcstandards-atcc.org/Products/All/HTB-94.aspx?geo\\_country=gb](https://www.lgcstandards-atcc.org/Products/All/HTB-94.aspx?geo_country=gb) (Accessed: 26/09/19).

Attur, M., Belitskaya-Lévy, I., Oh, C., Krasnokutsky, S., Greenberg, J., Samuels, J., Smiles, S., Lee, S., Patel, J., Al-Mussawir, H., McDaniel, G., Kraus, V.B. and Abramson, S.B. (2011) 'Increased interleukin-1 $\beta$  gene expression in peripheral blood leukocytes is associated with increased pain and predicts risk for progression of symptomatic knee osteoarthritis', *Arthritis Rheum*, 63(7), pp. 1908-17.

Babelova, A., Moreth, K., Tsalastra-Greul, W., Zeng-Brouwers, J., Eickelberg, O., Young, M.F., Bruckner, P., Pfeilschifter, J., Schaefer, R.M., Gröne, H.J. and Schaefer, L. (2009) 'Biglycan, a danger signal that activates the NLRP3 inflammasome via toll-like and P2X receptors', *J Biol Chem*, 284(36), pp. 24035-48.

- Bateman, J.F., Rowley, L., Belluoccio, D., Chan, B., Bell, K., Fosang, A.J. and Little, C.B. (2013) 'Transcriptomics of wild-type mice and mice lacking ADAMTS-5 activity identifies genes involved in osteoarthritis initiation and cartilage destruction', *Arthritis Rheum*, 65(6), pp. 1547-60.
- Blau, F. (1888) 'Die Destillation pyridinmonocarbonsaurer Salze', *Berichte der deutschen chemischen Gesellschaft*, 21, pp. 1077-1078.
- Booth, D.G., Takagi, M., Sanchez-Pulido, L., Petfalski, E., Vargiu, G., Samejima, K., Imamoto, N., Ponting, C.P., Tollervey, D., Earnshaw, W.C. and Vagnarelli, P. (2014) 'Ki-67 is a PP1-interacting protein that organises the mitotic chromosome periphery', *Elife*, 3, p. e01641.
- Boyan, B.D., Hart, D.A., Enoka, R.M., Nicolella, D.P., Resnick, E., Berkley, K.J., Sluka, K.A., Kwoh, C.K., Tosi, L.L., O'Connor, M.I., Coutts, R.D. and Kohrt, W.M. (2013a) 'Hormonal modulation of connective tissue homeostasis and sex differences in risk for osteoarthritis of the knee', *Biol Sex Differ*, 4(1), p. 3.
- Boyan, B.D., Tosi, L.L., Coutts, R.D., Enoka, R.M., Hart, D.A., Nicolella, D.P., Berkley, K.J., Sluka, K.A., Kwoh, C.K., O'Connor, M.I., Kohrt, W.M. and Resnick, E. (2013b) 'Addressing the gaps: sex differences in osteoarthritis of the knee', *Biol Sex Differ*, 4(1), p. 4.
- Breu, A., Sprinzing, B., Merkl, K., Bechmann, V., Kujat, R., Jenei-Lanzl, Z., Prantl, L. and Angele, P. (2011) 'Estrogen reduces cellular aging in human mesenchymal stem cells and chondrocytes', *J Orthop Res*, 29(10), pp. 1563-71.
- Brizova, H., Kalinova, M., Krskova, L., Mrhalova, M. and Kodet, R. (2010) 'A novel quantitative PCR of proliferation markers (Ki-67, topoisomerase IIalpha, and TPX2): an immunohistochemical correlation, testing, and optimizing for mantle cell lymphoma', *Virchows Arch*, 456(6), pp. 671-9.
- Brunet, L.J., McMahon, J.A., McMahon, A.P. and Harland, R.M. (1998) 'Noggin, cartilage morphogenesis, and joint formation in the mammalian skeleton', *Science*, 280(5368), pp. 1455-7.
- Burleigh, A., Chanalaris, A., Gardiner, M.D., Driscoll, C., Boruc, O., Saklatvala, J. and Vincent, T.L. (2012) 'Joint immobilization prevents murine osteoarthritis and reveals the highly mechanosensitive nature of protease expression in vivo', *Arthritis Rheum*, 64(7), pp. 2278-88.
- Bush, W.S. and Moore, J.H. (2012) 'Chapter 11: Genome-Wide Association Studies', *PLoS Computational Biology*, 8(12).
- Cao, L., Lee, V., Adams, M.E., Kiani, C., Zhang, Y., Hu, W. and Yang, B.B. (1999) 'beta-Integrin-collagen interaction reduces chondrocyte apoptosis', *Matrix Biol*, 18(4), pp. 343-55.

- Carlo, M.D. and Loeser, R.F. (2003) 'Increased oxidative stress with aging reduces chondrocyte survival: correlation with intracellular glutathione levels', *Arthritis Rheum*, 48(12), pp. 3419-30.
- Castano-Betancourt, M.C., Evans, D.S., Ramos, Y.F., Boer, C.G., Metrustry, S., Liu, Y., den Hollander, W., van Rooij, J., Kraus, V.B., Yau, M.S., Mitchell, B.D., Muir, K., Hofman, A., Doherty, M., Doherty, S., Zhang, W., Kraaij, R., Rivadeneira, F., Barrett-Connor, E., Maciewicz, R.A., Arden, N., Nelissen, R.G., Kloppenburg, M., Jordan, J.M., Nevitt, M.C., Slagboom, E.P., Hart, D.J., Lafeber, F., Styrkarsdottir, U., Zeggini, E., Evangelou, E., Spector, T.D., Uitterlinden, A.G., Lane, N.E., Meulenbelt, I., Valdes, A.M. and van Meurs, J.B. (2016) 'Novel Genetic Variants for Cartilage Thickness and Hip Osteoarthritis', *PLoS Genet*, 12(10), p. e1006260.
- Cawston, T., Billington, C., Cleaver, C., Elliott, S., Hui, W., Koshy, P., Shingleton, B. and Rowan, A. (1999) 'The regulation of MMPs and TIMPs in cartilage turnover', *Ann N Y Acad Sci*, 878, pp. 120-9.
- Cawston, T.E., Curry, V.A., Summers, C.A., Clark, I.M., Riley, G.P., Life, P.F., Spaul, J.R., Goldring, M.B., Koshy, P.J., Rowan, A.D. and Shingleton, W.D. (1998) 'The role of oncostatin M in animal and human connective tissue collagen turnover and its localization within the rheumatoid joint', *Arthritis Rheum*, 41(10), pp. 1760-71.
- Chambers, M.G., Bayliss, M.T. and Mason, R.M. (1997) 'Chondrocyte cytokine and growth factor expression in murine osteoarthritis', *Osteoarthritis Cartilage*, 5(5), pp. 301-8.
- Chan, C.M., Macdonald, C.D., Litherland, G.J., Wilkinson, D.J., Skelton, A., Europe-Finner, G.N. and Rowan, A.D. (2017) 'Cytokine-induced MMP13 Expression in Human Chondrocytes Is Dependent on Activating Transcription Factor 3 (ATF3) Regulation', *J Biol Chem*, 292(5), pp. 1625-1636.
- Chijimatsu, R. and Saito, T. (2019) 'Mechanisms of synovial joint and articular cartilage development', *Cell Mol Life Sci*, 76(20), pp. 3939-3952.
- Chin, J., Rupp, E., Cameron, P.M., MacNaul, K.L., Lotke, P.A., Tocci, M.J., Schmidt, J.A. and Bayne, E.K. (1988) 'Identification of a high-affinity receptor for interleukin 1 alpha and interleukin 1 beta on cultured human rheumatoid synovial cells', *J Clin Invest*, 82(2), pp. 420-6.
- Chowanadisai, W., Lönnardal, B. and Kelleher, S.L. (2006) 'Identification of a mutation in SLC30A2 (ZnT-2) in women with low milk zinc concentration that results in transient neonatal zinc deficiency', *J Biol Chem*, 281(51), pp. 39699-707.

Chun, J. (2017) 'Interleukin-1 $\beta$  effect on primary mouse articular chondrocytes' [Gene expression profiling by microarray]. 10/10/17. Gwangju: Gwangju Institute of Science and Technology. (Accessed: 18/09/2019).

Claassen, H., Steffen, R., Hassenpflug, J., Varoga, D., Wruck, C.J., Brandenburg, L.O. and Pufe, T. (2010) '17 $\beta$ -estradiol reduces expression of MMP-1, -3, and -13 in human primary articular chondrocytes from female patients cultured in a three dimensional alginate system', *Cell Tissue Res*, 342(2), pp. 283-93.

Clancy, R.M., Rediske, J., Tang, X., Nijher, N., Frenkel, S., Philips, M. and Abramson, S.B. (1997) 'Outside-in signaling in the chondrocyte. Nitric oxide disrupts fibronectin-induced assembly of a subplasmalemmal actin/rho A/focal adhesion kinase signaling complex', *J Clin Invest*, 100(7), pp. 1789-96.

Clements, K.M., Flannelly, J.K., Tart, J., Brockbank, S.M., Wardale, J., Freeth, J., Parker, A.E. and Newham, P. (2011) 'Matrix metalloproteinase 17 is necessary for cartilage aggrecan degradation in an inflammatory environment', *Ann Rheum Dis*, 70(4), pp. 683-9.

Comblain, F., Dubuc, J.E., Lambert, C., Sanchez, C., Lespoune, I., Serisier, S. and Henrotin, Y. (2016) 'Identification of Targets of a New Nutritional Mixture for Osteoarthritis Management Composed by Curcuminoids Extract, Hydrolyzed Collagen and Green Tea Extract', *PLoS One*, 11(6), p. e0156902.

Constable, E.C. and Housecroft, C.E. (2019) 'The Early Years of 2,2'-Bipyridine-A Ligand in Its Own Lifetime', *Molecules*, 24(21).

Cuvier, O. and Hirano, T. (2003) 'A role of topoisomerase II in linking DNA replication to chromosome condensation', *J Cell Biol*, 160(5), pp. 645-55.

Da Silva, J.A., Larbre, J.P., Spector, T.D., Perry, L.A., Scott, D.L. and Willoughby, D.A. (1993) 'Protective effect of androgens against inflammation induced cartilage degradation in male rodents', *Ann Rheum Dis*, 52(4), pp. 285-91.

Dallas, G.M. (2013) *Principal Component Analysis 4 Dummies: Eigenvectors, Eigenvalues and Dimension Reduction*. Available at: <https://georgemdallas.wordpress.com/2013/10/30/principal-component-analysis-4-dummies-eigenvectors-eigenvalues-and-dimension-reduction/>.

Davis, S.R. and Cousins, R.J. (2000) 'Metallothionein expression in animals: a physiological perspective on function', *J Nutr*, 130(5), pp. 1085-8.

de Lange-Brokaar, B.J., Ioan-Facsinay, A., van Osch, G.J., Zuurmond, A.M., Schoones, J., Toes, R.E., Huizinga, T.W. and Kloppenburg, M. (2012) 'Synovial inflammation, immune cells and their cytokines in osteoarthritis: a review', *Osteoarthritis Cartilage*, 20(12), pp. 1484-99.

Dinarello, C.A. (2003) *Interleukin-1 Family of Ligands and Receptors*. Lippincott Williams and Wilkins. Available at:

[http://lvts.fr/Pages\\_html/Encyclopedies/FundamentalImmunology/ramiCOMMAND=applyStylesheet\(interface.xsl,CH025S0216.pub\)&p\\_userid=pau&found=.html](http://lvts.fr/Pages_html/Encyclopedies/FundamentalImmunology/ramiCOMMAND=applyStylesheet(interface.xsl,CH025S0216.pub)&p_userid=pau&found=.html).

Dunn, S.L., Soul, J., Anand, S., Schwartz, J.M., Boot-Handford, R.P. and Hardingham, T.E. (2016) 'Gene expression changes in damaged osteoarthritic cartilage identify a signature of non-chondrogenic and mechanical responses', *Osteoarthritis Cartilage*, 24(8), pp. 1431-40.

Englund, M., Guermazi, A., Roemer, F.W., Aliabadi, P., Yang, M., Lewis, C.E., Torner, J., Nevitt, M.C., Sack, B. and Felson, D.T. (2009) 'Meniscal tear in knees without surgery and the development of radiographic osteoarthritis among middle-aged and elderly persons: The Multicenter Osteoarthritis Study', *Arthritis Rheum*, 60(3), pp. 831-9.

Esparza, J., Vilardell, C., Calvo, J., Juan, M., Vives, J., Urbano-Márquez, A., Yagüe, J. and Cid, M.C. (1999) 'Fibronectin upregulates gelatinase B (MMP-9) and induces coordinated expression of gelatinase A (MMP-2) and its activator MT1-MMP (MMP-14) by human T lymphocyte cell lines. A process repressed through RAS/MAP kinase signaling pathways', *Blood*, 94(8), pp. 2754-66.

Fell, H.B. and Jubb, R.W. (1977) 'The effect of synovial tissue on the breakdown of articular cartilage in organ culture', *Arthritis Rheum*, 20(7), pp. 1359-71.

Finger, F., Schorle, C., Zien, A., Gebhard, P., Goldring, M.B. and Aigner, T. (2003) 'Molecular phenotyping of human chondrocyte cell lines T/C-28a2, T/C-28a4, and C-28/12', *Arthritis Rheum*, 48(12), pp. 3395-403.

Fisch, K.M., Gamini, R., Alvarez-Garcia, O., Akagi, R., Saito, M., Muramatsu, Y., Sasho, T., Koziol, J.A., Su, A.I. and Lotz, M.K. (2018) 'Identification of transcription factors responsible for dysregulated networks in human osteoarthritis cartilage by global gene expression analysis', *Osteoarthritis Cartilage*, 26(11), pp. 1531-1538.

Fosang, A.J. and Beier, F. (2011) 'Emerging Frontiers in cartilage and chondrocyte biology', *Best Pract Res Clin Rheumatol*, 25(6), pp. 751-66.

- Fosang, A.J., Rogerson, F.M., East, C.J. and Stanton, H. (2008) 'ADAMTS-5: the story so far', *Eur Cell Mater*, 15, pp. 11-26.
- Fox, A.J., Bedi, A. and Rodeo, S.A. (2009) 'The basic science of articular cartilage: structure, composition, and function', *Sports Health*, 1(6), pp. 461-8.
- Fushimi, K., Troeberg, L., Nakamura, H., Lim, N.H. and Nagase, H. (2008) 'Functional differences of the catalytic and non-catalytic domains in human ADAMTS-4 and ADAMTS-5 in aggrecanolytic activity', *J Biol Chem*, 283(11), pp. 6706-16.
- Gadher, S.J., Eyre, D.R., Duance, V.C., Wotton, S.F., Heck, L.W., Schmid, T.M. and Woolley, D.E. (1988) 'Susceptibility of cartilage collagens type II, IX, X, and XI to human synovial collagenase and neutrophil elastase', *Eur J Biochem*, 175(1), pp. 1-7.
- Gebauer, M., Saas, J., Sohler, F., Haag, J., Soder, S., Pieper, M., Bartnik, E., Beninga, J., Zimmer, R. and Aigner, T. (2005) 'Comparison of the chondrosarcoma cell line SW1353 with primary human adult articular chondrocytes with regard to their gene expression profile and reactivity to IL-1beta', *Osteoarthritis Cartilage*, 13(8), pp. 697-708.
- Giedroc, D.P., Chen, X. and Apuy, J.L. (2001) 'Metal response element (MRE)-binding transcription factor-1 (MTF-1): structure, function, and regulation', *Antioxid Redox Signal*, 3(4), pp. 577-96.
- Girijashanker, K., He, L., Soleimani, M., Reed, J.M., Li, H., Liu, Z., Wang, B., Dalton, T.P. and Nebert, D.W. (2008) 'Slc39a14 gene encodes ZIP14, a metal/bicarbonate symporter: similarities to the ZIP8 transporter', *Mol Pharmacol*, 73(5), pp. 1413-23.
- Giunta, C., Elçioglu, N.H., Albrecht, B., Eich, G., Chambaz, C., Janecke, A.R., Yeowell, H., Weis, M., Eyre, D.R., Kraenzlin, M. and Steinmann, B. (2008) 'Spondylocheiro dysplastic form of the Ehlers-Danlos syndrome--an autosomal-recessive entity caused by mutations in the zinc transporter gene SLC39A13', *Am J Hum Genet*, 82(6), pp. 1290-305.
- Glasson, S.S. (2007) 'In vivo osteoarthritis target validation utilizing genetically-modified mice', *Curr Drug Targets*, 8(2), pp. 367-76.
- Glasson, S.S., Askew, R., Sheppard, B., Carito, B., Blanchet, T., Ma, H.L., Flannery, C.R., Peluso, D., Kanki, K., Yang, Z., Majumdar, M.K. and Morris, E.A. (2005) 'Deletion of active ADAMTS5 prevents cartilage degradation in a murine model of osteoarthritis', *Nature*, 434(7033), pp. 644-8.

Glasson, S.S., Askew, R., Sheppard, B., Carito, B.A., Blanchet, T., Ma, H.L., Flannery, C.R., Kanki, K., Wang, E., Peluso, D., Yang, Z., Majumdar, M.K. and Morris, E.A. (2004) 'Characterization of and osteoarthritis susceptibility in ADAMTS-4-knockout mice', *Arthritis Rheum*, 50(8), pp. 2547-58.

Glasson, S.S., Blanchet, T.J. and Morris, E.A. (2007) 'The surgical destabilization of the medial meniscus (DMM) model of osteoarthritis in the 129/SvEv mouse', *Osteoarthritis and Cartilage*, 15(9), pp. 1061-1069.

Goldring, M.B. (2012) 'Chondrogenesis, chondrocyte differentiation, and articular cartilage metabolism in health and osteoarthritis', *The Adv Musculoskelet Dis*, 4(4), pp. 269-85.

Goldring, M.B., Birkhead, J.R., Suen, L.F., Yamin, R., Mizuno, S., Glowacki, J., Arbiser, J.L. and Apperley, J.F. (1994a) 'Interleukin-1 beta-modulated gene expression in immortalized human chondrocytes', *J Clin Invest*, 94(6), pp. 2307-16.

Goldring, M.B., Fukuo, K., Birkhead, J.R., Dudek, E. and Sandell, L.J. (1994b) 'Transcriptional suppression by interleukin-1 and interferon-gamma of type II collagen gene expression in human chondrocytes', *J Cell Biochem*, 54(1), pp. 85-99.

Goldring, M.B. and Goldring, S.R. (2010) 'Articular cartilage and subchondral bone in the pathogenesis of osteoarthritis', *Ann N Y Acad Sci*, 1192, pp. 230-7.

Gordon-Betts, J., Young, K.A., Wise, J.A., Johnson, E., Poe, B., Kruse, D.H., Korol, O., Johnson, J.E., Womble, M. and DeSaix, P. (2013) 'Synovial Joints', in *Anatomy & Physiology*. Openstax. Available at: <https://opentextbc.ca/anatomyandphysiology/chapter/9-4-synovial-joints/>.

Grässel, S. and Aszodi, A. (2017) *Cartilage*. Springer International Publishing.

Gunther, V., Lindert, U. and Schaffner, W. (2012) 'The taste of heavy metals: gene regulation by MTF-1', *Biochim Biophys Acta*, 1823(9), pp. 1416-25.

Günes, C., Heuchel, R., Georgiev, O., Müller, K.H., Lichtlen, P., Blüthmann, H., Marino, S., Aguzzi, A. and Schaffner, W. (1998) 'Embryonic lethality and liver degeneration in mice lacking the metal-responsive transcriptional activator MTF-1', *EMBO J*, 17(10), pp. 2846-54.

Hara, T., Takeda, T.A., Takagishi, T., Fukue, K., Kambe, T. and Fukada, T. (2017) 'Physiological roles of zinc transporters: molecular and genetic importance in zinc homeostasis', *J Physiol Sci*, 67(2), pp. 283-301.

- Hare, D.J., New, E.J., de Jonge, M.D. and McColl, G. (2015) 'Imaging metals in biology: balancing sensitivity, selectivity and spatial resolution', *Chem Soc Rev*, 44(17), pp. 5941-58.
- Hojyo, S., Fukada, T., Shimoda, S., Ohashi, W., Bin, B.H., Koseki, H. and Hirano, T. (2011) 'The zinc transporter SLC39A14/ZIP14 controls G-protein coupled receptor-mediated signaling required for systemic growth', *PLoS One*, 6(3), p. e18059.
- Holder, N. (1977) 'An experimental investigation into the early development of the chick elbow joint', *J Embryol Exp Morphol*, 39, pp. 115-27.
- Holmbeck, K., Bianco, P., Caterina, J., Yamada, S., Kromer, M., Kuznetsov, S.A., Mankani, M., Robey, P.G., Poole, A.R., Pidoux, I., Ward, J.M. and Birkedal-Hansen, H. (1999) 'MT1-MMP-deficient mice develop dwarfism, osteopenia, arthritis, and connective tissue disease due to inadequate collagen turnover', *Cell*, 99(1), pp. 81-92.
- Homandberg, G.A. and Hui, F. (1996) 'Association of proteoglycan degradation with catabolic cytokine and stromelysin release from cartilage cultured with fibronectin fragments', *Arch Biochem Biophys*, 334(2), pp. 325-31.
- Homandberg, G.A., Meyers, R. and Williams, J.M. (1993) 'Intraarticular injection of fibronectin fragments causes severe depletion of cartilage proteoglycans in vivo', *J Rheumatol*, 20(8), pp. 1378-82.
- Homsher, R. and Zak, B. (1985) 'Spectrophotometric investigation of sensitive complexing agents for the determination of zinc in serum', *Clin Chem*, 31(8), pp. 1310-3.
- Huang, T.C., Chang, W.T., Hu, Y.C., Hsieh, B.S., Cheng, H.L., Yen, J.H., Chiu, P.R. and Chang, K.L. (2018) 'Zinc Protects Articular Chondrocytes through Changes in Nrf2-Mediated Antioxidants, Cytokines and Matrix Metalloproteinases', *Nutrients*, 10(4).
- Hunter, D.J. and Bierma-Zeinstra, S. (2019) 'Osteoarthritis', *The Lancet*, 393, pp. 1745-1759.
- Iwanaga, T., Shikichi, M., Kitamura, H., Yanase, H. and Nozawa-Inoue, K. (2000) 'Morphology and functional roles of synoviocytes in the joint', *Arch Histol Cytol*, 63(1), pp. 17-31.
- Karlsson, C., Dehne, T., Lindahl, A., Brittberg, M., Pruss, A., Sittering, M. and Ringe, J. (2010) 'Genome-wide expression profiling reveals new candidate genes associated with osteoarthritis', *Osteoarthritis Cartilage*, 18(4), pp. 581-92.

- Kevorkian, L., Young, D.A., Darrah, C., Donell, S.T., Shepstone, L., Porter, S., Brockbank, S.M., Edwards, D.R., Parker, A.E. and Clark, I.M. (2004) 'Expression profiling of metalloproteinases and their inhibitors in cartilage', *Arthritis Rheum*, 50(1), pp. 131-41.
- Kim, J.H., Jeon, J., Shin, M., Won, Y., Lee, M., Kwak, J.S., Lee, G., Rhee, J., Ryu, J.H., Chun, C.H. and Chun, J.S. (2014) 'Regulation of the catabolic cascade in osteoarthritis by the zinc-ZIP8-MTF1 axis', *Cell*, 156(4), pp. 730-43.
- Kim, S.H., Turnbull, J. and Guimond, S. (2011) 'Extracellular matrix and cell signalling: the dynamic cooperation of integrin, proteoglycan and growth factor receptor', *J Endocrinol*, 209(2), pp. 139-51.
- Kimura, T. and Kambe, T. (2016) 'The Functions of Metallothionein and ZIP and ZnT Transporters: An Overview and Perspective', *Int J Mol Sci*, 17(3), p. 336.
- King, L.K., March, L. and Anandacoomarasamy, A. (2013) 'Obesity & osteoarthritis', *Indian J Med Res*, 138, pp. 185-93.
- Kinney, R.C., Schwartz, Z., Week, K., Lotz, M.K. and Boyan, B.D. (2005) 'Human articular chondrocytes exhibit sexual dimorphism in their responses to 17beta-estradiol', *Osteoarthritis Cartilage*, 13(4), pp. 330-7.
- Knäuper, V., Will, H., López-Otin, C., Smith, B., Atkinson, S.J., Stanton, H., Hembry, R.M. and Murphy, G. (1996) 'Cellular mechanisms for human procollagenase-3 (MMP-13) activation. Evidence that MT1-MMP (MMP-14) and gelatinase a (MMP-2) are able to generate active enzyme', *J Biol Chem*, 271(29), pp. 17124-31.
- Koshy, P.J., Lundy, C.J., Rowan, A.D., Porter, S., Edwards, D.R., Hogan, A., Clark, I.M. and Cawston, T.E. (2002) 'The modulation of matrix metalloproteinase and ADAM gene expression in human chondrocytes by interleukin-1 and oncostatin M: a time-course study using real-time quantitative reverse transcription-polymerase chain reaction', *Arthritis Rheum*, 46(4), pp. 961-7.
- Koyama, E., Shibukawa, Y., Nagayama, M., Sugito, H., Young, B., Yuasa, T., Okabe, T., Ochiai, T., Kamiya, N., Rountree, R.B., Kingsley, D.M., Iwamoto, M., Enomoto-Iwamoto, M. and Pacifici, M. (2008) 'A distinct cohort of progenitor cells participates in synovial joint and articular cartilage formation during mouse limb skeletogenesis', *Dev Biol*, 316(1), pp. 62-73.
- Krachler, M., Domej, W. and Irgolic, K.J. (2000) 'Concentrations of trace elements in osteoarthritic knee-joint effusions', *Biol Trace Elem Res*, 75(1-3), pp. 253-63.

- Kraus, V.B. (2014) 'Osteoarthritis: The zinc link', *Nature*, 507(7493), pp. 441-2.
- Laberge, M.A., Baum, T., Virayavanich, W., Nardo, L., Nevitt, M.C., Lynch, J., McCulloch, C.E. and Link, T.M. (2012) 'Obesity increases the prevalence and severity of focal knee abnormalities diagnosed using 3T MRI in middle-aged subjects--data from the Osteoarthritis Initiative', *Skeletal Radiol*, 41(6), pp. 633-41.
- Lawyer, T.J., Jankowski, J., Russell, G.V. and Stronach, B.M. (2014) 'Prevalence of post-traumatic osteoarthritis in morbidly obese patients after acetabular fracture fixation', *J Long Term Eff Med Implants*, 24(2-3), pp. 225-31.
- Lefebvre, V., Peeters-Joris, C. and Vaes, G. (1990) 'Modulation by interleukin 1 and tumor necrosis factor alpha of production of collagenase, tissue inhibitor of metalloproteinases and collagen types in differentiated and dedifferentiated articular chondrocytes', *Biochim Biophys Acta*, 1052(3), pp. 366-78.
- Li, J. and Dong, S. (2016) 'The Signaling Pathways Involved in Chondrocyte Differentiation and Hypertrophic Differentiation', *Stem Cells Int*, 2016, p. 2470351.
- Little, C.B., Barai, A., Burkhardt, D., Smith, S.M., Fosang, A.J., Werb, Z., Shah, M. and Thompson, E.W. (2009) 'Matrix metalloproteinase 13-deficient mice are resistant to osteoarthritic cartilage erosion but not chondrocyte hypertrophy or osteophyte development', *Arthritis Rheum*, 60(12), pp. 3723-33.
- Little, C.B., Meeker, C.T., Golub, S.B., Lawlor, K.E., Farmer, P.J., Smith, S.M. and Fosang, A.J. (2007) 'Blocking aggrecanase cleavage in the aggrecan interglobular domain abrogates cartilage erosion and promotes cartilage repair', *J Clin Invest*, 117(6), pp. 1627-36.
- Little, C.B., Meeker, C.T., Hembry, R.M., Sims, N.A., Lawlor, K.E., Golub, S.B., Last, K. and Fosang, A.J. (2005) 'Matrix metalloproteinases are not essential for aggrecan turnover during normal skeletal growth and development', *Mol Cell Biol*, 25(8), pp. 3388-99.
- Liu, B., Balkwill, A., Banks, E., Cooper, C., Green, J. and Beral, V. (2007) 'Relationship of height, weight and body mass index to the risk of hip and knee replacements in middle-aged women', *Rheumatology (Oxford)*, 46(5), pp. 861-7.
- Liu, M.J., Bao, S., Gálvez-Peralta, M., Pyle, C.J., Rudawsky, A.C., Pavlovicz, R.E., Killilea, D.W., Li, C., Nebert, D.W., Wewers, M.D. and Knoell, D.L. (2013) 'ZIP8 regulates host defense through zinc-mediated inhibition of NF- $\kappa$ B', *Cell Rep*, 3(2), pp. 386-400.

Loeser, R.F. (2017) 'The Role of Aging in the Development of Osteoarthritis', *Trans Am Clin Climatol Assoc*, 128, pp. 44-54.

Loeser, R.F., Goldring, S.R., Scanzello, C.R. and Goldring, M.B. (2012) 'Osteoarthritis: a disease of the joint as an organ', *Arthritis Rheum*, 64(6), pp. 1697-707.

Lokau, J., Göttert, S., Arnold, P., Düsterhöft, S., Massa López, D., Grötzinger, J. and Garbers, C. (2018) 'The SNP rs4252548 (R112H) which is associated with reduced human height compromises the stability of IL-11', *Biochim Biophys Acta Mol Cell Res*, 1865(3), pp. 496-506.

Luc, B., Gribble, P.A. and Pietrosimone, B.G. (2014) 'Osteoarthritis prevalence following anterior cruciate ligament reconstruction: a systematic review and numbers-needed-to-treat analysis', *J Athl Train*, 49(6), pp. 806-19.

Lumen (2019) *Joints and Skeletal Movement*. Available at: [courses.lumenlearning.com/boundless-biology/chapter/joints-and-skeletal-movement/](https://courses.lumenlearning.com/boundless-biology/chapter/joints-and-skeletal-movement/) (Accessed: 13/07/2020).

Löffek, S., Schilling, O. and Franzke, C.W. (2011) 'Series "matrix metalloproteinases in lung health and disease": Biological role of matrix metalloproteinases: a critical balance', *Eur Respir J*, 38(1), pp. 191-208.

Mackie, E.J., Ahmed, Y.A., Tatarczuch, L., Chen, K.S. and Mirams, M. (2008) 'Endochondral ossification: how cartilage is converted into bone in the developing skeleton', *Int J Biochem Cell Biol*, 40(1), pp. 46-62.

Marouli, E., Graff, M., Medina-Gomez, C., Lo, K.S., Wood, A.R., Kjaer, T.R., Fine, R.S., Lu, Y., Schurmann, C., Highland, H.M., Rieger, S., Thorleifsson, G., Justice, A.E., Lamparter, D., Stirrups, K.E., Turcot, V., Young, K.L., Winkler, T.W., Esko, T., Karaderi, T., Locke, A.E., Masca, N.G., Ng, M.C., Mudgal, P., Rivas, M.A., Vedantam, S., Mahajan, A., Guo, X., Abecasis, G., Aben, K.K., Adair, L.S., Alam, D.S., Albrecht, E., Allin, K.H., Allison, M., Amouyel, P., Appel, E.V., Arveiler, D., Asselbergs, F.W., Auer, P.L., Balkau, B., Banas, B., Bang, L.E., Benn, M., Bergmann, S., Bielak, L.F., Blüher, M., Boeing, H., Boerwinkle, E., Böger, C.A., Bonnycastle, L.L., Bork-Jensen, J., Bots, M.L., Bottinger, E.P., Bowden, D.W., Brandslund, I., Breen, G., Brilliant, M.H., Broer, L., Burt, A.A., Butterworth, A.S., Carey, D.J., Caulfield, M.J., Chambers, J.C., Chasman, D.I., Chen, Y.I., Chowdhury, R., Christensen, C., Chu, A.Y., Cocca, M., Collins, F.S., Cook, J.P., Corley, J., Galbany, J.C., Cox, A.J., Cuellar-Partida, G., Danesh, J., Davies, G., de Bakker, P.I., de Borst, G.J., de Denu, S., de Groot, M.C., de Mutsert, R., Deary, I.J., Dedoussis, G., Demerath, E.W., den Hollander, A.I., Dennis, J.G., Di Angelantonio, E., Drenos, F., Du, M., Dunning, A.M., Easton, D.F., Ebeling, T., Edwards, T.L., Ellinor, P.T., Elliott, P., Evangelou, E.,

- Farmaki, A.E., Faul, J.D., et al. (2017) 'Rare and low-frequency coding variants alter human adult height', *Nature*, 542(7640), pp. 186-190.
- Martin, J.A. and Buckwalter, J.A. (1998) 'Effects of fibronectin on articular cartilage chondrocyte proteoglycan synthesis and response to insulin-like growth factor-I', *J Orthop Res*, 16(6), pp. 752-7.
- Matheson, T.D. and Kaufman, P.D. (2017) 'The p150N domain of chromatin assembly factor-1 regulates Ki-67 accumulation on the mitotic perichromosomal layer', *Mol Biol Cell*, 28(1), pp. 21-29.
- McMillan, J., Kinney, R.C., Ranly, D.M., Fatehi-Sedeh, S., Schwartz, Z. and Boyan, B.D. (2007) 'Osteoinductivity of demineralized bone matrix in immunocompromised mice and rats is decreased by ovariectomy and restored by estrogen replacement', *Bone*, 40(1), pp. 111-121.
- Miles, A.T., Hawksworth, G.M., Beattie, J.H. and Rodilla, V. (2000) 'Induction, regulation, degradation, and biological significance of mammalian metallothioneins', *Crit Rev Biochem Mol Biol*, 35(1), pp. 35-70.
- Miller, R.E., Lu, Y., Tortorella, M.D. and Malfait, A.M. (2013) 'Genetically Engineered Mouse Models Reveal the Importance of Proteases as Osteoarthritis Drug Targets', *Curr Rheumatol Rep*, 15(8), p. 350.
- Miwa, H.E., Gerken, T.A. and Hering, T.M. (2006) 'Effects of covalently attached chondroitin sulfate on aggrecan cleavage by ADAMTS-4 and MMP-13', *Matrix Biol*, 25(8), pp. 534-45.
- Moazedi-Fuerst, F.C., Gruber, G., Stradner, M.H., Guidolin, D., Jones, J.C., Bodo, K., Wagner, K., Peischler, D., Krischan, V., Weber, J., Sadoghi, P., Glehr, M., Leithner, A. and Graninger, W.B. (2016) 'Effect of Laminin-A4 inhibition on cluster formation of human osteoarthritic chondrocytes', *J Orthop Res*, 34(3), pp. 419-26.
- Moleirinho, A., Carneiro, J., Matthiesen, R., Silva, R.M., Amorim, A. and Azevedo, L. (2011) 'Gains, losses and changes of function after gene duplication: study of the metallothionein family', *PLoS One*, 6(4), p. e18487.
- Morgan, T.G., Rowan, A.D., Dickinson, S.C., Jones, D., Hollander, A.P., Deehan, D. and Cawston, T.E. (2006) 'Human nasal cartilage responds to oncostatin M in combination with interleukin 1 or tumour necrosis factor alpha by the release of collagen fragments via collagenases', *Ann Rheum Dis*, 65(2), pp. 184-90.
- Mosig, R.A., Dowling, O., DiFeo, A., Ramirez, M.C., Parker, I.C., Abe, E., Diouri, J., Aqeel, A.A., Wylie, J.D., Oblander, S.A., Madri, J., Bianco, P., Apte, S.S., Zaidi, M., Doty, S.B., Majeska, R.J., Schaffler, M.B.

and Martignetti, J.A. (2007) 'Loss of MMP-2 disrupts skeletal and craniofacial development and results in decreased bone mineralization, joint erosion and defects in osteoblast and osteoclast growth', *Hum Mol Genet*, 16(9), pp. 1113-23.

Moulharat, N., Lesur, C., Thomas, M., Rolland-Valognes, G., Pastoureau, P., Anract, P., De Ceuninck, F. and Sabatini, M. (2004) 'Effects of transforming growth factor-beta on aggrecanase production and proteoglycan degradation by human chondrocytes in vitro', *Osteoarthritis Cartilage*, 12(4), pp. 296-305.

Murphy, G. (2011) 'Tissue inhibitors of metalloproteinases', *Genome Biol*, 12(11), p. 233.

Ovesen, J., Møller-Madsen, B., Nielsen, P.T., Christensen, P.H., Simonsen, O., Hoeck, H.C., Laursen, M.B. and Thomsen, J.S. (2009) 'Differences in zinc status between patients with osteoarthritis and osteoporosis', *J Trace Elem Med Biol*, 23(1), pp. 1-8.

Pastinen, T. (2010) 'Genome-wide allele-specific analysis: insights into regulatory variation', *Nat Rev Genet*, 11(8), pp. 533-8.

Pearson, M.J., Philp, A.M., Heward, J.A., Roux, B.T., Walsh, D.A., Davis, E.T., Lindsay, M.A. and Jones, S.W. (2016) 'Long Intergenic Noncoding RNAs Mediate the Human Chondrocyte Inflammatory Response and Are Differentially Expressed in Osteoarthritis Cartilage', *Arthritis Rheumatol*, 68(4), pp. 845-56.

Poulet, B., Ulici, V., Stone, T.C., Pead, M., Gburcik, V., Constantinou, E., Palmer, D.B., Beier, F., Timmons, J.A. and Pitsillides, A.A. (2012) 'Time-series transcriptional profiling yields new perspectives on susceptibility to murine osteoarthritis', *Arthritis Rheum*, 64(10), pp. 3256-66.

PRASAD, A.S., HALSTED, J.A. and NADIMI, M. (1961) 'Syndrome of iron deficiency anemia, hepatosplenomegaly, hypogonadism, dwarfism and geophagia', *Am J Med*, 31, pp. 532-46.

Pratta, M.A., Tortorella, M.D. and Arner, E.C. (2000) 'Age-related changes in aggrecan glycosylation affect cleavage by aggrecanase', *J Biol Chem*, 275(50), pp. 39096-102.

Radtke, F., Georgiev, O., Müller, H.P., Brugnera, E. and Schaffner, W. (1995) 'Functional domains of the heavy metal-responsive transcription regulator MTF-1', *Nucleic Acids Res*, 23(12), pp. 2277-86.

Ramos, Y.F., Bos, S.D., van der Breggen, R., Kloppenburg, M., Ye, K., Lameijer, E.W., Nelissen, R.G., Slagboom, P.E. and Meulenbelt, I. (2015) 'A gain of function mutation in TNFRSF11B encoding osteoprotegerin causes osteoarthritis with chondrocalcinosis', *Ann Rheum Dis*, 74(9), pp. 1756-62.

- Ramos, Y.F., den Hollander, W., Bovee, J.V., Bomer, N., van der Breggen, R., Lakenberg, N., Keurentjes, J.C., Goeman, J.J., Slagboom, P.E., Nelissen, R.G., Bos, S.D. and Meulenbelt, I. (2014) 'Genes involved in the osteoarthritis process identified through genome wide expression analysis in articular cartilage; the RAAK study', *PLoS One*, 9(7), p. e103056.
- Raulin, J. (1869) 'Etudes chimiques sur la vegetation.', *Annales des sciences naturelles. Botanique et biologie végétale*, 11, pp. 92-299.
- Raz, P., Nasatzky, E., Boyan, B.D., Ornoy, A. and Schwartz, Z. (2005) 'Sexual dimorphism of growth plate prehypertrophic and hypertrophic chondrocytes in response to testosterone requires metabolism to dihydrotestosterone (DHT) by steroid 5-alpha reductase type 1', *J Cell Biochem*, 95(1), pp. 108-19.
- Regan, E.A., Bowler, R.P. and Crapo, J.D. (2008) 'Joint fluid antioxidants are decreased in osteoarthritic joints compared to joints with macroscopically intact cartilage and subacute injury', *Osteoarthritis Cartilage*, 16(4), pp. 515-21.
- Reynard, L.N., Barter, M.J. (2019) 'Osteoarthritis year in review 2019: genetics, genomics and epigenetics', *Osteoarthritis and Cartilage*.
- Rogers, E.L., Reynard, L.N. and Loughlin, J. (2015) 'The role of inflammation-related genes in osteoarthritis', *Osteoarthritis Cartilage*, 23(11), pp. 1933-8.
- Roschger, A., Hofstaetter, J.G., Pemmer, B., Zoeger, N., Wobraschek, P., Falkenberg, G., Simon, R., Berzlanovich, A., Thaler, H.W., Roschger, P., Klaushofer, K. and Strelci, C. (2013) 'Differential accumulation of lead and zinc in double-tidemarks of articular cartilage', *Osteoarthritis Cartilage*, 21(11), pp. 1707-15.
- Rose, B.J. and Kooyman, D.L. (2016) 'A Tale of Two Joints: The Role of Matrix Metalloproteases in Cartilage Biology', *Dis Markers*, 2016, p. 4895050.
- Roughley, P.J., Barnett, J., Zuo, F. and Mort, J.S. (2003) 'Variations in aggrecan structure modulate its susceptibility to aggrecanases', *Biochem J*, 375(Pt 1), pp. 183-9.
- Rowan, A.D., Hui, W., Cawston, T.E. and Richards, C.D. (2003) 'Adenoviral gene transfer of interleukin-1 in combination with oncostatin M induces significant joint damage in a murine model', *Am J Pathol*, 162(6), pp. 1975-84.

Rushton, M.D., Reynard, L.N., Barter, M.J., Refaie, R., Rankin, K.S., Young, D.A. and Loughlin, J. (2014) 'Characterization of the cartilage DNA methylome in knee and hip osteoarthritis', *Arthritis Rheumatol*, 66(9), pp. 2450-60.

Rushton, M.D., Young, D.A., Loughlin, J. and Reynard, L.N. (2015) 'Differential DNA methylation and expression of inflammatory and zinc transporter genes defines subgroups of osteoarthritic hip patients', *Ann Rheum Dis*, 74(9), pp. 1778-82.

Ruttkay-Nedecky, B., Nejdil, L., Gumulec, J., Zitka, O., Masarik, M., Eckschlager, T., Stiborova, M., Adam, V. and Kizek, R. (2013) 'The role of metallothionein in oxidative stress', *Int J Mol Sci*, 14(3), pp. 6044-66.

Saas, J., Haag, J., Rueger, D., Chubinskaya, S., Sohler, F., Zimmer, R., Bartnik, E. and Aigner, T. (2006) 'IL-1beta, but not BMP-7 leads to a dramatic change in the gene expression pattern of human adult articular chondrocytes--portraying the gene expression pattern in two donors', *Cytokine*, 36(1-2), pp. 90-9.

Salo, T., Mäkelä, M., Kylmäniemi, M., Autio-Harminen, H. and Larjava, H. (1994) 'Expression of matrix metalloproteinase-2 and -9 during early human wound healing', *Lab Invest*, 70(2), pp. 176-82.

Scanzello, C.R. and Goldring, S.R. (2012) 'The role of synovitis in osteoarthritis pathogenesis', *Bone*, 51(2), pp. 249-57.

Scanzello, C.R., McKeon, B., Swaim, B.H., DiCarlo, E., Asomugha, E.U., Kanda, V., Nair, A., Lee, D.M., Richmond, J.C., Katz, J.N., Crow, M.K. and Goldring, S.R. (2011) 'Synovial inflammation in patients undergoing arthroscopic meniscectomy: molecular characterization and relationship to symptoms', *Arthritis Rheum*, 63(2), pp. 391-400.

Scanzello, C.R., Umoh, E., Pessler, F., Diaz-Torne, C., Miles, T., DiCarlo, E., Potter, H.G., Mandl, L., Marx, R., Rodeo, S., Goldring, S.R. and Crow, M.K. (2009) 'Local cytokine profiles in knee osteoarthritis: elevated synovial fluid interleukin-15 differentiates early from end-stage disease', *Osteoarthritis Cartilage*, 17(8), pp. 1040-8.

Schett, G., Dayer, J.M. and Manger, B. (2016) 'Interleukin-1 function and role in rheumatic disease', *Nat Rev Rheumatol*, 12(1), pp. 14-24.

Schmitt, S., Küry, S., Giraud, M., Dréno, B., Kharfi, M. and Béziau, S. (2009) 'An update on mutations of the SLC39A4 gene in acrodermatitis enteropathica', *Hum Mutat*, 30(6), pp. 926-33.

Schneider, C.A., Rasband, W.S. and Eliceiri, K.W. (2012) 'NIH Image to ImageJ: 25 years of image analysis', *Nat Methods*, 9(7), pp. 671-5.

Scholzen, T. and Gerdes, J. (2000) 'The Ki-67 protein: from the known and the unknown', *J Cell Physiol*, 182(3), pp. 311-22.

Shiomi, T., Lemaître, V., D'Armiento, J. and Okada, Y. (2010) 'Matrix metalloproteinases, a disintegrin and metalloproteinases, and a disintegrin and metalloproteinases with thrombospondin motifs in non-neoplastic diseases', *Pathol Int*, 60(7), pp. 477-96.

Sim, D.L. and Chow, V.T. (1999) 'The novel human HUEL (C4orf1) gene maps to chromosome 4p12-p13 and encodes a nuclear protein containing the nuclear receptor interaction motif', *Genomics*, 59(2), pp. 224-33.

Snelling, S., Rout, R., Davidson, R., Clark, I., Carr, A., Hulley, P.A. and Price, A.J. (2014) 'A gene expression study of normal and damaged cartilage in anteromedial gonarthrosis, a phenotype of osteoarthritis', *Osteoarthritis Cartilage*, 22(2), pp. 334-43.

Sobecki, M., Mrouj, K., Camasses, A., Parisis, N., Nicolas, E., Llères, D., Gerbe, F., Prieto, S., Krasinska, L., David, A., Eguren, M., Birling, M.C., Urbach, S., Hem, S., Déjardin, J., Malumbres, M., Jay, P., Dulic, V., Lafontaine, D.L.j., Feil, R. and Fisher, D. (2016) 'The cell proliferation antigen Ki-67 organises heterochromatin', *Elife*, 5, p. e13722.

Sokolove, J. and Lepus, C.M. (2013) 'Role of inflammation in the pathogenesis of osteoarthritis: latest findings and interpretations', *Ther Adv Musculoskelet Dis*, 5(2), pp. 77-94.

Soul, J., Dunn, S.L., Anand, S., Serracino-Inglott, F., Schwartz, J.M., Boot-Handford, R.P. and Hardingham, T.E. (2018a) 'Stratification of knee osteoarthritis: two major patient subgroups identified by genome-wide expression analysis of articular cartilage', *Ann Rheum Dis*, 77(3), p. 423.

Soul, J., Hardingham, T., Boot-Handford, R. and Schwartz, J.M. (2018b) *SkeletalVis: An exploration and meta-analysis data portal of cross-species skeletal transcriptomics data*, *Bioinformatics*. Available at: <https://doi.org/10.1093/bioinformatics/bty947>.

Srikanth, V.K., Fryer, J.L., Zhai, G., Winzenberg, T.M., Hosmer, D. and Jones, G. (2005) 'A meta-analysis of sex differences prevalence, incidence and severity of osteoarthritis', *Osteoarthritis Cartilage*, 13(9), pp. 769-81.

Staines, K.A., Poulet, B., Wentworth, D.N. and Pitsillides, A.A. (2017) 'The STR/ort mouse model of spontaneous osteoarthritis - an update', *Osteoarthritis Cartilage*, 25(6), pp. 802-808.

Stanton, H., Rogerson, F.M., East, C.J., Golub, S.B., Lawlor, K.E., Meeker, C.T., Little, C.B., Last, K., Farmer, P.J., Campbell, I.K., Fourie, A.M. and Fosang, A.J. (2005) 'ADAMTS5 is the major aggrecanase in mouse cartilage in vivo and in vitro', *Nature*, 434(7033), pp. 648-52.

Steinberg, J., Southam, L., Butterfield, N.C., Roumeliotis, T.I., Fontalis, A., Clark, M.J., Jayasuriya, R.L., Swift, D., Shah, K.M., Curry, K.F., Brooks, R.A., McCaskie, A.W., Lelliott, C.J., Choudhary, J.S., Duncan Bassett, J.H., Williams, G.R., Wilkinson, J.M. and Zeggini, E. (2019) 'Decoding the genomic basis of osteoarthritis', 835850 [Online] DOI: <https://doi.org/10.1101/835850>.

Storm, E.E., Huynh, T.V., Copeland, N.G., Jenkins, N.A., Kingsley, D.M. and Lee, S.J. (1994) 'Limb alterations in brachypodism mice due to mutations in a new member of the TGF beta-superfamily', *Nature*, 368(6472), pp. 639-43.

Storm, E.E. and Kingsley, D.M. (1999) 'GDF5 coordinates bone and joint formation during digit development', *Dev Biol*, 209(1), pp. 11-27.

Stoytcheva, Z.R., Vladimirov, V., Douet, V., Stoychev, I. and Berry, M.J. (2010) 'Metal transcription factor-1 regulation via MREs in the transcribed regions of selenoprotein H and other metal-responsive genes', *Biochim Biophys Acta*, 1800(3), pp. 416-24.

Strong, L.C. (1944) 'Genetic Nature of the Constitutional States of Cancer Susceptibility and Resistance in Mice and Men', *Yale J Biol Med*, 17(1), pp. 289-99.

Styrkarsdottir, U., Lund, S.H., Thorleifsson, G., Zink, F., Stefansson, O.A., Sigurdsson, J.K., Juliusson, K., Bjarnadottir, K., Sigurbjornsdottir, S., Jonsson, S., Norland, K., Stefansdottir, L., Sigurdsson, A., Sveinbjornsson, G., Oddsson, A., Bjornsdottir, G., Gudmundsson, R.L., Halldorsson, G.H., Rafnar, T., Jonsdottir, I., Steingrimsson, E., Norddahl, G.L., Masson, G., Sulem, P., Jonsson, H., Ingvarsson, T., Gudbjartsson, D.F., Thorsteinsdottir, U. and Stefansson, K. (2018) 'Meta-analysis of Icelandic and UK data sets identifies missense variants in SMO, IL11, COL11A1 and 13 more new loci associated with osteoarthritis', *Nat Genet*, 50(12), pp. 1681-1687.

Sun, X. and Kaufman, P.D. (2018) 'Ki-67: more than a proliferation marker', *Chromosoma*, 127(2), pp. 175-186.

Tachmazidou, I., Hatzikotoulas, K., Southam, L., Esparza-Gordillo, J., Haberland, V., Zheng, J., Johnson, T., Koprulu, M., Zengini, E., Steinberg, J., Wilkinson, J.M., Bhatnagar, S., Hoffman, J.D., Buchan, N., Suveges, D., arc, O.C., Yerges-Armstrong, L., Smith, G.D., Gaunt, T.R., Scott, R.A., McCarthy, L.C. and

- Zeggini, E. (2019) 'Identification of new therapeutic targets for osteoarthritis through genome-wide analyses of UK Biobank data', *Nat Genet*, 51(2), pp. 230-236.
- Tang, C.H., Hsu, C.J. and Fong, Y.C. (2010) 'The CCL5/CCR5 axis promotes interleukin-6 production in human synovial fibroblasts', *Arthritis Rheum*, 62(12), pp. 3615-24.
- Thomas, A.C., Hubbard-Turner, T., Wikstrom, E.A. and Palmieri-Smith, R.M. (2017) 'Epidemiology of Posttraumatic Osteoarthritis', *J Athl Train*, 52(6), pp. 491-496.
- THOMAS, L. (1956) 'Reversible collapse of rabbit ears after intravenous papain, and prevention of recovery by cortisone', *J Exp Med*, 104(2), pp. 245-52.
- Todd, W.R., Elvehjem, C.A. and Hart, E.B. (1933) 'Zinc in the nutrition of the rat', *American Journal of Physiology*, 107(1), pp. 146-156.
- Tortorella, M.D., Burn, T.C., Pratta, M.A., Abbaszade, I., Hollis, J.M., Liu, R., Rosenfeld, S.A., Copeland, R.A., Decicco, C.P., Wynn, R., Rockwell, A., Yang, F., Duke, J.L., Solomon, K., George, H., Bruckner, R., Nagase, H., Itoh, Y., Ellis, D.M., Ross, H., Wiswall, B.H., Murphy, K., Hillman, M.C., Hollis, G.F., Newton, R.C., Magolda, R.L., Trzaskos, J.M. and Arner, E.C. (1999) 'Purification and cloning of aggrecanase-1: a member of the ADAMTS family of proteins', *Science*, 284(5420), pp. 1664-6.
- Tortorella, M.D., Liu, R.Q., Burn, T., Newton, R.C. and Arner, E. (2002) 'Characterization of human aggrecanase 2 (ADAM-TS5): substrate specificity studies and comparison with aggrecanase 1 (ADAM-TS4)', *Matrix Biol*, 21(6), pp. 499-511.
- Tuschl, K., Meyer, E., Valdivia, L.E., Zhao, N., Dadswell, C., Abdul-Sada, A., Hung, C.Y., Simpson, M.A., Chong, W.K., Jacques, T.S., Woltjer, R.L., Eaton, S., Gregory, A., Sanford, L., Kara, E., Houlden, H., Cuno, S.M., Prokisch, H., Valletta, L., Tiranti, V., Younis, R., Maher, E.R., Spencer, J., Straatman-Iwanowska, A., Gissen, P., Selim, L.A., Pintos-Morell, G., Coroleu-Lletget, W., Mohammad, S.S., Yoganathan, S., Dale, R.C., Thomas, M., Rihel, J., Bodamer, O.A., Enns, C.A., Hayflick, S.J., Clayton, P.T., Mills, P.B., Kurian, M.A. and Wilson, S.W. (2016) 'Mutations in SLC39A14 disrupt manganese homeostasis and cause childhood-onset parkinsonism-dystonia', *Nat Commun*, 7, p. 11601.
- Tyler, J.A. (1985) 'Articular cartilage cultured with catabolin (pig interleukin 1) synthesizes a decreased number of normal proteoglycan molecules', *Biochem J*, 227(3), pp. 869-78.
- van der Kraan, P.M., Buma, P., van Kuppevelt, T. and van den Berg, W.B. (2002) 'Interaction of chondrocytes, extracellular matrix and growth factors: relevance for articular cartilage tissue engineering', *Osteoarthritis Cartilage*, 10(8), pp. 631-7.

- Vance, D.D., Wang, L., Rampersaud, E., Lesniak, B.P., Vance, J.M., Pericak-Vance, M.A. and Kaplan, L.D. (2014) 'Dynamic gene expression profile changes in synovial fluid following meniscal injury; osteoarthritis (OA) markers found', *Journal of Exercise, Sports & Orthopedics*, 1, pp. 1-7.
- Verma, P. and Dalal, K. (2011) 'ADAMTS-4 and ADAMTS-5: key enzymes in osteoarthritis', *J Cell Biochem*, 112(12), pp. 3507-14.
- Verzijl, N., DeGroot, J., Ben, Z.C., Brau-Benjamin, O., Maroudas, A., Bank, R.A., Mizrahi, J., Schalkwijk, C.G., Thorpe, S.R., Baynes, J.W., Bijlsma, J.W., Lafeber, F.P. and TeKoppele, J.M. (2002) 'Crosslinking by advanced glycation end products increases the stiffness of the collagen network in human articular cartilage: a possible mechanism through which age is a risk factor for osteoarthritis', *Arthritis Rheum*, 46(1), pp. 114-23.
- Vincent, T.L., McLean, C.J., Full, L.E., Peston, D. and Saklatvala, J. (2007) 'FGF-2 is bound to perlecan in the pericellular matrix of articular cartilage, where it acts as a chondrocyte mechanotransducer', *Osteoarthritis Cartilage*, 15(7), pp. 752-63.
- Wadsworth, P. (2015) 'TPX2', *Curr Biol*, 25(24), pp. R1156-8.
- Wang, M., Sampson, E.R., Jin, H., Li, J., Ke, Q.H., Im, H.J. and Chen, D. (2013) 'MMP13 is a critical target gene during the progression of osteoarthritis', *Arthritis Res Ther*, 15(1), p. R5.
- Wang, Q., Rozelle, A.L., Lopus, C.M., Scanzello, C.R., Song, J.J., Larsen, D.M., Crish, J.F., Bebek, G., Ritter, S.Y., Lindstrom, T.M., Hwang, I., Wong, H.H., Punzi, L., Encarnacion, A., Shamloo, M., Goodman, S.B., Wyss-Coray, T., Goldring, S.R., Banda, N.K., Thurman, J.M., Gobeze, R., Crow, M.K., Holers, V.M., Lee, D.M. and Robinson, W.H. (2011) 'Identification of a central role for complement in osteoarthritis', *Nat Med*, 17(12), pp. 1674-9.
- Wentorf, F.A., Sudoh, K., Moses, C., Arendt, E.A. and Carlson, C.S. (2006) 'The effects of estrogen on material and mechanical properties of the intra- and extra-articular knee structures', *American Journal of Sports Medicine*, 34(12), pp. 1948-1952.
- Wimmer, U., Wang, Y., Georgiev, O. and Schaffner, W. (2005) 'Two major branches of anti-cadmium defense in the mouse: MTF-1/metallothioneins and glutathione', *Nucleic Acids Res*, 33(18), pp. 5715-27.
- Won, Y., Shin, Y., Chun, C.H., Cho, Y., Ha, C.W., Kim, J.H. and Chun, J.S. (2016) 'Pleiotropic roles of metallothioneins as regulators of chondrocyte apoptosis and catabolic and anabolic pathways during osteoarthritis pathogenesis', *Ann Rheum Dis*, 75(11), pp. 2045-2052.

Xu, T., Bianco, P., Fisher, L.W., Longenecker, G., Smith, E., Goldstein, S., Bonadio, J., Boskey, A., Heegaard, A.M., Sommer, B., Satomura, K., Dominguez, P., Zhao, C., Kulkarni, A.B., Robey, P.G. and Young, M.F. (1998) 'Targeted disruption of the biglycan gene leads to an osteoporosis-like phenotype in mice', *Nat Genet*, 20(1), pp. 78-82.

Xu, Y., Barter, M.J., Swan, D.C., Rankin, K.S., Rowan, A.D., Santibanez-Koref, M., Loughlin, J. and Young, D.A. (2012) 'Identification of the pathogenic pathways in osteoarthritic hip cartilage: commonality and discord between hip and knee OA', *Osteoarthritis Cartilage*, 20(9), pp. 1029-38.

Yang, Q., Mukundan, A., Thorsten, K., You Jin, L., Shoshana, Y., Zhongbo, L., Abramson, S.B. and Mignatti, P. (2015) 'Membrane-type 1 matrix metalloproteinase controls osteo- and chondrogenesis by a proteolysis-independent mechanism mediated by its cytoplasmic tail', *Osteoarthritis and Cartilage*, 23.

Yao, W., Balooch, G., Balooch, M., iang, Y., Nalla, R.K., Kinney, J., Wronski, T.J. and Lane, N.E. (2006) 'Sequential treatment of ovariectomized mice with bFGF and risedronate restored trabecular bone microarchitecture and mineralization', *Bone*, 39(3), pp. 460-469.

Yazar, M., Sarban, S., Kocyigit, A. and Isikan, U.E. (2005) 'Synovial fluid and plasma selenium, copper, zinc, and iron concentrations in patients with rheumatoid arthritis and osteoarthritis', *Biol Trace Elem Res*, 106(2), pp. 123-32.

Young, D.A., Lakey, R.L., Pennington, C.J., Jones, D., Kevorkian, L., Edwards, D.R., Cawston, T.E. and Clark, I.M. (2005) 'Histone deacetylase inhibitors modulate metalloproteinase gene expression in chondrocytes and block cartilage resorption', *Arthritis Res Ther*, 7(3), pp. R503-12.

Zengini, E., Hatzikotoulas, K., Tachmazidou, I., Steinberg, J., Hartwig, F.P., Southam, L., Hackinger, S., Boer, C.G., Styrkarsdottir, U., Gilly, A., Suveges, D., Killian, B., Ingvarsson, T., Jonsson, H., Babis, G.C., McCaskie, A., Uitterlinden, A.G., van Meurs, J.B.J., Thorsteinsdottir, U., Stefansson, K., Davey Smith, G., Wilkinson, J.M. and Zeggini, E. (2018) 'Genome-wide analyses using UK Biobank data provide insights into the genetic architecture of osteoarthritis', *Nat Genet*, 50(4), pp. 549-558.

Zhu, S., Makosa, D., Miller, B. and Griffin, T.M. (2020) 'Glutathione as a mediator of cartilage oxidative stress resistance and resilience during aging and osteoarthritis', *Connect Tissue Res*, 61(1), pp. 34-47.

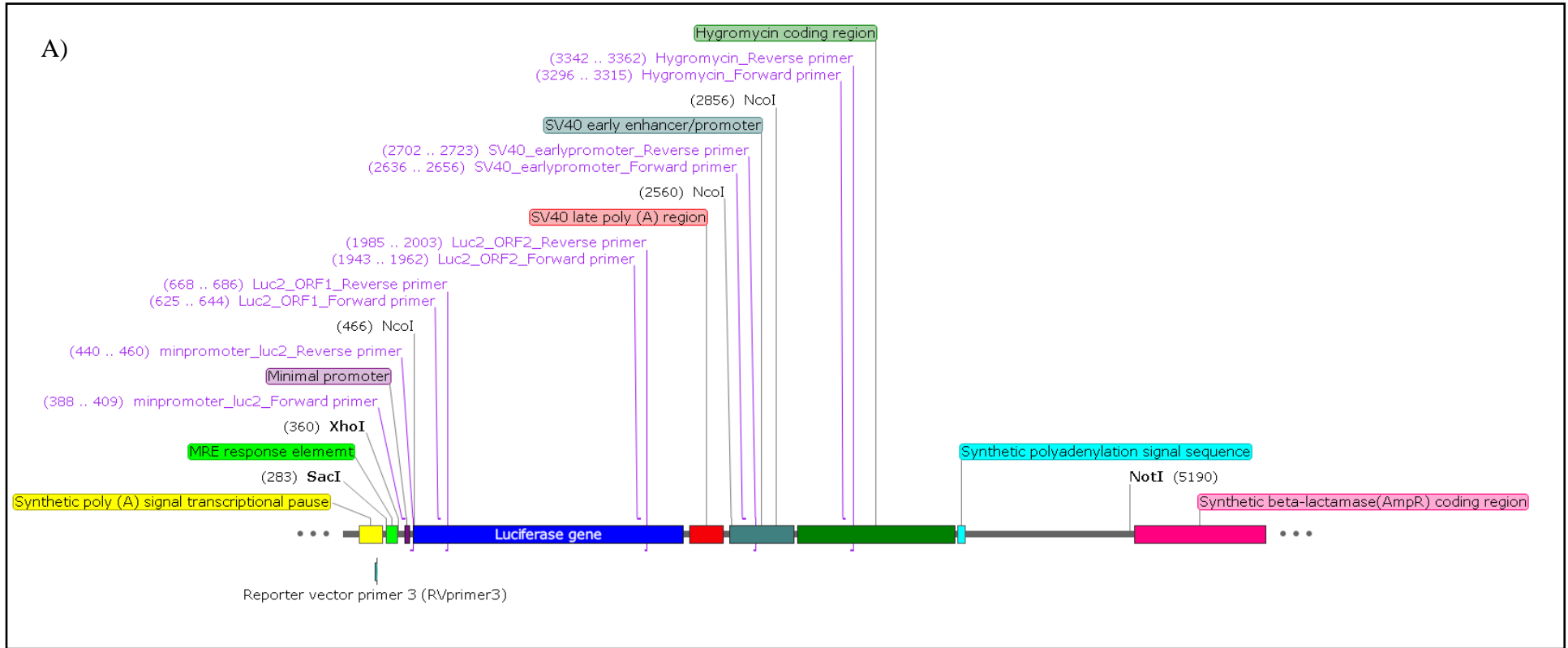
Ziller, A. and Fraissinet-Tachet, L. (2018) 'Metallothionein diversity and distribution in the tree of life: a multifunctional protein', *Metallomics*, 10(11), pp. 1549-1559.

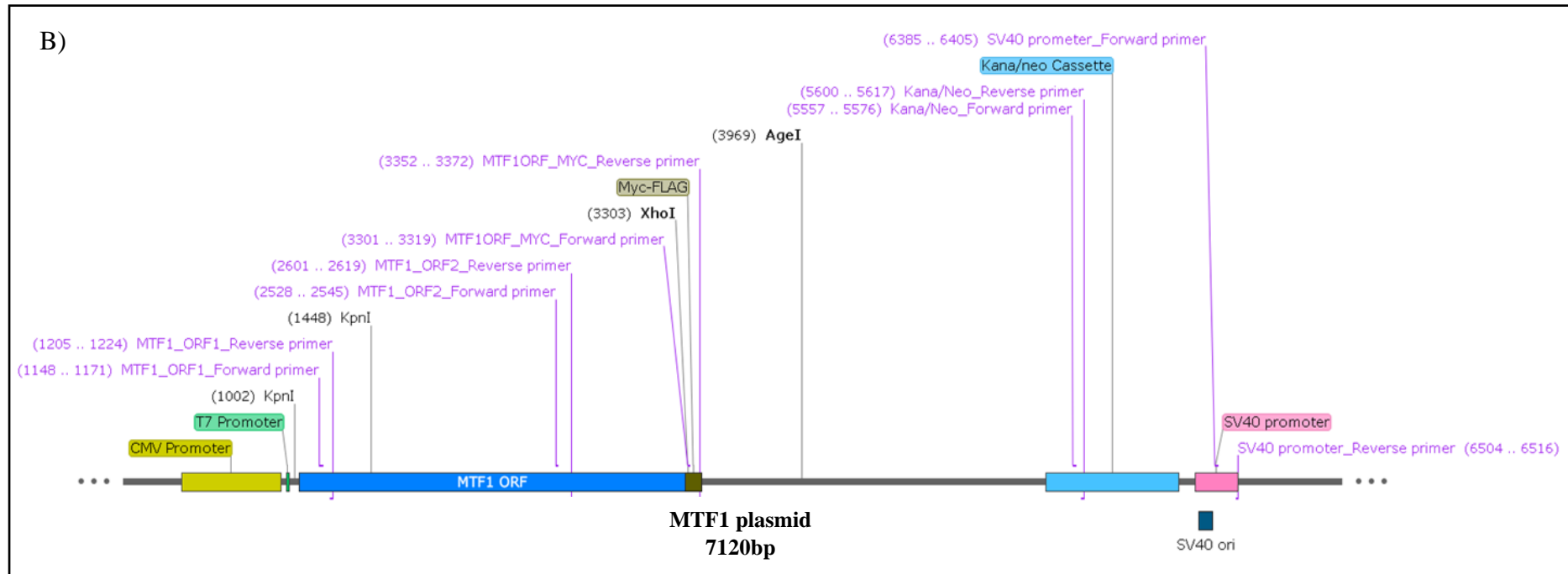
Øiestad, B.E., Engebretsen, L., Storheim, K. and Risberg, M.A. (2009) 'Knee osteoarthritis after anterior cruciate ligament injury: a systematic review', *Am J Sports Med*, 37(7), pp. 1434-43.



# Chapter 9. APPENDIX

275





**Plasmid maps for A) pGL4.40[luc2P/MRE/Hygro] and B) pCMV6-MTF1 plasmids generated in SnapGene Viewer (<https://www.snapgene.com/snapgene-viewer/>).** Plasmid maps were created initially using A Plasmid Editor Software (<http://jorgensen.biology.utah.edu/wayned/ape/>) and the .ape files were loaded into SnapGene Viewer and exported as Tiff images. The pGL4.4[luc2P/MRE/Hygro] plasmid MRE (light green) is flanked by SacI and XhoI restriction sites which were used to remove the metal response element (MRE) and was religated with the multiple cloning sequence (MCS). NotI or AgeI restriction enzymes were used for the preparation of linear pGL4.40[luc2P/MRE/Hygro] and pCM6-MTF1 plasmids respectively. NcoI or a combination of KpnI and XhoI was used to confirm the uptake of pGL4.40[luc2P/MRE/Hygro] and pCMV6-MTF1 plasmids respectively following bacterial transformation and DNA isolation. MluI restriction enzyme (not shown) was used to cut the empty control pGL4.40 plasmid after cloning the pGL4.40[luc2P/MRE/Hygro] plasmid. The antibiotic resistance genes are A) ampicillin (pink) and B) kanamycin/neomycin (light blue) ensuring *E. coli* survival after transformation. The hygromycin region in A) provides resistance to hygromycin B in pGL4.40[luc2P/MRE/Hygro] plasmid transfected eukaryotes. Neomycin (Kana/neo cassette in B) prevents MTF1 plasmid-transfected eukaryotic cells from dying in response to G418 antibiotic. Locations of restriction enzymes and qPCR primers are detailed and their position in the sequence map highlighted. Primer binding locations are highlighted on the plasmids in purple.

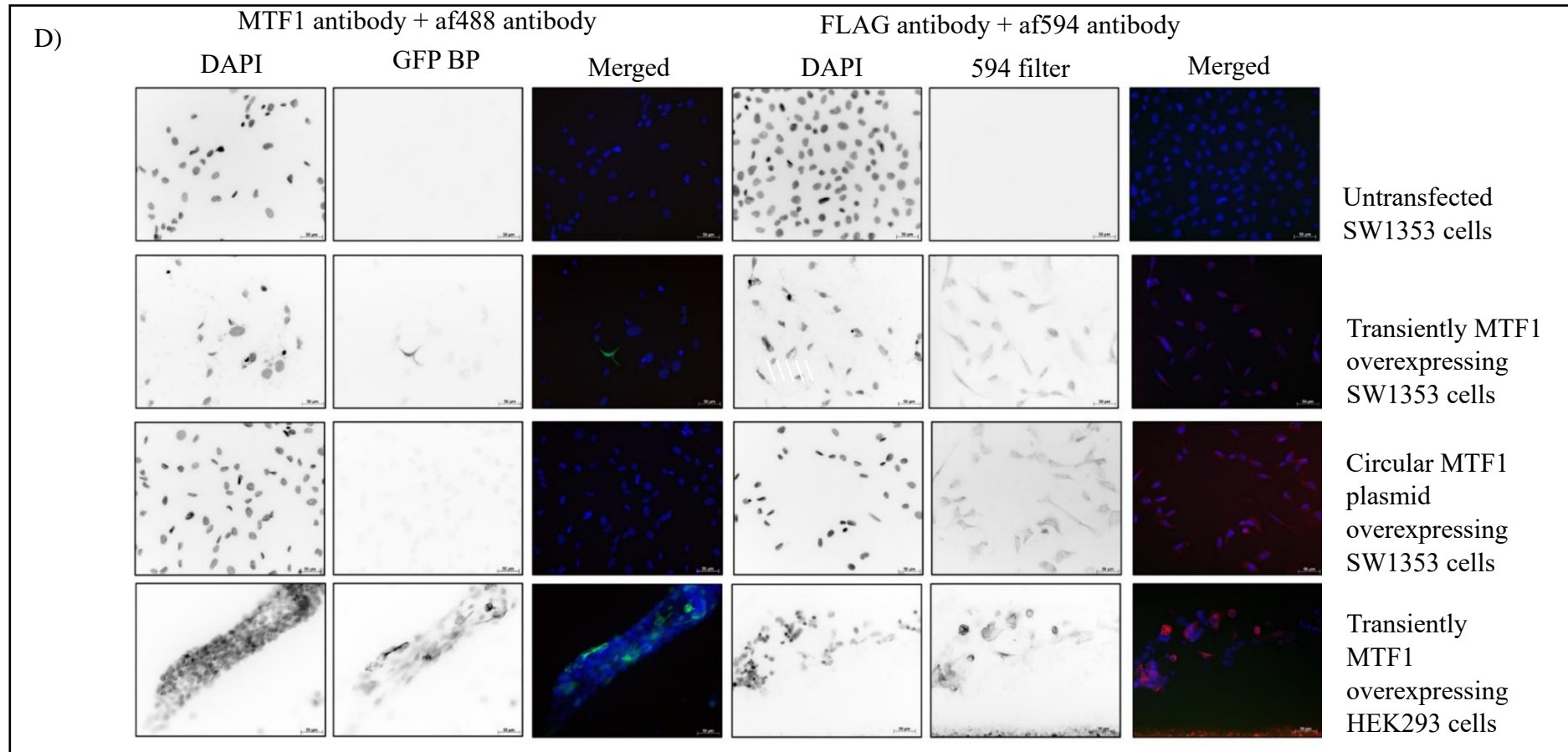
C) pGL4.40 luciferase plasmid

MTF1 plasmid

		plasmid ng			
Ct ratios		0.000008	0.0004	0.02	1
	Min promoter vs LUC2 ORF1	1.026	1.021	1.020	1.050
	Min promoter vs LUC2 ORF2	0.993	0.996	1.006	1.057
	Min promoter vs SV40 early promoter	1.075	1.062	0.989	1.082
	Min promoter vs hygro	1.030	1.098	0.994	1.022
	LUC2 ORF1 vs LUC2 ORF2	0.967	0.975	0.986	1.007
	LUC2 ORF1 vs SV40 early promoter	1.047	1.041	0.969	1.030
	LUC2 ORF1 vs hygro	1.003	1.075	0.975	0.973
	LUC2 ORF2 vs SV40 early promoter	1.082	1.067	0.983	1.023
	LUC2 ORF2 vs hygro	1.037	1.102	0.989	0.966
	SV40 early promoter vs hygro	0.958	1.033	1.006	0.944
Min promoter	min	0.993	0.996	0.989	1.022
	max	1.075	1.098	1.020	1.082
	median	<b>1.028</b>	<b>1.042</b>	<b>1.000</b>	<b>1.054</b>
LUC2 ORF1	min	0.967	0.975	0.969	0.973
	max	1.047	1.075	1.020	1.050
	median	<b>1.015</b>	<b>1.031</b>	<b>0.980</b>	<b>1.019</b>
Luc2 ORF2	min	0.967	0.975	0.983	0.966
	max	1.082	1.102	1.006	1.057
	median	<b>1.015</b>	<b>1.031</b>	<b>0.987</b>	<b>1.015</b>
SV40 early promoter	min	1.037	1.033	0.969	0.944
	max	1.082	1.102	0.989	1.082
	median	<b>1.061</b>	<b>1.065</b>	<b>0.986</b>	<b>1.027</b>
hygro	min	0.958	1.033	0.975	0.944
	max	1.082	1.067	1.006	1.023
	median	<b>1.042</b>	<b>1.069</b>	<b>0.989</b>	<b>1.026</b>

		plasmid ng			
Ct ratios		0.00000016	0.000008	0.0004	0.02
	MTF1_ORF1 vs MTF1_ORF2	0.928	0.923	0.932	0.936
	MTF1_ORF1 vs MTF1_Tag	0.976	0.955	0.947	0.951
	MTF1_ORF1 vs SV40	0.929	0.946	0.941	0.925
	MTF1_ORF1 vs kana/neo	0.953	0.953	0.950	0.952
	MTF1_ORF2 vs MTF1_Tag	1.052	1.034	1.016	1.015
	MTF1_ORF2 vs SV40	1.001	1.024	1.010	0.988
	MTF1_ORF2 vs kana/neo	1.028	1.032	1.020	1.017
	MTF1_Tag vs Sv40	0.951	0.991	0.994	0.973
	MTF1_Tag vs kana/neo	0.976	0.998	1.003	1.002
	SV40 vs kana/neo	1.026	1.008	1.010	1.029
MTF1_ORF1	min	0.929	0.923	0.932	0.925
	max	0.953	0.955	0.950	0.952
	median	<b>0.941</b>	<b>0.949</b>	<b>0.944</b>	<b>0.944</b>
MTF1_ORF2	min	0.936	0.923	0.932	0.936
	max	1.052	1.034	1.020	1.017
	median	<b>1.014</b>	<b>1.028</b>	<b>1.013</b>	<b>1.002</b>
MTF1_Tag	min	0.951	0.955	0.947	0.951
	max	1.052	1.034	1.016	1.015
	median	<b>0.964</b>	<b>0.994</b>	<b>0.998</b>	<b>0.987</b>
SV40	min	0.929	0.946	0.941	0.925
	max	1.001	1.024	1.010	1.002
	median	<b>0.964</b>	<b>0.994</b>	<b>0.998</b>	<b>0.981</b>
kana/neo	min	0.953	0.953	0.950	0.952
	max	1.052	1.034	1.016	1.029
	median	<b>0.965</b>	<b>0.976</b>	<b>0.977</b>	<b>0.970</b>

**qPCR plasmid primer assay validation for pGL4.40[luc2P/MRE/Hygro] and pCMV6-MTF1 plasmids respectively.** One or 0.02ng/μl of pGL4.40[luc2P/MRE/Hygro] or pCMV6-MTF1 plasmid were diluted 50-fold for four serial dilutions and used in separate qPCR reactions set up in technical triplicate with each respective primer pair listed in column one of each table. Theoretically, the C<sub>t</sub> ratio between the different amplified sequences from the plasmids should all be identical (approximately one) if the primers are working, because one sequence is not preferentially transcribed over any other. Thus, the C<sub>t</sub> ratios from the experiment were calculated for every possible primer combination from the separate reactions across the diluted plasmid series. The range (minimum and maximum) and median values were calculated and reported and so justified the use of all primers, but specifically the primers for the transcribed regions of *luciferase* and *MTF1*.



**ICC results from eight-well chamber slides containing untransfected, transiently MTF1-transfected, undigested circular MTF1 plasmid overexpressing SW1353 cells and transiently MTF1-transfected HEK293 cells.** Cells were stained with C-terminal MTF1 (Santa Cruz, 365090) or FLAG (CST, 2368) antibodies and the respective goat anti-mouse IgG 488 or goat anti-rabbit IgG af594 secondary antibodies. Cells were efficiently permeabilised and greater care taken with PBS washes gave greater cell numbers for counting. However, the FLAG antibody bound non-specifically in SW1353 cells transiently transfected with MTF1 plasmid. Camera exposure times were 1.344 and 0.656 seconds for the GFP BP and the 594 filter respectively. Images presented are representative for the whole well among 3-4 images taken per well per field of view. The magnification is x20 and the scale bars are 50 $\mu$ m.

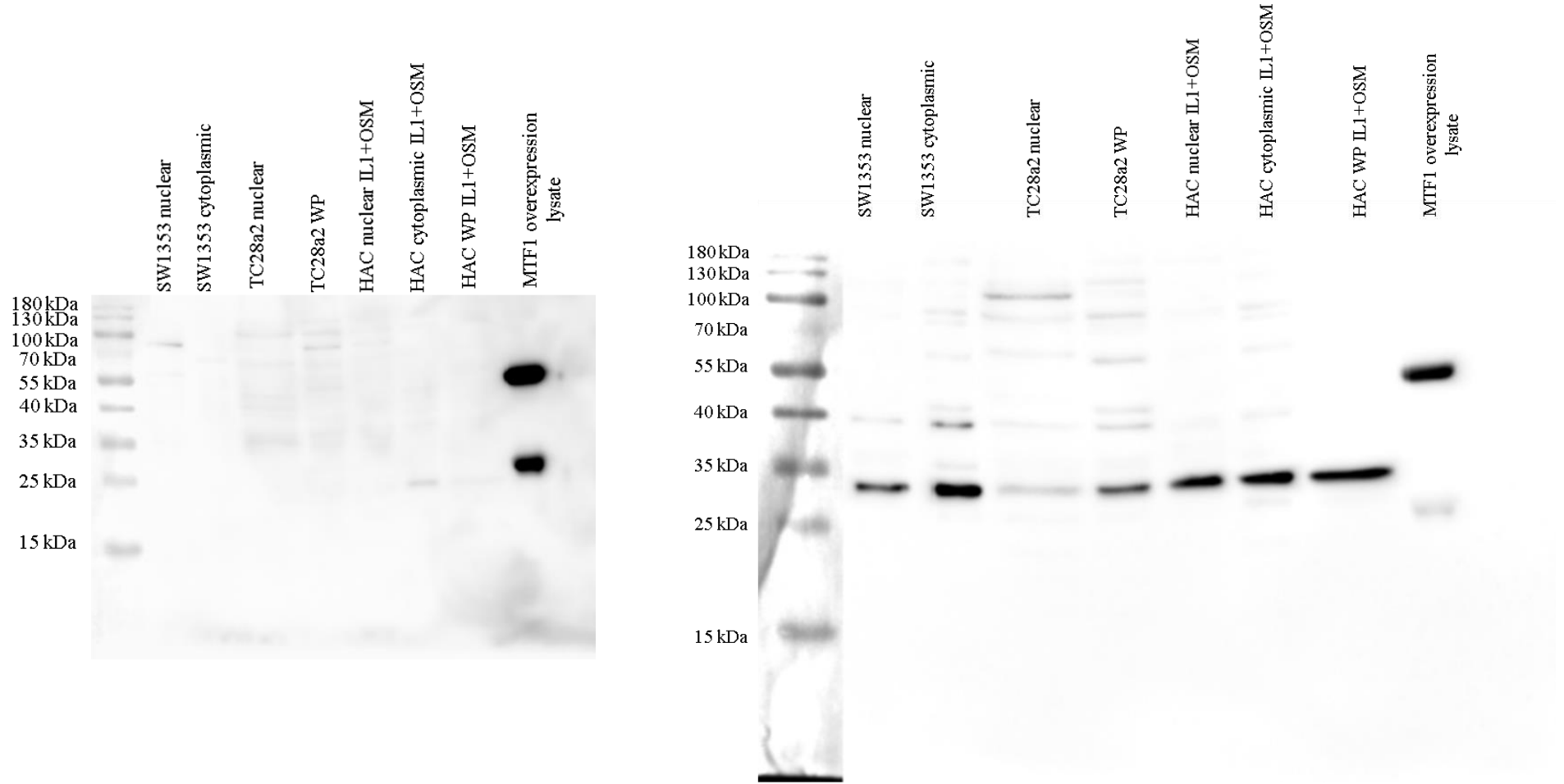
**T/C-28a2 gene expression fold changes relative to control flasks per passage from each experiment.** The table shows all fold changes and standard deviations of pro-inflammatory genes, *MTs*, *MTF1* and zinc transporters from all experiments and every sample derived from flasks from those experiments. Two experiments were conducted in which T/C-28a2 cells were treated with or without 0.25ng/ml IL-1 $\alpha$  for three passages, after which it was removed and the cells passaged for a further 72 hours. Four additional experiments were carried out for 72 hours only. Each experiment was conducted in biological triplicate per passage, but the RNA quality was poor during extraction of the second series of flasks (control and IL-1 $\alpha$ -treated) in experiment two and in the first pair of flasks in the series (control and IL-1 $\alpha$ -treated) from experiment one. N/A indicates genes that were not measured because of a problem of the quality of the RNA from a passage one control flask (experiment two sample from flask series three) after extraction, or where the standard deviation could not be calculated. Unprioritised genes were not measured (nm) in experiments conducted later in the PhD (experiments three-six). Values highlighted in red are outliers among the biological replicates. Data in bold is significant following either paired t-test of the normalised or log<sub>2</sub> transformed gene expression data or Wilcoxon t-test for non-normal IL-1 $\alpha$  and control pairings.

Genes E)	24 hours			Mean	S.D	P1 (72 hours)															Mean	S.D	P2 (144 hours)						Mean	S.D	P3 (216 hours)					Mean	S.D	P4 (288 hours)						
	IL-1 $\alpha$ present					IL-1 $\alpha$ present																	IL-1 $\alpha$ present								IL-1 $\alpha$ absent													
	Experiment					Experiment																	Experiment								Experiment													
	1	2	3			1	2	3	4	5	6	1	2	3	4	5	6	1	2	3			1	2	3	4	5	6			1	2	3	4	5			6	1	2	3	4	5	6
	Samples					Samples																	Samples								Samples													
<i>IL-6</i>	10.0	10.2	9.5	<b>9.9</b>	<b>0.34</b>	3.0	4.8	3.0	10.31	26.4	27.4	25.1	11.7	11.6	12.8	9.4	7.2	8.1	15.3	14.7	15.7	<b>12.9</b>	<b>7.72</b>	7.1	5.8	4.9	8.7	13.0	<b>7.9</b>	<b>3.18</b>	9.6	<b>2.3</b>	4.5	7.8	8.0	<b>7.5</b>	<b>2.15</b>	0.6	0.6	0.7	0.6	0.6	0.8	
<i>CXCL8</i>	86.4	99.1	98.5	<b>94.7</b>	<b>7.14</b>	6.2	6.9	6.0	51.8	102.8	77.5	101.2	67.5	65.0	76.1	25.5	22.0	21.1	237.1	246.4	300.5	<b>88.3</b>	<b>92.42</b>	37.3	24.9	22.9	95.0	109.1	<b>57.9</b>	<b>41.04</b>	63	<b>5.4</b>	49	66	70.1	<b>62.0</b>	<b>9.28</b>	0.8	0.7	0.8	0.9	0.8	0.07	
<i>CCL2</i>	9.0	6.1	7.4	<b>7.5</b>	<b>1.44</b>	4.8	6.2	6.4	12.0	8.7	7.0	7.7	7.3	7.0	7.8	16.7	15.4	13.8	24.0	25.7	23.0	<b>12.1</b>	<b>6.94</b>	11.4	11.7	12.0	21.4	23.4	<b>16.0</b>	<b>5.87</b>	17	<b>1.6</b>	13	19	23.8	<b>18.3</b>	<b>8.36</b>	3.6	1.6	0.8	1.5	1.8	1.19	
<i>ADAMTS5</i>	1.1	1.1	1.4	1.2	0.17	1.7	1.9	1.5	1.2	2.4	1.9	2.0	1.3	1.2	1.4	2.3	2.2	2.5	1.8	1.5	1.8	<b>1.8</b>	<b>0.42</b>	2.4	1.9	1.6	1.4	1.4	<b>1.8</b>	<b>0.42</b>	2.7	1.1	1.6	1.6	reverse transcription issue	1.7	0.66	1.2	1.2	1.0	1.3	1.2	0.16	
<i>MMP13</i>	2.2	2.6	2.7	2.5	0.27	1.7	2.2	1.8	2.4	3.3	2.9	3.2	2.2	1.9	2.2	2.6	2.2	2.5	3.1	3.0	3.4	<b>2.5</b>	<b>0.56</b>	3.5	2.1	1.9	2.6	3.0	2.6	0.66	5.3	1.3	2	2.1	reverse transcription issue	<b>2.7</b>	<b>1.78</b>	1.1	0.8	0.2	0.7	0.7	0.36	
<i>MTF1</i>	1.1	0.9	1.0	1.0	0.07	1.0	1.6	1.4	1.0	nm	nm	nm	nm	nm	nm	nm	nm	nm	nm	nm	1.2	0.30	1.1	0.9	0.8	1.1	0.8	0.9	0.13	1.2	1	0.8	1.3	reverse transcription issue	1.1	0.23	1.0	0.9	1.0	0.9	0.9	0.07		
<i>MT1A</i>	1.3	3.8	3.3	2.8	1.30	2.9	3.5	3.9	2.8	4.4	5.6	5.0	4.3	3.2	5.0	4.0	3.7	2.9	3.2	3.7	4.1	<b>3.9</b>	<b>0.82</b>	2.3	2.5	2.1	3.4	2.2	<b>2.5</b>	<b>0.53</b>	2.7	2.1	2.5	2.7	reverse transcription issue	2.5	0.31	1.1	0.9	1.3	0.7	1.0	0.28	
<i>MT1G</i>	2.4	2.5	2.4	2.5	0.08	2.8	2.2	2.2	1.2	2.7	2.5	2.1	1.2	1.2	1.4	0.9	0.9	0.7	1.7	1.3	2.1	<b>1.7</b>	<b>0.68</b>	0.5	1.7	1.1	1.3	0.7	1.1	0.46	1.3	1.1	1.5	1.6	reverse transcription issue	1.4	0.22	1.2	0.9	1.8	0.9	1.2	0.45	
<i>SLC30A1</i>	1.0	1.2	1.0	1.1	0.14	0.5	1.2	0.8	0.9	N/A	N/A	N/A	N/A	N/A	N/A	N/A	N/A	N/A	N/A	N/A	N/A	0.8	0.31	1.9	0.6	0.9	0.9	0.6	1.0	0.56	0.9	0.4	0.5	0.7	0.4	<b>0.6</b>	<b>0.22</b>	1.1	0.8	1.4	1.1	1.1	0.27	
<i>SLC30A2</i>	1.0	1.0	0.8	0.9	0.12	0.9	2.7	1.8	1.1	1.6	0.81	0.6	1.2	1.3	0.8	0.8	0.8	0.9	0.28	1.4	0.9	0.7	1.4	0.5	1.0	0.39	1.4	1.0	1.3	1.0	1.1	0.20												
<i>SLC30A3</i>	0.7	0.6	0.5	<b>0.6</b>	<b>0.07</b>	0.3	1.4	0.4	1.0	0.8	0.51	2.3	0.7	0.5	0.6	0.8	1.0	0.74	0.2	0.1	0.3	0.8	0.6	0.4	0.29	1.0	0.7	1.6	0.8	1.0	0.44													
<i>SLC30A5</i>	0.5	0.8	0.6	0.6	0.16	0.1	0.2	0.1	1.3	0.4	0.59	<b>12.6</b>	0.4	0.4	0.4	1.1	0.6	<b>0.34</b>	0.1	0.1	0.1	0.5	0.5	0.2	0.22	0.8	0.2	0.8	1.6	0.9	0.57													
<i>SLC30A6</i>	1.0	0.9	1.1	1.0	0.11	1.2	1.5	1.3	0.9	1.2	0.22	0.8	1.0	1.0	0.8	1.0	0.9	0.12	1.5	1.3	1.1	0.8	0.8	1.1	0.29	1.1	0.9	1.2	1.4	1.2	0.21													
<i>SLC30A7</i>	1.0	0.8	0.9	0.9	0.08	1.4	0.9	0.7	1.0	1.0	0.28	0.6	1.3	0.7	0.9	0.9	0.9	0.9	0.9	0.9	0.9	0.9	0.27	1.3	0.8	0.6	0.8	0.9	0.9	0.25	1.0	1.0	1.3	1.2	1.1	0.19								
<i>SLC30A9</i>	0.8	0.8	1.2	1.0	0.24	1.6	1.1	0.5	0.7	nm	nm	nm	nm	nm	nm	nm	nm	nm	nm	nm	nm	1.0	0.50	1.1	1.2	0.7	0.8	0.6	0.9	0.23	1.3	0.7	0.6	0.9	reverse transcription issue	0.9	0.32	1.0	0.8	0.2	0.4	0.6	0.33	
<i>SLC39A1</i>	1.2	1.0	0.7	0.9	0.25	0.8	0.9	0.7	1.4	0.9	0.29	1.7	1.0	1.4	1.0	0.9	1.2	0.31	0.5	0.9	1.2	0.8	0.6	0.8	0.26	1.3	1.0	0.8	0.7	1.0	0.28													
<i>SLC39A3</i>	1.2	1.0	0.9	1.0	0.12	1.0	1.0	1.1	1.4	1.1	0.17	1.3	1.0	1.2	1.0	0.9	1.1	0.18	1	1	0.9	0.9	0.7	0.9	0.13	0.8	0.6	1.0	0.9	<b>0.8</b>	<b>0.14</b>													
<i>SLC39A4</i>	1.1	nm	nm	1.1	n/a	1.0	<b>2.1</b>	0.8	nm	1.3	0.65	<b>2.4</b>	0.7	0.7	nm	nm	0.7	n/a	<b>1.6</b>	0.9	0.4	nm	nm	0.6	n/a	<b>1.4</b>	0.6	nm	nm	1.0	na													
<i>SLC39A6</i>	0.8	1.1	1.0	1.0	0.15	1.1	1.3	0.9	1.2	1.1	0.16	1.1	0.9	1.0	0.9	0.9	1.0	0.08	1.6	1.2	0.9	0.8	1.0	1.1	0.31	1.0	0.7	1.1	1.2	1.0	0.19													
<i>SLC39A7</i>	1.0	1.2	0.9	1.1	0.15	1.1	1.8	1.2	1.2	1.3	0.33	1.3	1.1	0.8	0.9	0.8	1.0	0.23	0.5	0.7	0.7	0.6	0.4	0.6	0.13	1.1	0.7	1.2	0.9	1.0	0.24													
<i>SLC39A8</i>	1.0	1.1	2.0	1.4	0.57	1.3	1.3	1.1	0.6	1.0	1.3	0.4	0.8	0.7	1.8	1.2	1.4	0.9	0.8	1.4	0.6	1.0	0.37	0.6	0.9	1.1	0.8	1.5	1.0	0.33	1.2	1.2	1	1.9	reverse transcription issue	1.3	0.39	1.0	1.0	0.5	1.3	1.0	0.33	
<i>SLC39A9</i>	0.7	1.0	0.9	0.9	0.13	0.9	1.5	0.9	0.9	1.1	0.30	1.3	0.9	0.9	0.7	0.9	0.24	1.4	1	0.8	1	0.8	1.0	0.27	0.9	0.8	1.0	1.0	0.9	1.0	0.9	0.10												
<i>SLC39A10</i>	0.8	0.9	1.0	0.9	0.13	0.9	1.1	1.0	0.7	nm	nm	nm	nm	nm	nm	nm	nm	nm	nm	nm	nm	0.9	0.17	1.1	1.1	1.0	1.0	0.8	1.0	0.12	1.3	0.9	1	0.8	reverse transcription issue	1.0	0.22	1.1	0.7	1.1	1.0	1.0	0.21	
<i>SLC39A11</i>	0.8	1.0	0.7	0.9	0.14	0.8	1.1	1.0	1.0	0.9	0.12	1.6	1.2	1.0	1.1	0.9	1.2	0.27	0.5	0.7	0.6	0.8	0.7	0.7	0.11	1.1	0.8	1.2	0.9	1.0	0.17													
<i>SLC39A13</i>	1.0	1.1	1.1	1.1	0.07	1.1	1.3	1.0	1.2	<b>1.2</b>	<b>0.14</b>	1.4	1.3	1.4	1.0	0.8	1.2	0.26	1.5	0.8	1.3	1.1	0.9	1.1	0.27	1.1	0.5	0.9	0.8	0.8	0.23													
<i>SLC39A14</i>	1.9	1.8	1.4	1.7	0.22	1.9	3.4	2.4	2.0	1.8	1.7	0.5	2.5	2.3	2.9	2.4	2.3	2.5	1.8	2.0	2.1	<b>2.2</b>	<b>0.62</b>	2.0	2.0	1.8	2.0	1.8	1.9	0.11	1.4	1.1	1.8	2.4	2.0	1.7	0.50	1.1	0.9	0.8	0.6	0.8	0.23	

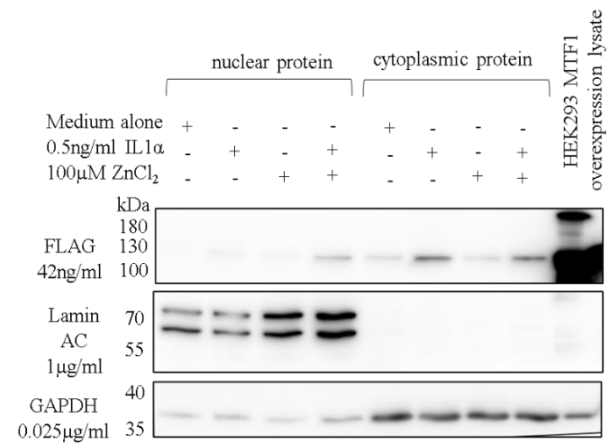
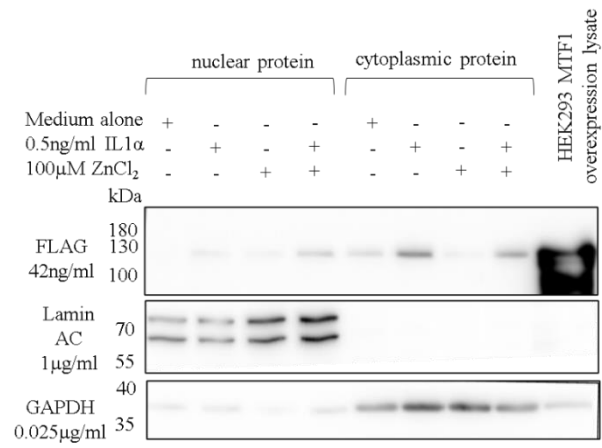
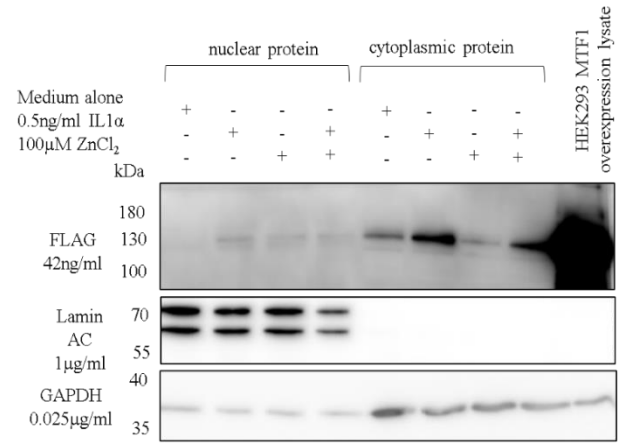
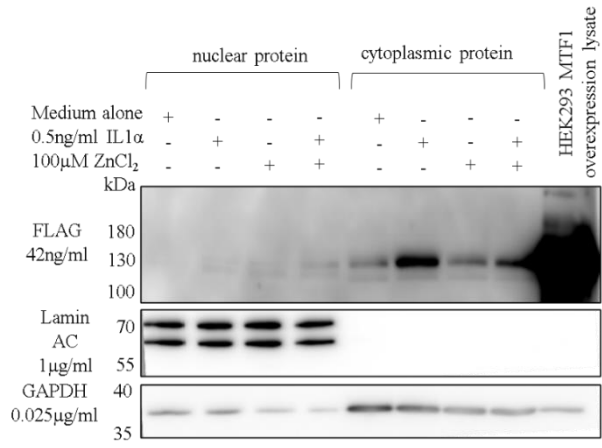


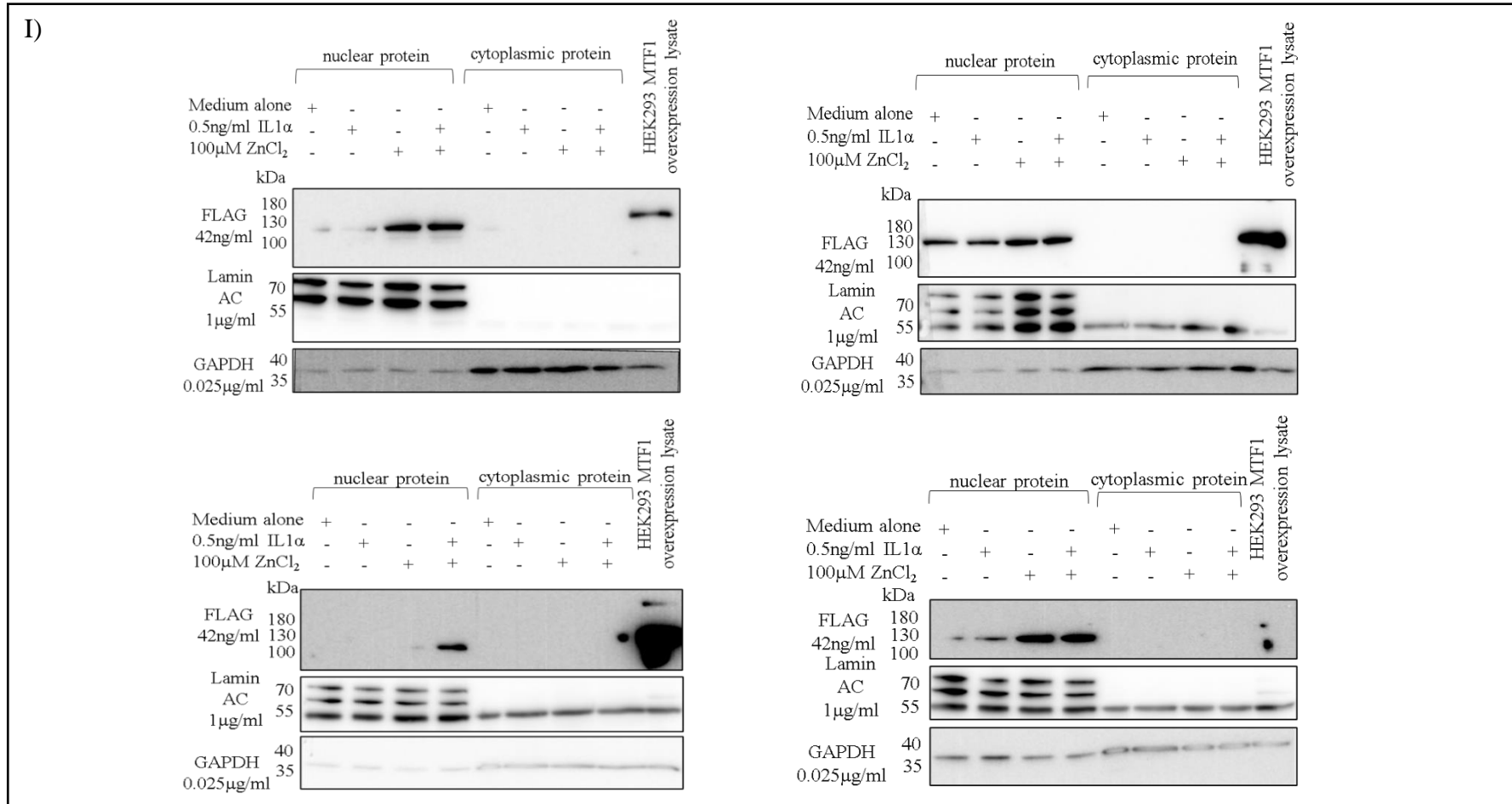
G)

**Uncropped western blot for MTF1 protein in HAC, SW1353 and T/C-28a2 lysates and overexpressed MTF1 in HEK293 lysate.** The blot to the left was first probed with C-terminal MTF1 antibody before later reprobing with N-terminal MTF1 antibody.



H)





Remaining nuclear and cytoplasmic western blots from AgeI-digested linear MTF1 overexpressing SW1353 cells treated with medium alone, IL-1 $\alpha$  and/or ZnCl $_2$  for G) 24 or H) 72 hours. Each row of western blots are biological replicates from the same 24 or 72 hour experiment. The band observed at 55kDa probed with lamin AC in the 72 hour blots is non-specific and was not included in the densitometry analysis of the data in Figure 6.19.

